

CURRENT PRACTICES AND TRENDS IN
INTELLIGENCE ANALYSIS

①

CURRENT PRACTICES AND TRENDS IN
INTELLIGENCE ANALYSIS
INTELLIGENCE ANALYSIS

AD-A226 670

DTIC
ELECTE
SEP 05 1990
S D G D

DTIC FILE COPY.

DISTRIBUTION STATEMENT A
Approved for public release
Distribution Unlimited

90 08 10 216

**CURRENT PRACTICES AND TRENDS
IN
MECHANICAL FAILURE PREVENTION**

**Proceedings of the 44th Meeting
of the
Mechanical Failures Prevention Group**

**Virginia Beach, Virginia
April 3-5, 1990**

**Compiled by
Henry C. Pusey
and
Sallie C. Pusey**

**A Publication of the
Vibration Institute**
A NOT-FOR-PROFIT CORPORATION



**THIS DOCUMENT CONTAINED
BLANK PAGES THAT HAVE
BEEN DELETED**

Copyright © 1990 by
Vibration Institute
6262 S. Kingery Highway
Willowbrook, Illinois 60514
All Rights Reserved

AVAILABLE FOR \$50.00 from Vibration
Institute 6262 S. Kingery Highway
Willowbrook, IL 60514
TELECON 9/4/90 VG

Special Notice

The U.S. Government retains a nonexclusive, royalty-free license to publish or reproduce, or allow others to publish or reproduce, the published forms of any papers in these proceedings authored by a government agency or a contractor to a government agency whenever such publication or reproduction is for U.S. Government purposes.



Accession For	
NTIS CRA&I	<input checked="" type="checkbox"/>
DTIC TAB	<input type="checkbox"/>
Unanno.	<input type="checkbox"/>
Justific	
By <u>50.00</u>	
Distributi. <u>price</u>	
Availability codes	
Dist	Availability for special
<u>A-1 21</u>	

TABLE OF CONTENTS

PREFACE	vii
FEATURED PAPERS	
→ The High Cost of Failure of Rotating Equipment <i>N. F. Rieger, T. H. McCloskey and R. P. Dewey</i>	3
Abstract: Structural Transfer Functions - "Real" vs. Digital <i>R. H. Lyon</i>	23
→ Legal Liability of the Design Engineer <i>T. H. Shunk</i>	25
→ Detection, Diagnosis, and Prognosis: An Evaluation of Current Technology <i>R. L. Eshleman</i>	33
→ Plasticity in Failure Mechanisms <i>C. D. Beachem</i>	43
MOTOR DRIVEN EQUIPMENT DIAGNOSTICS	
Induction Motor Fault Detection via Passive Current Monitoring - A Brief Survey <i>G. B. Kliman and J. Stein</i>	49
→ MOVATS Diagnostic Methodology <i>W. L. Lavalley and W. D. Romine</i>	67
Motor Current Signature Analysis(MCSA) <i>C. L. Thibault</i>	73
Cost-Effective On-Line Monitoring of Rotating Equipment Using Motor Current Analysis <i>D. J. Linehan, S. L. Bunch and B. B. Hanzelka</i>	81
Machine Monitoring via Motor-Current Demodulation Techniques <i>S. F. Smith, K. N. Castleberry and C. H. Nowlin</i>	87
Incipient Failure Prediction for Electrical Machines <i>J. L. Kohler, J. Sottile, F. C. Trutt and C. Santa Cruz</i>	97
Self-Learning Prognostic Systems <i>C. G. Kolbach</i>	111
OIL ANALYSIS IN MACHINERY DIAGNOSTICS	
Techniques to Evaluate the Remaining Useful Lubricant Life of Gas Turbine Engine Lubricating Oils <i>R. E. Kauffman</i>	121
On-Line Monitoring of Ferromagnetic Debris Concentration <i>P. Campbell</i>	131
High Power - Density Reduction Gearbox Lubrication Studies Using Positron Emission Tomography <i>V. Mashkin and M.R. Hawkesworth</i>	141

Impact of Microfiltration on Spectrometric Oil Analysis C.S. Saba	151
Summary of New Techniques to Improve the Ability of Emission Spectroscopy to Detect Large Wear Particles in Lubricating Oils M. Lukas and D.P. Anderson	161
METHODOLOGY FOR IMPROVED DURABILITY	
Remaining Life Assessment of Thermal Power Plant Components Using Fracture Mechanics Approach J. Pattabiraman and B. J. Sukanya	173
Design of Permanent Magnet Biased Magnetic Bearings for a Flexible Rotor C. K. Sortore, P. E. Allaire, E. H. Maslen, R. R. Humphris and P. A. Studer	183
FAULT DIAGNOSIS	
The Effect of Transformation from a Fixed to a Rotating Coordinate System on Excitation Frequency J. Neun and L. Hoogenboom	195
Pump Problems and Piping Participation (Real and Alleged) E. C. Goodling, Jr.	205
DATALERT: An Integrated Machinery Vibration Data Collection and Analysis System Used in Loss Prevention K. D. Bever and T. M. Raymond	215
Analysis of Gear Vibration in the Time-Frequency Domain B. D. Forrester	225
Vibration Signature and Fatigue Crack Growth Analysis of a Gear Tooth Bending Fatigue Failure H. J. Rose	235
CONDITION MONITORING	
Acoustic Emission Analysis for Bearing Condition Monitoring C. J. Li and S. Y. Li	249
Systems for Preventing Mechanical Failure of Machine Tools R. K. Wharton	259
Condition Monitoring of Operating Fluid Film Bearings with Ultrasonic Transducers F. C. Wiesinger Jr., G. T. Haramis Jr., W. E. Karberg, P. Rapone and R. E. Berris	273
Condition Based Maintenance for Shipboard Machinery G. W. Nickerson	285
A Condition Based Maintenance Monitoring System for Naval Shipboard Machinery C. P. Nemerich, W. W. Boblitt and D. W. Harrell	295

MECHANISMS OF FAILURE

Analysis of Crack Tip Blunting, Initiation and Growth of Aluminum SEN Specimens by Moire Interferometry <i>B. S. -J. Kang, V. Vaselenak and Q. -K. Liu</i>	307
--	-----

Advances in Preventing Premature Failure of PEEK Based Compressor Valve Plates <i>R. S. Klein, H. P. Wertheimer and D. Woollatt</i>	325
--	-----

Diagnostics Look at Engine Condition <i>J. L. Pettigrew</i>	335
--	-----

PREDICTIVE MAINTENANCE

Fifteen Proven Predictive Maintenance Technologies <i>J. W. Flude</i>	355
--	-----

APPENDIX

List of MFPG Publications	367
---------------------------	-----

PREFACE

The 44th meeting of the Mechanical Failures Prevention Group(MFPG) was sponsored by the Office of Naval Research(ONR) and held April 3-5, 1990 at the Cavalier Hotel in Virginia Beach, Virginia. Meeting management, program coordination, exhibit scheduling, tour arrangements and proceedings compilation were by the Vibration Institute. MFPG Council Chairman **Henry R. Hegner** of ECO, Inc. chaired the program committee and developed the two sessions on Motor Driven Equipment Diagnostics. **John J. Anderson**, CTS, Inc.; **Sudhamy Basu**, the Scientex Corporation; **Michael Behm**, Behm Balancing Devices; **Paul L. Howard**, Giordano Associates, Inc. and **T. Robert Shives**, National Institute of Standards and Technology were active members of the program committee. **Henry R. Hegner** chaired the Opening Session. Other session chairmen are identified on the section title pages in these proceedings.

Special thanks are due to **John L. Frarey** of Shaker Research Corporation for organizing a panel session on Detection of Bearing Failures and to **John S. Mitchell** of Palomar Technology International for conducting a workshop on Predictive Maintenance. Appreciation is extended to the Naval Aviation Depot, Norfolk, Virginia for arranging an excellent tour of their facilities on the day following the conference.

For more than 20 years, the proceedings of this distinguished series of MFPG meetings have been added to the archives of failure prevention technology. The proceedings of the 44th meeting are the first to be distributed at the conference. This accomplishment was made possible by the enthusiastic cooperation of all concerned; the MFPG Council, the Program Committee, the session chairmen and, especially, the authors/speakers. Very tight deadlines were set and met for the delivery of manuscripts. This volume is the result. It is my view that it was well worth the effort. I would be pleased to receive the opinions of others.

The Mechanical Failures Prevention Group was organized in 1967 under the sponsorship of the Office of Naval Research to focus on mechanical failure technology. Improved reliability, greater safety and economic savings were among the obvious goals to be achieved through a better understanding of mechanical failures. The original objectives continue to form the basis for the activities of the current technical committees. With the ever increasing complexities of equipment and systems and the shrinking federal budget, the goals of the MFPG become even more important.

The National Institute of Standards and Technology(formerly NBS) has had a long history of interest and activities in the field of failure analysis and prevention. It was natural, therefore, that as the membership and activities of the MFPG grew, ONR asked NBS for assistance. In 1971, NBS assumed the role of a primary sponsor of the MFPG and continued this function, with the support of other government agencies, through the 43rd MFPG Meeting. At the 44th Meeting, the Vibration Institute accepted the responsibility for conference management, with the ONR once again the principal sponsor. The MFPG Council is currently seeking additional sponsors from interested government agencies. They are also looking for motivated volunteers to participate in technical committee activities.

On behalf of Dr. Eshleman and the Vibration Institute, I want to thank the Office of Naval Research and the MFPG Council for inviting us to participate in the organization of the 44th MFPG meeting. It is our hope that this series of conferences will continue to provide a common meeting ground for those who have mechanical failure problems and those who are engaged in failure avoidance technology.

Henry C. Pusey
General Chairman, MFPG '90

FEATURED PAPERS

Keynote, Opening Session, Plenaries

Chairman: Henry R. Hegner
ECO, Inc.

The High Cost of Failure of Rotating Equipment

Neville F. Rieger
Stress Technology Inc.
Rochester, New York

Thomas H. McCloskey
Electric Power Research Institute
Palo Alto, California

Robert P. Dewey
Stress Technology Inc.
Rochester, New York

Abstract

Costs of several failures which occurred in rotating machinery are reviewed in terms of 1) machine damage costs and 2) loss of production costs. This information is based on reported damage costs from insurance companies, and on estimated replacement electric power costs based on specified data. The known causes of such failures are presented for discussion, and it is shown that in most instances replacement power costs from lost production represents the greatest source of financial loss in such events. Suggestions are offered for ways to reduce each of the above costs, in the event of rotating equipment failure.

1.0 INTRODUCTION

Rotating equipment failures cause millions of dollars of unrecovered costs in lost energy production, plus additional millions of dollars paid in replacement equipment costs paid by casualty insurers. During a loss event, efforts are usually focused on restoring the unit to service as quickly as possible. It is important that a comparable effort is made to understand the failure root-cause, and to apply the information gained by the failure experience. Experience has conclusively shown that where failed rotating members are simply replaced with identical components, the original problem is likely to be re-installed, and the failure scenario may be re-initiated.

Substantial financial risks are therefore inherent in the above approach, particularly if the remaining failure root cause involves a chronic problem. It is now well proven that the financial risks associated with any catastrophic failure far outweigh the investment typically required to identify a life-extension strategy to make the component failure-proof. The long term consequences of many failures can be controlled or prevented by the application of technology now available through most equipment manufacturers, research institutes, and specialized independent consultants.

This paper contains a discussion of five types of rotating equipment failures, each of which is important either from its relative frequency of failure, or from the extreme cost of such events. A scale is presented by which lost production costs, repair/replacement costs can be estimated from previous catastrophic events. Appropriate actions for preventing or controlling such events are then discussed. Such actions can be applied to the rotating equipment found in most turbine power plants, and the costs and failure scenarios apply generally to bladed turbomachinery. The paper utilizes certain cases of steam turbine failure to demonstrate the likely financial consequences of three basic types of failure; degradation, rupture and bursting as these apply to flow path components, to individual blades or blade groups, and to disks, integral rotors, and turbine generator drive trains. Downtime and associated costs have been obtained from EPRI sources and from Insurance Company reports published subsequent to the catastrophic events mentioned herein.

2.0 INDUSTRY PERSPECTIVE

Surveys of the power generation industry have consistently shown that, other than boiler problems, turbine outages represent the single largest contributor to lost productivity [1]. Generation loss statistics have shown that lost MW production represents the greatest source of immediate financial loss to utilities. Turbine failure statistics in particular are dominated by long forced outages in which unavailability of parts, repairs and installation costs have played a major role. For example, turbine problems associated with valves, piping, lubrication, or vibration typically require from 100 to 400 man hours to resolve. Blade failures (cracks in the roots, shrouds or vanes) have reportedly extended such outages by 500 to 1500 hours. If the blade or disk failure was catastrophic, with consequential damage to adjacent rows or casing, the outage could approach 6 to 12 months to repair.

A more extensive EPRI study [2] focussed on blade failures, as related to (300MW+) turbines. This survey showed that losses due to blade failure alone caused over two-hundred thousand hours of lost power production, estimated in value at 1.1 (1983) billion dollars, during the years 1970-1981. Blade, diaphragm and rotor replacement costs were correspondingly reported at \$87 million dollars. The average costs of blade failures over a 10 year period was 5,200 hours of unit downtime per reporting utility (or 2400 hours/unit) and \$2.1 million dollars in replacement parts (\$1.1 million per unit) in 1983 dollars.

The failure of a disk, of a rotor or of a generator is typically catastrophic, and will usually result in unit shut-downs of several months duration, depending largely on whether the component failure was contained within the turbine or generator

casing. One of the more striking findings of the EPRI survey was that few failure reports or records were available from the operators which contained a detailed discussion of the failure. In nearly half these instances, failures were reported as "cause unknown", or were attributed to the operating circumstances, as no other explanation was found. The original blade design was reinstalled in the unit without significant reworking. The success ratio of this approach was less than 60%. Although independent root-cause analysis is more widely practiced in the utility industry today, such analysis is still mostly limited to situations where repeated or periodic failures have continued.

3.0 CLASSIFICATION OF CASES

The most frequent turbine-generator unit failures can be classified into the five categories of increasing severity shown in Table 1.

Table 1
Causes of Turbine Damage and Failures

Classification	Mechanisms
1. Blade/diaphragm degradation	Solid particle erosion, corrosion, moisture erosion
2. Blade cracking/failure	Resonance, flutter, corrosion-fatigue, creep
3. Disk cracking/rupture	Stress corrosion cracking, resonance, water-cutting
4. Generator failure	Hydrogen embrittlement, catastrophic unbalance, retaining ring cracking, fire
5. Rotor burst	Whirl unbalance, misalignment, low-cycle fatigue

Blade/diaphragm degradation and blade cracking are the most commonly observed blading failures. Such degradation develops progressively, and is usually repaired during maintenance outages. When present it can result in significant losses in production and thermal efficiency. Erosion problems are generally confined to one or two HP stages of the turbine, and erosion/corrosion problems occur most frequently in the last three (wet) stages of the LP rotors. While degradation problems *per se* rarely cause a forced outage of a unit, the consequences can still be severe and on-going in terms of cost, as will be discussed.

As EPRI surveys have shown [3], disk cracking is not as rare as might be expected. This survey identified that 33 out of 72 operating nuclear plants had reported low pressure disk cracking by 1980, i.e. within the first 10-20 years of service. Within the same period, 32 out of 46 units experienced outages due to generator problems. Eighty five percent of all generator problems involved outages over 100 hours. Complete rewinds of a generator are similar in repair duration to those of a blade failure. The outage period typically lasts from 1500 to 2000 hours [3].

Turbine rotor bursts occur much less frequently and may be classified into those cases where the portion of the rim breaks off, or where the disk shatters into several pieces from the bore. Irrespectively, the consequences are severe because both situations produce large missiles. The destruction resulting from a disk burst is typically contained by the turbine casing, whereas a bore burst may release missiles into the turbine hall or beyond. Generator bursts are more likely to be contained, but the presence of cooling hydrogen may result in an explosive fire which may be prolonged by escaping lubricant from the generator bearings.

4.0 BASIS FOR ESTIMATED COSTS

The costs provided in this paper are based either on reported figures or have been estimated based on the figures which follow:

Table 2
Estimated Costs For Replacement Power in \$/KwH

	<u>Oil</u>	<u>Coal</u>	<u>Nuclear</u>
1970	0.03	0.03	0.02
1980	0.09	0.05	0.035
1990	0.06	0.08	0.06

Table 3
1990 Typical Costs of Replacement Blading \$1000.00

<u>Stage</u>	<u>100MW</u>	<u>300MW</u>	<u>500MW</u>
Control	50-100	90-175	150-300
HP	40-90	75-150	125-175
IP	50-100	80-175	150-200
LP	50-150	80-250	150-400

Table 4
Relative Costs Associated With Each Turbine Failure

Category	Event	Repair	Production
Blade Erosion	Erosion	\$ 0.05 M-\$ 0.15M	\$ 0.5 M - \$ 2.0 M (annual)
Blade Failure	Loss	\$ 0.1 M-\$ 0.5 M	\$ 2.0 M - \$ 8.0 M
Disk Failure	Burst	\$ 3.5 M-\$ 5.0 M	\$ 15.0 M - \$ 35.0 M
Rotor Failure	Burst	\$ 10.0 M-\$30.0 M	\$ 100.0 M - \$200.0 M
Generator	Burst	\$ 15.0 M-\$40.0 M	\$ 100.0 M - \$500.0 M

The source of the above figures are cited values from several utilities, and from many failure costs obtained over the past 15 years. Utilizing the above figures, the cost of any failure event or degradation replacement can be estimated on a consistent basis for comparison purposes. Examples of the use of these figures are given later in the text. Where known figures are available from authoritative sources, these figures are given with the reference.

The failures discussed herein occurred on turbine-generators ranging in size from 100MW to 600MW in capacity. The production losses shown reflect total loss estimates using data from Tables 3 and 4. The degradation problem reflects the average ongoing cost in lost performance during (1) year out of (10) years unit operation. The blade failure figures represent the consequence of a multiple event within a single year. The rotor and generator failures both result in extensive damage to the unit and to the associated plant, and have sometimes resulted in unit unavailability for up to two years. Evidently, all production losses are influenced by availability of replacement parts or rotors. While operation without blade rows may restrict MW output, unavailability of rotors shuts the unit down completely.

5.0 DEGRADATION OF FLOWPATH COMPONENTS

The costs presented for blade erosion are based on the power curtailment for a 100 MW turbine which has experienced severe erosion in three LP stages [4]. Examples of deposit build-up are shown in figure 1, and erosion/deposit damage is shown in figure 2. Erosion losses are associated with the following effects:

- Erosion of diaphragms disturbs the flow field by degrading the profile geometry, and by altering the velocity triangles. It is known that profile degradation losses are more severe for HP stages than LP stages, though the rates of degradation are often faster in LP stages.
- The erosion of diaphragm trailing edges also alters the flow exit angles and wake thickness, thereby affecting stage performance losses, and increasing blade excitation stimulus for at nozzle passing frequency.
- Deposit build-up also affects the airfoil surface roughness of both diaphragms and blades. Where deposit build-up occurs in Wilson Line stages, surface corrosion may be fostered, as shown in figure 2, with the deposits acting as nesting sites for trace chemicals within the steam chemistry. Such deposits are typically removed during scheduled overhauls.

Can blade degradation problems be prevented or controlled? In one case of a geothermal steam quality problem, a need existed to contend with a caustic flow environment. Initially, the costs associated with obtaining better control of the steam quality were viewed as being prohibitive and unnecessary. Units of similar design in other locations had not experienced such severe erosion. In hindsight, the estimated performance losses attributable to turbine inefficiency alone were estimated to be 14 million dollars over 11 years. Further, these losses were also occurring in several units operated by the utility, all of which experienced similar performance problems [4].

It is also becoming increasingly important for utilities to prepare Acceptance Criteria for Blading (and other) components which address the specific needs and operating conditions within their units. Blade life extension, or improvement strategies can also be planned and reviewed at the outset, prior to purchase of new or replacement blades. For example, blade designs may be selected in cooperation with the manufacturer which incorporate integral covers, or free standing airfoil designs, to minimize corrodent traps at tenon-cover failure locations. Coating techniques which have been pioneered by EPRI and Southern California Edison have demonstrated excellent results to date, and may be implemented with a view toward reducing the incidence of corrosion and erosion. The estimated production and degradation savings by one utility which has implemented such coatings is \$41.3 million over a five year period [5].

Sophisticated turbine performance codes such as STELLA (Steam Turbine Efficiency and Low pressure Loss Analysis) [6] have recently become available to verify performance and efficiency claims made for advanced or replacement stage geometries, for multiple stages throughout the steam or gas flow path. Such codes also allow both maintenance outage or replacement scheduling to

be planned based on the perceived cost of erosion losses vs overhaul and repair costs. An independent evaluation program has been used by several utilities to identify and select the most suitable flow path design from those proposed by several manufacturers, through a selection procedure which objectively evaluates claims concerning performance, reliability and cost.

6.0 BLADE FAILURES

Turbine blades are required to operate under severe conditions, typically involving static, dynamic and thermal loads. Most blades currently in operation can be expected to perform reliably for 20 years or more without requiring replacement. Potentially however, a single blade failure can result in significant losses in production, depending on whether blade cracking is identified during an inspection outage, or whether the component fails catastrophically during operation. It was therefore surprising to find in the EPRI blade failure survey [3] a significant number of repeat failure incidents which resulted from adopting unproven life-extension approaches presumably used for the sake of expediency. It is emphasized here that fix verification cannot be assured based on "similar" previous experience. Blade life improvement is a skilled technique. Statistics and experience clearly show that anything less than purposeful cause identification followed by careful replacement engineering will often lead to further failure.

A typical case is the failure of a low pressure steam turbine blade in the L-2 row of a 492MW nuclear unit. The initial forced outage was indicated by a stepped increase in vibration due to unbalance, detected at the bearing adjacent to the failed stage. Inspection showed that a blade had separated from the disk as shown in figure 3, failing in the first attachment hooks of the root. Blades of the original design were installed and the unit returned to service. It was stated at this time that 30 identical rows of blades had been in service for as long as ten years without such a failure occurring. Two years later, during a refueling outage, the blades were again inspected and once again were found to be cracked. The blade row was replaced and this time re-grouped in an attempt to correct a perceived tuning problem. Five months after the refueling outage, a third blade failure occurred. As shown in figure 4, a blade again separated from the disk, in a similar fashion to the original failure. Recognizing the need for a detailed investigation, each of the L-2, L-1 and L-0 blade rows was removed, and baffle plates were installed. (L-0 and L-1 rows had suffered consequential damage). This reduced the unit's MW production by 10% for a further 13 months which represented \$14.0 million dollars in lost revenue. ($492\text{MW} \times 0.1 \times 24 \text{ hours} \times 365 \text{ days} \times 13/12 \times \$0.03/\text{MWh}$).

A cooperative effort of analysis and testing by the manufacturer, utility and consultant determined that the problem had been caused by coupling between the lowest tangential blade mode with the generator torque pulsations, due to electrical network transients at 120hz. These pulsations caused high blade transient stresses, and eventually blade failure by high cycle fatigue. This hypothesis was established by analysis, verified by telemetry testing of the rotor, and confirmed by the manufacturer. During a scheduled fourth outage, a new blade design was installed which reduced both steady and dynamic stresses at the failure location. The unit has since operated for 14 years without a subsequent incident.

The high cost of such blade failures has now established the critical importance of root cause investigations to eliminate the risk of subsequent repeat failure outages. Approximately 3500 hours of unit outages were required for the blading work during the four outages described in the above example. For the machine this represents an estimated loss of \$35 million dollars in production, of which 75% was incurred between the third and fourth outages. This is in addition to the \$14 million loss due to restricted output noted above. The total cost in 1990 dollars would be about \$98 million. The cost of the independent root-cause diagnosis which was performed subsequent to the third outage was less than \$50 thousand dollars.

Real alternatives to a trial and error approach toward blading failures are now available through EPRI in the form of a customized software program "BLADE" (Blade Life Algorithm For Design Evaluation). BLADE is organized for use by turbine operators, with the capability to perform stress analyses, frequency calculations, and the ability to predict blade life based on the unit operating pattern [7]. As part of a verification effort, BLADE has now been used to assist host utilities identify the cause of a generic problem, and to select a suitable fix. In a typical application of BLADE, the estimated savings in replacement parts alone was valued by one utility at \$1.3 million dollars [8]. BLADE is scheduled to be released for EPRI membership use in late 1990, and will also be made available for licensing to non-EPRI members, on a fee basis.

It is strongly emphasized that blade replacement alone without supporting engineering amounts to "blade roulette". Good engineering demands thorough root cause analysis, following immediate replacement to restore production. Eventually a real fix based on the agreed root-cause must be devised and installed as soon as possible during a second (scheduled) outage.

7.0 DISK CRACKING AND RUPTURE

Disk cracking may occur at one of four locations; keyways, bores, rim attachments, and on the disk faces, if the critical conditions of flaw size, stress, corrosion, and operation are satisfied. Rim attachment failures are generally less catastrophic. These have been caused by stress corrosion cracking, and by resonant axial disk vibrations.

The modern era of disk bursts resulting from stress corrosion cracking began with the explosion of the disk of a 60MW nuclear unit in 1969. Subsequent studies revealed that a large number of identical operating rotors were also cracked in a similar manner, but had not yet burst. This launched an in-depth study for the root cause, and for its fix, which was eventually identified as stress corrosion cracking. Disk-bore failures typically involve either stress-corrosion and/or low cycle (start-stop) fatigue. Cracks have developed from bore keyways and from disk and rotor inclusions which have linked together and propagated within the disk under cycled hoop stresses during start-stop cycling. These cracks are intergranular and branched which demonstrates that a corrosive mechanism has contributed to the crack propagation (and also probably to crack initiation).

Figures 5 and 6 show sections of a disk which burst at each first stage of a 200 MW nuclear unit. The failure was not preceded by any measurable increase in vibration. The unit had accumulated approximately 134,000 hours of service. An investigation of the failure sponsored by EPRI showed that failure resulted from long-term growth of sub-critical cracks around the bore surface. Catastrophic rupture grew from two diametrically opposed locations. The failure of one disk is thought to have precipitated the failure of the second disk, resulting in additional severe internal damage to the turbine, though no missile fragments penetrated the outer casing. Magnetic particle testing showed a large number of sub-critical cracks oriented in a radial/axial direction, and located within two bands, one near each face of the disk. Crack indications ranged from less than 3mm up to 18mm. Several indications were co-planar, in close proximity to one another, and showed substantial overlap. Tensile residual stresses were measured at the disk bore surface, but were thought to have resulted from the residual shrinkage assembly stresses. Corrosive attack on the crack surfaces was indicated, but no evidence of pitting or general corrosive attack of the bore surface was apparent [9].

Can such failures be prevented or controlled? Improvements in ultrasonic testing have since allowed utilities to periodically monitor and record the number and growth of small cracks or inclusions within a disk, down to the bore. Programs such as EPRI's SAFER Code [10] have been developed to map the three-dimen-

sional location of indications and the distance between them to assist in determining whether indications are likely to link up under the action of the prevailing (calculated) stress field, and if so, whether these indications may reach critical size under cycling or corrosive conditions. Recent use of SAFER by Rochester Gas and Electric Corporation resulted in a \$1.0 million dollars savings by preventing the premature retirement of a rotor which had been condemned based on the raw ultrasonic data [11]. A similar application indicated that short-duration continued use of an L-0 row of rotating blades would be possible with an existing crack indication, provided no further up-down or MW load cycling was undertaken. The unit subsequently ran safely without blade failure for a further 6 months until a scheduled replacement outage, saving the utility an estimated \$12.5 million in replacement power costs.

8.0 ROTOR BURST

In 1987, a monoblock turbine rotor which had operated for approximately 58,000 hours, including 728 hot starts, and 110 cold starts, exploded without advanced warning. Failure originated in the second LP rotor section, which broke into approximately 80 pieces. The turbine was completely destroyed, as shown in figure 7. Consequential damage to the plant was extensive when fragments of the rotor tore through both the turbine casing, and through the plant roof. Two fragments weighing over one ton apiece were found in an adjacent field, more than one kilometer from the plant site. The single largest fragment of 24 tons, shown in figure 8 illustrates how the rotor split along the plane of the centerline. Faults from which the brittle fracture initiated are discernible from this photograph.

The estimated cost for repairs to the unit and plant were valued in the tens of millions of dollars. Based on the size of the machine, and its mode of operation, a single year of lost production was estimated to be about \$120 million. Despite the ferocity of the explosion, no one was injured.

Completed in 1969/70, the rotor represented the largest forged piece of its type manufactured in Germany up to that time. As part of acceptance tests for this rotor, ultrasonic examination had showed something "unusual" near the rotor axis, in the head section of the original steel casting. The rotor was overspeed tested and then re-examined by ultrasound in the area where the unusual readings had occurred. No change was indicated. Additional material strength analyses were performed, but it appears that a life prediction analysis based on the up-down cycling of the unit was not performed. It should be here recalled that life prediction is a constantly evolving technology, and that such analyses may not have been possible twenty years ago. However, during its last few years of operation, the turboset had been mainly used to cover peaking requirements.

This involves up-down cycling, possibly twice daily. Several overspeed tests were also conducted subsequent to the initial run [12].

Hindsight of course, suggests several possible actions which if undertaken may have warned of the impending burst. Regular ultrasound testing might have detected the growth of the crack as it began to progress. The rotor could have been bored to eliminate the non-homogeneous material, although this doubles the bore stresses. Conventional fracture mechanics could have been used to test the feasibility of cyclic operation in terms of stresses and remaining life. Without question, before the original service profile for the unit was changed, and ongoing up-down cycling began to degrade the rotor residual life, analytical/ultrasound reassessment of remaining life would have been prudent, as the RG&E example above (and others) have shown.

As the cost of capital equipment in the United States continues to grow, it is understandable that the average age of rotating equipment in the United States will also continue to increase as life-extension is preferred to replacement. Life extension strategies have therefore become of greater concern to utilities wishing to avoid new construction. The technology to address this situation is available, in large part through EPRI. Remaining life extension programs now allow rotor residual operating life to be evaluated with good success against the possibility of rotor failure. To study questions of life extension, computer programs such as the SAFER code described previously, and the FEATURE code for rotordynamic analysis may be used [12]. FEATURE is a micro-computer based program for the static and dynamic analysis of complex multi-rotor bearing systems. FEATURE was designed specifically to assist plant engineers in establishing and improving the dynamic performance of rotating machinery.

9.0 GENERATOR AND TURBINE ROTOR SYSTEM FAILURE

During the past 15 years, there have been several spectacular rotor system failures among the world's utilities. Although these events have been studied in great detail by the manufacturers and utilities concerned, little information has been reported on these occurrences. One case concerns a 600MW turboset which was restarted following a general overhaul and inspection outage. Before returning the unit to service, the electrical overspeed protection device was to be checked by running the unit to 110% overspeed. Just before reaching this speed, the turboset exploded. Leaking generator hydrogen and lubricating oil then ignited, causing a large fire. Subsequent inspection of the unit showed that the generator shaft had ruptured over half its length and was broken near its mid-point, as shown in figures 9 and 10. Two fractures had occurred at the overhung exciter end of the system. Portions of the exciter had cut through the casing and

were hurled into the machine hall. One piece weighing three tons struck the girder of an overhead crane, causing it to fall thereby creating a crater one meter in diameter in the floor. The entire exciter-generator-LP turbine shaft system train was catastrophically broken at eleven different locations. The turbine generator system was considered to be an 85% loss, resulting in repair and component replacement damages to approximately \$40 million dollars [14]. Corresponding power replacement losses for the for (2) year repair outage involved would have been over \$300 million.

The cause of this failure has been attributed to turboset instability, most likely created when the overhung exciter became unbalanced. Several studies of the system characteristics have been pursued subsequent to the basic failure, in which sophisticated rotordynamic models of the entire system have been used to examine in detail the three dimensional, non-linear behavior of the system in its bearings and foundation supports. These results illustrate the detail with which such complicated systems can now be investigated to evaluate their stability properties, and the extent to which system stability is influenced by rotor unbalance under non-linear bearing load conditions.

10.0 ACTIONS TO PREVENT OR CONTROL LOSSES

Some useful actions which may be taken to prevent the failures and losses described in this paper are:

1. Prepare appropriate acceptance specifications based on life analyses of anticipated operating conditions which address all recognized failure modes to which the equipment is subject. Such specifications should be prepared by the purchaser, and negotiated with the manufacturer prior to contracting for the unit or component.
2. Regular non-destructive examinations should be undertaken during inspection outages, to detect cracks at critical locations at an early stage where possible.
3. Spare rotor programs should be considered for base loaded units from the outset. Cost benefit studies show that spare rotor costs are recovered in efficiency gains, in reduced maintenance outages, and in crack detection to avoid catastrophic events.
4. Chronic repeating blade failures usually indicate a performance malfunction problem which should be addressed and corrected at the root cause level.
5. Root-cause diagnosis should be undertaken in parallel with short term blade replacement efforts when restoring a unit to service. The benefits of utilizing the

experience gained from a failure investigation can be applied directly in determining the a permanent fix.

As indicated, many advanced programs have recently been developed by EPRI and others which directly address most of the problems detailed herein. For next generation machinery, specifications prepared in advance can allow an operator to ask the pertinent questions regarding reliability or performance, and seek competitive bids from several suppliers. For existing machines life extension procedures based on sound engineering can be implemented for most types of rotating machinery. Procedures for cost-effective reblading and refurbishment of flow path components are now available to greatly extend and enhance the performance of existing equipment.

It is evident that when all costs are considered, component degradation can be prohibitively expensive, and failure of the system can be financially ruinous. Today, such costs can each be minimized or prevented directly through the application of appropriate investigative procedures and diagnostic technology, applied in advance of installation and during operation of turbine-generator equipment.

11. REFERENCES

- [1] Koppe,R.,Olson,E."Nuclear and Large Fossil Unit Operating Experience", EPRI NP 1191, Project 771-4, September 79
- [2] Dewey,R.,Rieger,N.,McCloskey,T."Survey of Steam Turbine Blade Failures", EPRI CS 3891, Project 1856-1, March 1985
- [3] Lyle,F.,Burghard,H."Steam Turbine Disk Cracking Experience", EPRI CS 3891, Project 1398-5, June 1982
- [4] Tsujimura,K.,Tagami,S.,Myazaki,M.,Randolf,J."Geothermal Steam Turbines" Chapter 3, Sawyer's Turbomachinery Maintenance Handbook, Volume 2, 1980
- [5] Ortalano,R.,McCloskey,T. "Development of Low Pressure Coatings Resistant to Steam Borne Corrodents", EPRI CS 3139, Project RP 1408-1, June 1983
- [6] Hong,C.,Subbiah,R. "STELLA Manual for The Estimation of Multi-Stage Steam Turbine Performance" STI Proprietary Computer Code, February 1989
- [7] Redding,M.,Lam,T.,Dewey,R.,Hesler,S. "The BLADE Program as a Diagnostic Tool For Turbine Blade Failures", EPRI Steam Turbine/Generator NDE Workshop, 1989

- [8] EPRI First Use "BLADE Code Helps SCE Select a New Blading Design" RP 1856, August 1989
- [10] Burghard, H. "Metallurgical Evaluation of A Failed LP Turbine Disk" EPRI NP 2738, Project 1398-6, December 1982
- [11] McCann,D.,Reichel,W.,Burton,W.,Grandjean,D. "Overboring Extends Life of Rotor Slated for Replacement by OEM" Power Magazine, January 1988
- [12] Schaden Spiegel "Largest Steam Turbine Loss in Germany" Munich Reinsurance Company, February 1988
- [13] Lee.C, Tecza,J.Zorzi,E. "FEATURE: Finite Element Analysis Tool For Utility Rotor Dynamic Evaluation", CS-3999-CCM, Project RP 1648
- [14] Schaden Spiegel "Catastrophic Loss At A Steam Power Plant" Munich Reinsurance Company, January 1982



Figure 1: Deposit buildup on inlet nozzles HP turbine stage.



Figure 2: Surface degradation and deposits LP flow guides.

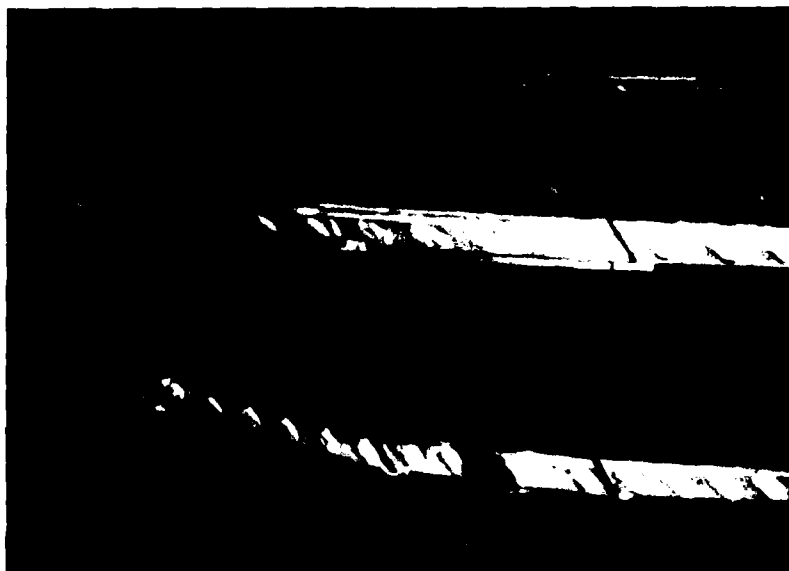


Figure 3: Rotating blade loss from L-2 row and consequential damage (initial failure).

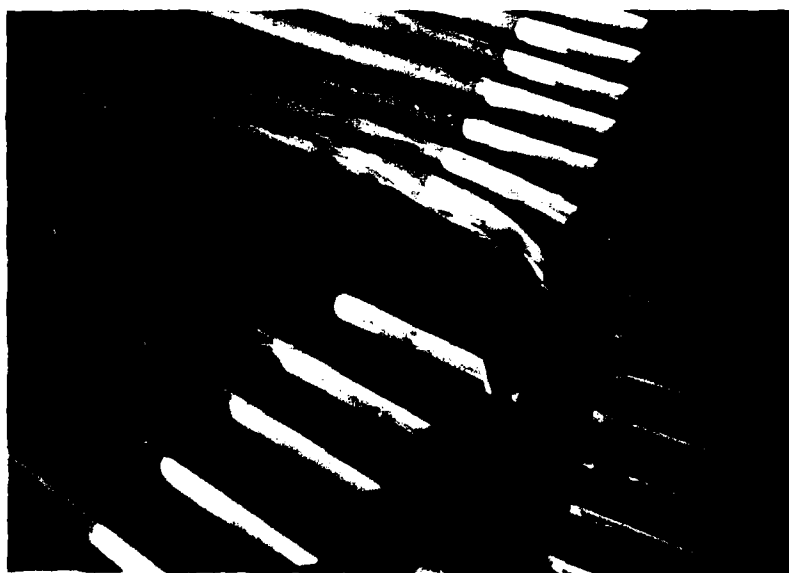


Figure 4: Rotating blade loss from L-2 row and consequential damage (3rd failure).

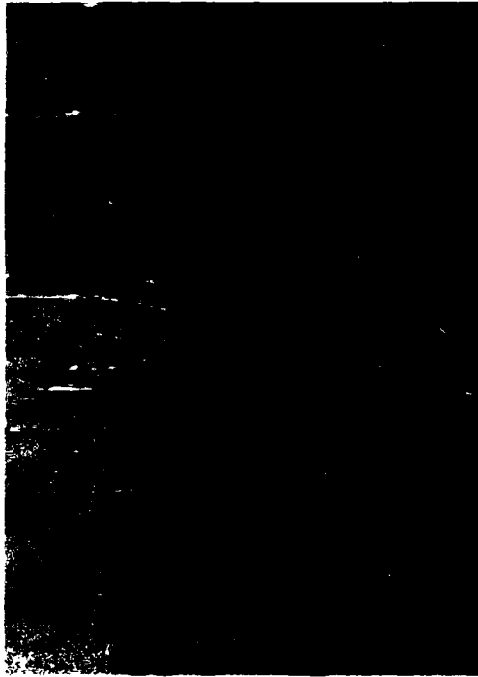


Figure 5: Radial crack from disk burst showing initiation sites at bore.



Figure 6: Disk segment from burst showing radial crack planes.



Figure 7: Wreckage of 330 MW Turbine-generator from LP rotor burst.

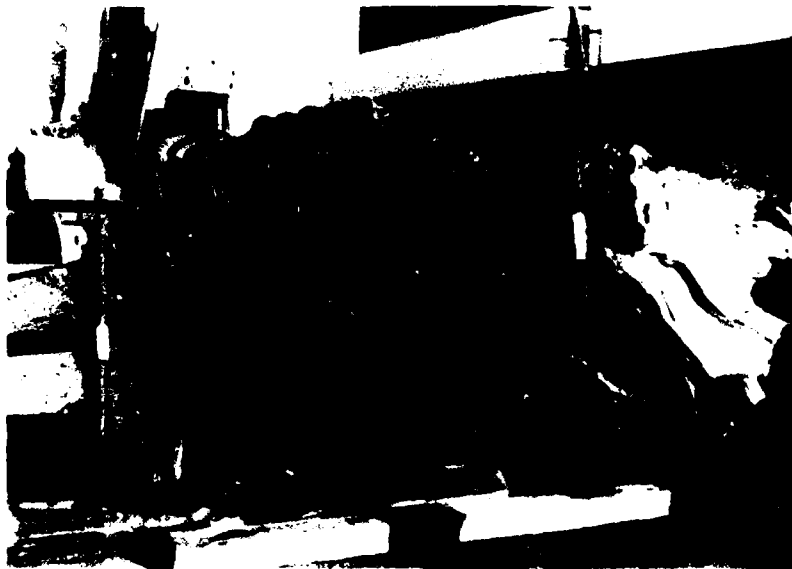


Figure 8: Burst rotor segment weighing 24 tons showing bore inclusions and cleavage planes.



Figure 9: Remains of 600 MW Generator showing shaft crack extending to coil slots.

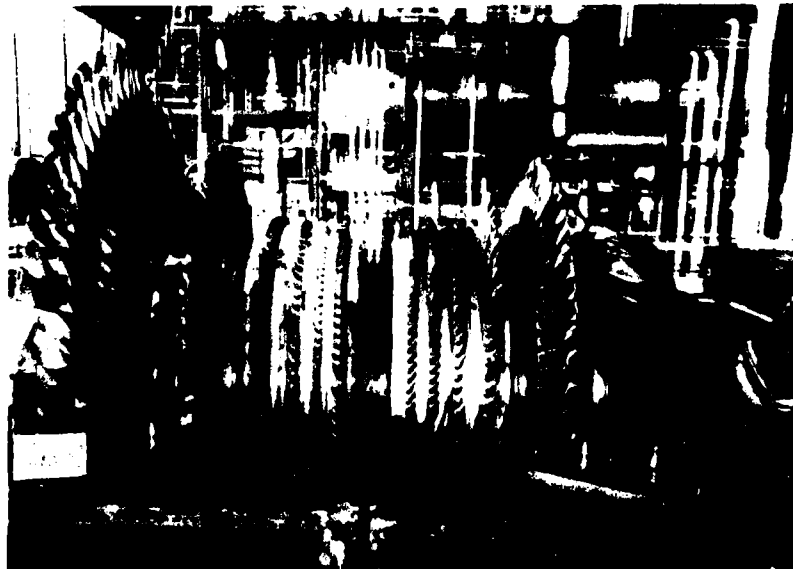


Figure 10: Damaged LP rotor showing blading rows stripped by excessive whirling.

STRUCTURAL TRANSFER FUNCTIONS - "REAL" VS. DIGITAL

Richard H. Lyon
RH Lyon Corporation
Belmont, MA 02178

Abstract: Structural transfer functions are the link between forces produced by mechanisms and the vibrations that are measured by sensors. Various analytical models such as polynomial ratios or modal expansions can be employed to represent a transfer function but, as models of real physical systems, the resonances and anti-resonances are represented by the poles and zeros of the transfer function. The phase and magnitude of the transfer function, as well as other related quantities such as group delay, can then be found in terms of the locations and residues of the poles and zeros. We refer to transfer functions based on pole - zero models as "real".

Digital procedures represent measured or computed impulse responses as sampled data sequences. Because of the nature of the processing involved, these data streams are truncated. Noise in the measurement or a desire for better resolution in the frequency domain will determine the truncation point in the record. Because of the nature of Discrete Fourier and Z transforms used for this truncated data, the models become all zero representations of the transfer function. The question then naturally arises, "in what ways is it possible for an all zero, finite impulse response system to represent the properties of a 'real' pole zero physical system?"

It seems clear that the amount of structural damping must be related to this equivalence. When the damping is large, the impulse response record length is shorter, and the truncation will be sooner. The number of samples in the record is fewer, and the number of zeros in the transfer function is also fewer. Alternately, in the pole - zero model, high damping means that the system poles (the resonances) are at a greater distance from the real frequency axis, and the details of the pole locations should become less important. The equivalence or consistency between the two worlds is expressed through certain asymptotic properties of the distribution of zero locations.

When digital processors are combined with physical systems in feedback loops, as in active vibration control, we need to be concerned about how one world can model the other. In this paper, we recall how pole - zero modeling leads to certain conclusions regarding signal transmission in machine structures. These understandings can then be the basis for processing methods in the recovery of fault signatures. Since the processing methods themselves will represent the transfer function in the digital world, this is another area where the adequacy of such a substituted reality needs to be investigated.

LEGAL LIABILITY OF THE DESIGN ENGINEER

By Thomas H. Shunk

Baker & Hostetler
3200 National City Center
Cleveland, Ohio 44114

Abstract: The legal liability of a design engineer and his company for devices that malfunction may come from three different sources--the law of negligence, the law of contracts, and the law of product liability. In most cases, the design engineer will be held responsible for damage directly caused by the product's design if the foreseeable risks associated with the design exceed the benefits associated with the design, or if the product, as designed, is more dangerous than an ordinary consumer would expect when used in an intended or reasonably foreseeable manner. Simple adherence to accepted industry standards of design does not relieve the design engineer from his duty to exercise reasonable care in designing the product. Proposed standards not yet adopted by industry committees may also be used by the courts to judge the sufficiency of a design. Also, the design engineer may have a duty to suggest improved design parameters even when the purchaser has established explicit specifications to the contrary.

Key Words: Government contractor defense; legal liability; specifications; standards.

1. Sources Of Design Engineer Liability

Design engineers may be held legally responsible for the economic and bodily damage caused by malfunctioning products they have designed. The legal theory upon which a design engineer's responsibility is based is a function of the relationship of the design engineer to the manufacturer and to the user of the product.¹

If the design engineer's company both designs and manufactures the product, the company will be subject to the laws of products liability. In most states, sellers of defective products are held strictly liable for injury directly caused by the malfunctioning of the product. A company that only provides design services and does not manufacture or sell the product will usually not be held strictly liable--instead, the court will inquire into the question of whether the design services were negligently provided.

¹ In general, individual persons working within the scope of their duties for a business entity are the legal agents of that entity, and their actions will be imputed to the business entity.

The manufacturer of a product is said to be "strictly liable" because the court will not inquire into the extent to which the manufacturer acted with reasonable care in making the product to determine whether the product was defective. Most states have approved the following description of the limits of strict liability:

- (1) *One who sells any product in a defective condition unreasonably dangerous to the user or consumer or to his property is subject to liability for physical harm thereby caused to the ultimate user or consumer, or to his property, if*
 - (a) *the seller is engaged in the businesses of selling the product, and*
 - (b) *it is expected to and does reach the consumer without substantial change in the condition in which it is sold.*
- (2) *The rule stated in Subsection (1) applies although*
 - (a) *the seller has exercised all possible care in the preparation and sale of his product, and*
 - (b) *the user and consumer has not bought the product from or entered into any contractual relation with the seller.*²

When the business entity with which the design engineer is associated does not manufacture the product, but only develops the product's design, the rules set out above applying strict liability are in most states replaced by the more familiar concept of responsibility for negligence. In such a case, the design engineer must exercise the care that would be exercised by a reasonably prudent design engineer skilled in the subject matter of the product being designed. From a practical standpoint, this usually means that the legal inquiry will concern itself with two issues--the extent to which better designs were known in the engineering community, usually as evidenced by current scientific literature, and the extent to which the design engineer could have foreseen the likely misuse of the product by the

² Restatement (Second) of Torts, (1965), Section 402 A.

consumer and developed a design to guard against that misuse.

Whether the business entity with which the design engineer is associated sells the designed product or not, it may also be responsible under theories of contract law and the law of implied warranty. The extent to which the design engineer is liable for injury in those cases is determined by the words of the contract, purchase order, or design specifications to which the design engineer has agreed in producing the product for a customer. Depending upon the situation, the engineer may also be responsible for oral agreements made in addition to the written documents about the operating parameters of the product, etc. Further, and particularly if the product is one sold to the public at large, the design engineer may be held to have made *implied* warranties of merchantability and fitness for use of the product in addition to any explicit agreements reached with the purchaser of the product.

"Merchantability" is essentially the extent to which the product is of the same general quality as other like products. "Fitness for use," as its name implies, is the extent to which the product matches the uses to which the product can be expected to be put. Theories of implied warranty, however, have generally been neglected in recent years because of the availability of strict liability and negligence theories to hold the design engineer responsible.

2. Design Considerations

While the design engineer may be faced with an apparently bewildering array of sources of legal liability, in many states the various legal theories generally reduce themselves to much the same question: Did the design engineer take into account everything he knew or should have known about the product and the design in light of currently-available information in order to produce a product whose benefits outweighed its risks?

The two key elements of the foregoing question are the issues of what the design engineer "should have known" and what constitutes "currently-available information."

The design engineer may be surprised by the type of information a court may conclude he "should have known." It is natural for the engineer to consult current industry standards when shaping the design of the product. A court, however, may hold the engineer responsible for knowing the details of *proposed* but

not yet adopted standards even when the usefulness of those standards is still the subject of much debate within the industry. This is particularly true if the design engineer's company participates in the industry association considering the proposed changes and has access to proposed draft revisions.

Similarly, a design engineer would naturally consider the normal uses to which the product may be put, estimating maximum loads and forces to which the product may be subjected in the course of its use. A court, however, will ask the engineer to go beyond normal and even maximum intended use considerations to a consideration of "foreseeable misuse." The doctrine of "foreseeable misuse" requires the design engineer to consider the ways in which the product may be put to uses alternative to those specified, as well as misused for its intended purpose.

A critical test of the foreseeability of the misuse is the presence of prior anecdotal incidents of the misuse. For this reason, a design engineer engaged in the improvement of a design should give careful study to reports of prior product misuse to determine whether additional safety guards or an improved design would either prevent the user from misusing the product or would render the product harmless in the face of misuse. Various loose-leaf product liability reporters, generally available through company law departments or outside counsel, can also provide information about typical product misuse patterns, at least insofar as those instances reach the stage of legal action on behalf of the injured party.

One common alternative to redesigning the product in light of past instances of misuse is the adoption of warning labels to be affixed to the product and included in literature concerning the product. There are significant risks associated with this alternative, however.

Superficially, warning labels may appear to be an inexpensive substitute for product redesign. The design engineer should be careful, however, in making the choice between warning against misuse and designing against misuse for a number of reasons. No matter how clear the design engineer may feel the product warning has been made, there will undoubtedly be users of the product who misinterpret or ignore the meaning, importance, or details of the warning. The product may also find its way into the hands of a person who, for reasons of youth, illiteracy, or language, cannot understand the warning. Warning

labels may also become obliterated over time with use of the product or suffer other degradation, rendering the warning ineffective.

Remember that the design engineer's response to a potential safety concern regarding the designed product will be judged by the design's reasonableness in light of the risks associated with the design and the benefits achieved from the design. Remember also that a jury, faced with an injured plaintiff, will tend to give little weight to economic design concerns in comparison to the risk of injury. This stems from the fact that, while injury is a possibility when considered at the design stage, it is a certainty when the case reaches the courtroom.

3. Designing To Specifications

Just as the design engineer should not rely blindly on current industry standards in developing product design, he should not rely unquestioningly on product specifications developed by the purchaser or user, even when the purchaser is exceedingly knowledgeable in regards to design, such as is the case with U. S. military procurement. The designer and manufacturer of the product are relieved from responsibility for a deficient design only when the user knowingly assumes the risk of using the product. This will occur only when the user has actual and detailed knowledge of the risk to which he is subjected in using the product and nevertheless chooses to use the product as designed and manufactured.

For this reason, the designer should be certain that each aspect of the user's specifications that does not measure up to the standards the designer himself would use in developing the product are pointed out to the user, with the specific indication of the defects in the design, expected risks, and alternative strategies. Unquestionably, the manufacturer and designer should advise the purchaser of these issues in writing so that a clear record has been made of the knowing decision by the purchaser to utilize the original specifications for the product.

This issue is of particular concern to government defense contractors, because of the availability to them of immunity from legal liability under certain conditions, when their products are designed to government specifications. The Supreme Court of the United States has recently reaffirmed the immunity of a government defense contractor from suit for injury caused by its product in the case of Boyle vs. United Technologies Corp., 108 S. Ct. 2510 (1988).

Essentially, the Supreme Court affirmed in that case that a contractor designing and manufacturing a product for government military use will be immune from suit for injuries if the product is one that has not previously been used in the stream of commerce or if it was designed for use by the government in a new or dangerous manner, and if the contractor has complied with the specifications without any negligence on its part. The latter means that the contractor has a duty to warn the government of any hazard of which it believes the government is unaware with regard to product design, and it has a duty to comply with the specifications in "all material respects." The key here is that the contractor may not blindly rely upon the government specification if the contractor has superior knowledge of the hazards of the specification and fails to warn of the risks associated with that design and of alternatives.

The Boyle case has been considered by some commentators on the law to imply that the government military contractor immunity may be extended to situations beyond traditional military procurement in the future. One commentator, for example, suggests that the doctrine will not be limited merely to military applications, but to any application in which "the product [is] needed for an important federal operation that is of such a magnitude that only the government can handle it. The existence of a statutory- or a judge-made limit on federal liability is an indication that the government program is of the requisite importance."³ It also appears that the immunity may be found to cover not only injuries sustained by members of the armed services from use of the product, but also by civilians who come in contact with the product, even outside the context of military engagement.

Any company faced with a product liability suit for a product made for use by the federal government should have their legal counsel give consideration to the question of the availability of the government contractor immunity defense based upon the apparent recent strengthening of this rule. In any event, companies producing products to government specifications should take the time to consider the appropriateness of those specifications and make written record of advice to the government procurement agency

³ Frumer, L.R. and Melvin I. Friedman, Products Liability, Vol. 3, pp. 25-82 to 25-83 (Mathew Bender, 1989).

of the limitations and difficulties that may be associated with those specifications.

4. Conclusion

Products must be designed to be reasonably safe in light of information that the design engineer knew or should have known at the time the product was designed. While application of good principles of engineering design will undoubtedly meet this goal to a large extent, the design engineer must keep in mind that the court may take a view of the current "state of the art" regarding the design of the product that differs from the view of the design engineer. Examples considered in this article include proposed but not yet adopted industry standards and specifications for products promulgated by apparently knowledgeable purchasers. Attention to these issues by the design engineer in the process of designing the product should result in a substantial lessening of the possibility of exposure of the design engineer to legal liability.

DETECTION, DIAGNOSIS, AND PROGNOSIS: AN EVALUATION OF CURRENT TECHNOLOGY

Ronald L. Eshleman
Vibration Institute
Willowbrook, IL 60514

Abstract: Current state-of-the technology in machine fault detection, diagnosis, and prognosis is evaluated. The role of sensors and analyzers used for detection and analysis is summarized, as are diagnostic techniques. Life estimation of machine components (prognosis) is reviewed. Fault diagnosis and prognosis techniques are not evolving as rapidly as instrumentation. Technical areas that must be developed include condition and fault mechanisms, modification of signal transmission paths, and signal analysis. Technologies from various disciplines must be combined in order to develop techniques for diagnosis and prognosis.

Key Words: Detection; diagnosis; expert systems; fault mechanisms; FFT analyzers; filters; gears; life estimation; rolling element bearings; sensors; signal transmission path

Introduction: Prevention of mechanical failure has grown in importance as lower manufacturing costs and quality products have become essential. Implementation of mechanical failure technology, which has evolved informally with electrical and mechanical engineering technologies, saves industry millions of dollars each year. Developments in detection, diagnosis, and prognosis are the result of empirical work carried out in government and industry. The evolution of fast, accurate digital computers for measurement has tended to drive the technology forward. However, the techniques required to perform diagnosis and prognosis seriously lag the tools available. Development of these techniques will require formal research on mechanisms, characteristics of signal transmission paths, signal analysis, and life estimation.

Because the techniques of mechanical failure analysis encompass many disciplines, research has not flourished at the university level or at research centers. Indeed, no formal research center is devoted to detection of mechanical failures, diagnosis, prognosis, and condition evaluation. However, research will be required to advance the state of the technology in these areas. In addition, little empirical work is presently being done to advance these techniques.

This paper contains a review of the current technology associated with detection, diagnosis, and prognosis. The type of research that will be required to advance the technology is summarized.

Detection: Sensors that convert mechanical vibration to electrical signals representing displacement, velocity, and acceleration have been highly developed to accurately reproduce their environment. As is true of all other instruments that transmit or process electrical signals, sensors have frequency response characteristics; that is, limitations exist in certain frequency ranges. Thus, no single sensor is useful over the entire frequency range or for every application. Selection of an appropriate sensor is dependent on the design of the machine and the nature of the fault or condition. For example, seismic measurement is used for rolling element bearings; machines with fluid-film bearings are best monitored with proximity probes that measure relative shaft displacement. The frequency of the fault often plays an important role in sensor selection. The most serious limitation of sensors has to do with low-frequency vibration. Low-frequency signals that approach the noise level of a machine are difficult to measure seismically, either because the strength of the transducer signal rolls off--as is true of velocity pickups--or because the signal is not sufficiently strong--as can occur with accelerometers. Special low-frequency accelerometers are currently available, but random noise signals occasionally exceed the magnitude of the measured signal.

In the past ten years digital instruments have almost replaced analog ones with the exception of analog oscilloscopes. Some of the high-performance digital oscilloscopes on the market permit detailed analysis of vibration signals. Development and miniaturization of digital computers have stimulated advances in vibration instrumentation, which now exceed the capabilities of the techniques used to diagnose problems. In the past ten years the fast Fourier transform (FFT) spectrum analyzer has replaced most swept filter analyzers because it has better resolution and a greater dynamic range. However, the FFT spectrum analyzer is not without pitfalls and limitations. Block processing of data has inherent limitations in applications requiring instantaneous results but does permit the examination of large quantities of data. Most FFT analysis is carried out with one or two channels, but multichannel processors have become popular for saving time and simultaneously analyzing many measurements. However, they are of no technical advantage in machine fault diagnosis and prognosis. FFT spectrum analyzers dominate today's market, but there are signs of emerging competitive analyzers that use other mathematical algorithms, digital filters (parallel filtering), and phase lock filters for resolution.

Diagnosis: Because the techniques for fault diagnosis have evolved more slowly than instrumentation in the past 15 years, the tools are far more advanced than the techniques. Three technical areas must be addressed:

- condition and fault mechanisms
- modification of signal transmission paths
- signal analysis

Condition and fault mechanisms are important technical areas because the faults of a machine cannot be diagnosed and its condition cannot be evaluated unless the mechanisms that result in vibration are quantified. In other words, the mechanical condition of a specific machine component

must be matched to the signal from the analyzer. A large rolling element bearing with a defect on the outer race and the corresponding time signal and frequency spectrum are shown in Figure 1. The pulses in the time signal are caused by the elements as they roll over the defect at a frequency equal to the ball pass frequency of the outer race. The frequency spectrum shows the ball pass frequency of the outer race and its orders at various magnitudes in inches per second. The pattern of vibration magnitudes at different frequencies provides information about the condition of the bearing.

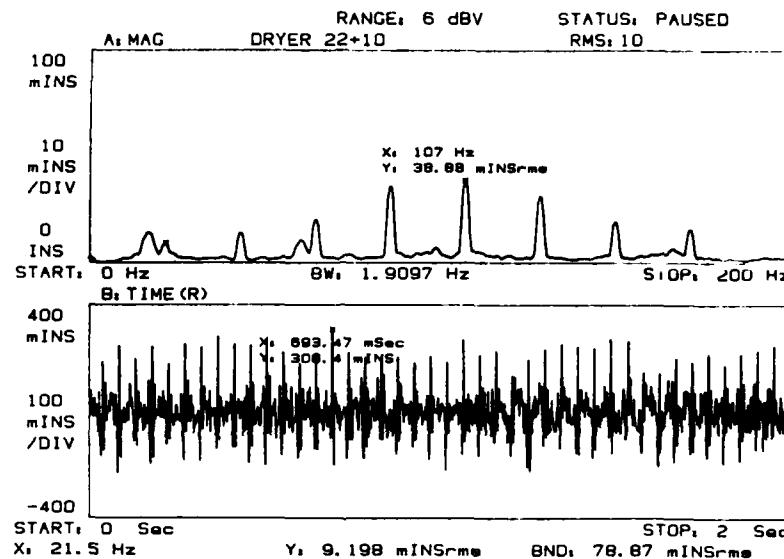


Figure 1. Rolling Element Bearing Defect in the Outer Race.

Condition evaluation requires quantification of the magnitudes of vibration and its frequencies in both the spectral and time domains. This process, called pattern recognition, has not yet been formalized. A so-called calibration requires that vibration information be compared to a known defect. The time domain signal must be considered in this process because the spectrum is not unique. Because phase is not considered when the spectrum is evaluated, it could represent two totally different mechanical conditions.

The two similarly shaped spectra shown in Figure 2 represent two different conditions in gearboxes. The upper spectrum is from a gearbox with a broken tooth; the lower spectrum is from a different gearbox in which the mesh binds and releases suddenly once per revolution. The mechanisms are much more clearly defined in the time domains (Figure 3). The sharp pulses from the broken tooth as it passes through the mesh are evident in the

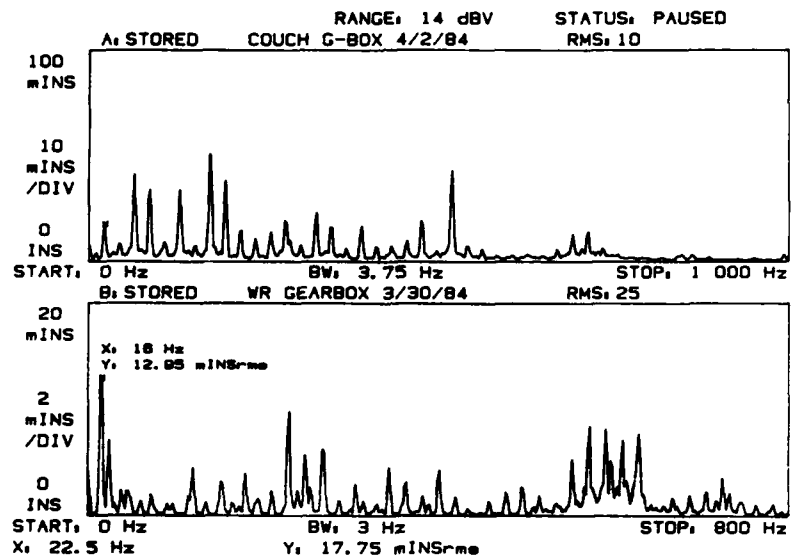


Figure 2. Gearbox Spectra for Broken Tooth and Mesh Binding.

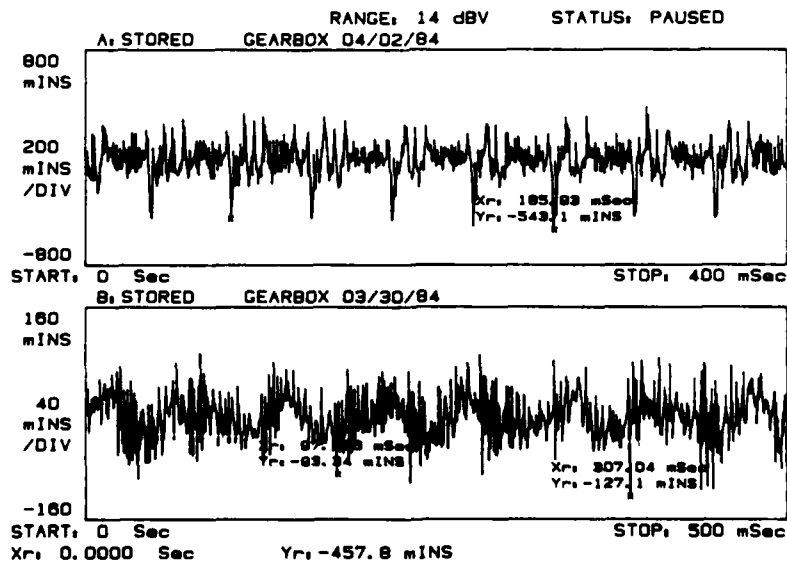


Figure 3. Gearbox Time Domain for Broken Tooth and Mesh Binding.

upper signal. In the lower signal the binding and releasing of the gear set as it rotates, while not so clearly defined, do have a distinctive pattern.

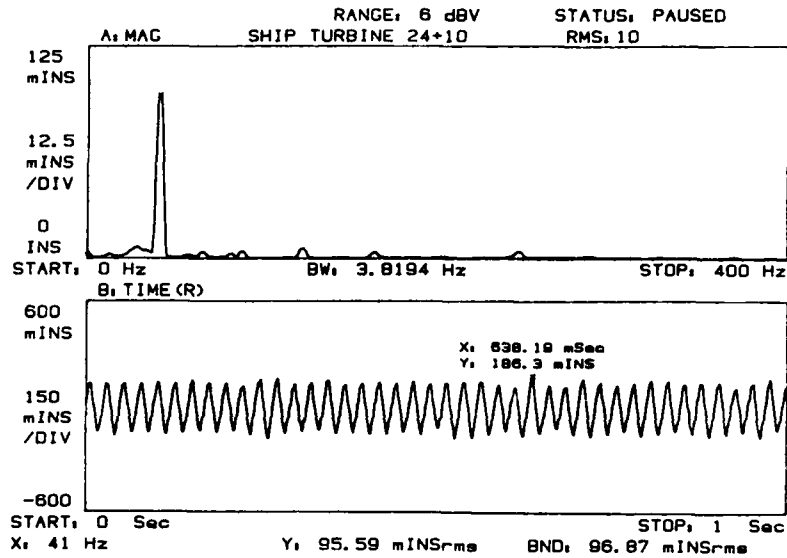
Modification of the signal transmission path is another technical area that must be addressed. During the time required for a vibration signal generated by a defect to progress from its origin to a sensor, the signal can be modified by joints and the mass-elastic-damping properties of the machine. Theoretically a transfer function between the source and the sensor location can be measured with a dual-channel FFT analyzer, but it is not yet practical to do so for operational machinery. Nonlinear joint and structural mechanisms complicate the process of formalizing the problem.

Signals clipped by passage through a machine joint cause more problems in fault diagnosis than do linear mass-elastic-damping modifications. The most functional solution to the problem would be to mathematically model the transmission path because the machine would not have to be shut down for experimental calibration. However, before such procedures are possible, better physical simulation will be required. The limiting factor today is the lack of joint stiffness models and damping data for mechanical systems.

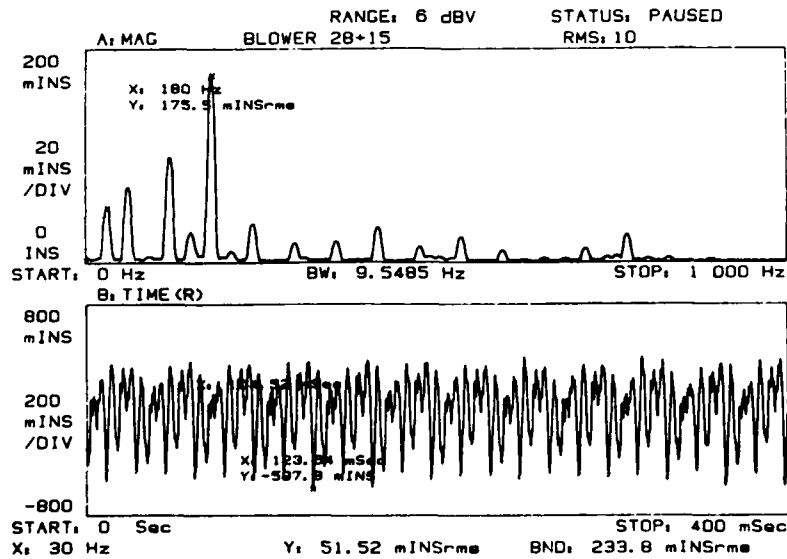
Processing and analyzing signals is the third technical area that must be addressed in diagnosing faults and evaluating machinery condition. Of primary importance is the measurement parameter. The most directly measurable parameter is used for fault analysis--relative shaft vibration when flexible bearings are used and absolute casing vibration when stiff bearings are used. The flexibility and damping of a machine support are affected not only by the bearings but also by the parameters of adjacent machine components; for example, shafts, pedestals, housing, foundations. Although microphones or some other noncontacting remote sensor might be convenient, the problem of the transmission path negates their practical application. The analysis techniques used today are based on identification of frequencies; these techniques have been used for years and have never been formalized. Measured frequencies are matched to the following: operating speeds of machines and their orders; sidebands; sum and difference frequencies; natural frequencies and critical speeds. Amplitude and frequency modulation and pulsation of the signal are often evaluated.

The operating speed of a machine is generally considered the reference frequency for analysis in the frequency identification process. Figure 4a is typical of mass unbalance; a high magnitude vibration occurs at the operating frequency of the machine. Figure 4b shows pulsation in a blower; the vibration is occurring at machine speed and its orders. A long sequence of difference frequencies at the running speed of an impacting printing press is shown in Figure 4c; this pattern is typical of impacts occurring in a machine. Figure 4d is a signature typical of misalignment--frequencies at shaft speed and two times shaft speed are present. The component at two times shaft speed is larger. Figure 4e shows a gear-mesh frequency at the pinion frequency; this pattern is typical of a faulty gear mesh. Techniques for processing and analyzing signals require time and spectral domains,

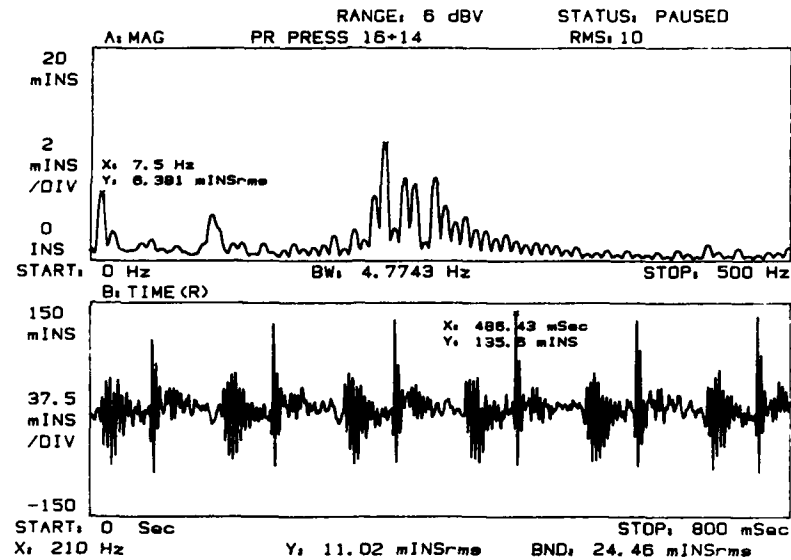
Figure 4. Frequency Identification Process: Examples
a. Turbine Mass Unbalance.



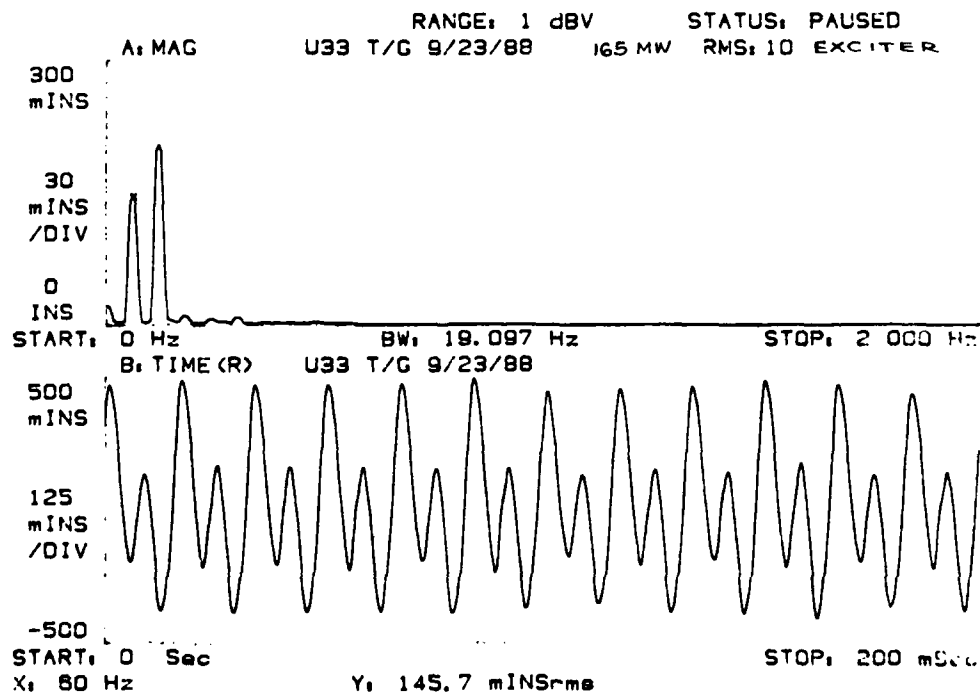
b. Blower Pulsation.



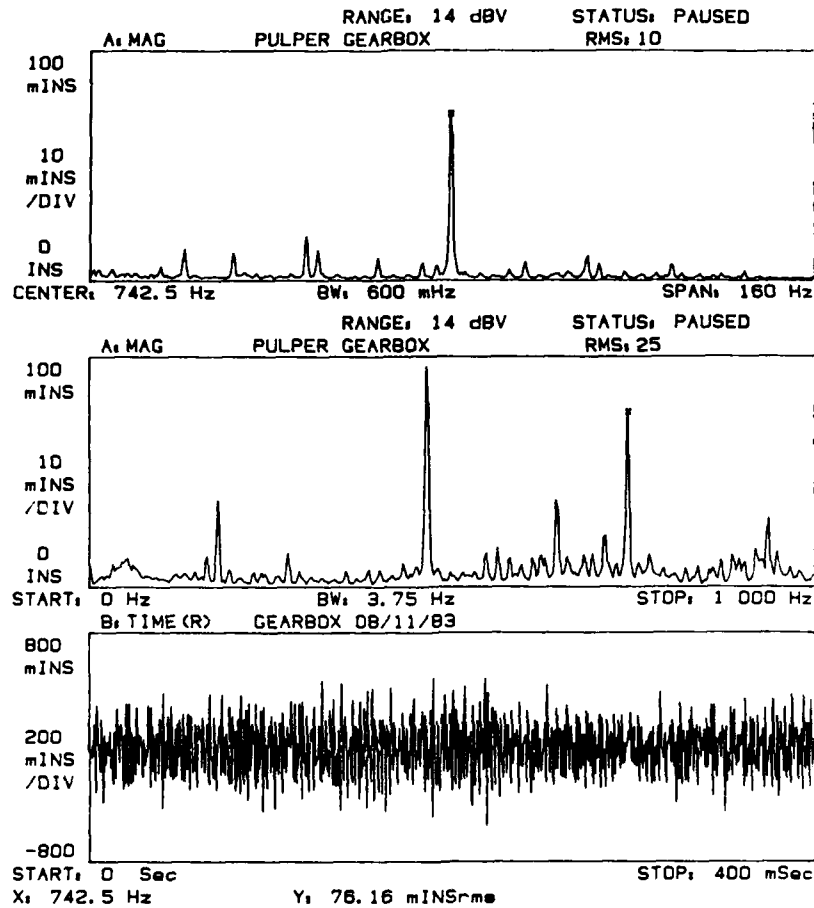
c. Printing Press Cylinder Impacts.



d. Exciter-Generator Misalignment.



e. Pulper Gearbox: Gear-Mesh Vibration.



orbits, start-up and coast-down data, and cascade diagrams. These techniques are currently being used informally with the exception of expert systems.

Expert systems for machine fault diagnosis are evolving, but developers will discover in the not-too-distant future that they have reached the limits of current knowledge of mechanisms and signal path transmission. Indeed, there is also a need to develop advanced data processing techniques and information identification techniques. Thus, expert systems cannot perform magic--they are bounded by available knowledge. When the reasoning and experience associated with current knowledge of machine mechanisms, identification of transmission paths, and data processing are finally formalized, expert systems will become more effective.

Prognosis: Procedures for prognosis of failures (life estimation) have been established only for turbine blading. Life estimation has usually been based on limited experience with failures of specific machine components. The remaining life of a machine or component must be based upon wear, the environment, and the history of stress cycles in the machine. These factors must also be considered when establishing its current condition. And only after the current condition of a machine is known can meaningful life estimates be made. Information about current condition can also be used to evaluate the effects of changes in components and wear in order to assess whether or not machine life can be extended. The techniques of prognosis involve diagnosis, condition models, and failure models (Figure 5).

Data from measurements are applied to a modal model to obtain the internal forces in a component or machine. These forces are used in a condition model along with measured data and the operational history of the machine to determine stresses, state of wear, and defects in the machine or its components. The current condition of the machine is then extrapolated from this information to predict time to failure using a failure model. The available failure models--Miner's law for example--are expressed in terms of number of cycles to failure.

Although some data exist for failure models, they are rarely applied. The reasons are the complexity of the process and a lack of information about the history of machine operation. Development of techniques for estimating the life of a machine and its components is a major challenge in the field of predictive maintenance. Whether analytical methods will be developed or a purely empirical approach will be followed remains to be seen. The empirical method requires gathering and processing a large quantity of data in a consistent way and then relating the data statistically to different types of component failures. It is possible that a combination of analytical and empirical methods will be necessary.

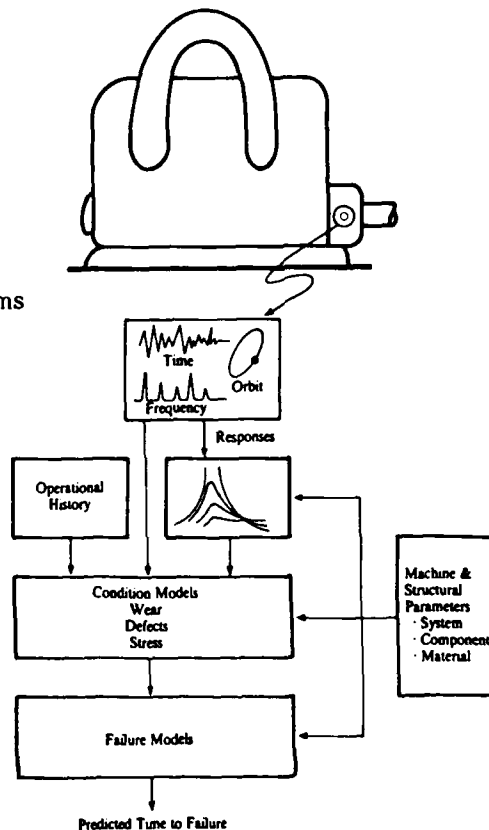


Figure 5.
Life Estimation Techniques.

Factors that affect machine life include steady and dynamic stresses of structural members, hardness and strength of materials, wear, life history of components, and cumulative damage. Development of models based on these factors, which determine the condition of a machine or a component when it responds to known forces or motions, is a challenge in predictive maintenance.

Failure models that predict time or cycles to failure have been available for materials and simple structures for years. But no failure models have been developed for factors other than stress and strength. Theoretically, structural failure models that are broken down into small elements can be applied to complex components and machines for the purpose of life prediction. Good results are now being obtained with computer models that have been experimentally verified and calibrated. However, the development of failure models and the data to implement them will be a challenge for engineers.

Conclusions: In my opinion the opportunities are many and varied in the field of mechanical failure technology. To date a lack of clear identity with a formal academic discipline has thwarted the development of techniques for machinery diagnosis and prognosis. Many engineering disciplines will have to become involved--mechanical, electrical, civil, chemical, and metallurgical. An imaginative synergistic approach will thus be necessary to bring about major breakthroughs. Advances in hardware will continue at a rapid pace, but they cannot be adequately exploited unless techniques evolve. Expert systems may appear to be technique-oriented, but the computer hardware and software that drives them is limited by the techniques now available. Unless new techniques are developed, expectations now being generated for expert systems cannot be fulfilled. These systems are bounded by the effectiveness of the best analysts currently available and fall short when reasoning is required.

PLASTICITY IN FAILURE MECHANISMS

C. D. Beachem
Naval Research Laboratory
Material Science and
Technology Division
Washington, DC 20375-5000

Abstract: Fracture and cracking mechanisms are explained in terms of varying degrees of extreme plasticity. The size of the plastic zone, the rate of strain within the plastic zone, the temperature of the deforming material, and chemical interaction in the process zone help determine the failure mode.

Key words: Failure analyses; fracture mechanisms; plasticity; evolution of theories; fractography.

Inhibitions to new theories: The main problem with increasing our knowledge of fracture and failure mechanisms is that our ability to think new thoughts is severely hampered by our need to survive. We need to get our paychecks, and unless we please our bosses, we won't be paid very long. We need to get passing grades in school, and we will surely fail unless we accede to our instructor's point of view. We need to publish and unless the editors substantially agree with what we write, we can forget publication.

These are some of the problems we face after we recognize that we have an original mechanism concept and are trying to do something useful with it. Trying to get the original concept in the first place is even more difficult.

We want to please. We very much need to please. It is highly disturbing to encounter displeasure in our parents in our formative years, in our teachers in grade school, in college and into our present selves.

Thus we intensively train ourselves for years to not challenge, to follow strictly laid down paths, and to accept what the revered elders and the respected professors say as law.

Thank goodness, of course. Such training goes a long way to keep us out of the hospital and jail. We accept as a fact that macroscopic properties are real, the 0.2% offset yield strength is the yield strength of all the material inside the standard 0.505 inch tensile specimens, for example. Of course, that's a lie. The tensile specimen is

composed of various constituents, crystals, and dissolved gas concentrations, each of which has its own different yield strengths and contributes in its own way to the average of the 0.505 specimen. Once we are educated beyond the P/A realm and learn some physical metallurgy, this type of mechanism refinement is straightforward.

Extrapolating from the standard tensile specimen to other structures, events, and theories is not at all pleasant. One finds that all our macroscopic concepts need to be challenged and in most cases are under some form of attack and modification. This leaves very little solid, familiar ground to stand upon. If what we think is secure in the physical theories of physics, chemistry, and metallurgy are now found to be constructed of the shifting sands of discovery, how do we find firm ground to place our feet? It would be much more comfortable to find a few spots of firm foothold to step upon as we cross a swamp or marsh.

As we try to advance our theories of crack growth and failure we find ourselves trying to stand upon old familiar standard concepts while we address, discover, and understand the unknowns of each failure analysis. Cleavage and ductility are two of a long list of familiar macroscopic terms that have been around for centuries, that form some of our most steadfast concepts, and give us considerable trouble in advancing our understanding of mechanisms. Their classical macroscopic concepts are unchanged and are still useful. However, use of the light microscope, the electron microscope, and other tools has forced us to understand that their small microscopic mechanisms cannot be predicted by extrapolating their macroscopic characteristics.

Cleavage: Cleavage was once thought to be the basic unit of fracture. It was visualized as separating a crystal into two parts by suddenly overcoming the attractive forces across a crystal plane such that all the forces simultaneously let go and all the atoms on one side of the plane simultaneously went one way and all the atoms on the other side simultaneously went another, all with no deformation at all. All sorts of theories were related to the concept. Fatigue was said to "crystallize" metal parts so that they broke by cleavage. Of course, the original classical concepts of cleavage were wrong. Also wrong were secondary and tertiary mechanisms based on these earlier concepts. From observations in the electron microscope we now know that cleavage can occur by fatigue, corrosion fatigue, stress corrosion cracking, hydrogen assisted cracking, and solid and liquid metal cracking and that some kind of highly intense and highly localized plasticity is involved during these cleavage processes.

A small but growing number of researchers are indicating

that the basic mechanism of "true", "brittle", "fast", "monotonic" classical cleavage - the same cleavage that used to form the basis for so many mechanisms - is itself accomplished by highly plastic mechanisms, either by short order dislocations or some form of melting. Professor Wilsdorf at The University of Virginia is leading some of this pioneering work. Such concepts such as "melting" sound strange only because early crystallographers and metallurgists were fond of sketching atoms when they had no way of actually seeing them. What we can all see and therefore we know it exists, is plasticity. What is wrong with extrapolating that which we know exists (plasticity) down into the atomic scale? There is nothing logically wrong with such an extrapolation. The primary difficulty is using the term plasticity to describe such fine scaled events.

Ductility: Plasticity has a comfortable home in the concept of ductility. We are all familiar with the soft tensile specimen that necks way down before it slips apart, and with the Charpy impact specimen that bends without breaking. That sort of plasticity is something we all recognize. It has been long described as occurring via dislocation generation and motions. A finer scale of plasticity is microvoid coalescence (MVC). Unfortunately, MVC has wrongly become a sort of standard for the presence of microplasticity. What we have to realize is that both cleavage and MVC are larger scaled results of finer scaled plasticity mechanisms.

Atomic scaled mechanisms: If we turn our backs to "pure" cleavage as a basic mechanism, what should we select as a replacement? Should we take the antithesis to be true - that the atomic mechanism, the basic mechanism, of fracture is plasticity? It would seem logical.

The problem here is that our concept of plasticity is befogged by our macroscopic concepts. If we allow a lot of latitude we might get away with calling it plasticity. Is melting a kind of plasticity? Again, melting is a concept which is usually experienced as a macroscopic event removed from crystallographic considerations. What about evaporation? It too is something we haven't substantially studied under the microscope.

It may be safest to say that the new basic form of fracture is plasticity, and that for the moment its exact microscopic nature is not known. It is, however, experienced on a scale smaller than microvoid coalescence and smaller than normal dislocations.

MOTOR DRIVEN EQUIPMENT DIAGNOSTICS
(I&II)

Chairmen: Henry R. Hegner
ECO, Inc.
and
Ronald C. Tate
David Taylor Research Center

INDUCTION MOTOR FAULT DETECTION VIA PASSIVE CURRENT MONITORING - A BRIEF SURVEY

G.B. Kliman

GE Corporate R & D

P.O. Box 8

Schenectady, New York 12301

J. Stein

Electric Power Research Institute

3412 Hillview Avenue

Palo Alto, California 94304

Abstract: Only in recent years has passive current monitoring for fault and incipient fault detection been achieving greater visibility even though many of the ideas have been in the literature for some years. This paper briefly reviews some of the theories and techniques employed in detecting stator and rotor faults in AC machines by analysis of the current. A related subject is the use of the motor current to detect problems in the load on the shaft or in the power supply.

Key words: Diagnostics; fault detection; fault monitoring; incipient failure detection; induction motors

Introduction: Passive current monitoring for fault or incipient fault detection has been achieving greater prominence recently. This is most likely the result of the confluence of a number of trends including a greater appreciation of the benefits of condition monitoring, the development of viable theories and the wide availability of low cost but powerful personal computers. For most purposes current monitoring can be implemented inexpensively on any size machine by utilizing the current transformers already in place in the motor control centers. Fig 1 is a schematic depiction of a typical current monitoring system. It is fortunate that the average current transformer, although designed only for line frequency operation, is usually capable of reasonably passing signals whose frequencies are well into the kilohertz range. This is, however, the case only for small signals superimposed on a large line frequency component as such transformers would quickly exceed their thermal limits with high-frequency currents of significant magnitude. Use of the existing current transformers makes it convenient to monitor numbers of motors remotely from one location.

In this paper we will first examine techniques to detect bar cracks or breaks in the rotors of induction motors. There are now several firms offering "broken-bar detectors" based on these techniques. The rapid growth of this industry and acceptance of the "broken-bar detector" by both electric utilities and industry has undoubtedly given a major impetus to the consideration of passive current monitoring in general, especially as only software changes in a computer-based instrument (as most of them are), will usually be needed to implement new fault detection algorithms with perhaps an added sensor or two. We will also discuss techniques for detecting stator faults. It is notable that no detectors are marketed for stator faults or incipient faults in the same way as that for rotor faults even though such faults are more common. There are good reasons for this state of affairs, which will be discussed later.

The second broad area of interest and the latest to receive attention is to utilize the motor as

a sensor to detect problems in the load on its shaft. Some commercialization efforts are now under way in this area but this is just starting. There is also some confusion as to what is appearing in the motor current and why. Hence we present a brief derivation to demonstrate more rigorously how load perturbations must appear in the current. These results also shed light on a problem of false alarms in some broken bar detectors.

Motor Fault Detection

Rotor faults: There is, by now, an extensive academic and commercial development of theory and instruments to detect problems in the rotor of an induction motor ¹⁻¹⁵. All of the instruments now on the market depend on the detection of particular components of the current spectrum that are directly related to rotor asymmetries. It has been shown that when a rotor asymmetry is present the airgap flux will be perturbed and this perturbation will rotate at shaft speed. Furthermore the spectrum of the airgap flux, as observed from the stator, will resemble Fig. 2. The frequencies of the spectral components are given by ⁷:

$$f = f_l \left[k / (p/2) * (1-s) \pm s \right] \quad (1)$$

where f_l = line frequency
 s = per unit slip
 p = number of poles
 k = 1, 2, 3, 4 ...

Note that the spectrum lines in Fig. 2, from Eq. 1, are actually two lines separated by twice the slip frequency (the actual frequency of currents in the rotor) but not resolved by the plotter. The shape of the airgap flux spectrum does not differ markedly for a broad selection of power plant motors. Note however, that the density of lines depends on the number of poles in the motor (8 poles in Fig. 2) and that there are lines at frequencies below 60 Hz. The stator winding, however, selects out and modifies the spectrum when observed from the stator terminals, such that only sidebands of the 5th, 7th, etc., harmonics appear with any magnitude. To illustrate this approach a measurement of the current sidebands near line frequency in a test motor with various numbers of broken bars is shown in Fig. 3 ^{1,14}. Here both an upper and lower sideband may be seen. The theory predicts only the lower sideband (marked by the vertical dashed line). The upper sideband is caused by the twice slip frequency speed oscillation induced by the broken bar currents.

Rotor asymmetry, due to a faulty bearing, rotor ellipticity, misalignment of the shaft with the cage, magnetic anisotropy, etc., result in similar spectra and must be distinguished from bar breaks. Two approaches have been taken. One approach ^{1,14} is to examine the relative behavior of the fundamental and higher harmonic sidebands. A rotating asymmetry will yield a line frequency sideband very much like that for a broken rotor bar. A broken bar may be distinguished from an asymmetry by examining the magnitudes of the harmonic sidebands. An asymmetry will typically result in a smooth variation of airgap flux density, i.e., the upper harmonic content will be low. In contrast, localized effects, such as a broken bar, result in large upper harmonics.

The second approach to distinguish broken bars from asymmetries relies on an examination of sidebands of the bar passing frequency. It has been shown ¹⁶⁻¹⁹ that both rotating and non-rotating eccentricity will give rise to current components at frequencies given by:

$$f = f_i \left[(kR \pm n_d) * (1-s)/(p/2) \pm n_w \right] \quad (2)$$

where R = number of rotor slots

n_d = 1, 2, 3, 4, 5 ...

n_w = 1, 3, 5, 7, 9 ...

An illustration of "bar passing" spectral components of the current is shown in Fig. 4 for a 4-pole motor with 51-rotor slots with and without a rotating (dynamic) eccentricity¹⁶. Note that the frequencies of interest are now much higher and could go above 6 kHz on large two-pole motors. Rotating eccentricity, such as a rotating airgap variation, will cause rotor currents and could be confused with a broken bar. A nonrotating asymmetry, such as an offset bearing, will not give rise to rotor currents.

Stator Faults: Stator faults are usually interpreted to mean only insulation related faults. These are turn-to-turn, phase-to-phase and phase-to-ground shorts. In most cases an outright failure of the insulation is not hard to detect. The new interest is focussed on the situation where the fault is just starting to develop in hopes of averting catastrophic destruction by "follow-through" currents. In some cases an outright failure may be hard to detect by conventional methods such as a turn-to-turn fault with no ground involvement.

The most common method of detecting faults is the "ground-fault detector" shown in Fig. 5. Kirchoff's current law dictates that the instantaneous sum of the currents in a three-phase system, without neutral connection, must always be zero. Hence a current transformer arranged with all three leads, as shown in Fig. 5, must always indicate zero unless there is an additional return path such as ground. Ground fault detectors can be made sensitive and rapid enough to be used for protection of personnel against shock hazards. The question now being raised is "Can this method be made sensitive enough to give reliable indication of incipient ground insulation failure?" Of course such an approach can yield no signal for unbalanced stator impedances such as would result from a turn-to-turn fault nor, for that matter, from any fault in the rotor. In the specialized case of mining equipment, where a high resistance neutral grounding connection is often used, there is a possibility that the current transformer approach may be of some utility²⁰.

A technique long used, is to trip on the presence of negative sequence currents as an indication of a major fault. In an attempt to provide a firmer basis for the setting of such trips and to lay the groundwork for improving sensitivity to the level of incipient faults detailed analyses of partial phase and phase-to-phase faults were done by an equivalent circuit method²¹. To implement the method it was necessary to calculate all of the partial self and mutual inductances of the motor. Accurate calculation of inductance is extremely difficult for the end windings and complicated for all others in the presence of saturation. Correlation of prediction and test then becomes problematical. Nonetheless, results were obtained that agreed well with the test in some respects. Figs. 6 and 7 show the comparison of prediction and test for "bolted" partial phase and phase-to-phase faults. It may be observed that, while the effect of such massive faults on the positive sequence components may not be possible to detect in the field, the negative sequence components are quite prominent and may become the basis for an incipient fault detector. A complicating factor in such detectors is that a faulted (broken bar) rotor will also give rise to significant negative sequence components in the current¹².

An approach to providing a sensitive instrument for detecting ground- and partial-phase faults was patented some time ago but has apparently not achieved significant market penetration, if

indeed, it was ever seriously marketed²². This instrument depends on detection of the phase current unbalance that must occur when there is a ground or phase fault in the motor. It is thus closely related to the negative sequence current methods and will also be affected by rotor faults.

It must be recognized that, unlike rotor faults, a stator insulation weakness will not give much warning in the line frequency current. Once a fault path develops the driving voltage and leakage, current will lead to a rapid increase in conductivity with large follow-through currents resulting in a catastrophic collapse and direct shorting. Active methods may yield average insulation quality checks but that is beyond the scope of this paper. It is possible that there may be detectable precursors, perhaps not at line frequency, but little or no research has been done to make this determination.

Model Fitting: A much different approach to passive methods utilizes the tools of optimal control theory. The published application¹⁵ was directed to rotor faults although it could also have been applied to other aspects of the motor.

The essence of this method is the fitting of a model, e.g., the standard equivalent circuit of Fig. 8. A series of measurements are made at various voltages or loads. Estimation techniques are then used to find the best fit of the model to the measurements. In the case of rotor faults a rotor resistance temperature compensation estimator is also utilized. Fig. 9 shows the results of one series of trials on a small motor. Three (presumably) identical rotors were tested in the same stator. Rotors #1 and #3 were left in original condition but rotor #2 had one bar completely broken. It was found that without the thermal compensation estimator, the results scattered over a range wider than that shown. Much remains to be done before this promising method can be a commercially viable tool.

Load Fault Sensing

Experience: The first papers describing the detection of problems in the shaft load of motors were published in 1982^{23,24}. This work was inspired by prior work on motor noise. The work reported by Steele and his associates was largely experimental, much in the spirit of prior mechanical signature analysis. Broken rotor bars were part of this investigation with results very similar to those already described. A variety of motors driving healthy and faulty loads were tested. In most cases the spectrum of the current was examined in an attempt to identify changes in the spectrum associated with specific faults. Statistical analysis of a filtered current signal was used to identify bearing problems.

Fig. 10 is one example of the test series. In this case a pump was driven by an induction motor. This figure compares the line current spectra when the pump was in presumably good condition, and when a deliberately damaged bearing was replaced into the pump. No attempt was made at this time, to identify spectrum lines with particular physical phenomena in the motor or pump. Also tested were small DC motors (windshield wiper drive, cam timer drive and a DC disk motor) with damaged gears or unbalanced load. As an illustration of the statistical method, Fig. 11 shows the results of a pulse-over-threshold analysis of the filtered drive motor current signal for various induced bearing faults in the driven pump.

A complementary aspect of load sensing may be seen in Fig. 3. The test loop for this experiment^{1,14} was powered by a 60 Hz motor-generator set driven by a synchronous motor. Notice the set of sidebands not marked by the computer, appearing in the second and third spectra,

but not in the first and third. This turned out to be due to a degenerating coupling on the m-g set. When the source was determined, reported, and the m-g set repaired the extra lines disappeared, as shown in the bottom spectrum.

More recently another approach to passive current monitoring has been developed with more emphasis on time domain analyses, in addition to the more traditional frequency domain analysis²⁵⁻²⁷. This approach was developed specifically for the diagnosis of motor-operated valves (MOV) commonly used in power plants. These methods may be applicable to other kinds of loads as well. Fig. 12 is an example of the identification of specific events in the operation of a MOV by a close examination of the average motor current as a function of time. On the other hand, frequency domain analysis displays quite different characteristics for the MOV driven by an induction motor, as illustrated in Fig. 13. Notice that in this case, care has been taken to associate spectrum lines with particular physical phenomena in the geared valve, which is the motor load.

Efforts are now under way to commercialize this technique under the name Motor Current Signature Analysis (MCSA). More information on licensing and commercial aspects may be obtained from the originators of the technique²⁵⁻²⁷. A caution in regard to Fig. 12 is in order. The spectrum line "c" marked motor shaft speed is referred to by licensees as the MCSA-motor speed and is apparently, believed to be a feature of the patented method. As shown in the next section, that spectrum line is not the shaft speed and therefore will not show in the same way or position in the spectrum for all induction motors.

One of the authors of this paper has developed a similar technique of motor current signature analysis but directed specifically to studying the behavior of hermetic rotary compressors. In such compressors the high- and low-pressure regions are separated by a vane in sliding contact with a metal ring being driven off axis by a 2-pole induction motor. This ring moves freely on an oil film between itself and the eccentric which is on the motor shaft. The dynamics of the ring motion are quite complex having both average and oscillating components. Passive current monitoring provided a convenient and accurate method of observing the average ring rotation in production compressors. Fig. 14 is an example of how the free rotation of the ring is manifested in the current. In the particular units under study the ring rotation speed appears as a first and second harmonic, of approximately equal amplitude, in sidebands about the line frequency. The other prominent local features are the results of (deliberate) asymmetry in the motor rotor (as in rotor faults) and the cyclic variation of the motor torque due to the compressor.

Shaft Speed Oscillation Spectra: To predict the current spectra due to speed oscillation we will start with the steady-state equivalent circuit of Fig. 8. It is assumed that the motor is operating in the sinusoidal steady state at line frequency but with a small, low-frequency torque and speed variation applied to the shaft by the load. In order to display the major effects, the equivalent circuit is simplified to include only the slip dependent rotor resistance. This assumption was checked by implementing a simulation using a full d-q axis representation of the motor that showed the frequency predictions of the simplified circuit to be correct over a remarkably wide range of inputs²⁸.

The shaft speed of the motor is assumed to consist of an average and an oscillating component given by Eq. 3:

$$n(t) = N_m \left[1 + \sum_k M_k \sin(2\pi k f_c t) \right] \quad (3)$$

The line voltage is assumed to be a pure sinusoid given by Eq. 4:

$$v(t) = V \sin(2\pi f_l t) \quad (4)$$

where N_m = unperturbed shaft speed (rpm)
 M_k = fourier components of the speed fluctuation
 f_c = fundamental frequency of the speed fluctuation
 V = voltage amplitude

When the shaft speed of Eq. 3 is used in calculating the slip, s , the line current, i_s , calculated in the simplified circuit, is given by Eq. (5):

$$i_s(t) = (V/R) * (N_m - N_o) / N_o * \sin(2\pi f_l t) + (V/R_r) * (N_m / N_o) * \sin(2\pi f_l t) \sum_k M_k \sin(2\pi k f_c t) \quad (5)$$

where N_o = mechanical synchronous speed (rpm)
 R_r = rotor resistance (Figure 8)

Notice that Eq. 5 consists of a line frequency component that is just that which would be present if there were no speed variation plus a symmetrical series of sidebands reflecting the shape of the shaft-speed variation as if the motor were acting as an amplitude modulator with line frequency as the carrier and the shaft speed as the modulating signal.

In the special case of the fundamental frequency, f_c , of the modulation being the shaft frequency itself, i.e., the load torque varies with shaft position, the frequencies of the harmonics may be expressed more simply in terms of the line frequency and slip alone.

$$f = f_l \left[k / (p/2) * (1-s) \pm 1 \right] \quad (6)$$

Table 1 compares the frequencies (Eq. 6) for 2- and 4-pole motors with the "broken bar" frequencies of Eq. 1. First, note that in a 4-pole motor there are two components very near to shaft frequency. One of the components should be the larger in magnitude since it is due to the fundamental. Second, note that there will always be a component at rotor frequency but it will be due to higher harmonics as the number of poles in the motor is increased. Third, for 2-pole motors, the shaft oscillation harmonics will be identical to those for broken bars with the exception of an interchange of line and rotor frequency components. Finally, there will be no such harmonics unless there is some oscillation in the shaft.

Conclusion: Several examples of passive current monitoring techniques have been described. The number of papers being published and companies getting into business indicate that this field is beginning to take off, and that such techniques will be routinely applied on a large scale. Clearly there is much research left to do for improving present methods, applying new methods, and developing techniques for other kinds of faults.

In this paper we did not review other methods now in use for fault and incipient fault

diagnosis such as RF emissions, vibrations, chemical analysis, flux sensors, temperature sensors, etc. In addition to developing these methods further as individual entities, the various technologies will have to be integrated into diagnostic systems, in which all aspects of the motor will be considered as a whole, for greater sensitivity and for the resolution of ambiguity, as well as for a broader coverage^{29,30}. Related to those approaches is system modeling, somewhat along the lines of the rotor-resistance technique described in Rotor Faults, but applied on a larger scale to entire drive systems and possibly to the total system, be it a power plant or an industrial process³¹.

Acknowledgment: The authors wish to thank GE Corporate Research and Development, and the Electric Power Research Institute for the use of their facilities in the preparation of this paper.

References:

- [1] Kliman, G.B. et al., "Noninvasive Detection of Broken Rotor Bars in Operating Induction Motors", *IEEE-PES, Trans. EC*, Vol. 3, No. 4, pp. 873-879, Dec. 1988.
- [2] Kliman, G.B., "The Detection of Faulted Rotor Bars in Operating Induction Motors", *Conf. Proc. ICEM '86*, Munich, Sept. 1986.
- [3] Kliman, G.B. et al., "Broken Bar Detector for Squirrel Cage Induction Motors", *Conf. Proc. MMDC*, Las Vegas, Sept. 1989.
- [4] Tavner, P.J., Armin, K.K. and Hargis, C., "An Electrical Technique for Monitoring Induction Motor Cages", *IEE Conf. on Electrical Machines and Drives, IEE Publication No. 282*, pp. 43-46, 1987.
- [5] Gaydon, B.G. and Tucker, C.F.J., "Detection of Rotor Defects in Induction Motors Using Minicomputer", *CEGB Report SE/SSD/RN/80/074*, June 1981.
- [6] Williamson, S. and Smith, A.C., "Steady State Analysis of 3-Phase Cage Motors With Rotor Bar and End Ring Faults", *IEE Proc.*, Vol. 129, Pt. B, No. 3, pp. 93-100, May 1982.
- [7] Deleroi, W., "Broken Bar in Squirrel Cage Rotor of an Induction Motor, Part 1: Description by Superimposed Fault Currents", *Arch. fur Elektrotechnik*, Vol. 67, pp. 91-99, 1984.
- [8] Mavridis, D., "On the Performance of Three-Phase Squirrel Cage Induction Motors During the Presence of Bar or Ring Breaks", Ph.D. thesis, Univ. of Hanover (Germany), 1963.
- [9] Kerzenbaum, I. and Landy, C.F., "The Existence of Large Interbar Currents in Three-Phase Squirrel Cage Motors With Rotor-Bar and/or End Ring Faults", *IEEE. PAS-103*, No. 7, July 1984.
- [10] Landy, C.F. and Moore, R., "Further Success in the Detection of Broken and/or Cracked Rotor Bars in Large Squirrel Cage Induction Motors", *IEE Conf. on Electrical Machines and Drives, IEE Publication No. 282*, pp. 145-149, 1987.
- [11] Hickiewicz, J., Symanic, S. and Wach, P., "Vibroacoustic Diagnosis of Electric Circuit Defects of 3-Phase Induction Motors", *Conf. Proc. ICEM '86*, Munich, Sept. 1986.

- [12] Vas, P., "Steady State and Transient Performance of Induction Motors With Rotor Asymmetry", *IEEE-PAS, Trans. PAS*, Vol. PAS-101. No. 9, pp. 3246-3251, Sept. 1982.
- [13] Thomson, W.T., Chalmers, S.J. and Rankin, "An On-Line Computer Based Current Monitoring System for Rotor Fault Diagnosis in 3-Phase Induction Motors", *Turbomachinery International*, pp. 17-24, Nov./Dec 1987.
- [14] Kliman, G.B. et al., "The Detection of Broken Bars in Motors", EPRI Report (in press), 1989.
- [15] Cho, K.R., Lang, J.H. and Umans, S.D., "Detection of Broken Rotor Bars in Induction Motors Using State and Parameter Estimation", *IEEE- IAS, Conf. Proc. IAS Annual Meeting*, San Diego, Oct. 1989.
- [16] Cameron, J.R., Thomson, W.T. and Dow, A.B., "Vibration and Current Monitoring for Detecting Airgap Eccentricity in Large Induction Motors", *IEE Proc.*, Vol. 133, Pt. B, No. 3, pp. 155-163, May 1986.
- [17] Cameron, J.R., Thomson, W.T. and Dow, A.B., "On-Line Current Monitoring of Induction Motors - A Method for Calculating the Level of Airgap Eccentricity", *Conf. on Electric Machines and Drives, IEE Publication No. 282*, pp. 173-178, 1987.
- [18] Verma, S.P. and Natarajan, R., "Effects of Eccentricity in Induction Machines", *Conf. Proc. ICREM*, Budapest, Sept. 1982.
- [19] Natarajan, J. and Ramanathan, R., "Investigations of Rotor Harmonics of Induction Motors", *Conf. Proc. 20th North American Power Symposium*, Sept. 1988.
- [20] Natarajan, R., "Failure Identification of Induction Motors by Sensing Unbalanced Stator Currents", *IEEE Trans Energy Conversion*, Vol. 4, No. 4, pp. 585-590, Dec. 1989.
- [21] Williamson, S. and Mirzoian, K., "Analysis of Cage Induction Motors With Stator Winding Faults", *IEEE-PES, Summer Power Meeting*, July 1984.
- [22] Hentschel, M., "Circuit Arrangement for Recognition of a Defect Caused by Phase Breakdown or Ground Short in the Current Supply of a Three-Phase Motor" U.S. Patent 3,824,430, July 1974.
- [23] Steele, M.E., Ashen, R.A. and Knight, L.G., "Applications of an Electrical Method for Condition Monitoring of Motors", *MOTORCON Proc.*, pp. 321-335, Sept. 1982.
- [24] Steele, M.E., Ashen, R.A. and Knight, "An Electrical Method for Condition Monitoring of Motors", *IEE Conf. on Electrical Machines - Design and Applications*, Pub. No. 213, July 1982.
- [25] Kryter, R.C. and Haynes, H.D., "Condition Monitoring of Machinery Using Motor Current Signature Analysis", *Sound and Vibration*, pp. 14-21, Sept. 1989.
- [26] Haynes, H.D. and Kryter, R.C., "Condition Monitoring of Machinery Using Motor Current Signature Analysis", *Conf. Proc., MMDC*, Las Vegas, pp. 690-695, Sept. 1989.
- [27] Haynes, H.D., "Aging and Service Wear of Electric Motor Operated Valves Used in Engineered Safety-Feature Systems of Nuclear Power Plants", ORNL Report, NUREG/CR-4234, ORNL-6170/V2, Vol. 2, Aug. 1989.
- [28] MacMinn, S.R., private communication.
- [29] Tavner, M.A., Gaydon, B.G. and Ward, B.A., "Monitoring Large Generators and Motors", *IEE Proc.*, Vol. 133, Pt. B, No. 3, pp. 169-179, May 1986.

- [30] Gonzalez, A.J. and Lowenfeld, S., "On-Line Diagnosis of Turbine- Generators Using Artificial Intelligence", *IEEE Trans. on Energy Conversion*, Vol. EC-1, No. 2, pp. 68-74, June 1986.
- [31] Isermann, R., "Process Fault Detection Based on Modeling and Estimation Methods - A Survey", *Automatica*, Vol. 20, No. 4, pp. 387-404, 1984.

Table 1
**Comparison of broken bar current spectrum and shaft
oscillation current spectra.**

K	Broken Bar	Speed Oscillation	
	2 Poles	2 Poles	4 Poles
1	$f_i, (1-2s)f_i$	$sf_i, (2-s)f_i$	$(1+s)/2f_i, (3-s)/2f_i$
2	$(2-s)f_i, (2-3s)f_i$	$(1-2s)f_i, (3-2s)f_i$	$sf_i, (2-s)f_i$
3	$(3-2s)f_i, (3-4s)f_i$	$(2-3s)f_i, (4-3s)f_i$	$(1-3s)/2f_i, (5-3s)/2f_i$
4	$(4-3s)f_i, (4-5s)f_i$	$(3-4s)f_i, (5-4s)f_i$	$(1-2s)f_i, (3-2s)f_i$

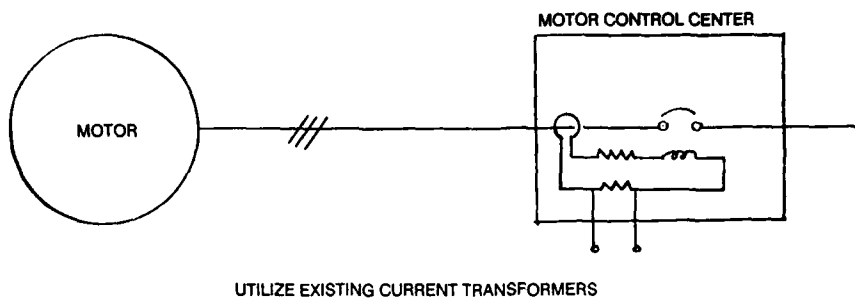


Figure 1. Current monitoring with existing facilities.

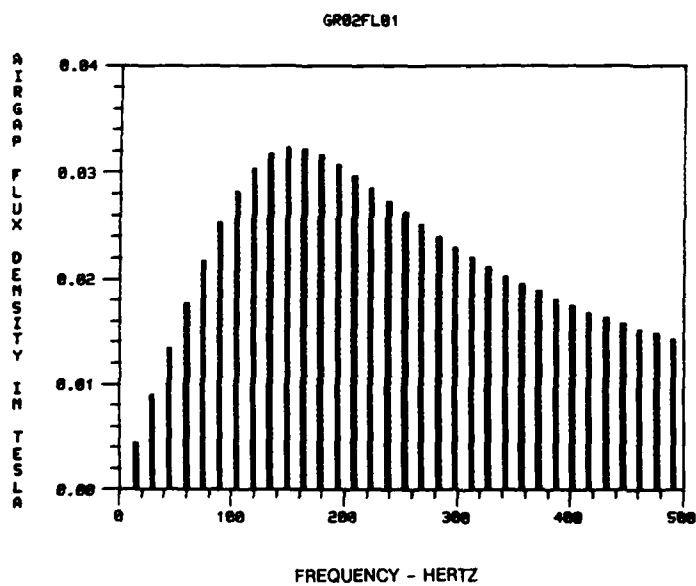
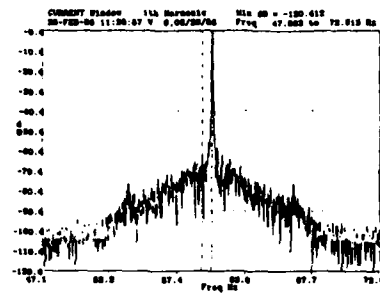
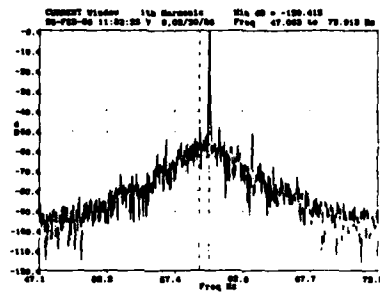


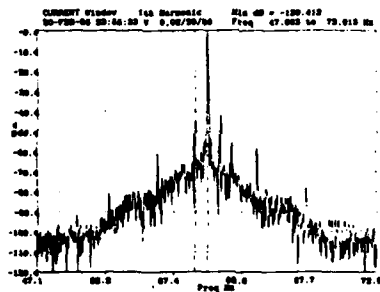
Figure 2. Airgap flux spectrum as seen from the stator for an 8-pole gas recirculation fan motor with one broken bar^{1,14}.



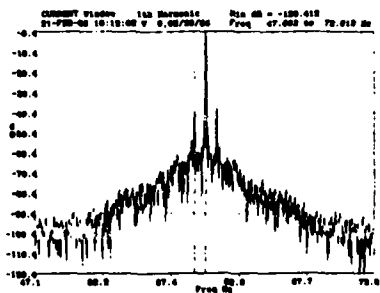
GOOD MOTOR
NO BROKEN BARS
NO OFFSET



ONE BROKEN BAR



TWO BROKEN BARS



THREE BROKEN BARS

Figure 3. Current spectra in the vicinity of the first harmonic (60 Hz) for several fault conditions on test motor^{1,14} (6 pole, ~ 25 hp).

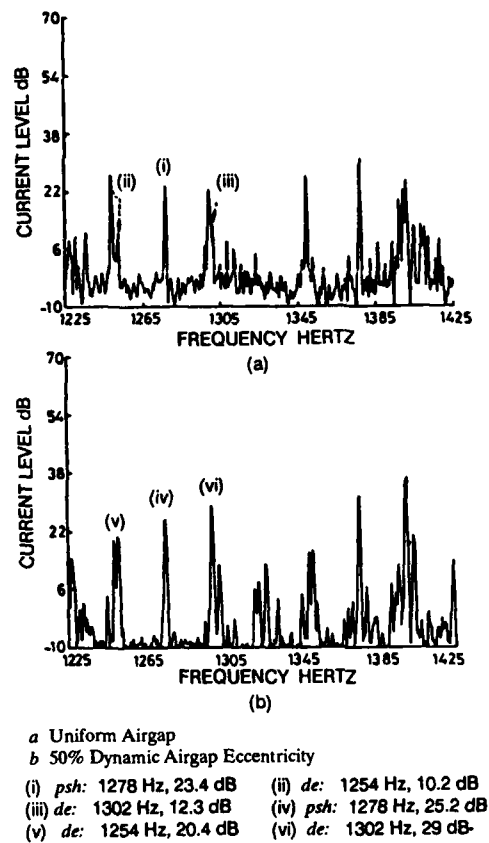


Figure 4. Example of the effect of a dynamic asymmetry in the current spectrum near the bar passing frequencies. Current zoom spectrum with 51-slot rotor (4 poles, 11 kW)¹⁷.

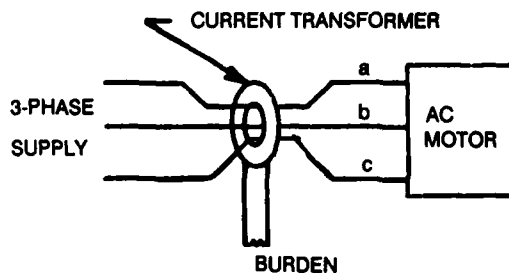


Figure 5. Typical circuit for ground fault protection.

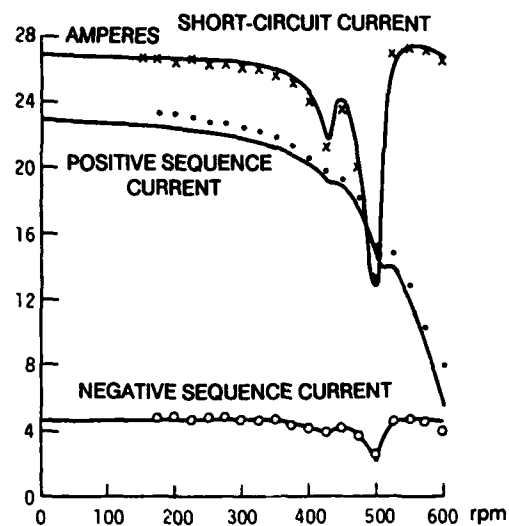


Figure 6. Predicted and measured currents for a phase-to-phase short circuit²¹ (10 poles).

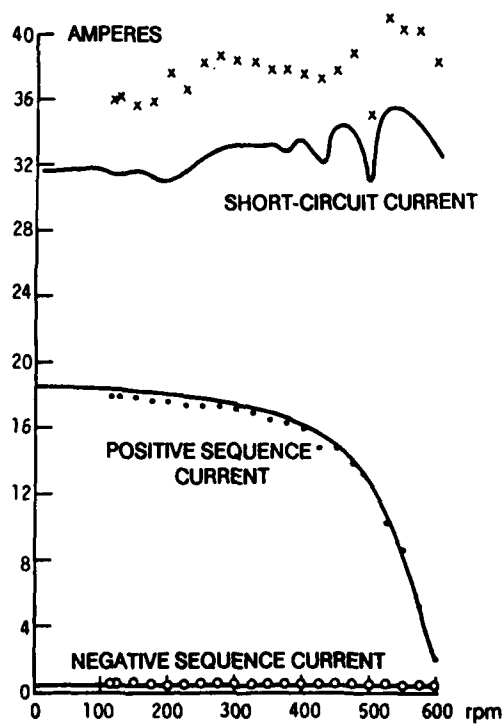


Figure 7. Predicted and measured currents for one coil short circuited²¹ (10 poles).

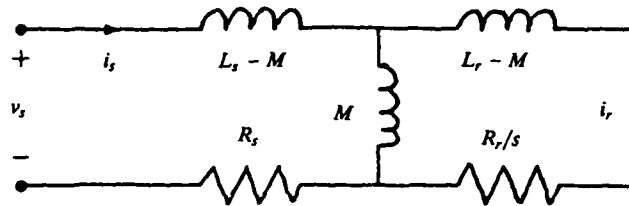


Figure 8. Balanced single-phase electrical model of an induction motor operating at constant velocity.

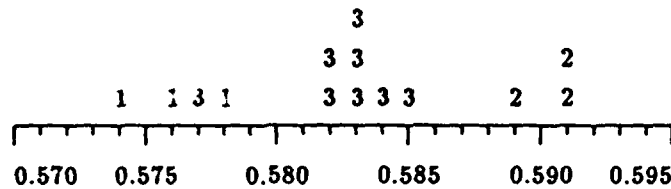


Figure 9. Estimated rotor resistance for motors with faulted (#2) and unfaulted (#1 and #3) rotors¹⁵.

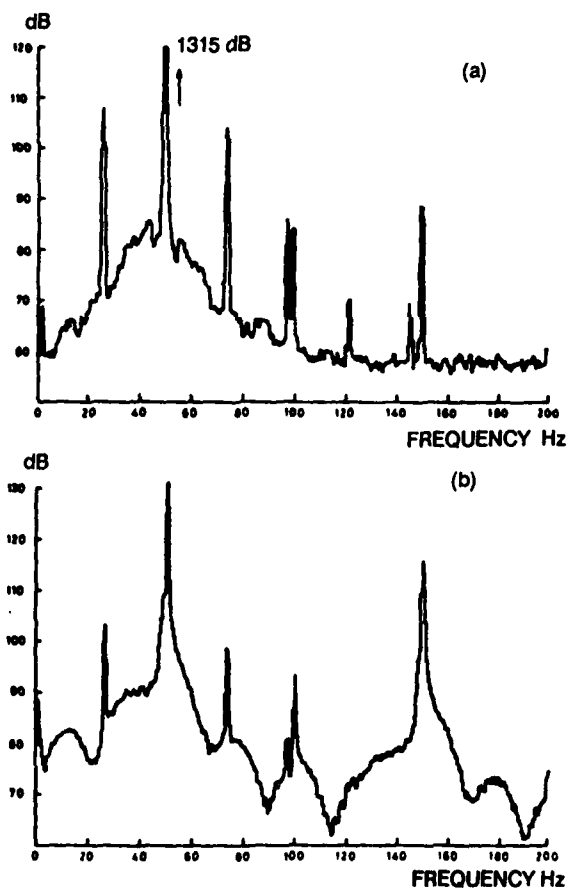


Figure 10. Comparison of current spectra for a pump with (a) good and (b) bad bearings^{23,24} (2.6 kW, 4 pole).

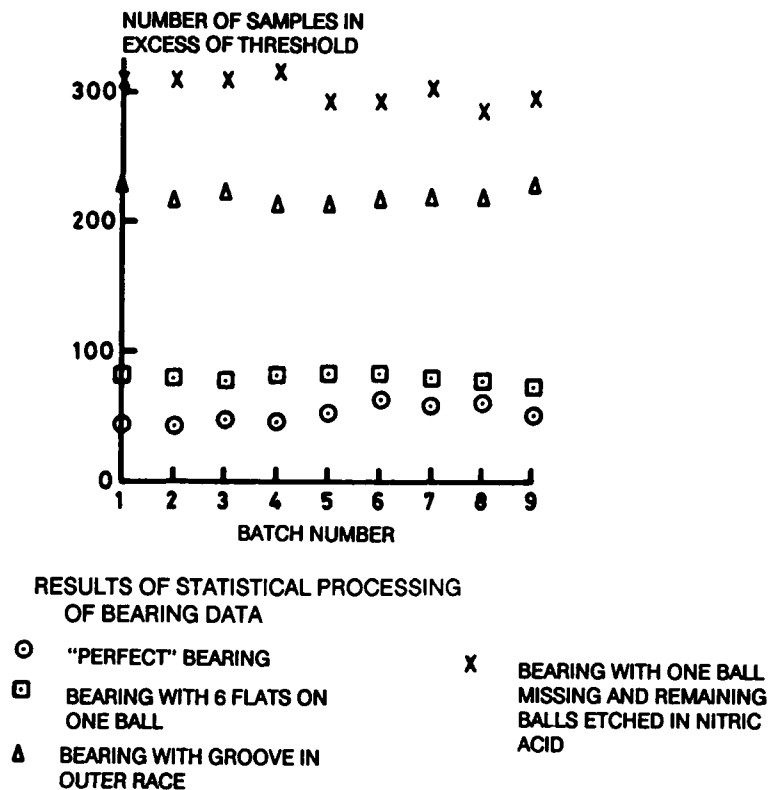


Figure 11. Results of a pulse-over-threshold analysis of the filtered current of a motor driving a pump having various defective bearings^{23,24} (2.6 kW, 4 pole).

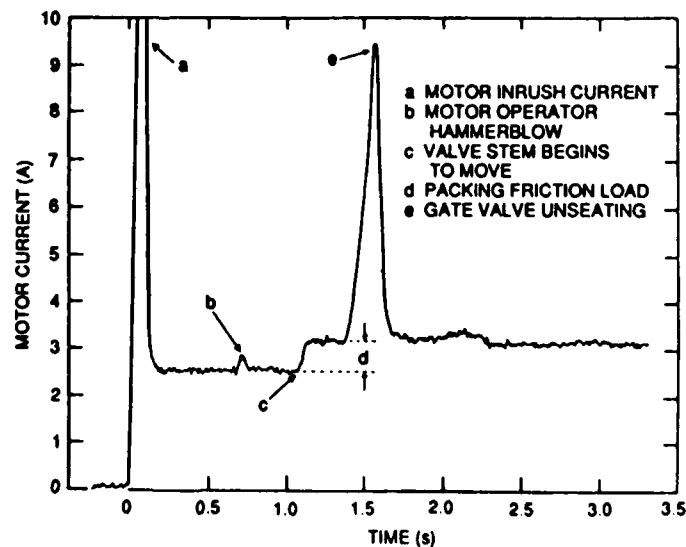


Figure 12. Typical transient features seen at the beginning of the close-to-open stroke of an MOV^{25,27} (4 hp, 4 pole).

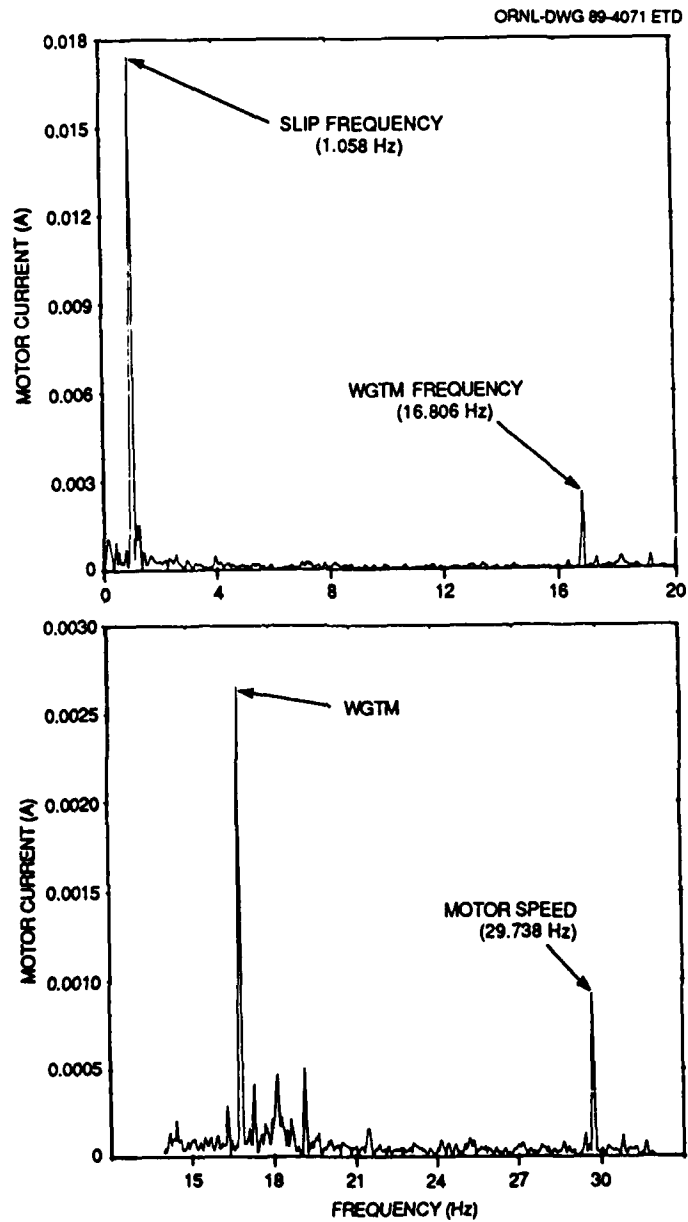


Figure 13. MOV200 motor current spectrum analysis (close-to-open stroke)²⁷ (4 hp, 4 pole).

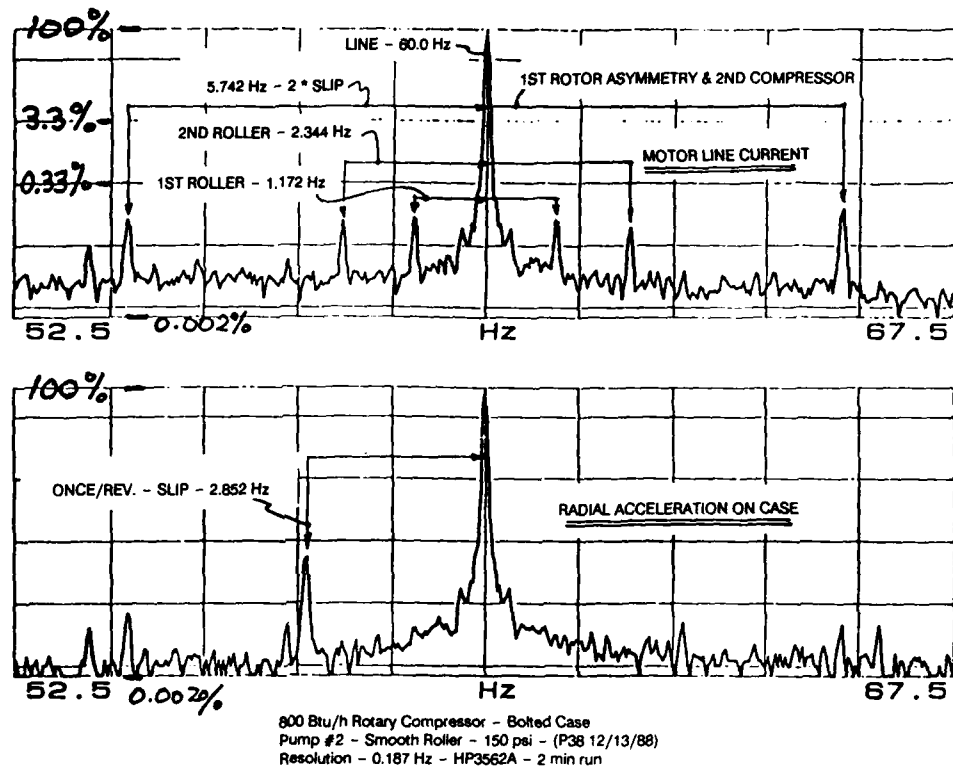


Figure 14. Typical current spectrum for a properly operating rotary compressor drive motor in the vicinity of line frequency (5 hp, 2 pole).

MOVATS DIAGNOSTIC METHODOLOGY

William L. Lavallee and W. Dean Romine
HENZE-MOVATS Incorporated
200 Chastain Center Boulevard, Suite 250
Kennesaw, Georgia 30144-5512

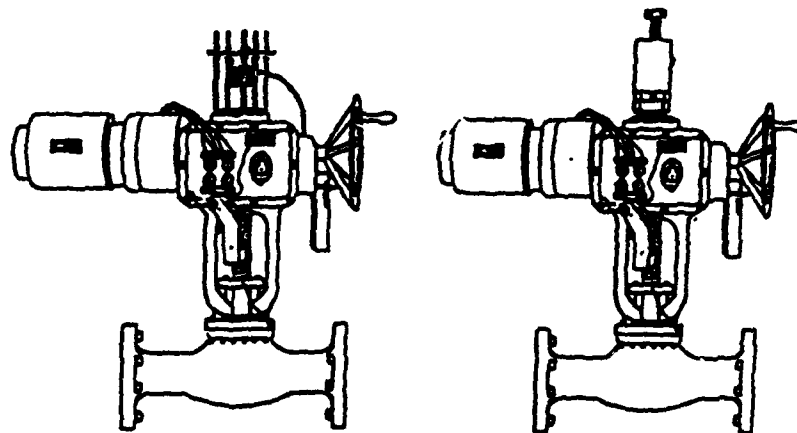
Abstract: The ability to ensure operability of Motor-Operated Valves (MOV) in nuclear power plants has been a concern of the Nuclear Regulatory Commission (NRC) for the past several years. The NRC recently issued Generic Letter 89-10, "Safety Related Motor-Operated Valve Testing and Surveillance", which requires nuclear power plants to develop and implement a program that ensures MOVs will be maintained and will operate under design-basis conditions for the life of the plant. This paper describes a system which obtains static and dynamic signatures of critical MOV parameters and provides a simple and effective method by which the data can be examined and any required corrective actions can be identified.

Key Words: Limit switch, load cell, motor current, motor load, motor-operated valve, spring pack, stem thrust, thrust measuring device, torque switch.

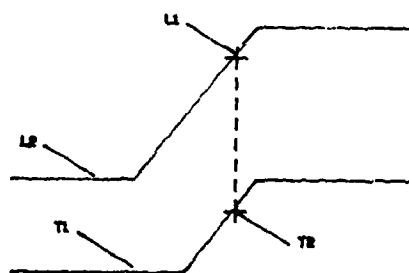
Introduction: The MOVATS Diagnostic Test System is an innovative and simple data acquisition and signature analysis method by which the general mechanical and electrical control setup of a motor-operated valve (MOV) can be accurately determined. Signatures of valve stem thrust, control switch actuation, motor current, and actuator status, all superimposed, through the use of portable diagnostic equipment can warn the user of incipient degradations occurring within the valve, actuator, control circuit, or motor, prior to actual failure. The system can also provide assurance that any previously identified concerns have actually been corrected.

The basis for the MOVATS Incorporated methodology is formulated on the concept that the greater the load being delivered to the valve stem, the greater the movement of the worm within the actuator. A linear variable differential transformer was installed in a device called the "Thrust Measuring Device", or TMD, to calibrate the movement to actual stem load throughout a valve cycle to produce a dynamic measurement of stem thrust. The TMD is installed on the actuator by removing the spring pack dust cover such that its stylus comes in contact with any part of the spring pack preload nut. Subsequent movement of the spring pack, caused by changes in stem load is translated into a voltage output of the TMD. Knowledge of the dynamic movement of the spring pack throughout the valve cycle provides information regarding the valve and actuator mechanical condition and can further be correlated to actual stem thrust. Knowledge of stem thrust allows the actuator to be set to achieve thrust required to actuate without exceeding the stress limits of the valve or actuator.

System Description: In order to calibrate the spring pack movement to actual stem thrust, a National Bureau of Standards (NBS) certified load cell is mounted such that it is in close proximity of the top of the valve stem. With the TMD installed and monitoring spring pack movement, and the load cell being connected to the portable two channel digital recording oscilloscope, the valve is opened electrically. As the valve stem contacts the load cell, the stem load rises dramatically with a corresponding spring pack movement. The spring movement signature can now be directly correlated to the thrust signature. The resultant curve is then used to determine pounds of stem thrust per inch of spring pack deflection.



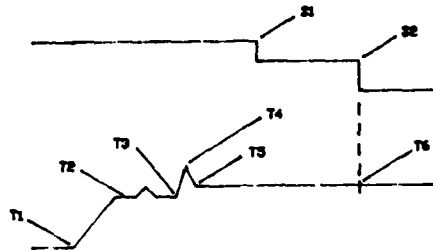
Load Cell Installation



Spring Pack Calibration Signature

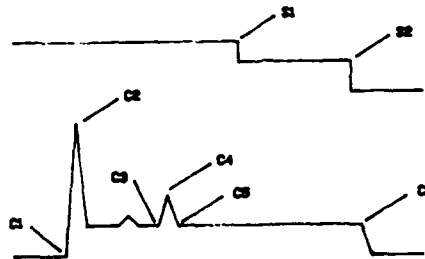
The spring pack calibration curve allows the user to determine the magnitude of thrust being delivered to the valve stem at any time during the valve cycle. The TMD can also be correlated to stem thrust using the MOVATS Stem Strain Ring (SSR) or Stem Strain Transducer (SST). These devices clamp directly onto the valve stem, either on the threads or the smooth stem area and can be used to measure closing stem thrust, unseating values, and packing loads accurately.

Control Switch Signature: Testing has shown that having the capability to determine the exact time and loading at which the control switch actuates is of great importance. This sub-system provides a signature which reflects the exact points within the valve cycle at which various switches actuate. By obtaining this signature simultaneously with the thrust signature, the loading condition at the time each switch trips can be determined.



Control Switch and Thrust Signature

Motor Current Signature: In measuring this parameter dynamically, a Simpson AC amp probe, or a Fluke AC/DC amp probe with analog output, is utilized. This parameter can be obtained either at the valve or the motor control center. Changes in motor current signatures can provide periodic indication of grossly degrading mechanical or electrical MOV conditions. It is also useful in determining the stroke time and contactor drop out time of the MOV.



Control Switch and Motor Current Signature

Motor Load Signature: This particular parameter can be measured at the motor control center or at MOV's with terminal blocks, with a simple, easy to install transducer. A relationship between motor load and actuator torque is established during baseline testing to enable the user to evaluate any degradations which may occur. This method involves comparison of the available thrust margin to baseline motor running load making allowances for stem factor degradation. Once these parameters are established, acceptable margins can be determined to evaluate changes over the trending period. An increase in the trended value indicates that either the stem load at running load has risen or degradations have occurred which have caused an increase in the motor torque required to provide the running load stem thrust. These events detract from the available thrust margin and the actuators ability to provide the required thrust.

Signature Analysis: From signatures taken during baseline testing and those taken at the motor control center, the following parameters can be determined:

- Apparent Running Load
- Minimum Available Thrust
- Valve cycle time
- Time of hammerblow
- Time of unseating
- Time at which close-to-open bypass switch opens
- Actuator inertia induced stem load
- Inrush motor current
- Running motor current
- Final motor current

With the above specific data signatures available, the following typical degradations or combinations thereof can be readily identified.

- Valve mechanical wear
- Actuator mechanical degradation
- Actuator gear wear
- Motor electrical degradation
- Improperly set bypass switches
- Improperly set torque switches
- Backseating conditions
- Torque switch relaxation
- Unbalanced torque switch
- Loose stem nut locknut
- Excessive stroke time
- Inadequate load available to operate valve under accident or design conditions
- Improper alignment of actuator to valve
- Excessive packing loads
- Improperly sized upper bearing housing gasket

Although all of the above information has proved to be quite helpful in diagnosing pending or existing degradations within the valve and actuator, one should not overlook the trending capabilities which the testing provides. Parameters such as motor load, cycle time, minimum available thrust, inertia, etc., can now be compared to previous data to identify slowly developing actuator degradations.

HENZE-MOVATS Incorporated: HENZE-MOVATS Incorporated Motor-Operated Valve (MOV) experience spans over six years of MOV testing, engineering, program reviews, and actuator/valve repairs within the nuclear industry. The first to bring a motor-operated valve analysis and testing system to the market, HENZE-MOVATS continues to be the leader in MOV services. To date, forty-eight U.S. utilities, the U.S. Government, and sixteen foreign utilities have utilized HENZE-MOVATS' services.

In 1983, MOVATS Incorporated (HENZE-MOVATS Incorporated) introduced the MOVATS Series 2000 Valve Analysis System which for the first time enabled utilities to monitor MOV performance. This new technology provided the ability to monitor MOV output (stem thrust, HBC torque, or actuator torque) and to detect numerous MOV degradations. HENZE-MOVATS Incorporated has averaged over eighty-three thousand man-hours per year testing MOVs and currently has over sixty-five qualified field service engineers who perform this service. In our continuing effort to advance MOV testing technology, HENZE-MOVATS Incorporated has recently introduced the MOVATS Series 3000 Valve Analysis System which is a computer based testing system fully compatible with all our testing transducers for rising stem and quarter turn valves.



The 3000 system consists of the Signature Analysis Module (SAM), Data Acquisition Module (DAM), a color video monitor, and a full function, full-size keyboard. The SAM receives data from up to eight transducers at once and simultaneously displays in real time any four traces in engineering units. The system utilizes a menu-driven software package that makes the acquisition and signature analysis essentially automatic.

Summary: Signature analysis of critical parameters associated with motor-operated valves has shown that developing mechanical and electrical concerns can be identified prior to actual loss of function or significant component damage. In many of the field tests, the signatures illustrated that although the valve appeared to be operating properly, changes in wear characteristics, packing loads, or system induced loads (pressure or flow), could challenge the operability of the valves. These concerns were eliminated by minor field adjustments. As for the mechanical and electrical degradations noted in the signatures, provide cognizant maintenance personnel a clear insight into not only which valves require closer attention, but specifically where within the valve or actuator the degradation most likely exists.

MOTOR CURRENT SIGNATURE ANALYSIS (MCSA)

Claude L. Thibault

Wyle Laboratories
7800 Governors Drive West
Huntsville, Alabama 35807-7777

Motor Current Signature Analysis (MCSA) is a powerful monitoring tool for electric motor driven equipment.

It was developed by ORNL to determine the effects of aging and service wear specifically on motor operated valves used in nuclear power plant safety systems, but is applicable to a broad range of machinery.

Wyle has been licensed on this system by ORNL in July of 1988.

Although the bulk of experience with MCSA has been in connection with motor operated valves, motor current signatures have been obtained from other devices (reciprocating pump, centrifugal pumps, fans, etc.)

Once the baseline data has been established, continued operability of the Motor Driven System can be verified, by monitoring Motor Current Signatures from the Motor Control Center. This can be accomplished using Motor Current Signature Analysis (MCSA). MCSA possesses several innovative features which include on-site computerized data acquisition, remote monitoring capability and the use of such instrumentation as signal conditioner and clamp-on ammeters for quick setup. The system identifies, characterizes, and trends over time the instantaneous load variation of mechanical equipment in order to diagnose changes in the condition of the equipment, which if allowed to continue, may lead to failure. The motor current noise signature is detected, amplified and further processed as needed to examine its time domain and frequency domain (spectral) characteristics.

MCSA is based on the recognition that an electric motor (a-c or d-c) driving a mechanical load acts as an efficient and permanently available transducer by sensing mechanical load variations, both large and small, long-term and rapid, and converting them into variations in the induced current generated in the motor windings. These motor current variations are carried by the electrical cables powering the motor and can be extracted at any convenient location and processed as desired. Motor current signatures, obtained in both time and frequency domains, provide equipment condition indicators that may be trended over time to provide early indication of degradation.

Parameters Measured: The motor current signature is obtained as the system operates. Motor current signatures provide diagnostic information on four different levels:

- o Mean value
- o Gross variations
- o Transients
- o Frequency spectrum

As an example, for a MOV, from the time domain signature, the following parameters are determined:

- o Inrush current
- o Running current
- o Seating Current
- o Hammerblow time and amplitude
- o Valve unseating, time and amplitude
- o Limit switch trip
- o Valve seating
- o Torque switch trip
- o Stroke time
- o Torque bypass switch

And from frequency domain, the following parameters are measured:

- o Motor slip frequency
- o Motor speed (RPM)
- o Worm gear tooth meshing (WGTM) frequency
- o Valve stem velocity
- o Operator gear ratios
- o Impact of packing tightness
- o Effects of stem damage

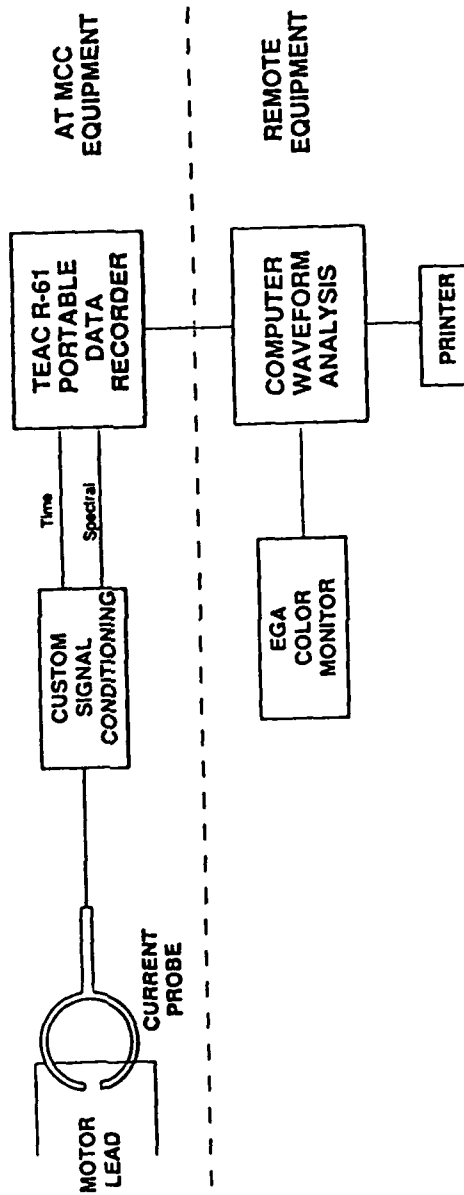
Samples of MCSA hard copy output are shown on the following pages. These plots are indicative of the flexibility and comprehensiveness of the MCSA data system output.

Conclusion: Although application experience of MCSA is concentrated on Motor Operated Valves, it is likely that MCSA will provide a highly sensitive, selective, and cost effective preventive maintenance means for on line monitoring of the condition of a wide variety of heavy machinery driven by electric motors.

References:

- o How to Monitor Motor-Driven Machinery by Analyzing Motor Current by R. C. Kryler and H. D. Haynes from ORNL.
- o Application of Diagnostics to Determine Motor-Operated Valve Operational Readiness by D. M. Eissenberg/ORNL for Publication in the Proceedings of the 14th Water Reactor Safety Information Meeting at the National Bureau of Standards, Gaithersburg, Maryland, October 27-31, 1986.

MCSA DIAGRAM



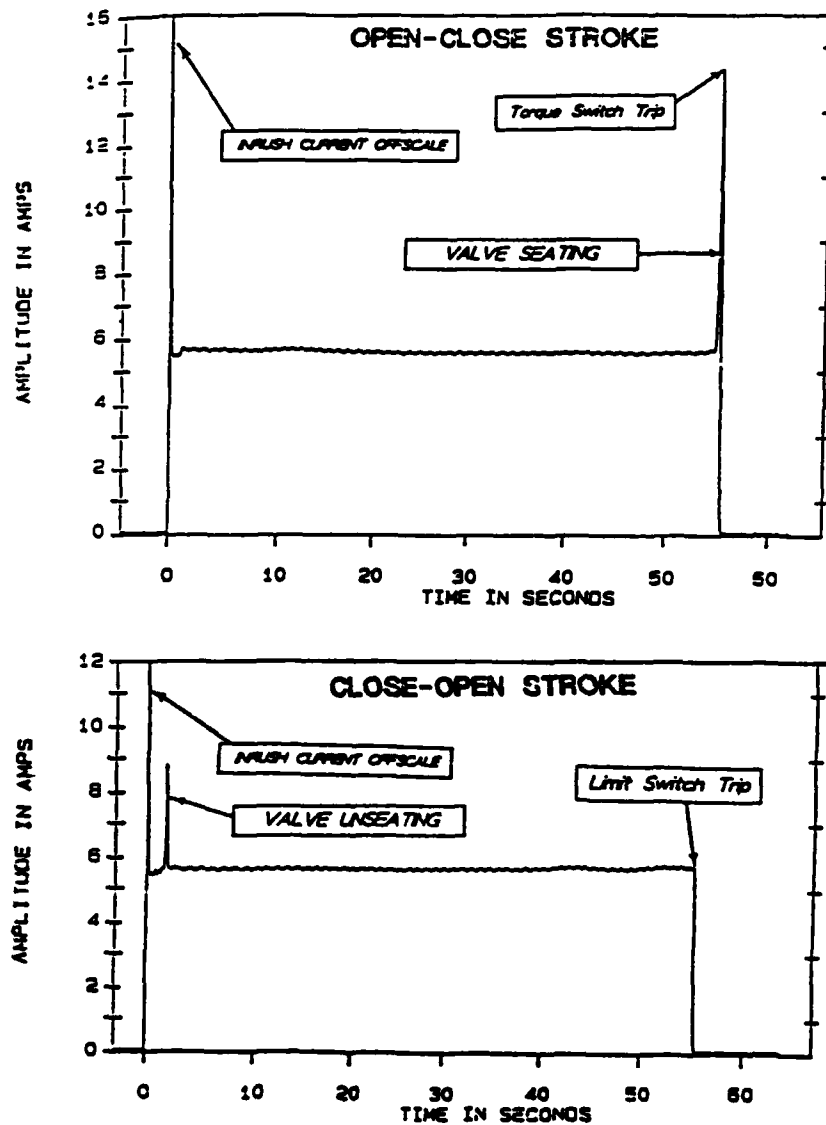


FIGURE 2: MOTOR CURRENT SIGNATURE--FULL STROKE

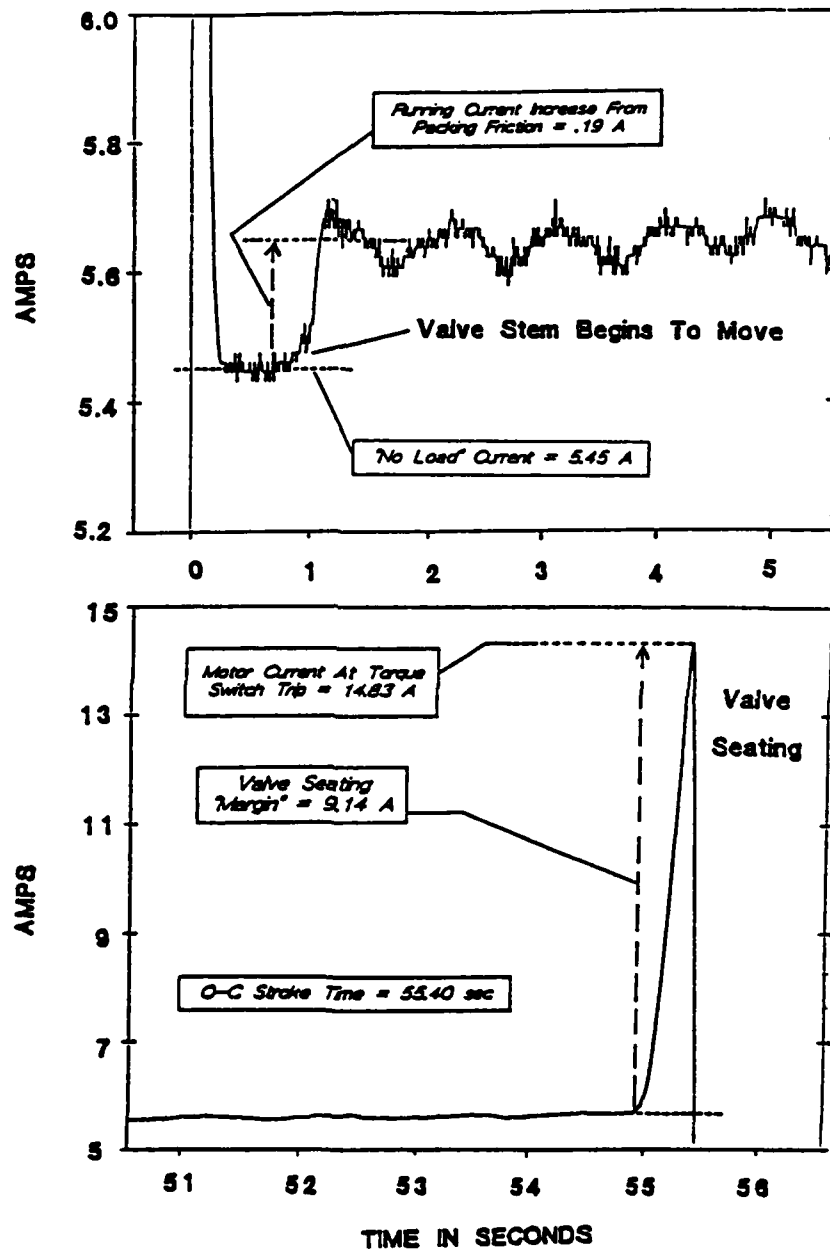


FIGURE 3: MOTOR CURRENT SIGNATURE--TRANSIENTS (O-C STROKE)

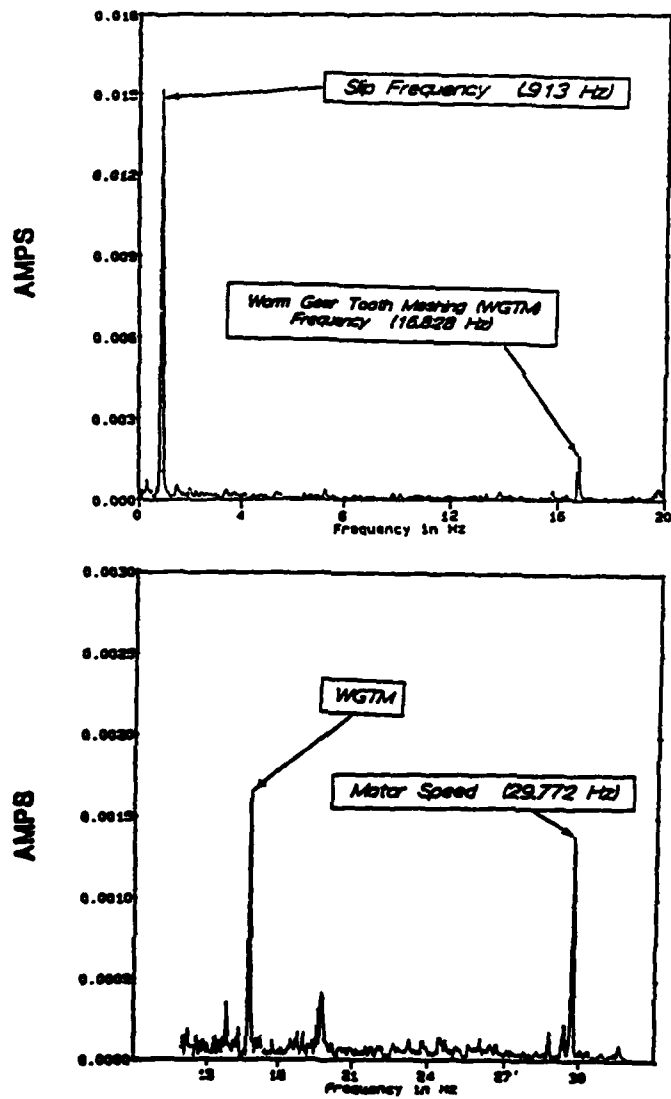


FIGURE 4: MOTOR CURRENT SPECTRUM ANALYSIS (O-C STROKE)

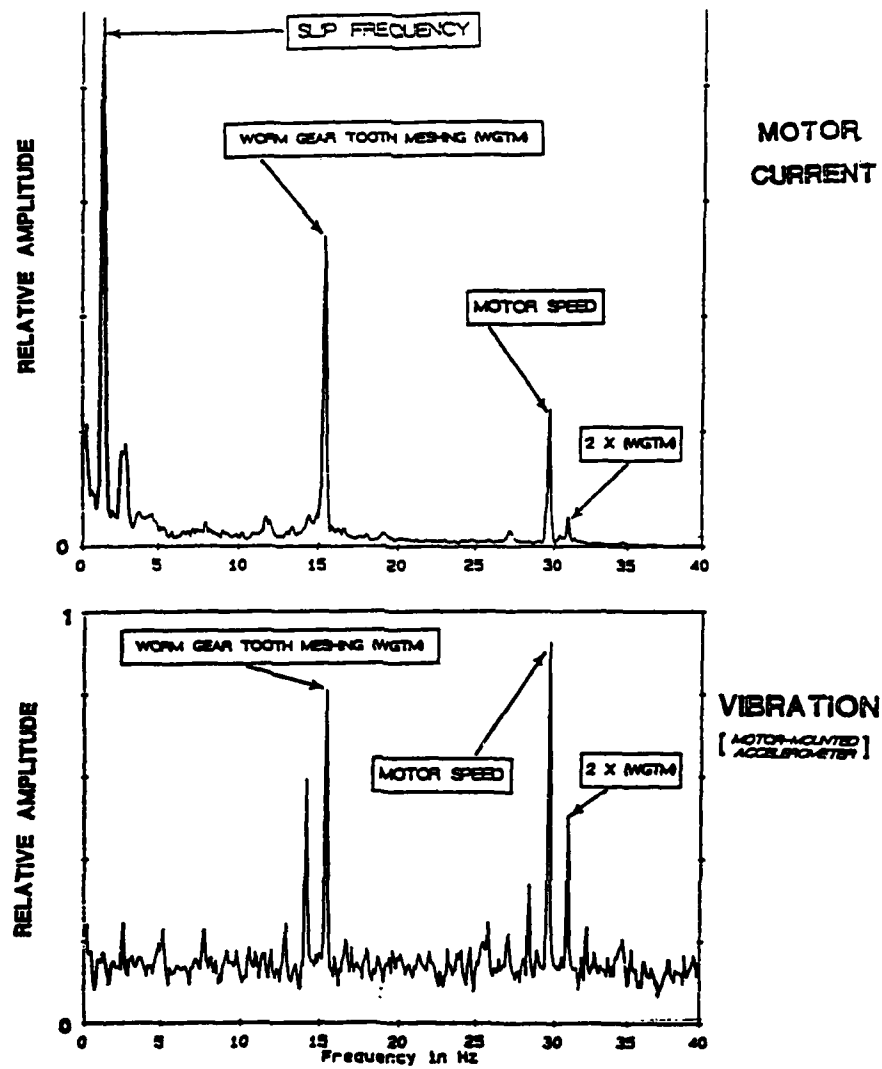


FIGURE 5: COMPARISON OF MOTOR CURRENT AND VIBRATION

COST-EFFECTIVE ON-LINE MONITORING OF ROTATING EQUIPMENT USING MOTOR CURRENT ANALYSIS

D.J. Linehan S.L. Bunch B.B. Hanzelka

Oak Ridge Y-12 Plant*
Martin Marietta Energy Systems, Inc.
Oak Ridge, TN 37831-8161

ABSTRACT: Motor current analysis can be used as an effective predictive maintenance tool for monitoring rotating equipment. Machine signatures can be acquired, nonintrusively, with this new technology and are comparable to those obtained with proven vibration analysis. In addition, motor current monitoring can be performed in a more cost-effective manner than can vibration monitoring. However, motor current analysis is still in the developmental stage and must be performed in conjunction with vibration analysis for accurate results to be achieved. This paper presents a history of this new technology and provides a cost analysis for a typical plant. In addition, a case study, comparing vibration and current signatures, is also discussed.

KEY WORDS: AC rotating equipment; cost-effective; current transformer; Fourier transform; motor current analysis; nonintrusive; on-line

INTRODUCTION: Predictive maintenance, the process of predicting required maintenance and determining the relative health of a piece of equipment, is at least 40% more cost-effective than either the preventive maintenance or the run-to-failure philosophies for a typical manufacturing plant. Further, savings from predictive maintenance are at least ten times greater than annual program costs for a typical plant. These cost savings (due mainly to fewer cases of catastrophic maintenance) and productivity improvements (resulting from less unscheduled maintenance) are two of the most important benefits associated with predictive maintenance; however, a positive impact on safety may also be realized^[1].

Each year, 10% of all large AC (alternating current) rotating equipment in a typical manufacturing facility will fail^[2]. For this reason, the Oak Ridge Y-12 Plant has implemented a predictive maintenance strategy in an effort to lower the failure rate of large AC rotating machinery using proven vibration analysis. This technology utilizes transducers, most often accelerometers, to transform mechanical vibrations into electrical signals. Accelerometer readings are observed at several locations on a machine and stored. Each recorded set of data is then converted from the time-domain to the frequency-domain (via the Fourier Transform) and analyzed. Peak values in this frequency data (or "signature") are characteristic of specific mechanical components associated with a particular machine. Component failures are predicted by observing the magnitudes of the peaks in the signature. By utilizing vibration analysis as a predictive maintenance tool, the failure rate of rotating equipment can be reduced to 5% each year assuming that every piece of equipment is monitored once per month^[3].

With all the benefits associated with vibration analysis, there are also several disadvantages. First, the collection of vibration signatures is labor-intensive. The technician must perform the iterative task of attaching the accelerometer to a specific location on the machine and recording the vibration data. Once all signatures are collected, the data must then be analyzed, the condition of the machine determined, and the required maintenance performed. Second, vibration analysis equipment is expensive. Accelerometer costs alone can constitute a major portion of the entire investment. While vibration analysis could be performed on-line without operator intervention, reducing labor costs, several accelerometers would be required for each machine monitored.

*Operated by Martin Marietta Energy Systems, Inc. for the U.S. Department of Energy under contract DE-AC05-84OR21400.

Motor current signature analysis (MCSA), developed at the Oak Ridge National Laboratory (ORNL), is a technology which has the potential to overcome many of the disadvantages associated with vibration analysis while retaining its benefits. MCSA is based on the principle that a motor attached to a load acts as a permanently available transducer whose output is present on any incoming motor phase^[4]. Experiments conducted by ORNL and the Oak Ridge Y-12 Plant have shown that a correlation exists between vibration and motor current signatures, supporting the basic idea that a motor can act as an accurate transducer^[5]. In addition, this special "transducer" provides a nonintrusive means of obtaining the signature of a machine at a single point by attaching a clamp-on current transformer to one of the motor leads^[6]. Because current meters contain current transformers, for those machines where metering capabilities already exist, motor current analysis may be performed with minimal interface hardware. Once the current data has been recorded, both the vibration and current signatures are obtained and analyzed in a similar fashion.

MCSA provides a more cost-effective method of performing predictive maintenance than does vibration analysis for large AC rotating machines since MCSA requires only one monitoring point for each piece of equipment. For the same reason, MCSA is also better suited for on-line monitoring of rotating machinery than is vibration analysis. In addition, by implementing an effective multiplexing scheme, several machines could be cost-effectively monitored on-line from a single processor since current transformers are relatively inexpensive. However, the primary pitfall associated with motor current analysis is that the relatively small motor current signature is combined with the large 60 Hertz power source, resulting in a signature with unacceptable resolution. Both ORNL and the Oak Ridge Y-12 Plant are developing highly sensitive hardware to achieve the resolution required to extract the motor current signature from the spectrum^[7].

COST ANALYSIS: Still in the experimental stage, MCSA must be used in conjunction with vibration analysis to obtain useful results. MCSA would provide a general alarm condition and vibration analysis would then be used to perform specific fault diagnosis. However, as more vibration and current data is analyzed, MCSA may eventually replace vibration analysis as the predictive maintenance tool of choice for rotating equipment.

Fig. 1 graphs cost verses time for two predictive maintenance scenarios, both of which assume a typical plant containing approximately two-hundred large AC rotating machines. The dotted line represents costs associated with a predictive maintenance strategy where vibration analysis is utilized exclusively and assumes each machine is monitored once per month. Initial costs include one piece of vibration analysis equipment and its associated interface hardware/software. The solid line represents costs associated with an approach where motor current and vibration analysis are used and assumes that eight machines are multiplexed to, and continually monitored by, one on-line MCSA system. While the initial investment is higher, since vibration and motor current analysis hardware/software must be obtained, these costs are recovered in approximately one year. Both scenarios include yearly costs associated with the labor-intensive task of data collection, while excluding that associated with run-to-failure and unscheduled maintenance. Including these items would only serve to shorten the time required for both lines to intersect, thus increasing

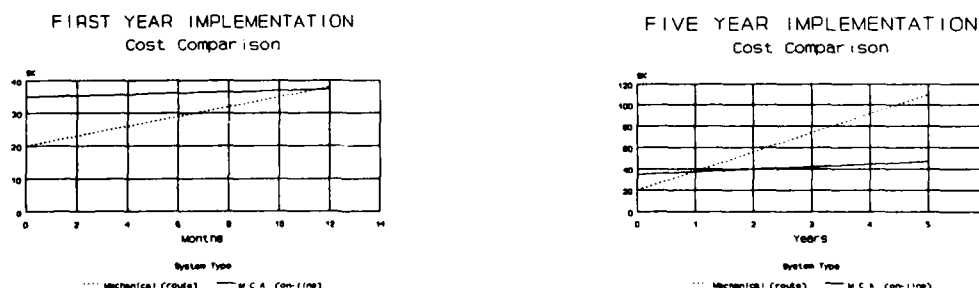


Fig. 1: Cost comparisons.

the benefit of employing MCSA. The yearly costs associated with collecting data is, therefore, the greatest advantage a predictive maintenance strategy utilizing motor current analysis has over one that does not.

Several items have been omitted from the previous discussion in an effort to present a conservative cost analysis. However, one further item, for which no data is available, requires consideration. The preceding analysis ignored the impact on failure rate as it applies to the increased monitoring frequency associated with on-line motor current analysis. Assuming that eight machines are multiplexed for every processor, each machine could be monitored several times per day. This would certainly have a positive impact on the failure rate since component problems could be discovered before a catastrophic failure occurs.

CASE STUDY: ORNL has conducted experiments comparing motor current and vibration spectra obtained from a reciprocating vacuum pump and has concluded that the two correlate well^[6]. Similar research performed at the Oak Ridge Y-12 Plant on larger, belt-driven, AC rotating machines has, so far, reinforced this observation. The following four figures provide both vibration and motor current signatures for one such machine.

Fig. 2 shows the spectrum of accelerometer data recorded near the fan of a particular machine. The peak near 5.5 Hertz corresponds to a vibration associated with the belt pass frequency, and that near 11.7 Hertz corresponds to a vibration associated with the fan speed. These two peaks can again be identified in the motor current spectrum of Fig. 3. Similarly, accelerometer data recorded at the motor of this machine is shown in Fig. 4, where a motor bearing vibration can be observed as a peak at 171.7 Hertz. The four additional maximums labeled in Fig. 4 are first and second order sidebands associated with the primary bearing vibration. The motor current spectrum of Fig. 5 also displays the primary motor bearing vibration peak.

As has been observed, a one-to-one mapping of peak frequencies exists between vibration and motor current spectra; however, peak magnitudes do not appear to map directly. In addition, load bearings, such as those coupled to the fan, have been difficult to ascertain. However, this may be due to the fact that those machines for which motor current data has been collected are primarily belt-driven as opposed to direct drive.

In addition to the previous case study, other researchers have conducted experiments based on inducing faults within the motor. Defects ranging from broken or cracked rotor bars to cut end rings in induction motors were all observed in the motor current spectra when severe enough. All these defects increase the magnitude of the slip frequency (and it's harmonics) since they increase motor resistance.^{[9],[10],[11]}

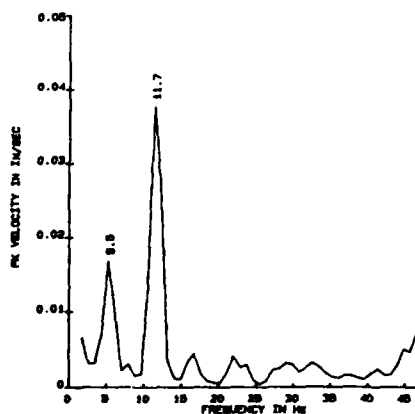


Fig. 2: Fan vibration spectrum.

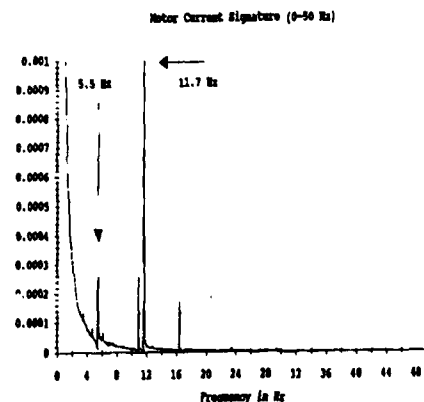


Fig. 3: MCSA, 0-50 Hertz.

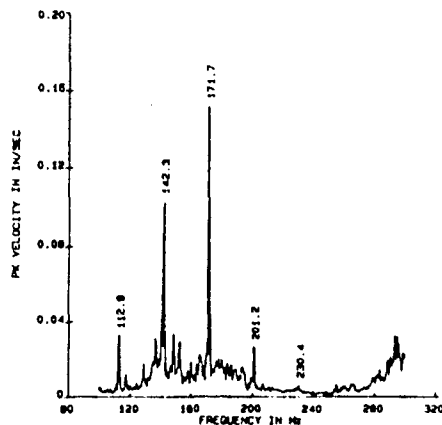


Fig. 4: Motor vibration spectrum.

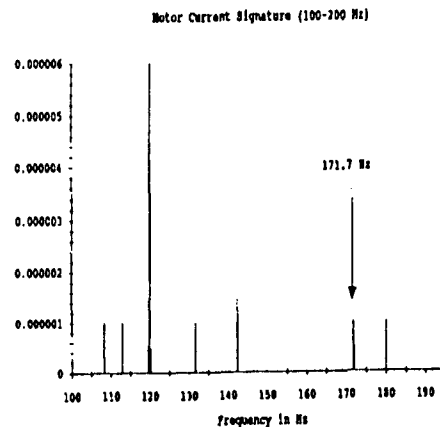


Fig. 5: MCSA, 100-200 Hertz.

DATA ACQUISITION AND ANALYSIS SYSTEMS: As has been stated, analysis of either motor current or vibration signals is very similar in that the time-domain data is converted into frequency-domain data where peak values are compared to previous signatures. This task is most easily accomplished by sampling the time-domain data (via an analog-to-digital convertor), storing it in a personal computer (PC), and executing a Fourier Transform software algorithm. However, the interface hardware for vibration analysis differs greatly from that for MCSA. The large 60 Hertz power signal combining with the small current signature, one of the aforementioned disadvantages of motor current analysis, is the impetus for the development of special MCSA interface hardware. Circuitry implemented at the Oak Ridge Y-12 Plant is based on the observation that useful information exists throughout the spectrum. Because the magnitude of the spectral data of interest is very small, little noise can be self-induced by the interface circuitry. In addition, a high resolution analog-to-digital convertor (ADC) must be utilized. With these constraints considered, resultant signatures obtained from this interface, valid for a wide range of frequencies, can exhibit enough resolution and dynamic range to distinguish very small component peaks, such as those produced by motor bearings. However, motor current analysis interface hardware is still in the experimental stage. Continued hardware/software research may produce a cost-effective interface with even higher resolution.

FUTURE DEVELOPMENTS: Both basic research and hardware and software developments must continued for motor current analysis to be a success. Algorithms must be implemented to detect and alarm on both new and enlarged peaks in the signature, relative to some standard, for each machine monitored. In addition, further research is required to determine whether specific component peaks can be accurately discerned from a motor current spectrum. If possible, algorithms could then be developed to not only provide a general alarm, but to also provide specific component failure predictions.

Basic research is required in two areas of motor current analysis. First an accurate motor model must be developed so that the ability of a motor to transduce mechanical vibrations can be judged. Second, motor current signal characteristics must be investigated more thoroughly so that appropriate signal conditioning can be performed. Researchers have used (with some success) the Wigner distribution for this purpose since it simultaneously extracts both time-domain and frequency-domain information from the motor current data^[12].

Interface hardware will likely change once these fundamental questions have been answered. In addition, if motor current analysis is to be performed on-line, hardware maintainability must also be considered. One method of implementing a maintainable interface, shown in Fig. 6, is to attach a white noise source to one of the multiplexed inputs. A signal of this type yields a predictable spectrum which is ubiquitous (and relatively flat) over a large range of frequencies for functioning

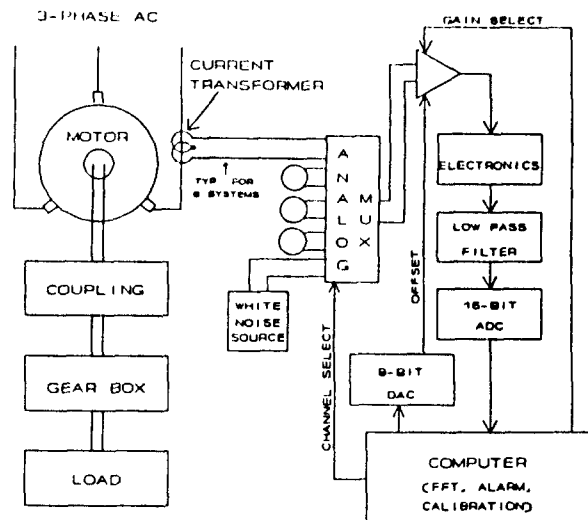


Fig. 6: Typical motor current analysis interface circuit.

hardware (and software). Any deviation from this characteristic spectrum can give discernable indications of hardware (or software) failures. A cost-effective white source can even be realized with digital circuits. Pseudo-random binary sequences, generated with shift registers and exclusive-or gates, provide a good approximation of white noise^[13].

Applications of MCSA may extend beyond those mentioned above. Experiments conducted by ORNL have demonstrated that motor current analysis is equally well suited for DC (direct current) rotating equipment^[14]. In addition, research is presently being conducted at the Oak Ridge Y-12 Plant to determine the feasibility of using MCSA on servo motor systems. In a broader scope, certain portions of motor current analysis may even be applicable to power distribution predictive maintenance.

CONCLUSIONS: Motor current signature analysis (MCSA) has proven its applicability as a valuable predictive maintenance tool for industrial applications. Correlations exist between spectral information obtained from motor current analysis and that obtained from vibration analysis. However, MCSA offers a more cost-effective means of acquiring signatures than does vibration analysis. In addition, on-line monitoring and diagnosing capability is also possible.

While still in the experimental stage, this new technology can have a positive impact on the failure rate of rotating equipment. In addition, applications of MCSA technology may extend to such areas as production equipment and power distribution. Further research, however, is required to explore all that motor current analysis has to offer.

REFERENCES

- [1] Computational Systems, Inc., *Predictive Maintenance Seminar and Workshop*, Knoxville, TN (April 1989).
- [2] Computational Systems, Inc.
- [3] Computational Systems, Inc.
- [4] Haynes, H.D.; R.C. Kryter, "Condition Monitoring of Machinery Using Motor Current Signature Analysis", *Sound and Vibration*, pp. 14-21 (September 1989).

- [5] Haynes.
- [6] Haynes.
- [7] Smith, S.F., D.E. Hendrix, Inventors, Patent Title: "A Demodulation Circuit for AC Motor Current Spectral Analysis" (Patent applied for Sept. 1988).
- [8] Haynes.
- [9] Reis, Jim, "Case Study of a Method for Diagnosing AC Induction Motors using Spectrum Analysis", *Proceedings of the 1st International Machinery Monitoring and Diagnostic Conference*, pp. 40-44 (September 1989).
- [10] Kliman, G.B., R.A. Koegl, A.V. Mohan Roa, J.F. Wolfinger, K. Roa, "Broken Bar Detector for Squirrel Cage Induction Motors", *Proceedings of the 1st International Machinery Monitoring and Diagnostic Conference*, pp. 674-682 (September 1989).
- [11] Thomson, W.T., S.J. Chalmers, D. Rankin, "An On-Line, Computer-Bases Current Monitoring System for Rotor Fault Diagnosis in 3-Phase Induction Motors", *Turbomachinery International*, pp. 17-24 (November/December 1987).
- [12] Meng, Q., L. Qu, Y. Shen, "Time-Frequency Distributions of Vibration Signals in Rotating Equipment", *Proceedings of the 1st International Machinery Monitoring and Diagnostic Conference*, pp. 918-924 (September 1989).
- [13] Golomb, S.W., *Digital Communications with Space Applications*, Prentice-Hall, Inc., Englewood Cliffs, New Jersey, 1964.
- [14] Haynes.

MACHINE MONITORING VIA MOTOR-CURRENT DEMODULATION TECHNIQUES

S. F. Smith, K. N. Castleberry, and C. H. Nowlin
Oak Ridge National Laboratory*
Post Office Box 2008
Oak Ridge, Tennessee 37831-6006

Abstract: The application of advanced linear demodulation techniques to the analysis of several motor-driven systems is discussed. The use of high-quality amplitude- and angle-demodulation circuitry has permitted remote status monitoring of several types of medium- and high-power gas compressors driven by 3-phase induction motors rated from 100 to 3500 hp, both with and without intervening speed increasers. Flow characteristics of the compressors, including various forms of abnormal behavior such as surging and rotating stall, produce at the output of the specialized detectors" specific time and frequency signatures which can be easily identified for monitoring, control, and fault-prevention purposes. The resultant data are similar in form to information obtained via standard vibration-sensing techniques and can be analyzed using essentially identical methods. In addition, other machinery such as refrigeration compressors, brine pumps, vacuum pumps, fans, and electric motors have been characterized via the specialized detectors to identify numerous types of mechanical and electrical faults. A detailed study of the theoretical aspects of motor-current modulation is described, and the general design of a custom integrated circuit to perform the desired signal-processing tasks to implement an inexpensive portable analyzer instrument is provided.

Key words: Demodulation; amplitude demodulation; phase demodulation; motor slip; imbalance; surging; rotating stall; vibration monitoring; modeling; integrated circuit; remote sensing.

Introduction: In 1985 and 1986, investigations aimed at developing better means of monitoring the condition of critical motor-operated valves in nuclear power plants were conducted in the Engineering Technology Division of the Oak Ridge National Laboratory (ORNL) under the sponsorship of the U.S. Nuclear Regulatory Commission. The most significant result of that study was the observation that the ac power lines to the actuating motors contained numerous signals resulting from motor/valve interactions that could be analyzed through time and frequency analysis techniques similar to those already universally employed in conventional vibration monitoring. The systematic analysis package resulting from this work, known as Motor-Current Signature Analysis (MCSA), has been made available to commercial and industrial firms through the Technology Transfer Office at ORNL and has been described previously in the open literature.¹

In mid-1986, investigators from the ORNL Instrumentation and Controls Division and the Oak Ridge Gaseous Diffusion Plant developed additional refinements* to the original MCSA measurement techniques to provide improved resolution and sensitivity in the

*Operated by Martin Marietta Energy Systems, Inc., for the U.S. Department of Energy under Contract No. DE-AC05-84OR21400.

"Patent being applied for.

characterization of motor-driven systems including pumps, fans, and gas compressors such as those employed in U.S. gaseous diffusion uranium enrichment plants. Central to these advancements was the observation that cyclic variations in the mechanical load presented to an ac motor will in general produce cyclic amplitude and angle (phase and frequency) modulations (AM, PM, and FM) of the current drawn by the motor from its power source. In theory, any load variation seen (or induced) by the motor will result in simultaneous amplitude and angle modulations of the motor current that will exhibit the frequency components of the mechanical load changes.² This basic principle is shown diagrammatically in Fig. 1; here, for the idealized case above, the single-frequency load modulation is clearly seen on the motor current signal envelope (not to time scale). Such a simple modulation will give rise to a single set of AM sidebands (as shown in the upper-right box of Fig. 1). Obviously, real-world systems produce more complex modulated-signal spectra (more like those presented in the lower plot). Note, however, that in actual signals there can exist a very large difference between the carrier (power-line) and its associated sideband-frequency amplitudes; the difference in some cases has been measured to be on the order of 100 dB (a 10^5 ratio). Such a dynamic range between components clearly exceeds the capabilities of modern spectrum analyzers and data recorders and represents a major impediment in the analysis of other than direct-coupled loads.

Demodulator Design: Fortunately, standard analog communications theory has exhaustively described the various AM, PM, and FM demodulation processes required to extract the desired vibration- or load-induced components from the modulated motor load current. From the general detector equations it has been determined that synchronous AM and wideband PM demodulators offer excellent linearity and adequate frequency response for the vast majority of applications. Figure 2 is a block diagram of a representative motor-current analyzer unit. Here, the motor signal is sampled by a conventional current probe and subsequently amplified and filtered to remove the power-line harmonic signals (and their associated sidebands), which would produce aliasing in the downstream AM and

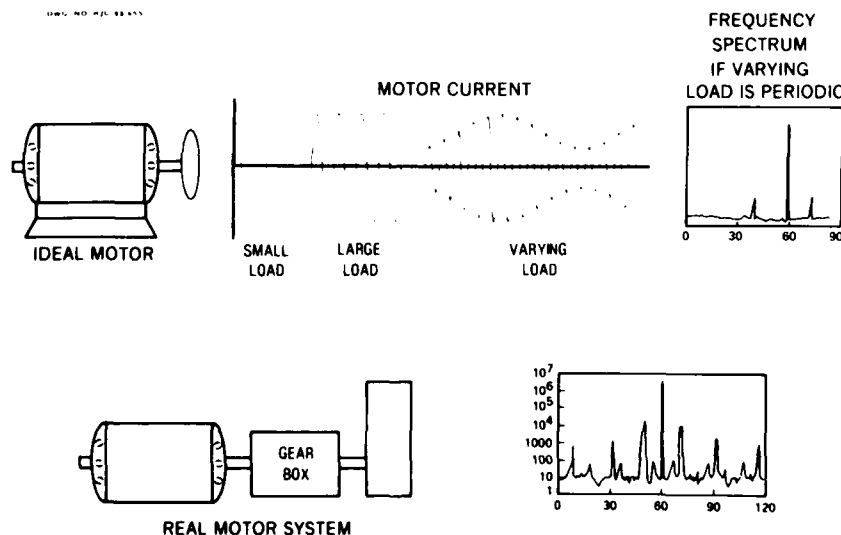


Fig. 1. Basic concepts of ac motor current spectral analysis.

²U.S. Patent pending.

PM detectors. For those applications that do not require demodulation, there are two alternative wideband paths: one direct-coupled for flat frequency response to beyond the audio range, and the other with notch filters to eliminate the 60-Hz primary power-line component (and optionally its 120-Hz second harmonic). The normal path (through the predetection low-pass filter) splits to feed a high-quality synchronous AM demodulator and a phase-locked loop-based PM detector, both of which possess less than 0.1% nonlinearity and an overall dynamic range of the order of 110 dB (carrier amplitude to noise floor).

For the original demonstration of the usefulness of motor-current demodulation techniques in machine analysis, a series of laboratory experiments was conducted to establish a representative correlation between standard accelerometer-derived vibration information and data obtained by probing the electrical current drawn by a typical small-capacity vacuum pump. Sampling the pump electrical input was accomplished by an ordinary current probe (such as those available as accessories to a standard multimeter); the probe output signal was then amplified and fed to a pair of prototype demodulators (both AM and PM). The spectra of the accelerometer, current probe, and demodulator outputs are compared in the plots of Fig. 3. In Fig. 3a the pump (P), belt (B), and motor slip (S) peaks and their respective harmonics are identified. The high-frequency rolloffs evident in the AM and PM demodulated spectra (Fig. 3b) are due to the sharp-cutoff postdetection low-pass filters used to remove potential high-frequency artifacts caused by signal aliasing (with power-line harmonics) and the usual detector products (principally in the range of 120 Hz).

Plant Applications: Once the technique was benchmarked with the vacuum pump and several other small laboratory-scale machines, the demodulator circuitry was converted to a self-contained field unit and transported to DOE's gaseous diffusion plant in Paducah, Kentucky. There data were acquired on several large UF_6 cascade compressors, including two 900-hp centrifugal booster pumps and several "00" size (1700-hp) axial-flow stage compressors, all during normal operation. All current signals were monitored via standard 0- to 5-A loops driving panelboard ammeters in the area control rooms. In these and

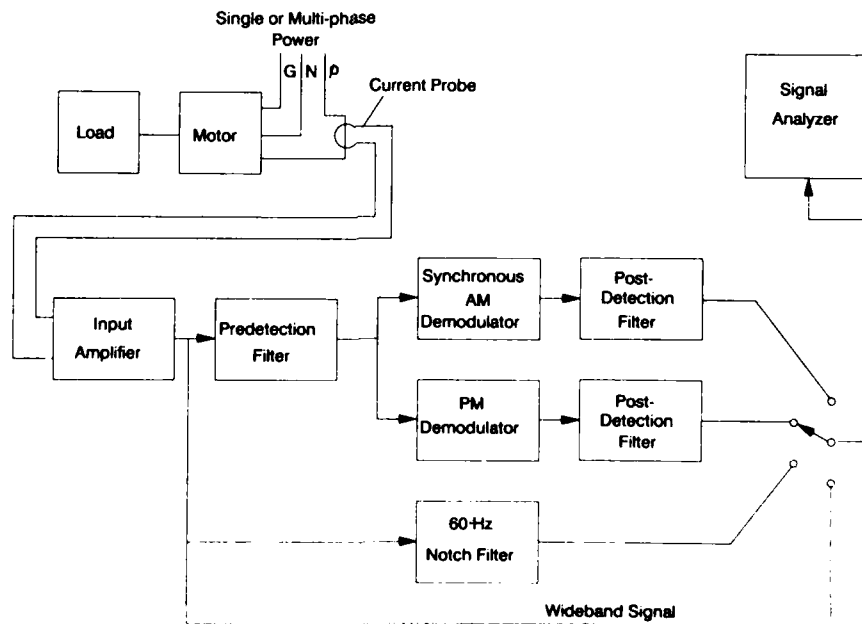


Fig. 2. Block diagram of motor current analyzer unit.

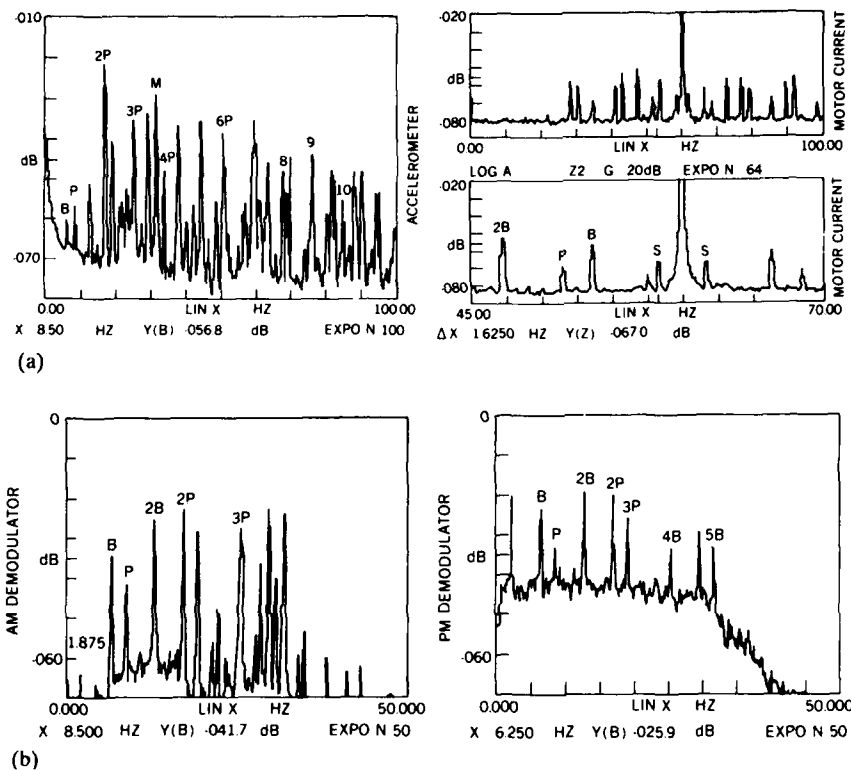


Fig. 3. Vacuum pump: Comparison of accelerometer, current probe, and demodulator outputs.

subsequent tests in the diffusion plants, the only local signals obtained at the machines were the reference mechanical vibration data (via accelerometers and proximity probes). In all cases the current signals were picked up hundreds of feet away in the control rooms. A significant improvement in the ability to detect a specific (and potentially damaging) type of axial compressor flow abnormality (called "secondary" or "rotating-stall" operation), was observed using the demodulators as shown in Figs. 4, 5, and 6.³ During rotating stall, no significant indications of the problem are evident on the normal process compressor vibration probes or in the stage motor ammeters; thus the condition often goes undetected for long periods of time, resulting in compressor blade fatigue damage. A shaft proximity probe (Fig. 4) barely shows the spectral peak characteristic of "secondary" (rotating stall) near 13 Hz; in contrast, the demodulator plots in Figs. 5 and 6 reveal a vivid portrait of the condition. The peaks near 8, 30 (running speed), and 33 Hz are the usual components traditionally observed during compressor operation; the 13- and 26-Hz components are due to the rotating stall (its fundamental and second harmonic), and the motor slip peak appears at just under 1 Hz. Corresponding tests subsequently performed at the DOE plant at Portsmouth, Ohio, on similar compressors over a wide range of power levels yielded essentially identical results. In every case, the 13-Hz peak was clearly evident in the demodulated signals on machines in the "secondary" state.

Another form of axial-flow compressor instability that is often difficult to detect with the usual motor-end accelerometer or velocity sensor is known as "B-barrel surge," in which the discharge ("B") barrel of the compressors lacks a volume flow adequate to achieve

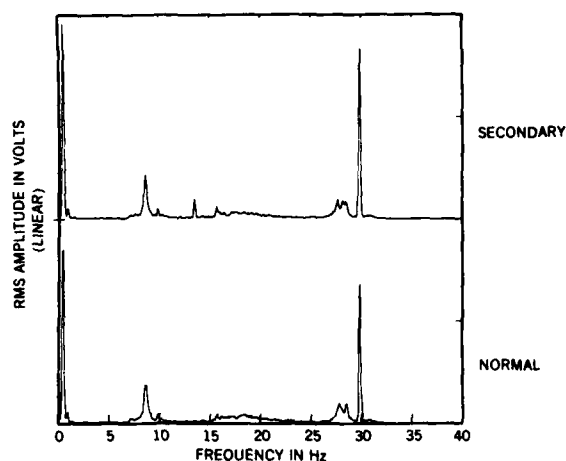


Fig. 4. PGDP cascade test: shaft proximity probe signals.

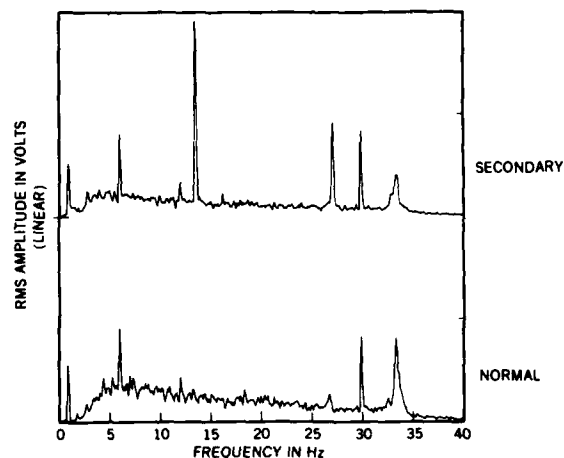


Fig. 5. PGDP cascade test: AM-demodulated motor current spectra.

aerodynamic stability. The resultant localized surging is much less pronounced than the more common primary (full-machine) surge and generally does not cause a noticeable deflection of the stage motor ammeter. Nevertheless, the surge oscillation frequency of roughly 1.25 Hz (shown by the cursor symbol) and several of its harmonics are evident in the demodulated spectral plot of Fig. 7. Note that in this larger size ("000") compressor (rated at 3300 hp), the machine balance is so close that no significant fundamental running-speed component (at 20 Hz/1200 rpm) is visible above the background level.

Another interesting and useful application of the motor-current demodulator is in the monitoring of centrifugal compressors, particularly those handling variable molecular-weight gases. Units with ratings up to 950 hp were probed via their remote motor ammeter loops, and in every case a prominent slip-related peak was observed in both AM- and PM-demodulated spectra. The frequency of this peak varied according to the average molecular weight of the process gas being handled at the time. Since the system controls tended to keep the compressor inlet pressures constant, it is presumed that the slip is actually proportional to the overall loading or to the effective process gas density. The

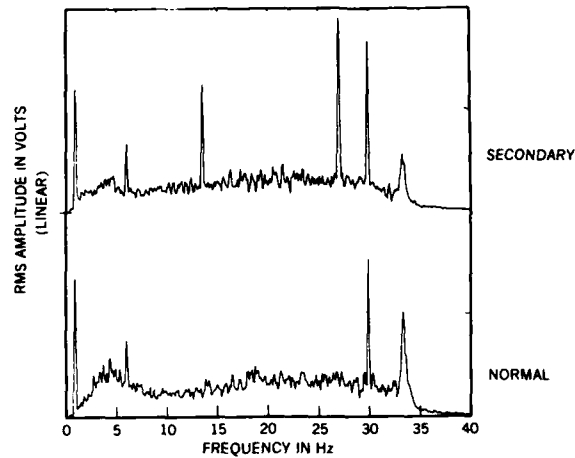


Fig. 6. PGDP cascade test: PM-demodulated motor current spectra.

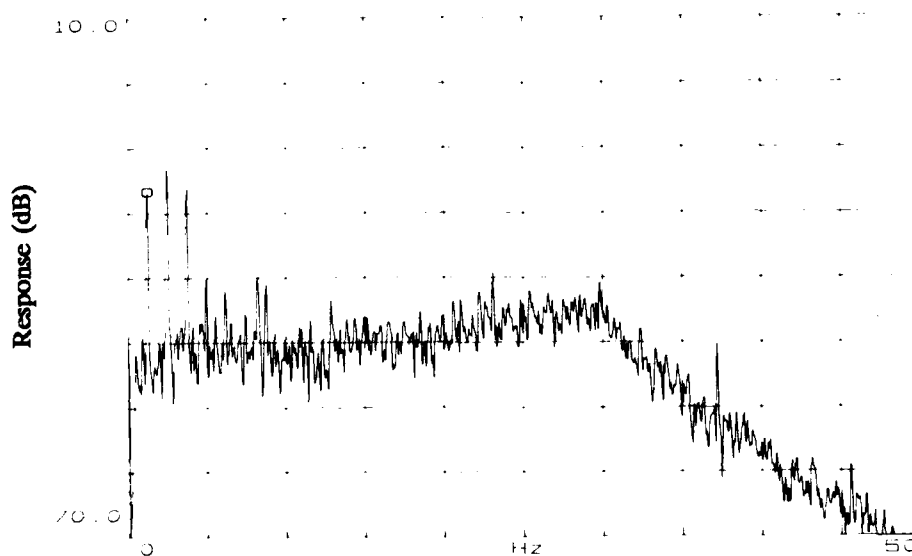


Fig. 7. PGDP "000" compressor in B-barrel surge.

ratio of the peak frequency to the true motor slip rate was found to be on the order of the number of compressor impeller vanes but, since the correlation is not exact, additional studies related to this relationship are continuing. A significant application of motor-current analysis is being explored in the purge cascade area of the Portsmouth plant, where the demodulated data have been able to track major process molecular-weight shifts ("front" movements) with great speed and accuracy. In Fig. 8, a typical 200-hp process compressor motor has been sampled and demodulated; for this case of higher molecular weight gas, the slip-related peak is at roughly 17.75 Hz. In Fig. 9, after a movement of the gas front, the same machine is now handling a lighter gas mixture. As expected, the decreased motor loading has reduced the slip, and its related peak has now dropped in frequency to about 12 Hz.

Other types of machinery have also been examined. Figure 10 shows the AM-demodulated spectrum of a 1700-hp refrigeration compressor with incipient bearing oil whirl. Another compressor of the same type was recorded during a major surging incident; the time plot of the current envelope is shown in Fig. 11. Finally, a normally operating 500-hp brine pump spectrum is shown in Fig. 12, with the slip peak at nearly 1 Hz marked at the left. The running-speed component at just under 30 Hz (1800 rpm) is clearly evident; any increase in its level over the baseline case would indicate an imbalance problem such as that caused by a deteriorated shaft coupling.

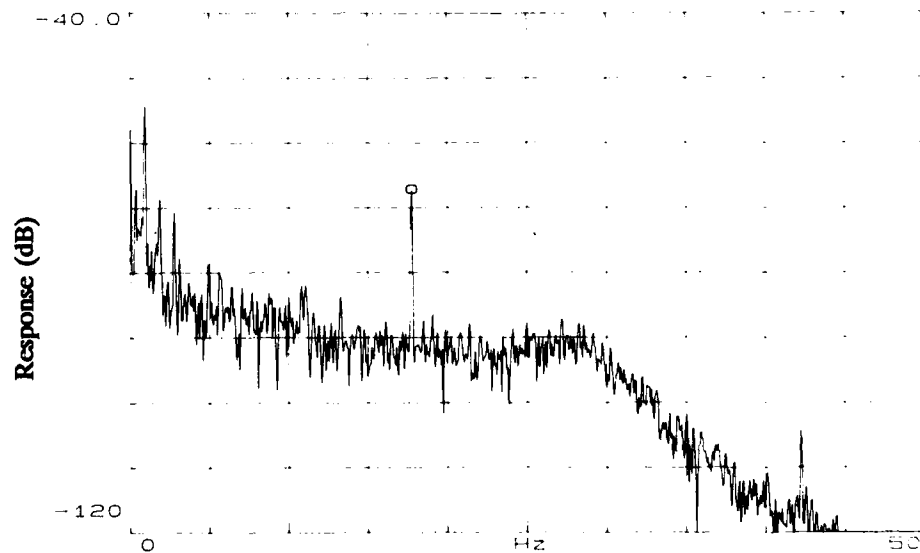


Fig. 8. Process centrifugal compressor (high molecular weight).

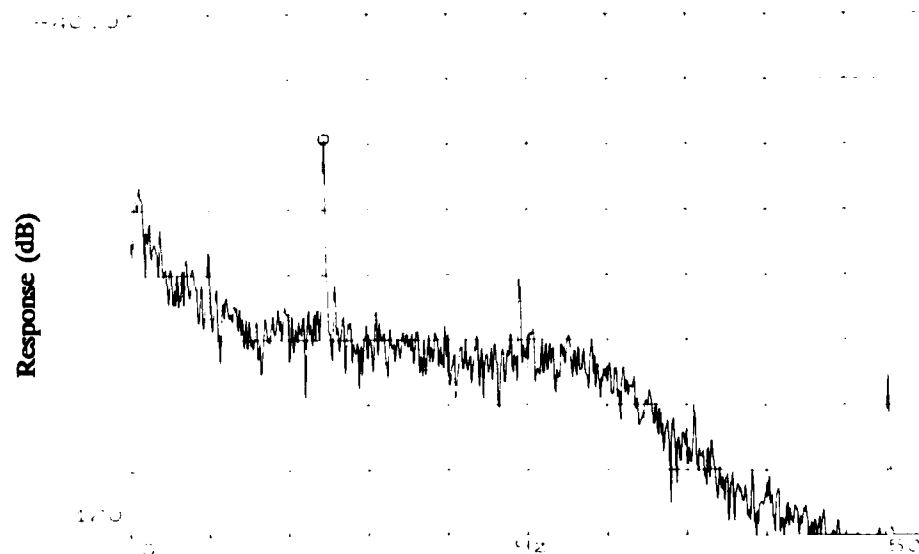


Fig. 9. Process centrifugal compressor (low molecular weight).

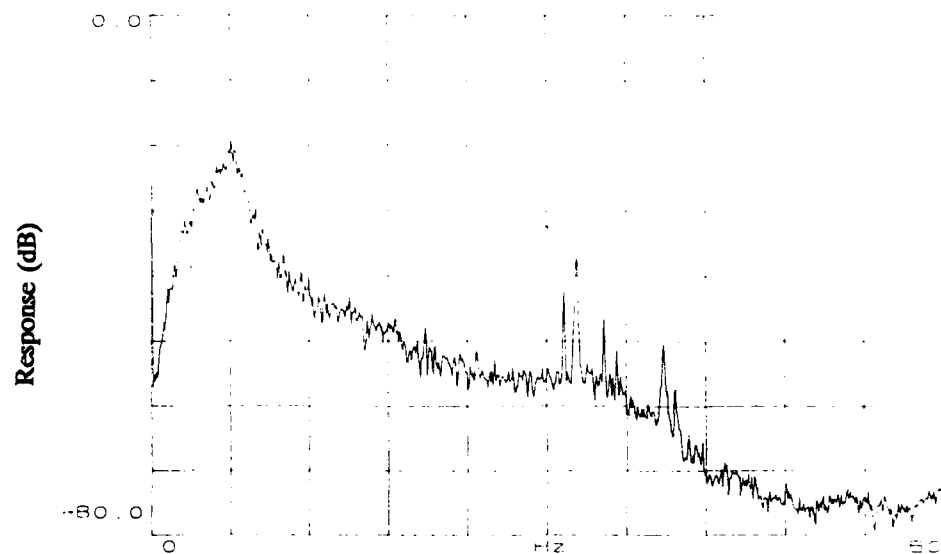


Fig. 10. 1700-hp refrigeration compressor AM-demodulated spectrum.

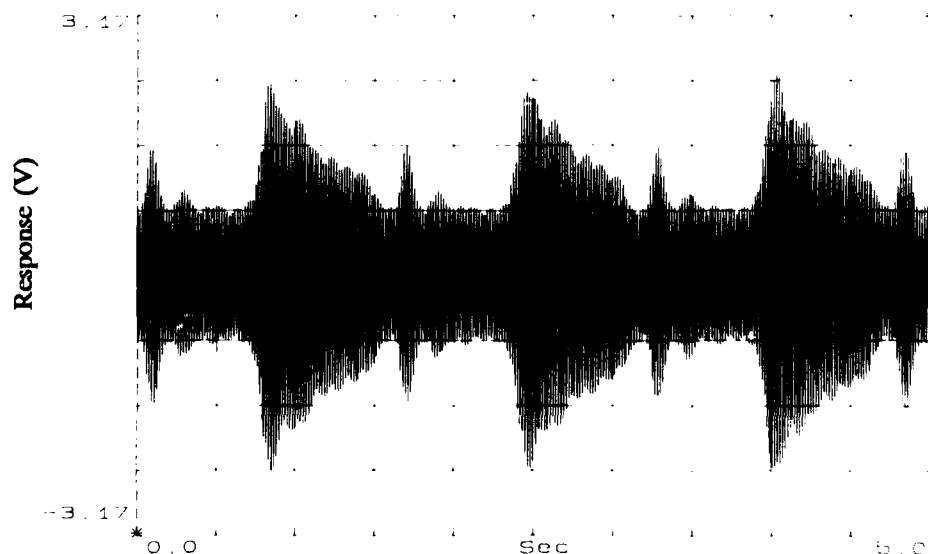


Fig. 11. Refrigeration compressor current envelope.

Chip Implementation: ORNL is presently pursuing the design of a self-contained power-line analysis device in the form of a custom mixed-analog/digital CMOS integrated circuit. It will contain the salient circuitry required to implement a high-quality combination AM/PM motor-current demodulator, complete with the necessary filtering and detection circuitry to perform simple spectral-sensing tasks with only a few passive external components. The initial application of the device is expected to be in the DOE gaseous diffusion plants, but the unit is being configured to handle a wide range of other motor-current monitoring tasks as well.

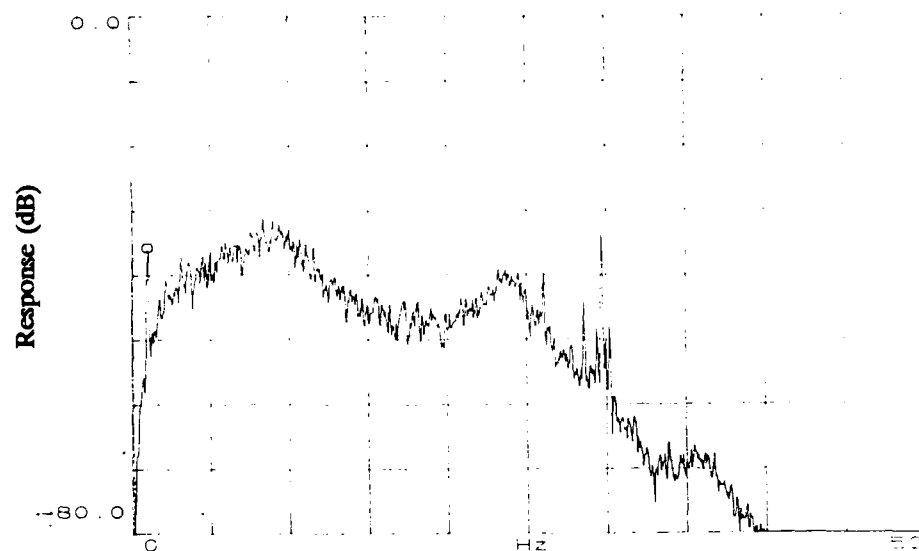


Fig. 12. 500-hp brine pump AM-demodulated spectrum.

A block diagram of the demodulator chip is shown in Fig. 13. The input signal, as shown at the left of the diagram, is boosted by a gain-controlled differential amplifier. The motor-current signal, now at a level of roughly 200 mV peak-to-peak, is applied to a switched-capacitor elliptic state-variable low-pass filter (which removes frequencies greater than roughly 100 Hz to prevent detector aliasing). Alternately, the amplifier output is available for external wideband analysis when demodulation is not required. The combined AM/PM detector is a synchronous quadrature switching type, where the necessary demodulator drive logic signals are derived from the digital timing logic block shown at the top of the diagram.

The postdetection low-pass filter is also a state-variable, sharp-cutoff elliptic type that removes the high-frequency beats emerging from the detector circuitry, leaving a clean AM- or PM-demodulated signal with a bandwidth of roughly 30 Hz. The master clock oscillator, which provides for time-synchronous operation of the filters and demodulator switches, is divided by internal state-machine logic circuitry and is phase-locked to the incoming power-line carrier (nominally 60 Hz). This chip will permit a host of low-cost, high-accuracy applications to be accommodated with very little power consumption and will facilitate development of several types of powerful portable analysis and diagnostic instrumentation.

Theoretical Efforts: To acquire an improved theoretical understanding of motor-current modulation, a mathematical modeling study was initiated to analytically determine the modulation components produced by an idealized 2-pole, 3-phase ac motor with a 1-Hz slip frequency and known mechanical shaft load modulation frequencies. For this derivation, the usual motor analyses were abandoned in favor of the more fundamental solutions beginning with Maxwell's equations. The motor mechanical load was modulated by fixed-frequency sinusoids, each at a 1% modulation index, and the resultant analytic motor current signal was subjected to a 2048-point Fourier transform analysis. Besides the predominant 60-Hz power-line component, a significant spectral peak was found at 58 Hz (twice the shaft speed minus the 60-Hz line frequency), which itself exhibited modulation sidebands corresponding to the mechanical load variations. Mathematical calculations of both amplitude (synchronous AM) and angle (PM/FM) demodulations applied to the

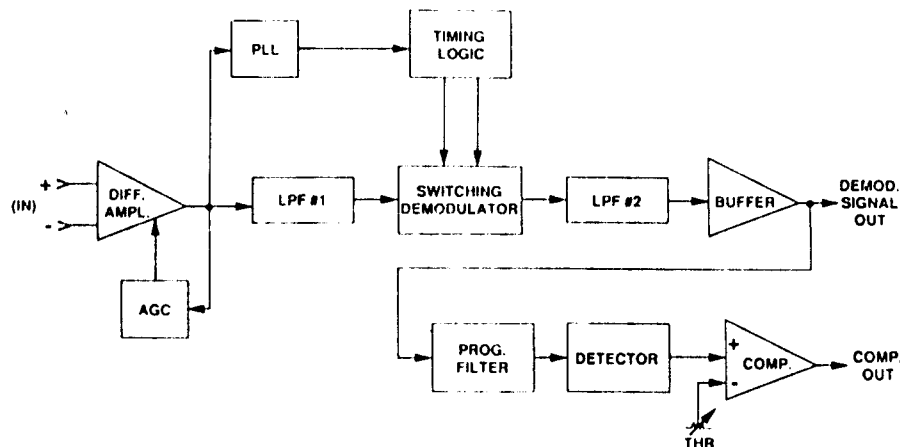


Fig. 13. Block diagram of motor-current demodulator chip.

motor-current waveform have indicated that the PM spectrum was somewhat "cleaner" (i.e., showed less intermodulation distortion) than did its ideal AM counterpart. Further theoretical efforts, complemented by a recently fabricated 3-phase motor laboratory test fixture with specialized load-synthesis hardware and signal analysis capabilities, are under way to assess the utility of more advanced detection techniques in the analysis of ac motor-driven systems.

Final Comments: The ORNL demodulation system also has been successfully applied to the study of faults in large 3-phase gaseous diffusion stage motors (up to 3500 hp), along the lines described by several researchers in the United Kingdom.⁴ In this case, however, the ORNL circuitry has provided a useful improvement in sensitivity over the direct spectral analysis techniques reported in those earlier efforts. Several additional equipment studies are also under way to apply the demodulation technology to other types of motor-driven processes, particularly those in hostile environments or with poor accessibility for conventional vibration analysis.

Numerous other applications of motor-current analysis, with particular emphasis on the demodulation techniques described, are presently being pursued at ORNL as well as other DOE sites, with considerable interest in the technology being expressed by other government and private organizations.

REFERENCES

1. R. C. Kryter and H. D. Haynes, "Condition Monitoring of Machinery Using Motor Current Signature Analysis," *Sound and Vibration* 23(9), 14 (1989).
2. D. E. Hendrix and S. F. Smith, U.S. Patent Application, "Demodulation Circuit for AC Motor Current Spectral Analysis."
3. K. N. Castleberry and S. F. Smith, Report of Possible Subject Invention, "Detector for Flow Abnormalities in Gaseous-Diffusion Plant Compressors," Martin Marietta Energy Systems, Inc., January 15, 1990.
4. W. T. Thomson, S. J. Chalmers, and D. Rankin, "An On-Line, Computer-Based Current Monitoring System for Rotor Fault Analysis in 3-Phase Induction Motors," *Turbomachinery International*, November/December 1987.

INCIPIENT FAILURE PREDICTION FOR ELECTRICAL MACHINES

Jeffery L. Kohler and Joseph Sottile
The Pennsylvania State University
Mine Electrical Laboratory
Academic Activities Building
University Park, PA 16802

Frederick C. Trutt
University of Kentucky
Department of Electrical Engineering
779 Anderson Hall
Lexington, KY 40506

Carlos Santa Cruz
The Pennsylvania State University
Mine Electrical Laboratory

Abstract: It is a widely accepted fact that the corrective maintenance actions facilitated by predictive maintenance testing reduces the probability of costly catastrophic failures and improves system safety. In the case of electrical machinery, mechanical testing practices have become increasingly sophisticated over the years. Electrical tests, for predictive maintenance purposes have changed little over the past several decades, despite advances in enabling technologies. While it is true that sophisticated techniques are employed for very large and crucial machines, e.g. power plant generators, the vast majority of motors are still subjected to little more than insulation resistance (IR) measurements, on a periodic basis. The purpose of this paper is to briefly review the strengths and weaknesses of the traditional test methods, and then to present new alternatives which could be used to significantly enhance existing predictive maintenance programs.

Key words: Motor Testing; Failure Prediction

Periodic Tests: There are a number of well established procedures for the periodic assessment of induction-motor electrical integrity. Insulation evaluation techniques such as "megger" testing are popular and have been performed for many years. These tests, along with a detailed discussion of the relative merits, were discussed in reference 3; a brief summary is provided here.

Periodic test methods, i.e., manually-acquired measurements taken from time to time, rather than continuously, can be divided into three groups based on the characteristic of

the excitation source used in the test. These are direct current, alternating current, and surge tests.

Direct-current methods are the most widely used in motor insulation testing, probably because of their convenience of use, as much as anything else. The test apparatus is lightweight and portable, the tests are relatively safe, and very large values of resistance (megohms) can be measured. A megohmmeter is typically used for performing the tests although hypots (i.e., high-potential testers) may also be used.

Three types of DC tests are typically employed: the time resistance test, the dielectric absorption ratio, and the step voltage test.

In the time resistance method, two or more readings are taken over the duration of the test time (i.e., five or ten minutes). If the insulation is in good condition, there should be a gradual increase in resistance. If the insulation is contaminated, the resistance will not increase during the test period.

The dielectric absorption ratio is a ratio of two time-resistance readings, for example 60-seconds/30-seconds. This ratio is utilized to show the effects of absorption current in good insulation. Tabulated values and experience guide maintenance personnel as to what is acceptable.

Some maintenance personnel establish a step-voltage test for evaluating insulation well above the rated AC voltage of the equipment. It is believed that such DC tests are capable of revealing incipient problems which could not otherwise be found. The technique for performing this type of analysis consists of applying two or more DC voltages and observing any reduction in insulation values at the higher voltage levels.

Because DC methods measure such high values of resistance, many factors involving both the condition of the insulation, and the test procedure affect the results. Typically, the commonest problems are from temperature, moisture content of the insulation, and poorly executed test procedures.

The results of DC tests are relative, and therefore evaluation is based on trends over time, rather than on the specific value of one reading. For this reason, it is best to observe the trend of the readings by plotting the resistance over time for each piece of equipment. However, there are several quantitative guidelines that have been established, such as the 'one-meg rule' which limits the minimum ground insulation to one megohm plus one megohm for each kV terminal rating of the machine.

DC tests have several advantages if properly performed. The insulation can be evaluated in terms of a spot resistance, resistance versus voltage, ratios of resistances, and so forth. Each of these tests will yield specific information about the machine insulation. This makes DC tests very attractive for testing low voltage motors if the user can establish a meaningful procedure to interpret the results.

In general, DC tests are effective at detecting insulation anomalies between phase and ground, whether these anomalies are due to insulation degradation or temporary conditions, such as the presence of moisture. However, they are not able to detect phase-phase problems unless each phase winding can be electrically isolated and separated from the others. Also, DC tests are incapable of detecting turn-turn degradation.

In addition to DC tests, other tests exist which identify specific parameters which relate to insulation degradation or failure. For example, partial discharge tests detect charge transfer in the insulation voids under an applied AC voltage. Power factor tests measure the dielectric power factor and use it as the evaluation parameter. Surge tests use impedance matching under an applied surge to detect winding failures. The test apparatus is typically expensive and the test procedures are difficult to employ. In many cases, these tests are justifiable only for larger, more expensive motors.

The periodic tests summarized here can provide valuable information on aspects of a motor's condition. Indeed, in many plants, IR testing using a megohmmeter, has been practiced for years with satisfactory results. Despite the advantages of these periodic tests they have inherent weaknesses, other than cost or problems relating to use in a plant environment. Principally, these methods require taking the motor off-line. This is an inconvenience and results in infrequent testing of a specific motor. Another weakness of almost equal importance is that the methods may not be sensitive to some prevalent modes of deterioration or modes which only become apparent when the motor is operating. Because of these limitations, many researchers have attempted to develop new techniques which would overcome the inherent disadvantages of the aforementioned tests. The most promising efforts are those which relate to actual motor performance, are sensitive to all modes of deterioration, and can be applied while the motor is operating.

Sequence Tests: The analytical method of symmetrical components provides a tool to analyze unbalanced power systems [4]. However, the symmetrical components of the voltages and currents are more than mathematical

conveniences; they are physical quantities which can be measured [5]. Further it is known that the presence of sequence currents in power systems can cause problems. The negative sequence current, for example, sets up a magnetic field in a motor which is rotating in the opposite direction to the field produced by the positive sequence. While the resulting reduction in mechanical power is negligible, the increased heating may not be inconsequential [6].

The use of symmetrical component-based relaying is also well known. However, it is now known that it can also be useful for predictive purposes. It has been found through both computer simulation and experimental investigations, that the negative sequence current is a good indicator of low levels of deterioration within three-phase induction motors.

Sequence Current Predictor: One of the simplest techniques which can be used to detect deterioration in motors is to monitor the negative sequence current. Tests have indicated that for high-impedance leakage paths within motor windings, negative sequence current is directly proportional to the leakage current at constant (fault) voltages. Additionally, for constant leakage currents, the level of negative sequence current increases with increasing potential. This reflects the increasing deterioration severity, in as much as the power dissipated is concerned. Figure 1 illustrates these two points.

In general, the negative sequence current increases with the power dissipated in the leakage path, but no direct relationship between negative sequence current and fault power has been formulated. However, a definite linear trend between the two exists. This relationship is shown clearly in Figure 2 for two motors which differ only in the stator connection, one being delta-, and the other wye-connected.

Although a generalized mathematical relationship between negative sequence current and fault power has yet to be determined, negative sequence current is still useful as an inexpensive continuous monitoring technique that could detect motor problems which might otherwise go undetected. Also, negative sequence monitoring can be applied in areas of the mining or processing industries where other test techniques cannot be economically utilized. It is stressed here that negative sequence monitoring should not be used as a substitute for more extensive and revealing test techniques. A fundamental limitation of this predictor is the requirement for a balanced voltage supply to the motor. If the supply becomes unbalanced then, because of the motor's low negative sequence impedance, a negative sequence current will flow. It is impossible to distinguish that part of the total negative sequence

current arising from the unbalanced voltage from the part due to motor deterioration with only current measurements. Because slightly unbalanced supplies, changing in time, are relatively common in industrial power systems, this constraint on the predictor is serious. However, for only slightly more effort this constraint can be overcome.

Sequence Impedance Predictor: The ratio of a sequence voltage to the same sequence current defines that sequence's effective impedance. The measured sequence voltages and currents can be used to compute the effective sequence impedances. While the positive-sequence impedance will change for a variety of reasons, including temperature, speed, and loading, the negative sequence impedance will remain nearly constant, unless deterioration is taking place within the motor. Because the negative sequence impedance is relatively insensitive to speed changes it is a good candidate for monitoring purposes.

The method of symmetrical components provides a procedure for computing the motor currents resulting from an unbalanced voltage supply impressed on an unfaulted motor (because the currents of the two sequences do not react upon each other.) Consequently, the effects of supply unbalances can be accounted for in an unfaulted motor. If the currents which flow cannot be accounted for, another mechanism must be at work: deterioration in the motor.

Based on the relative insensitivity of the motor's negative sequence impedance to speed changes and its ability to account for supply unbalances, the effective negative sequence impedance monitoring can be a very simple yet effective parameter to monitor.

An initial value for a motor's negative sequence impedance can be obtained from the manufacturer or simply by performing the measurements and subsequent calculation when the motor is put into service. Even for motors already in service these measurements could be performed, and then the motors could be tracked for signs of change in the effective negative sequence impedance.

This predictor is simple, inexpensive to obtain, and it accurately detects low levels of turn-turn, winding-winding, and turn-to-ground insulation deterioration. Additionally, certain rotor defects will also result in an increased negative sequence current. The authors believe that its implementation would significantly improve existing predictive maintenance capabilities. Notwithstanding, this predictor has its own limitations. Most notable is the inability to discriminate among the modes of deterioration. This limitation can be overcome by utilizing a more comprehensive set of predictors available from the decision-function method.

Decision Function Method: The decision function method is a result of efforts to develop continuous monitoring methods to assess the integrity of mine power systems [1,2]. Over the years the scope of the research was broadened to include motor applications in other industries, including shipboard usage.

This method also requires the measurement of the voltage and current phasors; the measurements must always be made at the same level of loading on the motor, or at the same motor speed. The sampled phasors are processed to extract a number of predictors and performance measures. These can be used to assess the operational aspect of the motor in addition to detecting specific identifiable modes of deterioration. The theory of this method is described in reference 7 and will be summarized here.

Theory: The measured phasors are used to calculate complex power, impedance, and the symmetrical components of voltage, current, and impedance. A set of features are obtained from the real and imaginary components of the complex power and impedance; these are active power, P, reactive power, Q, power factor, PF, resistance, R, and reactance, X. The magnitude of the current phasor, I, is included in this set of features. Each of these features exist for phase A, B, and C. Thus the jth feature for phase p is X_{pj} , where p=A, B, or C. The use of the symmetrical component values will be described later.

A common basis for detecting problems in many predictive techniques is the premise that a deteriorating component will exhibit changes in a measured value when compared to a reference value. The interpretation of IR test data is often based on a comparison of the present measurement to past measurements, rather than on absolute values. This premise is also applied here; any deterioration which has occurred will be apparent as

$$S_{pj} = X_{pj} - X'_{pj} \quad (1)$$

where S_{pj} is the incremental change of the jth feature type in phase p. The reference value, X'_{pj} , can be provided by the user from experimental observation or analytical computation. In practice, this measure is unreliable for small levels of deterioration because it is sensitive to winding temperature, terminal voltage, and phasor sampling constraints, among others. It has been determined that the difference in magnitude among each of the phases, or the interphase distance, is insensitive to the aforementioned factors. As such it is better suited to revealing low levels of deterioration. The transformation to achieve this is defined by

$$K_{1j} = (X_{aj} - X_{bj}) - (X'_{aj} - X'_{bj}) \quad (2)$$

$$K_{2j} = (X_{bj} - X_{cj}) - (X'_{bj} - X'_{cj}) \quad (3)$$

$$K_{3j} = (X_{cj} - X_{aj}) - (X'_{cj} - X'_{aj}) \quad (4)$$

These transform values form a pattern vector; the symmetrical component values are also included as elements to form the pattern vector which can be mapped into a decision space. The decision space is partitioned by type of deterioration, e.g. turn-turn, phase-phase, or phase-ground, and by the phase involved, e.g. A, B, B-C, C-GND, etc.

The pattern classification algorithm is in the experimental stage and it is therefore not widely available. Although the algorithm is able to classify the pattern vectors, a lack of development funds will delay its introduction. Nonetheless, the transform values themselves can be tracked over time.

Discussion: The application of this method also requires the measurement of voltage and current phasors. Unlike the sequence predictors, however, a significant number of computations must be performed to extract the relevant performance measures and failure predictors. The computational capability of a personal computer is required. The benefit available through this increase in complexity, over the previously discussed tests, is increased sensitivity to deterioration, and the possibility of identifying the specific mode of deterioration and the particular phases involved in the degradation process. The accuracy of such a deterioration detection and classification system could be enhanced by using additional predictors related to electrically-excited vibrations, temperature, magnetic field, and so on [8]. Unfortunately, the process of identifying the specific mechanism of deterioration and the phase involvement has not been automated at this time, although there is information available to guide a manual classification process [9].

Software is available to provide the information presented in Figure 3, if the user can measure the voltage and current phasors. Additionally, computer models are described in reference 1 which can be used to simulate various deterioration modes in motors and cables. The results of these simulations can be compared against actual measurements to determine the mode of an observed deterioration process. Another application of one of these, the motor model, will be described in the next section of this paper.

Voltage Unbalance Compensation: One of the more difficult problems to overcome in the application of this technique is that of dealing with the voltage unbalances which occur in the power system. The unbalances are constantly

changing; and very small unbalances can obscure the effects of a low-level leakage path. In fact, voltage unbalance factors (VUF) of 0.10% can have a detrimental effect on the procedure. Moreover, a dynamic approach must be taken because of the possibility of supply fluctuations. Thus it was necessary to develop a technique to compensate for bus voltage unbalances.

In most industrial settings, small unbalances in supply voltage cause little or no problems. However, in a predictive setting these small unbalances are quite problematic because of the low negative-sequence impedance of the motor; and there is no simple means of correcting for the unbalance. Voltage unbalances can be manifested in an infinite variety of magnitude and angle changes. While the scalar quantity of voltage unbalance factor is useful in characterizing power system performance, it is unable to reflect the effect of voltage unbalance on the predictors. Accordingly, it is not possible to correct the predictors based on a scalar value such as a correction factor for 0.1% VUF, 0.2% VUF, and so on. A more sophisticated approach was required.

Correction Technique: This technique consists of a software algorithm which is used to develop the corrected input phasors for the decision-function method. The corrected phasors are those which would have resulted if the voltage supply had been balanced. The procedure is as follows.

First the correction algorithm takes the measured voltage phasors and extracts the positive sequence voltage. The positive sequence voltage is then used to calculate a base case. This base case yields the current phasors which would occur if the supply were balanced and the motor were undergoing no deterioration. Then a second case is simulated. In this case, the tuned motor model computes the current phasors using the measured voltage phasors, but assumes that the motor is undergoing no deterioration. Finally, the algorithm linearly recombines the two cases to extract the current phasors which would exist if the supply were balanced. This algorithm accurately predicts the corrected current phasors, insofar as the decision-function method is concerned, as long as the motor does not have a low impedance fault. This is not viewed as a constraint because the purpose is to detect incipient failures, not faults which are becoming severe.

Implementation: It is recommended that any of the aforementioned predictors be implemented either as a supplement to or replacement of the traditional periodic tests. However, the strongest recommendation would be to utilize the negative sequence predictor immediately, and then to phase-in the decision function method, as resources allow. Specific issues related to these follow.

Measurement: The measurements may be performed on a periodic basis with portable instruments, or a monitor can be permanently located on an individual motor bus. The sequence impedance test requires a knowledge of the negative sequence current and voltage. These two quantities can be measured directly using commercially available meters, and the negative sequence impedance can be calculated. Alternatively, a simple circuit could be constructed to combine the measurement and calculation so that the impedance would be displayed. Yet another option is to measure the current and voltage phasors. Once these are available, the sequence quantities can be computed, or a circuit could be constructed to combine the measurement and calculation, allowing the negative sequence impedance to be directly displayed. Of course, the decision function method requires the phasor values.

Sensitivity: The two practical concerns about sensitivity relate to the smallest level of deterioration which can be detected, and the required sensitivity to detect a specific level of deterioration. The question of what level of deterioration should be detectable is mainly economic, since the tradeoff is measurement sophistication against measurement cost. If virtually unlimited funds are available, then existing technology can be used to detect the earliest stages of deterioration within a motor. In most cases, however, this could not be justified. At the other extreme, it is known that industrial motors can be found operating "satisfactorily" with a twenty-five percent unbalance in currents, or motors with an IR reading of less than 5000 Ohms. While such instances can be found, it would be difficult to justify delaying maintenance actions on these motors. The authors have found it useful to apply the following guidelines in determining what the minimum detectable level should be.

First, the deterioration should be detected early enough to allow for the scheduling and implementation of a corrective maintenance action. For example, detecting a deteriorating condition a few minutes before failure would be of limited value. Detecting the deterioration weeks or months in advance would be more useful, and should be the goal. Second, the deterioration should be detected before the degradation process has caused a safety hazard. Third, as a practical matter, the deterioration must be detected well in advance of the visual and auditory signs that would alert personnel to a problem within the motor.

The differences in motor construction and operation combined with the variability of degradation processes within motors make it difficult to quantify the remaining life, given the value of a specific predictor, such as negative sequence impedance, or even an IR reading. If a particular test or predictor is utilized over a period of time, a body of statistical data can be developed to

determine remaining life. This has been done for some periodic tests such as insulation resistance, power factor, and charge loop. Despite the body of data there are still many problems associated with failure prediction in these tests. The sequence-impedance predictor and the decision-function test do not have the benefit of such a body of historical evidence. Accordingly it is necessary to utilize estimates based on modelling and experimental data.

An insulation failure within a motor may involve turns on an individual winding, but most likely involves a winding and ground or two windings. However, it is believed that the original deterioration process, in most cases, probably originates with the degradation of insulation between turns. As such this would be an important event to detect so that a future failure could be prevented. This is fairly difficult to detect, although a few more difficult scenarios can be imagined and certainly many more less difficult ones can be envisioned. As such this one will be used to address the question of required sensitivity.

Although random-wound motors avoid high potentials between adjacent coil turns, and even though additional phase insulation is added for winding-to-winding protection, as well as to ground, problems still develop. Thermal, mechanical, and environmental stresses are exacerbated in the end turns, making them particularly susceptible to deterioration. While the impedance of any leakage path between two turns may be relatively constant, the potential across that impedance is dependent upon which turns are involved. For example, if a 500 Ohm path occurs between adjacent turns with a potential of a few volts, the leakage path will be impossible to detect and is at an inconsequential stage. However, if the same path is across two turns having a potential difference of 200 volts, then the degradation will be quite detectable and will progress to failure quickly, due to the power levels involved. Based on experimental investigations it appears that a detection capability of 0.002 A per unit will be sufficient. Ongoing work indicates that even higher levels of sensitivity can be achieved by using a sequence segregating network which will only pass the negative sequence parameters.

Conclusions: The use of the negative sequence impedance test is recommended for in-plant predictive maintenance applications. This test is sensitive to a wide-range of degradation mechanisms which will ultimately result in motor failure, and its use can allow for timely repair of the motor before costly downtime or a catastrophic failure is incurred. Furthermore, the technique can be applied while the motor is in operation. It is recommended that this predictor be monitored continuously, rather than being applied on a periodic basis, since an appropriate interval between tests cannot yet be defined.

The use of the decision-function method will allow a more detailed analysis of motor performance and condition. The possibility of including electrically-excited vibrations in the method further expands its capabilities, and will improve the sensitivity and accuracy of the technique. Although this technique can be used periodically, it is recommended that it be applied in a continuous monitoring system.

REFERENCES

- [1] L.A. Morley and J.L. Kohler, Coal Mine Electrical System Evaluation - Continuous Monitoring, Annual Report on BOM Grant GO155003, NTIS PB 283 491/AS, 270 p., Jan. 1977.
- [2] J.L. Kohler and F.C. Trutt, Prediction of Incipient Electrical Component Failure, Final Report on BOM Contract JO338028, NTIS PB 88-213590, 371 p., Mar. 1987.
- [3] J. Sottile and J.L. Kohler, "Techniques for Improved Predictive Maintenance of Industrial Power Systems," IEEE Transactions on Industry Applications, IA-25, no. 6, Nov./Dec. 1989.
- [4] C.F. Wagner and R.D. Evans, Symmetrical Components, McGraw-Hill Book Company, New York, 1933, 437.
- [5] C.F. Wagner and R.D. Evans, Symmetrical Components, McGraw-Hill Book Company, New York, 1933, p 271-327.
- [6] C.F. Wagner and R.D. Evans, Symmetrical Components, McGraw-Hill Book Company, New York, 1933, p 351.
- [7] J.L. Kohler, "A Decision-Theoretic Method for the Classification of Incipient-Failure Patterns Which are Characteristic of Deteriorating Mine Power-System Components," an unpublished Ph.D. thesis, The Pennsylvania State University, University Park, PA, March 1983, 141 p.
- [8] F.L. Ding and F.C. Trutt, "Calculation of Frequency Spectra of Electromagnetic Vibration For Wound-Rotor Induction Machines with Winding Faults," Electric Machine and Power Systems, vol 14, no. 3, 1988.
- [9] C. Santa Cruz, "The Characterization of Incipient Failure Patterns for Three-Phase Induction Motors and the Development of Classification Methods for Predictive Maintenance Applications in the Mining Industry," an unpublished Ph.D. thesis, The Pennsylvania State University, University Park, PA, May 1990.

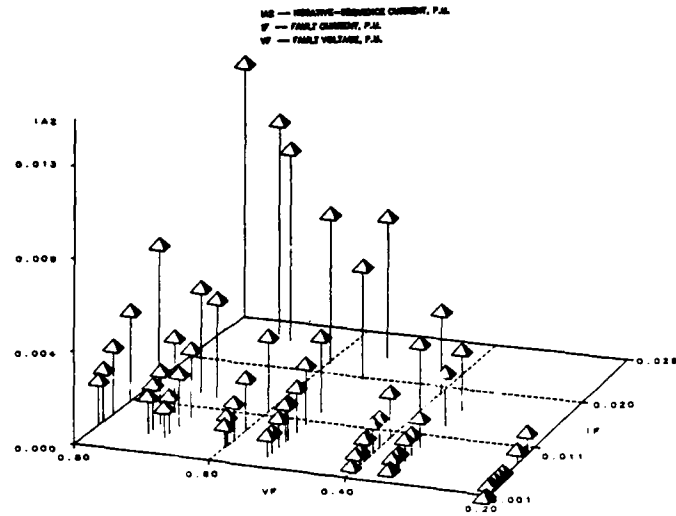


Figure 1. Change in the negative-sequence predictor as a function of deterioration level (I_f) and location of deterioration (V_f) for stator-winding deterioration modes not involving ground.

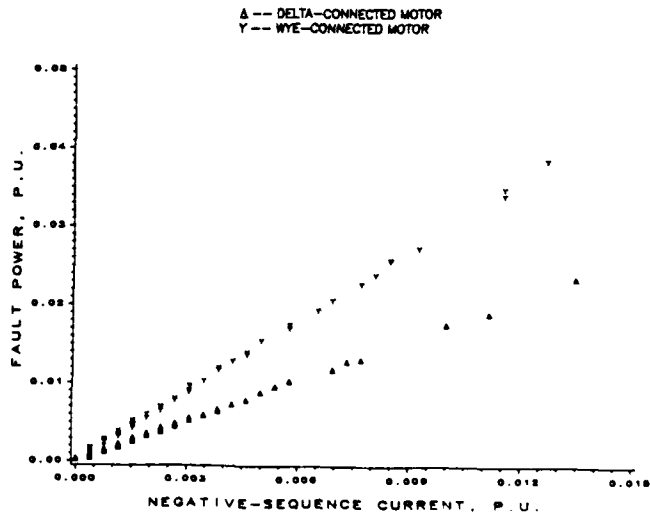


Figure 2. Change in the negative-sequence predictor as a function of deterioration severity (Fault Power) for stator-winding deterioration not involving ground.

PENN STATE MINE ELECTRICAL LABORATORY
FEATURE AND KAPPA VALUES

DRIVE MOTOR No. 5KL84AL217C 1/7/89

THE INPUT PHASORS FOR THIS ANALYSIS WHERE:

MAG(1) = 1.12 ANGLE(1) = -41.6
MAG(2) = 1.11 ANGLE(2) = -161.1
MAG(3) = 1.13 ANGLE(3) = -280.5
MAG(4) = 1.02 ANGLE(4) = 0.0
MAG(5) = 1.02 ANGLE(5) = -120.5
MAG(6) = 1.01 ANGLE(6) = -240.3

ALL VALUES ARE IN PER UNIT; THE BASES ARE:
VBASE = 277.13626099 PBASE = 1245.0000
IBASE = 4.49237490 ZBASE = 61.6904
MOTOR RATED HORSE POWER = 5.00
RATED VOLTAGE = 480.00
EFFECTIVE NEGATIVE-SEQUENCE IMPEDANCE = 0.5

FEATURE VALUES

FEATURE	PHASE A	PHASE B	PHASE C
I	1.115	1.114	1.133
S	1.135	1.137	1.146
P	0.848	0.862	0.875
Q	0.754	0.741	0.740
PF	0.747	0.758	0.764
Z	0.913	0.915	0.892
R	0.682	0.694	0.681
X	0.607	0.597	0.576
SYI	1.121	0.011	0.007
SYV	1.016	0.005	0.000

KAPPA TRANSFORM VALUES

FEATURE	KAPPA 1	KAPPA 2	KAPPA 3
I	0.001	-0.019	0.018
S	-0.002	-0.009	0.011
P	-0.014	-0.013	0.027
Q	0.013	0.001	-0.014
PF	-0.011	-0.005	0.016
Z	-0.003	0.023	-0.021
R	-0.012	0.013	-0.001
X	0.010	0.021	-0.030

Figure 3. Example output using the decision-function method.

SELF-LEARNING PROGNOSTIC SYSTEMS

Charles G. Kolbach
Predictive Technologies Inc.
19 E. Central Avenue Paoli, Pennsylvania 19301

Abstract: An AI-based prognostic system is described that develops and updates its knowledge base, proactively, from the operating experiences of the system being monitored. A cooperating interface between this dynamic knowledge base and a rules-based operational knowledge base allows the expert system to learn and to respond to relational changes, in the operating characteristics and the environment, that predict failure.

Key words: prognostic system; expert system; learning; data acquisition; statistical algorithm.

1. Predicting Failure: Since the industrial revolution, industry has relied on two basic kinds of maintenance to keep its equipment working: run-to-failure, where repairs are made only when the equipment breaks down, and preventive maintenance, where repairs are made according to a time schedule based on previous failure data. Both methods have serious limitations. Run-to-failure almost guarantees expensive repairs, costly downtime and, in process lines, product waste. Preventive maintenance often requires the unnecessary investment in time, money and resources in repairing equipment that did not require repair.

A number of techniques to predict maintenance needs directly from the actual equipment conditions have been developed. A powerful tool for determining the internal faults of equipment having rotating parts is vibration signal analysis. Analyzers are now available for continuous monitoring for "signatures" indicating potential maintenance problems. Methods of correlating other kinds of equipment behavior to indicators of fault are not as well developed, and the traditional approach to verifying the correct operation of a system is still monitoring with sensors to a predetermined set of alarm thresholds.

2. Failure Prediction with Expert Systems: The logical extension of the monitoring for predictors of failure is the diagnosis of the fault itself, and a number of expert systems have been developed for this purpose. See Dvorak's survey of the area of monitoring and control [2]. There have been two distinct approaches to

automating the diagnostic process. One uses heuristic-based expert systems and the other is model-based. Heuristic methods are efficient but their fixed symptom-failure rules can not deal with cases that are not covered in the knowledge-base. Model-based methods reason on the usually better understood system structure and functions. The procedure is to look for outputs that violate the expectations in the model and then use the structure knowledge to find a set of components that might be responsible for the symptoms.

Although there is no standard architecture for an expert system, a typical architecture is shown in figure 1. It includes:

A Knowledge Base (KB): This part of the system carries the expertise which many represent discrete knowledge or heuristic rules of thumb from the expert's

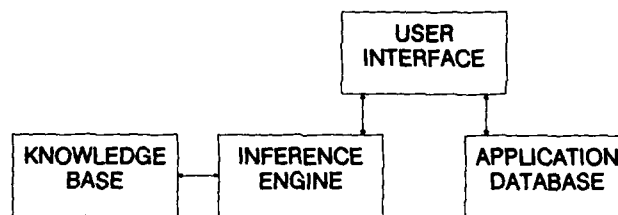


Figure 1. Expert System, Typical Architecture

experience. Typically, these rules are modeled as If-Then clauses, such as "If switch S1 is closed then motor M1 will operate", but they don't have to be and can be presented in any format that best meets the need of the specific application. The attributes expressed in the rules can be discretely stated, expressed probabilistically, or be the results of procedures which are called during use. It is desirable that the KB be flexible for maintainability or update purposes and, theoretically, the system should be able to process any KB written in the same format. KB's are expensive to write and maintain and, as all expert knowledge, subject to technical obsolescence.

An Application Database: The information concerning the system that the expertise is being provided to can be input directly, reside in another data base, or be read-in from a data acquisition system. Depending on the system needs, access to one or all of these information sources may be required.

An Inference Engine: The inference engine carries out the reasoning functions that use the rules in the knowledge base to interpret the "application" described in the Application Database. General problem solving knowledge capability resides mainly in the inference engine, allowing it to reason with different knowledge bases. There are three main methods of applying this reasoning. Forward chaining, also called data-driven, uses application input information to infer a conclusion; backward chaining, or goal driven, uses a hypothesis and infers if

the facts in the application make the hypothesis true; and sideways chaining, or rule-value, seeks to verify a hypothesis in an optimal order determined by the current application hypothesis and input information. Most inference engines have a means to explain the conclusions, they have made, to the user and to allow the content of the reasoning chain to be reviewed before an advised action is taken.

A User Interface: An expert system requires an interface that will permit the user to query the system, provide information, and receive advice. The information should be presented to the user in a way that conforms to the user's model of the task and his expectations.

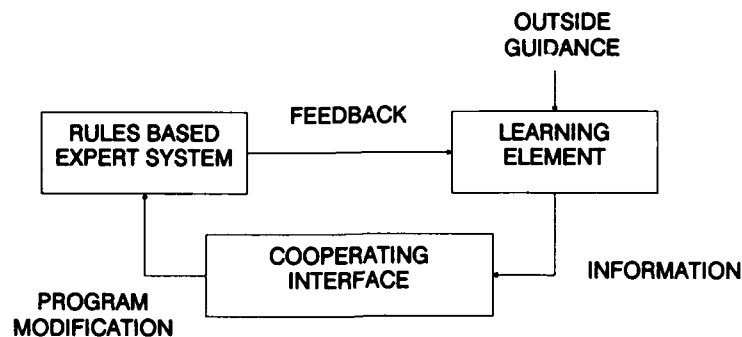


Figure 2. General Learning Model

3. Machine Learning: As previously observed, the expertise in a expert system, like that of a human expert, is subject to technical obsolescence. It is therefore not surprising that there is a strong research effort in the field of machine learning towards enhancing the process of generating and maintaining the costly expert system knowledge base. An excellent view of the field is provided in the two volumes by Michalski, Carbonell, and Mitchell [3]. Machine learning like human learning can take several forms. These include rote learning, being instructed, learning by analogy, learning from examples, learning by observation and discovery, and learning by experience. Although there are many machine learning methods, they generally fall into two broad categories: black box systems and cognitive systems. The black box methods rely on precise mathematical formulation of the learning system while the cognitive systems more closely approach the way humans learn. A general learning model is diagrammed in figure 2. The AI system is functionally divided into a rules based expert system and a learning element. The expert system performs the normal operational tasks while the learning element combines outside information, and feedback from guidance into learning that will be used to improve performance. A key role is played by the cooperating interface which must integrate new learning into the expert system knowledge without disrupting any still viable rule structures. The importance

of the feedback to the learning system can not be overemphasized. Without feedback the system can not gain the experience that permits it to modify its actions to enhance its performance.

4. Problems with Prognostic Systems: Whether the predictive monitoring is performed traditionally or by the latest AI techniques, the deficiency with the use of discrete alarm thresholds is the same. Sensor readings are essentially numbers, the only information they carry are in implied relationships. To then use selected discrete values as the focus of the monitoring puts the major emphasis on the process that selects the thresholds rather than on the dynamic process that is being monitored. Real systems have varying internal and environmental interactions that are not well represented by fixed threshold values. To paraphrase Ross Ashby's definition of a "machine" [1], real systems "have an internal state and exist in an environment, which is also a state. These two states define uniquely the next internal state, at all times". The PREFIX monitor to be described, later in this paper, avoids these problems by transforming the monitored sensory data into dynamic system relationships that essentially provide alarm thresholds that characterize the full acceptable operating range of the system.

Another concern in threshold monitoring is the selection of the specific sensor inputs to use for determining the system characteristics to be monitored. The tendency is to monitor only the sensors that measure the more obvious system characteristics, whereas other neglected sensors may give more subtle but much earlier indicators of failure. The PREFIX monitor can look at a wide array of sensor outputs and then from learned experience, select those that show relationships to the fault being monitored.

5. PREFIX-A Self-learning Prognostic System: There are two basic modules in the PREFIX system: a learning module and a performance module. See Figure 3. Each of these modules are served by their own microprocessor. Data describing the behavior of the system being monitored is available to the learning module from a data acquisition system. The learning module, using rules and standards provided in the expert knowledge base of the performance module, monitors the data to detect deviations in the normal operating relationships. If these deviations were not anticipated in the existing expertise of the expert or experience knowledge bases then the new information is presented through the cooperating interface to the operator interface. The resulting dialogue will indicate whether the deviations are due to deliberate system changes or not. The experience knowledge base will be updated accordingly. When this new state information has been verified by additional experience or dictate, the cooperating interface permits the appropriate update of effected rules in the expert knowledge base. Executive control of PREFIX by the operator is provided by the performance

module. System performance and the review of any new learning is available at any time.

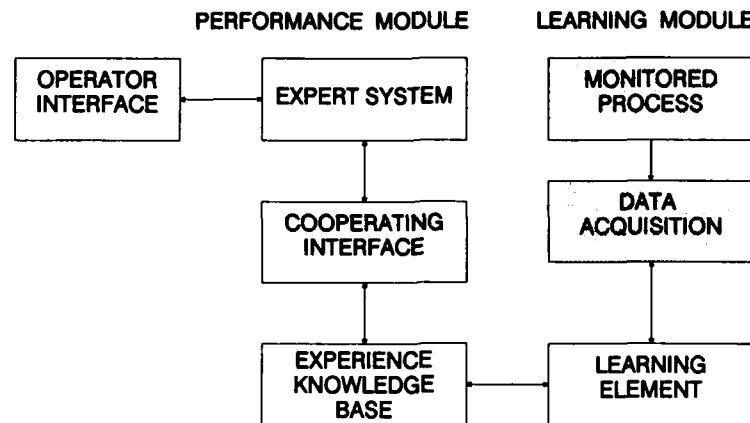


FIGURE 3. PREFIX SELF-LEARNING PROGNOSTIC SYSTEM

5.1 Learning Module:

Data Acquisition: PREFIX can accommodate monitored system data, in any combination, from data bases, transducer driven data, or manual input. Usually the system to be monitored is already instrumented for machine control purposes. While many control signals can be used for prognostic monitoring, it usually is necessary to augment this data with sensory outputs that are more related to overall system interactions and changing environmental states. Providing sensors to the often inaccessible locations in these in-place systems often requires indirect measuring techniques to be utilized. In these techniques, a sensor output, that correlates with the property that can not be directly measured, is chosen to express the same system relationships. If necessary, the "learning" aspect of PREFIX can mimic the response characteristics of the original inaccessible signal, but in most cases we are concerned with only the system relationship values. Except in the most simple prognostic systems, the data acquisition function should be independent. The behavior to be sensed must be appropriate to the needs of the prognostic system, but tasks such as signal conditioning and sampling routines are better performed by a stand-alone data acquisition system. PREFIX usually accesses its monitored system data through the database of the acquisition system.

Learning Element: The learning module monitors the process at a sampling rate dictated by the specific application. Usually, the knowledge base will provide the necessary system information to define a learning strategy. The depth of the in-

formation provided will vary with application and can range from complete control logic and fault trees to, a minimum, the definition of the events to be monitored and the system output standards. However, to better understand the powerful self-learning capabilities of PREFIX, let us assume that the learning module doesn't know anything about the system it is monitoring except the values of the raw data being received from the data acquisition system. As we are concerned with relationships rather than data, proprietary statistical algorithms are applied to develop the dynamic attributes of the data, and these values are combined into a state vector that essentially represents a pattern of the dynamic behavior of the system at that time. Without experience or knowledge the state vector is not referenced to the system, nor is there any way of determining if it represents abnormal behavior. Lacking direction, the module defaults to a mode in which a linear sequential estimator is used to discover stable states of incoming data. When distinct stable states are identified the module will associate a normal state vector and a triggering system event with each. In the absence of the identification of an event to tie to the state vector, the vector is stamped with time and date to provide a reference to the operating personnel when they now must define what stable states and system triggers should be monitored. This technique allows PREFIX to deal with systems that are not well understood and actually help the operating personnel develop the basic operating knowledge needed.

Once significant states have been identified, they are monitored for deviations from these states. When deviations are observed, the operator will be advised of the characteristics of the deviation and the system relationships that have been altered. The advisement is presented in a format that permits operator response. If the deviation from normal was caused by a deliberate change such as a new set point selection in a controller, this fact is stored with the new state vector and is made part of the general learning. If not, the system will mark the state vector for continued monitoring as to its effect on overall system performance. As this continuous learning by observation and by operator input progresses, the learning system becomes educated as to what signals represent normal operation and what signals are associated with positive or negative system performances.

Experience Knowledge Base: PREFIX uses a frame based knowledge system as a method of organizing and packaging data and procedures into its knowledge structure. Frames, first advanced by Marvin Minsky [4], have the advantage that they can efficiently express relationships. The essential feature of a frame is that it contains "slots" that can be filled with values that describe frame properties, link other frames, and invoke procedures whenever a slot is read or modified.

During the setup of the specific application, a frame is constructed in the experience knowledge base for each data source. Although, there are hundreds of types of transducers, they can all usually be accommodated by five standard frame templates according to their presence/absence, positioning, inspection, condition measuring, and identification sensing functions. Typically, the frames

will carry slots for data values, relative location on the system flow path, and other system identification elements. In continuous processes the system flow is referenced from raw material inputs to product output; in mechanical equipment the flow criteria is from energy input to functional output.

5.2 Performance Module:

Expert System: PREFIX uses its expert system for providing its own learning tool with the expert guidance it needs to understand the configuration, operation, and objectives of the monitored system, and for providing the user with an expert interpretation of the operating information learned by the learning tool. For this reason, the inference engine has both forward and backward chaining capabilities. The expert knowledge bases to be used are written in a standard format on a word processor or on the built-in editor. During the setup of the specific application, a parsing utility will automatically read and debug the knowledge base, construct the appropriate frames, and enter the rule information into the correct slots of these frames. A menu-driven utility then presents each frame in turn to the user and prompts for any additional information needed.

Cooperating Interface: The frame structure of the expert system knowledge base is connected to the frame structure of the experience base through the cooperating interface. The interface acts as a blackboard for the passing of information between the two bases, and as a mechanism for updating the knowledge base as required to reflect configuration changes or new knowledge learned from the monitored system. The interface communicates with the operating personnel through the expert system user interface to obtain modification permissions and advise of learned system relationships that indicate potential problems or opportunities for system improvement.

Conclusion: PREFIX, a self learning prognostic monitoring system has been described. The emphasis was placed on its ability to detect subtle changes that indicate potential failure in monitored systems having multiple states of behavior and interacting with changing environments. However, this same ability allows PREFIX to determine the positive relationships that would lead to a more optimal operation. Opportunities normally buried in large volumes of system data are quickly recognized and implemented. The Predictive Technology described will create a new category of products which will achieve levels of performance not presently possible.

References:

- [1] Ashby, W.R., *An Introduction to Cybernetics.*, New York, NY: Wiley, 1961.
- [2] Dvorak, D.D., *Expert Systems for Monitoring and Control.*, Technical Report AI 87-55, Department of Computer Sciences, The University of Texas at Austin, May 1987.
- [3] Michalski, R.S., J.G. Carbonell; T.M. Mitchell., *Machine Learning: A Guide to Current Research.*, Boston, Mass: Kluwer, 1986.
Machine Learning: An Artificial Intelligence Approach, Volume II., Palo Alto, CA.: Morgan Kaufman, 1986.
- [4] Minsky, M. A., *A Framework for Representing Knowledge.*, In P. Winston (Ed.), *The Psychology of Computer Vision.*, New York, N.Y.: McGraw Hill, 1975.

OIL ANALYSIS IN MACHINERY DIAGNOSTICS

Chairman: Phillip W. Centers
Wright Research & Development Center

TECHNIQUES TO EVALUATE THE REMAINING USEFUL
LUBRICANT LIFE OF GAS TURBINE ENGINE
LUBRICATING OILS

Robert E. Kauffman

University of Dayton Research Institute
300 College Park
Dayton, Ohio 45469-0001

Abstract: This paper presents a review of the research conducted to develop and evaluate a remaining useful lubricant life evaluation technique (RULLET) for MIL-L-7808 and MIL-L-23699 type gas turbine engine lubricating oils. A RULLET has the potential to enable oil analysis programs to reduce material and labor costs by eliminating scheduled oil changes and by detecting abnormal operating equipment prior to component malfunction. The RULLET candidates were developed from thermal analysis, hydroperoxide titration, and cyclic voltammetric techniques. A comparative study of the RULLET candidates determined that the cyclic voltammetric technique was the most suitable for use by oil analysis programs. The operation of the cyclic voltammetric technique requires less than ten seconds, requires a small amount of sample (100 μ l), is easy to operate and uses inexpensive equipment.

A field test of the cyclic voltammetric based RULLET was then performed by Air Force personnel. The results of the field test showed that the RULLET can be operated by nontechnical personnel to determine correct oil change intervals for normal operating engines and to detect abnormal operating engines prior to malfunction. The RULLET was especially successful in detecting abnormal C-130 aircraft engines prior to malfunction.

Key words: Condition monitoring; cyclic voltammetry; gas turbine engine; lubricating oil; oil analysis technique; remaining useful lubricant life

Introduction: This paper describes the research designed to develop a RULLET for use by the Air Force. (1-4) Remaining useful lubricant life (RULL) is the length of engine operating time from the time a lubricant is sampled until large changes in the basestock's physical properties

occur, i.e., the useful life of the lubricant ends (Figure 1). To ensure that a lubricant is not used past the end of its useful life which would result in excessive oil degradation, component wear, and eventual engine malfunction, the Air Force changes oil periodically, usually during phase inspection. Because the periodic oil changes are inherently conservative, lubricants with RULL are discarded. Therefore, the ability to predict the RULL of lubricants would eliminate the need for scheduled changes providing savings in operating costs to the Air Force. The ability to predict the RULL of lubricants could also be used to identify lubricants being degraded at an accelerated rate by abnormal operating engines. The ability to identify abnormal operating engines prior to engine malfunction would provide additional savings to the Air Force.

However, the only tests currently available to the Air Force for determining the RULL of a lubricant are long term stability tests. The analytical techniques used to detect changes in the physiochemical properties (viscosity, total acid number, color, etc.) of a lubricant (Figure 1) are dependent on the lubricant's formula and the stressing conditions, and consequently, are incapable of determining the lubricant's RULL.

Therefore, techniques were developed to enable the Air Force to evaluate the RULL of different type lubricants.⁽¹⁾ The investigation focused on developing a RULLET for gas turbine engine lubricating oils. To be suitable for use by the Air Force, the RULLET must be easy and inexpensive to operate, require less than 10 minutes to perform, require a small amount of sample (less than 1 cc), and be performed using inexpensive instrumentation.

The research to develop a RULLET for used MIL-L-7808 and MIL-L-23699 type gas turbine engine lubricating oils was performed in two stages. In the first stage analytical techniques were developed then evaluated for use by the Air Force using laboratory stressed and authentic used gas turbine engine lubricating oils. In the second stage the selected RULLET candidate was field tested by Air Force personnel to determine the RULL values and RULL depletion rates produced by normal and abnormal operating conditions for different types of military aircraft engines.

Experimental

Used Oils for RULLET Evaluation: Except for a series of used MIL-L-7808 type lubricating oil samples obtained from a normal operating engine test stand, the series of used MIL-L-7808 and MIL-L-23699 type lubricating oil samples analyzed during this work were obtained from abnormal operating Air Force gas turbine aircraft engines prior to engine malfunction.

Used Oils for RULLET Field Test: The used gas turbine engine lubricating oils analyzed during the field test were MIL-L-7808 and MIL-L-23699 type oils and were obtained from Air Force A-10 and C-130 aircraft engines.

Cyclic Voltammetric Method: A fresh MIL-L-23699 type oil was used as the 100% standard and the solvent system was used as the 0% standard to calibrate the RULLET for % RULL determinations. The RULLET was constructed from a commercially available, microcomputer controlled voltammograph which was equipped with a glassy carbon working electrode, a platinum wire reference electrode, and a platinum wire auxiliary electrode^(4,6) (Figure 2).

The oil samples (100 μ l) were diluted with acetone (3 ml) containing an electrolyte and an organic base. The voltage of the auxiliary electrode was scanned from 0.0 to 1.0 V then back to 0.0 V for six cycles at a rate of 6.0 V/second. The % RULL of the oil sample was calculated as described in detail in References (4-6).

Field Test Description: The field test was performed by placing RULLETs at three Air Force bases. The A-10 aircraft used oil samples analyzed during the field test were obtained from the Air Force Spectrometric Oil Analysis Program (SOAP). After the wear metal concentrations of the used oil samples were determined by the SOAP, a portion of the remaining used oil sample was analyzed by the RULLET (100 μ l sample size required). Since the SOAP did not monitor the C-130 aircraft at the selected Air Force bases, used oil samples (5 ml, sampled cold) were obtained specifically for RULLET analysis.

The % RULL and hours since oil change (HSOC) values of the analyzed used oil samples were recorded by aircraft type and engine serial number. The % RULL values were then plotted versus the HSOC values for each series (2-15 samples obtained from same engine) of used oil samples to determine the % RULL values and depletion rates for different types of normal and abnormal operating engines.

Results and Discussion

Comparison of RULLET Candidates: During this investigation⁽¹⁾ three RULLET candidates were developed, based on thermal analysis⁽²⁾, hydroperoxide titration⁽³⁾, and cyclic voltammetric⁽⁴⁾ methods using fresh and laboratory stressed MIL-L-7808 type lubricating oils. To select the RULLET candidate most suitable for use by the Air Force, the experimental parameters of the candidates were compared to the RULLET criteria listed in Table 1. Except for the cost criteria (costs of cyclic voltammetric and hydroperoxide titration methods are similar), the cyclic voltammetric candidate best meets the criteria for development into a RULLET.

The cyclic voltammetric candidate has the additional advantage of requiring less than one minute to perform regardless of the oil sample's RULL or formulation. The thermal analysis⁽²⁾ and titration⁽³⁾ candidates required up to ten minutes to analyze the fresh and stressed MIL-L-7808 type oils (Table 1).

Therefore, the cyclic voltammetric method was selected as the RULLET candidate most suitable for use by the Air Force and other gas turbine engine users.

Cyclic Voltammetric Analyses of Used Oil Samples

Introduction: To initially evaluate the potential of the cyclic voltammetric RULLET candidate for use by the Air Force, three types of used oil samples were analyzed: (i) Routines - Normal wear detected by the Air Force SOAP and verified by maintenance personnel, (ii) Hits - Abnormal wear detected by the Air Force SOAP and verified by maintenance personnel, and (iii) Failures - Obtained prior to engine failure unpredicted by the Air Force SOAP. The three types of used oil samples were used to evaluate the capability of the cyclic voltammetric candidate to determine the RULL of MIL-L-7808 and MIL-L-23699 type oil samples obtained from normal (Routine) and abnormal operating (Hits and Failures) engines.

Analysis of Routine Used Oil Samples: To determine the potential of the cyclic voltammetric candidate to evaluate the RULL of used oil samples obtained from normal operating engines, a series of Routine used oil samples obtained from a engine test of a MIL-L-7808 type oil was analyzed. The plots of the % RULL, viscosity (40°C) and total acid number (TAN) measurements versus hours of engine operating time for the Routine used MIL-L-7808 type oil sample series are shown in Figure 3. The viscosity and TAN measurements were performed by the test engine personnel.

The % RULL versus hours of engine operating time plot in Figure 3 shows that for a normal operating engine, the % RULL of the obtained samples decrease at a moderate, fairly constant rate during the testing period of 175 hours. The inflection points present in the % RULL plot (especially at 175 hours) are indicative of oil additions. After the rise upon initial stressing, the viscosity and TAN plots in Figure 3 are level throughout the test confirming that the oil's useful life had not been exceeded (Figure 1). The viscosity and TAN plots in Figure 3 also show that physiochemical property measurements are unsuitable for the RULL evaluations of gas turbine engine oils, i.e., % RULL of oil samples decreased 25% during the test while the viscosity and TAN measurements remained level.

To further confirm the presence of normal operating conditions for the Routine used oil sample series, particle size distribution and particle composition analyses of the wear debris in the used oil samples were performed using a modified emission spectrometer⁽⁷⁾. For all of the Routine used oil samples, no wear metal particles were detected (normal wear mode).

Analysis of Failure and Hit Used Oil Samples: To initially evaluate the potential of the cyclic voltammetric candidate to detect abnormal operating conditions prior to engine malfunction, numerous series of Failure and Hit used oil samples obtained from abnormal operating engines were analyzed. The % RULL versus HSOC plots for the majority of the Failure and Hit used oil sample series exhibited rapid decreases in the % RULL values several flight hours prior to engine malfunction (Figure 4).

In contrast to the % RULL versus HSOC plots which exhibit rapid decreases in Figure 4, several Hit used oil sample series taken from C-130 aircraft engines had 0% RULL several hours prior to SOAP recommended engine removal (Figure 4). The remaining Failure and Hit used oil sample series produced % RULL versus HSOC plots that were unaffected by the presence of abnormal operating conditions, i.e., plots were similar to those in Figure 3.

The presence of abnormal operating conditions were confirmed for each Failure and Hit used oil sample series by the detection of wear metal particles in the oil samples taken several hours prior to engine malfunction⁽⁷⁾.

Field Test

A-10 Aircraft: During the three months of testing, over 1,000 samples were obtained from approximately 200 different A-10 aircraft engines. The RULL values of the different oil sample series (2-9 samples per series) ranged from 96-102% for 192 of the engines and from 90-95% for 8 engines. The HSOC of the used oil samples obtained from the A-10 aircraft engines ranged from 0 to 200 hours [(200 hours: oil change interval)].

To compare the % RULL versus HSOC trends for the A-10 aircraft engines operating at % RULL values above 95% with those operating at % RULL values below 95%, the % RULL were plotted versus the HSOC for the different oil sample series. The % RULL versus HSOC plots for the representative A-10 aircraft engine oil samples are presented in Figure 5.

The used oil sample series in Figure 5 with % RULL above 95% range between 102-97% and the % RULL versus HSOC plots exhibit moderate decreases or increases (oil additions) between samples. All of the A-10 aircraft engines with

% RULL above 95% were classified as normal operating engines (SOAP analyses normal) during the field test.

The used oil sample series labeled A-1 and A-2 in Figure 5 had % RULL values below 95% and their % RULL plots exhibited rapid decreases between oil samples. The SOAP recommended the A-1 engine for inspection due to a rapid increase in the iron concentrations of the oil samples taken at 22 and 24 HSOC. Maintenance personnel removed the engine for inspection and verified that the engine was experiencing abnormal wear. The maintenance report detailing the replaced engine components was not made available. The A-2 engine was removed for routine maintenance at 182 HSOC and underwent unspecified component replacement. The A-1 and A-2 engines were not placed back into service during the field test.

The % RULL plots of the other A-10 aircraft engines with % RULL values below 95% exhibited moderate decreases or increases between oil samples similar to the normal A-10 sample series in Figure 5 and were classified normal by the SOAP.

C-130 Aircraft: In contrast to the RULL values obtained for the A-10 aircraft, the RULL values obtained by Air Force personnel were below 95% for several C-130 aircraft engine oil samples. The 93 used oil samples analyzed by the Air Force personnel were obtained from 50 different C-130 aircraft engines. Except for two engines, labeled C-1 and C-2, the RULL values of the used oil samples obtained from the C-130 aircraft engine ranged from 89 to 103% with the RULL values decreasing slightly with engine operating time (Figure 6). However, the used oil samples obtained from the C-1 and C-2 aircraft engines produced RULL values between 29-45% and 64-80%, respectively, and the RULL values decreased rapidly with engine operating time (Figure 6).

Due to the low RULL values, the C-1 engine was removed for inspection at 195 HSOC by Air Force maintenance personnel. The maintenance personnel discovered that the back carbon seal was cracked. The cracked seal could account for the rapid degradation of the oil (rapid decreases in the % RULL values) since hot air would be able to interact with the oil accelerating its thermal-oxidation. The seal was repaired and the C-1 engine was placed back into service. The % RULL value of the oil sample obtained from the repaired C-1 engine was 93% at 90 HSOC further indicating the cracked seal was the cause of the low % RULL values.

The C-2 engine was removed for unscheduled maintenance at 600 HSOC and was not returned to service during the field test. The maintenance records for the C-2 engine were not available during the field test.

Summary: The results of the developmental research and field test have shown that the cyclic voltammetric RULLET can be operated by nontechnical personnel to detect abnormal operating equipment prior to malfunction and to determine correct oil change intervals for normal operating engines. As with most predictive maintenance techniques, histories must be developed for each type of gas turbine engine being monitored in order for an oil analysis program to detect abnormal operating engines.

For the A-10 aircraft engines monitored during the field test, the short length of time (1-2 HSOC) between samples and the frequent oil additions produced % RULL which remained above 93% for normal as well as abnormal operating engines. Thus, the initial results of the field test for A-10 engines demonstrated that the oil change intervals [of 200 HSOC] for the A-10 aircraft were very conservative. The depletion rates of the % RULL values, and not the actual % RULL values, were better suited for detecting abnormal operating engines (Figure 5). The oil change intervals were extended [to 400 HSOC] soon after the field test was completed.

For the C-130 aircraft engines studied during the developmental research and monitored during the field test, the RULLET was very successful in detecting abnormal operating engines prior to component failure. The % RULL values and the % RULL depletion rates could both be used to detect the abnormal operating engines (Figures 4 and 6).

The fact that % RULL values below 85% are indicative of abnormal operating conditions indicates that physiochemical property measurements which are insensitive to % RULL changes during the useful life of the lubricant (Figures 1 and 3) would be incapable of detecting the initiation of abnormal operating conditions. Only after the antioxidant capacity of the used oil has become depleted (0% RULL in Figure 1) are the physiochemical property measurements capable of detecting abnormal operating conditions.

Therefore, the developmental research and field test have shown that the RULLET has the capability to improve the Air Force's SOAP by assisting in the detection of abnormal operating conditions which rapidly degrade the oil without necessarily increasing the wear metal concentrations used by SOAP to detect severe wearing components. The RULLET can also be used to determine the correct oil change intervals for the different type engines used by the Air Force.

The rapidness, ease of operation, small amount of required sample, and accuracy of the cyclic voltammetric based RULLET analyses make it much more suitable for incorporation into oil analysis programs than the commonly used viscosity or TAN measurement techniques (Figure 1). Of

the aircraft studied during the field test, the capability of the RULLET to detect abnormal C-130 aircraft engines has the largest potential for reducing material and labor costs due to the worldwide use of C-130 aircraft. Further field testing of the RULLET is needed to determine the full potential of a RULLET for use by the Air Force and other gas turbine engine users.

Acknowledgements: This work was supported by the Aero Propulsion and Power Laboratory, Air Force Wright Aeronautical Laboratories, Wright-Patterson Air Force Base, Ohio with Lynne M. Nelson as the Project Engineer. The comments and suggestions of G. A. Beane IV and Phillip W. Centers (WRDC/POSL) are appreciated.

References

1. This paper was taken in part from : R.E. Kauffman and W.E. Rhine, "Assessment of Remaining Lubricant Life," Report No. AFWAL-TR-86-2024, November 1986.
2. Kauffman, R.E. and Rhine, W. E., "Development of a Remaining Useful Life of a Lubricant Evaluation Technique. Part I: Differential Scanning Calorimetric Techniques," Lub. Eng., 44, 2, pp 154-161 (1988).
3. Kauffman, R.E. and Rhine, W.E., "Development of a RULLET. Part II: Colorimetric Method," Lub. Eng., 44, 2, pp. 162-167 (1988).
4. Kauffman, R.E., "Development of A Remaining Useful Life of a Lubricant Evaluation Technique. Part III: Cyclic Voltammetric Methods," Lub. Eng., 45, 11, pp. 709-716, (1989).
5. Kauffman, R.E., "Method for Evaluating the Remaining Useful Life of a Lubricant," U.S. Patent 4,744,870 (May 17, 1988).
6. Saba, C.S., et al., "Lubricant Performance and Evaluation," Report No. AFWAL-TR-87-2025, June 1987.
7. Kauffman, R.E., "Particle Size and Composition Analyses of Wear Debris Using Atomic Emission Spectrometry," Lub. Eng., 45, 3, pp. 147-153 (1989).

Figure Captions

- Fig. 1. Plots of the Viscosity (40°C) and Total Acid Number (TAN) versus Hours of Stressing Time and Remaining Useful Lubricant Life at 370°F for a Typical Gas Turbine Engine Lubricating Oil.
- Fig. 2. Voltammograph and Three Electrode Systems Developed to Perform the Cyclic Voltammetric Methods.
- Fig. 3. Plots of the Percent Remaining Useful Lubricant Life, Viscosity (40°C), and Total Acid Number (TAN) versus Hours of Engine Operation for a Series of Used MIL-L-7808 Type Oils Obtained from a Normal Operating Gas Turbine Engine Test Stand.

- Fig. 4. Plots of the Percent Remaining Useful Lubricant Life versus Hours Since Last Oil Change for Series of Failure and Hit Used Oils Obtained from Abnormal Operating Gas Turbine Engines.
- Fig. 5. Plots of Percent Remaining Useful Lubricant Life versus the Hours Since Last Oil Change for Used Oil Sample Series Obtained from Normal and Abnormal Operating A-10 Aircraft Engines.
- Fig. 6. Plots of Percent Remaining Useful Lubricant Life versus the Hours Since Last Oil Change for Used Oil Sample Series Obtained from Normal and Abnormal Operating C-130 Aircraft Engines.

TABLE 1
COMPARISON OF RULLET CRITERIA WITH RULLET CANDIDATES'
PERFORMANCE CHARACTERISTICS

<u>Criteria</u>	<u>Cyclic Voltammetric</u>	<u>Thermal Analysis</u>	<u>Hydroperoxide Titration</u>
<u>Cost</u>			
Instrumental	Less than \$2K	Less than \$2 K	Greater than \$20 K
Operational	As low as possible	\$0.04	\$0.30
			\$0.08
<u>Ease of Operation</u>			
Sample Size	Less than 5 ml	100 μ l	2.5 μ l
Sample Preparation	Minimal	Minimal	No
Instrumental Procedure	Simple	Simple	Complex
Safety Requirements	Minimal	Minimal	Yes ^a
			Yes ^b
<u>Analysis Time</u>	Less than 10 minutes	Less than 1 minute	1-10 minutes
<u>Linear Relationship with RULL</u>	Yes	Yes	Yes
			No ^c

^aHigh temperature and oxygen pressure used.

^bToxic chemicals used.

^cLinear between inflection points.

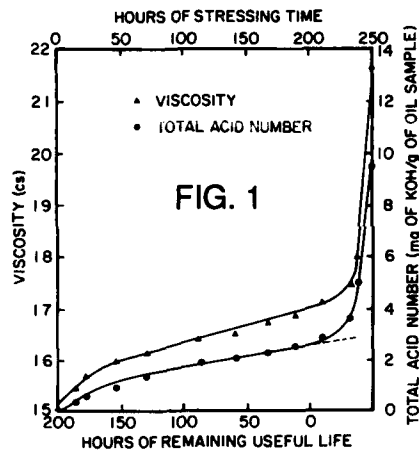
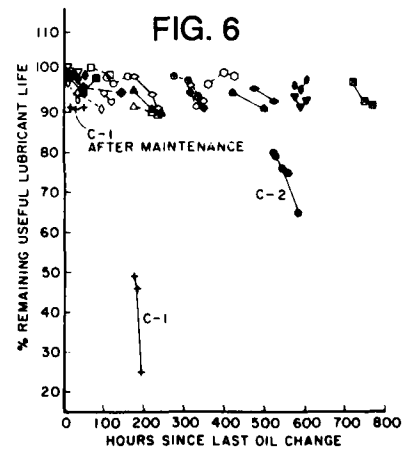
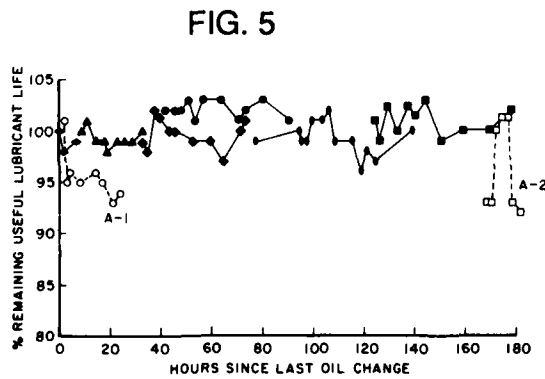
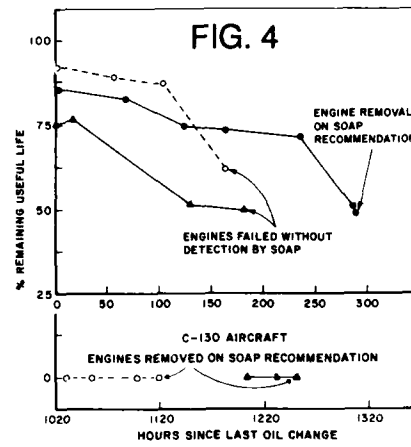
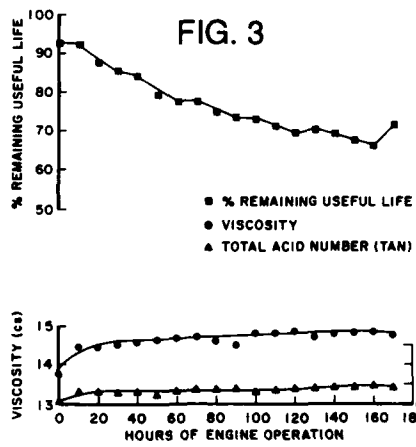
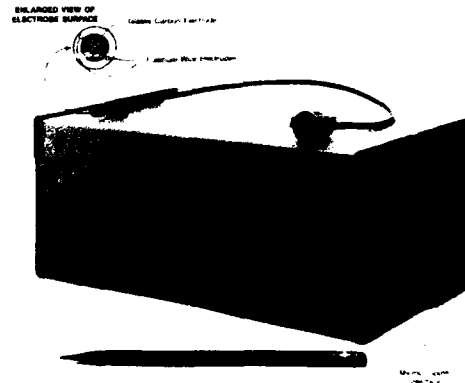


FIG. 2



ON-LINE MONITORING OF FERROMAGNETIC DEBRIS CONCENTRATION

Phil Campbell

SENSYS, 36 Bentley Ave.
Nepean, Ontario
Canada K2E 6T8

Abstract: The efforts of sensor technology development groups over the past five, ten, fifteen years, has been to develop an on-line device that will quantitatively indicate the approach to failure of a mechanical component.

There are two approaches to this problem. These are, count the number of large particles generated when the mechanical component fails, or measure the concentration of the material in the fluid. The latter method has the advantage that it is monitoring the approach to failure while the former method monitors the actual event.

This paper discusses the technology behind a ferromagnetic concentration monitor. This technology was developed by Atomic Energy of Canada in cooperation with the Department of National Defence of Canada.

The technology is based on a sensing coil being placed between the two poles of an electromagnet. The rate of build up of material across the coil is directly proportional to the concentration of ferromagnetic material in the oil.

This paper will explain the parameters that influence the operation and performance of the sensor.

In conclusion some statements will be presented as to the viability of making measurements of ferromagnetic concentration on system with fine filters and where failures are expected to take place in a very short time period.

Introduction: Wear debris is generated during the normal operation of rotating equipment and during abnormal events when components are failing due to a variety of mechanisms. The task of on-line monitoring is to inform the maintenance engineer about both of the above situations. If the concentration of normal wear debris gets too high then it can cause failures to occur, therefore continual information about the baseline concentrations must be known. In addition, the generation of debris from unusual events must be detectable above the normal baseline.

Measuring the concentration of ferromagnetic debris allows both of the above to be achieved. This paper describes the technical basis of the sensor, and the laboratory tests.

It also introduces a new technology that generates a higher level of information available to the predictive maintenance engineer. The oral presentation related to this subject will contain details of applications, where field trial results will be reported, as well as introducing new methods of packing the technology.

Principles of Operation: FerroSCAN consists of a sensor coil, a trapping magnet and a microcontroller. The fluid sample stream passes through a cylindrical sensor coil which is the inductive component of a radio frequency oscillator. When the ferromagnetic content within the active volume of the coil is changed, the inductance in the RF circuit changes resulting in a change in oscillator frequency. For a simple series circuit consisting of an inductance, L, and capacitance, C, the resonance frequency is given by:

$$f = 1/2\pi \sqrt{LC} \quad (1)$$

Thus, if the ferromagnetic content within the sensor coil is increased the inductance L, will increase and the frequency of the oscillator, f , will decrease.

To collect ferromagnetic material, an electromagnet is built around the sensor coil. When the magnet is energized, ferromagnetic debris collects over the coil and the oscillator frequency decreases until the trapping magnet is de-energized. The ratio obtained by dividing the frequency change by the trapping interval is a linear function of the bulk concentration of ferromagnetic debris.

The operation of FerroSCAN is best described with the help of the frequency/time profile shown in Figure 1. When the trapping magnet is energized, the oscillator frequency undergoes a step change from $f(B)$ to $f(C)$ due to change of magnetic permeability of the magnetic material surrounding the sensing coil. As ferromagnetic wear debris is trapped against the inside of the sensor coil winding, the frequency decreases progressively from $f(C)$ to $f(F)$ due to a steady increase in inductance. When the magnet is de-energized, the trapped ferromagnetic material is released and the oscillator frequency decreases. The slope, s , of the frequency ramp measured within the trapping interval $[t(E)-t(D)]$ is given by:

$$s = [f(D) - f(E)] / [t(E) - t(D)] \quad (2)$$

and it is a linear function of the bulk concentration of suspended ferromagnetic particulate material. A natural limit exists to the amount of material that can be trapped as the trapping interval is being extended. This is the result of a reduction in the magnetic field gradient as ferromagnetic particles build-up across the pole gap and in the corresponding reduction in trapping efficiency. It is found, however, that the drop in frequency required to make

precise measurements of $[f(D) - f(E)]$ is small enough that the variation of frequency with trapping interval over the range of interest can be considered linear. The frequency changes are typically a few kHz and a linear approximation over this range is a good one.

FerroSCAN could be operated in several modes depending on the application. The first mode involves measuring the frequency change for a fixed trapping interval. The advantage of this approach is that it provides a fixed cycle time and enables a single controller to monitor many sensors with ease. However, using a trapping interval of 10 seconds, non-linearity in response becomes significant at concentrations in excess of approximately 150 ppm.

In a second mode of operation, the trapping interval is measured for a fixed change in frequency, Δf . Thus, the trap is energized until Δf has been attained, then it is de-energized and the resulting trapping interval used to compute the slope, s . In this manner, the sensor always operates in its linear trapping range whether the ferromagnetic particulate concentration is low (long trapping interval) or high (short trapping intervals).

The third and preferred mode of operation is a combination of the above two, where the trapping period is variable between upper and lower limits and can adjust to changes in concentration. This combination enables FerroSCAN to respond satisfactorily over a large dynamic range covering very clean (long trapping times) and very dirty (short trapping times) systems.

Sensor Calibration: The sensors are calibrated on an oil loop at constant temperature and flow, using 6-9 μm size particles.

As known weight of particles is added to the oil and several sensor readings are logged. As sedimentation of particles in the loop can not be avoided, oil samples are extracted from the loop for subsequent chemical analysis (atomic absorption). A calibration curve relating the results from chemical analysis to FerroSCAN readings is determined by the least-square method, and the precision is quoted as one standard division, typically representing $\approx 1\text{ppm}$.

For test purposes the oil loop permits varying oil temperature and flow velocity, adds air, uses particles of different sizes and vibrates the sensor assembly.

Sensor Manufacture and Installation: The sensor comprises a magnetic coil, a sensing coil and a ferromagnetic shell. When the current is applied to the windings, the electromagnet is activated. There is a mechanical seal between the sensing coil and the shell. As well, the electromagnet cavity is filled with an epoxy potting material.

This sensor can withstand extended pressure cycling to 600 psig at -55°C to $+125^{\circ}\text{C}$. The sensor is installed directly in line on pipes up to about 1 1/4" diameter. The installation can be by welding or through fittings and no obstruction is caused in the line.

Factors Effecting Response:

Trapping Efficiency: The trapping efficiency, Σ , of the sensor is defined by the expression

$$\Sigma = 1 - c'/c \quad (3)$$

Where c , c' are the concentrations of suspended ferromagnetic particulate material upstream and downstream of the trapping magnet, respectively.

The five principal factors which determine trapping efficiency are inner diameter of the sensor, the radial gradient of the magnetic field particle size, linear flow velocity and viscosity. An approximate theoretical treatment indicates that trapping efficiency should vary inversely as the sensor inner diameter, viscosity and linear flow velocity, directly as the radial component of the magnetic field strength and as the square of the particle radius.

Oscillator Frequency - Temperature Effects: From electromagnetic theory, the inductance of a coil having cylindrical geometry can be expressed in terms of the magnetic permeability of the material within its core, μ , the number of turns per unit length, n , and the core volume, v , as follows:

$$L = \mu n^2 v \quad (4)$$

Substituting this expression for L into equation (1) and differentiating with respect to μ gives

$$\Delta f / f = 1/2 \mu \quad (5)$$

The quantity $\Delta f / \Delta \mu$ can be regarded as the sensitivity of the sensor to changes in the ferromagnetic content of the material within the core of the sensor coil. Thus from equation (5), sensor sensitivity will, for a given value of μ (material within the core), be directly proportional to the frequency of the RF oscillator.

Oscillator frequency is also affected by changes in the dimensions of the sensor coil as a result of thermal expansion and by temperature induced changes in the magnetic permeability of the material within the core of the sensor coil.

Net thermal expansion/contraction is determined by the balance of heat dissipated by the magnet winding, heat flow from the oil stream and external cooling. Thus, if the temperature of the sensor coil increases, the coil's volume will increase and the oscillator frequency will decrease in accordance with equation (5) above: conversely, a decrease in temperature will result in an increase in oscillator frequency.

Changes of dielectric constant of the medium within the active region of a sensor also effects the resonance frequency. Thus the presence of two-phase flow (air/oil mixture) is observed as increased signal noise from the sensor.

Temperature change induced effects are minimized by hardware selections, which reduce the temperature induced changes of resonance frequency to $\approx 20\text{ppm}/^{\circ}\text{C}$, for the temperature range 25 to 125°C , and by a correction in software. Referring to Figure 1, the change in the oscillator base frequency

$$B = [(A) - (H)] / [t(H) - t(A)] \quad (6)$$

is subtracted from the slope calculated in eq. (2) to separate the signal due to ferrous debris from other contributions. This operation however, results in larger signal noise.

Flow Velocity: The sensor performance depends on the fluid's ability to remove debris from the trapping surface after the completion of a trapping cycle. At very low flow velocities this ability is impaired and the sensor displays a sharp dependence of sensitivity on flow velocity. At velocities between 0.3 to 1.5 m/s the trapping efficiency for debris is approximately constant and the sensor's sensitivity increases linearly with flow, as a larger volume of fluid is being sampled.

At higher fluid velocities ($>1.5\text{m/s}$) the trapping efficiency decreases, as the magnetic force trapping the particles competes with increased fluid drag. Correspondingly, the sensor sensitivity gradually decreases (Figure 2). In applications, where relative change of velocity is small this phenomenon is not significant.

Viscosity: As viscosity increases (oil temperature decreases) the fluid drag increases and again the sensor sensitivity decreases. (Figure 3).

Particle Size: The magnetic force trapping the particles is proportional to particle volume, i.e. it increases as third power of the particle size. In contrast, forces due to fluid exhibit weaker dependence on particle size. Consequently, sensor trapping efficiency increases with

particle size (figure 4).

Low trapping efficiency (several percent) indicates that the sensor samples only a narrow annular region of the pipe, approximately 0.1 to 1mm thick.

As wear is demonstrated by the increase in both particle number and their size this phenomenon augments the utility of trending information to detecting wear.

Air-Oil Mixture: When air is introduced into oil, a number of different flow regimes can exist. Whatever the regime, FerroSCAN will continue to trap the ferromagnetic debris. However, depending on the regime, the debris will transfer through the pipe in different ways. In some cases, the debris will concentrate at the interface between the two phases. The mixed phase regime will impose a heterogeneous debris distribution. Therefore, more scattered responses should be expected. Figure 5 illustrates this point. Relative insensitivity of sensor response to vibrations up to 8g of acceleration is also demonstrated.

Data Reporting: FerroSCAN measures the concentration of ferromagnetic debris in the oil line. Any fluctuation in the debris will be monitored by the sensor. The sensors are sending data to a controller, where they are logged, producing a complete profile of ferrous debris concentration in the oil system. Stored data can be downloaded into a computer where they are displayed in graphic format or as a data file. The data presentation package, FerroPLOT permits easy data manipulation.

The dependence of sensor trapping efficiency on particle size is used to provide qualitative information on particle size distribution. Sensors are operated at two strengths of trapping magnetic field. The difference of trends for those two sets of data is indicative of the change in particle size distribution. There is a lot of information contained in the trends produced by our software package FerroPLOT. This information becomes invaluable in understanding the dynamic nature of operating equipment.

Conclusion: The FerroSCAN technology is under intense scrutiny by the oil condition monitoring community. It has undergone a dramatic evolution since SENSYS was started three years ago, and we are proud of the technical, advances we have made in our effort to meet our clients' needs. The more our clients use it, the more we are able to incorporate the market needs and the better the product will be. We have come a long way in a short time.

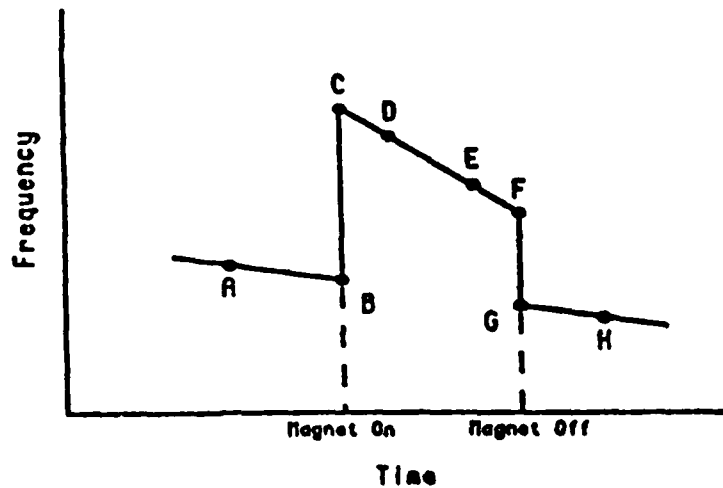


Figure 1:
Schematic of Sensor Operation
(refer to text)

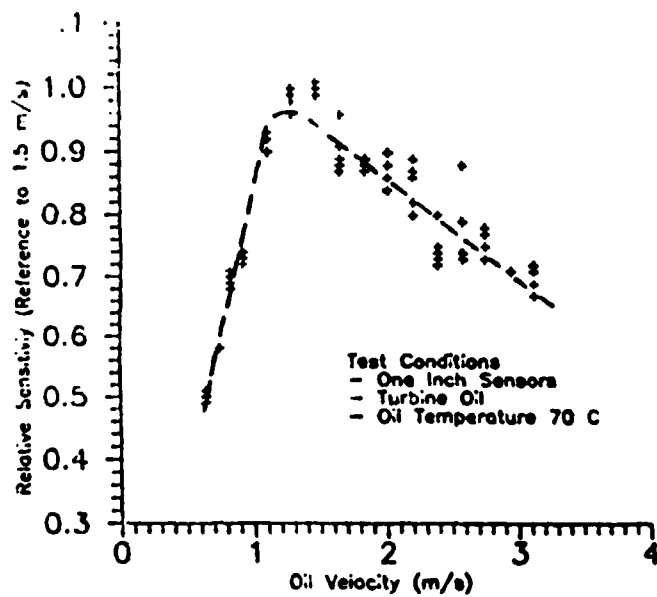


Figure 2:
Dependence of Sensor Sensitivity
on Linear Flow Rate

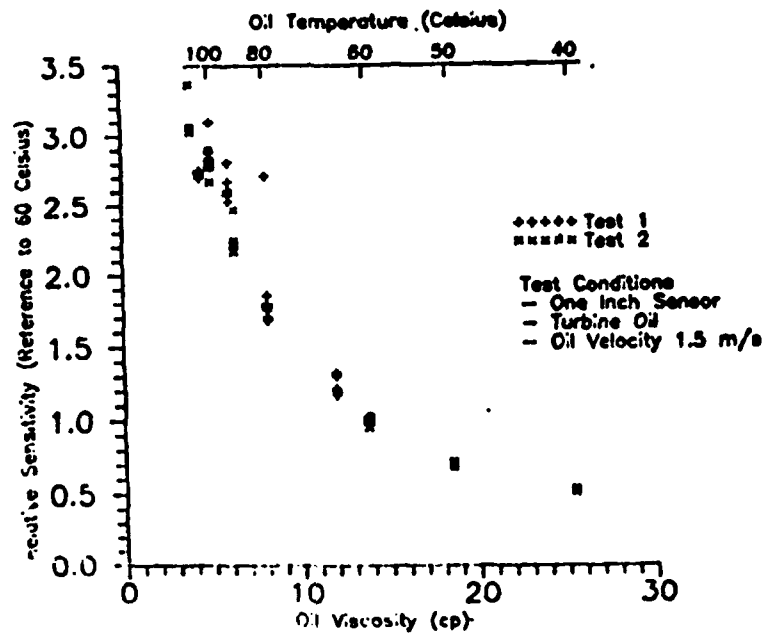
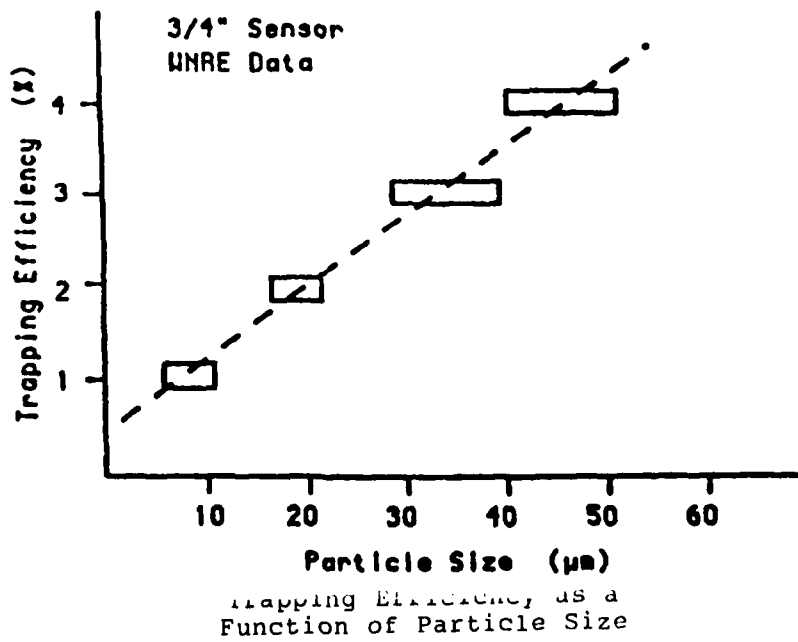
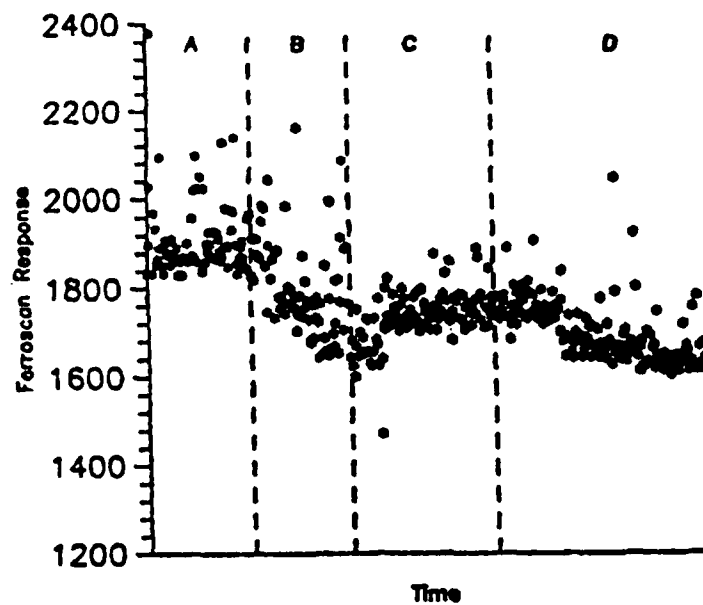


Figure 3:
 Sensor Sensitivity as a
 Function of Oil Viscosity





Test Conditions
 -- Half Inch Sensor Mounted Vertically
 -- Oil Velocity 2.2 m/s
 -- Turbine Oil
 A -- No Vibration & No Air Injection
 B -- No Vibration With Air Injection
 C -- 8G at 45 Hz & No Air Injection
 D -- 8G at 45 Hz With Air Injection

Figure 5:
 Effect of Air and Vibration on Sensor Response

HIGH POWER - DENSITY REDUCTION GEARBOX LUBRICATION
STUDIES USING POSITRON EMISSION TOMOGRAPHY

V. Mashkin
Textron Lycoming
550 Main Street
Stratford, CT 06497 U.S.A.

M.R. Hawkesworth
School of Physics
University of Birmingham
Birmingham, B15 2TT U.K.

Abstract. The efficiency of high power density gearboxes depends primarily on the lubrication system. Excessive oil flow leads to increased speed-related parasitic losses and consequently high gear teeth temperatures which may result in lube film breakdown causing tooth scuffing and premature failure. To investigate speed related power losses and methods for their reduction, a diagnostic tool capable of identifying oil distribution patterns within actual gearboxes at full operating conditions is required. The new technique of positron emission tomography is being developed at the University of Birmingham, UK to be just such a tool. Prior to this work it had already been successfully demonstrated in studies involving solid oil distributions, but had not been used to identify oil collection areas and scavenge patterns in air-oil mist environments typical of high power-density reduction gearboxes.

A test rig for a typical turbofan engine gearbox has been designed and built at Textron in order to investigate its oil and air-oil mist distribution under operating conditions using PET. A series of static tests were conducted initially in Birmingham to prove basic feasibility before proceeding to high speed work in a test cell. A selection of the results is discussed following a summary of the principle underlying PET and a brief description of the University of Birmingham's mobile positron "camera" being developed for wide industrial application.

Key Words: High power-density gearbox lubrication; industrial positron emission tomography; mobile positron camera.

Introduction: Positron emission tomography (PET) is a new non-invasive technique capable of furnishing quantitative three-dimensional information on fluid distributions within opaque structures. In this technique the fluid of interest is labelled with a positron-emitting radioisotope. Each positron emitted very quickly combines with a nearby electron and annihilates into two gamma rays travelling in diametrically opposite directions. If two positron-sensitive gamma ray detectors are placed on each side of the subject, a pair of rays may be assigned to a single positron annihilation by their (approximately) simultaneous or coincident, detection and the spatial coordinates of the points of

detection recorded. The gamma ray path may then be calculated, and the intersections of many such paths provide a three-dimensional map of the location of the positron-emitting isotope and, hence, of the host fluid (figure 1). Prior to the Birmingham programme PET had only been developed for medical application [1], but it is, in fact, particularly interesting for engineering studies, since the positron-electron annihilation gammas always have an initial energy of 511keV, offering useful penetration of structural materials. Moreover, the amount of radioisotope used and the data-logging time may be much greater than in medicine, with the result that tomographs may contain much more detail and be separated from one another with greater efficiency.

The Birmingham positron camera for engineering research:

The design and operating principles of the positron camera for engineering research at the University of Birmingham are detailed elsewhere [2,3]. At present the camera has two detectors each of which is a multiwire proportional chamber of 20 anode-cathode planes stacked behind one another. The timing signal for coincidence recognition, or rejection, is provided by the anodes, and the positron of each gamma ray detected is given by the cathodes, the wires of the cathodes on each side of an anode being orthogonal to give both x and y coordinates which are read using the delay-line principle. The cathode "wires" are, in fact, strips of lead (2.2mm wide with 0.8mm gaps) 50mm thick, to give a 511keV gamma-detection efficiency of about 10 percent. The overall efficiency for detecting a pair of annihilation gammas from a source between the detectors is, therefore, about one percent reduced by a geometrical factor which depends on detector separation and on whether data processing includes steps to equalize detector response over a large fraction of the sensitive area of 600mm x 300mm. The delay-line readout is set to provide 256 x 128 pixel resolution, i.e., each gamma ray detected is assigned to a 2.34mm square cell in a 256 x 128 cell array in the data logger, which is the main factor limiting the spatial resolving power of the camera to about 6mm (full width at half maximum intensity (FWHM) of the image of a point source), though features of interest can usually be located with much greater accuracy than this figure might suggest. In addition to the condition that a gamma ray recording in one detector must have an associated event within, typically, 10ns in the other detector for the two to be considered coincident and therefore arising from the same positron, a number of other data validation tests are supplied prior to recording [2,3].

Positron-Emitting Radiolabels for Engineering Research

A positron emitter for flow studies needs a chemical form which is compatible with the fluids involved, an activity sufficient to give good images in an acceptable time, and a half-life long enough for satisfactory measurements to be made but short enough to avoid persistent radioactivity in the test object. Gallium-68 (half-life 68 minutes) has been used for most of our work on

lubricants; it is eluted as required from a generator carrying the parent nuclide germanium-68 (half-life 271 days). The generator principle for producing relatively short-lived radioisotopes is well known in nuclear medicine and provides in gallium-68 a convenient and readily transportable source of positron-emitting label for engineering studies needing a mobile positron camera.

Fluorine-18 produced at the University of Birmingham has now been used for several studies on operating engines at Rolls-Royce test bed [4].

Tomograph Construction

The basic method of image production in PET is to project each gamma ray path calculated from the detection position coordinates (x_1y_1 and x_2y_2 from the cathode readouts, and z_1 and z_2 from the anode positions) backwards onto a series of planes, or slices, through the object lying parallel to the detector faces (Figure 1). The number and position of these slices are chosen by the operator; at present 64 are normally selected 2.34 mm apart to provide a final three-dimensional (3D), image of 256 x 128 x 64 cubic voxels. Such back-projection images or tomographs are, however, only the first step in providing 3D information with a positron camera. Various processing routines may be applied to sharpen each tomograph and remove to some extent the background from gammas actually emitted closer to other tomographs. The tomographs may also be corrected for photon attenuation and selected ranges of signal intensity colour-coded to aid analysis. Finally, each tomograph is overlaid with a simplified engineering drawing of the appropriate plane of the object taken from its 3D digital representation previously entered into the computer [5].

Experimental Results

The gearbox placed between two PET detectors is schematically shown in Figure 2. The actual gearbox test rig is presented in Figure 3. The first series of tests were conducted to ascertain the basic feasibility of PET to identify minute quantities of oil inside the gearbox. For this purpose a 0.020 in. internal diameter plastic tube, filled with a radioisotoped oil, was placed at the specified location in the gearbox as shown in Figure 4. The tube was bonded to the lubrication ring and the ends pulled out of the gearbox through the holes, specially provided for this purpose.

The corresponding oil distribution image is also shown in Figure 4a. The image corresponds accurately to both the location and configuration of the plastic tube.

(Oil concentrations are conveyed by light tones in the black and white images presented here, but in practice the intensity/oil concentration is color-coded for greater accuracy.) In the next test, the plastic tube was detached from the lubrication ring and pushed into the gearbox on both ends so that it could take an

arbitrary new profile. The image corresponding to this profile is shown in Figure 4b. The inferences from these initial tests were:

- Radioisotope concentration in the oil was sufficient to create a signal of the intensity required to generate clear images,
- Gamma rays penetrated the metallic parts of the gearbox adequately,
- Small amounts of oil can be detected by PET cameras,
- PET-generated images show the actual oil locations as well as oil concentrations.

The actual oil distribution in the gearbox under static conditions were further recorded. Figure 5a shows the end view of the oil distribution at the lower part of the gearbox and the scavenging strut. The overlay of this picture is shown in Figure 5b.

The next series of tests were performed at different gearbox speeds and oil flow rates in a test cell. Examples of the oil distribution images generated during this phase of the testing are given in Figure 6, 7 and 8. The oil distribution at the end view from the fan side at 10,000 RPM and 2,900 PPH oil flow rate is shown in Figure 6. The pronounced oil collection areas were identified between the ring gear outside surface and the casing as well as in the triangles, formed by the ring and the sun gear and adjacent planets. Figure 7 describes the oil scavenge pattern typical for slow rotation (up to 5,000 rpm). Oil escapes from the gearbox through the left side of the strut. The oil scavenge pattern is completely different at 10,000 rpm rotational speed (see Figure 8). The oil clearly travels from the left to the right side of the gearbox through the planet axle bores. The most pronounced oil collections being on the right side of the carrier in the area of the planet right side bearings (zone B). Scavenging is quite poor (low white color density in zone C). Most oil scavenges from the strut right side (zone A). The test results indicated that both oil distribution and scavenge patterns are the function of rotational speed, rather than the oil flow rate. The series of the tests conducted prove that the PET technique is a powerful diagnostic tool capable of discovering the oil distribution patterns inside enclosed volumes, thus creating a solid background for the optimization of high power-density gearbox lubrication systems.

Acknowledgements

The authors wish to thank Textron Lycoming and Rolls-Royce plc for the support of this work and for permission to publish results.

References:

1. E.J. Hoffman, M.E. Phelps and S.C. Huang, "Performance Evaluation of a Positron Tomograph Designed for Brain Imaging", J. Nucl. Med. 24, 245-257, (1983).
2. J.E. Bateman, J.F. Connolly, R. Stephenson, G.J. Tappern and A.C. Flesher, "The Rutherford Appleton Laboratory's Mark I Multiwire Proportional Counter Positron Camera", Nucl. and Meth. 225, 209-231, (1984).
3. M.R. Hawkesworth, M.A. O'Dwyer, J. Walker, P. Fowles, J. Heritage, P.A.E. Stewart, R.C. Witcomb, J.E. Bateman, J.F. Connolly and R. Stephenson, "A Positron Camera for Industrial Application", Nucl. Instr. and Meth. A253, 145-157, (1986).
4. P.A.E. Stewart, J.D. Rogers, R.T. Skelton, P.L. Salter, M.J. Allen, R. Parker, P. Davies, P. Fowles, M.R. Hawkesworth, M.A. O'Dwyer, J. Walker and R. Stephenson, "Positron Emission Tomography - a New Technique for Observing Fluid Behaviour in Engineering Systems", in: Non-destructive Testing: Proc. 4th European Conf. London, September 1987. (J.M. Farley and R.W. Nichols, eds.), Vol. 4, pp. 2718-2726, Pergamon Press, Oxford.
5. M.A. O'Dwyer, M.R. Hawkesworth and J. Walker, "Aspects of the Application of Positron Emission Tomography to Engineering Studies: Drawing Overlays and Correction for Photon Attenuation", Nucl. Instr. and Meth. A273, 898-903, (1988).

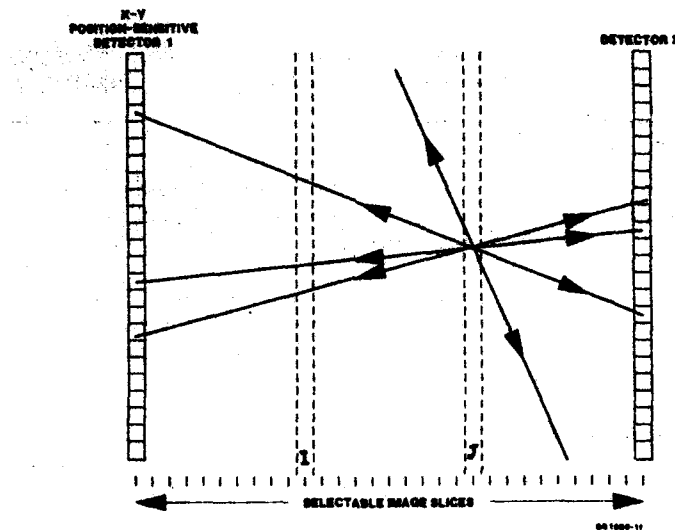


Figure 1. Illustration of the basic principle underlying the production of three-dimensional images in Positron Emission Tomography. A strong sharp image is forming in the tomograph J, which actually contains a point source.

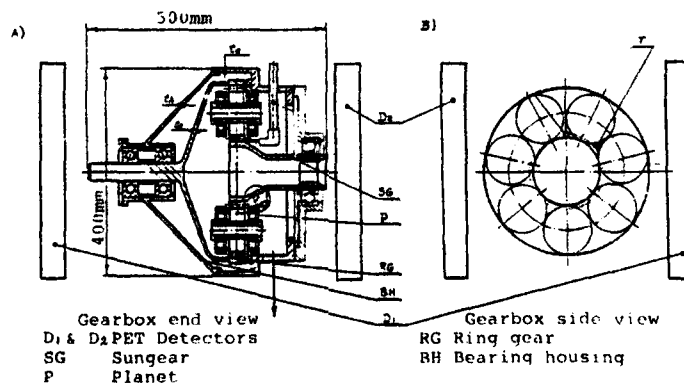


Figure 2. Schematic representation of the gearbox test rig showing the position of the gamma ray detectors for the end (left) and side (right) views studies.



Figure 3. Photograph of the gearbox test rig with the gamma ray detectors aligned at opposite ends of the gearbox shaft in preparation for the dynamic tests.

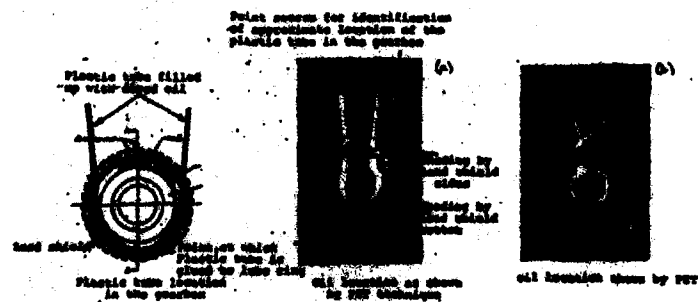


Figure 4. Illustration of the basic feasibility test that reveals (right (a) and left (b)) the location of a filled with radiolabelled oil plastic tube, which has been glued to the lube ring.



Figure 5. End elevation of the lower region of the stationary gearbox with oil draining under gravity. The figure illustrates the need to overlay the tomograph (a) with a simplified drawing of the gearbox (b) to aid interpretation.

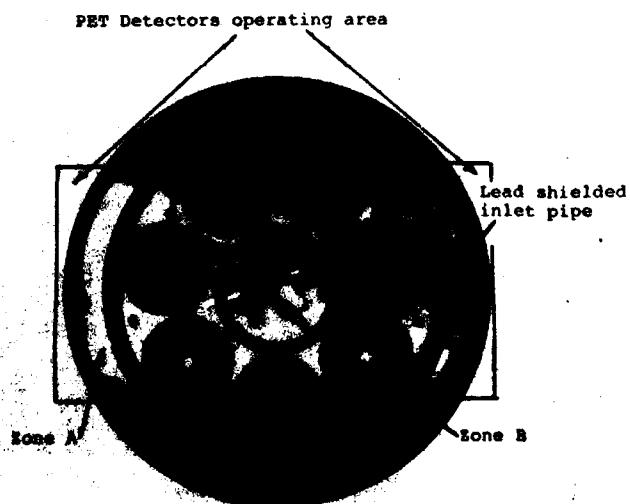


Figure 6. Oil collection pattern in the gearbox at 10,000RPM and an oil flow rate of 2,900PPH. The gearbox end view from the fan side of the cross section through the planet centerlines.

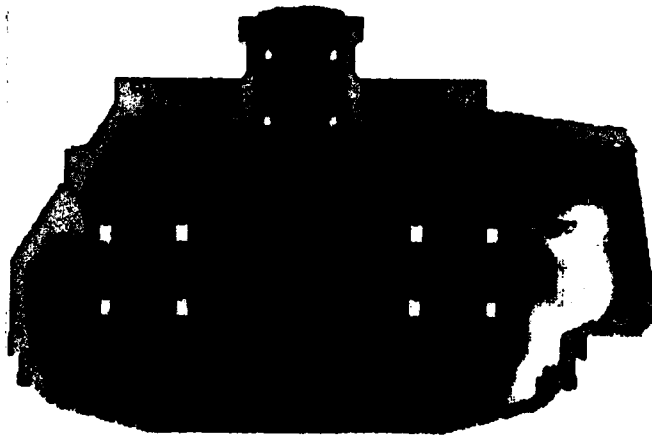


Figure 7.

The centerline tomograph with a gearbox overlay showing oil collection at the top of the "6 o'clock" drain strut at 5,000RPM and an oil flow rate of 2,900PPH.

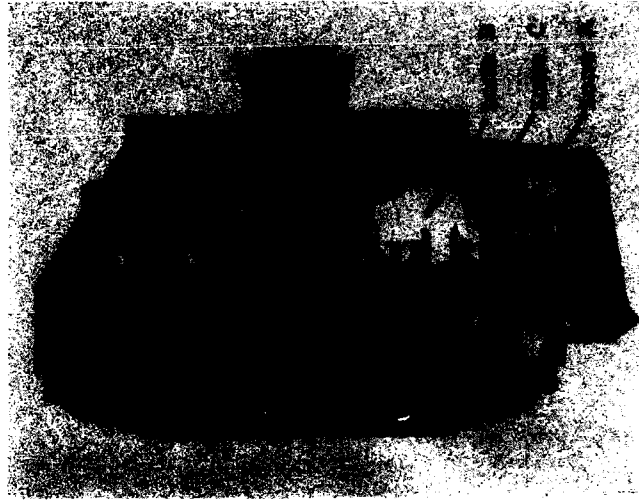


Figure 8.

The centerline tomograph with the gearbox overlay showing an oil build at the planet axle exits at 10,000RPM and the oil flow rate of 2,900PPH.

IMPACT OF MICROFILTRATION ON SPECTROMETRIC OIL ANALYSIS

Costandy S. Saba
University of Dayton Research Institute
300 College Park
Dayton, Ohio 45469-0001

Abstract: A 7-gallon oil capacity filtration test rig was designed and built to study the effect of a 3-micron filtration on spectrometric oil analysis. Several used oil samples were filtered and the wear debris in the pre-filtered and post-filtered samples was studied using ferrography and its particle size distribution was determined using other filtration techniques. Several spectrometers were used to evaluate the impact of fine filtration on Spectrometric Oil Analysis Program. The data will demonstrate the effect of fine filtration on particle size and concentration as well as the spectrometer response. The results show that the 3-micron filter is very efficient in removing particles above 3 microns from the main stream of lubricant.

Key Words: Ferrography; fine filtration; microfiltration; particle size distribution; spectrometric oil analysis

Introduction: Introducing fine filtration in lubrication systems may be beneficial in reducing the amount and size of wear debris, minimizing three-body wear and increasing the time between oil changes. However, the impact of using fine filtration (3-10 micron) in aircraft lubrication systems is of primary concern here because it removes larger size wear particles from the main stream of lubrication systems. Since wear particles carry within them important information about the health of oil-wetted parts, their removal through filtration may result in losing valuable information about engine wear. Another factor of concern is the effect of fine filtration on the threshold values already established for the Spectrometric Oil Analysis Program (SOAP). The U.S. Military Services rely on these guidelines to determine the health of their operating engines. Any change within the lubrication system such as filtration could have an impact on the analytical results and the present threshold values and guidelines may have to be revised.

Within the last decade ultrafine filtration has been introduced into several new engines by retrofitting micron size filters into these engines. The primary objective is to extend component life by reducing the amount and size of wear debris in the lubrication system. The development of the first known 3 micron absolute oil filter for the T53 gas turbine lubrication system is described by Lynch and Cooper.¹ The filter was tested from approximately 300 hours without clogging. Its use provided a cleaner lubrication environment, longer oil drains and decreased abrasive wear. As a result of this project a more extensive testing program for this filter was² established at Fort Rucker in 1978 for the Bell UH-1/AH-1 helicopters.

Wansong³ deals with the maintainability benefits of 3 micron filtration on the General Electric T700 engine which powers the H-60 series and AH-64 Helicopters. This is the first production engine that incorporates 3 micron lube oil filters from its inception.

Since analysis for wear debris has proven to be a valuable diagnostic tool for determining the health of an engine, the use of fine filtration would raise an important question as to the effectiveness of spectrometric oil analysis due to the filter's "removal" of debris detectable by the spectrometer. Therefore, one of the main objectives of this task was to determine the impact of microfiltration on Spectrometric Oil Analysis Program (SOAP). In this work, a microfiltration test rig was designed and built during the first phase of this program. Six different oil samples were filtered through the 3 micron filter. The wear debris was characterized in the pre-filtered and post-filtered samples and the particle size distribution was determined. Spectrometric oil analysis was also performed to evaluate the impact of microfiltration on SOAP.

Test Rig Assembly: The microfiltration test rig was built on a rolling bench assembly. The high pressure gear pump with constant speed drive motor and the scavenger pump were installed at the lower level of the rolling bench assembly. The schematic in Figure 1 shows the configuration (not exact dimensions) of the actual construction of the rig including valves, flowmeters, pumps, thermocouples, pressure transducers, test filter and reservoirs. For some of the samples wear metal produced from a wear test device was used.

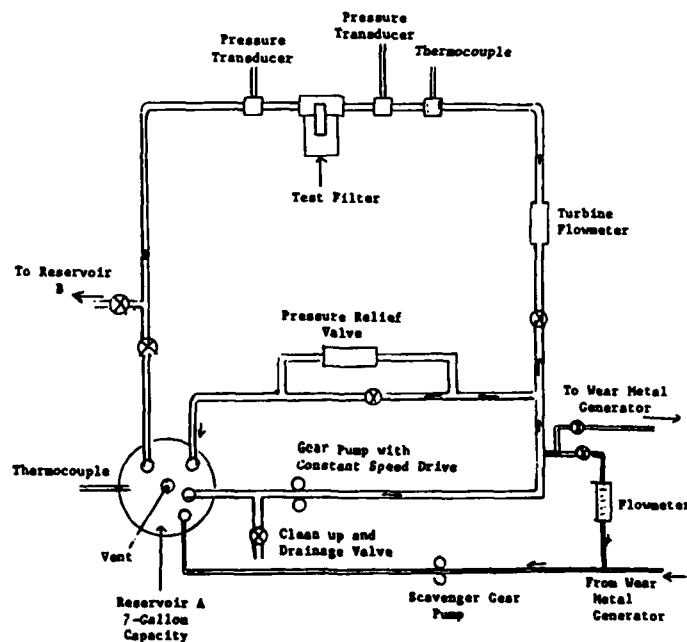


Figure 1. Schematic of the Microfiltration Test Rig

Wear Metal Generator: Wear metals were generated using the pin-on-disk, gear and four-ball wear test configurations. The particle size distributions were determined for the above wear debris from the three different tests using a filtration technique. Aliquots of the oil sample containing the wear debris were filtered through 0.4-, 1-, 2-, 3-, 5-, 8-, 12-micron Nuclepore membranes. A 2-g aliquot of the oil sample was diluted with pentane prior to filtration. A total of 10 grams were filtered for each filter pore size. Pentane was allowed to evaporate and the remaining oil (filtrate) was analyzed for total Fe content using AA and the acid dissolution method.⁴ The particle size distribution of particles indicates that the pin-on-disk wear test produced the smallest size particles while the gear test produced the largest particles. Initial filtration using the test rig will be performed using the wear debris generated from the pin-on-disk wear test.

Test Lubricants: Table 1 describes the six oils used in the microfiltration test rig. Used engine oils as well as fresh MIL-L-7808 oil were doped with wear metals generated from a pin-on-disk wear test. Unless otherwise mentioned, each sample was filtered four times and the nomenclature of the pre-filtered and post-filtered samples for each pass are described in Table 2.

Microfiltration Testing: Table 3 reports typical parameters monitored during each test of the microfiltration test rig operation. Microfiltration study of all six samples is described in detail elsewhere.⁵ Only Test No. 2 is described here to illustrate the various analyses performed on the pre- and post-filtered samples. Approximately 6 gallons of Qual-11E (MIL-L-7808) was doped with 1.2 g of Fe wear debris prior to filtration testing. The Fe wear was collected from several pin-on-disk wear tests using 1018 steel specimen. The pin-on-disk wear sample was sonically agitated and vigorously handshaken prior to addition to the rig's oil tank (A). The oil in the rig was allowed to circulate in the bypass mode for 30 minutes at 100°C. Approximately 300 mL (Sample A-1) was sampled before filtering at the sampling valve. The oil was allowed to pass once through the rig's 3 micron filter and was collected in a 7-gallon container (Tank B). It took approximately 15 seconds to filter 6 gallons of oil at 18.7 GPM. A 300-ml aliquot (A-2) was taken from the container (Tank B) immediately after filtration. Similar size aliquots were taken before and after filtering for the second and third passes. These samples were analyzed to determine the capturing efficiency of the rig's 3 micron filter and the particle size distribution of the wear particles.

Spectrometric Analysis: Samples taken before and after microfiltration were analyzed for iron wear debris using atomic absorption (AA), atomic emission (AE) and acid dissolution method (ADM). Analytical results are illustrated in Figure 2. The acid dissolution method data shows a significant amount of debris was captured by the filter after the first pass (55%). However, a smaller amount of wear debris was captured in the second (22%) and third pass (5%). Similar trending in direct AA and AE analytical results were

TABLE 1
DESCRIPTION OF MICROFILTRATION TEST FLUIDS

Test No.	Description of Test Fluid
1	Qualification No. 11E (MIL-L-7808), containing pin-on-disk wear metal generated from Falex wear test of O-86-2.
2	Oil from Test No. 1, with additional pin-on-disk wear metal.
3	Used MIL-L-7808 lubricant from a test stand J57 aircraft engine.
4	Qualification No. 05A (MIL-L-23699), with wear debris taken from engine simulator.
5	Used 10W30 weight automotive lubricant, containing visibly large amount of debris.
6	Used MIL-L-23699 lubricant from T56 aircraft engine gearboxes.

TABLE 2
DESCRIPTION OF NOMENCLATURE OF MICROFILTRATION TEST SAMPLES

Test Sample	Description
A-1	Pre-filter, first pass
A-2	Post-filter, first pass
B-1	Pre-filter, second pass
B-2	Post-filter, second pass
C-1	Pre-filter, third pass
C-2	Post-filter, third pass
D-1	Pre-filter, fourth pass
D-2	Post-filter, fourth pass

TABLE 3
PARAMETERS MONITORED DURING THE MICROFILTRATION
TEST RIG OPERATION

	1st Pass	2nd Pass	3rd Pass	4th Pass
Flow rate (GPM)	18.5	18.5	18.4	18.5
P_1 (psi) ^a	26.3	26.2	26.7	26.5
P_2 (psi) ^b	10.4	10.7	10.7	10.9
Tank Temp (°C)	102	102	101	100
Line Temp at Filter (°C)	101	102	101	100

^a P_1 = Pressure upstream of filter; ^b P_2 = Pressure downstream of filter

obtained for the filtered and unfiltered samples of the three passes but with lower values than the ADM. However, it is clearly shown that the 3 micron filter removes the large particles of wear debris after the first pass and that the amount of Fe in the filtrate remains constant except for B-1. Possible cross contamination from the lines and pump could have contributed to this increase in Fe.

Particle Size Distribution: The particle size distribution (PSD) was determined for the unfiltered and filtered samples in order to determine the effective particle size of the filter. The effective particle size of the filter is the particle size that is larger than the pore size of the filter. Therefore, wear particles with sizes larger than the effective size of the filter will be captured by the filter. Figure 3 shows the PSD for the pre- and post-filtered samples of Test No. 2 using ADM, Portable Wear Metal Analyzer (PWMA) and AE. Again it is seen that the microfiltration test rig filter is effective in retaining particles larger than 3 micron.

The PSD as shown by the ADM curves indicate that this sample has smaller particles than Test No. 1 sample. For this reason microfiltration did not impact the AA results (Figure 2) but differences are still seen by the AE, PWMA and ADM.

Ferrographic Analyses: Analytical ferrographic analyses showed the debris to contain a major quantity of small normal wear particles and minor quantities of larger severe wear and nonmetallic particles and fibers. After the first pass, the debris in all subsequent samples consisted of small normal wear and some nonmetallic debris. Optical density readings and L/S (ratio of large to small particles) values given in Table 4 show that L/S values did not change after the first pass. The DR Ferrograph data agreed with the analytical ferrograph.

TABLE 4

OPTICAL DENSITY READINGS OF ANALYTICAL FERROGRAMS
(1mL and Diluted Samples)

Sample	Entry	% Area Covered - Incident Light Ferrogram Position					L/S ^a
		50 mm	40 mm	30 mm	20 mm	10 mm	
A-1 (Pass 1 Before Filter, 0.1 mL Sample)	46.9	27.0	14.0	10.3	9.3	7.6	1.74
A-1 (Pass 1 Before Filter, 0.05 mL Sample)	31.4	21.2	8.7	7.1	6.7	9.3	1.48
A-2 (Pass 1 After Filter, 1 mL Sample)	55.1	53.8	48.9	39.2	34.3	34.0	1.02
A-2 (Pass 1 After Filter, 0.1 mL Sample)	17.0	14.5	9.5	7.4	7.0	9.1	1.17
B-1 (Pass 2 Before Filter, 0.1 mL Sample)	28.2	21.2	17.5	13.6	15.8	15.4	1.37
B-2 (Pass 2 After Filter, 0.1 mL Sample)	11.6	17.6	11.4	12.0	5.7	7.6	0.66
C-1 (Pass 3 Before Filter, 0.1 mL Sample)	16.0	14.2	9.2	6.3	6.8	13.6	1.13
C-2 (Pass 3 After Filter, 0.1 mL Sample)	8.7	10.1	7.2	9.1	8.2	14.9	0.86

^aL/S-Ratio of large particles (entry position) to small particles (50 mm position)

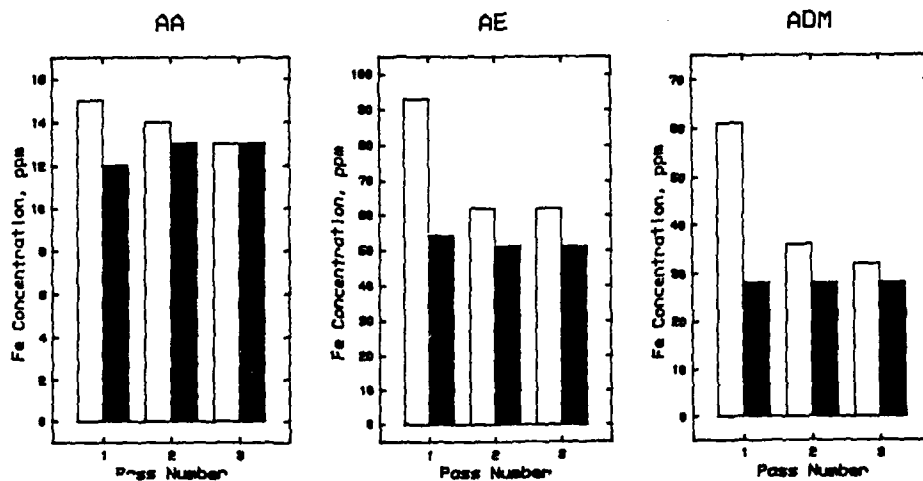


Figure 2. Iron Concentration of Pre- and Post-filter Samples for the First, Second and Third Passes of Microfiltration Test No. 2 Using AA, AE and ADM; □ = Pre-filter, ■ = Post-filter (MIL-L-7808 Oil from Test No. 1 with Additional Pin-On-Disk Wear Debris)

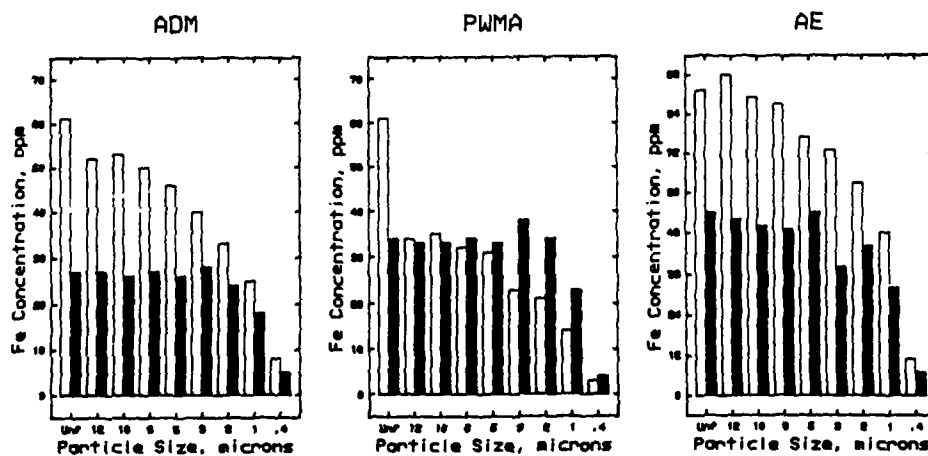


Figure 3. Particle Size Distribution of Iron Wear Debris in Pre- and Post-filter Samples from Microfiltration Test No. 2 Using ADM, PWMA and AE; □ = Pre-filter, ■ = Post-filter

Correlation of Microfiltration Testing: The correlation of all microfiltration test data is shown in Figures 4 thru 6. Figure 4 shows the correlation of percent iron having particle size greater than 3 microns with percent of iron captured by the MFR 3 micron filter, the percent decrease in L/S values using the Analytical Ferrograph and percent decrease in L/S values using the DR Ferrograph with the iron analyses being made by ADM for the six filtration tests. Very good correlation is shown between the percent iron removed by the 3 micron filter and the theoretical value which should have been removed based on ADM/particle size analyses. The L/S values obtained using the Analytical Ferrograph gave good correlation between the percent change of L/S values with percent iron above 3 microns but showed a small reversal for Tests No. 3 and No. 5 which contained very few large particles. No correlation is shown for the percent iron above 3 microns and percent change in L/S values using the DR Ferrograph.

Figure 5 shows the correlation of percent iron having particle size greater than 3 microns with percent of iron captured by the MFR filter and percent change in Analytical and DR Ferrograph L/S values when the iron analyses were conducted using AE. This data shows that correlation still exists between the percent iron removed by the MFR filter versus percent iron above 3 microns. However, when using AE analyses, a shift is shown as the percent particles above 3 microns is increased. This is due to the decrease in AE sensitivity (detector response) for large particles. The L/S values obtained using the Analytical Ferrograph showed correlation between the percent change of L/S values with percent iron above 3 microns except for the samples having very few large particles. The data shown for the DR ferrograph using AE iron analyses is very similar to that obtained when using ADM with no correlation in DR L/S values with percent iron particles above 3 microns.

Figure 6 shows the correlation of iron having particle size greater than 3 microns with the percent of iron captured by the MFR filter and percent change in Analytical and DR Ferrograph L/S values when the iron analyses were conducted using the PWMA. Samples from Tests No. 4 and No. 5 were not investigated using the PWMA. The data shows similar trending for the all three parameters (% iron captured by MFR filter and the change in L/S values for the Analytical and DR Ferrographs) when the percent iron is determined using the PWMA. However, samples from Tests No. 2 and No. 6 show a small reversal in ranking relative to the percent of iron captured by the MFR filter based on ADM analyses.

Figure 7 shows the correlation of percent iron greater than 3 microns determined by ADM with percent captured by the MFR as determined by AE, PWMA and AA analyses. Data for the AE analyses is very similar to Figure 4 (a) except for a small decrease in percent particles captured by the MFR which is due to decrease in sensitivity of AE to increasing particle size for the samples containing large particles. The data for the PWMA analyses show similar trend as that for AE except for a reversal for Test No. 6. Data for AA analyses shows distinct bias against large particles which has previously been noted (Figure 4).

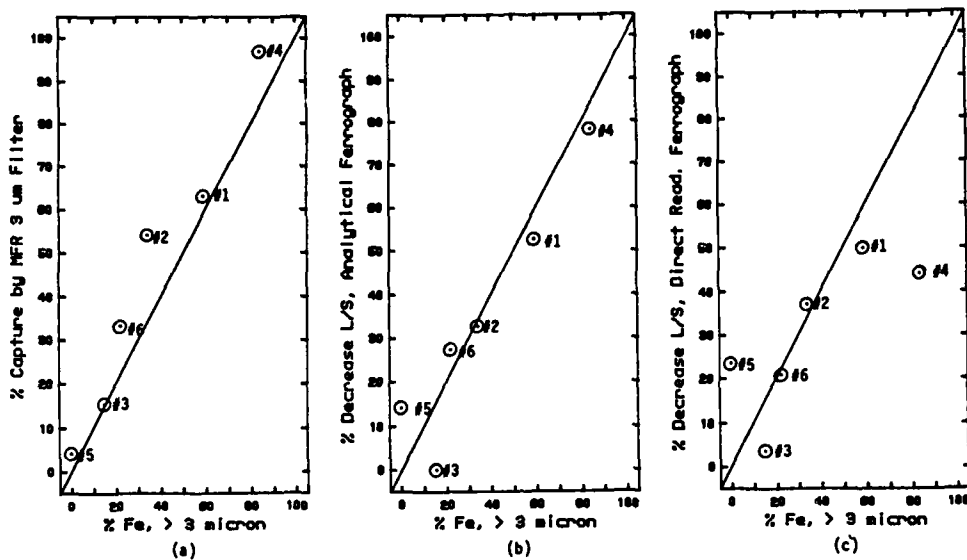


Figure 4. Correlation of % Iron Greater than 3 Microns with % Iron Captured by the MFR 3 Micron Filter and % Decrease in L/S Values Using the Analytical & DR Ferrographs with % Iron Being Determined by ADM (#1, #2, ... Indicate MFR Test No.)

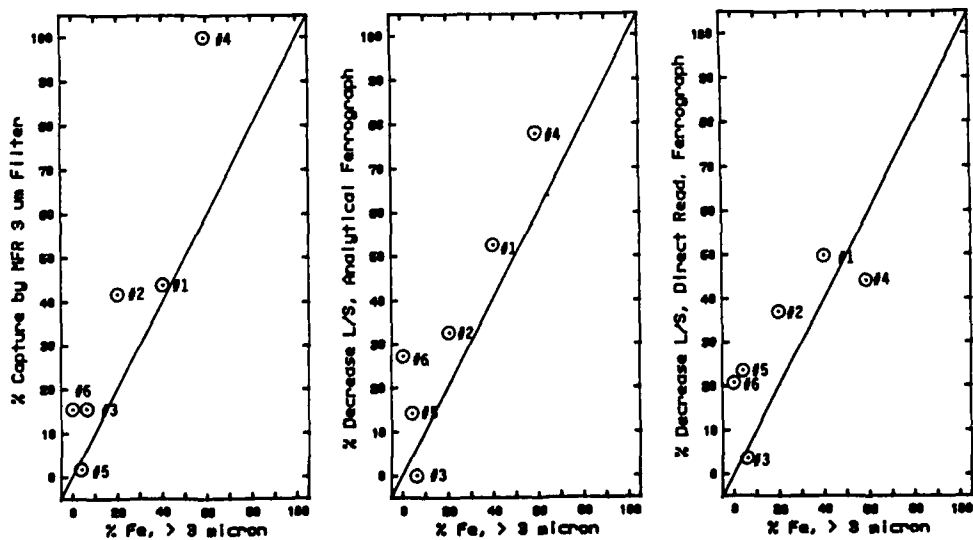


Figure 5. Correlation of % Iron Greater than 3 Microns with % Iron Captured by the MFR 3 Micron Filter and % Decrease in L/S Values Using the Analytical and DR Ferrographs with % Iron Being Determined by AE (#1, #2, ... Indicate MFR Test No.)

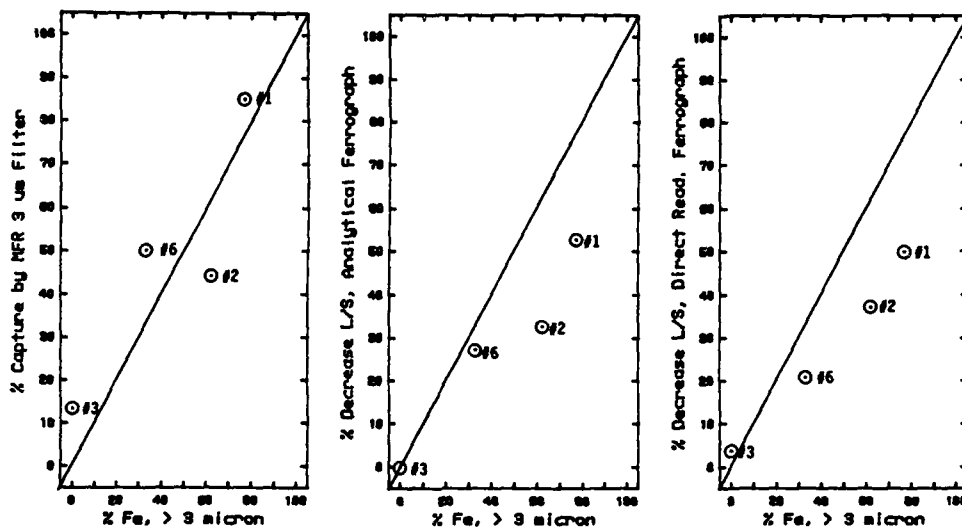


Figure 6. Correlation of % Iron Greater than 3 Microns with % Iron Captured by the MFR 3 Micron Filter and % Decrease in L/S Values Using the Analytical and DR Ferrographs with % Iron Being Determined by the PMMA (#1, #2, ... Indicate MFR Test No.)

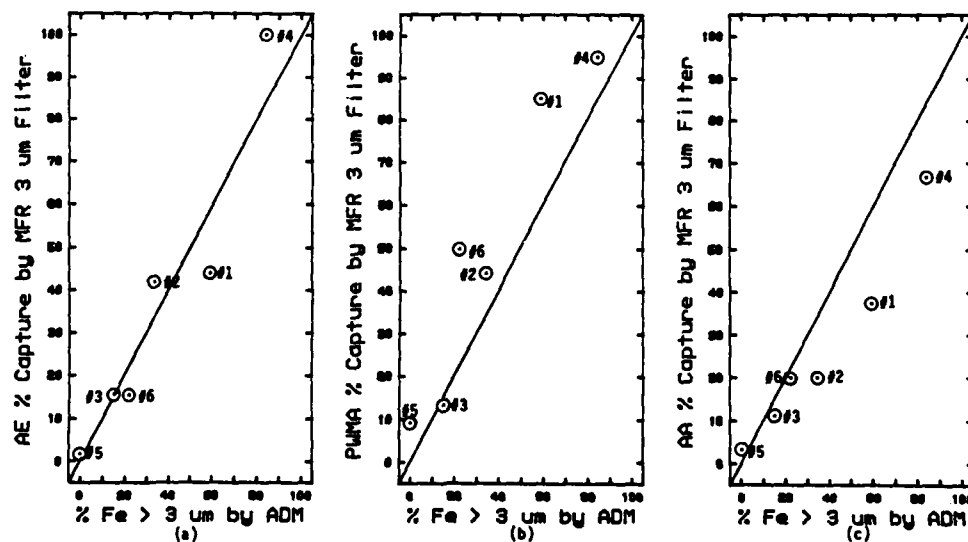


Figure 7. Correlation of % Iron Greater than 3 Microns Determined by ADM with % Iron Captured by the MFR as Determined by AE, PMMA and AA Analyses (#1, #2, ... Indicate MFR Test No.)

Conclusions: (a) Operating parameters monitored during the six tests indicate that microfiltration can be used in lubrication systems where different types of oils are used such as Mil-L-7808 and MIL-L-23699.

(b) Impact of microfiltration on SOAP cannot be fully identified based on microfiltration of limited number and type of samples used. However, the results of this study showed that SOAP threshold values may be influenced by the use of microfiltration, especially in samples with particle size >3 micron.

(c) Spectrometric methods also revealed that the level of contaminants after the first pass (even after one hour of recycling the oil at about 18 GPM, Test No. 4) remained constant.

(d) Spectrometric methods showed that the efficiency of 3 micron absolute filtration is almost 100% in removing iron wear debris larger than 3 micron. Efficiency for non-wear debris was not determined.

(e) Comparative analytical techniques showed that SOAP instruments (AA and AE) were able to detect significant changes in the concentration of wear debris after the first pass through the 3 micron absolute filter for samples containing substantial amount of Fe debris greater than 3 micron. However, analytical methods including AA and AE showed no change in concentration for the first and subsequent passes for samples containing Fe wear debris less than 3 micron provided the original concentration was not altered.

Acknowledgement: This work was sponsored by the Aero Propulsion and Power Laboratory, Wright Research and Development Center, Air Force Systems Command, Wright-Patterson Air Force Base, OH 45433-6563 under Contract No. F33615-85C-2507.

REFERENCES

1. Lynch, C.W. and Cooper, R.B., "The Development of a Three-Micron Absolute Main Oil Filter for the T53 Gas Turbine," ASME Journal of Lubrication Technology, 93, p 430 (1971).
2. Tauber, T., Hudgins, W.A. and Lee, R.S., "Oil Debris Assessment and Fine Filtration in Helicopter Propulsion Systems," Oil Analysis Workshop-Symposium, Pensacola, Florida, May 1983.
3. Wansong, J.F., "T700 Engine-Designed for the Pilot and Mechanic" Presented at the 39th Annual Forum of the American Helicopter Society, May 9-11, 1983.
4. Kauffman, R.E., Saba, C.S., Rhine, W.E. and Eisentraut, K.J., "Quantitative Multielement Determination of Metallic Wear Species in Lubricating Oils and Hydraulic Fluids," Anal. Chem., 54, p 975 (1982).
5. Saba, C.S., Smith, H.A., Keller, M.A., Jain, V.K. and Kauffman, R.E., "Lubricant Performance and Evaluation," Final Technical Report AFWAL-TR-89-2008, April 1989.

SUMMARY OF NEW TECHNIQUES TO IMPROVE THE ABILITY OF EMISSION SPECTROSCOPY TO DETECT LARGE WEAR PARTICLES IN LUBRICATING OILS

Malte Lukas & Daniel P. Anderson
Spectro Incorporated
160 Ayer Road
Littleton, MA 01460

ABSTRACT: Machine condition monitoring through oil analysis is a proven and cost-effective maintenance management technique. Periodically, however, the ability and the need of the analytical techniques to detect large wear particles is questioned. Today there is general consensus as to the maximum wear particle size capability of atomic emission spectrometers (AES) and atomic absorption spectrometers (AAS), but few agree on the alternatives to improve them.

This paper discusses three techniques that can be used to improve the ability of optical emission spectrometers to detect and quantify large wear particles in lubricating oil. They are the "Single Spark," "Ashing Rotrode" and "Acid Digestion Differential" techniques.

The single spark technique is based on an atomic emission spectrometer readout system that stores the intensity of individual excitation sparks for each element and presents the data as a particle size distribution. The system can operate in real time and provide information on each analysis, or the output can be suppressed and the user alerted only if wear particles exceed a preset size limit. Test data has shown an ability to detect and identify wear particles up to 40µm in size.

The ashing rotrode technique is based on a sample introduction and analysis system in which the oil sample is deposited on a graphite electrode, then resistively heated to desolvate the oil matrix. The desolvated matrix is subsequently excited by a pulsed D.C. arc and the spectra is analyzed by a polychromator. This technique minimizes matrix effects, enhances spectral sensitivity, and greatly improves detection of large wear particles.

The acid digestion differential technique is based on two analyses of the same oil sample. The sample is analyzed with and without acid to dissolve wear particles. The difference in the two readings indicates the presence of large wear particles.

All three techniques discussed in this paper improve the ability of spectrometric techniques to detect, quantify and identify wear particles. Capabilities and limitations of each are discussed. The technique of choice varies with the requirements and philosophy of the analytical laboratory.

KEY WORDS: oil analysis, wear metal particles, ICP, inductively coupled plasma, atomic emission spectrometer, AES, atomic absorption spectrometer, AAS, rotating disc excitation, RDE, single spark, ashing rotrode, acid digestion

INTRODUCTION: Many excellent reports and articles have been written on the subject of oil analysis and its historic evolution. Simply stated, oil analysis is a diagnostic maintenance tool used to detect and quantify wear metals and contaminants in the lubricant of oil wetted systems. It is based on the fact that a representative sample of lubricant, when periodically analyzed, provides important information on the condition of the wearing surfaces. It is a test that helps to determine whether a mechanical system is in a normal wear mode, or whether a potentially serious problem exists.

Wear particles are generated as a result of friction and the continuous wearing away of contacting surfaces. They enter the lubricant in the form of metallic particles from submicrometer to millimeter in size. Although present day oil analysis enjoys a high rate of success, existing emission spectrometric techniques are blind to large wear particles [1,2]. The particle size limitation varies with the analytical technique but general agreement places it at particle sizes in the range of 5 to 10 micrometers [2,3].

The particle size limitation of spectrometric techniques was first identified and openly discussed in great detail at an oil analysis symposium in 1978 [1,2]. Since that time, several studies have been done on the subject. Unfortunately, this phenomenon suffers from inadequate public relations and the analytical size limitation of atomic emission spectrometers seems to have been rediscovered about every two years since then.

This paper presents several methods that have been developed over the last ten years to improve the large particle detection capabilities of emission spectrometers. The ultimate goal is to detect the relatively small percentage of failures missed by routine spectrometric oil analysis techniques.

DEFINITION OF THE PROBLEM: Detection of large particles by atomic emission spectroscopy is influenced by a number of factors [4]. The most important factors are described below.

1. **Representative Sample** - If a system is in a severe wear mode and generating large wear particles, the oil sample taken to the laboratory for analysis must contain a representative quantity and size distribution of particles. The size of the sample and good sample taking technique can be an important factor. Likewise, the sample must be vigorously shaken to resuspend particles before measurements are made in the laboratory.
2. **Excitation Parameters** - The type of excitation influences the particle size detection capability of spectrometric techniques. Excitation power to dissociate a particle is the key factor. However, the hottest source, an inductively coupled plasma (ICP), is limited by short sample residence time in the plasma. Depending on composition, particles may not be in the plasma long enough to dissociate and vaporize. For the rotating disk electrode (RDE) method, an arc source has better efficiency for certain elements, but for others, a spark source is preferred.
3. **Oil Viscosity** - For the RDE method, the viscosity of the oil has an effect on the quantity of the sample reaching the excitation process and thus the quantity of wear particles carried with it. This is further influenced by the porosity of the disc electrode. Viscosity is less of a factor with AAS or ICP-AES since most oil samples must be diluted prior to analysis, eliminating viscosity as a major variable.
4. **Morphology of Wear Particles** - The shape of a particle has an effect on the efficiency of the spectrometric technique. For example, rubbing wear particles have a length to thickness ratio of about 10:1. Powdered metals are often more-or-less spherical. If both types are described by their major dimension, spherical particles of the same dimension as wear particles will be more difficult to excite.
5. **Lubricant Composition** - It has been shown that the efficiency of the analytical technique varies between hydrocarbon oils and ester oils [1].
6. **Quantity of Sample Introduced into the Excitation Process** - The ability to measure large wear particles presumes that they are present in the small quantity of sample that is actually excited. For a typical 1 ml oil sample, 100% of it is subjected to analysis with the ashing technique (discussed in this paper), less than 50% for the RDE method and only a few percent for the ICP method. If there are only a few large particles present

per milliliter of sample, the probability of detecting those particles is thus greatest for the ashing technique.

7. Method of Sample Introduction - In the ICP method, the sample is nebulized to form an aerosol. By the time the aerosol reaches the plasma, the droplet size is very fine, typically less than 5 μm . Consequently, wear particles larger than 5 μm have no chance of being detected.

8. Standard Samples for Particle Size Investigations - A recurring problem in experimental work with wear particles is obtaining oil samples which contain wear particles of defined sizes. In some of the work described below, powdered metals were purchased, separated according to size with a sonic sifter and nuclepore filters at 5, 10 and 20 micrometers to obtain separate filtrates with known maximum particle size. These powders were subsequently mixed, by weight, with MIL-L-7808 or MIL-L-23699 synthetic lubricant. The particle size distributions were then verified using a particle counter and by scanning electron microscopy.

Any new method to improve the large wear particle detection capabilities and efficiency of the AES techniques must address many of the above influencing factors. Several such methods are described below.

SINGLE SPARK: The single spark technique is not a new development, it is a new application for an existing spectrometer data readout system [5]. It is based on the principle that if metallic particles are present in a fluid and are excited with a single arc or a spark, the intensity of light emission will be proportional to the size of the particle.

A single spark system can be used with almost any spectrometer. It takes the output from the photomultiplier tubes and utilizes fast integrators to store and quantify the intensities of up to 2,000 individual sparks for each element during an analysis. In a production environment, the actual data from such a system is not displayed during the analysis cycle. The spectrometer provides normal data readout in parts per million, and single spark data is used to provide an alarm or other type of indication if the intensity (particle size) for an element exceeded an operator adjustable threshold.

Raw data for a single spark system is in the form of an intensity distribution. Increasing intensity corresponds to larger particle size. Readout is available on a CRT, or on a printer for hard copy. A typical readout for one element is shown in Figure 1. The abscissa shows, from left to right, increasing intensity of individual sparks and corresponds to particle size. The scale can be calibrated to actual particle size. The ordinate corresponds to the number of sparks at each intensity. It is therefore a plot of particle size versus the number of particles at each size.

The single spark software has a menu to allow the user to select from a number of statistical variables such as total sparks, mean, median, integral, maximum, etc. Excitation source parameters can also be varied by the software to select either 60, 120 or 240 sparks per second. For the experimental work presented in this paper, 120 sparks per second was used with a total integration of 1,000 individual sparks. Therefore, analysis time for each sample was less than 9 seconds.

Analytical Results: Initial tests were performed with a conventional rotating disc sample introduction system. Oil samples, prepared to contain the various particle sizes were analyzed and very little, if any, difference was noted in the intensity readouts for samples with particles greater than 10 micrometers. These results reconfirmed one of the wear particle related shortcomings of the RDE technique, namely that there are large particle transport difficulties.

The single spark system is ineffective without an efficient sample introduction system. Experimental modifications to the sample introduction system were an immediate

focal point of additional work. To allow more of the metallic particles to enter the area of excitation, several techniques were tried including hollow counter electrodes to direct the sample onto the disc electrode, scalloped discs to "shovel" more of the sample into the excitation, and discs with varying porosity. These experiments led to a very simple and practical solution. Square electrodes were manufactured with a "trough" to contain and hold, for each analysis, the same quantity of oil sample. This solved the problem of carrying all of the sample into the arc. Furthermore, after a few minutes the porous graphite electrode absorbed the oil, leaving only the analyte.

In order to obtain a base level for the analytical data, the single spark signature for MIL-L-7808 without any metal particles was determined. In Figure 1 the intensities closest to the origin and in the first two decades were determined to be background signal. The background is similar for most elements and is attributable mostly to the electrodes themselves.

With an understanding of the background signal, the readout for oil samples with actual metallic particles is easier to understand. Figure 1 is a single spark signature for the analysis of 100 ppm chromium oil samples with metallic particles at <10, <20, and <74 μm in size.

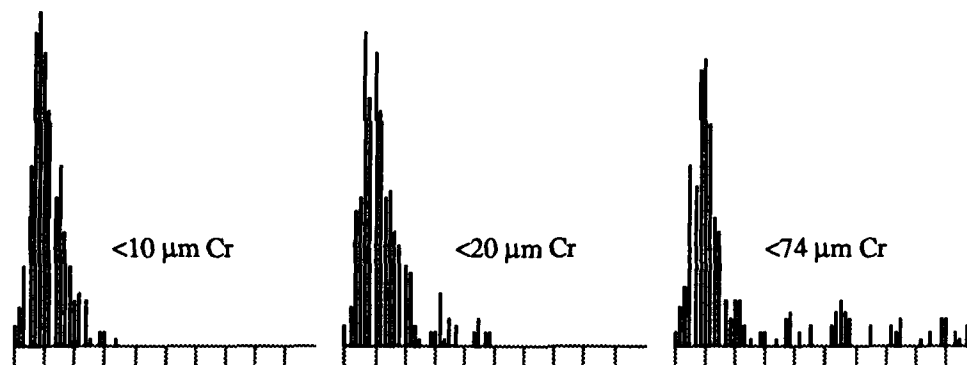


Figure 1. Single Spark Signature for Chromium Particles in Oil at Various Size levels.

The figures clearly show that there is an increase in the intensity distribution that corresponds to particle size. The background signal for chromium (figure 2) has all spark intensities within the first two decades. The sample with particles below 10 μm has spark intensities which extend well into the third and fourth decades. The 20 μm sample contains spark intensities over five decades. Finally the sample with particles up to 74 μm covers all decades with spark intensities.

All three samples were prepared to contain, by weight, 100 ppm of chromium. One would, therefore, expect that the integral of the intensities, which corresponds to normal ppm readout, to be the same. Although the integral was within experimental error for the samples with the smaller particles, it was only half as much for the sample with the particle distribution of up to 74 μm . Repeated analyses produced similar results. It is therefore probable that although some of the larger particles are excited by the spark and provide an intensity readout, many of the particles are too large to be completely volatilized.

The experiments were repeated for other elements, and similar single spark signatures depicting large particles were obtained thus demonstrating that with proper sample introduction, the single spark technique works well to identify large particles which are otherwise not detected.

A similar system, based on the same principle, was discussed by Kaufman [6] in the development of a multi-element data acquisition system. He demonstrated that by monitoring voltage buildups on integrating capacitors, the spectrometer could differentiate between dissolved wear species produced by normal wear modes and wear debris produced by abnormal wear modes. Qualitative particle size distributions and particle composition analyses were performed on metal powders prepared in MIL-L-23699 lubricating oil. As in the work described above, the efficiency of the spark source to fully vaporize large wear particles was also questioned. Nevertheless, the system was shown to have the potential to improve abnormal wear detection capabilities of oil analysis programs.

ASHING ROTRODE TECHNIQUE: Another method, the ashing rotrode technique, was also investigated toward improving the particle size detection capabilities of emission spectrometers. In this technique, the oil sample is deposited directly on a graphite electrode, then resistively heated to desolvate the oil matrix. The desolvated ash is then excited by a pulsed d.c. arc. The resultant spectra is analyzed by simultaneous AES. Preliminary experimental data shows that the the ashing rotrode technique improves detection of large wear particles, minimizes matrix effects and enhances spectral sensitivity.

The ashing rotrode technique was based on earlier work which had shown that manipulations to excitation source parameters and sample introduction systems will improve particle detection capabilities of AES. It had been determined that true improvements in detection capabilities were possible with slower disc electrode speeds, higher excitation potential, and by excitation of samples after the oil was absorbed into the pores of the electrode [4,5]. In developing a particle detection system, it was decided that the first step was to desolvate the oil matrix, followed by exposure of the analyte to an excitation plasma suitable for efficient vaporization of the elements of interest.

Preliminary work on this method showed that it was possible to quantitatively analyze wear particles up to 40 μm in size by manual and time consuming ashing techniques [7]. Through desolvation and concentration of analyte, the ashing rotrode technique could produce a limit of detection for most elements at the sub part per million level. This concept, coupled with further automation, led to the ashing rotrode system.

Description of The Ashing Rotrode: Preliminary research into the development of the ashing rotrode technique revealed that variations in specific density of individual graphite electrodes would produce inconsistent ash residue [8]. To minimize this effect, 12.5 mm diameter graphite stock was cut to lengths of 100 mm and machined such that 10 individual electrode surfaces of 5 mm in width were spaced 2.5 mm apart. This became the ten sample ashing rotrode as shown in Figure 2. The rotrode was then mounted horizontally between two chucks in the spectrometer's sample excitation chamber. The chucks were driven by a synchronous motor which rotates the electrodes and provides electrical contact to an ashing source.

The second graphite electrode is 6 mm in diameter and acts as the counter electrode and anode. It is mounted on a slide mechanism which moves parallel to the ashing rotrode. This permits the anode to be positioned over any of the ten electrode surfaces for sequential analysis of up to ten separate oil samples. An optical quartz fiber mounted on the slide mechanism follows the movement of the counter electrode and directs the light from the excitation process into a polychromator.

The procedure to ash and analyze an oil sample begins while the electrode is rotating with the deposition of 30 μl of oil with a Teflon tipped positive displacement pipet on the first lobe. When all 9 samples have been applied, the ashing current is automatically initiated and timing is controlled by a built in microprocessor. Typical ashing time for ten samples is 60 seconds. The analytical cycle is the same as in a normal RDE-AES and can be performed sequentially for each lobe, and immediately

after the ashing step. Analysis of each lobe takes 30 seconds during which time the electrode rotates one complete revolution.

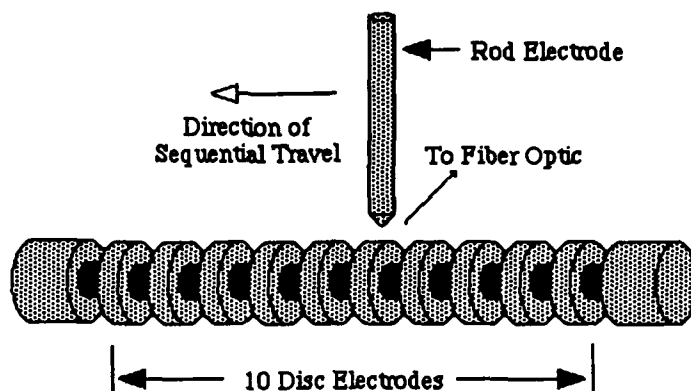


Figure 2, Ten Sample Ashing Rotrode and Counter Electrode

Analytical Performance: It was apparent from the outset that proper sample deposition techniques had to be developed in order to obtain good experimental data. The performance obtained with the ashing rotrode technique was excellent and can be summarized as follows.

1. **Detection Limit** - Initial data produced excellent detection limits. In most cases, the detection limits were an improvement over those of the conventional rotating disc technique. The detection limits also appeared to be a function of the quantity of wear particles on the electrode lobe, since it was possible to improve and vary them by adding more of the oil.
2. **Matrix Effect** - The ashing rotrode technique eliminates to a great extent the matrix effect cause by varying types of lubricants. A background correction system is therefore not required.
3. **Precision** - At times a precision of 2-3% RSD had been achieved, but an average precision is more in the vicinity of 4-5% RSD. The reason for this appears to be a lack of sufficient knowledge regarding variables, such as optimum ashing process and electrical contact of the electrodes. The type, grade and manufacturing process of the electrode has also shown to be a contributing factor.
4. **Accuracy** - The accuracy of the ashing rotrode on metallo-organic standards can be stated in general terms for most elements as 0.5 ppm, or 5% of the concentration, whichever is greater. The ashing rotrode, however, was not developed to analyze oil standards. It was developed to provide quantitative analysis of oil samples containing wear particles not readily detectable by existing instrumentation. For this reason, it is possible to provide analytical results on used oil samples not always consistent with other techniques. The technique was used as part of a study for the DoD Joint Oil Analysis Program, where it displayed good correlation to standard samples and those with additive concentrations in sub micron components. In used oil samples containing particles, the ashing rotrode always predicted higher concentration as compared to existing analytical techniques. This is to be expected if the technique is more efficient in detecting wear particles, but it is not entirely clear if all of the differences are due to actual wear particles alone.

The ashing rotrode technique has been proven to be an effective method to improve the large wear particle detection capability of analytical instruments. It has, however, also raised some additional questions which must be answered or explained before it is placed into routine service in an oil analysis laboratory.

ACID DIGESTION DIFFERENTIAL METHOD: It was recognized more than 10 years ago that in spite of the extensive application of spectrometers for oil analysis, no analytical procedure was available which satisfied all requirements in regard to speed of analysis, precision, accuracy, sensitivity, convenience of sample preparation and cost per analysis. Inductively coupled plasma (ICP) spectrometry was shown by Fassel, et al.[9] to be more capable in satisfying all of these requirements. However the ICP method, as routinely applied, has very poor particle sensitivity. An oil sample, diluted by solvent to lower viscosity, is nebulized to create an aerosol which flows through a spray chamber before reaching the plasma. The spray chamber removes all but the finest droplets by settling and impaction, so that the maximum droplet size reaching the plasma is approximately 5 μm . Consequently, particles in the sample larger than 5 μm have no chance of being detected.

Justification for Acid Digestion Differential Method: If spectrometric measurements are made as a function of time after an engine oil change, the wear metals concentration will continue to increase indefinitely, as shown in Figure 3, as long as clean make-up oil is not added to the engine. In fact, for spectrometric measurements to be meaningful, the time since the last oil change must be known since it is the increase in wear metals concentration during a given operating period that is of significance. Spectrometric data for aircraft gas turbine engines is a special case. Absolute maximum concentration levels apply to gas turbine engines because even though the oil in most gas turbine engines is not changed, the wear metals concentration reaches a maximum due to the frequent addition of make-up oil. Kjer [10] describes the mathematics of wear particle concentration for small particles, large particles and for topping-off.

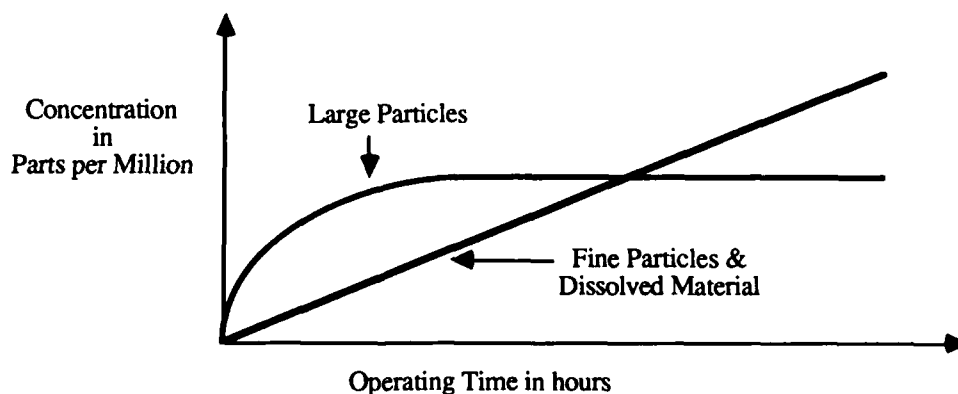


Figure 3. Particle Concentration as a Function of Time

From the foregoing discussion, it may be seen that the total metals concentration in a lubricating oil sample is the total of two components; the fine particle and chemically dissolved portion and the large particle portion. The concentration of the fine particle and chemically dissolved fraction continues to increase between oil changes, but the large particle fraction reaches a dynamic equilibrium concentration, wherein the contribution of generated wear particles is offset by the loss of large particles to filters, settling or comminution. The concentration of large particles is of the greatest interest in regard to abnormal wear, because the quantity and size of large particles increases substantially for many, and probably most, abnormal wear modes. Also, the contribution of the large particles to the total wear metals concentration is often a

much smaller fraction than the contribution of the fine particles and dissolved material [11].

For spectrometric analysis, then, to be as effective as possible at monitoring the condition of various equipment, especially in regard to providing the earliest possible indication of abnormal wear conditions, it is not sufficient to monitor only the total wear metals concentration by a particle size independent method. This is providing a method which met all desired procedural and analytical requirements existed.

Anderson [12] suggests that a differential method be considered, at least for critical equipment having a history of rapidly developing failure modes, wherein two measurements are made on each sample. An ICP spectrometer is recommended for this procedure because of its superior precision, accuracy and limits of detection. One measurement is made by directly introducing the sample to the plasma after diluting it with solvent by an appropriate ratio. This measurement gives the fine particle fraction. The second measurement is made using a particle size independent method to arrive at a total metals concentration. The difference between the two measurements is an indication of large particle fraction.

The large particle fraction is expected to remain within certain limits during trouble free operation, even as the lubricant experiences more operating time. Abnormal wear modes, filter clogging, contaminant ingestion, lubricant failure, etc, are expected to significantly increase the large particle fraction.

Analytical Results: Two series of oil samples were obtained from reciprocating engine test stands. Series A samples show no increase in the severity of wear during the course of the test as determined by ferrographic analysis. The quantity of large particles is approximately the same in all Series A samples. Ferrograms prepared for Series B samples show a substantial increase in the concentration of large particles as the test proceeds.

Each sample from Series A and Series B was heated, homogenized by shaking, and split into two portions. One portion was left as is, an acid digestion following the method of Kauffman, et al, [13] was performed on the other portion. All portions were weighed on an electronic balance, as was the acid and solvent (kerosene) added to each portion, so that concentration data could be accurately calculated. Each portion was then analyzed by ICP-AES so that two measurements were obtained for each sample as follows:

- 1) ICP-AES without acid digestion.
- 2) ICP-AES with acid digestion.

For Series A samples, little difference is obtained between measurements with and without acid digestion. Figure 4 shows progressively greater difference between the two methods for Series B samples.

The power of this differential acid digestion technique is that it is able to quantify the presence of large particles in situations where the concentration is increasing, as measured either by routine techniques or particle size independent techniques. In one case, Series A, there is no increase in large particles, only normal wear may be said to be ongoing, whereas in Series B, a progressive increase in wear severity is occurring. Without differential measurements, either case appears to show an increasing trend.

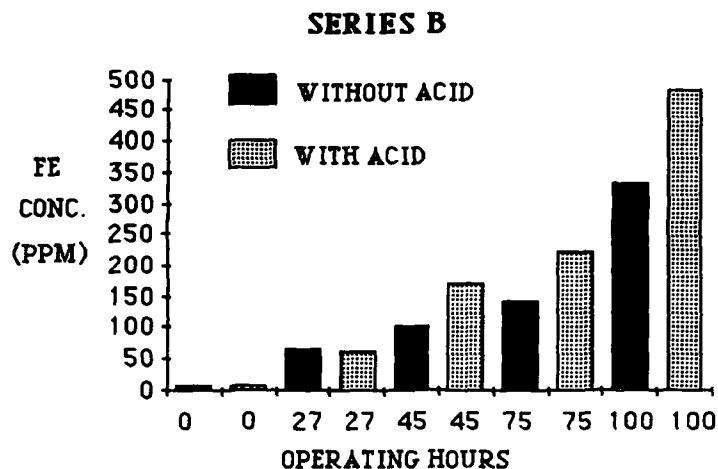


Figure 4- Fe results for Series B.

CONCLUSION: There is little doubt that the weakest link in the analysis of oil samples with today's modern spectrometers is the sample introduction system. This is true for the RDE technique and much more so for the ICP. Two methods which improve the RDE technique were discussed in this paper along with a more time consuming method for the ICP based on the dissolution of the wear particles.

During the last decade, the ICP has gained popularity in some applications for oil analysis where more precision is required. Development work continues on sample introduction systems based on the Babington nebulizer which has been shown to be clog free for the introduction of particle suspensions into flames [14]. One such sample introduction system, which has been optimized for the analysis of coal slurries, should also improve wear particle analysis efficiencies in oil samples. A series of tests to verify this will have to be conducted.

It has been shown that:

1. The single spark technique is very effective in detecting and quantifying large wear particles in oil samples. It will work with a standard RDE-AES spectrometer, however to be effective, the sample introduction system has to be modified.
2. The ashing rotrode shows the most promise as a separate analytical technique. It can be incorporated into a modified RDE-AES spectrometer, but additional laboratory work is required to fully understand its capabilities.
3. The acid differential technique can provide multi-element quantification of the presence large wear particles in lubricating oil samples. It is a two step method, because the particle size independent technique by itself does not necessarily provide the needed information about abnormal wear.

Although the wear particle size limitation of atomic emission techniques is periodically "rediscovered", it is now safe to say that methods exist which circumvent this so called limitation. This paper has shown three methods developed by the author's company and others that improve the particle detection capability to varying degrees. The overall efficiency of oil analysis can be improved if any of these methods are applied. The method of choice varies with actual requirements and the philosophy of the laboratory.

REFERENCES

- [1] Lukas, M., Giering, L.P., "The Effects of Metal Particle Size in the Analysis for Wear Metals using the Rotating Disc Atomic Emission Technique", Presented at the International Symposium on Oil Analysis, Erding, Germany, July 1978.
- [2] Eisentraut, K.J., Thornton, T.J., Rhine, W.E., Costandy, S.B., Brown, J.R., and Fair, P.S., "Comparison of the Analysis Capability of Plasma Source Spectrometers vs. Rotating Disc Atomic Emission and Atomic Absorption Spectrometry for Wear Particles in Oil: Effect of Wear Particle Size", Presented at the International Symposium on Oil Analysis, Erding, Germany, July 1978.
- [3] Rhine, W.E., Saba, C.S., and Kaufman, R.E., "Metal Particle Detection Capabilities of Rotating-Disc Emission Spectrometers", *Lubrication Engineering*, Vol. 42, No.12, p 755, 1986.
- [4] Rhine, W.E., Saba, C.S., and Kaufman, R.E. "Spectrometer Sensitivity Investigations of the Spectrometric Oil Analysis Program", NAEC Report 92-169 Naval Air Engineering Center, 22 April 1983.
- [5] Lukas, M., "Development of a Particle Size Independent Method for Wear Metal Analysis", Presented to the International Oil Analysis Symposium, Department of Defense, Pensacola, Florida, May 1983.
- [6] Kauffman, R.E. "Particle Size and Composition Analyses of Wear Debris Using Atomic Emission Spectrometry", *Lubrication Engineering*, Vol. 45, No.3, p 147, 1989
- [7] Gilbert, T.R., Sandoval, J.E., Yurko, R.J., "Direct Determination of Wear Metals in Used Lubricating Oils by Arc Emission Spectroscopy Using a Novel Rotating Disc Electrode", Presented at the 37th Pittsburgh Conference & Exposition on Analytical Chemistry and applied Spectroscopy, Atlantic City, New Jersey, March 12, 1986.
- [8] Yurko, R. J., Gilbert, T. R., and Sandoval, J. E., "Direct Analysis of Wear Particulates by the Ashing Rotrode Technique", *Proceedings of Condition Monitoring '87*, University College of Swansea, Wales, Pineridge Press, Swansea, Wales, U.K., 1987.
- [9] Fasel, V.A., Petersen, C.A., Abercombie, F.N., and Kniseley, R.N., "Simultaneous Determinations of Wear Metals In Lubricating Oils by Inductively Coupled Plasma Atomic Emission Spectroscopy", *Analytical Chemistry*, 48, pp 516-519, 1976.
- [10] Kjer, T.E., "Wear Rate and Concentration of Wear Particles in Lubricating Oil", *Wear*, 67, pp 217-226, 1981.
- [11] Taken in Part from, Anderson, D.P., "A Quantitative Method for the Determination of Large Particles in Lubricating Oil Samples Using ICP Spectrometer", Presented at the 1989 Condition Monitoring and Preventive Maintenance Conference, Atlanta, Georgia, May 1-4, 1989.
- [12] Anderson, D.P., "Condition Monitoring by Wear Metal Analysis Using ICP Spectrometry", *Proceedings of Condition Monitoring '87*, University College of Swansea, Wales, Pineridge Press, Swansea, Wales, U.K., 1987.
- [13] Brown, J.R., Saba, C.S., Rhine, W.E., and Eisentraut, K.J., "Particle Size Independent Spectrometric Determination of Wear Metals in Aircraft Lubricating Oils", *Analytical Chemistry*, 52, pp 2365-2370, 1980.
- [14] McCurdy, D.L., Fry, R.C., "Adaptation of the Slurry Nebulizer Technique of Solid Samples to Inductively Coupled Plasmas", Presented at 1985 Pittsburgh Conference and Exposition on Analytical Chemistry and Applied Spectroscopy, New Orleans, LA, February 27, 1985.

METHODOLOGY FOR IMPROVED DURABILITY

Chairman: Sudhamy Basu
The Scientex Corporation

REMAINING LIFE ASSESSMENT OF THERMAL POWER PLANT
COMPONENTS USING FRACTURE MECHANICS APPROACH

J.Pattabiraman and B.J.Sukanya
Tata Consulting Engineers
Bangalore, India 560 001

Abstract: The subject of residual life assessment of critical components of thermal power plants is becoming increasingly important in view of the techno-economic advantages of extending the useful life of an older power plant. The methodology of residual life estimation takes inputs from several interdisciplinary areas of plant engineering such as materials science, design, stress analysis, power plant operations, inspection (NDE) and destructive testing. Analytical estimates based on damage mechanics calculations provides a figure on the degree of damage undergone by a severely stressed zone in a critical component which confines itself to the crack initiation phase. It is acknowledged that there could be a significant amount of useful service life still left in components even with crack present in them. Fracture Mechanics recognises the presence of cracks in materials and drawing data from design, operation, stress analysis and inspection, provides two important practical guidelines to the plant operation: Firstly, by providing an advance warning indication on impending failures of critical parts by scientifically assessing the time required for the crack to propagate and grow to a critical size and secondly, in helping operator to identify those parameters which should be closely monitored, so that the crack growth rate is retarded and more service life could be extracted from such components.

This paper outlines a general methodology applicable to estimate useful service life left in critical components of thermal power plants like headers, drums, steam pipes, turbine rotors and casings, using fracture mechanics. Based on this, and keeping economics as well as safety in view, it is possible to decide on the alternative as whether to repair and continue operation or to repair and continue operation with a reduced inspection interval or to continue operation for a limited period till the planned replacement or retire forthwith.

Key words: Crack growth rate; critical crack length; clustering technique; creep fatigue; damage fraction; fatigue with hold time; fracture toughness; high temperature operations; inspection; life assessment methodology; stress intensity factor; thermal power plant.

Introduction: Thermal power plants have traditionally been built with an assumed normal design life of about 30 years after which the utilities are expected to replace older equipment with new to meet load growth requirements and to deliver power at a lower cost. However, the uncertainty in forecasting load growth, escalating construction costs, applicability of more stringent environmental standards and the life extension being a low cost (10-25%) alternative have considerably altered this approach. Utilities have recognised that potential life time for components in an existing plant may be far in excess of the

nominal design life owing to a number of factors that include use of minimum property in design, factor of safety in design, conservative data extrapolation, over estimation of oxidation effects, etc. With this trend towards operating power plant components far beyond their design lives, utilities need a scientific basis and a methodology for assessing the exhausted lives. The present day requirements demand that the materials used exhibit optimal performance, provide a long life, permit economy and at the same time ensure safety and reliability of components and systems. The early success of fracture mechanics in correlating fatigue crack growth in metals has led to a number of research efforts to study crack growth at high temperature where creep and environmental effects (corrosion for e.g.) which are time dependent interact with fatigue. Successful application of fracture mechanics for life estimation is possible for those components having a crack length of at least 1 mm and thickness at least 2.5 (K_{Ic}/\sqrt{YS}) and free from bulk damage. The basic data required are those of material property, plant operations, NDE and component geometry and these are discussed below. Utilising these data, using latest published information on fracture mechanics, a procedure is presented to estimate residual life.

Material Property Data: One of the major reasons for the uncertainty in life estimation is due to the non-availability of accurate material property data. The exposure of material to elevated temperature and corrosive environment leads to inservice degradation of mechanical properties. Therefore, it is important to get the present (latest) value of fracture toughness and other conventional mechanical properties of the degraded specimen. The value of fracture toughness and yield stress are required as a function of temperature. The critical crack size is a function of the square of fracture toughness. Errors in assessment of toughness could lead to large errors in computation of critical crack size and correspondingly errors in life estimation. Where measurement on actual sample is not feasible, the material properties available in literature could be used with a reasonable judgement using factors of safety to account for their inservice deterioration. The value of toughness at temperature below 850°C may be determined using a linear interpolation. For heat affected zones and weld metal, the Larson Miller stress temperature plots may be used in arriving at the property data.

Plant Operation Data : The pattern of operation along with data on number of operating hours, operating sequence, operating temperature and pressure should be obtained for both transients and steady state operations. Transients include start-ups, shut down, load changes and the number of occurrences of overspeed, excursions above the permissible temperature and pressure margins. The pattern of operation includes data on variation of operating parameters over time for all typical transients/steady state operation encountered.

Geometry Data: Geometry data can be obtained from design drawings or from physical measurement of components. Changes in dimensions of the component during the service should be arrived at by comparing the dimensions of the component "as built" vs "as observed" and any stress analysis should be carried out on the basis of "as observed" dimensions.

Inspection Data: The NDE techniques are powerful tools in detecting the size, shape and location of a defect. NDE techniques can be combined to compliment one another so that the operator is more confident of measurement of the flaw. Clustering technique can be applied to connect adjacent flaws so as to act as a single large flaw depending upon their size, the stress, temperature and material property. This process has to be repeated until no more linking of such flaws is possible. The clustering technique can be based on ligament yield/rupture model which assumes that once the ligament between adjacent indications yields, the ligament is no longer given any credit for load carrying ability and the two flaws are linked as a single large flaw.

Determination of Critical Regions: This is the first step involved in any life assessment methodology. The details of design construction and operating history are reviewed and a preliminary inspection is carried out. Potential sites for inspection includes elbows, transition in cross sections if any, areas adjacent to supports, seam welds, dissimilar weld etc. At welds, the location should be so chosen as to include the weld metals, heat affected zone, fusion line intersection between longitudinal and girth welds and the transition between heat affected zone and base metal. Maximum permissible stress (σ_p) and maximum permissible crack size (a_p) using the expressions given in Equation Set (I) should be computed. Stress intensity factor for the regions having stress greater than permissible maximum stress or crack size greater than permissible maximum crack length should be computed. Fracture Mechanics parameters like stress intensity factor, J Integral, and C_t parameter can be determined by using the expressions available in standard handbooks. The critical region is decided on the basis of high values of stress intensity factors corresponding to such regions.

Stress Analysis: Stresses generated due to various types of loading such as thermal, mechanical, self weight and pressure together with fluctuations in such loads have to be determined. It is not possible to calculate the temperature and stress distribution analytically through closed form solutions using elementary principles of heat transfer and elasticity in bodies with complex geometries. In such cases, finite element method needs to be adopted for stress and thermal analysis. Initially, elastic thermal stress analysis has to be performed. This includes calculation of transient and steady state temperature distributions for components. The next step is to use these temperature values as inputs to compute the thermal stresses. Components of stresses due to thermal, mechanical, pressure and centrifugal loadings both during transients and steady states are then determined along the three principal directions and combined appropriately directionwise. The principal stresses are determined and the numerically largest of these is of importance since the crack always propagates normal to the direction of largest principal stress occurring at the crack tip at a particular time instant.

In the next para, a stepwise procedure is presented using the above data as inputs, for assessing the residual life of a component.

Stepwise Procedure for Estimation of Remaining Life

1. Determine the following data: (a) Material property, (b) Future loading and operation pattern, (c) Component and location geometry.
2. Perform a preliminary stress analysis and inspection in the selected region. Regions can be selected based on guidelines provided earlier. Apply clustering technique and prepare the final list of flaws.
3. Using the equation set (I) furnished below and fracture toughness data, compute permissible stress (\sqrt{P}) corresponding to maximum crack length, and maximum permissible crack length (a_p) corresponding to maximum stress prevailing in the component.

Equation Set (I)

(i) Opening mode of crack propagation

$$(P = (3-4\nu) \text{ for plane strain, } P = \frac{(3-\nu)}{(1+\nu)} \text{ for plane stress})$$

$$\begin{aligned} \text{a) } a_{cr} &= \frac{8\mu S_{cr}}{(P-1)\sqrt{V_{cr}}} \\ \text{b) } a_{cr} &= \left[\frac{K_{Ic}}{\sqrt{V_{max}}} \right]^2 \frac{1}{\pi F} \\ \text{c) } a_{cr} &= \frac{K_{Ic} \left[\phi^2 - 0.212 \left(\frac{V_{max}}{V_{ys}} \right)^2 \right]}{1.21 \pi \sqrt{V_{max}}} \\ \text{d) } a_{cr} &= 0.2 \left[\frac{K_{Isc}}{\sqrt{V_{ys}}} \right]^2 \end{aligned}$$

(ii) Sliding mode of crack propagation

$$a_{cr} = \left[\frac{192 \mu S_{cr}}{\tau_{cr}^2 (-P^2 + 14P - 1)} \right]$$

(iii) Mixed mode of crack propagation

$$\begin{aligned} S &= A_{11}K_I^2 + 2A_{12}K_I K_{II} + A_{22}K_{II}^2 + A_{33}K_{III}^2 \\ \text{where, } A_{11} &= (1/16\mu) \left[(1 + \cos\theta)(P - \cos\theta) \right] \\ A_{12} &= (1/16\mu) \left\{ \sin\theta \left[2\cos\theta - (P+1) \right] \right\} \\ A_{22} &= (1/16\mu) \left[(P+1)(1 - \cos\theta) + (1 + \cos\theta)(3\cos\theta - 1) \right] \\ A_{33} &= (4/16\mu) \end{aligned}$$

The relation between strain-energy-density and crack length is obtained by substituting in the above relation the expressions for K_I , K_{II} and K_{III} in terms of a critical strain energy density for a given stress level.

Equation recommended under following conditions.

- i) a when S_{cr} is available for the material.
b,c when K_{Ic} is available for the material.
d when the material is subjected to stress corrosion and when K_{Isc} is available for the material.
- ii) when S_{cr} is available for the material subject to second mode of crack propagation.
- iii) when S_{cr} is available for the material subjected to mixed mode of crack propagation.

4. Compute stress intensity factor based on standard references or using finite element method for all the cracks having crack-length greater than permissible crack length and stress greater than permissible stress. Decide critical region as the region having highest stress intensity factor.

5. Divide the total future operating (loading) time into suitable, number of intervals to take into account (a) degradation of mechanical property with time and (b) crack growth.

6. Perform detailed stress analysis at the critical region corresponding to the loading at each interval of time and compute all the components of stress. It is to be noted that initially the crack length as observed during the inspection would be used for calculations. In the subsequent time intervals, this is updated by computed values depending upon the rate of crack growth per time interval or per cycle using the latest value of K_{Ic} or S_{cr} at that interval of time. The actual value of crack length based on inspection would replace the theoretical value computed earlier. Fresh calculation and decisions made on this basis should supercede the previous ones.

7. Decide at each stage on the basis of guidelines given below and in equation set (II) whether elastic plastic analysis is needed. If needed, compute fictitious crack length and use this to compute SIF, J - integral and C_t - integral.

Guidelines for Elastic Plastic fracture mechanics

a) The plastic zone size is considerable under following conditions:

- i) The radius of crack-tip is large
- ii) Rate of loading (strain rate) is extremely low
- iii) The material is sufficiently ductile
- iv) Operating temperature is high

b) First obtain the stress intensity factor for crack in stressed medium assuming elastic conditions to prevail.

c) The plastic zone size is calculated using equation set (II). If $r_p < a/50$, then only LEFM is valid.

d) If the crack tip plastic zone enclave size is less than crack length and net area available, the crack size is fictitiously increased by half of plastic zone size.

e) This fictitious crack size is then subsequently used in analysis using LEFM procedure.

f) If the plastic zone size is large, in case of creep the governing parameter is J -Integral for brittle material and C_t parameter for ductile material. For brittle materials, r_p will be very small.

Equation Set (II) (For plastic zone computation)

Stress distribution in the immediate vicinity of sharp crack tip is given by the following expression

a) For an ideal Slit

$$S_{ij} = \frac{K_s}{\sqrt{2\pi r}} f_{sij}(\theta)$$

b) For a crack with tip radius - ρ

$$S_{ij} = \left[K_1 / (\sqrt{2\pi r}) \right] f_{sij} \left(\frac{\rho}{r}, \theta \right)$$

$$g(\theta) = \frac{1}{2} \left\{ \left[f_{sxx}(\theta) - f_{syy}(\theta) \right]^2 + \left[f_{syy}(\theta) - f_{szz}(\theta) \right]^2 + \left[f_{szz}(\theta) - f_{sxx}(\theta) \right]^2 + \left[f_{sxy}^2(\theta) + f_{syx}^2(\theta) + f_{syz}^2(\theta) \right] \sigma \right\}$$

The plastic zone boundary is defined by coordinate r_y in terms of SIF and θ

a) Ideal Slit

$$r_y = \frac{g(\theta)}{2\pi} \left(\frac{K_s}{V_{YS}} \right)^2$$

b) Considering the effect of crack tip radius

$$r_y = g \left(\frac{\rho}{r}, \theta \right) \left(\frac{K_1}{V_{YS}} \right)^2 \left(\frac{1}{2\pi} \right)$$

Monotonic plastic zone size at maximum load

$$r_m = \frac{1}{(1+n')\pi} \left(\frac{K_{max}}{V_0} \right)^2$$

Cyclic plastic zone size

$$r_c = \frac{1}{4(1+n')} \left(\frac{1}{\pi} \right) \left(\frac{\Delta K}{V_0} \right)^2$$

where, $V = V_0 \left(\frac{\epsilon}{\epsilon_0} \right)^{n'}$ For $V \geq V_0$; $V = E \epsilon$ for $V < V_0$

8. Compute critical crack length at each stress level and time interval using expressions furnished in Equation Set (I) given in Step 3.

9. Check if, $a_i \leq a_{cr}$, $a_i > a_{cr}$

If $a_i \leq a_{cr}$, there is no left over life and component should be retired immediately. Otherwise, proceed further.

10. Determine the direction of crack growth using expressions given in Equation Set (III).

Equation Set (III): (To determine the direction of crack - propagation)

i) Strain energy criterion for mixed mode crack - propagation: The fracture angle θ_0 is obtained by solving the following equation:

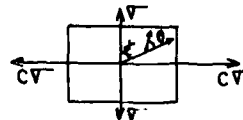
$$K_1^2 [\sin 2\theta_0 - \sin \theta_0] + 2K_1 K_2 [2 \cos 2\theta_0 - \cos \theta_0] - K_2^2 [-3 \sin 2\theta + \sin \theta] = 0$$

ii) Maximum strain energy density criterion: The crack propagates through an angle $\theta = \theta_0$ which satisfy the following condition:

$$\frac{\partial S}{\partial \theta_0} = 0; \quad \frac{\partial^2 S}{\partial \theta_0^2} > 0$$

iii) Maximum energy release rate criterion: The direction of crack growth θ_0 is defined by the condition:

$$\frac{\partial G}{\partial \theta} = 0 \quad \text{and} \quad \frac{\partial^2 G}{\partial \theta^2} < 0 \quad \text{at } \theta = \theta_0$$



iv) Maximum tensile stress criterion

$$\sqrt{\sigma_{\theta\theta}} = \frac{1}{4\sqrt{2\pi r}} \left[K (3 \cos \theta_0/2 + \cos 3\theta_0/2) - 3K (\sin \theta_0/2 + \sin 3\theta_0/2) \right] + L_1 \sin^2 \theta_0$$

The crack grows in the direction $\theta = \theta_0$ which satisfies the condition:

$$\frac{d\sqrt{\theta\theta}}{d\theta} = 0 ; \quad \frac{d^2\sqrt{\theta\theta}}{d\theta^2} < 0 ; \quad L = \sqrt{(1-C)\cos 2\alpha}$$

$$K_I = \frac{\sqrt{\pi a}}{2} [(1+C) - (1-C)\cos 2\alpha] ; K_{II} = \frac{\sqrt{\pi a}}{2} (1-C) \sin 2\alpha$$

11. Determine the rate of crack growth in fatigue, creep and fatigue with hold-time using Equation Set (IV).

Equation Set (IV) - (to determine the rate of crack growth):

i) Paris - Law:

$$\frac{da}{dN} = C (\Delta K)^m$$

ii) Rate of crack propagation as a function of R:

$$\frac{da}{dN} = \frac{A' (\Delta K)^{m'}}{(1-R) K_c - \Delta K}$$

iii) Crack growth rate as a function of strain energy density:

$$\frac{da}{dN} = \text{EXP} \left[\frac{C [A \ln(\alpha \Delta S) - B]}{[A \ln(\alpha \Delta S) - B]} \right] A [\ln(\alpha \Delta S) - B]^n + C_2 [A \ln(\alpha \Delta S) - B]^2 + C_3 [A \ln(\alpha \Delta S) - B] + C_4$$

$$\Delta S = S_{\max} - S_{\min}$$

$$\alpha = \frac{(1+R)}{1+R \left[\frac{\sqrt{U}}{\sqrt{YS}} \frac{(1+RA)}{YS} \right]^2}$$

$$R = \frac{\sqrt{v_{\min}}}{\sqrt{v_{\max}}}$$

iv) Crack growth rate as a function of mean stress:

$$\frac{\Delta a}{\Delta N} = C' (\Delta S_{\min})^n \quad \Delta S_{\min} = S(\theta_0 \sqrt{v_{\max}}) - S(\theta_0 \sqrt{v_{\min}})$$

$$\Delta S_{\min} = A_{11}(\theta_0) [(K_1)_{\max}^2 - (K_1)_{\min}^2] + 2 A_{12}(\theta_0) [\bar{K}_2 \Delta K_1 + \bar{K}_1 \Delta K_2] + A_{22}(\theta_0) K_2 \Delta K_2 + A_{33}(\theta_0) K_3 \Delta K_3$$

v) Fatigue with hold-time:

$$\frac{da}{dN} = A_1 (\Delta K)^{n1} + A_2 (\Delta K)^{n2} t_n^{m1} + A_3 C^* t_h$$

vi) Creep-crack-growth:

$$\frac{da}{dt} = M(J) \propto \beta$$

β varies from 1 to 3

$$J = \frac{B}{E} \left[K_1^2 + K_2^2 \right] + \frac{(1+\nu)}{E} K_3^2$$

$\propto \beta = 1$ for large value of n

M - material constant

$$t_c = \frac{K^2 (1-\nu^2)}{E(n+1) J^*} \quad \propto = \frac{1}{n+1}$$

vii) Creep-crack growth:

$$\frac{da}{dt} = C'' (c_t)^{m''} \quad c_t = \frac{4(1-\nu^2) K^4}{E(n-1) W} (E A)^{\frac{2}{(n-1)}} t^{\frac{(n-3)}{(n-1)}} \frac{F'}{F} + C^*$$

$$F = 11.6 \sqrt{\frac{a}{W}} \left[0.95 + 1.301 \left(\frac{a}{W} \right) + 10.66 \left(\frac{a}{W} \right)^2 - 55.02 \left(\frac{a}{W} \right)^3 + 75.56 \left(\frac{a}{W} \right)^4 \right]$$

$$F' = \frac{dF}{d\left(\frac{a}{W}\right)} \quad \propto = \frac{1}{2\pi} \left[\frac{(n+1)^2}{2n\alpha_n^{n+1}} \right]^{\frac{2}{(n+1)}}$$

α_n^{n+1} - A factor with a value of 0.69 for value of n between 3 & 10.

viii) When crack growth rate plots are available for materials of components having similar operating conditions such as load, frequency, temperature and environment, they can be directly made use of to compute the crack growth rate.

12. Determine the number of cycles required for failure in case of fatigue, fatigue with hold-time and time required for rupture in case of creep at each stress level for each interval of time as appropriate using Equation Set (V).

Equation Set (V) (Cumulative damage theories)

To determine number of cycles required for failure

$$N_i = (a_{cr} - a_i) \frac{da}{dn}$$

$$(N_i)_{th} = (a_{cr} - a_i) \left(\frac{da}{dt} \right)_{thi}$$

To determine the time required for failure

$$t_f = (a_{cr} - a_i) \left(\frac{da}{dt} \right)_i$$

(i) Palmgren-Miner hypothesis or linear-damage rule
(used widely in practice and is also simple to use)

(a) Fatigue

$$D_F = \sum \frac{n_{ij}}{N_{ij}}$$

(b) Creep

$$D_C = \sum \frac{t_{ij}}{T_{ij}}$$

(c) Creep-fatigue

$$D_{FC} = \sum \frac{n_{ij}}{N_{ij}} + \sum \frac{t_{ij}}{T_{ij}}$$

ii) Henry Cumulative damage theory (used for spectrum loadings)

$$D_i = \sum \frac{\left(\frac{N_i}{n_i} \right)}{1 + \left(\frac{E_i}{S_i - E_i} \right) \left(1 - \frac{n}{N} \right)}$$

iii) Macro-Starkey cumulative damage theory (used for spectrum loadings)

$$D = \sum \frac{n}{N} = \int_0^1 \left[1 + \frac{N_1}{N_2} + \frac{N_1}{N_3} + \dots + \frac{N_1}{N_i} \right] db'$$

$$\left[1 + \frac{N_1}{N_2} r_2 D_i' \frac{(r_2 - 1)}{r_2} + \dots + \frac{N_1}{N_i} r_i D_i' \frac{(r_i - 1)}{r_i} \right]$$

iv) Marin cumulative damage theory (used when operation takes place at different stress amplitudes in regular sequence)

$$D = \left(\frac{n_1}{N_1} \right) + \left(\frac{n_2}{N_2} \right) \left(\frac{S_2}{S_1} \right)^q + \left(\frac{n_3}{N_3} \right) \left(\frac{S_3}{S_1} \right)^q + \dots + \left(\frac{n_i}{N_i} \right) \left(\frac{S_i}{S_1} \right)^q = 1$$

$$\left(\frac{n_1}{N_1} \right) + \left(\frac{n_2}{N_1} \right) \left(\frac{S_2}{S_1} \right)^y + \dots + \left(\frac{n_i}{N_1} \right) \left(\frac{S_i}{S_1} \right)^y = 1 \quad \text{where } q = y - x$$

S^xN = K Approximation of S-N curve

$$\text{The remaining life } n_{lr} = N_i \left[1 - \frac{n_1}{N_1} \left(\frac{S_1}{S_i} \right)^q - \left(\frac{n_2}{N_2} \right) \left(\frac{S_2}{S_i} \right)^q - \dots - \left(\frac{n_{i-1}}{N_{i-1}} \right) \left(\frac{S_{i-1}}{S_i} \right)^q \right]$$

13. Determine the fraction of life exhausted in case of creep, or fatigue or fatigue with hold-time applying the appropriate cumulative damage theory using Equation Set (V).

14. Total number of cycles required for failure in case of fatigue and fatigue with hold time

$$= \sum_{ij} n_{ij} \times FS$$

Total time required for failure in case of fatigue and fatigue with hold time = $\sum n_{ij} FS \times \text{period of each cycle.}$

Total time required for failure in case of pure creep = $\sum t_{ij}$

Guidelines for inspection schedules: Based on the foregoing discussions, the schedule for inspection could be drawn up on the following basis:

a) It is to be noted that the size of the "tolerable" subcritical flaw vary with the location of flaw, metallurgical structure and loading. Hence, specific guidelines for inspection programme are generally developed by utilities based on their previous experience and currently available technical data and calculations.

b) If computations show that size of flaw is tolerable, it could be repaired locally by grinding, welding or patching. Periodic measurement of flaw size during further service of the component is recommended after assessing the economic viability of a reinspection program vs replacement.

c) The intervals of reinspection are so selected to assure that the largest flaw left in service or missed by inspection does not grow to cause leak or rupture in that period. The confidence level of remaining life calculations is also an influencing factor. Flaws which have been left in service could be reinspected within an interval in which they can be expected to grow further by 0.1 inch. This is based upon the assumption that 0.1 inch is the smallest detectable crack length.

d) If calculations show that flaw is large and that it could grow to critical size rapidly, then replacement is the only alternative and that should be carried out immediately.

Conclusion Computations for estimations of residual service life of a flawed component using fracture mechanics is thus possible for thermal power plant components and the utilities could well exploit the potential of fracture mechanics fully in arriving at decisions concerning the future operation of the plant duly supported by a scientific methodology.

Nomenclature

A, C', X, Y		Klsc	Fracture toughness for stress corrosion cracking
m, m', n'	Material constants		
B	Breadth of component	N	Number of fatigue cycles required for failure
C^*, C_t	C-Integral (for creep)		
D	Damage ratio	R	Ratio of min. to max. stress in a fatigue cycle
E	Youngs Modulus		
F	Form factor	RA	Reduction in area (%)
Jlc	Critical value of J - integral	S	Strain energy density
		Scr	Critical strain energy density
K_I, K_{II}, K_{III}	Stress Intensity Factors for first, second and third mode of cracks propagation respectively	T	Time required for failure under constant load
		W	Width of the component
Klc	Plane strain fracture toughness for first mode of crack propagation	a	Half length of the crack
		n	Number of fatigue cycles applied.

r	Plastic zone size	ρ	Radius of the crack tip
t	Duration of application of constant load	ν	Poisson's ratio
\sqrt{VS}	Yield stress	μ	Shear Modulus
ϵ	Strain	α	Angle between the crack length & the direction of applied stress.
τ	Shear stress	θ	Angle between crack length and direction of crack extension
τ_{cr}	Critical shear stress		
σ_U	Ultimate stress	ϕ	crack shape parameter

References

1. 'Life assessment and repair of steam turbine casings', workshop proceedings, EPRI CS 4676 SB July 1986.
2. 'Remaining life estimation of boiler pressure parts crack growth studies', EPRI CS 4676 SB July 1986.
3. Pattabiraman, J. 'Stress analysis of piping system to aid TC start-ups in large thermal power plants', Proceedings of the 40th meeting of the Mechanical Failures Prevention Group, National Bureau of Standards, Gaithersburg, Maryland, April 16-18, 1985.
4. 'Generic guide lines for the life extension of fossil fuel power plants', EPRI CS 4778 Nov 1986.
5. 'Guidelines for the evaluation of seam welded steam pipes', EPRI CS 4774 Feb.1987
6. 'Life assessment methodology for turbo-generators and rotors', Vol.1, Vol.2, Vol.3, EPRI CS/EL 5523 (1988).
7. 'Pattabiraman, J. 'Residual life prediction of power plants components', Electrical India, 30th Sept.1987.
8. Osgood, C. 'A course on fracture creep and cyclic creep cracks propagation in 1 Cr-Mo-V steel', Inst Mech Engrs Conference Publication (1973).
9. Sundararajan, G. et al, "Evaluation of residual life of critical components of thermal power plant equipment by on line monitoring", paper No.8A.3, Proceedings of the International Conference on Residual Life of Power Plant Equipment Prediction and Extension - LIPREX 89, Hyderabad, India. Jan.1989.

DESIGN OF PERMANENT MAGNET BIASED MAGNETIC BEARINGS FOR A FLEXIBLE ROTOR†

Christopher K. Sortore‡, Paul E. Allaire, Eric H. Maslen and Robert R. Humphris
University of Virginia
School of Engineering and Applied Science
Department of Mechanical and Aerospace Engineering
Charlottesville, VA 22901

Philip A. Studer
Magnetic Concepts
Silver Springs, MD 20901

Abstract: Magnetic suspension technology has advanced to the point of being able to offer a number of advantages to a variety of applications in the rotating machinery and aerospace fields. One strong advantage of magnetic bearings over conventional bearings is the decrease in power consumption. The use of permanent magnets, along with electromagnets, is one appealing option which can further reduce the power consumption of the bearing.

The design and construction of a set of permanent magnet biased, actively controlled magnetic bearings for a flexible rotor is presented. Both permanent magnets and electromagnets are used in a configuration which effectively provides the necessary fluxes in the appropriate air gaps, while simultaneously keeping the undesirable destabilizing forces to a minimum. The design includes two radial bearings and a thrust bearing.

The theoretical development behind the design is briefly discussed. Experimental performance results for a set of operating prototype bearings is presented. The results include measurements of load capacity, bearing stiffness and damping and the dynamic response of the rotor. With few exceptions, the experimental measurements matched very well with the predicted performance. The power consumption of these bearings was found to be significantly reduced from that for a comparable set of all electromagnetic bearings.

Key Words: Magnetic bearings; magnetic suspension; permanent magnets; electromagnets; low power bearings; feedback control

Introduction: Magnetic bearings have a number of strong advantages. One most obvious advantage is their non-contacting, virtually friction-free characteristics. Entire lubrication systems and the need for mechanical oil seals, which add to friction losses and instabilities associated with cross coupled bearing coefficients, can be eliminated by using these types of bearings. The life expectancy of a magnetic bearing, in many

† This work was funded by Sundstrand Corp., Rockford, IL 61125

‡ Now employed with Aura Systems, Inc., El Segundo, CA 90245

cases, can be much higher than that of a conventional bearing. Due to the non-contacting nature of the bearings, mechanical parts do not wear out. This can obviously increase system reliability and decrease costly repairs and necessary maintenance which interrupt profitable machine operation. If designed properly, a magnetic bearing can perform under much harsher conditions and environments for extended periods of time which would not be possible with other types of bearings. One further advantage of the frictionless characteristic of these bearings is that of power loss. The power consumption of a conventional fluid-film bearing is in many all cases much more than for a magnetic bearing. Power loss reductions of one order of magnitude or more can be expected when a machine is converted from using conventional bearings to magnetic bearings.

A variety of work has been accomplished on a number of different applications and aspects of magnetic bearings. An extensive amount of research has been performed by a number of university and industry researchers on the development of magnetic bearings in an industrial canned motor pump [1]. A number of other successful industrial applications of magnetic bearings has been reported by Weise [2]. Burrows *et. al.* [3] presents the development and application of a magnetic bearing specifically designed for the vibration control of a flexible rotor. Keith, *et. al.* [4] successfully developed a PC-based digital controller for magnetic bearings. Continuing research is being performed in the areas of digital and adaptive controls for magnetic bearings.

In researching the use of permanent magnets in combination with electromagnets, of particular interest are two patents credited to Philip Studer [5, 6]. These patents contain a number of features, primarily dealing with permanent magnets, which have useful application to the bearings discussed in this paper. Wilson and Studer [7] have also applied the permanent magnet bias concept to a linear motion bearing. Ohkami *et. al.* [8] have performed some interesting comparison studies of magnetic bearings of various configurations which use permanent magnets. Another paper by Tsuchiya *et. al.* [9] studies and comments on the stability of a high speed rotor which is suspended in magnetic bearings biased with permanent magnets. Meeks [10] has also performed a comparison of the various magnetic bearing design approaches and concludes that the combining of actively controlled electromagnets with permanent magnets results in a superior magnetic bearing in terms of size, weight and power consumption. The rare earth permanent magnets of today, in particular Sm-Co and Nd-Fe-Bc magnets, offer very high performance characteristics in terms of magnetic strength, energy product and thermal qualities. The magnet designer is able to concentrate a very large amount of magnetic energy in a small package, making more efficient use of available space.

The design concept for the permanent magnet biased magnetic bearing design discussed in this paper is a variation on research and development reported by Studer [5, 6]. The following two sections give a brief description of how the bearings conceptually operate.

Radial Magnetic Bearing Description: A diagram of a permanent magnet biased radial magnetic bearing is shown in Figure 1. This bearing is designed to operate at one end of the rotor and control radial forces only. Four axially magnetized arc segment magnets are positioned circumferentially adjacent to the stator. The bias flux generated by the permanent magnets passes down the laminated stator pole leg, through the working air gap, axially along the shaft, then returns to the permanent magnet via a radial bias pole piece. The active control flux generated by the coils also passes down the stator pole leg and through the working air gap. The return path for the active flux is then

circumferentially around the stator, as shown in Figure 1. This design requires only four poles and four coils, unlike an all electromagnetic design which generally requires eight. In addition, since the coils for each bearing axis are connected in series, the bearing control system requires only five current amplifier channels, which is half as many as required of the all electromagnetic bearing.

Combination Radial/Thrust Magnetic Bearing Description: A schematic of this bearing design, revealing the various magnetic paths, is shown in Figure 2. This bearing combines control of both radial and thrust forces. The radial portion of the bearing is identical to that which was described in the previous section. The thrust control however, is implemented by a unique magnetic flux configuration. The permanent magnet bias flux passing along the shaft splits equally between the two thrust poles before returning to the permanent magnet. A single active coil produces a magnetic flux, in the shape of a toroid, which symmetrically adds or subtracts to the bias flux in the working air gaps between the thrust disk and thrust poles.

Design Concept: The bearings designed for this project are different from all electromagnetic bearing designs in that they employ both permanent magnets and electromagnets. Permanent magnets generate the bias flux in the working air gaps and electromagnets are used to modulate this flux.

The purpose of establishing a bias flux in the working air gaps is to linearize the governing force equation of the magnetic actuator. The bias flux is a nominal flux density about which the control flux is varied. If a bias flux of zero is used, (only one opposing actuator is operated at a time,) then the force generated by the actuator on the rotor follows a quadratic force law, i.e., the force will be proportional to the square of the flux density in the air gaps. Consequently, the force slew rate will be zero when the rotor is in the nominal balanced position and the transient response will be adversely effected. If, however, the bearing fluxes are modulated about a non-zero bias flux, (with opposing actuators symmetrically perturbed,) it is easily shown that the force becomes linearly related to the control flux. The following section demonstrates this important relation.

Force Relationships: The force generated in an air gap of area A_g and length g by a magnetic actuator can be expressed by the direct relation

$$F = \frac{1}{2\mu_0}(B_g)^2 A_g \quad (1)$$

where B_g is the flux density in the air gap and μ_0 is the permeability of free space. If only a single axis of the bearing is considered, then the net force acting on the shaft will be the difference of the two opposite acting actuator forces. Assuming the areas of the two opposing air gaps are the same, the force acting on the shaft by the magnetic bearing can be expressed as

$$F_{shaft} = \frac{1}{2\mu_0}(B_{g1}^2 - B_{g2}^2)A_g \quad (2)$$

The flux density in the air gaps is being supplied by two sources, i.e., the permanent magnet and the coil. In order to properly provide differential control, the fluxes in the two gaps are symmetrically perturbed so that the flux in one gap is increased while the flux in the opposite gap is decreased by the same amount. This implies that

$$B_{g1} = B_{pm} + B_c \text{ and } B_{g2} = B_{pm} - B_c \quad (3,4)$$

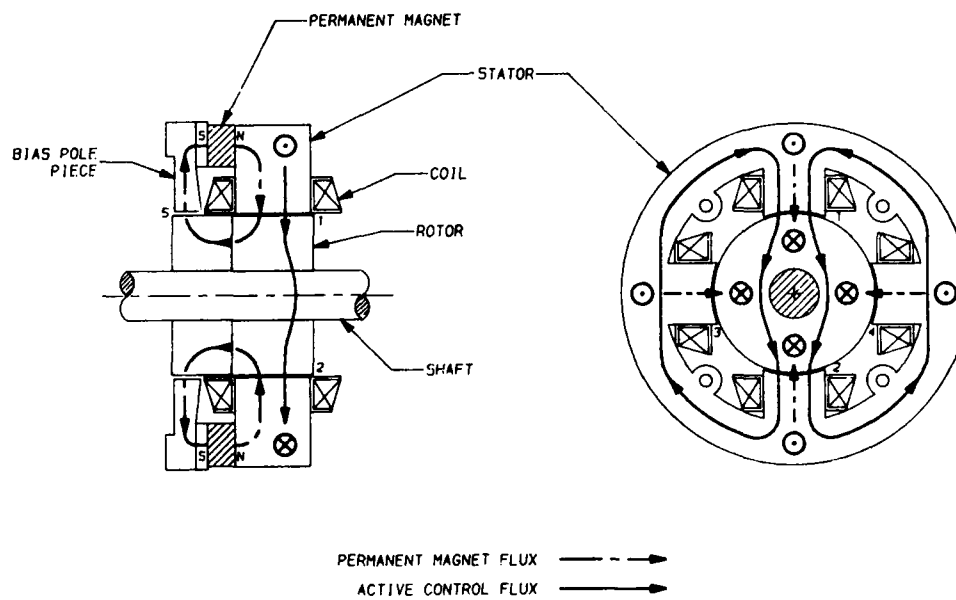


Figure 1 - Permanent Magnet Biased Radial Magnetic Bearing Flux Paths

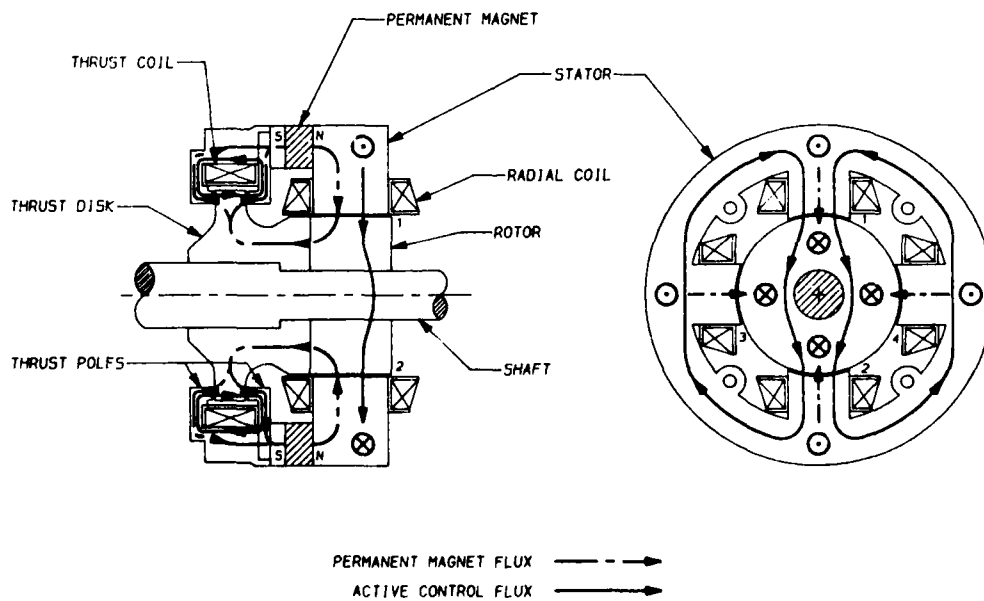


Figure 2 - Permanent Magnet Biased Radial/Thrust Magnetic Bearing Flux Paths

where B_{pm} is the flux density generated by the permanent magnet and B_c is the flux density generated by the coil. Substituting Eqs. (3, 4) into Eq. (2), expanding and simplifying, the force acting on the shaft can now be expressed as

$$F_{shaft} = \frac{2}{\mu_0} B_{pm} B_c A_g \quad (5)$$

By expressing the equation for the force on the shaft in this form, it is interesting to note that the force is not only proportional to the bias level, B_{pm} , but it is also linearized with respect to the control flux, B_c .

Open Loop Stiffness and Actuator Gain: The force generated by the bearing in the horizontal direction, F_x , can be accurately approximated by the truncated Taylor series expansion in the following way:

$$F_x \approx F_x \Big|_{x=0, i_c=0} + \frac{\partial F}{\partial x} \Big|_{x=0, i_c=0} x + \frac{\partial F}{\partial i_c} \Big|_{x=0, i_c=0} i_c \quad (6)$$

If the magnetic circuit is balanced, then the first term in Eq. (6) is equal to zero and

$$F_x \approx K_x x + K_i i_c \quad (7)$$

where x represents the rotor displacement and i_c represents the control current in the electromagnetic coil. The parameters K_x and K_i are defined as

$$K_x \equiv \frac{\partial F_x}{\partial x} \Big|_{x=0, i_c=0} \quad \text{and} \quad K_i \equiv \frac{\partial F_x}{\partial i_c} \Big|_{x=0, i_c=0} \quad (8,9)$$

The quantity K_x is referred to as the open loop stiffness and represents the change in the horizontal force due to horizontal displacement. The open loop stiffness is always negative which implies that the bearing is unstable in the open loop control configuration. Unlike a actual spring with a positive stiffness, a positive displacement of the rotor toward the magnet will increase the attractive force. The quantity K_i represents the actuator gain of the bearing. It represents changes in the horizontal force due to control current, i_c . Equivalent expressions exist for the components of the vertical force expression.

Expressions for the open loop stiffness and the actuator gain are determined by performing the appropriate differentiation of the force expression. These expressions take on the form

$$K_x = - \frac{2\mu_0 L^2 H^2 A_g}{g^3} \quad (10)$$

and

$$K_i = \frac{\mu_0 L H N A_g}{g^2} \quad (11)$$

where L and H represent the length and demagnetization force, respectively, of the permanent magnet and N is the number of turns in the electromagnetic coil.

Control System Description: The control elements of this system are those components which detect the motion of the shaft, determine the required control force and generate a coil current required by the magnetic bearing to generate this force. The

magnetic bearing system consists of four distinct components: the magnetic actuator, the displacement sensors and associated conditioning circuits, the analog PID controller and the power amplifier.

The actual magnetic bearing mainly consists of the electromagnetic coils, iron pole pieces, rotor and permanent magnets. The signal conditioning component consists of the eddy current induction displacement sensors, signal amplification and coordinate transformation circuits. The analog controller primarily consists of three separate components. The components take the form of proportional (P), integral (I) and derivative (D) compensation networks. These three parallel stages are added together through a summing amplifier to produce the output of the analog controller. The last component in the control loop is the power amplifier. The amplifier, upon request of the controller, supplies the required current to magnetic coils to produce the necessary fluxes in the bearing.

The dynamics of the bearing-rotor system can be combined with the operating characteristics of the control electronics to form a closed-loop control system. This control system is shown in a simplified block diagram form in Figure 3. The displacement sensor characteristics, analog controller and amplifier make up the relatively complex transfer function of the feedback controller, $G_c(s)$. The feedback controller relates the rotor position to the actuator current. The closed-loop transfer function for this magnetic bearing system, as determined from this block diagram, is given by

$$\frac{X(s)}{F_x(s)} = \frac{1}{ms^2 + K_x + K_i G_c(s)} \quad (12)$$

where m is the mass of the rotor supported by the bearing.

Prototype Bearing Construction: The four-pole radial bearing stators, as shown in the diagrams of Figures 1 and 2, were designed to be identical for both bearings. The stators and rotors were constructed of 3% silicon-iron lamination material which had a thickness of 0.007 inches. Each laminated component consists of approximately 100 laminations. The laminations were glued together using a two part activator/resin adhesive and the shape was machined by wire EDM (electric discharge machining.) The bearing stators have an outside diameter of approximately 3.0 inches and an axial length of approximately 0.7 inches. The outside diameter of the laminated rotor is approximately 1.5 inches. The thrust bearing components were machined from soft magnet iron. The high energy permanent magnets, made out of a Neodymium-Iron-Boron alloy, have a maximum energy product of 30 MG-Oe. The bearings support a shaft weighing approximately 3.7 lbm.

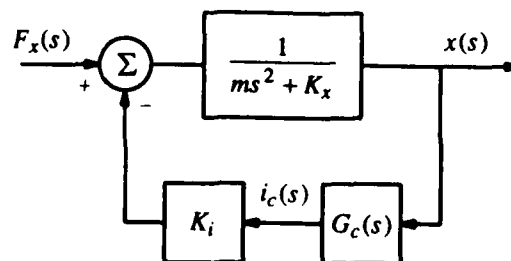


Figure 3 - Closed-Loop Magnetic Bearing Control System

Load Capacity: Measurements of the maximum load applied to the shaft, before falling out of support, are plotted as a function of proportional controller gain, K_p , in Figure 4. The force in this test was applied by hanging weights on the shaft. A pulley system was constructed in such a way that the force could be applied in the desired direction. The force in the plots represents forces applied along the bearing axes.

The variation of the maximum load at lower proportional gains is actually a measure of the stability threshold of the system. It is noted in Eq. (8) that the open loop stiffness, K_x is defined at a nominal operating point, i.e., rotor position and control current equal to zero. However, as the bearing is loaded with a static force, the steady state current begins to increase. It can be shown analytically that K_x is a function of the operating point of the control current. That is, as the control current increases, K_x also increases. Increasing proportional gain has the effect of compensating for this increase in K_x and consequently increasing the stability of the system.

The measurements made at higher proportional gains represent a more accurate measure of the actual load capacity of the bearing. Enough stability is provided so that magnetic saturation is reached in the bearing pole structures. The maximum predicted loads in the plots of Figure 4 are calculated at the point of magnetic saturation.

Equivalent Bearing Stiffness and Damping: Measurements of the equivalent stiffness of the bearings are shown in Figure 5. This simple measurement was performed by applying a constant force, ΔF , and noting the displacement, Δx , of the shaft (controller integrators turned off.) The stiffness then is given simply by $K_{eq} = \Delta F / \Delta x$. A linear regression was performed on the measured data, which resulted in very good correlation, as can be observed in the plots. It is noted that the proportional gain has a direct effect on the stiffness of the bearings, as has been previously demonstrated by Humphris, *et. al.* [11].

Relative damping in the bearings was investigated from a white noise frequency response analysis of the bearing and rotor. The analysis was performed by injecting noise, composed of all frequencies of interest, into one axis of the turbine-end radial bearing, and performing a FFT (Fast Fourier Transform) analysis on the vibration response of that axis. This linear frequency response, composed of 100 averages, is shown in Figure 6. The derivative controller gain, K_r , was varied through a range of values as noted in the plot. As expected, the derivative gain had a direct effect on the damping in the bearings [11]. The first large spike represents the first two modes of shaft vibration. They are very close together in frequency and essentially indistinguishable. The frequency of the second spike is the third mode of vibration and the third small spike at approximately 60,000 cpm is the fourth mode. It is noted that the variation of the derivative gain strongly effects the first two modes, has a small effect on the third mode and virtually no influence on the vibration amplitude of the fourth mode.

Critical Speeds and Rotor Response: The damped synchronous critical speeds of the flexible shaft supported by these bearings can be approximately determined from the white noise frequency response plots of Figure 6. These values, however, represent the zero speed natural frequencies, and the gyroscopic stiffening effects of any attached disks would not be included. Since the natural frequency is given by $\omega_n = \sqrt{k/m}$, where k is the shaft stiffness and m is the modal mass of the rotor, it is of course expected that the observed critical speeds, when the shaft was spinning, would be higher.

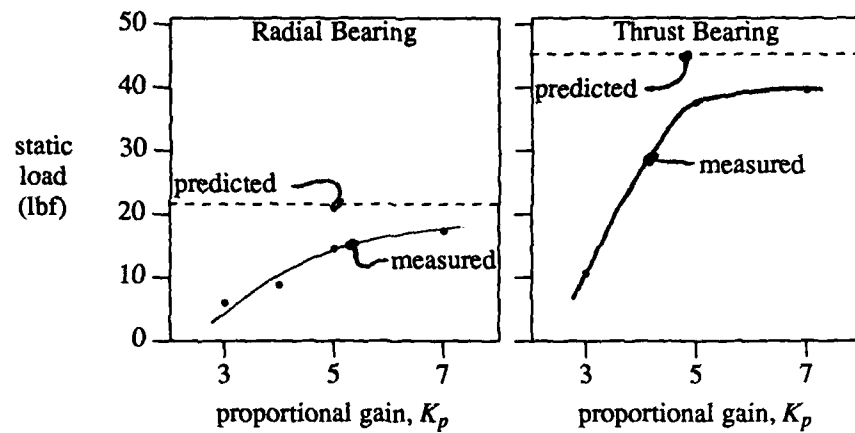


Figure 4 - Maximum Load Capacity

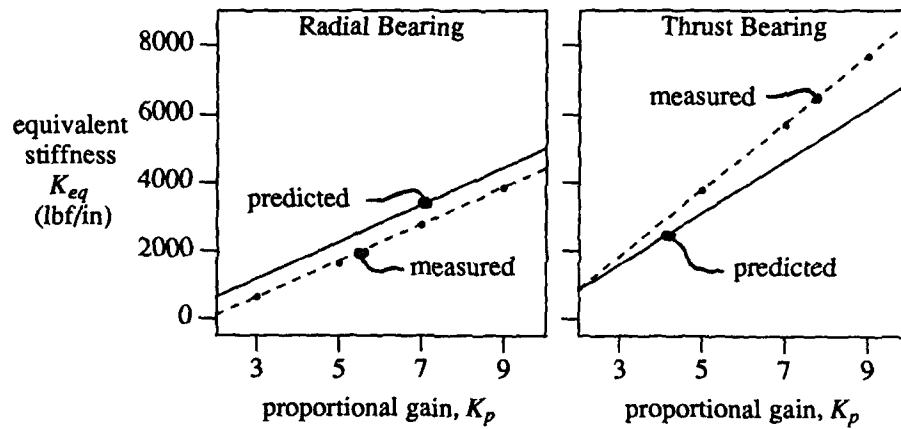


Figure 5 - Equivalent Bearing Stiffness

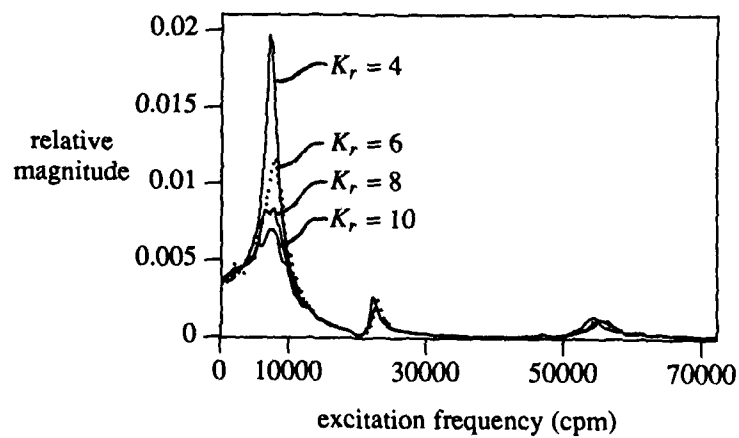


Figure 6 - Measured White Noise Linear Frequency Response

Plots showing the vibration magnitude and phase for the shaft speeds that were obtained is included in Figure 7. Amplitude information was taken directly from the magnetic bearing sensors and a key-phase sensor was used to provide the phase information. According to the maximum vibration amplitudes observed in Figure 7, the first vibration mode is observed to occur at approximately 10,000 rpm and the second at approximately 13,000 rpm.

Power Consumption: Finally, a number of power consumption measurements were made. Measurements of the power were taken with a wattmeter for a number of cases. This meter is used with the assumption that the measured voltage and current being supplied to the control electronics is sinusoidal in nature. In addition, it is realized that it represents a somewhat gross measurement as it includes all the inefficiencies of the various electronic components. Table 1 summarizes the results. The non-essential electronic diagnostic components of the bearing system were observed to consume only about 7 watts. These measurements represent a significant improvement over the 500 watts of approximate total power consumed by a comparable current biased all

Table 1 - Magnetic Bearing Power Consumption

	Shaft out of support	Shaft in support	at 20,000 rpm
diagnostic equipment connected	148 W	193 W	207 W
diagnostic equipment disconnected	141 W	187 W	

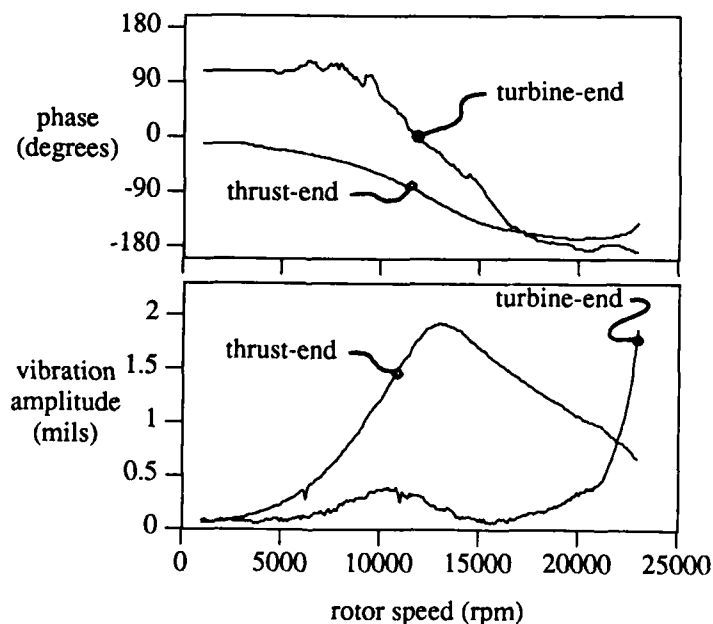


Figure 7 - Rotor Runup Response

electromagnetic bearing design.

Conclusions: The brief theory which was presented in this paper established the basic electromagnetic and mechanical relationships necessary to develop a set of permanent magnet biased magnetic bearings. The design involved both radial and thrust bearings. The availability of newer rare-earth high energy permanent magnets made it possible to effectively provide the necessary bias fluxes in the bearing.

The bearings and rotor were successfully constructed and operated. A number of tests and experiments were performed on the bearing-rotor system. The tests consisted of load capacity, stiffness and damping measurements. The results proved to be very positive in that the theoretical predictions and the observed performance matched reasonably well, giving credibility to the models which were used to perform the analysis. Of particular interest for this study was the measured power consumption of the bearings. It clearly demonstrates that the use of permanent magnets can improve the operating efficiency of an active magnetic bearing.

It was successfully observed and demonstrated that these bearings have strong potential for future use as efficient, reliable bearings. However, further research and development is required in the areas of controls, magnetic materials and actuator design before it is possible to install them into a useful industrial application.

References:

1. Allaire P., J. Imlach, J. McDonald, R. Humphris, D. Lewis, B. Banerjee, B. Blair, J. Clayton, R. Flack, "Design, Construction and Test of Magnetic Bearings in an Industrial Canned Motor Pump," Pump Users Symposium, Texas A & M, Houston, TX, May 1989.
2. Weise, D. A., "Present Industrial Applications of Active Magnetic Bearings," Presented at the 22nd Intersociety Energy Conversion Engineering Conference, Philadelphia, Pennsylvania, August 1987.
3. Burrows, C. R., N. Sahinkaya, A. Traxler and G. Schweitzer, "Design and Application of a Magnetic Bearing for Vibration Control and Stabilization of a Flexible Rotor," Proceedings of the First International Magnetic Bearings Symposium, ETH Zurich, Switzerland, June 1988.
4. Keith F. J., R. D. Williams, P. E. Allaire and R. M. Schafer, "Digital Control of Magnetic Bearings Supporting a Multimass Flexible Rotor," Presented at the Magnetic Suspension Technology Workshop, Hampton, Virginia, February 1988.
5. Studer, P. A., NASA, **Magnetic Bearing**, Patent 3865442, Patent Application 100637, February 1975.
6. Studer, P. A., NASA, **Linear Magnetic Bearing**, Patent 4387935, Patent Application 214361, December 1980.
7. Wilson, M. and P. A. Studer, "Linear Magnetic Bearings," Presented at the International Workshop on Rare Earth-Cobalt Magnets and Their Applications, Roanoke, Virginia, June 1981.
8. Ohkami, Y., O. Okamoto, T. Kida, C. Murakami, A. Nakajima, S. Hagihara and K. Yabuuchi, "A Comparison Study of Various Types of Magnetic Bearings Utilizing Permanent Magnets," Presented at the International Workshop on Rare Earth-Cobalt Permanent Magnets and Their Applications, Roanoke, Virginia, June 1981.
9. Tsuchiya, K. and M. Inoue, A. Nakajima, Y. Ohkami, and C. Murakami, "On Stability of Magnetically Suspended Rotor at High Rotational Speed,," Presented at the Aerospace Sciences Meeting, Reno, Nevada, January 1989.
10. Meeks, C., "Trends in Magnetic Bearing Design," Paper presented at Naval Sea Systems Command Magnetic Bearing Forum, Washington, D. C., July 1989.
11. Humphris, R. R., R. D. Kelm, D. W. Lewis and P. E. Allaire, "Effect of Control Algorithms on Magnetic Journal Bearing Properties," *Journal of Engineering for Gas Turbines and Power*, Vol. 108, October 1986.

FAULT DIAGNOSIS

Chairman: Howard A. Gaberson
Naval Civil Engineering Laboratory

THE EFFECT OF TRANSFORMATION FROM A FIXED TO A ROTATING COORDINATE SYSTEM ON EXCITATION FREQUENCY

John Neun, P.E. and Leo Hoogenboom
Mechanical Technology Inc.
Latham, New York 12110

ABSTRACT: Many measurements involve the application of strain gages to rotating members such as drive shafts. If a shaft were instrumented for bending and excited by an external force in a fixed direction at frequency F , the measured frequency is not F but two new frequencies displaced from F by plus and minus the shaft rotational speed. This paper describes this suppressed carrier modulation phenomenon as well as tests that confirm the frequency shift. The suppressed carrier not only applies to an external force acting on a rotating measurement system, but also to vibrations occurring on a rotating structure as measured from a fixed reference frame. This latter case applies to the detection of a vibrating blade by a sensor mounted on a shaft's bearing cap. In such a measurement, noise levels can be high. Understanding the suppressed carrier modulation phenomenon can make the difference between detecting the vibrating blade and losing the signal in the noise. Once the single-frequency excitation has been detected as a response at two frequencies, rules must be developed to determine the actual bending in the shaft. Interesting and confusing results can be obtained if one of the sidebands falls on a shaft resonance.

KEY WORDS: Frequency spectrum; modulation; sideband frequency; suppressed carrier; vibration

INTRODUCTION: For an accurate determination of the dynamic load and vibration characteristics of a drive shaft while in operation, it is desirable to make direct measurements on the shaft itself. In particular, the torsional behavior of a shaft is of interest, and for many applications, especially marine operation, dynamic thrust loading is important. Such measurements are best made with sensors mounted directly on the shaft. The direct nature of the results is worth the trouble caused by the logistical problems presented, such as how to get a wideband signal from the rotating reference frame of the shaft to the stationary reference frame of the observer. This problem is generally solved with slip rings which can be temperamental and are usually expensive. There are also more subtle ramifications of mixing reference frames. If a sinusoidally varying load originating from a fixed point in the fixed (not shaft) reference frame is applied to the rotating shaft, the observed frequency of the load is not necessarily as expected. A frequency spectrum of the load observed from the shaft may not contain a peak at the load frequency, but instead consist of two peaks equidistant from the load frequency, with spacing equal to the

shaft speed, depending on the nature of the load. The frequency of oscillation of the load is the carrier frequency, and it is in effect modulated by the frequency of shaft rotation. The carrier frequency is suppressed in the spectrum; the phenomenon is therefore called suppressed carrier modulation.

An experiment was performed to test a force sensor before its installation on a drive shaft and to quantify the suppressed carrier phenomenon.

SETUP: Figure 1 schematically depicts the experimental setup used.

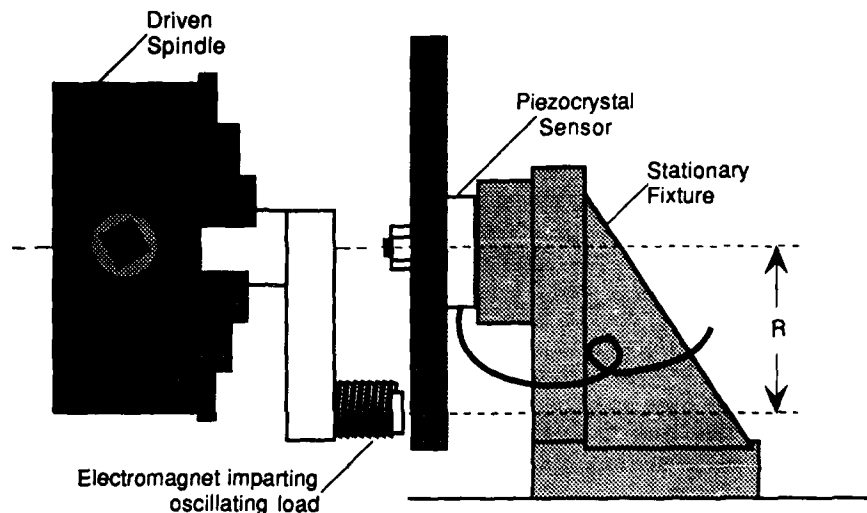


Figure 1: Experimental Setup, With Electromagnet Creating Oscillating Axial Load

The sensor was a piezocrystal load washer capable of measuring load in two dimensions: force along its centerline (F_z) and moment about its centerline (M_z). The nominal force range was ± 20 kN ($\pm 4,500$ lbf) with a nominal sensitivity of 1.8 picocoulombs/Newton (pC/N) (8 pC/lbf). The experiments described in this paper were concerned only with the F_z axis. As a point of interest, the nominal moment range was ± 200 Nm (± 150 ft-lbf), with a nominal sensitivity of 1.6 pC/Ncm (21 pC/ft-lbf). The oscillating load was created with an electromagnet. Because it was much more expedient to transmit the power to the electromagnet instead of the signal from the load washer through slip rings, the washer was mounted in a stationary fixture and the load generating electromagnet was rotated. Even though in the actual application on a shaft the sensor rotates and the load is fixed, the experiment was relevant because it is the relationship between the sensor and the load reference frames that is germane.

A lathe was used to provide controlled rotation of the load and accurate and substantial mounting for the sensor. The electromagnet was mounted on

an arm held in the lathe chuck. Power was transmitted to the electromagnet via slip rings (not shown in the figure). The load washer was preloaded to 500 kg by a tie bolt between a plate and a mounting fixture bolted to the cross slide of the lathe. The load cell was aligned with the spindle centerline.

The electromagnet acted through an air gap on the plate. All surfaces mating with the load washer were ground flat to ensure uniform pressure on the washer. The lathe was run at 240 rpm (4 Hertz), and the electromagnet generated a force at 308 Hertz. The distance of the electromagnet's center from the centerline of the lathe, L , could be varied from 0 to 6.3 cm (2.5 in). Running was possible at $R = 0$ cm; the nut shown on the centerline of the plate in Figure 1 in actuality did not interfere with the load application. A spectrum analyzer was used to evaluate the data.

A second configuration using the same equipment but with the electromagnet turned to impart a radial load to the sensor

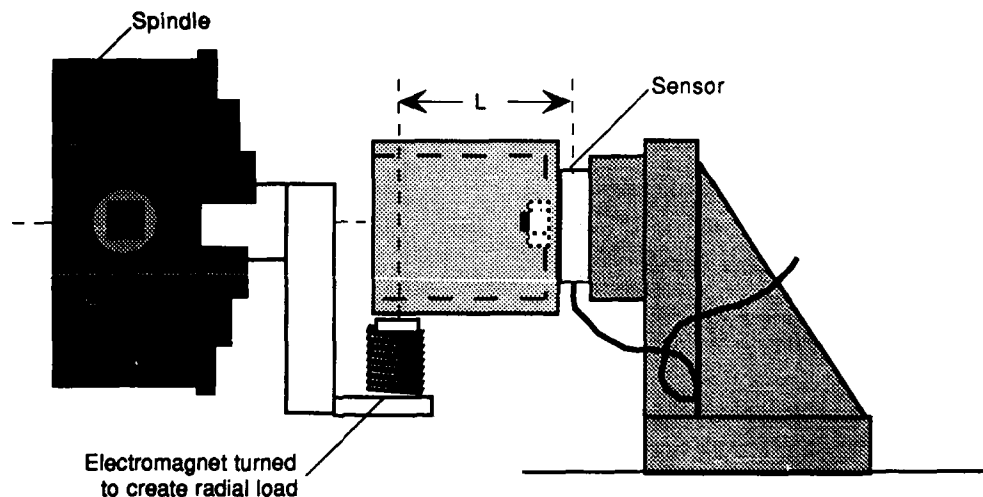


Figure 2: Setup for Radial Load

arrangement is shown in Figure 2. Note that the resultant moment on the sensor from the electromagnetic load can be compared to the moment generated in Figure 1 by ratioing the moment arms R and L . Also, the F_z response of the cell should have theoretically been zero, because no load in that direction should have been produced.

EXPERIMENTS: The first set of tests was performed with the axial force setup shown in Figure 1, with $R = 6.3$ cm. While the magnet was energized, the axial response of the sensor, F_z , was examined. The sensor should have reacted directly to the force because the force was in the direction of the measurement axis. To ascertain the magnitude of the force generated by the electromagnet, the signal was analyzed with the lathe

spindle not rotating. Figure 3 is a spectrum summarizing the result. It is an average of 16 instantaneous spectra; 4 were taken at each of 4 angular positions of the spindle (0° , 90° , 180° , and 270°) to eliminate differences within one revolution of the magnet. The chuck was rotated by hand between sets of averages. The figure shows that the magnet generated an average of 25 grams-force at 308 Hertz. It was observed that the force signal varied approximately ± 4 grams-force as the magnet was rotated. Two possible reasons for this variation were hypothesized, and both were probably responsible for some contribution. First, a difference in the gap between the magnet and the plate on which it acted could have caused a variation in the applied force, since the magnetic pull diminishes as the gap increases, and vice versa. The second cause could have been parasitical effects in the load washer.

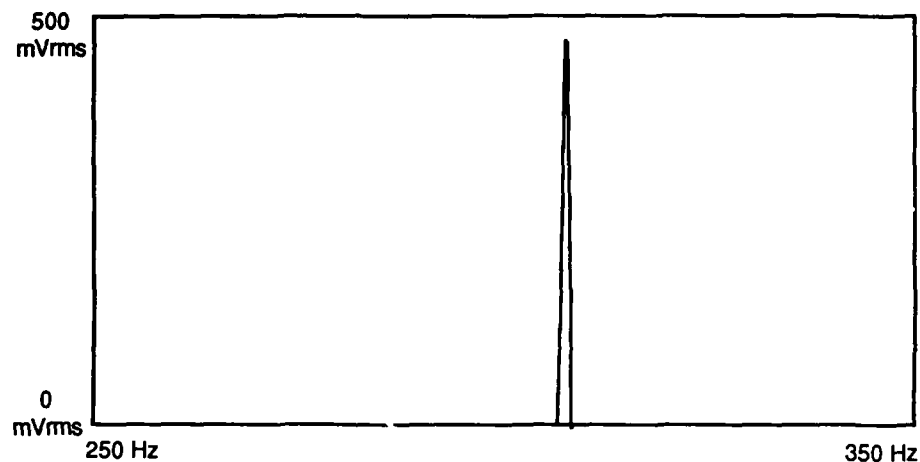


Figure 3: Axial response to axial force, not rotating, 25 grams at 308 Hertz

Load washers are designed to maximize their response to forces in the measurement direction and to minimize response to forces and moments in all other directions (see Reference 1). The washer used contains a number of quartz disks mounted in a regular pattern around the centerline of the washer such that the F_z load is perpendicular to all of them. They are designed to all respond equally to the F_z force. The response of all the disks is summed to create the output of the sensor. If the force is off-axis and a moment about a line perpendicular to the sensor centerline is present, the moment effect is cancelled because it puts half of the disks in tension and half in compression, such that tensile and compressive charge outputs sum to zero. This effect is illustrated in Figure 4. Theoretically, the orientation of the moment axis makes no difference to the measurement;

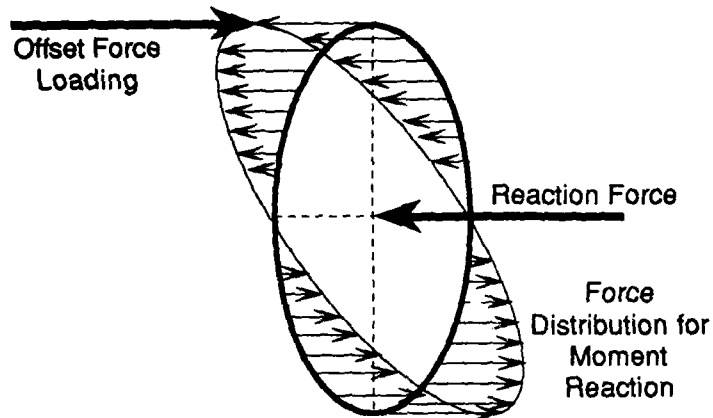


Figure 4: The distribution of reaction forces in a load washer due to an off-center load

the moment-induced outputs should cancel no matter where the off-axis load is applied. Actual measurements show that the output depends on the pressure distribution across the washer surfaces. When the distribution is changed, there may be a small net gain or loss in output even though the total input load is kept constant. The reason for this behavior is that part of the load is carried by the case of the cell and the pre-loading bolt. When, for fixed load input, this load sharing changes, all output also changes. The preload on the cell is intended to ensure that all piezo-ceramic disks in the cell participated equally in carrying load, to minimize the degree of cross-axis sensitivity, but an inherent error remains. "Crosstalk," the response of the sensor to loads other than those in the measurement direction, is inevitably seen, and furthermore, it is not consistent in all directions. The angular variation in the crosstalk response is probably a contributor to the uneven response which causes the need for the 4-pole average.

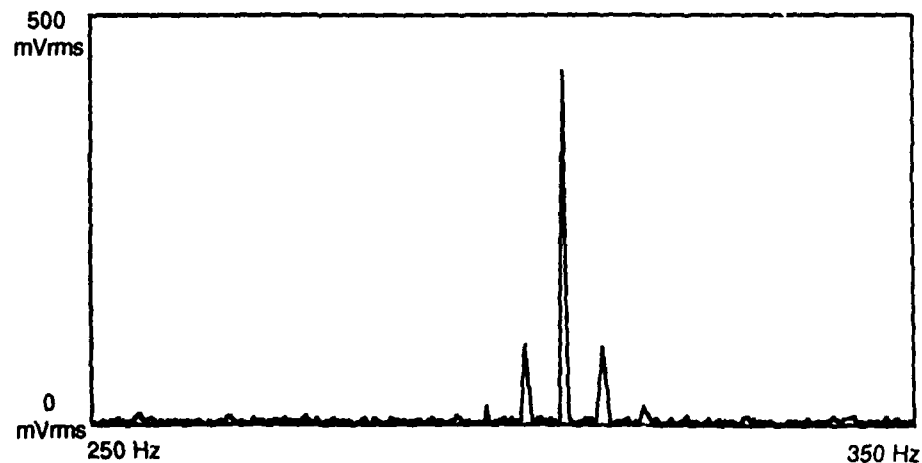


Figure 5: Axial response to axial load, rotating at 240 rpm, 24 grams at 308 Hertz, 3 grams at 304 Hertz and 312 Hertz.

Figure 5 is a spectrum taken with the axial load configuration (Figure 1) while the force rotated at 240 rpm (4 Hertz). Again, the figure is an average of 16 spectra generated from the F_z channel of the load washer. Note the presence of the sidebands at the rotating frequency, 4 Hertz, on either side of the carrier frequency, 308 Hertz. Also note that the carrier amplitude is 24 grams-force, which is about equal to the amplitude of the 308 Hertz peak in Figure 3, as is expected. The signal was modulated, causing the sidebands, but the carrier was not suppressed.

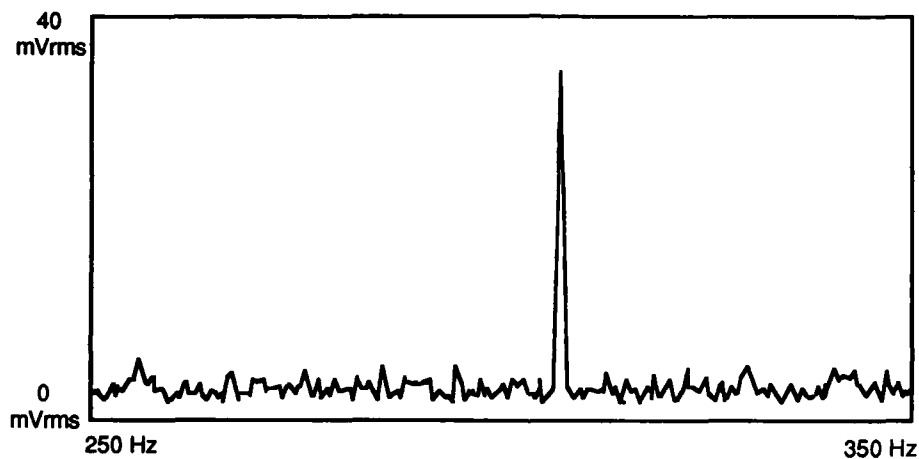


Figure 6: Axial response to radial load, not rotating, 1.8 grams at 308 Hertz.

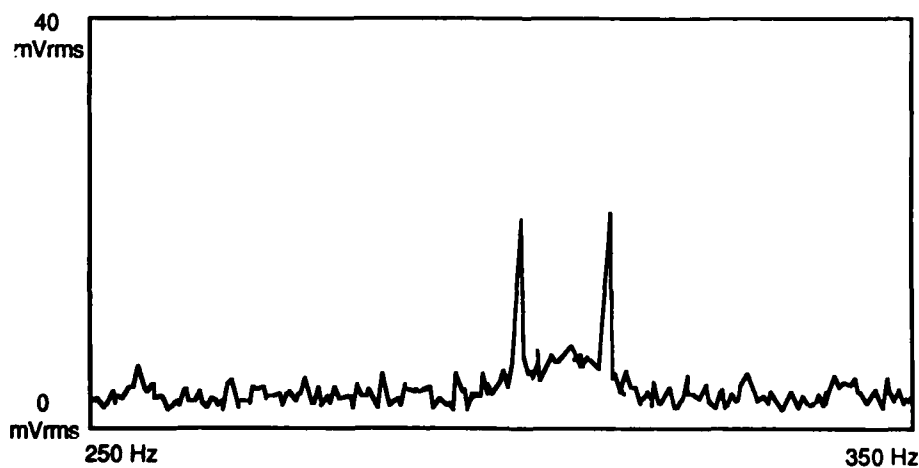


Figure 7: Axial Response to radial load rotating at 240 rpm, .6 grams at 308 Hertz, 1.2 grams at 304 Hertz and 312 Hertz.

Figures 6 and 7 replicate the results summarized in Figures 3 and 4, except that the radial load setup (Figure 2) was used. Note that the axial response is much less. There should theoretically be no response in the F_z direction, since there is no load in that direction. All response was due to error such as the crosstalk discussed above. Even though the response is much less, it is still easily measurable and definitely significant. With the nonrotating load, the amplitude at 308 Hertz is 1.8 grams-force. With the load rotating, the carrier amplitude is attenuated to 0.6 grams-force, one half of the sideband amplitude. The carrier peak in Figure 7 is nearly buried in the noise.

DISCUSSION OF RESULTS: The equation for a modulated sine wave is

$$f(t) = [K + m \sin(2\pi f_m t)] \sin(2\pi f_c t + \phi) \quad (1a)$$

or

$$f(t) = K \sin[2\pi f_c t + \phi] + \frac{m}{2} \sin[2\pi(f_c - f_m)t + \phi] + \frac{m}{2} \sin[2\pi(f_c + f_m)t + \phi] \quad (1b)$$

where

f_c = the carrier frequency (Hertz)
 f_m = the modulating frequency (Hertz)
 ϕ = the phase angle (radians)
 m = fractional modulation depth
 K = constant.

Note that if the first term of Equation 1a, $K + m \sin(2\pi f_m t)$, is replaced by a constant, A , the resulting equation is

$$f(t) = A \sin(2\pi f_c t + \phi) \quad (2)$$

which is a simple sinusoidal signal. The first term thus represents the time dependency of the amplitude, i.e., the modulation. When the carrier term in Equation 1b, $\sin[2\pi f_c t + \phi]$, goes to zero, the carrier is suppressed.

Figure 8 is an illustration of two signals. The shaded line represents a plain, nonmodulated sine wave. The black-lined signal represents a modulated signal with f_c equal to the frequency of the shaded sine wave. The carrier is suppressed. The most telling characteristic of the suppressed carrier signal is the phase reversal when the modulating component passes through zero. When the carrier is suppressed, the f_c term in Equation 1b becomes zero. In Equation 1a, therefore, the first term in the brackets, 1, disappears.

The phase flip in Figure 8 can be understood by examining Equation 1a with a suppressed carrier, i.e., with the K eliminated. The sine terms are

multiplied. As long as the modulating term, the "long" modulating wave in Figure 8, remains constant in sign, whether plus or minus, the sign of the product is determined by the carrier term, the "short" carrier wave in Figure 8. When the amplitude of the modulated carrier goes through zero, as it does at the two points of Figure 8, that relationship is reversed. For the left-hand quarter of Figure 8, the sign of the carrier is positive. This is reversed to negative for the middle half, and again is positive for the last quarter. The apparent phase of the signal is thus flipped 180° for the middle half.

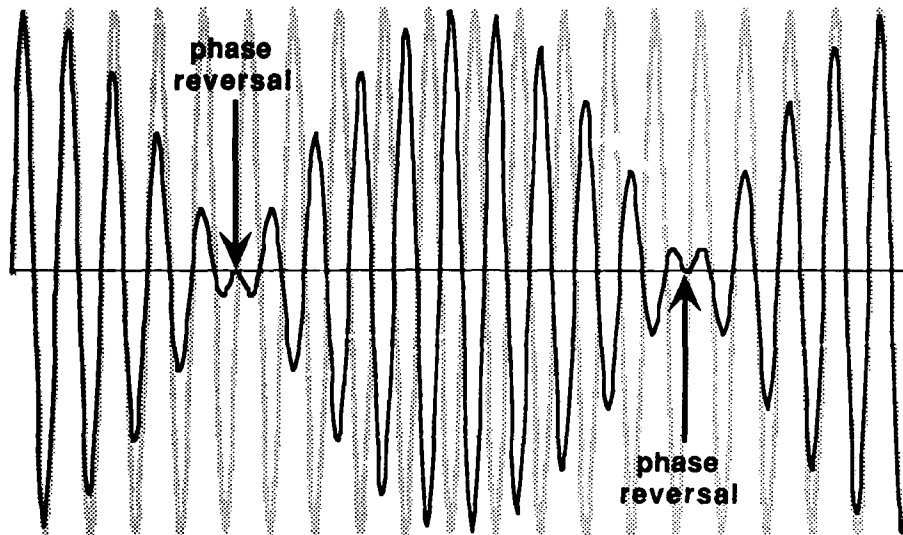


Figure 8: Two waveforms; the heavy line represents a modulated signal with suppressed carrier. The shaded line is a non-modulated signal at the carrier frequency. Note the phase flip at either end of the center area of the modulated signal.

The results of the tests with the first (axial) setup showed a conventional modulated signal. The sensor responded directly to the force parallel to the axis of measurement. The signal had some modulation due to the offset moment response and setup errors. Regardless of radial offset, the axially positioned magnet resulted in responses similar to those shown in Figures 3 and 5.

The second (radial) setup did not cause any load parallel to the F_z sensor axis. There was no fixed amplitude load in the z direction; all of the response in F_z was parasitic and therefore varied with angular position of the load. If B = crosstalk magnitude, then B was a function of angular position. Given the known pressure dependence of the load cell and its circular shape, the likely shape of the function can be approximated by the equation

$$B(\phi) = B_0 + B_1 \sin(\phi) \quad (3)$$

where

$B(\phi)$ = the magnitude of the crosstalk as a function of ϕ

$\phi = 2\pi f_m t$ = the angular position on the load cell determined by f_m

Multiplication of B with the force at the carrier frequency results in Equation 1b. For $B_0 = 0$, the carrier frequency is suppressed and only the sidebands remain. If the expression for the function is more complex, that is, if it is not simply sinusoidal, then more sidebands occur at integer multiples of f_m above and below the carrier frequency.

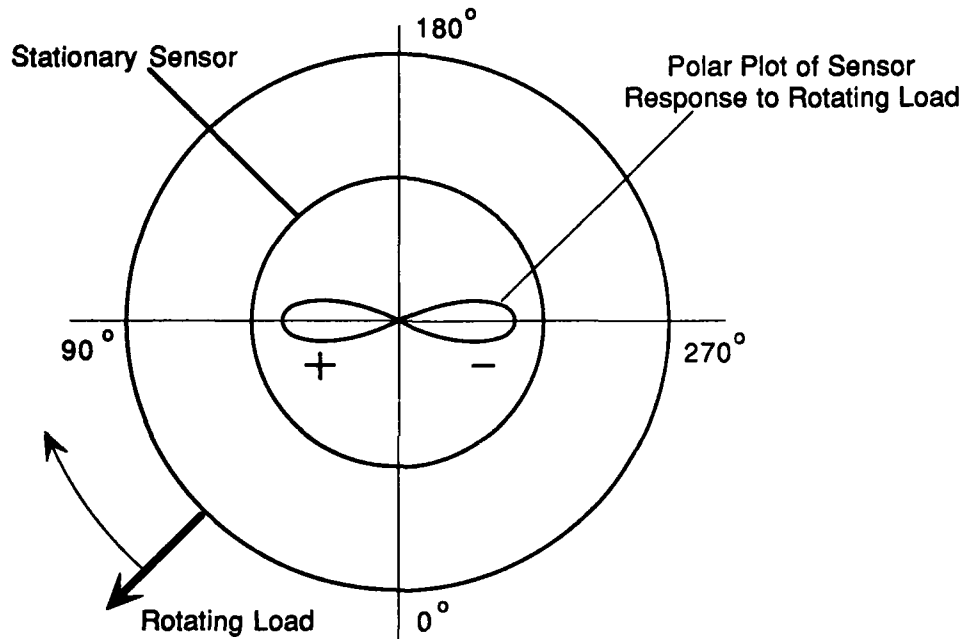


Figure 9: Response of a Stationary Sensor to a Rotating, Alternating Load

To visualize why for $B_0 = 0$ the carrier vanishes, consider the magnetic force in the radial setup of Figure 2. The magnetic force is always radially outward. Figure 9 shows how the force acts on the sensor arrangement. For the distribution given in equation (3), with $B_0 = 0$ there is a maximum response at $\phi = \pm 90^\circ$ and a zero response at 0° and 180° . The carrier is suppressed because as the load rotates, the sensor response reverses sign when the modulating function passes through zero (center in the polar plot). For exactly equal numbers of cycles of opposing signs at the carrier frequency occurring in alternation, the analyzer responds with zero amplitude for the symmetric part (at f_c), and a positive amplitude for the non-symmetric part (at $f_c \pm f_m$).

As the sensor rotates 180° , its response also shifts 180° in phase with respect to itself, and therefore cancels itself. The only vestige of the signal in the spectrum is therefore the modulating frequency, (the rotational speed), since the carrier frequency is suppressed.

APPLICATION: The experiments discussed indicate that care must be taken when nonstationary reference frames are used. The application for which these tests were performed required very sensitive measurements in the Z (axial) direction. It was found that a side force could have an important effect on that measurement. More importantly, the effect was manifested at frequencies not immediately obvious: the side force frequency was not seen in the Z-axis spectrum because of the suppressed carrier phenomenon. Rather, it became apparent with the sidebands around the invisible carrier frequency.

An analogous application is blade vibration in a turbine. A fixed sensor on a turbine bearing cap and a blade on a spinning turbine are in reference frames related to each other as described above. Even if the resonant frequency of the blade is known, it is not evident in a spectrum generated from the sensor. Instead, sidebands at the turbine speed appear in symmetry with the invisible blade vibration frequency. Normally, one searches for modulation effects by looking for a carrier and sidebands. It is difficult to spot the sidebands without the carrier frequency unless the investigator is specifically looking for them. If one of the sidebands falls on a resonance of the structure, the effect is even more difficult to spot because the amplitude of the sidebands could be quite nonsymmetrical. It is also difficult to find the source of excitation of the resonance, because the carrier frequency is hidden in the spectrum.

REFERENCES

- 1) Kistler Instruments Corporation, *"Measure Cutting Forces? No Problem With Quartz Multi-component Dynamometers,"* 1983, Kistler Instruments Corporation, Amherst, New York.
- 2) Fink, D.G., and Christiansen, D., eds., *"Electronics Engineers' Handbook,"* 1989, McGraw-Hill, New York.

**PUMP PROBLEMS AND PIPING PARTICIPATION
(REAL AND ALLEGED)**

Evans C. Goodling, Jr.
Gilbert/Commonwealth, Inc.
Box 1498
Reading, PA 19603

Abstract: At a steam electric power plant, whenever a pump becomes misaligned with its drive turbine or motor, begins to vibrate excessively or its bearings heat up and fail prematurely, initial blame is often directed toward the connected piping. Although high piping reactions at the pump connections can cause casing distortion and consequent problems with alignment and bearing wear, the root cause often lies elsewhere.

This paper discusses actual experiences resolving problems with pumps in a variety of fossil and nuclear power plants. The paper presents nine case histories of pump problems in which piping reactions were thought to be a primary factor. In some cases, the pipe did turn out to play a significant role, but in others it did not. Even where piping reactions were found to produce excessive forces and moments on pump casings, the piping reactions were found to be a symptom of deeper trouble. The paper then provides a checklist of suggested actions for the piping engineer who has been called in after everyone else has been given a chance to guess at what is causing a pump installation problem.

Key words: Coupling vibration; piping reactions; pipe restraint; pump bearing failure; pump casing distortion; pump shaft alignment; pump shaft vibration; pump vibration.

Introduction: Whenever a large high speed pump develops vibration or coupling alignment problems, high bearing temperatures, premature bearing failures, or material failures in the rotor or casing, the investigation often focuses on the connected piping. The problem might be identified as a vibrating pipe causing the pump to vibrate, thermal expansion that causes the pipe to twist the pump connections, or pipe restraints out of adjustment allowing the pipe to put too much force on the pump casing. What typically follows is a general discussion about the different things a pipe can do to a pump casing, sometimes even without the piping engineer present. There is sometimes so much initial emphasis on the piping that the real problem remains unidentified until the piping design has been exonerated.

For each of the following case histories, the type of plant is identified, followed by a description of the type of pump and its function in the plant systems. The vibration or other malfunctions are described, followed by a discussion of preliminary findings and a tentative diagnosis of the problem, which almost always identify the piping as the primary trouble source. There is a description of the piping investigation which was undertaken either to confirm the original diagnosis or to exonerate the piping. Following the details of the piping investigation is a discussion of the results of further

evaluation of other possible problem areas. Each case history then describes the corrective action taken and presents brief conclusions regarding the investigations and findings.

The case histories include some anecdotal commentary about operating personnel being misled into spending time trying to correct alleged piping problems. These are often futile attempts to resolve pump vibration and coupling alignment problems or material failures that inadvertently overlook the real problem source.

Case Histories

Case 1:

Location: Coal-fired power plant

System : Boiler feedwater, turbine-driven pump

Symptoms: Excessive vibration at pump bearings, premature bearing failures.

Preliminary findings: Shaft coupling misalignment; pipe reactions believed to be the cause.

Piping investigation: Thermal flexibility analysis of the piping showed that the nozzle reactions were well within the limits set by the pump manufacturer. However, at the request of the pump manufacturer, the torsional moment imposed by the piping at the pump discharge was reduced by about 50% by means of a spring-loaded horizontal torsion arm tied to a nearby building column. There was no improvement in pump operation after the torsion arm was installed. The plant owner contracted for extensive measurement and evaluation of vibration signatures before deciding to focus on the pump/turbine foundation and shaft coupling alignment.

Eventual findings: The pump sole plate was found to have been poorly grouted in place, and the structural steel mounting frame was found to deflect under normal operating conditions, thereby making it impossible to maintain proper alignment of pump and drive turbine shaft during operation.

Final action: The pump sole plate was chipped loose from the concrete slab and regouted into position. Stiffening gussets were added to the pump support frame to increase its lateral stiffness. The result was a significant decrease in the number of premature bearing failures.

Conclusion: A pump has a better chance of performing properly if it is installed correctly on a rigid support structure.

Case 2:

Location: Coal-fired power plant

System: Boiler feedwater, turbine-driven pump

Symptoms: Pump vibration and premature bearing failure

Preliminary findings: Piping believed to impose excessive moment on pump casing.

Piping investigation: Thermal flexibility analysis of the piping showed that the nozzle reactions were well within the limits set by the pump manufacturer. However, at the request of the plant owner, thermal restraints were added to the feedwater discharge piping in order to further reduce pump nozzle reactions.

Eventual findings: This pump design was unique; it was developed by modifying the design of a lower capacity pump to rerate it for higher flow.

Final action: Several pump modifications were later made, including installation of increased thrust bearing capacity and larger diameter rotor shaft. The pump problems have apparently been solved, but no single modification can be credited.

Conclusion: Uprating an existing design is not always the most economical way to get a higher capacity pump.

Case 3:

Location: Oil-fired power plant

System: Boiler feedwater, turbine-driven pump

Symptoms: High shaft vibration

Preliminary findings: Pump and turbine shafts always moved out of alignment shortly after startup, resulting in excessive vibration.
in the drive shaft assembly.

Piping investigation: Since the pump and turbine had been aligned strictly in accordance with the manufacturer's procedures, the piping reactions were suspected as the cause of misalignment and vibration after startup. However, review of pipe stress analysis results and project correspondence showed that the turbine manufacturer (who was responsible for the installation design) had certified the acceptability of the piping reactions.

Eventual findings: It was later discovered that the turbine manufacturer had considered only the pump inlet connection reactions in designing the structural frame on which the pump assembly was mounted, inadvertently ignoring the far higher discharge pipe reactions. When the pipe was cut, a large amount of cold spring was discovered in the direction opposite that which was specified on the piping erection drawing.

Final action: The pump mounting frame was redesigned and modified to carry the combined inlet/outlet connection piping reactions without deflecting under load or causing shaft misalignment and consequent vibration during operation. The pipe was reconnected with the proper amount of cold spring.

Conclusion: In this case, four parties were involved: the pump manufacturer, the turbine manufacturer, the piping erector, and the piping engineer. The piping engineer took initial blame until documentation and the pipe cut revealed the improper cold spring. Proper placement of responsibility for fixing a pump problem often depends upon how well you maintain your project documentation files.

Case 4:

Location: Coal-fired power plant

System: Boiler feedwater, turbine-driven pump

Symptoms: Large shaft misalignment, high vibration levels.

Preliminary findings: Pump and turbine shafts moved out of alignment shortly after startup.

Piping investigation: Since the pump and turbine had been aligned in accordance with the manufacturer's procedures, the piping reactions were suspected as the cause of misalignment and vibration after startup. However, review of the pipe stress analysis showed that reactions at the pump connections were within the pump manufacturer's allowable levels. Piping reaction was still the prime suspect due to the fact that some 3/4" alignment dowels were sheared off as soon as the pump and piping heated up to operating temperature.

Eventual findings: The pipe connection to the pump was cut loose and found to have been sprung circumferentially by 1/8", which on the 20" discharge pipe amounted to a torsional misalignment of 0.7 degree. It was then revealed that due to tight construction schedule and late valve delivery, the piping had been installed with a spool piece in place of the missing valve. When the valve was finally delivered, it was apparently installed with improper welding fitup, and consequent differential cooling and shrinkage caused the torsional misalignment.

Final action: Although no cold spring was specified by the design, cold spring was incorporated into the discharge piping to minimize the reactions at the pump connection. The shaft alignment problems and vibrations did not appear during subsequent operation.

Conclusion: Improper pipe fitup and welding techniques can severely affect pump alignment in a properly designed system.

Case 5:

Location: Oil/coal-fired power plant

System: Spare boiler feedwater system, motor-driven pump

Symptoms: Difficulty in achieving precise alignment between speed coupling and pump shaft.

Preliminary findings: The alignment indicator readings on the coupling flanges kept changing even while no adjustments were being made.

Piping: A casual remark about settings on variable spring hangers supporting the pump discharge piping led to a review of the piping and nozzle reactions. No discrepancies were found, and since nozzle reactions during pump shutdown were very low, the piping was eliminated as a cause.

Eventual findings: The pump was still warm from earlier operation when the alignment check was initiated. As the pump cooled, there was enough movement of the casing to be read on the dial indicators on the coupling flange.

Final Action: The pump was allowed to cool to ambient temperature before alignment procedures were resumed.

Conclusion: Changing temperatures in the pump casing can significantly affect shaft coupling alignment readings.

Case 6:

Location: Coal-fired power plant

System: Boiler circulating water piping, motor-driven pump

Symptoms: Cracks found in pump casing flanges of several pumps.

Preliminary findings: Several possible causes were suggested by the boiler manufacturer, including maladjusted variable spring hangers on the piping, pressure stress in the pump, and piping vibration.

Piping investigation: Pipe stress analysis for dead load and thermal expansion showed that the pipe stresses were well within B31.1 Power Piping Code allowable levels, and that pump casing stresses imposed by piping and operating pressure were less than eight percent of yield stress. It was determined also that minor adjustment discrepancies in the variable spring hangers on the piping had very little effect on pipe stresses or reactions on the pump connections.

Eventual findings: Other possible findings were suggested after the piping was exonerated, such as over-tightening of flange connection stud nuts, thermal gradients across the flange faces,

or residual stresses in poor quality pump castings. It was also learned that the pumps were purchased without any established allowable reactions at the piping connections, which had the possible effect of voiding any warranty for a pump subject to normal operating reactions from connected piping.

Final Action: The casing cracks were monitored in order to determine if they were growing, and the affected pumps scheduled for eventual replacement.

Conclusion: Casing cracks are not caused by normal pipe reactions; their presence is most likely due to a defective casting. Pumps should never be purchased without a written understanding as to what piping reactions are permitted at the connections. Otherwise, it may be very difficult to assign liability for resolving subsequent pump problems, regardless of whether piping reactions play any part.

Case 7:

Location: PWR nuclear power plant

System: Decay heat, motor-driven pump

Symptoms: Vibration, shaft coupling misalignment, pump shaft failures, severe piping vibration and broken restraints

Preliminary findings: It was originally thought that the pump problems stemmed from manufacturing discrepancies resulting in a distorted casing leading to pump shaft failures at both the drive end and the impeller end.

Piping investigation: The pump/motor shaft alignment was carried out with the piping empty. During subsequent filling, the alignment was found to change. The shafts were not realigned after filling. There was also some speculation that residual cold spring in the piping may be present and cause some casing distortion.

Eventual findings: It was believed that low water levels in the reactor coolant system had permitted vortices to form at the entrance to the pump suction piping, introducing air into the pump intake. Whenever air passes through the pump, large unbalanced forces are imposed on the pump impeller and shaft. The air induction into the pump plus the failure to realign the shafts after system filling are both believed to have contributed to the shaft failures.

Final action: All damaged pipe supports were repaired, the alignment procedures were changed to require final shaft alignment after the system is filled, and other action was taken to minimize the possibility of inducing air into the pump inlet piping.

Conclusions: Since the system operates with the piping full of water, it makes sense to make the pump drive shaft alignments with the

piping full of water. Also, it is very important to keep the inlet piping full of water without any induced or trapped air or vapor pockets.

Case 8:

Location: PWR nuclear power plant

System: Feedwater piping, turbine-driven pumps

Symptoms: Difficulty in aligning shaft coupling ends, vibration in pump bearings and in discharge piping

Preliminary findings: There were reports that the piping from three pumps in parallel would resonate when all three pumps were run at the same speed. One pump had earlier sustained a shaft break, which was said to have been caused by fatigue due possibly to coupling misalignment. Axial vibration at the pump bearings was found to exceed recommended levels by 80 percent. After shutdown, a coupling misalignment of 140 mils was measured.

Piping: There were no discrepancies found in either the piping or its supports and restraints. Pump/turbine shaft alignment was performed as specified in vendor instructions. Stress analysis demonstrated that piping reactions at the pump connections were within the allowable levels set by the pump manufacturer.

Eventual findings: The vibrations were determined not to be due to piping reactions or flow conditions, but are thought to be due to shaft misalignment or problems with the couplings themselves.

Final action: Replacement of couplings with new ones machined to close tolerances, more frequent lubrication of the couplings, and minor adjustment of operating speed have been tried. Vibrations have been reduced to more acceptable levels, but further investigation is continuing.

Conclusions: The piping reactions and flow conditions, at one time the prime suspects, have apparently been eliminated as primary causes.

Case 9:

Location: BWR nuclear power plant

System: Feedwater piping, turbine-driven pumps

Symptoms: One of three pumps was observed to be far out of alignment with its drive turbine.

Preliminary findings: Proper shaft alignment within established tolerances could not be obtained by the use of specified procedures.

Piping: In the course of making some pipe hanger adjustments, a pair of parallel rigid struts were disconnected on the pump discharge pipe, permitting the pipe to move an estimated two inches. Examination of struts on the suction piping showed that the pin-to-pin dimensions did not match those specified on the strut installation drawing. There were pipe wrench marks on the strut barrel implying that at some time in the past adjustments had been attempted in order to force the piping and pump into alignment.

Eventual findings: It was concluded that the pipe was cold-sprung at one time although no cold spring was specified on the piping erection drawings. There were unconfirmed reports that although this plant was started up in 1982, the affected feedwater pump had never been properly aligned. There were other reports that alignment had been achieved at one time but could not be maintained.

Final action: Pipe stress analysis showed that the struts were required in order to keep reactions at the pump connections down to acceptable levels. All rigid struts on the suction and discharge piping to all three pumps were disconnected during a shutdown and then readjusted and connected with no load imposed on the cold piping. The pumps were aligned in accordance with recommended procedures to bring the shafts and drive couplings to within specified tolerances, and were then observed during subsequent startup. The pumps again appeared to be pushed out of alignment as the piping heated up, but the magnitude of misalignment was substantially less than before the struts were adjusted to the cold no-load condition. There is additional action planned to further adjust the rigid struts in order to produce a cold offset that will enable the pumps to achieve acceptable shaft alignment as operating temperatures are reached.

Conclusions: This was a case of cold spring found to exist where none was specified or expected. Undocumented maintenance actions in the past had failed to solve the alignment problem, which was then ignored until it came to the attention of responsible management. Intelligent team work among engineering and maintenance personnel is now moving the problem toward a satisfactory resolution.

General Conclusions: The above case histories of pump problems initially attributed to piping reactions were shown to involve a variety of actual causes including inadequate design of pump structural support, improper cold spring in the piping, poor fitup and welding of the piping connection to the pump, shaft rotor and thrust bearing design, flow conditions, thermal expansion of the pump casing, and faulty pump castings. In no case was piping design the fundamental cause of the problems cited.

For anyone who is faced with determining the cause of vibration or shaft and coupling alignment problems in large high speed pumps where piping

reactions are considered suspect, the following checklist of investigative activities is recommended:

1. Review the pipe stress analysis to assure that reactions at the pump connections are not excessive when compared to the pump vendor's recommended maximum levels or when compared to levels permitted for other pumps of similar size and construction. See Cases 1, 2, 3, 4, 6, 8, and 9.
2. Review the piping erection drawings to determine whether cold spring was specified for the installation of the piping. Determine whether cold spring was correctly considered in the analysis and qualification of the piping connections to the pump. See Cases 1, 2, 3, and 4.
3. Survey the piping, supports and restraints to assure that they conform to the design used in the pipe stress analysis model. Examine the supports and restraints to assure that they are located and adjusted as designed. See Cases 6, 7, 8, and 9.
4. Look for evidence of piping reactions that significantly exceed the levels predicted by analysis. Large reactions may make it impossible to align the pump shaft and coupling and may manifest themselves in sheared alignment dowels or buckled pipe restraints. Such evidence may indicate improper or excessive cold spring or poor fitup during welding of piping attachment to the pump. At this point, it may be necessary to cut the pipe to confirm the actual amount of cold spring in the pipe. See Cases 3, 4 and 9.

If the piping and pipe supports pass the above review, they can probably be eliminated as the primary cause of any pump or shaft alignment problems. However, if discrepancies are found, they should be evaluated, corrected, or otherwise disposed of before moving on to the next steps.

5. Examine the pump foundation to determine if the pump is adequately anchored to the concrete slab or pedestal. See Case 1.
6. Confirm or observe the procedures used in aligning the power transmission shafts and shaft coupling to assure that alignment has been performed precisely as specified in the manufacturers' alignment procedures. See Cases 5 and 7.

If the problems still exist after it has been determined that the pump and its driver have been installed and aligned in accordance with specified procedures, then -

7. Monitor any deflection of the pump or its supporting structure during startup and operation to determine if there is enough movement to cause shaft misalignment. If this still occurs, the pump manufacturer should be consulted to review the design of the support structure and anchorage designs. See Cases 1 and 3.

If the problem remains after proceeding through the above steps, it is fairly certain that the piping has no significant role, and that the cause may be found in flow-induced transients or vibrations (Case 7), or material deficiencies in the pump casing, rotor, or shaft coupling (Cases 2, 6 and 8).

SUMMARY OF CASE HISTORIES

Case	Pump Speed (rpm)	Flow rate (gpm)	Discharge pressure (psig)	Driven by	Normal power (bhp)	Speed (rpm)	Piping reactions involved?
1	5800	5650	4735	Steam turbine	17947	5800	Yes ¹
2	6000	3310	4450	Steam turbine	9940	6000	No
3	5980	6958	3140	Steam turbine	13637	5980	Yes ²
4	5250	6400	2870	Steam turbine	12080	5250	Yes ³
5	5200	9000	3010	Induction motor	25000	1750	No
6	1750	7100	2400	Induction motor	300	1750	No
7	1750	3000	450	Induction motor	400	1750	No
8	4950	9600	1250	Steam turbine	6200	4950	No
9	5150	12500	1125	Steam turbine	8600	5150	Yes ⁴

Primary causes of piping problems:

¹Pump frame flexibility and poor condition of sole plate grouting.

²Pump frame flexibility and improper cold springing of discharge pipe.

³Improper weld fitup and residual torsion in discharge pipe.

⁴Improper cold spring in discharge pipe and adjustment of restraints.

In closing, it is recommended that an experienced piping engineer participate in the investigation from the very beginning. The piping engineer will most probably be able to promptly identify and confirm any piping characteristics that may involved, and may also be able to exonerate the piping or correct any support discrepancies so that attention can be directed toward finding the real cause of any reported pump problems. Because of its visibility, piping often becomes the prime suspect. Therefore, the initial investigation should be aimed at investigating and eliminating all piping and support discrepancies without delay.

Acknowledgments: The assistance of the following individuals who shared their experiences in the preparation of this paper is gratefully acknowledged: Randall Perry, James Yarger and James Muldoon of Gilbert/Commonwealth, Inc. and Gene Delp of Technicon Enterprises.

**DATALERT:
AN INTEGRATED MACHINERY VIBRATION
DATA COLLECTION AND ANALYSIS SYSTEM
USED IN LOSS PREVENTION**

**Kenneth D. Bever and Thomas M. Raymond
The Hartford Steam Boiler
Inspection and Insurance Company
One State Street
Hartford, CT 06102**

Abstract: DATALERT is an unique, integrated machinery vibration data collection and analysis system developed by a boiler and machinery insurer to assist customers in preventing rotating machine losses. Periodic vibration readings are taken remotely by plant personnel using hand-held, pre-programmed vibration data collectors. The readings are then transmitted to a central minicomputer using a modem over standard telephone lines. Without human intervention, the computer system processes the vibration measurements to highlight machines which are in alarm or are trending toward an alarm. The alarm reports, trend reports, and spectral plots are then summarized into a prioritized list of potential problems and recommendations. Plant staff can then take appropriate corrective action. A centralized database stores the data on-line for future access by both human and computerized expert analyses.

Key words: Integrated predictive maintenance system; automated vibration monitoring program; diagnostic expert system

Introduction: Periodic vibration monitoring is widely recognized as a reliable method of dynamically determining the health of rotating machinery (Hartley and Flanders, 1985; E.P.R.I., 1985).

Analysis of the overall vibration levels and associated vibration frequency signatures can result in the early detection and isolation of common machinery problems (IRD, 1975). These problems encompass misalignment, imbalance, anti-friction bearing defects, improper clearances and mechanical looseness among others. This early detection allows corrective maintenance to be prioritized and scheduled during non-critical periods, resulting in increased machinery availability and significant savings in both replacement parts and labor costs (Jackson, 1979). Production is therefore maximized and the risk of premature failure diminished.

In the mid 1970's, The Hartford Steam Boiler Inspection and Insurance Company established a Failure Analysis Laboratory to analyze machinery and equipment failure causes and help prevent recurrences. The laboratory was staffed with metallurgists, mechanical engineers, and vibration experts. A research program was implemented to establish the benefits of machinery monitoring as a loss prevention measure. Over the years, a substantial amount of loss data established the value of monitoring machinery conditions to help predict failures.

Hartford Steam Boiler combined this expertise with the available computer technology to develop an integrated vibration data collection system known as DATALERTTM.

DATALERT collects, processes, and analyzes machinery vibration data and resulting vibration frequency signatures as part of an integrated predictive maintenance system. All categories of rotating machines (except reciprocating) can be monitored. These machines typically have operating speeds from 100 to 20,000 revolutions per minute and are usually rated above 30 horsepower.

The system is not designed to replace permanently installed vibration monitoring systems on critical machinery. Instead, it augments these systems, which often do not provide historical information or spectral data. The most common problems that can be detected on machinery are: imbalance, looseness, misalignment, rolling element bearing defects, and seal rubs. DATALERT can help identify potential problems, indicate their severity, and assist in predicting how long a machine can operate before a failure is likely. It does this by comparing current measurements, as well as historical trend data, with a set of pre-defined alarm set points.

DATALERT is unique for the following reasons:

1. It includes a large, centralized database with machinery data from various facilities around the world. This enables trends and common machinery problems to be traced and analyzed on-line.
2. It provides an automated Analysis Summary Report which offers a preliminary diagnosis and a vibration analyst's recommendations for machinery suffering stress.
3. It eliminates the time consuming manual processing of vibration data into useful information. The savings has been estimated at three hours for each set of data.
4. It provides streamlined alarm reports, estimated time to alarm reports, selected overall vibration trend plots and frequency spectra.
5. It allows direct personal computer access to the central computer for immediate review of all report information.
6. It will incorporate a vibration analyst expert system to employ the expertise and knowledge of machinery vibration specialists.

The central computer and staff along with plant personnel and machinery collectively make up the DATALERT system. Hartford Steam Boiler assists in the training of the customer personnel and processes the data into useful information to provide insight into the causes of machinery vibration. The customer incorporates this insight into its predictive maintenance program to ensure continued maximum production.

Figure 1 summarizes the basic cycle of the program. The components of the program involve four areas:

1. Route development
2. Data collection and transmission
3. Reporting and plot generation
4. Expert analysis and corrective action recommendations provided to maintenance personnel

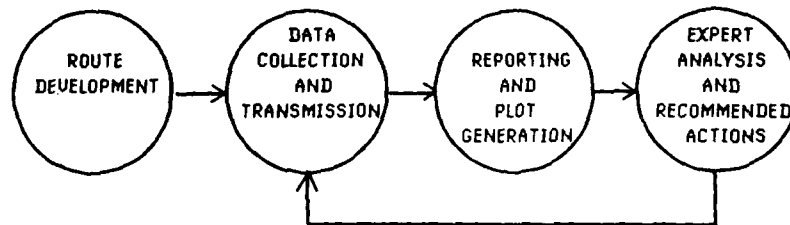


Figure 1

Route Development: A route is the order in which periodic measurement data is collected for each machine. Each route defines certain information about the machines to be monitored, where they are located in the plant, and the type of measurements to collect. Routes normally consist of the measurement information for approximately twenty-five machines. Each location or site usually has numerous routes. Once this information is stored in the central computer's database, the monitoring process can begin.

Machine Train Identification: The first step in developing a route is to identify the machines which should be monitored and establish their priority. Identifying the machines to monitor begins with a review of the plant layout and the compilation of a list of all of the machine trains in the plant. Certain machines, such as reciprocating machines, are not good candidates for this preventive monitoring program. Machine train types and component types that have been monitored in the project typically have operating speeds from approximately 100 to 20,000 RPM and are usually rated above 30 HP.

This list is then prioritized relative to the effect that the loss of a particular machine will have on production and maintenance costs. The different machines in the plant may or may not require the same amount of attention. Some machines are considered high priority or critical to production. These will require more attention than a machine that is of little consequence to production or is easily replaced.

The program classifies machines into three priorities: unspared critical (priority 1), spared critical (priority 2) and non-critical (priority 3). Unspared critical machines are defined as machines which are not spared and whose outage would result in total or partial loss of production for an extended period of time. Examples of these include turbine generators and syn-gas compressors. Spared critical machines refer to machines which are spared but whose loss would result in a complete or partial loss of production for some period of time. ID and FD fans may fall into this category. Non-critical machines are defined as those machines whose outage would not immediately affect production and which could be replaced before production loss would occur.

Machine Train Data Compilation: Once this list is prioritized, information about each train is compiled. This information will be used to identify possible sources of vibration. Nameplate data is collected, along with maintenance records, blueprints and OEM (original equipment manufacturer) documentation necessary to get sufficient information related to the number of blades, the number of balls or rollers in a bearing, number of gear teeth, etc. Information about the cylindrical and conical modes of vibration of rigid rotors and the bending critical modes of flexible rotors, if known, is also collected. Machines built to API specifications, require that much of this information be identified on the test stand at the OEMs before shipment. Certain machines operate in a variable speed mode through various schemes of governors or controllers. This requires that the operating speed range of these machines be compiled for later use in analysis. The information collected for each machine train is used to identify the machines to be monitored and the sources of vibration within each. Hartford Steam Boiler provides forms to collect this information.

On the forms, the information related to a specific machine to be monitored is noted. This information usually includes machine name, manufacturer, serial number, model number, speed, horsepower, type of bearings, and critical speeds.

Other information needed to help identify sources of vibration may or may not be readily available. This information is usually compiled over a longer period of time, as needed or during maintenance. Examples of this type of information include the bearing manufacturer, the number of gear teeth on a gear, and the number of impeller vanes.

Measurement Point Identification And Alarm Level Determination: The third step in the route development process involves establishing the measurement points on a machine train to be monitored and determining the alarm levels for these points. Measurement points are normally located as close to a machine's bearings as possible. Each position is clearly marked on the bearing housing. It is also numbered and given an orientation, such as vertical, horizontal, or axial. If only one measurement orientation is possible at a specific position, the plane of highest amplitude is selected. Next, all units of vibration to be taken at a machine train position are identified. Some measurements are more meaningful to an analyst if they are reported in particular units. For example, when severity

of vibration is desired, the preferred unit of measurement is inches/second or G's. Ball pass frequency measurements are useful in evaluating the condition of low-speed machinery with ball or roller bearings.

Three levels of alarm set points are used by the computer system. A **warning level** notifies plant personnel that a machine is in potential distress. A more severe **alert level** indicates that a machine is definitely in distress and requires prompt attention. The most severe **danger level** indicates that the machine is in imminent danger of failure. Once a machine exhibits the first distress level, the frequency of data collection can be increased to provide more accurate trending of this data over time. The data is then extrapolated to determine when the danger level is likely to be reached. This procedure allows for a planned shutdown to investigate and repair the problem.

These alarm levels are determined for each measurement position by using industry standards such as ISO Standards 3945 and 2372, API Standards 541, 613 and 612, or the Rathbone chart (Jackson, 1979).

Route Machine Train Identification: The fourth step in developing routes is to define the machine trains which compose a data collection route. Certain machine trains are grouped together on a route and monitored on a periodic basis, based on the criticality of the machines. Measurements are normally collected every two weeks for most machines.

The measurement collection device used in the program is a hand-held, battery-operated data collector. Along with the data collector, an accelerometer and associated mounting devices (magnet and hand-held probe) are provided for collecting vibration measurements. The data collector can be pre-programmed to facilitate the gathering of machinery data on a regular basis. Up to 270 data gathering points (about 25 machine trains) specifying a particular machine, measurement point, unit, and direction can be loaded into the data collector. The data collector also accepts certain alarm set points which trigger the collection of spectral data.

Computerized Database Storage: The final step in the development of a route is the storage of all machinery data collected in a large multi-user relational database located on a large minicomputer. This database is designed to optimize the storage of all the machinery component data and information related to a route. The information in the database includes such items as the machine name, measurement locations, operating speed, nameplate data, and the maintenance performed on a machine.

A customer accesses the database through a personal computer and a modem. An on-line database utility allows easy entry of the information about the machine trains in the DATALERT program and the routes to be followed. The user can later use this same utility to modify an existing machine train's measurement locations, alarm levels, or points to be monitored. The customer can also view or download summary reports of a specific machine train or an entire route directly from this utility.

The database also stores all vibration measurements and operating parameters collected from all monitored machines. A machinery history data file is maintained on-line for an appropriate period. This allows for the observation of trends on specific machines, as well as failure analysis across various types of machinery components.

Data Collection and Transmission: After training plant personnel in route development, an operator downloads an initial route from the central computer in order to take the first set of vibration readings. After the initial loading, the software automatically schedules the next route to be loaded into the collector based on the frequency of the routes and the last time data was received for each route.

The operator proceeds to capture vibration measurements from the specified points and directions shown on the data collector and may re-take any points or skip past a machine which is currently out of service. After this has been completed, these measurement and spectra readings are transferred from the collector to the central computer through a modem connected to an outside telephone line. After all data is received, the next route is sent back to the collector. Figure 2 illustrates the information flow between the various components of the DATALEERT system.

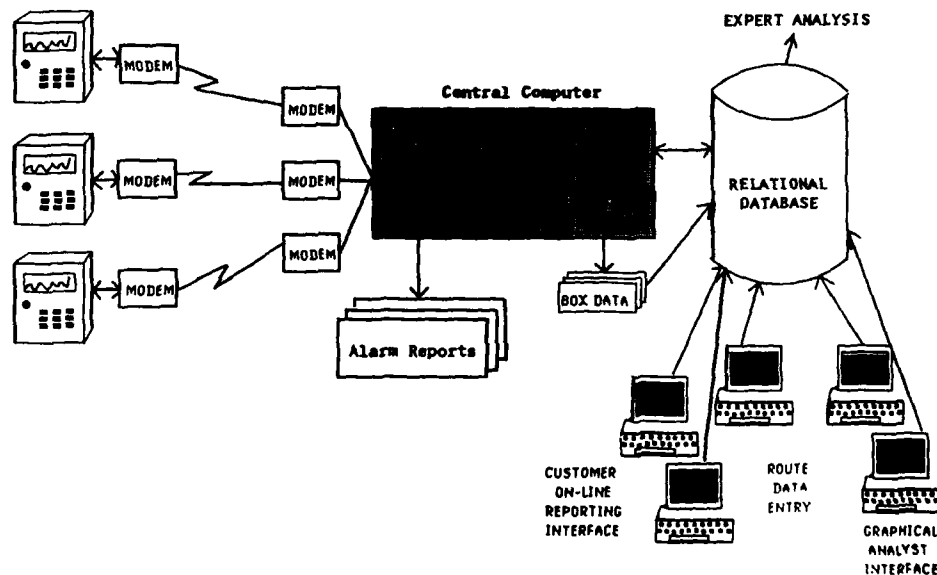


Figure 2

Reporting and Plot Generation: Following the successful loading of data, the software automatically starts the reporting and plot generation routines. These reports provide a condensed view of those machines which are currently in alarm or are trending toward an alarm.

Route Report Summary: The purpose of this report is to provide the plant with a summary of the measurements collected and the status of machines which have reached an alarm level during this route run or during the previous route run. The information includes a section with all machines in alarm categorized as follows:

Added -- The machine train previously had measurement positions which were in alarm and currently has positions which exceeded an alarm.

Removed -- The machine train does not currently have positions in alarm, but during the previous route run the machine train was in alarm.

Unchanged -- The machine train currently has measurement positions which are in alarm and previously had positions which were in alarm.

Overall Vibration Alarm Report: This report is a list of those measurement positions which exceeded an overall vibration alarm level as shown in Figure 3. The measurement position name, position number, direction of measurement, unit of measurement, alarm code triggered, current measurement, and last measurement are first listed. The heading "Alm" refers to the name of the alarm that was triggered: W for warning, A for alert, and D for danger. The column "% Ovr Alarm" indicates the percentage that the measurement exceeded the alarm level. The heading "Alarm Level" refers to the numerical value of the alarm that was triggered. Finally, the "Msrmt Date" column is the date that the measurements were transmitted for processing.

Overall Vibration Alarm Report									
Facility: Power Plant Corporation									
Route: Station A									
Facility ID: PPA									
Route ID: STATA									
Date: 24-Feb-1989									
Time: 14:46									
Measurement Position	Pos	Dir	Unit	Alm	Curnt Msrmt	Last Msrmt	% Ovr Alarm	Alarm Level	Msrmt Date
Machine Train: C-1103 Motor/GB/Compressor					ID: C-1103			Prio: 3	
Gearbox Motor End	3	A	g's	W	2.60	3.00	4	2.50	02/24/89
Gearbox Compressor End	4	V	g's	W	2.90	2.60	16	2.50	02/24/89
Machine Train: C-1104 Motor/GB/Compressor					ID: C-1104			Prio: 3	
Gearbox Motor End	3	V	g's	W	2.70	1.90	8	2.50	02/24/89
Gearbox Compressor End	4	H	g's	W	2.70	1.60	8	2.50	02/24/89

Figure 3

Estimated Time to Alarm Report: The purpose of this report is to provide a list of machine trains which have measurement positions which might exceed the danger level within the next three months. Only the last five measurements are used to calculate the estimated time to alarm. Machine trains which are currently listed on the Overall Vibration Alarm Report are not included on this report.

Vibration Measurements Report: The purpose of this report is to give a detailed listing of all the vibration measurements which were collected on a route. This report has the same headings as the "Overall Vibration Alarm Report" with the exception of "percent change" column. This column gives the percentage of change between the last measurement taken at the position and the current measurement reading.

Trend and Spectra Plots: DATALENT automatically generates overall vibration level trend plots and frequency spectra plots for those measurement positions which have exceeded an alarm. The system will produce a trend plot and spectra plot for each direction and unit taken at an alarming measurement position, even if only one direction exceeded an alarm for use in data analysis. Figure 4 shows an example of both types of plots. The spectra data is processed to reduce the data to spectra peaks for easier review.

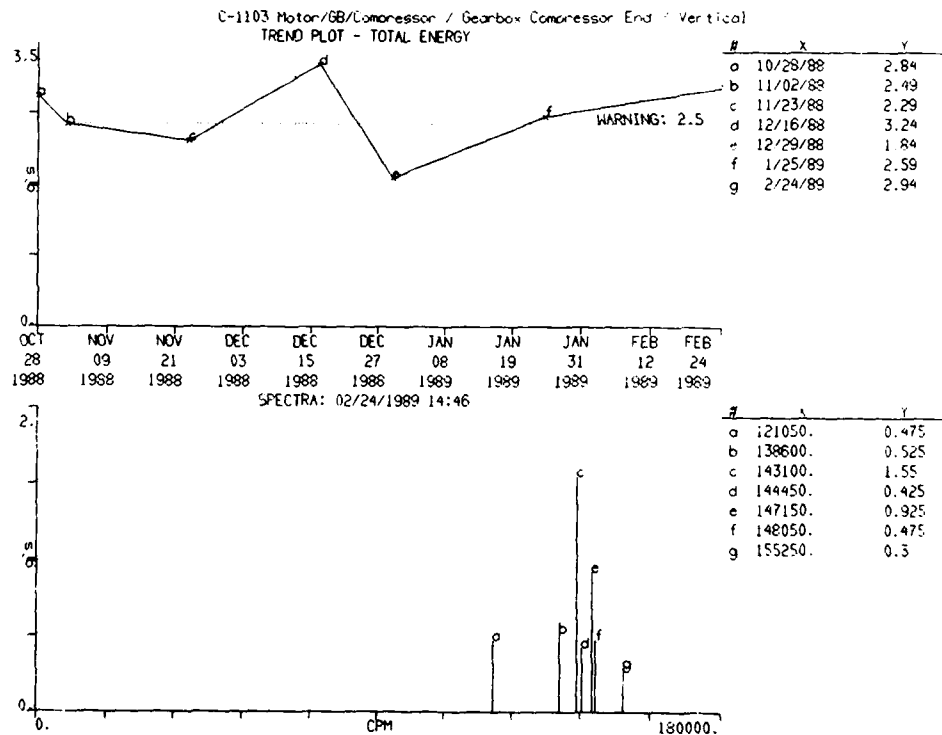


Figure 4

Expert Analysis and Corrective Action Recommendations: A vibration expert currently reviews the reports and issues a summary analysis report with a preliminary diagnosis and corrective action recommendations. This function is currently being incorporated in a computerized knowledge-based expert system which will have a basic knowledge of machinery vibration analysis to make a preliminary diagnosis and provide corrective action recommendations. This diagnostic expert system will contain five components:

1. Vibration diagnostic knowledge base containing the rules of vibration diagnosis
2. Vibration and spectra data for the machine trains which had measurement positions in alarm
3. Machine train component data for these machine trains
4. Corrective action knowledge base containing the proper corrective actions and recommendation rules based on the overall vibration levels and history of the machine train
5. Rule-processing program which matches the diagnostic rule set against the vibration and component data to make a list of possible causes.

The vibration diagnostic knowledge base is the principal module of the expert system. It will contain the heuristics developed from interviewing several experienced vibration analysts. The completed knowledge base will be able to do preliminary vibration diagnosis based on the spectra content of the measurement positions and historical information about the machine train (Weiss and Kulikowski, 1984).

The current vibration and spectra data for each machine train can be obtained directly from the database, along with previous history data on the measurement positions which are currently in alarm. This will be used to make recommendations based on trends found in the data.

The machine train component data is also available in the database. Information such as component type, bearing type, bearing frequencies, and shaft rotational speed can be retrieved for use by the rule-processing program.

The corrective action knowledge base will incorporate general guidelines and recommendations made by vibration analysts during the last two years in a similar vibration monitoring program. The corrective action knowledge base contains a list of corrective actions for each possible source of vibration and severity level of the vibration. These are collected to form a prioritized list of recommended actions based on the ease of performing each action.

The final component of the expert system is the rule-processing program. This program will attempt to move through the potential set of causes and narrow down the possible causes to the most probable using the vibration diagnostic knowledge base, the vibration and spectra readings, and the machine train component data. After the potential causes are identified, they will be ranked from the most likely to the least likely (Merritt, 1987). Finally, the rule-processing program moves through the corrective action knowledge base and selects the list of recommended corrective actions to take based on the possible causes identified.

Conclusion: DATALERT is an an integrated machinery vibration monitoring and analysis system that allows a comprehensive predictive maintenance program. The automated nature of the system and the incorporation of years of vibration analyst experience into a systematic, formalized computer system are key features of this system.

References:

E.P.R.I., Utility Machinery Vibration Monitoring Guide, NP-4346, 1985.

Hartley, W., and Flanders, E. E., "A Planned Approach to Machinery Vibration and Monitoring Diagnostics", TAPPI Journal, Sept. 1985.

IRD Mechoanalysis Inc., "General Machinery Vibration Severity Chart", 1975.

Jackson, C., The Practical Vibration Primer, Gulf Publishing Co., 1979.

Merritt, B., "Anatomy of a Diagnostic System", AI Expert, Vol. 2, No. 9, Sept. 1987, pp. 52-63.

Weiss, S., and Kulikowski, C., A Practical Guide to Designing Expert Systems, Rowman & Allanheld, Totowa, NJ, 1984.

ANALYSIS OF GEAR VIBRATION IN THE TIME-FREQUENCY DOMAIN

B. David Forrester
Aeronautical Research Laboratory
P.O. Box 4331, Melbourne
Australia, 3001

Abstract: A method for early fault detection in gears by analysing vibration signals using a joint time-frequency distribution is presented. The method provides a description of how the spectral content of the vibration signal is changing in time. Comparison with other vibration analysis techniques using actual fault data shows the advantages of time-frequency domain analysis.

Key words: Diagnostics; gears; helicopters; signal processing; vibration analysis

Introduction: At the Aeronautical Research Laboratory (ARL), research on methods for detecting faults in helicopter transmission systems has been in progress for over a decade. In helicopters, the transmission system is one of the most safety critical components, for which duplication is impractical and damaging loads are difficult to predict. Failure of transmission components can have catastrophic results and therefore it is vital to detect incipient failure very early. As well as the safety aspect, early failure detection can substantially reduce operational costs. If a fault can be identified in its early stages, repairs can be scheduled with minimum disruption to the normal operations of the aircraft.

Vibration analysis is playing an increasingly important role in early fault detection in transmissions systems. Recent advances in the application of time synchronous averaging and enhancement techniques have enabled the meshing behaviour of individual gears to be examined, allowing the detection of individual tooth faults. However, it is shown that with these methods there are difficulties in distinguishing the type and extent of tooth damage present, which can have a significant bearing on the expected time to failure of the gear.

The signal enhancement techniques currently in use have two major drawbacks:

- (a) they require selective filtering or removal of part of the signal average; and
- (b) they can only accurately portray signals in which the average frequency content does not vary in time.

With most tooth faults, both the amplitude and frequency content of the signal will change during the period in which the damaged tooth is in mesh. The nature of these short-term variations would be expected to give an indication of the type and extent of fault present.

To overcome the drawbacks of the current enhancement techniques, we look at the use of the Wigner-Ville distribution of the signal average. The Wigner-Ville distribution gives a representation of the signal jointly in both the time and frequency domains, providing a description of how the spectral content of the signal is changing in time.

Practical examples showing the use of the Wigner-Ville distribution to detect faults in Wessex helicopter main rotor gearboxes and an ARL epicyclic gearbox test rig are presented. Comparison is made with two of the existing methods used for helicopter gearbox fault diagnosis.

Time-frequency distributions: The basic goal of a joint time-frequency distribution is to provide a representation of the energy or intensity of a signal simultaneously in time and frequency. For a time based signal $s(t)$, the instantaneous energy (intensity per unit time) is the absolute value of the signal squared,

$$|s(t)|^2 = \text{intensity per unit time at time } t. \quad (1)$$

The energy density spectrum (intensity per unit frequency) is the absolute value of the Fourier transform squared,

$$|S(f)|^2 = \text{intensity per unit frequency at frequency } f \quad (2)$$

where $S(f)$ is the Fourier transform of $s(t)$

$$S(f) = \int_{-\infty}^{+\infty} s(t)e^{-j2\pi ft} dt \quad (3)$$

A joint time-frequency distribution $P(t,f)$ should represent the intensity per unit time per unit frequency at time t and frequency f ,

$$P(t,f) = \text{intensity at time } t \text{ and frequency } f \quad (4)$$

Ideally the summation of $P(t,f)$ for all frequencies at a particular time would give the instantaneous energy (1), and the summing up over all times at a particular frequency would give the energy density spectrum (2),

$$\int_{-\infty}^{+\infty} P(t,f) df = |s(t)|^2 \quad (5)$$

$$\int_{-\infty}^{+\infty} P(t,f) dt = |S(f)|^2 \quad (6)$$

Equations 5 and 6 are termed the 'marginals' and are conditions which should be met by a time-frequency distribution.

The Wigner-Ville distribution: One time-frequency distribution which meets the marginals is the Wigner-Ville distribution (WVD). The Wigner-Ville distribution is the most popular time-frequency distribution and its properties have been well documented (Boashash, 1987). For a complex time signal $s(t)$, the Wigner-Ville distribution $W(t,f)$ is defined as,

$$W(t,f) = \int_{-\infty}^{+\infty} s(t+\gamma/2)s^*(t-\gamma/2)e^{-j2\pi f\gamma}d\gamma \quad (7)$$

where $s^*(t)$ is the complex conjugate of $s(t)$.

The complex signal $s(t)$ can be derived by forming the analytic signal of a real signal $x(t)$,

$$s(t) = x(t) + jH[x(t)], \quad (8)$$

where $H[x(t)]$ is the Hilbert transform (Bendat) of $x(t)$:

$$H[x(t)] = \frac{1}{\pi} \int_{-\infty}^{+\infty} \frac{x(\mu)}{t-\mu} d\mu \quad (9)$$

The distribution $W(t,f)$ is real valued for all t and f , but is not necessarily positive.

Visual Representation: The WVD is displayed in this paper by using intensity to represent the logarithmic amplitude of the signal. The negative values have been excluded. The axes are the frequency in orders (one order represents the rotational frequency of the gear shaft) and the rotation of the gear in degrees.

For a gear in good condition the frequency content of the signal should be fairly uniform, resulting in predominantly vertical lines in the WVD (e.g. Figure 2). Where damage is present, the frequency content of the signal will vary. In the WVD this will be seen as variations in the horizontal direction (e.g. Figure 6).

Review of Existing Techniques: Two of the currently used signal enhancement techniques are also examined for comparison with the Wigner-Ville distribution.

Narrow band enhancement: The narrow band enhancement technique (McFadden, 1986) involves the narrow band filtering of the signal average about one of the dominant tooth meshing harmonics and removal of that meshing harmonic. The envelope of the remaining signal is then calculated. This is thought to represent the amplitude modulation function of the selected tooth mesh harmonic, and should highlight any change in the tooth meshing behaviour.

The kurtosis (normalized fourth statistical moment) of the enhanced signal is used as a measure of localised tooth damage. The kurtosis will respond to short term peaks which indicate that the meshing behaviour over a small portion of the gear is different from that of the rest of the gear.

As a guide, a kurtosis of less than 3.5 would indicate no local damage, between 3.5 and 4.5 would indicate minor local damage and greater than 4.5 indicates major local damage.

FM4 Enhancement: The FM4 (Figure of Merit number 4) involves the removal of what is considered the 'regular' signal for the gear from the signal average (Stewart, 1977). The 'regular' signal includes the tooth mesh frequency and its harmonics and possibly their upper and lower sidebands.

The remaining 'residual' signal is assumed to represent the deviation in the tooth meshing pattern from that of a normal gear.

The kurtosis of the residual signal is then used as an indicator of localised damage as above.

Both the Narrow Band and FM4 enhancements are represented here as plots of the enhanced signal average amplitude versus the rotation of the gear. The actual amplitudes are not given as we are interested here in the shape of the signal rather than its level. The kurtosis values for each enhancement are given as a measure of perceived damage.

Wessex Input Pinion: The input spiral bevel pinion of the Wessex main rotor gearbox has 22 teeth. It would be expected that this would give a vibration signal with major components at the tooth mesh frequency (22 orders) and its harmonics ($n \times 22$).

Undamaged pinion: Figure 1 shows the narrow band and FM4 enhancements for a normal Wessex input pinion.

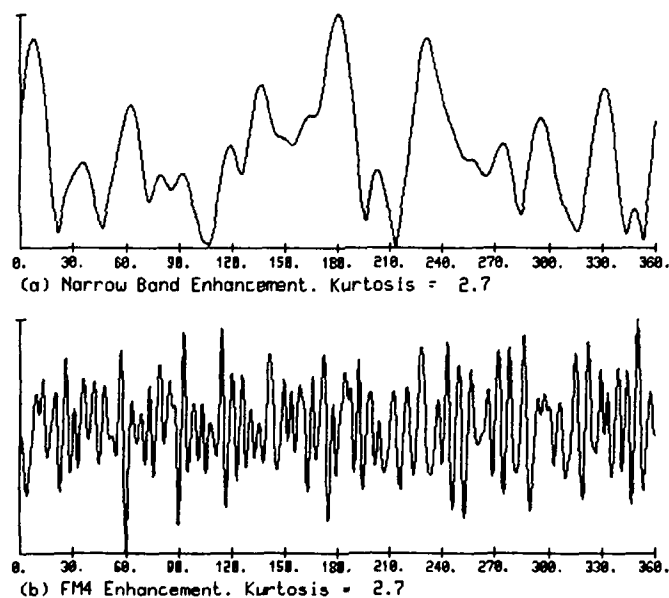


Figure 1. Undamaged Pinion.

As would be expected, both enhancements give kurtosis values of less than 3.5, indicating that no local tooth damage is present.

Figure 2 shows the corresponding WVD. The major meshing components can be seen at 22 and 66 orders, with a smaller component at 44 orders which also includes a component due to the cross-products of the 22 and 66 order components. Other patterns can be seen which indicate minor variations in the meshing action of the gear. These variations are normal and can be clearly distinguished from gear faults as will be seen later.

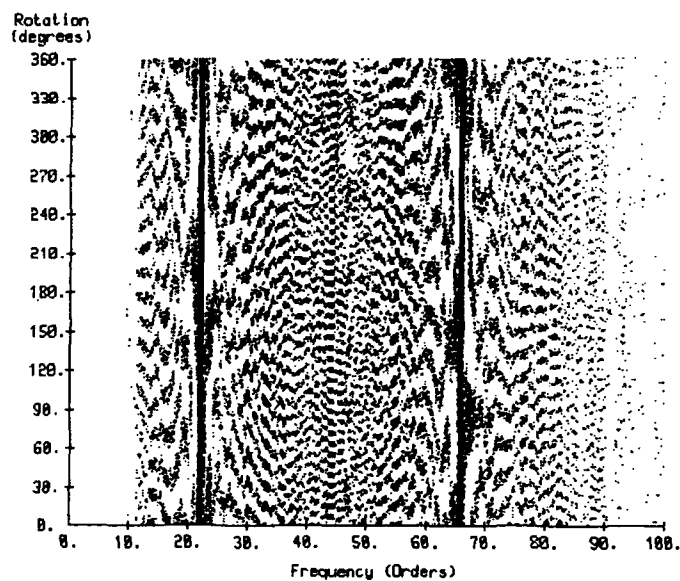


Figure 2. WVD of Undamaged Pinion.

Fatigue crack: Figures 3 and 4 show the narrow band and FM4 enhancements for a Wessex input pinion with a fatigue crack at 103 and 42 hours before failure respectively.

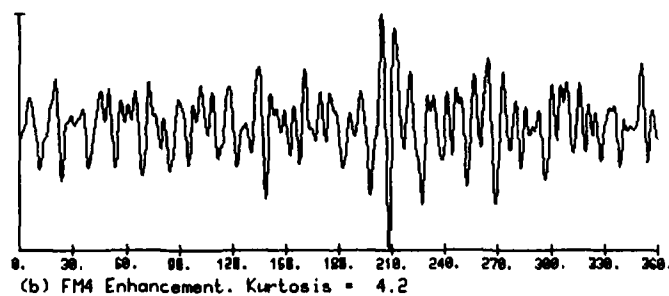
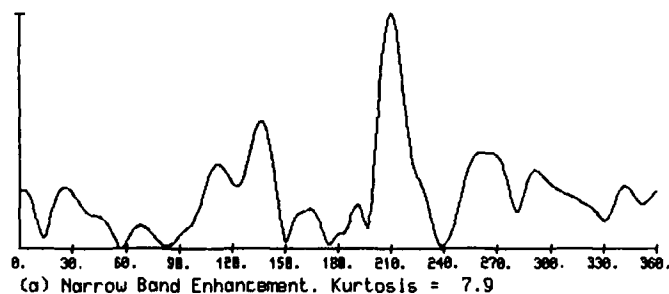


Figure 3. Cracked Pinion 103 hours before failure

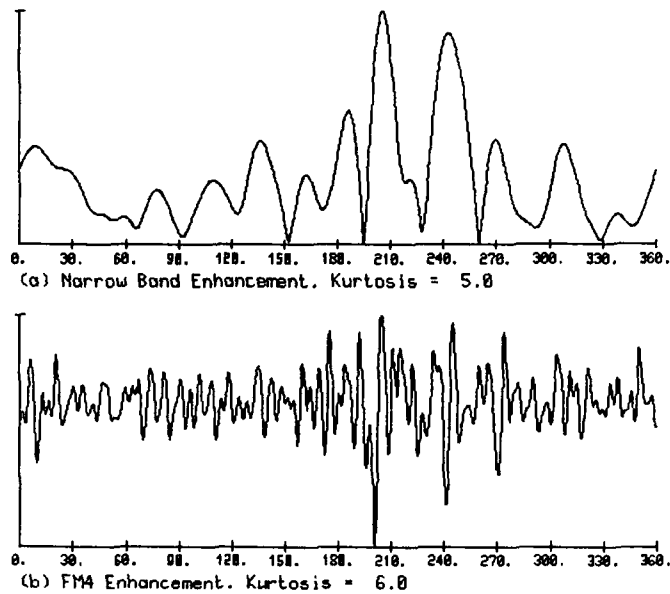


Figure 4. Cracked pinion 42 hours before failure

The narrow band enhancement gives a clear indication of the presence of the crack at 103 hours before failure with a kurtosis level of 7.9 however, the kurtosis drops to 5.0 as the crack progresses. FM4 gives a warning of the crack (kurtosis of 4.2) at 103 hours before failure with the kurtosis increasing to 6.0 as the crack progresses.

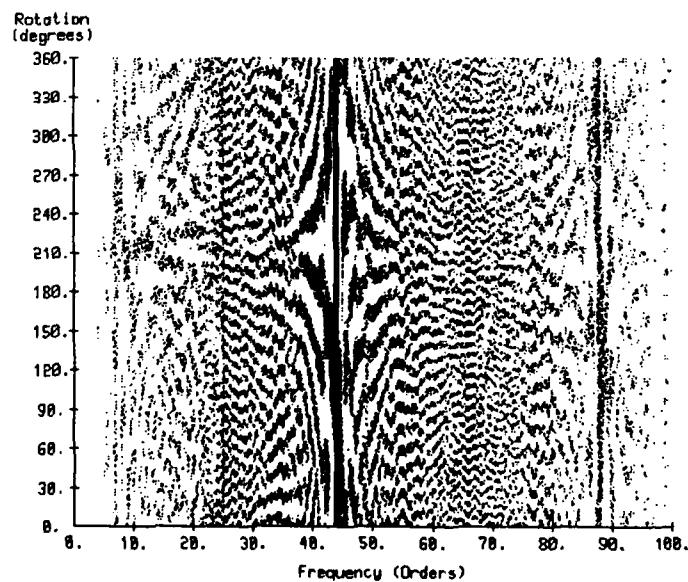


Figure 5. WVD of Cracked Pinion 103 hours before failure

The corresponding WVDs are shown in Figures 5 and 6. By comparing these with Figure 2, it can be seen that the crack is easily detectable at 103 hours before failure and the progression of damage is clearly evident at 42 hours before failure.

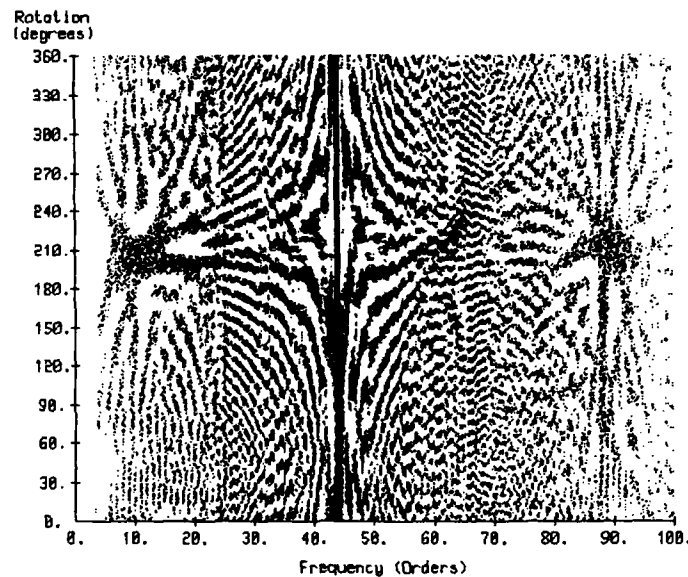


Figure 6. WVD of Cracked Pinion
42 hours before failure

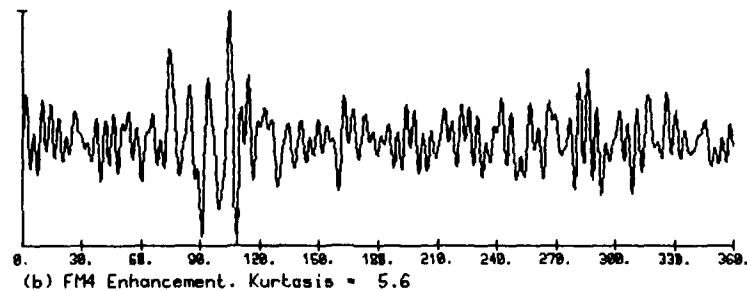
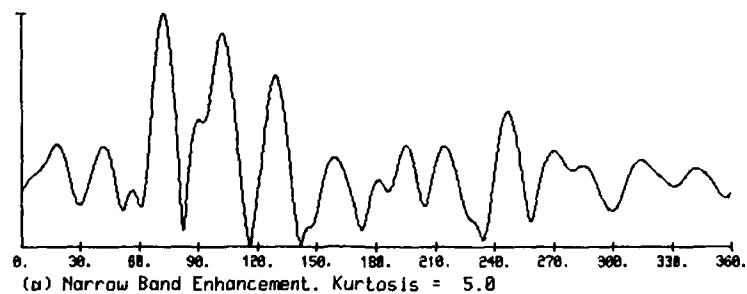


Figure 7. Spalled Pinion

Spalling: Figure 7 shows the narrow band and FM4 enhancements for a gear with spalling damage to the teeth. Both methods indicate the presence of tooth damage (kurtosis of 5.0 and 5.6 respectively) however, it is virtually impossible to distinguish the spalling from the tooth crack shown in Figures 3 and 4. This is of some importance as the spalled gear in Figure 7 continued in service for a further 200 hours without incident, whereas the gear seen in Figure 4 failed 42 hours later, causing a crash in which two lives were lost.

The corresponding WVD to Figure 7 is shown in Figure 8. The disturbance caused by the spalling is clearly detectable (compare Figure 2) and is also clearly distinguishable from the WVDs for the cracked gear (Figures 5 and 6).

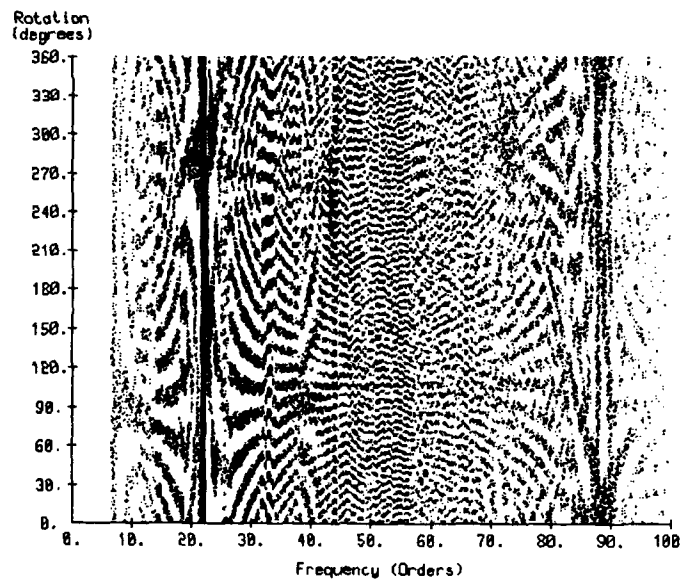


Figure 8. WVD of Spalled Pinion

Epicyclic Test Rig Planet Gear: The following examples are of epicyclic planet gear signal averages obtained from an ARL test rig using specialised signal averaging techniques developed at ARL. The gearbox has three planet gears each with 32 teeth which would be expected to produce vibration signals with major components at the tooth mesh frequency (32 orders) and its harmonics ($n \times 32$).

Damaged planet: A simulated fault was introduced into one of the planet gears by grinding 0.002 inches off one of the teeth. The narrow band and FM4 enhancements for the signal average of the damaged planet are shown in Figure 9.

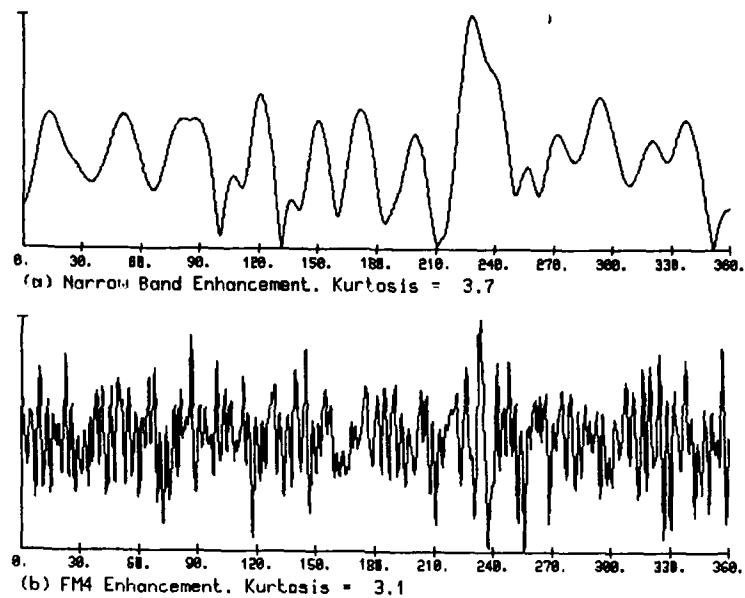


Figure 9. Damaged Planet Gear

The narrow band enhancement gives a warning of the damage (kurtosis of 3.7) and FM4 does not give any indication (kurtosis of 3.1) although it is possible to detect the change in meshing pattern by visual inspection of the FM4 signal (with hindsight).

The corresponding WVD is shown in Figure 10. Here the damage is clearly detectable.

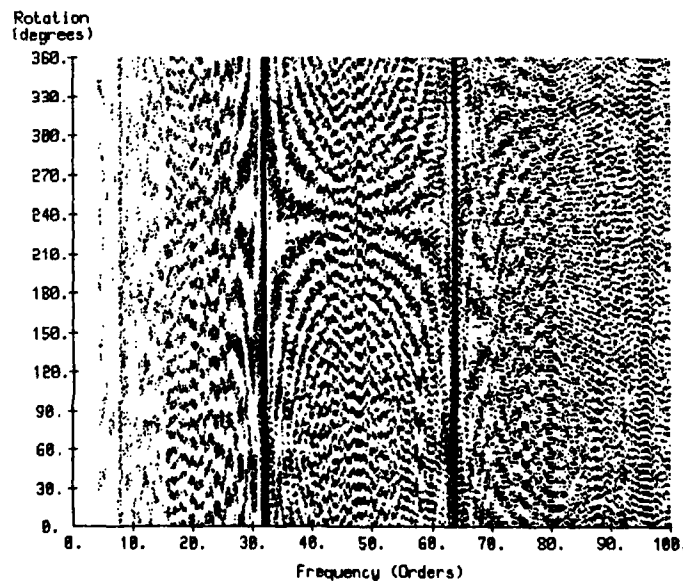


Figure 10. WVD of Damaged Planet Gear

Conclusions: It has been shown that the signal enhancement techniques currently used for the detection of local tooth faults are incapable of distinguishing tooth cracking from spalling and can be misleading in their indications of the extent of the fault.

The Wigner-Ville distribution has been applied to the signal averages of gears with and without faults and indications are that it is capable of detecting both the type and extent of faults simply by the patterns produced. No attempt has been made to give a full analysis of these patterns as this is outside the scope of this paper. However, the fact that the patterns can be clearly detected and distinguished by eye indicate that pattern recognition techniques for automatic gear fault detection could be implemented using the Wigner-Ville distribution as a basis.

REFERENCES:

Bendat, J.S. The Hilbert Transform and Applications to Correlation Measurements, Bruel and Kjaer, Copenhagen.

Boashash, B. (1987). Non-Stationary Signals and the Wigner-Ville Distributions: A Review. IASTED International Symposium on Signal Processing and its Applications - ISSPA 87 Vol.1 pp 261-268.

Forrester, B.D. (1990). Time-Frequency Domain Analysis of Helicopter Transmission Vibration. ARL Propulsion Report 180.

McFadden, P.D. (1986). Examination of a Technique for the Early Detection of Failure in Gears by Signal Processing of the Time Domain Average of the Meshing Vibration. ARL Aero Propulsion Technical Memorandum 434.

Peyrin, F. and Prost, R. (1986). A Unified Definition for the Discrete-Time, Discrete-Frequency, and Discrete-Time/Frequency Wigner Distributions. IEEE Trans. on Acoustics, Speech, and Signal Processing Vol.34 No.4. Aug. pp 858-866

Stewart, R.M. (1977) Some Useful Data Analysis Techniques for Gearbox Diagnostics. I.S.V.R., Univ. of Southampton Report MHM/R/10/77.

VIBRATION SIGNATURE AND FATIGUE CRACK GROWTH ANALYSIS OF A GEAR TOOTH BENDING FATIGUE FAILURE

H. John Rose
Drive System Design Specialist
Boeing Helicopters
P.O. Box 16858
Philadelphia, Pa. 19142

Abstract: This paper presents the results of vibration signature analysis and fatigue crack growth cycle measurements performed on a CH-47D helicopter combiner transmission input pinion gear. The spiral bevel input pinion gear experienced a classic bending fatigue failure during overload bench testing. Throughout this testing, vibration signatures of the combiner and one engine transmission were continuously recorded for later analysis on a Boeing Helicopters, Stewart Hughes-Mechanical Systems Diagnostic Analyzer (MSDA). After the failure, the pinion gear was metallurgically analyzed in the Boeing Helicopters materials engineering laboratory.

The intent of this paper is to present a summary of these test results in an effort to understand the propagation of the failure during the test, while comparing the discrete changes in the vibration signature. This work was performed in an effort to validate real time vibration signature analysis as a technique on which to base an airborne helicopter transmission vibration diagnostic system.

Key Words: Computer diagnostic analysis, Fault detection system, Transmission vibration diagnostic system, Vibration diagnostics, and Vibration signature analysis.

Introduction: In March 1989, during an engineering overload bench test of a non-shotpeened CH-47D helicopter combiner transmission spiral bevel input pinion gear, a classic bending fatigue failure occurred. Vibration signatures (signals) on the combiner and the engine transmission on the test side were routinely recorded during the test. Two separate analog high-speed magnetic tape recorders were utilized to record the vibration signatures for later analysis, should any type of a failure occur. In addition to the vibration signals, a phase accurate, one per revolution, speed sensor signal from the high speed input shaft, and a time code were also recorded.

During the subsequent failure investigation, it was determined that the failure origin was in the maximum stress section of the root of the gear tooth at a small subsurface inclusion. The type and size of this inclusion was within the acceptable limits for aircraft quality gear steels. The metallurgical and heat treat properties of the failed gear were found to be acceptable. Fatigue crack striation counting across the fracture face and extensive vibration signature analysis (both conventional level/spectrum and pattern recognition methods), were all accomplished. Results of this investigation revealed the cause of failure to be due to overload with no other extenuating circumstances.

The test load was 156% of the single engine power rating. The pinion gear sustained this overload for a period of 4.2 hours (3,090,276 cycles). The test was stopped, due to a sudden increase in the test cell external noise level. The following paper will attempt to compare the results of the metallurgical laboratory analysis of the gear tooth fracture, the test stand operators log sheet records, and the vibration signature analysis results.

CH-47D Engine and Combiner Transmission Description: The engine transmission consists of a single spiral bevel gear right angle mesh with a single engine input design power of 4600 HP at an input speed of 15,063 rpm and an output speed of 12,263 rpm. The combiner transmission consists of right hand and left hand spiral bevel input pinion gears at right angles to a common spiral bevel collector gear. The combiner transmission is designed for a single engine input power of 4600 HP or a dual engine input power of 7500 HP at an input speed of 12,263 rpm and an output speed of 6912 rpm. Figure 1 shows a sectioned view of both engine and combiner transmissions.

Test Stand Description: The transmission bench test stand utilized for this testing is of the "four square" locked-in torque type, where the test stand has the exact gear ratio as that of the test transmissions. Two aircraft engine transmissions and a combiner transmission are tested in the stand as a unit. Different torques can be applied to either engine transmission loop. Figure 2 shows a schematic arrangement of the three aircraft test transmissions, as well as the location of the accelerometer and speed sensor instrumentation.

Analysis Technique Definition: Some of the earliest work using the techniques of vibration signature pattern analysis, as a means of machinery health monitoring, was performed by a research group at Southampton University (UK) in the early 1970's. Most of the engineers in this group left the university in 1980, and formed Stewart Hughes Ltd., where they developed the Mechanical Systems Diagnostic Analyzer (MSDA). The analyzer was originally developed as an aid in vibration diagnostics for fault detection of helicopter transmissions. It has since been applied successfully to many other types of machinery. The MSDA is a very broad based, versatile, analog/digital computer analyzer, intended for the laboratory analysis of vibration signatures of complex machinery. As originally configured, the MSDA is equipped with thirty two standard vibration diagnostic analysis techniques for gears and shafts, and can be programmed to perform any additionally required methods.

The thirty two standard analysis routines consist of nineteen techniques based on signature analysis (pattern recognition) and thirteen techniques based on power spectrum (energy) analysis. These thirty two standard analysis techniques are identical or very similar to most of the known methods utilized worldwide for fault detection by means of vibration signature analysis. It was not the intent of this author to try to develop numerous new analysis techniques but rather to practically evaluate the entire concept of helicopter transmission fault detection, in a timely manner, using vibration signature analysis. The intent of this work is to eventually develop a real time, airborne, vibration diagnostic capability that will be able to completely and reliably indicate impending helicopter transmission internal fatigue failures, thus providing ample time for a safe landing, and prevent catastrophic accidents.

Of the thirty two MSDA analysis techniques evaluated during this test, ten showed positive indications of this particular failure progressing with time. Each produced positive early warning times ranging from 10.4 to 3.8 minutes at the 156% test torque level. "Positive indication," refers to a signal analysis value that displays a positive and continuous change from a long term value developed during a period of normal operation, prior to the initiation of the microcrack. This type of response, in any proposed analysis technique, is necessary in order to develop a real-time, computer based, fault detection system, which will respond to a fault in a timely manner and not produce false warnings. Figure 3 lists the ten most positive failure indicators (Stewart Hughes nomenclature) demonstrated during this test, as well as a brief description of the analysis technique employed by each.

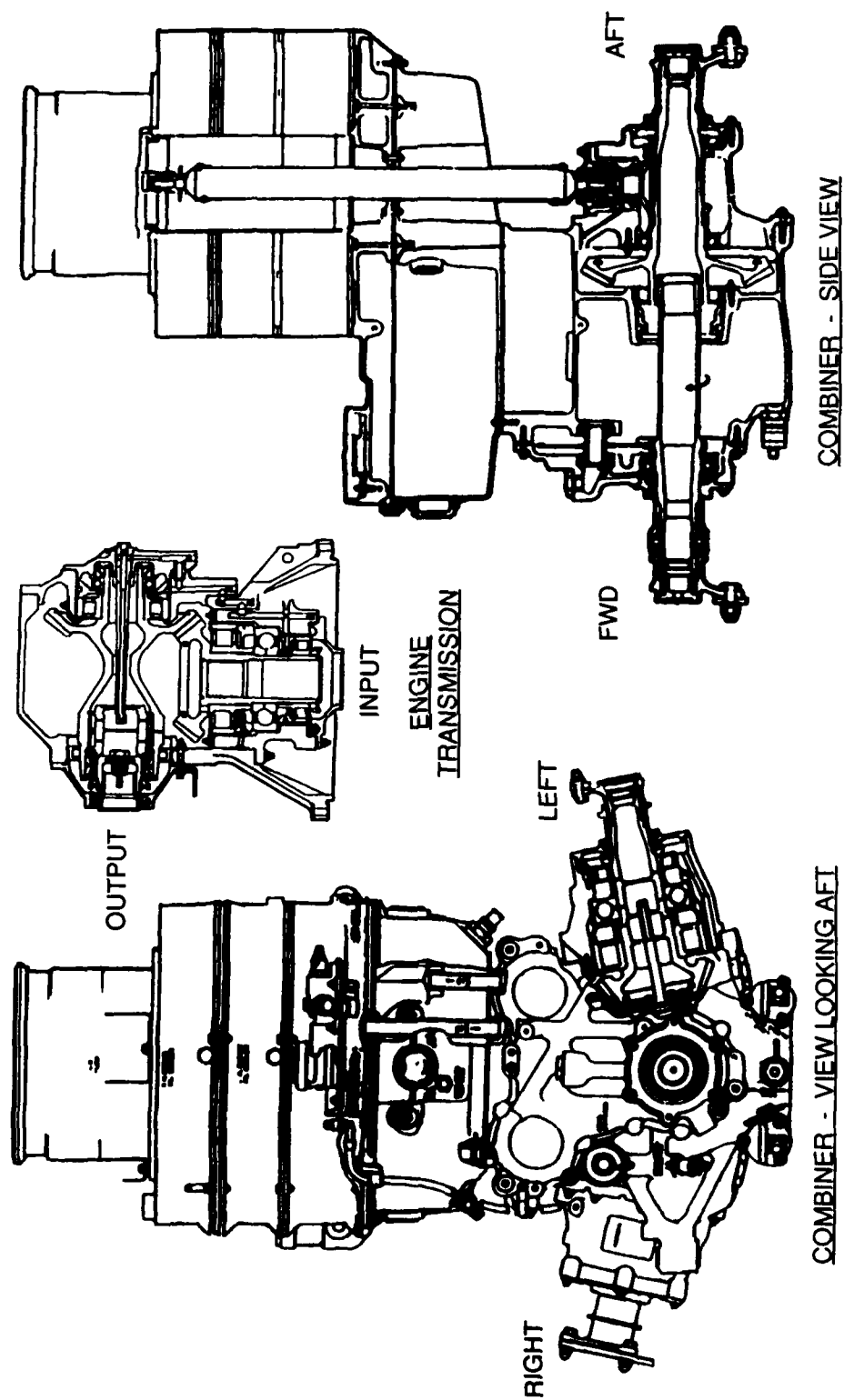


FIGURE 1 - CH-47D ENGINE / COMBINER TRANSMISSION SECTIONED VIEWS

FIGURE 2 - CH-47D COMBINER XMSN OVERLOAD TEST INSTRUMENTATION LOCATION

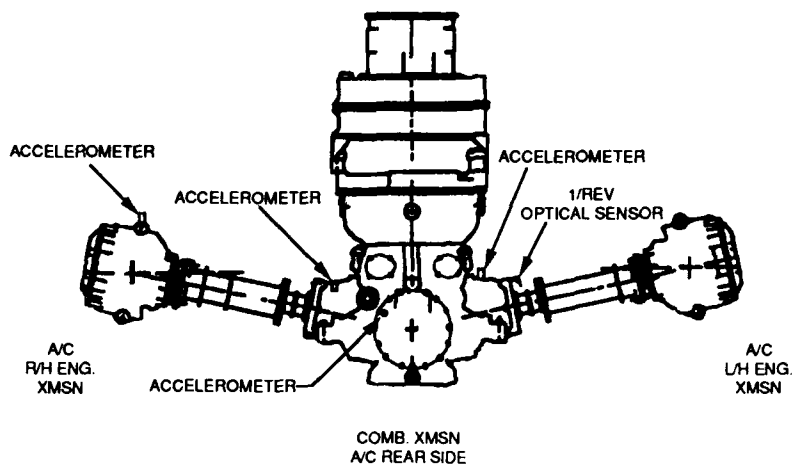
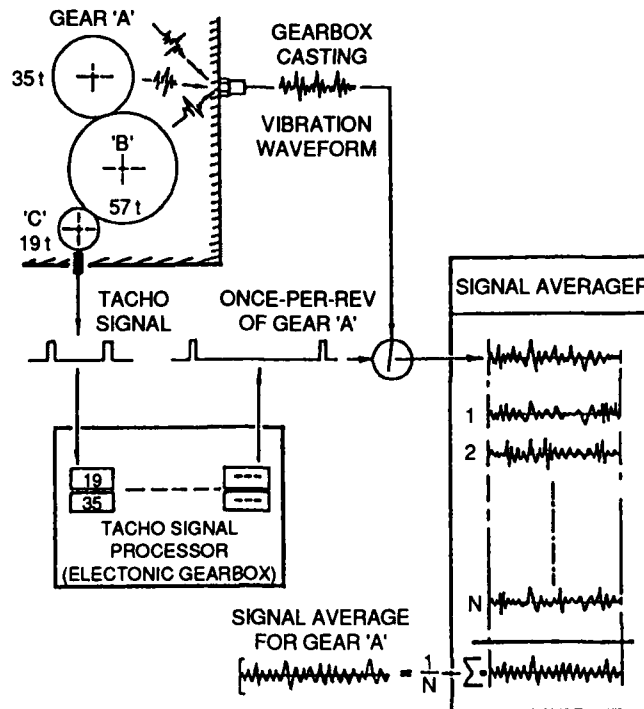


FIGURE 3 - MSDA ANALYSIS TECHNIQUE DEFINITION

SGAV (SIGNAL AVERAGE)		BBPS (BASEBAND POWER SPECTRUM)	
S02	-- ENERGY LEVEL AT TWICE PER REVOLUTION	RMS	-- ROOT MEAN SQUARE OF THE RAW SIGNATURE
FM4B	-- ENERGY LEVEL ATTRIBUTABLE TO THE NON-LOCALIZED AREA OF THE SIGNAL AVERAGE	WHT	-- VALUE OF THE PURE RANDOM NOISE
ACH	-- VALUE OF THE CHANGE IN THE RMS LEVEL OF THE SIGNAL AVERAGE FROM THE BASELINE	TEO-G	-- VALUE OF THE CHANGE IN THE RMS LEVEL OF THE POWER SPECTRUM FROM THE BASELINE
WCH	-- VALUE OF THE MEAN CHANGE IN THE LEVELS OF A PRESET NUMBER OF SHAFT ORDERS	TEO-P	-- MEASUREMENT OF THE MEAN CHANGE IN THE LEVELS OF A PRESET NUMBER OF SHAFT ORDERS
SCH	-- VALUE OF THE STABILITY OF A PRESET NUMBER OF SHAFT ORDERS	TEO-PK	-- THE MAXIMUM POSITIVE VALUE OF TEO-P

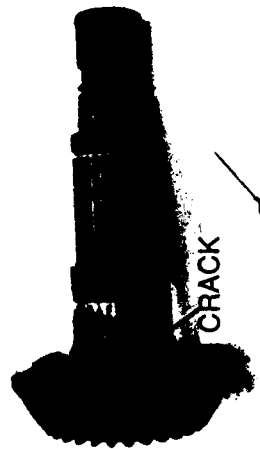
FIGURE 4 - TYPICAL GEARBOX VIBRATION SIGNAL AVERAGING



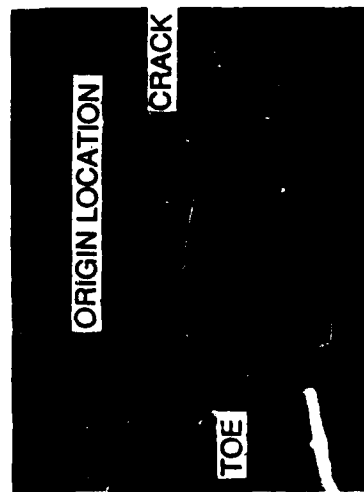
Typical Signal Averaging Method: Figure 4 pictorially depicts the operation of the signal averager. Basically, with the use of an electronically clean, wide frequency range (5-20,000 HZ) vibration signal, coupled with a sharp (square wave) phase accurate speed sensor signal, the signal is averaged by the following means: First, the electronic tachometer signal processor is set at the exact frequency of the gear or shaft being analyzed by using the exact gear tooth ratios between the component and the one per revolution speed sensor. Then, the vibration signal is electronically "chopped-up" at once per component revolution and overlayed on itself for as many signal averages as are required to stabilize the signal.

By utilizing this method of developing a clean, true, signal average of the component to be analyzed, all instantaneous and extraneous signals can be eliminated, so that a representative component signal remains for computer analysis fault detection. The authors experience has taught that too much time can never be devoted to the electronic and mechanical details of the accelerometer and speed sensor installations. If these sensors are not applied properly and their signals recorded or transferred in real time to an analyzer correctly, then no analysis technique in the world has a chance of detecting impending failures, nor eliminating "false warnings".

Pinion Fracture Face Description: A photograph of the combiner transmission input pinion, and that of the actual fractured gear tooth, is shown in figure 5. An enlarged photograph of the fracture face is shown in figure 6, with the origin and the end of the fatigue fracture denoted. Some typical failure progression lines are marked with the distance from the origin noted, along with the percentage of the gear area fractured by the time the failure had progressed to that point.



PINION GEAR



FRACTURED TOOTH

FIGURE 5 - CH-47D COMBINER TRANSMISSION
INPUT PINION

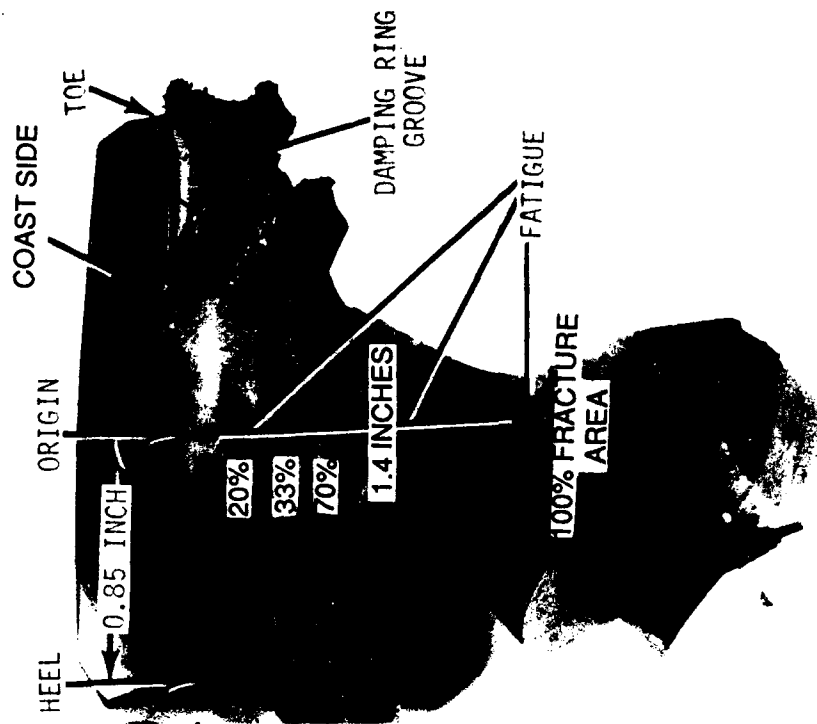


FIGURE 6 - FRACTURE FACE DENOTING
FATIGUE ORIGIN

Striation Counting Procedure and Results: Acetate replicas were made of the fracture surface at various distances from the origin. Standard two-stage chrome/carbon replicas were then prepared from the acetate replicas. The chrome/carbon replicas were placed on a copper grid, and subsequently examined utilizing a transmission electron microscope (TEM) at 5,000 to 30,000 magnification. In all, fatigue striation spacing was measured at eighteen different locations from the origin. This data is presented graphically in Figure 7, and extrapolated from the origin to the end of the fracture face. By integrating the varying striation spacing over the entire 1.4 inch length of the fracture surface, an approximate total number of fatigue cycles may be calculated. In this case, the total number is estimated to be 162,134 cycles.

Estimated Time and Cycles to Failure: The combiner transmission input pinion gear operates at 12,263 rpm at 100% rotor speed. This equates to 204.383 revolutions per second or 4.893 milliseconds per cycle of tooth loading. By taking the estimated 162,134 fatigue fracture cycles between microcrack initiation and failure (test stoppage), derived from the striation counting, and the time per cycle above, it can be estimated that the first microcrack developed approximately 13.25 minutes prior to failure (test stoppage).

Crack Growth Rate/Stress Intensity Projections: Figure 8 contains crack propagation rate versus stress intensity data for the double vacuum melt BMS 7-223 (VASCO-X2M) gear steel. By taking the mean striation spacing (in./cycle) for the entire fracture face, and equating the corresponding stress intensity to the gear tooth bending stress at the 156% single engine torque level of the test, the stress intensity equivalent for 100% and 65% twin engine torques can be calculated, and the correspondingly lower crack growth rates estimated.

From figure 8 it may be seen that a torque level of 100% twin engine would equate to a crack growth rate of 33.3% of the actual test conditions, while a 65% twin engine growth rate would equate to 14.9% of the test condition.

For example, at a typical CH-47D helicopter high gross weight torque level of 65% twin engine, it would take the failure experienced during this test 6.71 times longer to propagate. This data was used to develop the additional scales shown at the bottom of figure 10, so that a failure warning at normal torque levels could be estimated.

Analysis Technique Evaluation: Figure 9 contains plots of four typical analysis technique results versus time with the gear failure (test stoppage) shown at the right of the chart and the test clock time in minutes at the bottom. A leader is shown at the estimated microcrack initiation point determined by the striation counting at 13.25 minutes real time before failure.

A 5 Sigma(5 standard deviations) exceedance level on the mean of the data, prior to the microcrack initiation, was established as an extremely conservative approach to the initiation of a fault warning for all analysis techniques evaluated. Where each analysis technique value exceeded the 5 Sigma level, a vertical line has been drawn and marked with the warning time prior to failure. This method was utilized for all the thirty two analysis techniques evaluated as a result of this work.

Figure 10 is a summary chart of all the work generated during this evaluation, presenting the 5 Sigma exceedance levels for the ten analysis techniques (Stewart Hughes nomenclature) showing the most positive indications/warnings prior to failure.

FIGURE 7 - FATIGUE CYCLE STRIATION SPACING

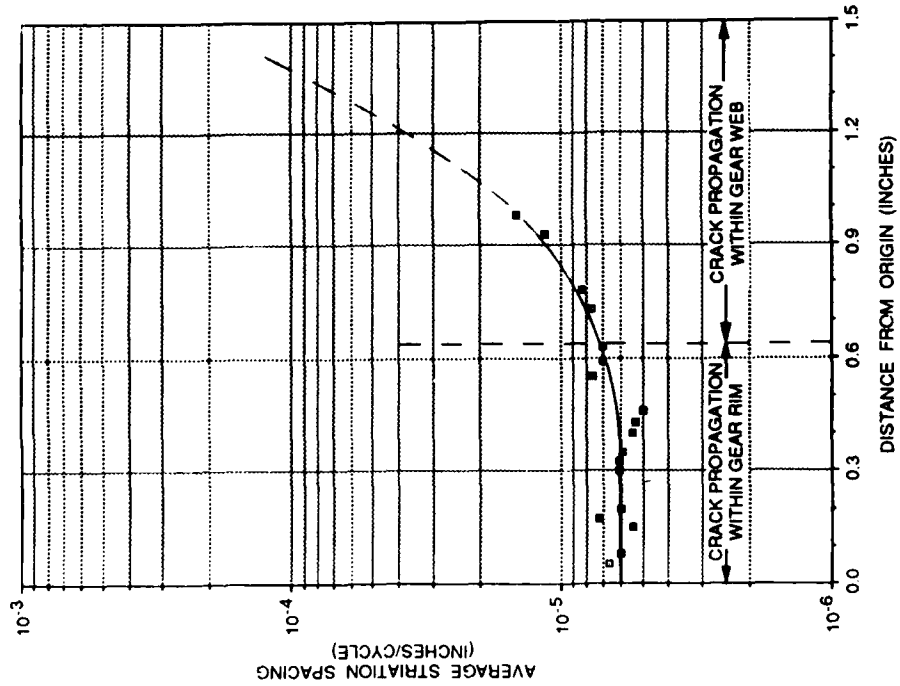
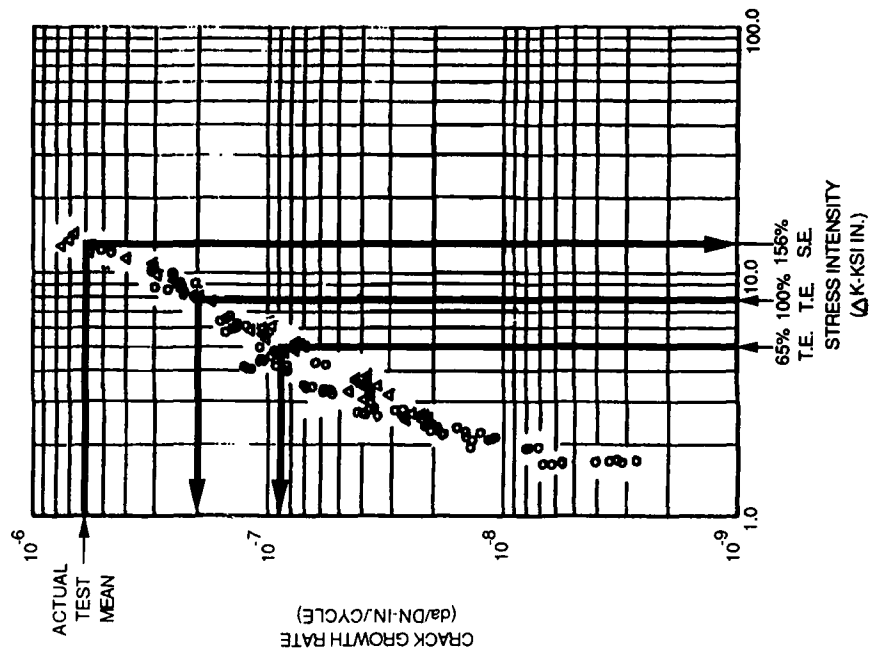


FIGURE 8 - VASCO-X2M DOUBLE VACUUM MELT STEEL
CRACK PROPAGATION



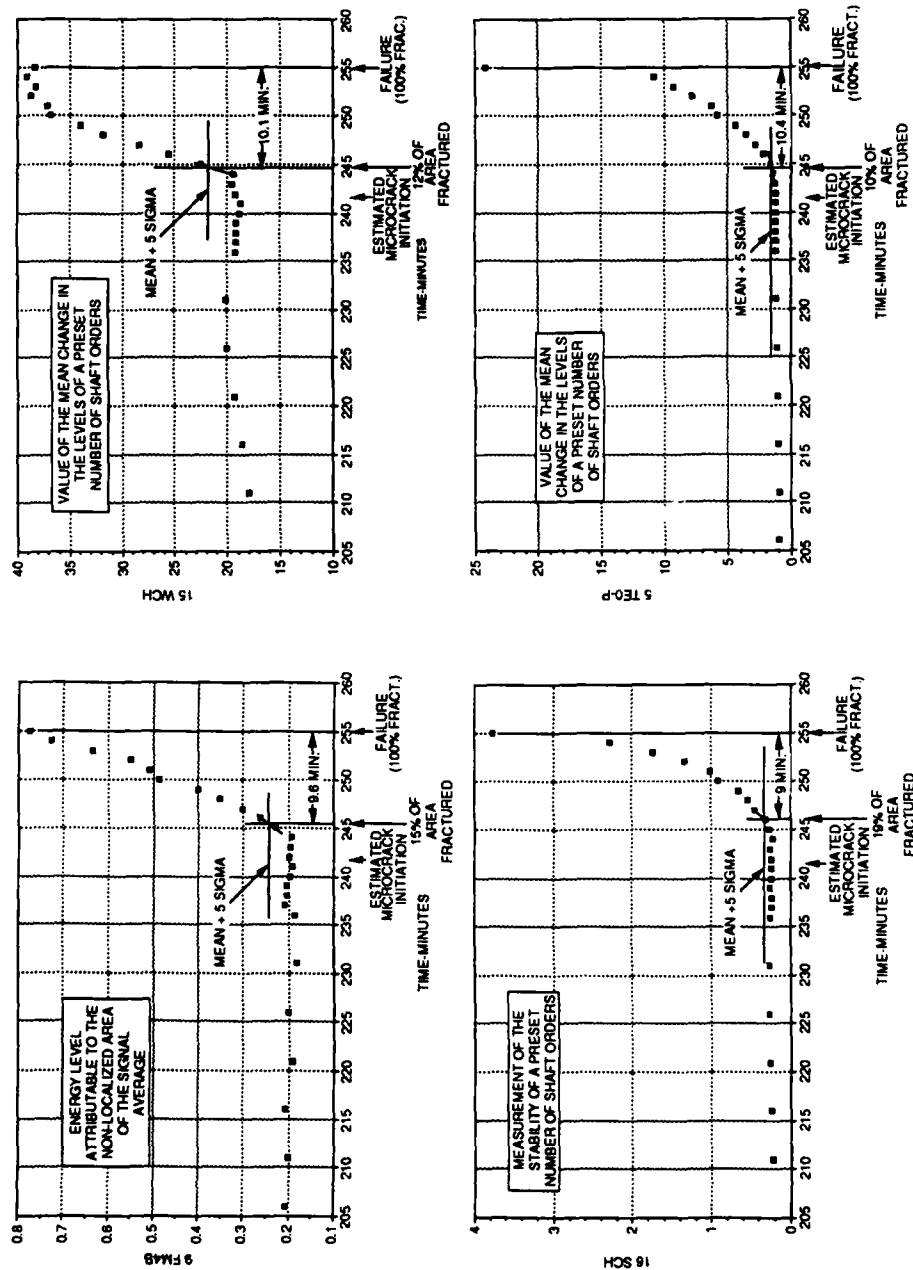
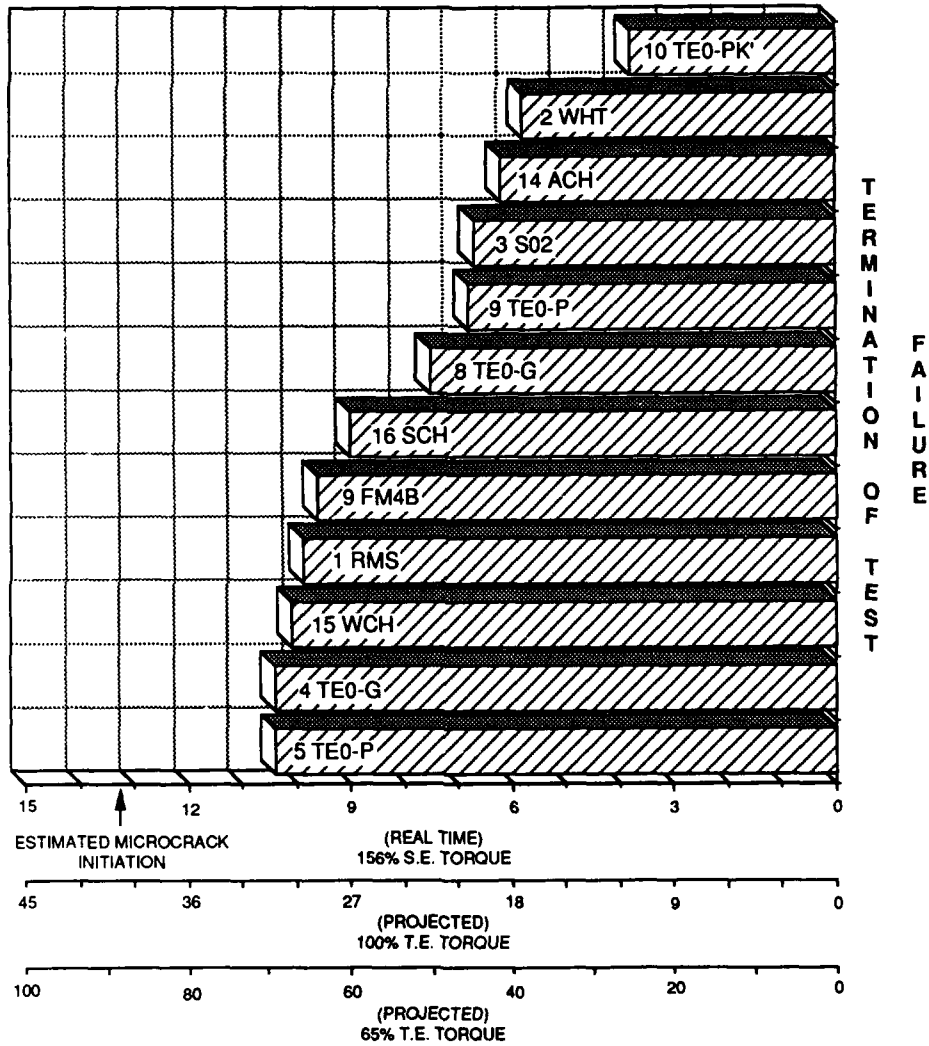


FIGURE 9 - TYPICAL ANALYSIS TECHNIQUE RESULTS CH-47D COMBINER PINION FAILURE

**FIGURE 10 - ANALYSIS TECHNIQUE EVALUATION
(STEWART HUGHES NOMENCLATURE)**



NOTE: TIME SCALES CALCULATED FROM VASCO-X2M DVM CRACK PROPAGATION RATE DATA

Conclusion: The results of this test, and other similar tests performed at Boeing Helicopters, strongly indicates the successful use of vibration diagnostics for detection of impending fatigue failures in helicopter transmission major dynamic components. This work concurs with that performed in the United Kingdom, under Royal Navy funding, over the last twelve or more years. Some of the released UK technical papers are listed in references 1-7.

In looking at the projected 65% twin engine torque level time scale in figure 10 it can be seen that from the time a microcrack initiates until a failure occurs, at a reasonable operational load, could be as short as 66 minutes after the triggering of the four most sensitive analysis techniques. Although this type of failure progression could be faster or slower, depending on the speed (cyclical rate) of the particular component, it clearly demonstrates the need for a real time airborne warning system, as opposed to a ground based "post-flight" system, since most normal flights are in excess of sixty six minutes. In order to develop a production airborne transmission vibration diagnostic system, seeded-fault transmission bench load testing, in conjunction with, aircraft flight testing, must be performed.

The bench testing can be used to further refine the most consistently sensitive of the various analysis techniques for multi-mesh rotor transmissions with epicyclic gear meshes, as well as for single and dual mesh transmissions. This testing will also help reduce the total number of techniques required for complete diagnostics, thus freeing up computer time to perform more analyses of each component in any given time span.

The flight testing is required, in order to understand the potential of the operating aircraft dynamic vibrations, environmental conditions, or other aircraft systems, towards producing "false" warnings. An airborne fatigue failure warning system that is troubled by "false" warnings can be as potentially dangerous, due to the requirement for inadvertant landings in a hostile (militarily or environmentally) site, as the rare occurrence of an undetected fatigue failure in an aircraft without such a system.

References:

1. Stewart, R. M., "Some Useful Data Analysis Techniques for Gearbox Diagnostics", Applications and Time Series Analysis Conference, ISVR, Southampton University, Southampton, England, September 1977.
2. Stewart, R. M. et al., "MSDA-1 Gear Monitoring Technology", Stewart Hughes Ltd. Document SHL/19, September 1981.
3. Gadd, P. and Mitchell, P. J., "Condition Monitoring of Helicopter Gearboxes Using Automatic Vibration Analysis Techniques", AGARD Conference Proceedings No. 369, HMSO London, England, 1984.
4. Stewart, R. M. et al, "Monitoring of Rotorcraft Dynamic Systems", Stewart Hughes Ltd. Document SHL/162, February 1985.
5. Brougham, M. J. and Gadd, P., "The Integration of Health Monitoring Techniques for Helicopter Gearboxes", Eleventh European Rotorcraft Forum, London, England, September 1985.
6. Collier-Marsh, M. E. and Astridge, D. G., "Operational Experience with the Advanced Transmission Health Monitoring Techniques on the Westland 30 Helicopter", Eleventh European Rotorcraft Forum, London, England, September 1985.
7. Astridge, D. G., "Helicopter Manufacturer's Requirements and Experience with Advanced HUM Systems on Westland Helicopters", IMechEng Aerospace Industries Division Publication, "Health and Usage Monitoring in Helicopter Mechanical Systems", April 1986.
8. Astridge, D. G., "Vibration Health Monitoring of the Westland 30 Helicopter Transmission - Development and Service Experience", 41st MFPG Meeting, NATC Patuxent River, Maryland, USA, October 1986.

CONDITION MONITORING

Chairman: John J. Anderson
CTS, Inc.

ACOUSTIC EMISSION ANALYSIS FOR BEARING CONDITION MONITORING

C. James Li

and

S. Y. Li

Assistant Professor
Department of Mechanical Engineering
Columbia University
New York, N. Y. 10027

Associate Professor
Department of Precision Machinery
and Instruments
Changsha Institute of Technology
Changsha, Hunan, PRC

Abstract: For automatic detection/diagnosis of localized defects in bearings, a pattern recognition analysis scheme was developed for investigating Acoustic Emissions (AE) of bearings. Two normalized and dimensionless features are extracted by short-time signal processing techniques. Employing these two features, a linear discriminant function has been established to detect defects on the outer race of bearings. Based on the experimental data of imposed bearing defects, the technique has a rate of success for the detection of defects of 98%. AE is also found to be a better signal than vibrations while the transducers have to be placed remotely from the bearing. It takes 20 seconds for data processing and fault diagnosis on a PC-AT on-line implementation.

Key words: Acoustic emissions, Bearing, localized defects, monitoring, pattern recognition analysis

INTRODUCTION: Rolling element bearing condition monitoring has received considerable attention for many years because the majority of problems in rotating machines are caused by faulty bearings. The classical failure mode of rolling element bearings is localized defects, in which a sizable piece of the contact surface is dislodged during operation, mostly by fatigue cracking in the bearing metal under cyclic contact stressing [1]. Thus, failure alarms for a rolling element bearing are often based on the detection of the onset of localized defects.

During the bearing operation, bursts of Acoustic Emissions (AE) result from the passage of the defect through the rolling element-race way contacts. Defects at different locations of a bearing (inner-race, roller and outer-race) will have characteristic frequencies at which bursts are generated. Theoretical estimations of these frequencies are denoted as characteristic defect frequencies (Appendix A). Therefore, the signal of a damaged bearing consists of periodic bursts of AE. The signal is usually considered as being amplitude modulated at the characteristic defect frequency.

Modulation of the AE by the characteristic defect frequency makes it possible to detect the presence of a defect and diagnose in what part of the bearing the defect appears. One may conclude that there are localized defects on the outer-race of a bearing if one sees a series of AE bursts occurring at a rate close to the theoretic estimation of the characteristic defect frequency for defects on the outer-race.

Traditional techniques for detecting localized defects are mainly based upon the processing of vibration and sound measured at the close by of the bearing. Examples of time domain

techniques are peak level, r.m.s. value [2], crest factor analysis[3], kurtosis analysis[4] and shock pulse counting [5]. A number of frequency domain techniques have been developed to detect the train of impulses occurring at some characteristic defect frequency from the waveform of the bearing signal. Examples among these approaches are spectrum analysis, synchronized averaging [6], cepstrum analysis, sum and difference frequencies analysis [7] [8], and high frequency resonance analysis (HFRT) [9-12].

The principal purpose of this research is to investigate the possibility of enhancing the early detection of bearing failures utilizing acoustic emissions and more sophisticated signal processing techniques. The pattern recognition based monitoring scheme employs short-time signal processing techniques to extract useful features from bearing AE signals [13]. These features are used by the pattern classifier to detect and diagnose bearing defects.

Short-time signal processing techniques use windowed segments of the bearing signals to facilitate the estimation of the rate and the strength of impulsive AE, which may be the result of a localized defect. If the estimated impulse generating rate is close to any one of the characteristic defect frequencies and the strength of the impulse train is significant, the designed pattern classifier will classify the bearing into damaged category. Due to the uniqueness of each characteristic defect frequency, the diagnosis regarding the location of the defect is also provided through the proposed scheme.

The rate of success for classifying bearings of known condition is used to measure the effectiveness of the designed scheme. An on-line implementation of the designed scheme is also presented.

2. BEARING CONDITION MONITORING VIA PATTERN RECOGNITION ANALYSIS

2.1 Feature Extraction: A sequence of samples (200,000 samples/sec.) representing a typical outer-race damaged bearing AE signal is shown in Fig. 2a. It is evident from this figure that the properties of the bearing signal change with time. For example, there are significant fluctuations in the peak amplitude of the signal, and there are also considerable variations of frequency contents. The fact that periodic impulses generated by damaged bearing are the sources of these time dependent variations suggests that time-domain processing techniques should be suitable for the processing of bearing signals.

The underlying fact is that the properties useful for estimating the impulse generating rate change relatively slowly with time. This leads to a variety of "short-time" processing methods in which short segments of the bearing signal are isolated and processed as if they were short segments from a sustained bearing signal with fixed properties. This is repeated periodically as often as desired. Often these short segments overlap one another. The result of the processing on each frame may be either a single number, or a set of numbers. Therefore, such processing produces a new time-dependent sequence which can serve as a representation of the signal [14-16].

Among others, short-time energy function, short-time average zero crossing rate and median smoothing are employed by the proposed scheme. The definition of the short-time energy function is

$$E_n = \sum_{m=-\infty}^{\infty} x^2(m)w(n-m) \quad (1)$$

where $x(n)$ is the sampled signal and $w(n) = 1$ if $0 \leq n \leq N-1$, $=0$ otherwise (N is the width of window).

In the context of discrete-time signals, a zero-crossing is said to occur if successive samples have different algebraic signs. The rate at which zero crossings occur is a simple measure of the frequency content of a signal. Its definition is

$$Z_n = \sum_{m=-\infty}^{\infty} |\text{sgn}[x(m)] - \text{sgn}[x(m-1)]| w(n-m) \quad (2)$$

where $\text{sgn}[x(n)] = 1$ if $x(n) \geq 0$, $= -1$ if $x(n) < 0$, and $w(n) = 1/2N$ for $0 \leq n \leq N-1$, $= 0$ otherwise. However, Eq. (2) makes the computation of Z_n appear more complex than it really is. All that is required is to check samples in pairs to determine where the zero-crossings occur with the average being computed over N consecutive samples.

The output of the median operator, M , on a segment of signal containing an odd number of samples is simply their middle number (Ex. : 7 in the series 1, 4, 7, 16, 43). Running medians have the desirable property that they will follow the discontinuities in the signal without smearing them out. The definition of median smoothing is

$$M_n = M[x(m)w(n-m)] \Big|_{m=-\infty}^{\infty} \quad (3)$$

where $w(n) = 1$ if $0 \leq n \leq N-1$, and not valid otherwise. This property makes median smoothing useful for prior processing of the bearing signal because short-time energy function and short-time average zero crossing rate are sensitive to the discontinuities in the signal. The signal discontinuities can be removed by subtracting the output of the median smoother from the signal.

The tactic for feature extraction is based upon the estimation of the rate and the strength of impulse generation from bearing signals. The estimation is performed by highlighting the occurrence of defect related AE bursts in the signal and computing their rate of occurrence and strength. If this estimated impulse generating rate happens to coincide with any of the characteristic defect frequencies and the strength of AE bursts is significant, the existence of a localized defect is concluded.

A bearing signal dominated by defect induced AE bursts reveals the occurrence of roller/defect impacts in the fluctuations of its amplitude. These amplitude fluctuations are made more prominent by computing their short-time energy functions.

On the other hand, the defect induced AE bursts oscillating at a much higher frequency than the AE generated by other machine elements will introduce variations in frequency content of bearing signals. Variations of this type may be easily revealed by the computation of average zero-crossing rate of bearing signals.

After all defect related AE bursts have been made more prominent in both the short-time energy function and short-time average zero-crossing rate, their rate of occurrence is estimated by computing the autocorrelation functions. The complete block diagram for the defect detection/diagnosis scheme is presented in Fig. 1.

The signal measured from an outer-race damaged bearing is shown in Fig. 2a. It contains visible AE bursts resulted from the passing on the defect by rollers. The characteristic defect frequency computed by equation (A1) is 110Hz.

Figures 2c and 2e are the short-time energy functions and the zero crossing rate computed from the signal in Fig. 2a. It can be seen that the bursts in the bearing signal are properly highlighted by peaks in both of them. Thus the impulse generating rate can be estimated from the rate of peak occurrence in both of them. Autocorrelation functions were used for the estimation of this rate.

Autocorrelation functions computed from the short-time energy function and zero crossing rate are plotted in Fig. 2d and 2f respectively. The first peak in Fig. 2d is at the lag of 0.0089 second which is equivalent to an impulse generating rate of 112Hz. This is close to the computed characteristic defect frequency. The autocorrelation function of the zero crossing rate indicates a similar rate. These two rates are denoted as f_{SE} and f_{ZC} respectively. SE stands for the short time energy and ZC stands for the zero crossing.

To obtain the features, the "peaks and valleys" (local maxima and minima) are located within the appropriate range around each characteristic defect frequency in two autocorrelation functions. The amplitudes of these two local maxima relative to their respective lower neighboring valleys indicate the strength of impulse trains generated by the damaged bearing. They are denoted as P_{SE} and P_{ZC} in Fig. 2d and Fig. 2f.

The impulse generating rate is defined as the weighted average of f_{SE} and f_{ZC} . Impulse Generating Rate = $(P_{SE} f_{SE} + P_{ZC} f_{ZC}) / (P_{SE} + P_{ZC})$. The frequency comparator compares the Impulse Generating Rate with all three characteristic defect frequencies (see Appendix 1). Should a match is found, the pattern classifier will carry out the classification of the condition of the bearing based on P_{SE} and P_{ZC} .

2.2 Pattern Classifier Design: Since the magnitude of P_{SE} and P_{ZC} is a measure of the strength of the damage related impulse train, it is obvious that the larger the magnitude the more confident one is about the presence of a correspondent localized defect. Coordinate pairs, (P_{SE}, P_{ZC}) , computed from a good bearing should fall into a region near the origin of the plane formed by P_{SE} and P_{ZC} . On the other hand, damaged bearings are characterized by (P_{SE}, P_{ZC}) far away from the origin.

A number of (P_{SE}, P_{ZC}) were obtained from two bearings of known condition. Fig. 3 presents their distribution in the plane formed by P_{SE} and P_{ZC} . The diamonds and blank squares represent coordinate pairs computed from a good bearing and a damaged bearing respectively. These two group of coordinate pairs are distinctly separated from each other and can be separated by a straight line x-x. In the context of pattern recognition, a linear function used to separate different clusters are termed as linear discriminant function. If the pattern vector is defined as $y = (P_{SE}, P_{ZC})$. A linear discriminant function takes the form

$$d_i(y) = a_i^t y + a_0 \quad (4)$$

where a_i^t is a weight vector for the discriminant function and a_0 is the additional component of the weight vector that corresponds to the intersecting point between $d_i(y)$ and axis.

2.3 Classifier Training: The problem of classifier training is equivalent to finding the coefficient set of the linear discriminant function using a labeled training set. A labeled training set actually consists of a set of available pattern vectors measured from bearings with known condition.

The approach for finding such a coefficient set with a given training set will be to define a criterion function $J(a)$ that is minimized if a is a solution vector. This reduces the problem to one of minimizing a scalar function, a problem that can often be solved by a gradient descent procedure.

Consider now the problem of constructing a criterion function, J , for solving the linear inequality: $a^t y + a_0 > 0$ if y comes from a damaged bearing and $a^t y + a_0 < 0$ if y comes from a good bearing. Without losing any generality, one may define a new pattern vector $y' = [y, 1]$ and add a minus sign to all the pattern vectors computed from a good bearing. Thus the problem becomes finding a coefficient set for the inequality $a^t y' > 0$ for all the training data available.

A common choice of the criterion function is the *perceptron criterion function* [17].

$$J_p(\mathbf{a}) = \sum_{\mathbf{y}' \in \mathbf{y}} (-\mathbf{a}^t \mathbf{y}') \quad (5)$$

where \mathbf{y} is the set of samples misclassified by \mathbf{a} . (If no samples are misclassified, J_p is defined to be zero.) Since $\mathbf{a}^t \mathbf{y}' \leq 0$ if \mathbf{y}' is misclassified, $J_p(\mathbf{a})$ is never negative, being zero only if \mathbf{a} is a solution vector.

Since the j th component of the gradient of J_p is $\partial J_p / \partial a_j$, one can see from Eq. 5 that

$$\nabla J_p(\mathbf{a}) = \sum_{\mathbf{y}' \in \mathbf{y}} (-\mathbf{y}') \quad (6)$$

and hence the basic gradient descent algorithm becomes

$$\mathbf{a}_{k+1} = \mathbf{a}_k + \sum_{\mathbf{y}' \in \mathbf{y}_k} (\mathbf{y}') \quad (7)$$

where \mathbf{y}_k is the set of samples misclassified by \mathbf{a}_k . Thus, the descent procedure for finding a solution vector can be stated as follows: the next weight vector is obtained by adding some multiple of the sum of the misclassified samples to the present weight vector.

This gradient search algorithm was programmed into Fortran programming language. When it is provided with all the training data shown in Fig. 3, line x-x in the figure was the *linear discriminant function* yield by this algorithm.

3. EXPERIMENTAL SETUP: The experimental setup consisted of a spindle driven by a variable speed motor and a stand-by bearing test rig. The spindle can be driven up to 2200 rpm. The investigated bearing is mounted on a mechanical platform which enables the adjustment of the following three: the thrust load, the angular misalignment, and the position of the center of the bearing.

Simulated localized defects were produced on two bearings' outer-race by electric-discharge machine to keep their size and depth under precise control. The size of the artificial defects is 60/1000 inch in diameter by 5/1000 inch in depth which is typical [1] and a groove 2mm wide across the outer race. The three bearings were (1) a good bearing, (2) a bearing with the groove, and (3) a bearing with single roller defect. AE signals were picked up in the radial direction by a transducer. The bandpass filtered (20k-90k) output signal of the sensor was sent to an A/D converter installed on an IBM PC-AT for data sampling.

4. DEFECT DETECTION/DIAGNOSIS: The rate of success for classifying the condition of the bearing was used to test the effectiveness of the proposed scheme. Forty one bearing signals were measured under different load and speed from the three bearings. The rate of success for the proposed scheme is 97.5% which is 6% better than the best among the state of the art based on applying a similar scheme to the processing of vibration signals of bearings [13]. This indicates that AE may be a better physical variable to measure than vibrations for assessing the condition of rolling element bearings. Fig. 4 shows a vibration signal and an AE signal measured 1 foot away from the second bearing. It is obvious that AE has a larger part of its energy caused by the presence of localized defects than that of vibrations. Therefore, AE is a better signal than vibrations while the transducers have to be placed remotely from a bearing.

5. ON-LINE IMPLEMENTATION

5.1 System Organization: On-line monitoring implies automatic data processing without human intervention. AE, picked up by sensors, is transmitted to a monitoring system where they are processed for information extraction. The on-line system comprises a data acquisition stage, where analog bearing signals are converted into digital form and a data processing stage, where modular software algorithms are employed to perform the designed algorithm under the guidance of a supervisor program.

The data acquisition stage comprises 1) an AE transducer, 2) an amplifier, 3) a band pass filter, and 4) an analog to digital converter. The data processing stage consists of three functional units: supervisor, defect detection/diagnosis unit, and data base.

The block diagram which illustrates the organization of the complete system is shown in Fig.5. The supervisor is responsible for: 1) the proper logic sequence of system operation, 2) the data flow control between the defect detection/diagnosis units and the global data base, and 3) global data base management.

A global data base is constructed to hold all the information to be relayed among the data acquisition stage, the functional units of data processing stage, and the system's human-machine interface. It comprises 3 data files: 1) General purpose data file, 2) Raw bearing signal data file, and 3) Pattern vector data file.

One important reason for having a global data base is that the external data files will preserve important data just prior to any unforeseen shutdown of the monitored system or bearing monitoring system itself.

The interface is responsible for the human-monitoring system communication. The necessary input information consists of a) bearing geometry, b) bearing rotational speed, and c) sampling rate. The output quantities through the interface consists of alarm and diagnosis.

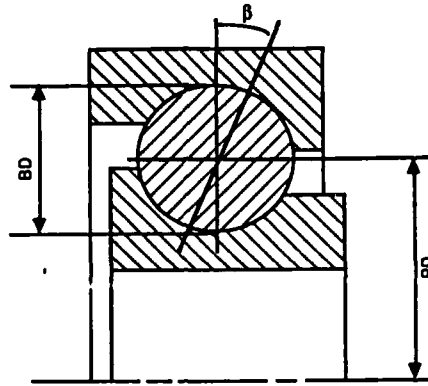
5.2 System Operation Logic: The actual sampling rate of the system may be varied and it is set by a programmable clock which is an integral part of the A/D converter. The supervisor first reads in the necessary inputs from the human operator. Then the data acquisition stage activates the A/D converter according to this information. Once the converter is initiated, it supplies discrete data elements to the system at the selected rate until a specified number of samples has been generated. The data are formulated into records and written onto the peripheral disk memory (data file #2).

The data will be processed by the defect detection/diagnosis unit. The loop of data measuring and processing will be continuously carried out until any kind of localized defect is detected and diagnosed. In the case of such an event, the pattern vector, estimated impulse generating rate, and classifier output will be displayed on the CRT to alert the operator.

6. CONCLUSIONS: A bearing condition monitoring technique based on the processing of acoustic emissions measured at the near by of a bearing was investigated. The development and application of the monitoring technique were carried out successfully in an on-line implementation. The scheme was proven to be more effective than vibration based techniques under most conditions. The advantages of the scheme are summarized as follows:

1. It provides a better alternative to the traditional sound/vibration bearing condition monitoring schemes.
2. It allows the diagnosis of the locations of localized defects on bearings.
3. It can be easily implemented with microprocessor hardware for on-line implementation.

Appendix A: Bearing characteristic defect frequencies [1]



$$f_{or} = \frac{n}{2} f_r \left(1 - \frac{BD}{PD} \cos(\beta)\right) \quad (A1)$$

$$f_{ir} = \frac{n}{2} f_r \left(1 + \frac{BD}{PD} \cos(\beta)\right) \quad (A2)$$

$$f_{ro} = \frac{BD}{PD} f_r \left(1 + \left(\frac{PD}{BD}\right)^2 \cos(\beta)\right) \quad (A3)$$

where

f_{or} = characteristic defect frequency for defect on outer-race
 f_{ir} = characteristic defect frequency for defect on inner-race
 f_{ro} = characteristic defect frequency for defect on roller
 BD = roller diameter
 PD = bearing pitch diameter
 f_r = bearing rotating speed
 β = contact angle between race and ball
 n = number of rollers

7. REFERENCES

1. Widner, R. L. and Littmann, W. E., "Bearing Damage Analysis," National Bureau of Standard special publication No. 423, April 1976
2. Downham, E., and Woods, R., "The Rationale of Monitoring Vibration on Rotating Machinery in Continuously Operating Process Plant", ASME paper No. 71-Vibr-96
3. Weichbrodt, B., and Bowden, J., "Instrument for Predicting Bearing Damage," GE Co. Report, March 1970, S-70-1021 AD 869633
4. Dyer, D. and Stewart, R.M.; "Detection of rolling element bearing damage by statistical vibration analysis," J. of Mechanical Design, Vol 100; 1978, p-229
5. Gustafsson O.G. and Tallian, T. "Detection of damage in assembled rolling bearings", Trans. ASLE, 5, 62 1962, P-197
6. Braun, S. and Datner, B., "Analysis of roller/ball bearing vibrations," J. of Mechanical Design, Jan. 1979, Vol 101; p-121
7. Ehrich, F.F.; "Sum and difference frequencies in vibration of high speed rotating machinery," J. of Engineering for Industry, Vol. 94, No. 1, Feb. 1972, p-181.
8. Eshleman, R.L., "The use of sum and difference frequencies in rotating machinery analysis," Proc. of Machinery Vibration Seminar IV, Cherry Hill, N.J., Vibration Institute Nov. 1980.
9. Mcfadden, P.D. and Smith, J.D., "Vibration monitoring of rolling element bearings by

- the high frequency resonance technique-a review," Tribology International Jan. 1984; p-3.
10. Broderick, J.J., Burchill, R.F. and Clark, H.L., "Design and fabrication of prototype system for early warning of impending bearing failure," NASA CR- 123717 Jan. 1972.
 11. Burchill, R.F., "Resonant structure techniques for bearing fault analysis," National Bureau of Standards NBSIR 73-252 1973.
 12. Darlow, M.S., Badgley, R.H. and Hogg, G.W., "Applications of high frequency resonance techniques for bearing diagnostics in helicopter gearboxes," USAAMRDL-TR-74-77, 1974.
 13. C. James Li and S. M. Wu, On-line Detection of Localized Defects in Bearings by Pattern Recognition Analysis, ASME J. of Engineering for Industry, Nov. 1989.
 14. J.M. Baker, " A New Time-Domain Analysis of Human Speech and Other Complex Waveforms," Ph.D Dissertation, Carnegie-Mellon Univ., Pittsburgh, PA., 1975
 15. J.B. Allen, "Short-Term Spectral Analysis and Synthesis and Modification by Discrete Fourier Transform," IEEE Trans. Acoustics, Speech and Signal Processing, Vol. Assp-25, No.3, pp235-238, June 1977.
 16. L.D. Erman, "An Environment and System for Machine Understanding of Connected Speech," Ph.D. Dissertation, Carnegie-Mellon University, Pittsburgh, PA, 1975
 17. Rosenblatt, F., "The Perceptron-A Perceiving and Recognizing Automation," Report 85-460-1, Cornell Aeronautical Laboratory, Ithaca, N.Y., 1957

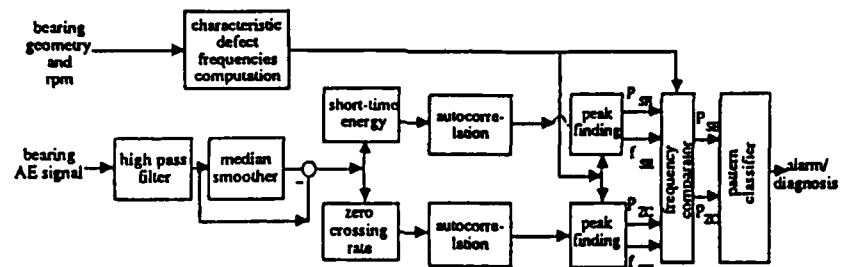


Fig. 1 Block diagram of defect detection/diagnosis scheme

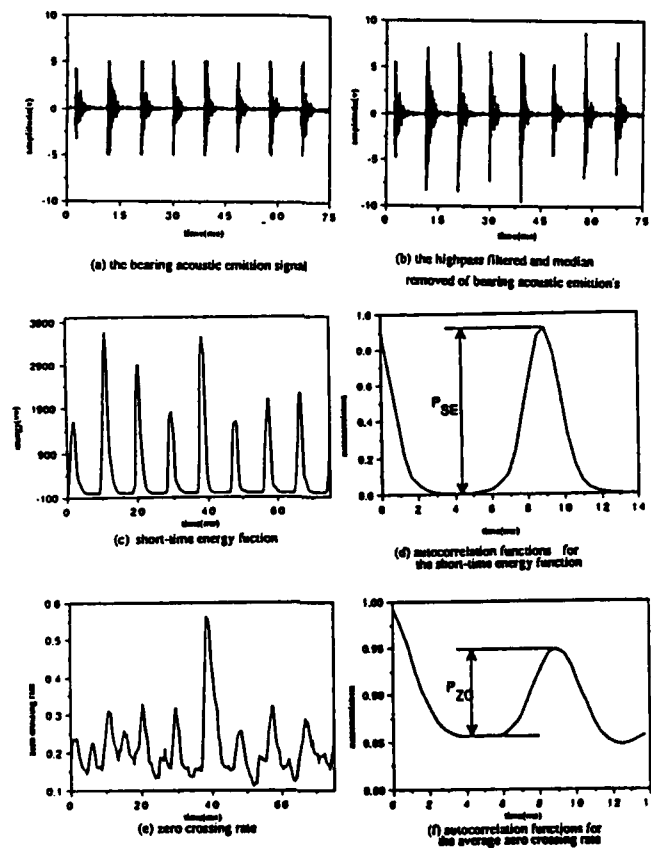


Fig. 2 The data processing results for the proposed scheme

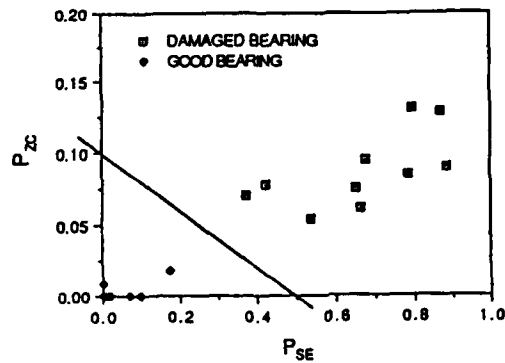


Fig. 3 Feature vector Distribution

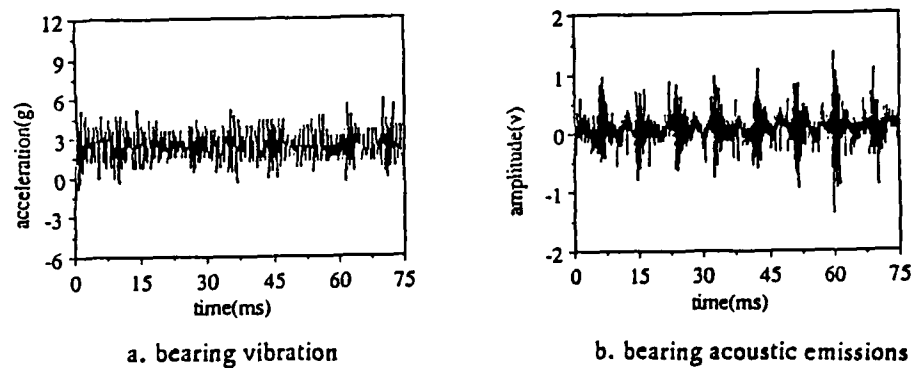


Fig. 4 Bearing signals measured away from the bearing:

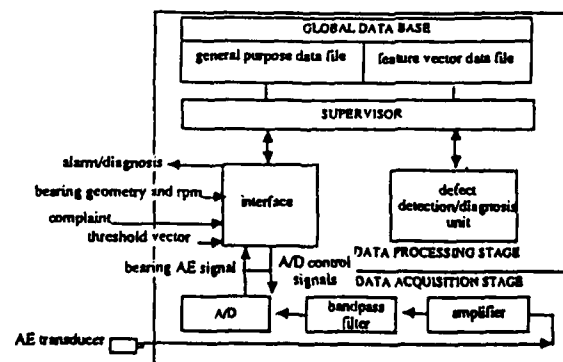


Fig. 5 Block diagram representation of the on-line bearing monitoring system

SYSTEMS FOR PREVENTING MECHANICAL
FAILURE OF MACHINE TOOLS*

Ronald K. Wharton
Benet Laboratories
Watervliet Arsenal
Watervliet, New York 12189-4050

Abstract: Two unique types of supervisory systems have been installed and implemented. The first of these, a Machinery Condition Surveillance System (MCSS), evaluates measurement data that has been generated from the operation of a 3-axis machining center. Specific internal mechanisms and variables are characterized; spindle, spindle motor-vibration, gearbox-oil temperature, z-axis motor-current, and cutting tool coolant-flow rate.

The second, a Broach Tool Condition System (BTCS), measures and displays forces produced by the cutting action of a 12 station broach machine. Destruction to tooling is minimized by frequent re-evaluation of analog force plots and the most recent threshold estimates for wear and breakage.

Key Words: Breakage; broaching machine; cutters; forces; free-state; internal mechanisms; machining center; mechanical failure; metal cutting; multi-parameters; performance characteristics; wear.

Introduction: An ordnance manufacturing arsenal has many diverse types of machine tool applications. Over a period of time, some units will experience incipient mechanical problems and wear of internal components. The conditions can signal the potential for catastrophic mechanism failure.

Similarly, during broach machining, forces of acceptable magnitude that are normally produced by the interaction of cutter and workpiece can suddenly rise above safe limits. The condition suggests severe dulling of cutting edges with the possibility for tool destruction. There is also the likelihood that product surface finish integrity shall be adversely affected.

Procedure: Efforts were undertaken to investigate and find methods for monitoring machinery and tooling.

*This work was supported by the U.S. Department of Defense, (MANTECH) Project A6888546 and related efforts.

Applications: In the first application, (figure 1a-1c), a pilot Machinery Condition Surveillance System continuously surveys measurements taken during the operation of a 3-axis machining system. An integrated monitoring technique features collection, storage, and retrieval of multi-parameter data generated from non-machining and dynamic metal removal activity.

Analyses of the following variables were performed; vibration, coolant flow, gearbox oil temperature, motor current, and spindle speed. Trended parameter performance plots and management reports describe the machine tools' current "health."

In the second application, (figures 2a-2c), the broach (rifler) holder and ram head assembly of a rifling machine are instrumented with force measuring-load sensitive and linear (displacement) transducers. During the broaching process, each cutter edge of the entire broach tool length engages material. The forces generated are measured in real-time. Simultaneously, a microprocessor performs A/D conversion and analysis of the data and produces a graphic display of force versus broach location. A hard copy plot is subsequently issued.

Results: Machinery Condition Surveillance System. The discussions that follow are interpretations of data taken from a limited set of randomly selected measurements.

Cross-correlation of analyses from each measured variable offered the best inference and prediction capabilities.

Time-varying vibration signal data: Using digital filtering and analysis algorithms, major oscillations were searched out, characterized, and linked to specific machine tool components.

1. In (figures 3a and 3b), when tracking the fluctuations in spindle motor current and spindle motor speed over a 7 day period, the variations noted are typical machine running responses, i.e., increases and decreases in current produce corresponding changes in speed.

2. In the crossplot (figure 3c) of spindle motor current vs. spindle motor speed, it is verified that speed increases as the current was increased, i.e., data cluster points at 1900 RPM and 3350 RPM. In (figure 3d), the crossplot of gearbox vibration g's (Peak) vs. spindle motor speed; the change in the overall vibration level is attributed to gear loading forces; i.e., cluster of data points at 1900 RPM and 3350 RPM.

3. In (figures 4a, 4b), peak vibration measurements were taken over the same one week time period. In (figure 4a), the vibration level for the free-state ranged from approximately .003g to .026g's. An arbitrary vibration threshold of .020g's was programmed to alert when the signal was considered high. In (figure 4b), during metal cutting activity; a 2.0 inch end mill produced variations ranging from .011 to .016 g's; a significant lowering in the vibration level. These changes are attributed to closer regulation of speed and load.

4. In (figures 4c, 4d), the gearbox oil temperature and cutting coolant flow serve as indicators of the machinery's overall operational performance. The variations noted are attributed to normal ambient temperature changes in the manufacturing area and the manual intervention by machine operator to regulate coolant flow rate.

Broach Tool Condition System. During broaching, the forces generated by 12 consecutive cutting tool stations of a single rifling machine were monitored. Each freshly sharpened cutter generated its own special signature of "force vs. broach tool length."

For each tool station, wear and breakage threshold limits in excess of the measured baseline real-time force signature level was arbitrarily assigned and programmed. Some examples of forces measured together with programmed wear/breakage boundary limits for stations, 1, 2, 3 and 7 are plotted (Figures 5a - 5d).

In figures 5a - 5c, representing cutting stations 1-3, the peak force magnitudes (55-40 kN) are the largest since larger volumes of metal are removed in earlier stages of broaching. In contrast, (Figure 5d), for cutting station 7, the force level is appreciably lower, approximately (20kN).

Summary: Technological benefits to be derived from utilizing the Machinery Condition Surveillance and Broach Tool Condition Systems:

- a. Use of automatic on-line monitoring for enhancing management's ability to foresee impending machine tool/process problems.
- b. Detection of early machinery component and cutting tool wear/degeneration.
- c. Improve on production uptime and make possible the adoption of scheduled maintenance.
- d. Improve the quality of surface finishes and accuracy of dimensions for weaponry.

The requirement for full plant coverage would require extensive considerations involving a much larger capacity surveillance system. To properly manage this task involves the use of an existing centralized DEC/VAX computer system, LAN-ETHERNET, timesharing, and adequate staffing of trained personnel.

The Broach Tool Condition System shall extend useful life of the cutters and serve as a standard for evaluating the effectiveness of the broach cutter regrinding process and the quality of broach tooling. Full implementation and optimization of the system shall be accomplished upon establishing a reliable database of dynamic force measurements and "teach-in" modification of safe wear/breakage force limits. The technology is expected to offer many "spin-off" applications.

Figure 1 - Machinery Condition Surveillance System(MCSS)

The Information contained in the photos represents a pilot machinery condition surveillance system dedicated to the health monitoring of a single machine tool continuously.

Figure 1a - Candidate Giddings & Lewis 3-Axis Machining Center Being Monitored

Figure 1b - Control Cabinet of Machining Center Showing MCSS Microprocessor(closed arrow) and CRT Monitor Unit(open arrow). The technician is performing on-site "Field" testing and debugging functions.

Figure 1c - The MCSS Engineering Analysis Computer shown is remotely located from the Machining Center. The technician performs continuous surveillance of multi-parameter measurements and is generating "Health" statistic reports.

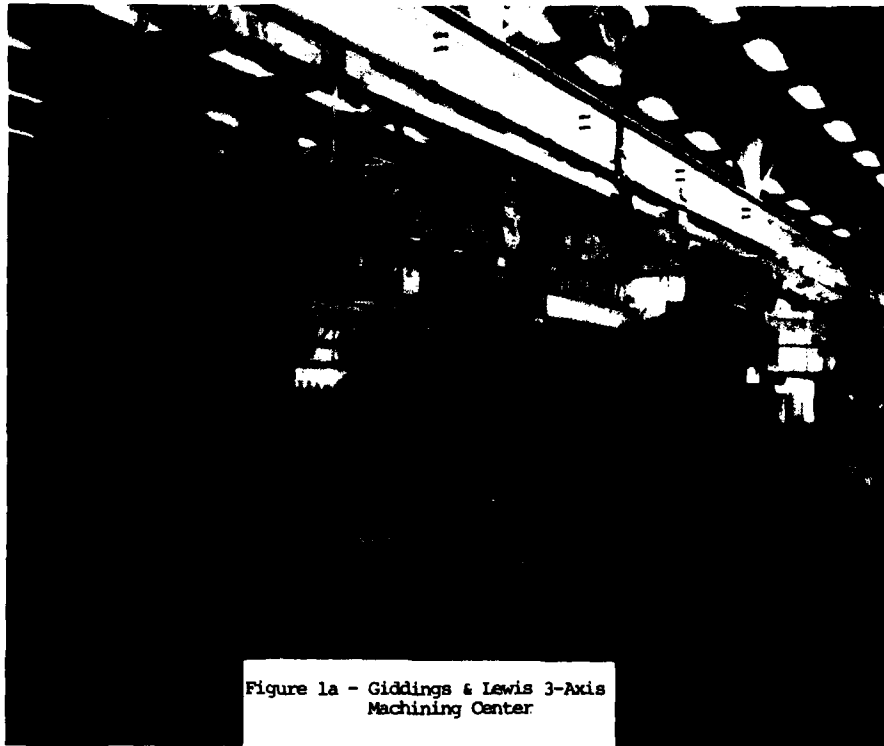


Figure 1a - Giddings & Lewis 3-Axis
Machining Center

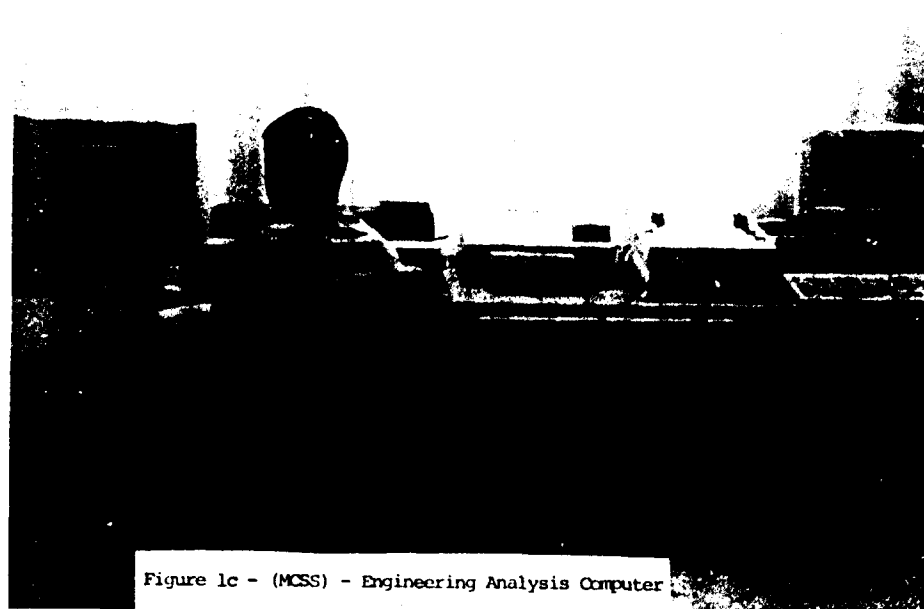
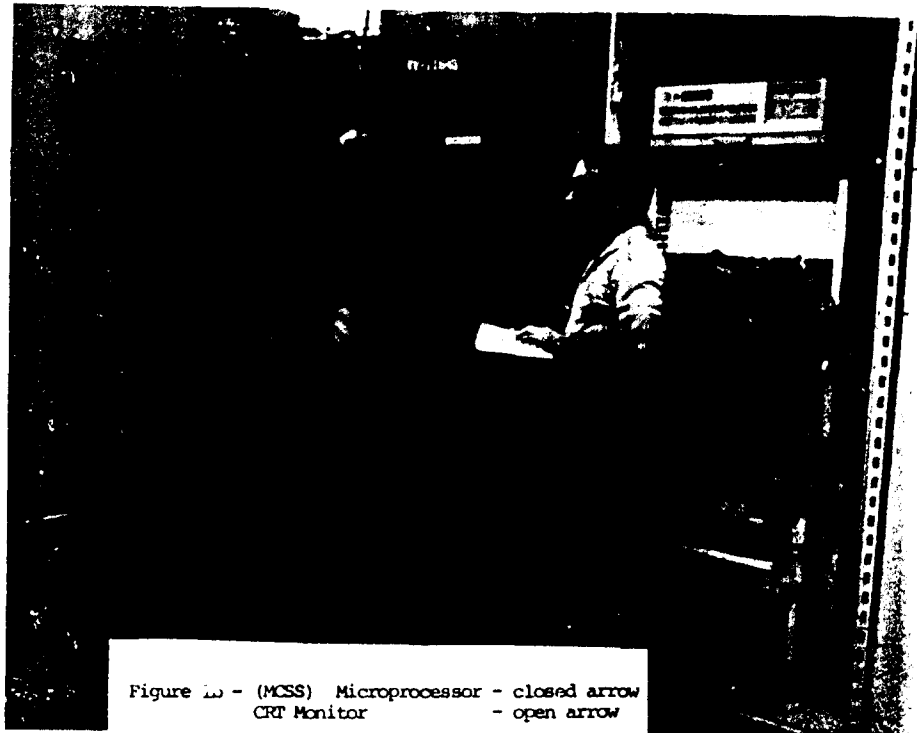


Figure 2 - Broach Tool Condition System

Figure 2a - A 12-Station Colonial Broach Machine Performing "Rifling" Operations on Ordnance Components

Figure 2b - Located at the Broach Machine, a Dedicated Microprocessor and CRT Monitor. The screen is indicating three traces of the dynamic rifling process. Bottom trace represents actual "force levels" produced. The upper traces are pre-programmed threshold levels offering boundary conditions for cautionary and imminent cutter failure protection(see Figure 3).

Figure 2c - Two Broach Cutter Inserts. The lower insert is new and without apparent defects. The upper cutters' extreme right edge has experienced wear/failure.

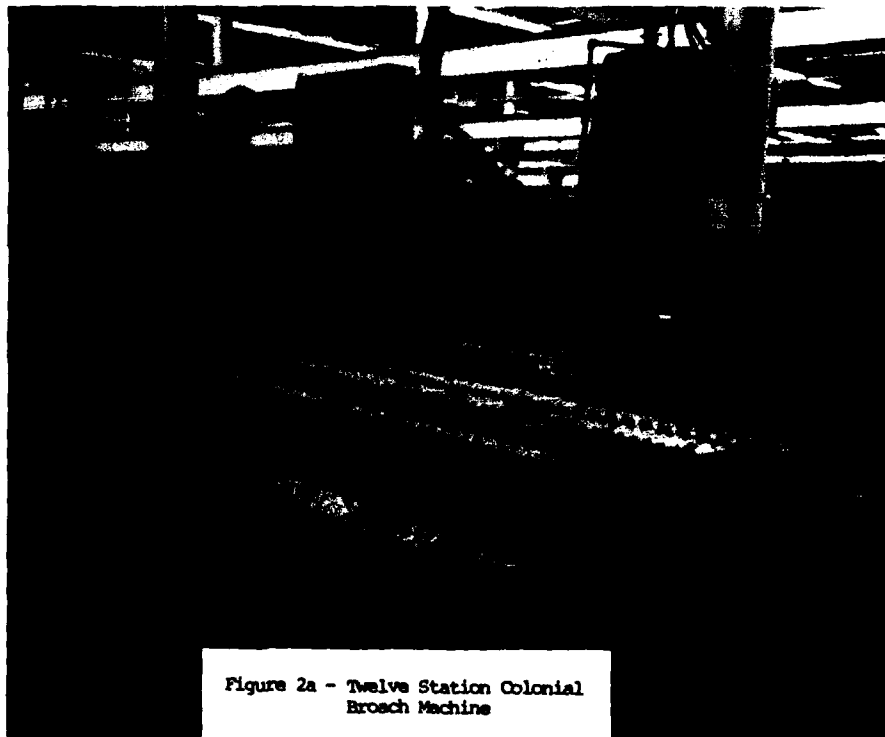
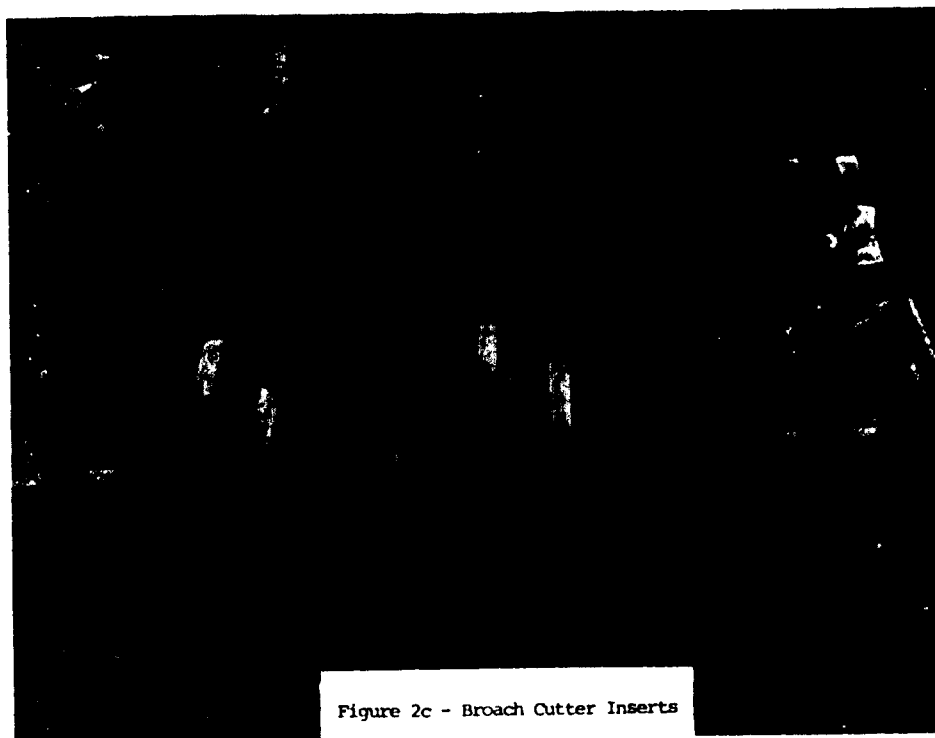
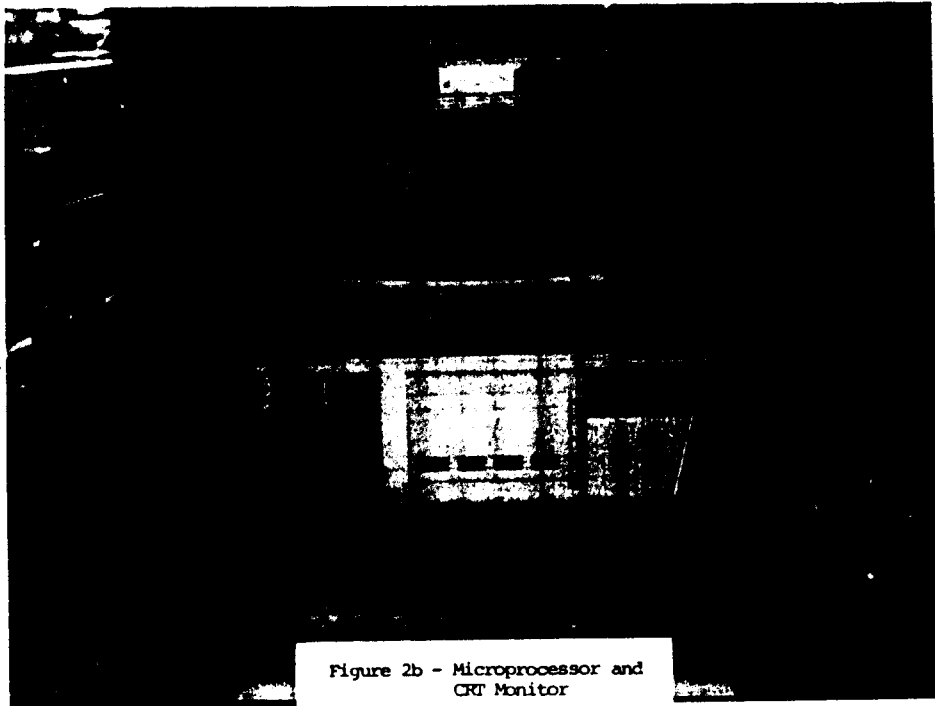
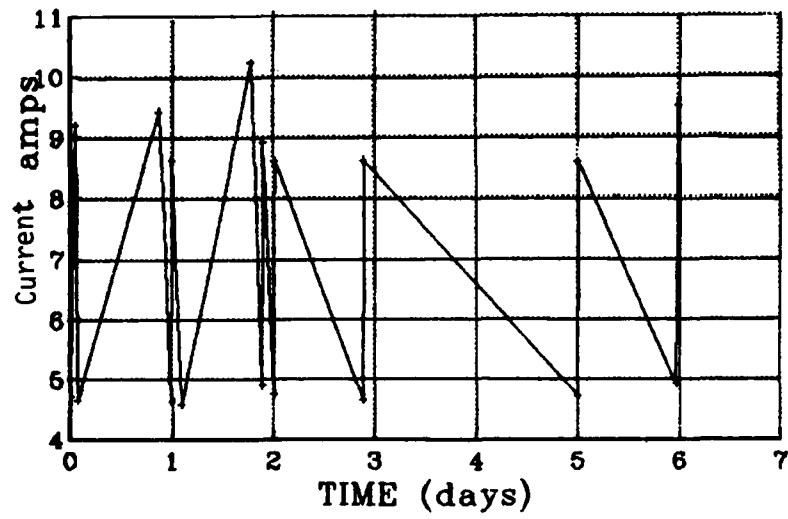


Figure 2a - Twelve Station Colonial Broach Machine



Y VARIABLE
Free State -
Spindle Motor Current

Figure 3A

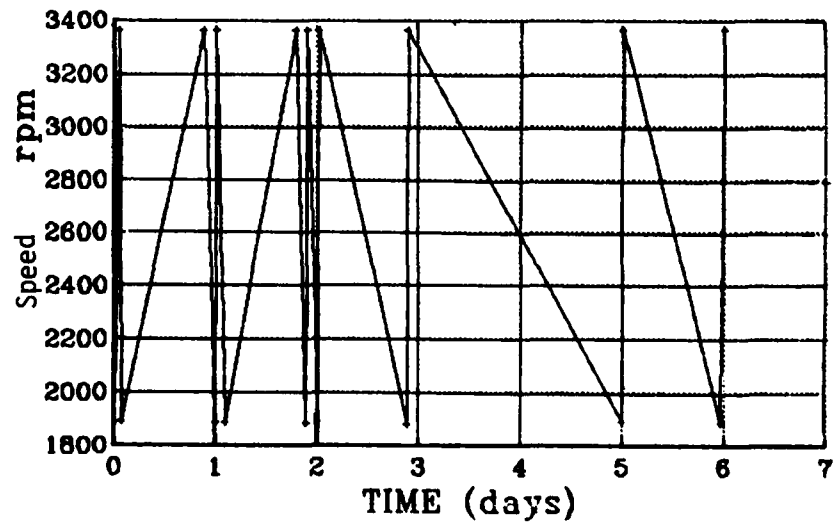


06/22/89 12:54:38

06/28/89 13:03:44

Y VARIABLE
Free State -
Spindle Motor Speed

Figure 3B



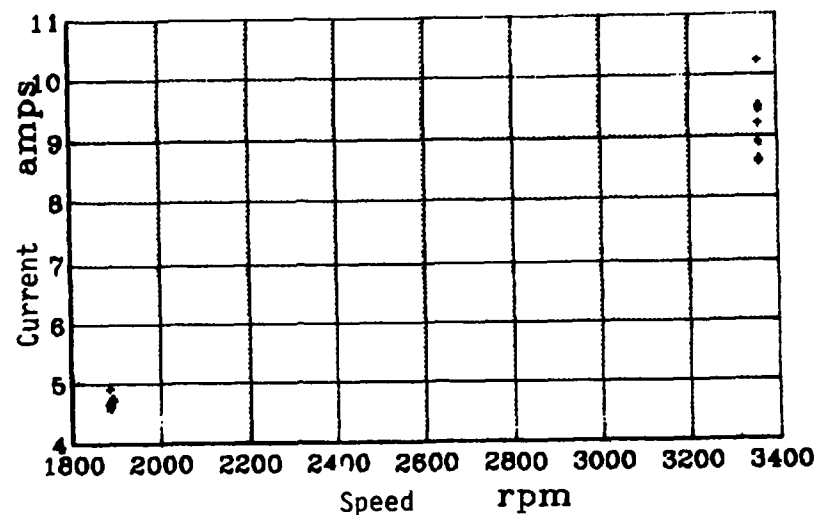
06/22/89 12:54:34

06/28/89 13:03:42

Y VARIABLE
Free State -
Spindle Motor Current

X VARIABLE
Free State -
Spindle Motor Speed

Figure 3C



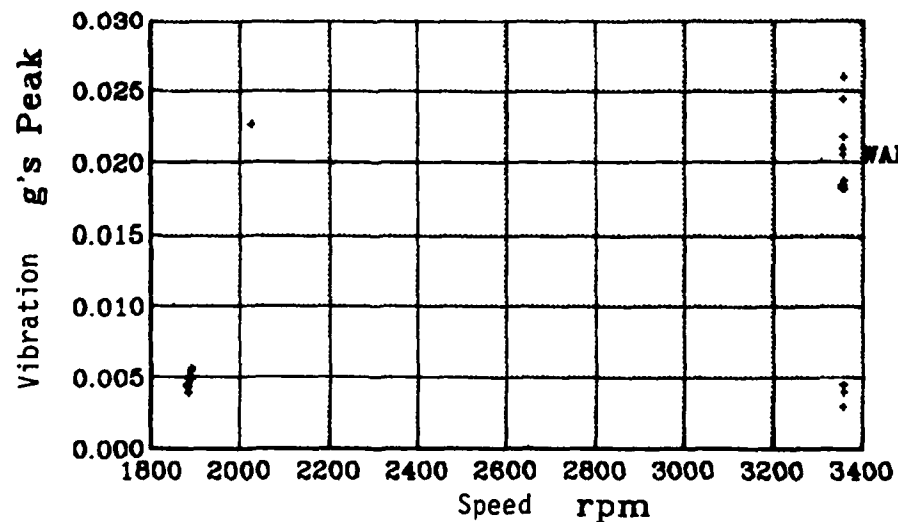
06/22/89 12:54:34

06/28/89 13:03:46

Y VARIABLE
Free State -
Gearbox Vibration
Freq 525.0 to 587.5 Hz

X VARIABLE
Free State -
Spindle Motor Speed

Figure 3D

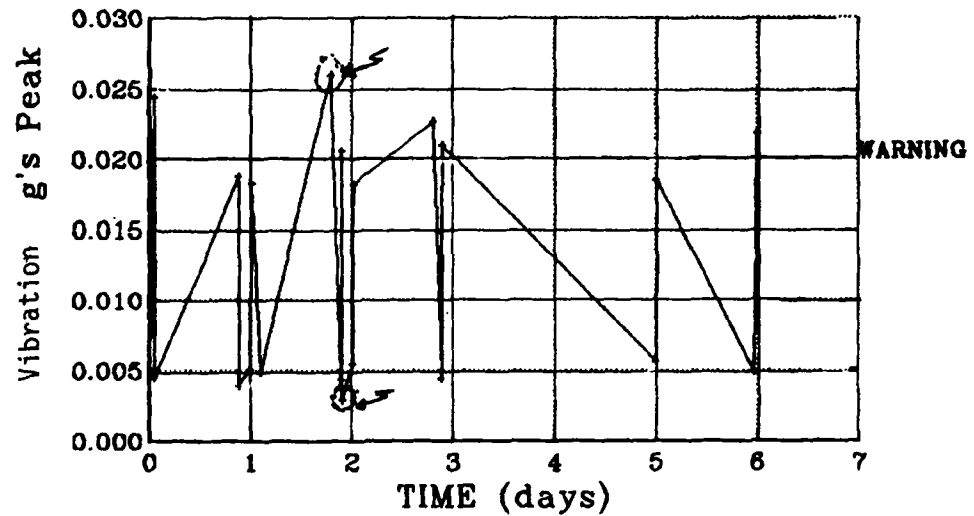


06/22/89 12:54:33

06/28/89 13:03:43

Y VARIABLE
 Free State -
 Gearbox Vibration
 Freq 525.0 to 587.5 Hz

Figure 4A

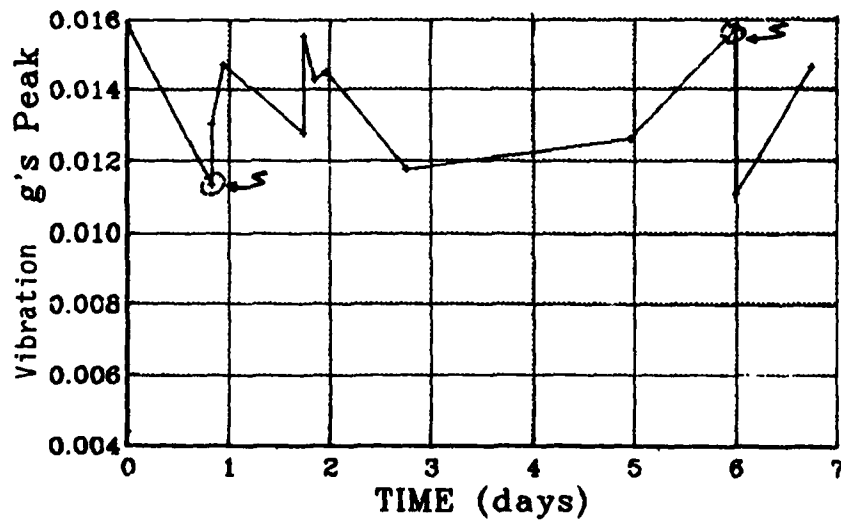


06/22/89 12:54:33

06/28/89 13:03:41

Y VARIABLE
 2.0" End Mill
 Gearbox Vibration
 Freq 550.0 to 575.0 Hz

Figure 4B

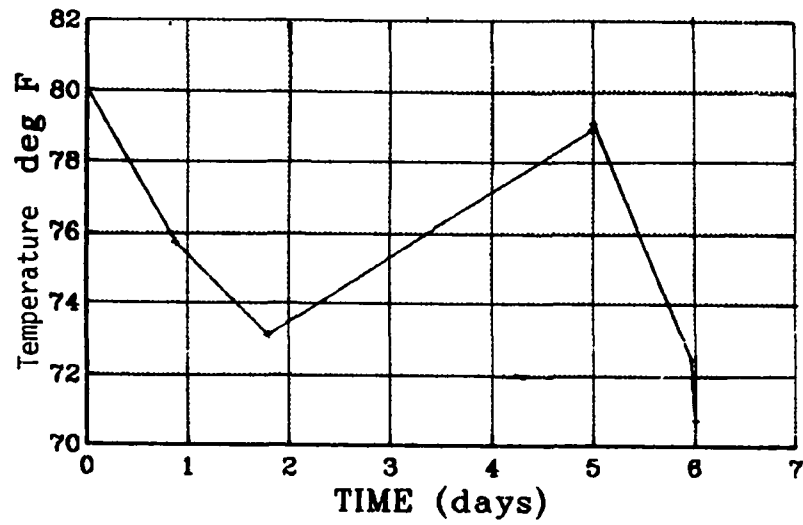


06/22/89 14:15:30

06/29/89 08:20:27

Y VARIABLE
Free State -
Oil Temperature

Figure 4C

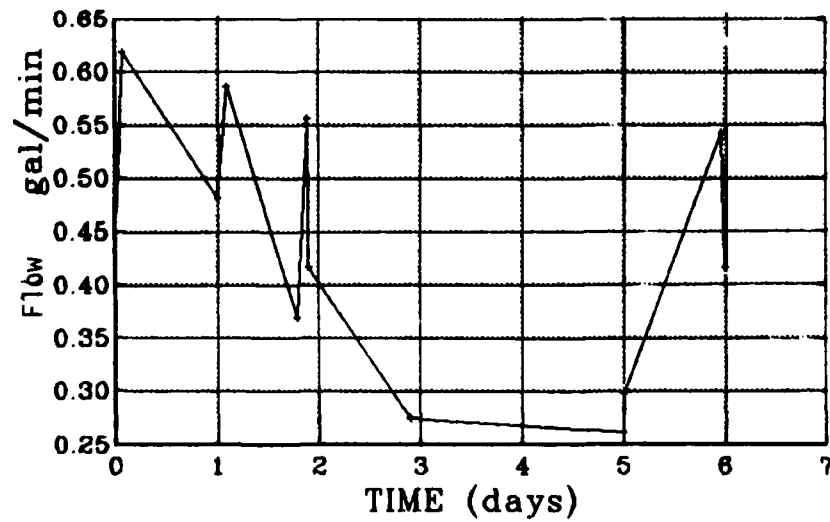


06/22/89 12:54:34

06/28/89 13:03:42

Y VARIABLE
Free State -
Cutting Coolant Flow

Figure 4D



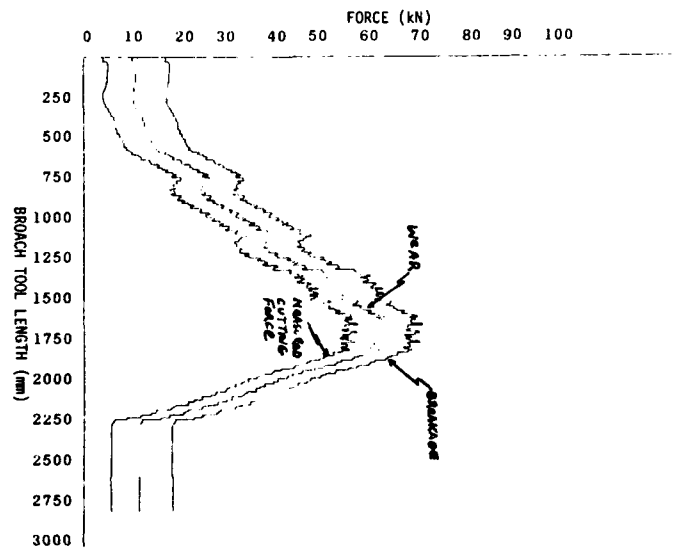
06/22/89 12:54:34

06/28/89 13:03:42

08238902.DAT 1. series 08/23/1989 02:41 285 values

Figure 5A

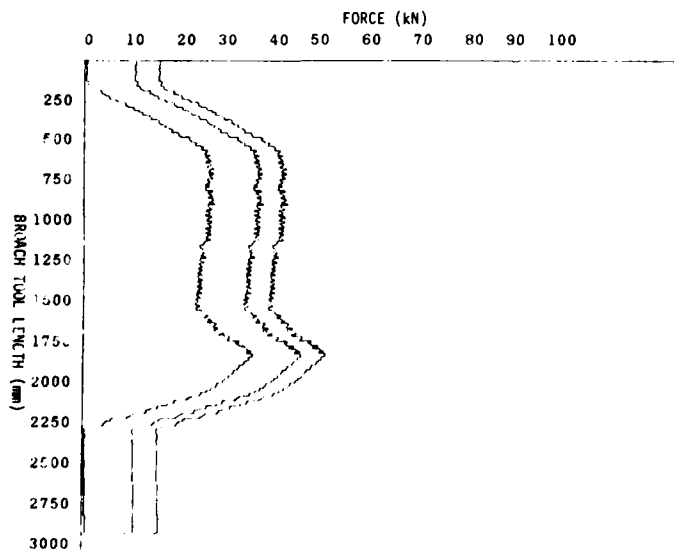
tool : 1
length of path-slice mm : 10
breakage-addition % : 18
wear-addition % : 10
tolerance : 5
error-code (piece ok) : 0
operating mode : AUTOMATIC



08238901.DAT 2. series 08/23/1989 10:25 295 values

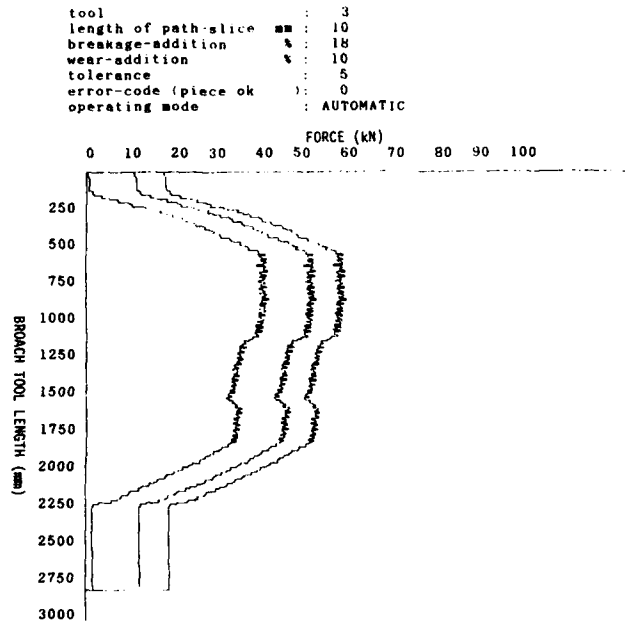
Figure 5B

tool : 2
length of path-slice mm : 10
breakage-addition % : 18
wear-addition % : 10
tolerance : 0
error-code (piece ok) : 0
operating mode : LEARNING



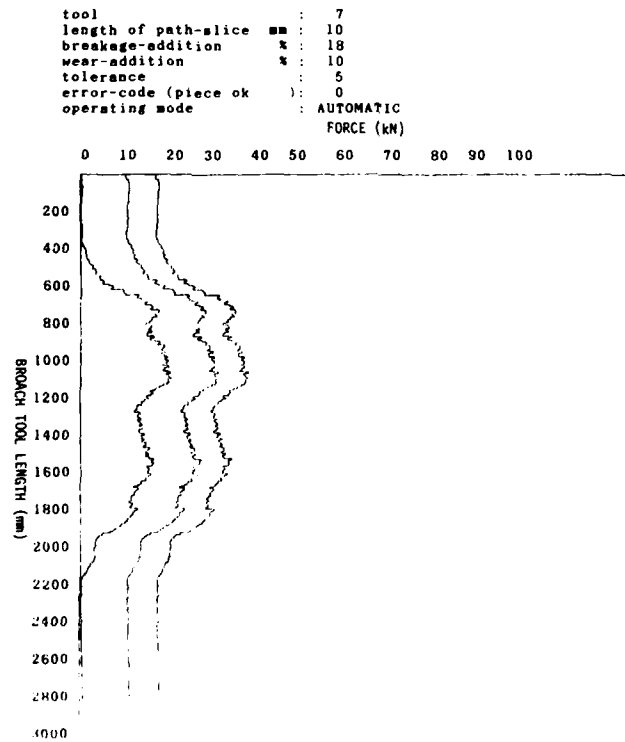
08238902.DAT 3. series 08/23/1989 02:48 285 values

Figure 5C



08238902.DAT 7. series 08/23/1989 03:03 285 values

Figure 5D



CONDITION MONITORING OF OPERATING FLUID FILM BEARINGS WITH ULTRASONIC TRANSDUCERS

Frederick C. Wiesinger Jr.

Kingsbury, Inc.
Philadelphia, Pennsylvania 19154

G. T. Haramis Jr.

TecSonics Inc.
Twinsburg, Ohio 44087

W. E. Karberg

Centerior Energy
Cleveland, Ohio 44101

Phil Rapone

Kingsbury, Inc.
Philadelphia, Pennsylvania 19154

R. E. Berris

Berris Electronics
Chagrin Falls, Ohio 44022

Abstract: Bearing wear is monitored in operating fluid film bearings with ultrasonic transducers. The transducers measure material loss from the surface of the bearing within a normal operational accuracy of $\pm .0002$ in. The high degree of accuracy permits the detection of wear from its earliest stages. Periodic or continuous inspection of the bearings while the equipment is running gives an immediate indication of the current condition of the bearing. An evaluation of the rate of change of the condition of the bearing is made from trending individual measurements. From this information an estimation of the bearing's remaining safe operating life can be made.

There are discussions of how the system works, the effect of temperature variations on the system, data from case histories of installations in two generator steam turbines, testing programs for the system, and proposed applications in naval bearing systems.

Key words: Ultrasonic transducers; on-line bearing wear measurement; bearing condition monitoring; fluid film bearings; tilting pad bearings; tapered land bearings; naval bearing systems.

Introduction: A fluid film bearing that is properly designed, manufactured, installed, and operated will never wear. An aligned bearing that is operating at its design

speeds and loads that has a good supply of proper clean cool oil will not actually come in contact with the shaft or the thrust surface and should therefore not experience any wear. There are many cases where bearings have operated trouble free for many years. There are also many cases where one of these key operating parameters have not been met and the bearings have worn.

Inspecting the bearings to determine their condition has traditionally been an expensive, time consuming and risky necessary evil. Equipment users in many industries have made significant efforts to reduce these risks and expenses thru application of instrumentation to obtain an indication of the condition of their bearings while their equipment is running. The application of thermocouples, vibration instrumentation, and oil analysis to determine bearing condition and performance is increasing dramatically. One industry estimate indicates that the use of thermocouples in bearings has increased by 60 times over the last twenty years.

Each of these technologies, however, evaluate the results of symptoms of a bearing problem that has already occurred. Often an indication of a bearing problem is obtained only after the bearing is well on its way to failure.

An ultrasonic transducer system installed in the bearing can track a lengthy process of wear. Measurement of the loss of material from the surface of the bearing due to abrasive or adhesive wear, corrosion and erosion can be tracked from the inception of the problem through the point of bearing instability. With this system bearing condition is determined thru evaluation of the dimensional change of the bearing rather than thru evaluation of shaft movement, shaft/bearing gap, temperature, or oil sample data.

The ultrasonic transducer system provides the ability to monitor the changing condition of the bearing so that maintenance can be planned to avoid unsafe operating conditions, forced outages, and equipment damage.

How the system works: The principal in this ultrasonic system is to time the travel of an acoustic signal from its emission at the piezoelectric crystal thru its travel to the bearing surface and its reflection back to the crystal. With known characteristics of the material and the acoustic signal the measured time can be converted into distance. Any reduction in that distance indicates bearing wear. The system is essentially an acoustic micrometer.

Measurements are independent of most equipment operation parameters such as rotational speed, vibration, clearance, and lube oil properties. Temperature does have an effect on the system. This will be discussed later. Electronic gating of the returning signal prevents false readings from echos from the oil or shaft.

Transducers designed for the bearing wear monitor system are specifically engineered for use in a variety of bearings. In current installations they are made with tips typically the same or similar material as the bearing surface. For example brass transducers are used in bronze bearings and babbitt tipped transducers

are installed in babbitt lined bearings.

Several transducers, each about the size of a pencil eraser and each containing a piezoelectric crystal, are installed in known or anticipated wear areas. In each case the tip of the transducer becomes an integral part of the bearing so that during equipment operation the tip of the transducer wears at the same rate as the surface of the bearing.

System instrumentation sends a sharp voltage pulse to the piezoelectric crystal mounted in the transducer. The crystal, in turn, emits a sonic pulse that travels to the face of the transducer and "bounces" or "echoes" back. The echo re-excites the crystal and is converted back to a voltage pulse that travels back to the system instrumentation. Specially designed circuitry in the electronics system identifies and qualifies the echo, and then measures the time from signal emission to echo receipt. The signal qualification process prevents false readings. The measured time difference translates accurately into distance.

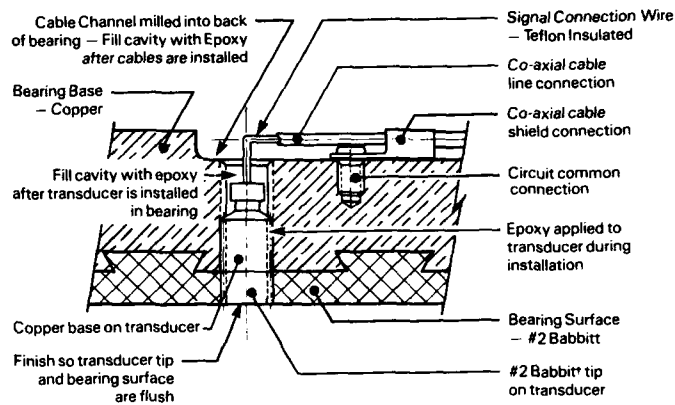


Figure 1. Typical Transducer Installation Cross Section

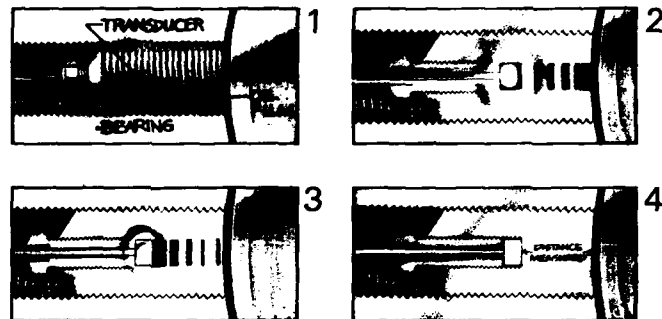


Figure 2. Transducer Operational Sequence

1. The transducer is mounted in the bearing in such a way that it becomes an integral part of the bearing surface.
2. A high-frequency sound wave emitted by the piezoelectric crystal travels to the face of the transducer and echoes back.
3. The echo re-excites the crystal and a signal travels back to the system instrumentation.
4. The instrument measures the time difference from pulse initiation to echo receipt then converts this time difference to distance.

Compensation for Temperature Differences: Variations in temperature have a dramatic effect on results obtained with ultrasonic transducers. Temperature changes

impact the transducers two ways: (1) when measurements are made in the 0.0001 inch range growth or shrinkage of the material due to temperature changes can be observed with the ultrasonic system, and (2) the speed of sound in a material changes with the change of temperature in the material. For these two reasons it is necessary to compensate for temperature variations in order to achieve measurement accuracies that make the use of the ultrasonic system an effective tool for indicating bearing condition. Tilting pad thrust bearings provide a special challenge for temperature compensation. In this type of bearing for a steady state operating condition there are broad temperature variations across the face of each pad (See Figure No. 3).

11000, RPM, 500 PSI, 100PCT T75/75 = 270°F TMAX = 297°F

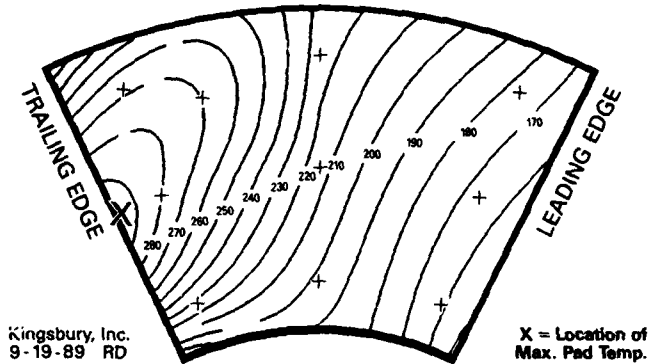


Figure 3. 10-1/2" 6-Shoe Thrust Bearing Pad Isotherms
Standard Bearing Fitted with Ultrasonic Probes

The temperature at a given point in the bearing also varies significantly for different operating conditions (See Figure No. 4).

An effective way to compensate for the broad temperature variations in the pad surface is to make the transducer so that it has its own temperature compensation capabilities. To do this a reference point has been located below the surface of the transducer. This reference point reflects the ultrasonic signal back to the piezoelectric crystal in the same way the ultrasonic signal is reflected from the surface of the transducer. Since the reference point is below the surface of the transducer its location is not effected by wear but the reference point is at a temperature

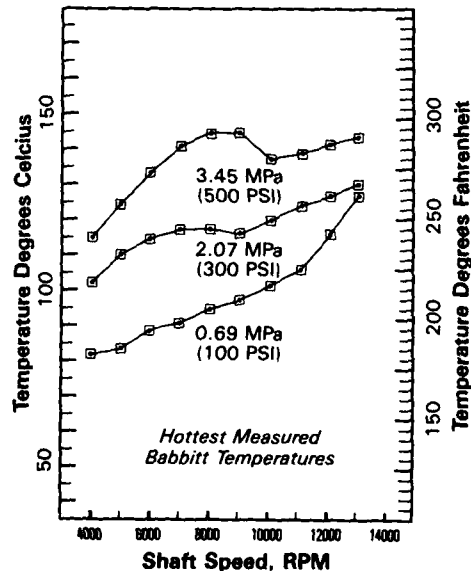
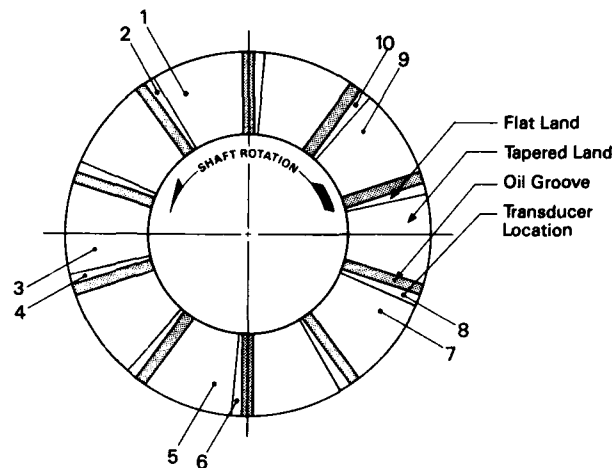


Figure 4. Hottest Babbitt Temperatures at the 75% / 75% Point of a 10.5 Inch Diameter Thrust Bearing

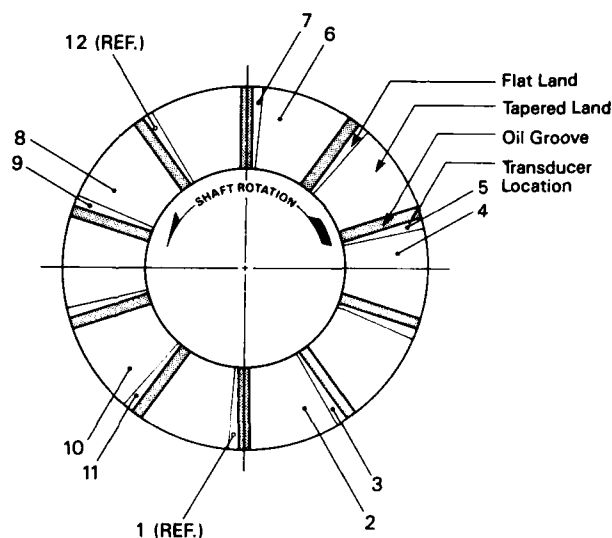
that is close to the that of the surface of the bearing. Any change in the measured position of the reference point would be due to temperature variations in the bearing. A reading is taken at the reference point with the system instrumentation, the instrument is then adjusted to match a baseline reading taken for the reference point. This adjustment calibrates the instrument for accurate measurement of the end of the transducer. Any change in the reading at the end of the transducer will then be due to wear in the transducer and correspondingly the bearing. Testing of this system in tilting pad bearings, described in the next section, indicates that measurement consistency achieved with self-referencing transducers are in the 0.00004 inch range.

Another way to compensate for temperature changes is to install a reference transducer in a bearing in such a way so that it never sees wear (See Figure No. 5). In a bearing that has relatively small temperature variations the readings from a transducer that is known not to be wearing effectively serves as a temperature reference point for the other transducers in the bearing.

The use of reference transducers reduces reading variations considerably. Figure No. 6 shows a series of readings from the transducer showing the most wear in an installation in the thrust bearing of a 250MW steam turbine at the Cleveland



NO REFERENCE TRANSDUCERS
Eastlake Unit No. 4
Turbine Side-Active Thrust Bearing



WITH REFERENCE TRANSDUCERS
Eddystone Unit No. 2
Generator Side-Active Thrust Bearing

Figure 5. Bearing Face after Restoration showing Transducer Locations

Electric Eastlake No. 4 Unit. In this installation there are no temperature reference transducers or self referencing transducers.

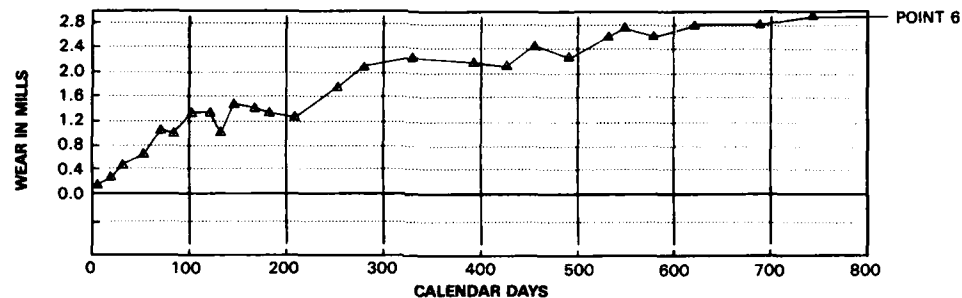


Figure 6.

NO REFERENCE TRANSDUCER
Eastlake Unit No. 4 • Turbine Side-Active Thrust Bearing

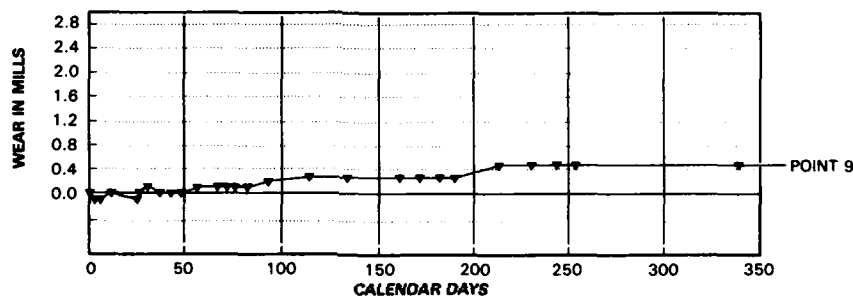


Figure 7.

WITH REFERENCE TRANSDUCER
Eddystone Unit No. 2 • Generator Side-Active Thrust Bearing

The readings stay within a $\pm .2$ mil accuracy but due primarily to temperature shifts in the bearing they tend to wander within that accuracy.

Figure No. 7 shows a series of readings from one transducer installed in the active thrust bearing of a 350MW steam turbine at the Philadelphia Electric Company Eddystone No. 2 Unit. The system was installed as part of the work supported by the EPRI On-Line Diagnostic Monitoring Center.

Two reference transducers have been installed in no-wear orientations in this bearing (See Figure No. 5). Although little wear is indicated in the first year of operation of the bearing, the data in Figure No. 7 reveals that the bearing temperature differences have been compensated for with the reference transducers and the wear is measured as a smooth progression instead of showing relatively dramatic jumps due to temperature.

System Test to Verify Accuracy: Shop tests to check the ability of the transducers to accurately measure the material lost from their surface were conducted. To simulate bearing wear, material was moved from the ends of transducers via a milling machine. The amount removed was measured with the ultrasonic transducer and

then a dial micrometer. The results are shown in Figure No. 8. The instrument used for this test was calibrated for solid bronze transducers. The system readings for the bronze transducers correlated closely with the micrometer readings. The babbitt tipped transducer readings vary from the micrometer readings by a linear value because the speed of sound in babbitt is slightly different than the speed of sound in bronze.

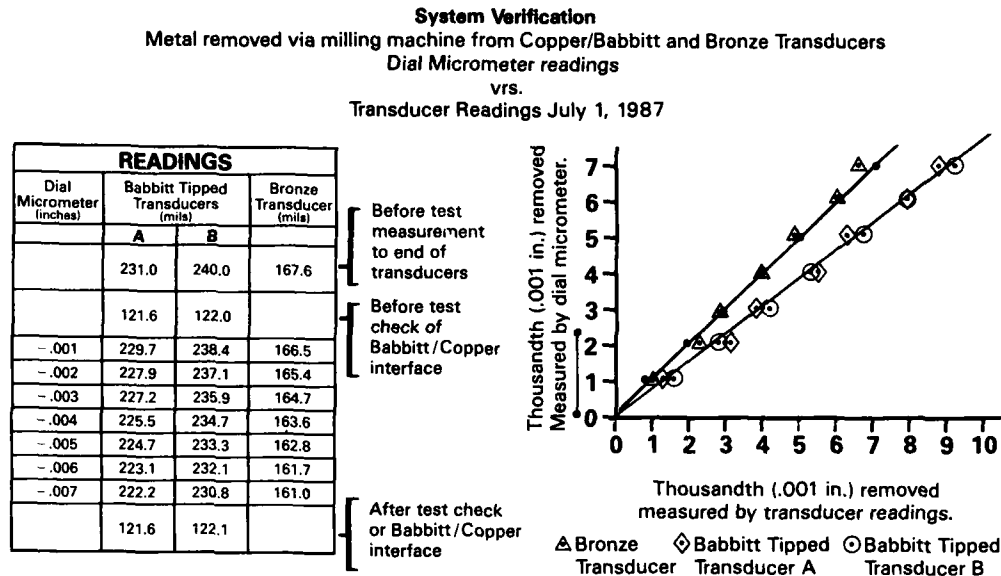


Figure 8. Accuracy Test Data

Testing of Self Referencing Transducers on Tilting Pad Thrust Bearings: A series of tests have been conducted at the Kingsbury, Inc. Test Facility in Philadelphia, Pennsylvania.

The purpose of these tests was to determine the ability of the ultrasonic on-line bearing condition monitoring system to function on a tilting pad thrust bearing through wide variations of speed, temperature and load.

The test bearing was a 10-1/2 inch double thrust bearing consisting of active and inactive elements (See Figure No. 9). The bearing surface of each side consisted of six pads with a babbitt OD of 10.5 inches (267mm) and a bore of 5.25 inches (133mm) having a total bearing area of 55.1 square inches (356 sqcm). Three of the active pads were modified for the installation of the ultrasonic transducers. The other three pads were heavily instrumented with thermocouples (ten thermocouples per pad).

The placement of any bearing instrumentation must be carefully considered. Based on previous testing, it was decided to locate the transducers in the 75/75 location (75% from the leading edge and 75% up from the inner radius). This is the region of the bearing surface that will be exposed to the highest combinations of pressure and temperature. Because of this pressure-temperature combination, this area of the bearing has the highest risk of bearing distress (See Figure No. 10).

An additional transducer was installed at the 25/75 position to check the accuracy of the self-referencing transducer under various temperature conditions.

The bearing was lubricated by a pressurized supply to create a flooded condition. The bearing was fed a specified volume of oil to an annular channel surrounding the bearing at the back end of the assembly. The oil then flows radially inward and axially between the bearing and rotating shaft until it reaches the working babbitt surface.

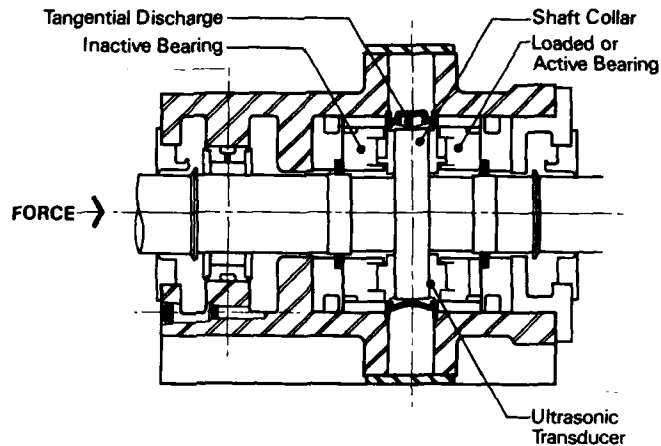


Figure 9. Test Tilting Pad Thrust Bearing

The main drive for the test bearings is an 1100 hp gas turbine engine capable of speeds from 2000 rpm to 14,000 rpm. The load to the bearings is applied with a hydraulic cylinder. Test data is stored in a data acquisition system then transferred onto computer disks. This provides immediate access to all test information for accurate data reduction and comparison.

The applied loads for the initial test in February 1989 were 0 psi to 500 psi in increments of 100 psi, at speeds of 4000, 8000, and 12,000 rpm. A second test was conducted in April 1989 to confirm the transducer system accuracy and repeatability. The transducer equipped pads were removed from the test stand between the two tests. The second test was run at 4000 to 13,000 rpm in increments of 1000 rpm. The loads were again 0 psi to 500 psi in 100 psi increments for each speed.

Prior to the first running test, a static test was conducted. In this test the pads were lapped to remove a small amount of babbitt from the bearing surface. Before lapping, the pad heights were measured with gages capable of detecting variations in the shoe pads to within an accuracy of $\pm .0001$ inches. The amount of babbitt being removed by the lapping operation was continually monitored by the ultrasonic measurement instrument until a total of .001 inches was removed. The pads were again measured with the gages to verify the surface removal reported by the ultrasonic measurement system. The results agreed for both measurement systems.

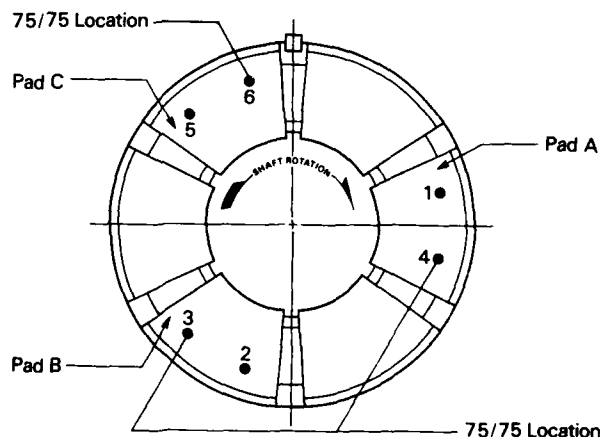


Figure 10. Locations of Ultrasonic Transducers in the Tilting Pad Thrust Test Bearing

During the testing, the transducers were exposed to a wide range of temperatures. Thermocouples embedded in the babbitt of the test bearing indicated variations at the 75/75 location from 160°F at low speed and load to over 280°F at the higher speed and load combinations (See Figure No. 4). In addition, during operation each shoe sees substantial thermal gradients across the bearing surface. Figure No. 3 represents a typical bearing surface temperature map during operation.

As expected, throughout the running tests of the active bearing with the ultrasonic transducers, it was necessary to adjust the reference reading of the electronic measurement instrument. With every increase in load on the active bearing there was a corresponding increase in temperature and pressure on the bearing surface causing the reference reading to change. The self-referencing capabilities of the transducers provide a fixed reference to allow an adjustment of the instrument to its original setting. The results of all the compiled data consistently indicated that there was no apparent wear during the tests. The transducer readings were within a few one hundred thousandths of an inch through all the loads and speeds. Figure No. 11 shows the transducer readings (in mils) indicated by the transducers in the April tests.

Inspection of the pads after both tests confirmed that there was no wear on the pads. In both running tests, transducers with self-referencing capabilities were able to compensate for extreme temperature variations created by changes of loads and speeds.

	PAD A				PAD B				PAD C				
TRANSDUCER	#1		#4		#2		#3		#5		#6		
	REF	SURF	REF	SURF	REF	SURF	REF	SURF	REF	SURF	REF	SURF	PSI
	129.87	175.83	128.65	174.62	136.60	178.43	120.41	164.47	127.10	173.78	126.76	175.15	0
	129.88	175.85	128.65	174.54	136.59	178.34	120.40	164.42	127.10	173.71	126.77	175.13	100
	129.89	175.84	128.65	174.59	136.59	178.36	120.40	164.44	127.10	173.71	126.78	175.14	200
	129.88	175.86	128.64	174.61	136.59	178.39	120.39	164.34	127.10	173.70	126.79	175.17	300
	129.88	175.85	128.64	174.62	136.58	178.38	120.38	164.36	127.10	173.72	126.79	175.19	400
	129.88	175.85	128.65	174.61	136.58	178.38	120.38	164.40	127.11	173.73	126.79	175.18	500

Note: All Measurements in Mils

Figure 11. Tilting Pad Thrust Bearing Transducer Measurements taken at 11,000 RPM

Naval Applications for Ultrasonic Wear Transducers: Fluid film bearings are used extensively on every ship in the U.S. Navy. In the propulsion system alone, fluid film thrust and journal bearings are used in the turbines, reduction gearboxes, and line shafting. Fluid film bearings are also used in the primary and stand-by power generation equipment as well as auxiliaries such as pumps and blowers. In each case, the bearing selection was based on the reliability and long life provided by fluid film bearings.

This inspection method is limited three ways:

- 1) It does not alert the machinery operator to any problems that occur between routine inspections.
- 2) It can only be performed while the shaft is secured.
- 3) Any indication of a problem still requires complete disassembly and inspection of the bearing components.

The use of ultrasonic transducers as shown in Figure No. 14 would provide an immediate indication of a problem and save both the labor and downtime associated with routine inspections.

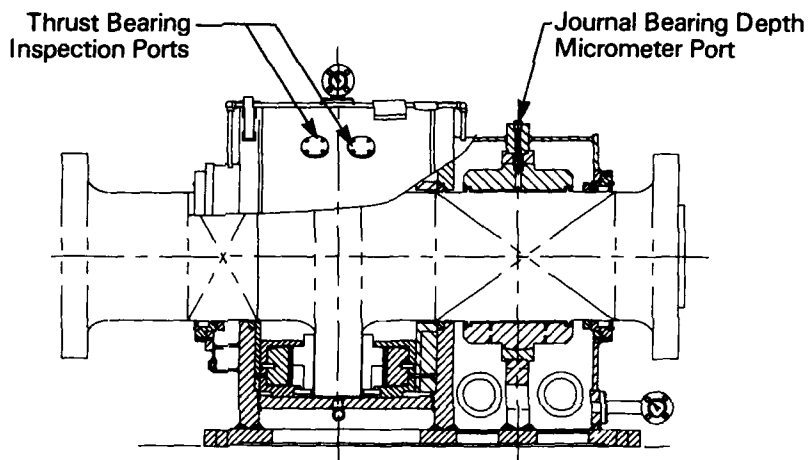


Figure 13. Existing Construction

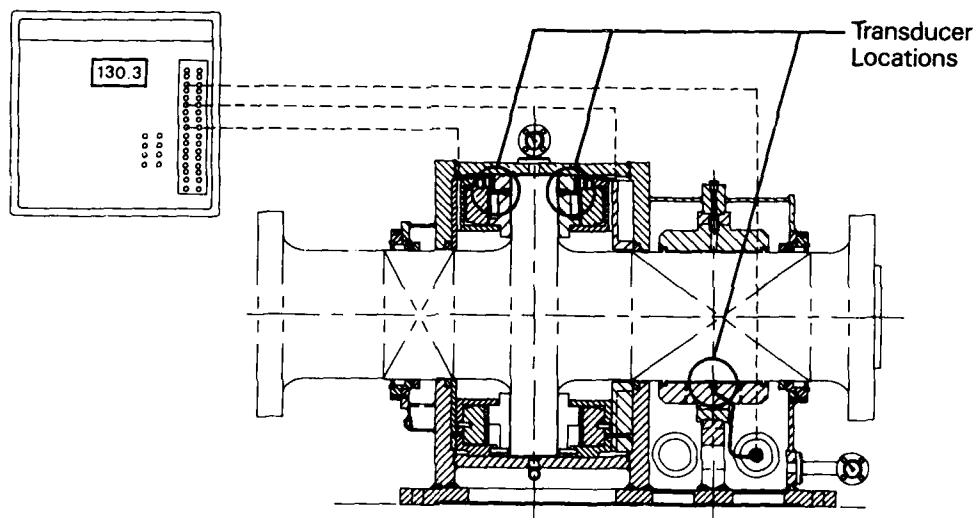


Figure 14. Ultrasonic Transducer Installation

Part of the routine maintenance for this equipment is inspection of the bearings for wear. As discussed in the introduction of this paper, wear occurs when one or more of the original design constraints have been exceeded. This can be caused by misalignment, overload, insufficient or contaminated lube oil supply, or improper cooling of the oil. In most cases, the original cause of bearing wear can never be determined. This is due to the fact that the wear will not even be noticed until the next scheduled inspection, provided there is not a catastrophic failure in the meantime.

The procedure for inspecting bearings for wear varies depending upon the equipment. Many specifications like MIL-T-17600D for line shaft bearings, require provisions to measure the static shaft position without removing the bearing cap. More complex equipment, such as main propulsion thrust bearings or reduction gearbox bearings still require disassembly to inspect the bearings.

Installation of ultrasonic transducers in any of these bearings would provide a continuous on-line indication of bearing condition.

Ultrasonic Transducers for Line Shaft Bearings: Figure No. 12 shows a schematic representation of the 18 line shaft bearings used on the Nimitz Class aircraft carriers. Each of these bearings has a provision to measure shaft position to approximate bearing wear. As shown, the bearings are distributed throughout the aft section of the hull. As there is no access from compartment to compartment in the shaft alleys, it is necessary to climb 3 or 4 deck levels in order to travel from bearing to bearing. Not only is this time consuming, but wear measurements can still only be accomplished while the shaft is not turning. Installation of ultrasonic transducers would provide continuous readings for all of the bearings at one location.

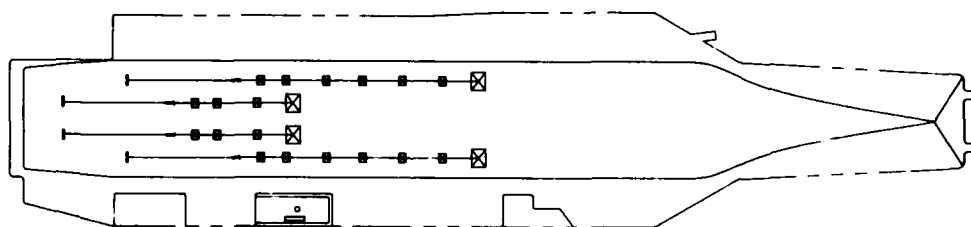


Figure 12. Line Shaft Bearing Layout Nimitz Class Aircraft Carrier CVN 68 Shown

Ultrasonic Transducers for Main Propulsion Thrust Bearings: Figure No. 13 shows a cross section of the main propulsion thrust bearing for the DDG-51 Class destroyer. Bath Iron Works Specification #450-244-05A required the depth micrometer provision shown to measure journal wear. There are two inspection ports that allow visual inspection of the leading edge of one shoe, the trailing edge of the adjacent shoe and the thrust collar surface between the shoes on both the forward and astern thrust bearings.

Summary: This new innovative monitoring technology can provide the crew of a Navy ship with more on-line bearing information than previously possible. This is accomplished thru direct, continuous, accurate measurement of material loss from the bearing surface rather than monitoring some other phenomenon of bearing distress. This additional information can eliminate second guessing instrumentation and/or unnecessary machinery tear downs.

Continuous tracking of bearing wear can provide valuable insight into a machine's response to varying duty cycles. It may be possible to change certain operating procedures to eliminate or at least minimize conditions that cause bearing wear. In this manner the period between required bearing replacement may be extended.

Precise wear information can alert the machine operator to pending problems, even small changes on the rate of wear can now be measured over the life of a bearing and trended.

This information can be used to predict when bearing replacement will be necessary so that required maintenance can be scheduled before the point of unsafe equipment operation is reached. The use of ultrasonic wear indication can reduce costly unscheduled downtime as well major equipment failures.

Acknowledgments: The development and application of the TecSonics technology is the result of a team effort. Significant contributions to this effort have been added by:

Dr. Dov Hazony - Case Western Reserve University
Wayne Tuttle - J. W. Harley Inc.
Bill Verwey - J. W. Harley Inc.
Jack Harley - TecSonics Inc.
Steve DeCrow - Renewal Parts Maintenance Inc.
Steve Trager - Centerior Energy
John McElroy - Philadelphia Electric Company
Rich Colsher - EPRI

References:

- (1) Haramis, G.T. et al., "On-Line Bearing Condition Monitoring With Ultrasonic Transducers", Plant Maintenance Technology Conference, Houston, Texas, November 14-16, 1989.
- (2) Haramis, G.T. et al., "Ultrasonic On-Line Bearing Condition Monitoring Technology", International Machinery Monitoring and Diagnostic Conference, Las Vegas, Nevada, September 11-14, 1989.
- (3) Karberg, W.E. et al., "On-Line Bearing Monitor Technology", ASME Pumping Machinery Symposium, 3rd Joint ASCE/ASME Mechanical Conference, San Diego, California, July 10 - 12, 1989.
- (4) Harley, J.W. et al., "Diagnostic Method for Bearing Wear Detection", Symposium Proceedings: Power Plant Pumps, EPRI CS-5857, Project 1884-25, Proceedings June 1988, pages 3-23 thru 3-33
- (5) Missana, A. et al., "Performance Of Tapered Land Thrust Bearings For Large Steam Turbines", ASLE Transactions, Vol. 14, No. 4, October 1971, pages 301 thru 306

CONDITION BASED MAINTENANCE FOR SHIPBOARD MACHINERY

G. William Nickerson
David Taylor Research Center
Annapolis, Maryland 21402

Abstract: The David Taylor Research Center under the sponsorship of the Office of Naval Technology Logistics Block has undertaken a program to develop condition based maintenance (CBM) technologies for shipboard machinery. The specifics of our program to date are discussed in another paper at this conference by Nemarich, Boblitt, and Harrell. This paper focuses on the issues of why condition based maintenance is needed and on the characteristics necessary to make the system viable. The content of this technology is described. Known DoD initiatives that this development supports are outlined. The benefits and the drivers to develop this technology at this time are described. The pitfalls that must be avoided to field a viable system are outlined. The philosophy of the program we have undertaken in this area is described. Finally, a vision of a shipboard integrated CBM system is described in a narrative description of a scene aboard a ship in 2015.

Key Words: Computer aided acquisition and logistic support; concurrent engineering; condition based maintenance; information management systems; mechanical diagnostics; mechanical prognostics; mechanical testability; reliability centered maintenance; system engineering; system integration

Introduction: Mechanical system condition based maintenance (CBM) encompasses a broad range of disciplines and components. Monitoring systems must be in place to measure parameters of interest. Algorithms must be available to convert the data obtained from the monitoring system into information about the indicated state of that machine relative to its design performance. Different algorithms must be available to diagnose machinery problems based upon deviation of measured state from the design condition. Processing power must be available to perform the necessary calculations. Forecasting methodologies must be in place to predict the future state of the machine based on its present state and to recommend maintenance actions or operational constraints to prevent consequential failures.

Implementation of a system of this type on a vehicle such as a naval ship could easily result in a monitoring system that costs more than the system being monitored. Thus, trades must be made in the conceptual phase to determine which systems, subsystems, and components warrant inclusion in such a system and which parameters in a particular equipment should be monitored. These trades must be made at the earliest stages of a

system's development and only those systems and parameters that meet predefined criteria should be included.

Previous efforts to implement monitoring systems and diagnostic systems on existing equipments have often been less than satisfactory. A primary reason for the problems with these monitoring and diagnostic systems can be attributed to limited testability in the original design of the equipment. Testability has not been given adequate attention at the early stages of system development. Attempts to add testability on after a machine has been designed (and built) will be unsatisfactory and expensive. Future mechanical systems must be developed in an environment where testability is considered at the beginning of the development process.

Achievement of the maximum benefit requires an integrated shipboard system. This entails efficient use of monitoring, data transmission, display, and control resources. Other programs are working to develop a shipboard data bus and other elements of the system. Among these programs are the Machinery Monitoring and Control System (MM&CS) and Damage Control Monitoring System (DCMS) programs. Coordination among all of these programs is critical and will be achieved.

Relation to DoD Initiatives: The Computer Aided Acquisition and Logistic Support (CALS) initiative provides an umbrella under which several other initiatives related to CBM may be included. The Office of the Secretary of Defense, through the National Security Industrial Association Task 86-1, has developed Mechanical System Condition Monitoring Design Guidelines. They address the mechanical testability and diagnostic technology base aspects of CBM. A draft of these guidelines is now being reviewed by industry and government prior to release in the near future.

Concurrent Engineering is a change in the culture of system development whose time has come. No longer can we afford to develop systems in a sequential manner where the "ilities", including testability, are appended at the end of the design process. They must be considered a performance attribute of the system and be given attention equal to the traditional performance attributes (i.e., weight, volume, efficiency, ...) in the initial stages of the design. The computer aided design tools either exist or can be developed now to allow us to effectively implement the Concurrent Engineering philosophy.

Reliability Centered Maintenance (RCM) provides a framework in which we can trade-off the cost of maintenance and monitoring against the benefits accrued. In the RCM concept, maintenance decisions (and in this case monitoring decisions) are based on an analysis of the consequences of failure, the cost of maintenance actions to prevent (or of the monitoring system to detect) the failure, and the ability of maintenance action to prevent (or of the monitoring system to predict) the failure. These trade-offs must be made as a part of the system development and the indicated actions taken at the earliest stages of design. If not, machinery diagnostics will not be a part of the solution but rather an additional problem.

Benefits of Condition Based Maintenance: The additional cost of providing monitoring and diagnostic capability must be offset by greater benefits to the customer. A few benefits which can be realized if these concepts are effectively implemented on a naval shipboard system are outlined below.

Manning levels of naval ships have obvious acquisition and operating cost implications. People aboard ship must be provided with berthing and living space. This translates to increased ship size and cost. The Ship Operational Characteristics Study (SOCS) found that condition based maintenance on surface combatants could result in a 12% reduction in required manning. The same study also found that CBM could allow a 15% increase in the ship volume available for the combat system.

If future mission requirements are to be met at reduced force levels and in a severely resource constrained environment the operational availability (Ao) of our systems must be improved. Ao is a function of Mean Time Between Failure (MTBF), Mean Time to Repair (MTTR), and Mean Logistic Delay Time (MLDT). CBM can effect Ao by reducing the MLDT and by increasing the effective MTBF.

When a component fails in service, the maintainer must diagnose the problem, identify the solution, order the parts, and make the repair. If the maintainer made an accurate diagnosis and ordered the correct parts, the repair will be completed in the time originally planned. If, however, the problem is misdiagnosed and the wrong parts ordered, the correct parts must be reordered. The down time is extended by the MLDT again. Thus, misdiagnosis of failed equipment results in failure of demonstrated Ao to meet design Ao. A good CBM system can improve the accuracy of diagnosis.

The most significant component of the Ao equation is MTBF. While monitoring cannot of itself improve MTBF, CBM can enhance MTBF in several ways. It can enable failures to be "designed out" of the system, it can reduce the consequential damage of failure, and it can extend the useful life of a damaged machine. Each of these are explained further.

If the diagnostics are **embedded** in the design phase, they can be used to isolate problems before the system is built. The indicated design improvements may be incorporated into the design to eliminate that problem. The MTBF of the fielded system will be increased.

In a fielded system, an effective CBM system will detect impending failure of a machine before failure occurs. This prevents consequential damage and resultant failure propagation. The CBM system should also recommend an alternative operational procedure that will allow the machine to operate at some reduced capacity for a longer time. An example would be to put the failing machine in the lag position of a lead/lag system. The failing machine thus remains available and the effective MTBF of the system is increased. Parts can then be ordered in advance of failure and maintenance actions can be scheduled for a convenient time to repair.

A perhaps more important benefit of a CBM system as described is the ability to provide the Commanding Officer (CO) with near-real-time readiness assessment of his ship system. The CBM system must be properly integrated with the machinery monitoring and control system and the damage control monitoring system in an architecture that provides distributed access to the information contained in the three systems. The CO will be able to assess the material condition of his system, make operational decisions based on improved information, and make optimal use of maintenance resources. Such a system is described later.

Why the time has come for CBM: Many technological advances and real world conditions have come together to make the CBM concept more attractive than in the recent past. Demographics, computer & communication technology explosion, increasing complexity of equipment to meet more rigorous operational requirements, and budget constraints have all conspired to make this concept attractive. These conditions are recognized by the DoD and USN and reflected in recent initiatives and directives. These drivers will be discussed further.

Demographics will make recruitment and retention of quality people more difficult. In the 1980's the number of 18-24 year olds decreased while the size of the labor pool increased. The trend will continue through the turn of the century. These are not projections -they are fact. All the 18 year olds that can be born in this century are already born! This maturing of the workforce will have profound effects on our society. In particular, while the numbers of people are certainly sufficient to meet the needs of the military, competition with the private sector for the best of them will intensify. Thus, it is important to invest in technologies like CBM that can relieve the need for increasing manning.

Computer and communications technologies continue an exponential growth in their cost effectiveness. This enables us to cost effectively introduce systems which even relatively recently would not have been possible. These technologies are key to implementation of a CBM system.

Complexity and sophistication of the equipment we install on our ships is increasing to meet ever higher performance requirements. This condition acts in direct opposition to our problems in attracting and retaining quality people. One goal of the CBM system is to embed training and data interpretation to such a degree that the diagnostic process becomes "technician transparent". Specialists will be required less (or not at all) and any maintainer will be able to quickly diagnose problems with any equipment.

All of these forces are driving the military at a time when budget constraints are becoming increasingly stringent.

Several studies have pointed to the value of this concept. The revolution at sea SOCS study identified the need for and benefits of condition based maintenance. That study identified CBM as an "imperative characteristic" of the 21st century combatant. A

Naval Research Advisory Council summer study on automation in 1988 outlined a Distributed Integrated Ship Control system including CBM, DCMS, and MM&CS functions and identified the benefits resulting from it.

The time to develop CBM is now.

Characteristics of a Viable System: There are many opportunities in implementation of these kinds of information management systems to exacerbate the present situation. System engineering is the key to making an effectively integrated solution. History has many examples where systems like this were fielded with disappointing results. Avoiding some of the most obvious pitfalls will increase the likelihood of success.

- Sensor proliferation: The CBM system must not result in uncontrolled growth of the installed sensor suite. Studies like RCM must be conducted to ensure that conscious decisions are made to include only those sensors which can be justified.

- Sensor calibration: We must not reduce equipment maintenance worktime by adding sensor maintenance workload. The sensors used in the system must be robust. They must be stable, reliable, inexpensive, and rugged to survive the shipboard environment. Features like self calibration are critical.

- Affordability: The ship system affordability must not be compromised inclusion of CBM. Thus, the minimum number of sensors must be employed and the cost of those sensors must be reduced. Further, testability of the equipments must be "designed in" so that most effective use of valuable sensor resources may be made.

- User confidence: The ship operators must have an extremely high degree of confidence in the information provided by this system. Without confidence, the problem is made worse - we've just added another system that must be bought and maintained without gaining any operational advantage. The required level of user confidence can only be achieved through systematic implementation. The details of this approach will be discussed further.

Integrated System: The CBM system described must be seamlessly integrated into the ship information management system. Future ships will have installed data bus resources and distributed control capability. The totality of shipboard information should be available on this bus. Specifically in the Hull, Mechanical, and Electrical (HM&E) area three information management systems are involved:

- Machinery monitoring and control system provides near real time machinery plant control and realignment in the event of changes in operational needs or in response to casualty.

- Damage control monitoring system provides readiness information about the ship and its systems allowing the operator to take action to mitigate damage from casu-

alty.

- Condition based maintenance system will allow the operator to efficiently manage the availability of his plant and allocation of maintenance resources in response to the effects of system degradation and failures.

These three systems need much of the same information. For example, it matters little whether the reason a particular piece of equipment is unavailable when needed is because of a material failure or a result of casualty. Thus the same information is necessary for both the DCMS and CBM system and the same sensors should be used.

Given that these integrated systems share a common databus, the finite capacity of that bus must be recognized so that data will not exceed its capacity. Thus, reasoned decisions must be made at the conceptual phase as to the level of distributed processing to be employed. Information, not data, should be placed on the bus. Some reasonable level of local processing must be employed.

Finally, the system must be "user friendly." Shipboard operators, at all levels from Commanding Officer to the machinery maintainer, will be presented with an ever increasing information load. This system must incorporate human engineering from the outset to ensure that the man/machine interface is elegant enough to enable the man to quickly and efficiently process the information he needs to make correct decisions and efficiently perform the task at hand.

Development of the concept described requires a coordinated effort. The philosophy must be an evolutionary development of a revolutionary concept. The technologies should be applied to individual equipments on existing and near term ships. The concurrent longer term maturing of the system will enable implementation on far term ships to realize the full potential.

DTRC/ONT Program: The program presently underway at DTRC is funded by the Navy Logistics Exploratory Development Block Program. It started in January 1989. The effort to date is described fully in another paper by Nemarich, Boblitt, and Harrell presented at this conference. I will describe some of the underlying philosophy of the program.

The initial focus of the effort was to implement a monitoring system on real navy equipment in the shortest possible time. We chose an oil lubricated high pressure air compressor (HPAC). This selection was driven by two main criteria. First, the equipment was already installed at DTRC and could be made available without a significant capital investment. Second, the HPAC is a known maintenance problem. Much maintenance and reliability data are available and any success that allows improvement to the HPAC will be valuable.

It should be noted, however, that it is not the goal of the present program to develop a

monitoring or CBM system for the HPAC. Our purposes are to develop and maintain a system on which we can demonstrate capabilities of various CBM technologies, concepts, and components.

Another important aspect of our work is that our initial focus is on parameters other than vibration. We recognize that vibration is an important parameter for assessing the health of a mechanical system and that much information is available in the vibration signal. But, for two reasons, our focus was primarily on process parameters. First, we used mainly the parameters already sensed on the system so we did not need to install additional measurement points on the system. Second, most work in the area of mechanical system condition monitoring to date has concentrated on vibration as the main signal of interest. Important machine condition information is be more directly available from analysis of the system process parameters. The intention is to incorporate vibration technology later.

I described above the need to establish confidence in a system such as this through an evolutionary approach. The technology should be installed incrementally on existing equipments and ships. If this is the only approach taken, an effectively integrated system will be impossible to achieve. Thus, the integrated system must be developed offline in parallel with the equipment specific technologies.

The program at DTRC will maintain its focus on the far term integrated whole ship system developing the technologies necessary to reach that goal. Along the way, however, specific solutions that could be implemented with some reasonable engineering development are expected. These solutions will transition to machinery development programs and be implemented in the fleet using processes such as the MACHALT program.

The Future: The following is a narrative description of a scene that might happen on a future ship that incorporates all of the concepts described. The scenario is quite "blue-sky" but is achievable if the commitment is made today.

It is the spring of 2015. The Battle Force Combatant USS BLUESKY (BFC 27) is operating in the Caribbean on an ASW training exercise with the Russian Submarine GREEN NOVEMBER.

The CO approaches one of many terminals on the ship. It may be in his stateroom, the Engineering Log Room, the Bridge, CIC, or the Quarterdeck - it doesn't matter, the terminals are all the same.

He identifies himself to the terminal by voice and the computer responds by showing him a graphical display of his ship and its mission areas. All parts of the ship and mission areas are Green, all is well. As he looks at the screen, the ASW mission area indicator goes from green to yellow and at the same time an area in the forward end of the ship goes from green to yellow.

This indicates that his ASW mission capability is being compromised by something located in the forward end of the ship.

He touches the yellow area of the ASW mission area indicator and is shown a graphical display of all of the equipments necessary to that mission area. He notes that all elements are green except for the sonar equipment room.

He touches the yellow indicator on the sonar equipment room and is shown a graphical display of the equipment in that room. All of the elements are green except for one seawater cooling pump.

He touches the yellow indicator on the seawater cooling pump and receives a report that the shaft bearing on the number 2 cooling pump is beginning to fail. He is told that under the current operating conditions, the pump will fail in 6 hours and is given a recommendation that the seawater cooling system alignment be changed from "Pump 2 lead" to "Pump 1 lead" to extend the expected life of the pump from 6 to 48 hours. He knows that this will allow him to complete his training exercise so he touches an ACCEPT button on the screen to execute the recommendation and acknowledge the situation. The MM&CS system then realigns the system to place pump #1 in the lead position.

Meanwhile, the Chief Engineer (CHENG) is in the log room. He is "logged in" to the terminal there and is looking at his top level display of the machinery plant. He notices that all main machinery systems (propulsion, electrical, and auxiliary) are green. While he is looking at it, the Auxiliary System turns yellow. He touches the yellow area.

He is shown a display of all subsystems in the Auxiliary system. All are green except the Seawater Cooling system. He touches the seawater cooling system.

He is shown a mimic of the seawater cooling system. All elements are green except for the #2 Seawater Cooling Pump in the Sonar Equipment room. He touches that area of the screen.

He is shown the same diagnostic screen that the CO is looking at. While he is looking at it he notices that the CO is also looking at it and makes the decision to realign the system to extend the pumps predicted life past the end of the current exercise. He breathes a sigh of relief.

He acknowledges the situation and is shown a recommendation for a repair action. The parts necessary to repair the impending failure are displayed and the manpower necessary to effect the repair. It will take 3 man-hours of a machinist mate to complete the repair. He presses the stock query button.

He is shown that all of the parts necessary for the repair are available on the ship except

for the main grease seal. It is available in Norfolk Supply Center and can be to him in 27 hours. He presses the button to order the part. He presses the manpower availability button.

He is shown a graph of the loading of his maintainers capable of performing the repair. He notes that all are fully scheduled for the next three days. He does not want to allow the pump to fail so he looks at the loading of his best machinist mate. He notes that he is scheduled for a three hour training session on lube oil pump overhaul tomorrow afternoon. This timing is not critical since the training is computer based and available at any time.

He reschedules the machinist mate to perform the repair action tomorrow afternoon knowing that the parts will be available, the present training exercise will be over, and he will be able to have the pump repaired by 1700 tomorrow. He acknowledges this plan and returns to the top level machinery system screen confident that the impending problem is handled.

The CO meanwhile has gone back to his top level screen. He receives an indication that an information message is available for him. He presses the button to read it and is told that the CHENG has acknowledged the impending failure of the seawater pump, ordered the parts necessary to effect repair of it, scheduled manpower necessary to repair it, and that the system should be returned to fully operational status by 1700 tomorrow without a loss of his ability to perform his ASW mission.

Conclusions: The navy is being driven in the direction of this concept by forces outside its control. If we do not recognize these forces and respond with a systematic development program, we have little chance of meeting the requirements of the future.

The Condition Based Maintenance for Shipboard Machinery concept requires significant effort in the following areas:

- sensors
- machinery diagnostics
- forecasting technologies
- man/machine interface
- information system integration
- machinery testability

DTRC is committed to meeting the challenge.

**A CONDITION BASED
MAINTENANCE MONITORING SYSTEM FOR
NAVAL SHIPBOARD MACHINERY**

Christopher P. Nemarich
Wayne W. Boblitt
David W. Harrell

David Taylor Research Center
U.S. Navy
Annapolis, Maryland 21402

Abstract: A demonstration model of a Condition Based Maintenance (CBM) monitoring system has been developed and installed on a high pressure air compressor. The CBM model is a distributed, microprocessor-based system incorporating graphical man/machine interface, expert system and local area network software. The CBM model integrates commercially available hardware and software packages with software, sensors and monitoring techniques currently under development. The intent is to apply CBM broadly to naval shipboard machinery for fault detection, diagnosis and prognosis (DD&P). The knowledge gained by implementing increasingly sophisticated systems will be used to develop generic CBM guidelines for naval machinery and ship system designs. This report presents a detailed description of the CBM monitoring system and discusses design issues. This report also presents future development plans for CBM.

Key Words: Automated machine monitoring ; condition based maintenance; distributed monitoring expert system; fault detection; fault diagnosis; machine health; process control; prognosis; shipboard machinery

Introduction: One of the roles of the David Taylor Research Center (DTRC) is to conduct research and development in the area of naval shipboard propulsion and auxiliary systems. DTRC also develops sensors and controls for these systems. Because of this expertise, the Logistics Block Program manager tasked the Center to create a technology push in the area of Condition Based Maintenance (CBM) monitoring. The expected benefits of CBM are improved maintenance procedures and scheduling, increased machinery operational readiness, and reduced logistics support cost.

As part of this effort, DTRC has developed a demonstration model of a CBM monitoring system. This demonstration model integrates commercially available hardware and software with developing technologies. The model demonstrates machinery fault detection, diagnosis and prognosis (DD&P) capabilities as applied to naval shipboard systems. The demonstration model makes use of new sensor types, programmable logic control, and industrial process control hardware and software. The model also includes local area networking, graphical man/machine interface and diagnostic software. Expert system software and the results from research in machinery modeling will be used for DD&P.

The near term goals of this program are to successively develop CBM systems for

existing machineries and integrate them to form larger systems. The long range goal is to develop generic CBM guidelines for future machinery developments and naval ship system designs.

This paper discusses the CBM demonstration system and some issues involved with the design of naval shipboard monitoring systems.

Background: The United States Navy now uses the Planned Maintenance System (PMS) for the upkeep of shipboard system machinery. This involves the periodic overhauling of machinery on a scheduled basis. The operation and maintenance of propulsion and auxiliary systems has steadily become more difficult, costly and labor intensive with the increasing diversity and complexity of these systems. In this era of shrinking maintenance budgets and skilled labor pool, the current means of maintaining and operating Navy ships has come under attack.

Efforts are being made to reduce the number of scheduled overhauls through the periodic monitoring of shipboard machinery health and performance. Data obtained from periodic monitoring helps the ships' forces diagnose machinery problems, determine machinery wear condition, and reduce maintenance procedures. This approach, however, will not solve the Navy's operating and maintenance problems.

The solution is an integrated shipboard machinery monitoring and control system that includes CBM. The Condition Based Maintenance concept encompasses more than just periodic condition monitoring. CBM is an approach that incorporates all aspects of automated machinery failure detection, diagnosis and prognosis. It has been shown by a task group of the Advanced Testing Technology Committee [1] that applying CBM to shipboard hull, mechanical and electrical systems can produce the following benefits:

- | | |
|--|-----|
| • reduce maintenance induced failures | 50% |
| • reduce maintenance actions | 35% |
| • increase availability | 20% |
| • reduce inspection and repair hours | 20% |
| • reduce spare parts provisioning | 20% |
| • reduce good parts removal | 10% |
| • extend equipment life/overhaul cycle | 10% |

CBM can produce these benefits but it requires an effective resolution of the issues involved with automated shipboard monitoring. The Navy has determined that CBM is an "Imperative Characteristic" [2].

CBM System Concept: An established approach is to develop the top-down system concept identifying the pertinent design issues. Once this has been done, the system is implemented from the bottom-up [3]. This is the approach that DTRC is taking.

Some of the issues addressed in the design of the CBM system are the man machine interface, distributed versus centralized processing and data base management, design

flexibility and adaptability to shipboard environments.

The overall CBM shipboard system concept developed is shown in Figure 1. This system has four levels. Level 1 is the programmable logic controllers (PLC). The PLCs reside at the machinery and provide digital machine control and collect and digitize sensor data.

The industrialized PC/ATs at level 2 reside with the PLCs in the machinery spaces. They provide the operator at the graphical man/machine interface with machine control through the PLCs. The operator has access to all information, alarms and control necessary to the operation of their machinery space.

Level 3 is a supervisory level consisting of PC/AT type workstations. These workstations, located in the engineering spaces, contain the historical database for the ship machinery and provide a high level of access to ship engineering system data and control.

Level 4, the highest level, provides managerial access to each workstation and industrial PC/AT. This level consists of a central VAX/VMS system or equivalent. It performs ship wide data management and control and other tasks required of the ship's most senior officers. Other ship functions would tie into this level.

This is a general system concept. It addresses the issues of distributed control and database management and can be applied easily to a ship environment. It is flexible and is not limited to the technologies listed here. This is the framework from which the CBM system will evolve.

CBM Demonstration Model: A Worthington high pressure air compressor (HPAC) installed in the laboratory provides a means of effectively demonstrating CBM on an actual shipboard auxiliary. The HPAC is a motor-driven, oil-lubricated, water-cooled, four-cylinder air compressor. Because it is complex and has a variety of subsystems, the HPAC is ideally suited for demonstrating CBM.

The CBM demonstration model is shown in Figure 2. It consists of a pair of i386 PC/AT computers and a Gould 984 programmable logic controller with 32 channels of A/D. A commercially available process control software package by Intellution Inc. called FIX/DMACS (TM) is used for the system control, data management and display. It supports the communication with the PLC, the diagnosis and prognosis software, and the local area network (LAN) software.

The CBM model developed to date works as follows. Analog signals from the HPAC sensor suite are digitized by the A/D modules in the Gould 984 PLC. The HPAC is outfitted with the standard shipboard gages and controls augmented with easily added transducers for data acquisition purposes. In order to aid in the acceptance of the new displays and controls provided by CBM, it is installed alongside the original HPAC gages and meters which have not been removed. The PLC provides limited microprocessor capabilities for data messaging, buffering and control. It communicates with the industrial PC/AT through the IBM realtime coprocessor.

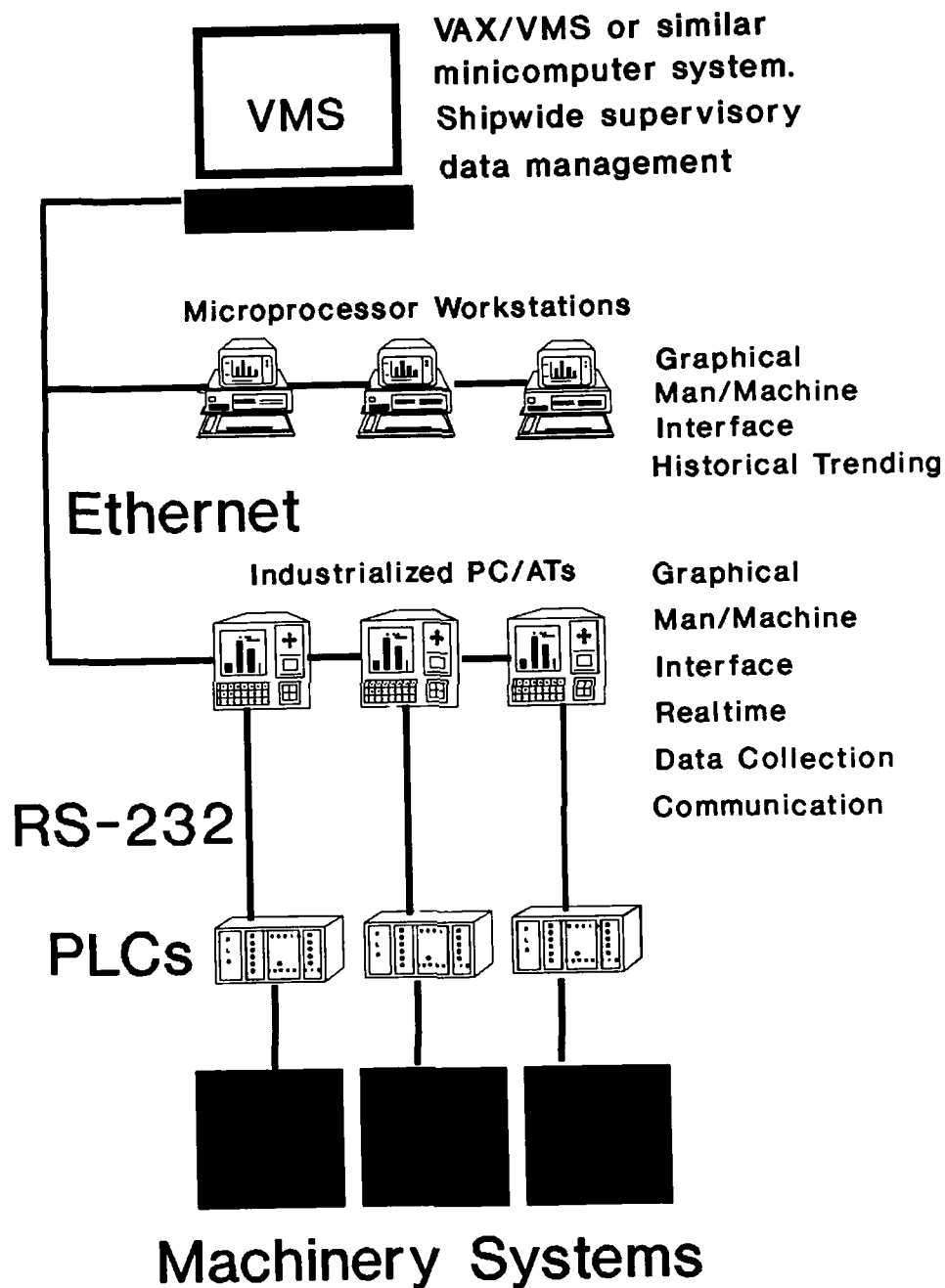


Figure 1 CBM System Concept

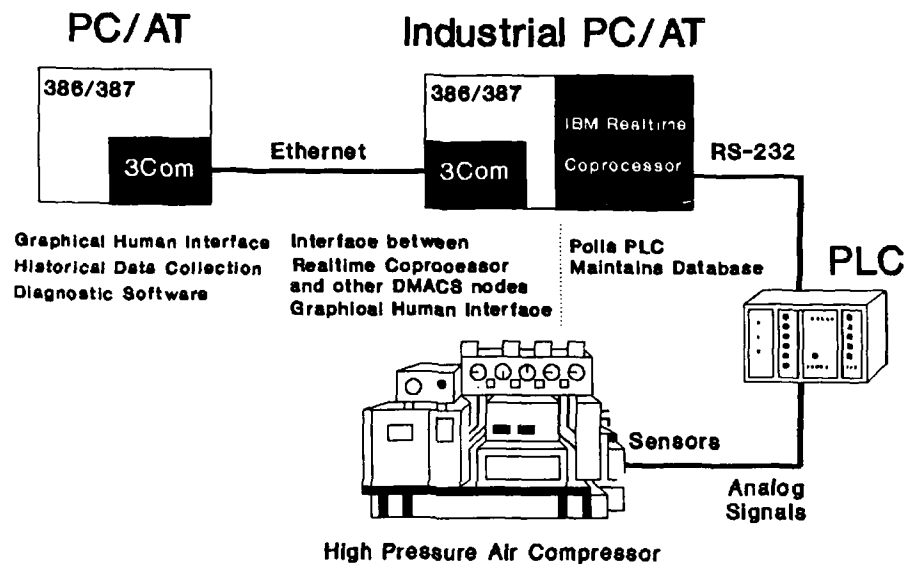


Figure 2 CBM Demonstration Model

The IBM realtime coprocessor is referred to as an Artic card. The Artic card, via its RS-232 serial port, reads the bank of memory addresses corresponding to the various transducer data channels. It comprises one of the three nodes in the CBM model. The realtime coprocessor executes the SCADA portion of FIX/DMACS software. SCADA is a mnemonic for Scan, Control, Alarm and Data Acquisition. The FIX/DMACS software is installed on both PC/ATs and provides communication between the PCs and the Artic card. This forms a three node FIX/DMACS system.

HPAC condition information is processed by FIX/DMACS and displayed on the EGA screen for the HPAC operator. This information is also available remotely at the workstation which is in another area of the building. The communication between the PC/AT at the HPAC and the remote workstation is via Ethernet and 3Com hardware.

The remote workstation maintains and stores the HPAC database and provides the operator with access to all information available to the machine operator. Messages can be passed between these nodes.

Ultimately, the workstation will also run a rule-based expert system for the detection, diagnosis and prognosis of HPAC faults. Failure prediction algorithms are being

developed for this. At the present time, only C-coded diagnostic rules run at this node.

Graphic man/machine Interface: A crucial portion of any automated monitoring system is the man/machine interface. The information flow from machine to man must be dealt with effectively to prevent information overload. Yet it must provide all the necessary data to the system operator. This is one of the central issue to the demonstration CBM system.

A variety of graphic display screens have been designed for CBM. Figures 3, 4, 5, and 6 show the major HPAC system screens. Figure 3 is the ANALOG DISPLAY screen. This screen is the main display and shows the HPAC operator information in an easy to read graphical format. At this screen, air temperatures and pressures for each stage of compression are displayed. The values are displayed relative to their respective alarm and warning states in a bar graph format. A digital screen, not shown, is also available which displays the values of these sensors in a numerical format. The digital screen shows all sensor data including the AC motor speed, current, voltage and power and rate of oil lubrication to the compression cylinders.

If any parameter exceeds either a warning or alarm threshold, the Machine Health box, located in the upper right corner of the display, changes color. Green is normal. Yellow is warning. Red is alarm. The operator can reach any major screen by selecting any of the large boxes at the bottom with the touch screen. The diagnostic box will change color to instruct the operator to go to the diagnostic screen to receive further instructions generated by the expert system.

The AIR SYSTEM screen is shown in Figure 4. This screen provides a mimic of the HPAC air system. The color of the boxes at each stage of compression represent the condition. Again, the operator can reach any other screen from here.

The OIL SYSTEM screen is shown in Figure 5. The HPAC oil system consists of a pump for distributing oil to main bearing and crank assembly and an auxiliary oil distribution system for cylinder lubrication. The concept of this screen is similar to the others. This screen, however, incorporates data from a unique fiber optic drop counter sensor. This sensor monitors the rate of drop lubrication to the HPAC cylinders from the auxiliary lube system.

The WATER SYSTEM screen, shown in Figure 6, displays cooling water inlet temperature and discharge temperature. The pressure at the condensate drain accumulator is also shown.

From the major screens, a graphical time history of a sensor value may be displayed. The user simply touches the screen element associated with that sensor. The data is displayed as in Figure 7.

Expert System Diagnosis: The CBM model is designed to use an expert system software package, NEXPERT (TM), to analyze sensor data and provide a diagnosis of HPAC faults. The intention is for the expert system to obtain sensor data from the SCADA

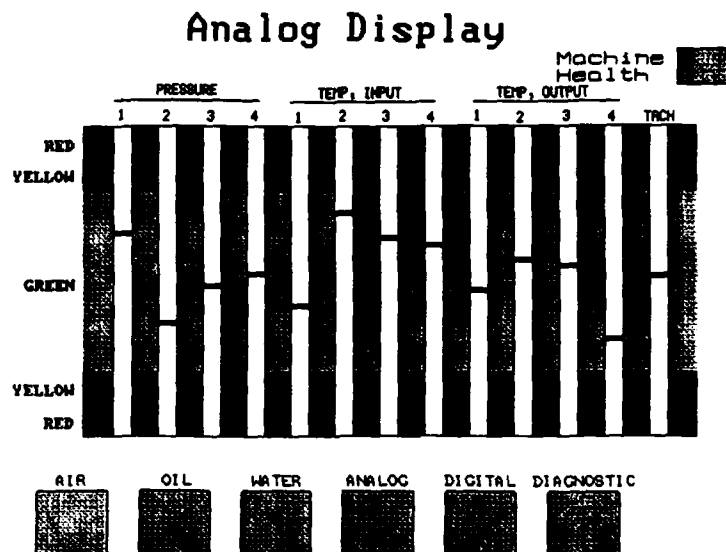


Figure 3 Analog Display Screen

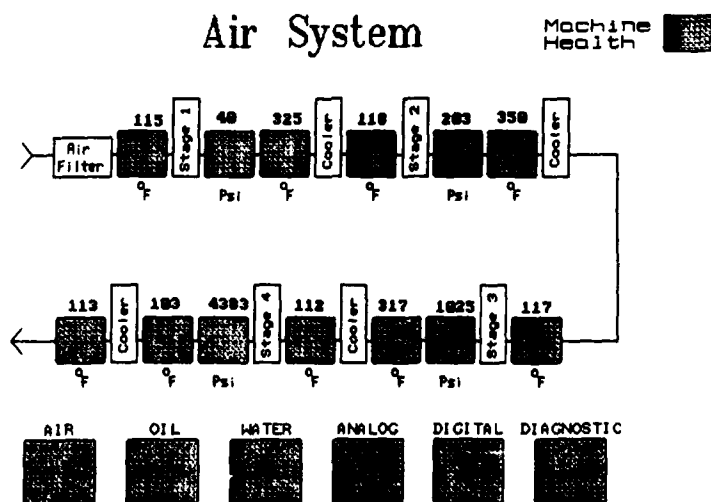


Figure 4 Air System Screen

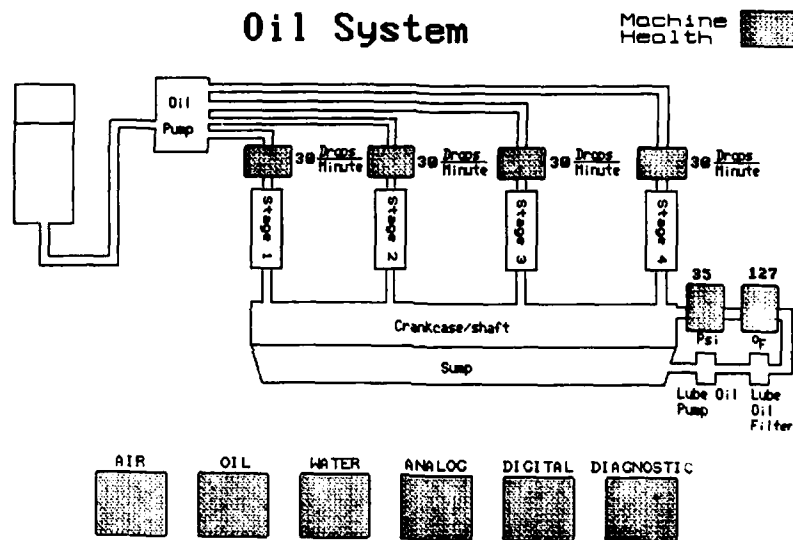


Figure 5 Oil System Screen

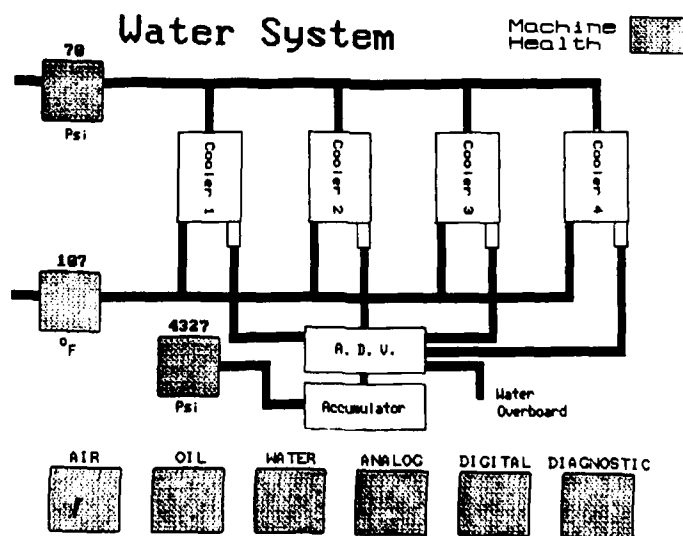


Figure 6 Water System Screen

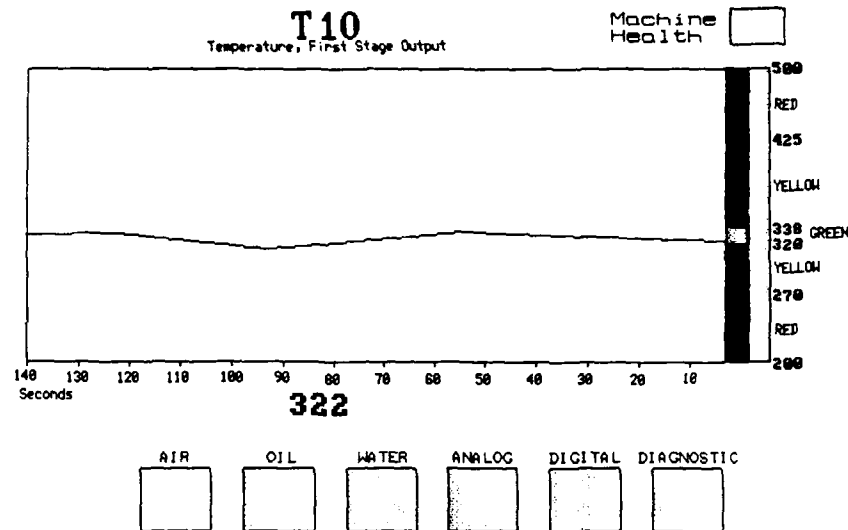


Figure 7 Example Data Display Screen

node database. FIX/DMACS provides access to the database via C function calls which are executable on any FIX/DMACS node. With the appropriate knowledge base, NEXPERT can analyze the data and communicate its results back to FIX/DMACS via C function calls.

This plan was postponed because of problems getting FIX/DMACS and NEXPERT to coexist on the same DOS node due to system memory constraints. A temporary solution has been adopted. Diagnostic rules are hard coded within a C program. The C program replaces the expert system with 24 hard coded rules arranged in order of decreasing severity. These rules are developed from the HPAC system manual and equipment experts. Once a rule fires, indicating a fault, a diagnostic number uniquely indicating the fault is immediately sent to FIX/DMACS for display on the screen. The color of the diagnostic box is controlled by this number. A yellow or red diagnostic box indicates the fault severity and directs the operator to the diagnostic screen. Even though more than one fault may be present, only the most severe is reported.

The C program provides piecewise linear scaling of data for the ANALOG DISPLAY, and controls the color of the MACHINE HEALTH box and major screen boxes on each display. Future CBM systems will use an expert system rather than hard coded rules in order to support larger rule bases.

Expert System Prognosis: The final element in the CBM model is the prognosis capability. Prognosis projects future machine health based on current and past condition. The expert system software will be extended to provide prognosis. It will use a knowledge base developed for the machine along with a probabilistic model of the HPAC to provide predictions of future machine health. Probabilities will be assigned to these predictions to give the operator an indication of the degree of confidence with which the prediction is made. The development of probabilistic machine models are crucial in order to provide more than a limited prognosis capability.

Work is being done at Columbia University on the method of state space machinery models. Data collected from the machine will be used to establish normal and abnormal state spaces. Algorithms will be developed to construct a multidimensional state space model of the HPAC. Although beyond the scope of this paper, this method has the potential of providing sophisticated prognostics.

Future Plans: The plans for CBM are to expand the present system to include the extended diagnosis and the prognosis capabilities discussed. Work will continue on the integration of the process control and expert system software. CBM may be extended to other operating systems with greater multitasking capabilities and larger memory models in order to accomplish this.

CBM will use the knowledge gained in developing the diagnosis and prognosis features to expand and refine the HPAC sensor suite. Sensor technologies will be developed as necessary for the detection of machinery health problems. Finally, CBM will be continually refined and expanded to include other shipboard machineries.

Conclusion: The CBM demonstration model will provide the Navy with the vehicle to improve its maintenance procedures and reduce costs. The challenge is to integrate CBM into the naval shipboard environment by using the knowledge gained from this effort to generate the guidelines for future machinery development and ship system designs.

References:

1. "Industry/Joint Services ATE Project", Final Report, Advanced Testing Technology Committee, Task Group 1d, Electronic Test of Non-Electronic Equipment, Revision C, 1 April 1979
2. Laird, W.C., "U.S. Navy Testing/Diagnostic RDT&E Program Plan", NOSC Technical Document 1646, Sept 1989, Naval Ocean Systems Center, San Diego, CA. 92152-5000
3. "Human Integrated Manufacturing in CIM Applications", Chilton's IC&S, Vol 62, No 11, November 1989, pp 67-70.

MECHANISMS OF FAILURE

Chairman: T. Robert Shives
National Institute of Standards and Technology

ANALYSIS OF CRACK TIP BLUNTING, INITIATION AND GROWTH OF ALUMINUM
SEN SPECIMENS BY MOIRE INTERFEROMETRY

B S.-J. Kang, V. Vaselenak and Q.-K. Liu

Department of Mechanical and Aerospace Engineering
West Virginia University
Morgantown, WV 26506

Abstract: Moire interferometry was applied to study ductile fracture of aluminum alloys. Sequential records of both u- and v-displacement fields associated with crack tip blunting, initiation and growth in 5052-H32 and 2024-T3 single edge notched (SEN) specimens with a/w ratios of 0.23, 0.47 and 0.67 were obtained and analyzed. Detailed v-displacement profiles along the crack line and their corresponding rotational factors, r_t , during the loading stages, e.g. blunting, initiation and growth were constructed and determined based on the moire fringe patterns. The results indicate similar blunting and initial crack growth process for the three Al 5052-H32 SEN specimens of different a/w ratios. The effect of a/w ratio and material strain hardening on r_t was also assessed. Finally J- Δa (J_R) and COD- Δa resistance curves were constructed for the aluminum specimens. The results show that J_R and COD resistance curves are independent of specimen a/w ratio up to approximate 1 mm initial crack growth.

Key Words: moire interferometry; J-integral; COD; CMOD; crack tip profile; rotational factor, r_t ; J- Δa and COD- Δa resistance curves.

Introduction: Crack growth in ductile material can be divided into three stages, namely, 1) crack tip blunting and the onset of stable crack growth, 2) stable crack growth and 3) rapid tearing. Numerous fracture parameters which characterize stable crack growth under small-scale yielding condition, such as average crack opening angle (COA) [1], crack tip opening angle (CTOA) [2], crack tip opening displacement (CTOD) [3], critical strain [4,5], energy release rate [6], crack tip force [7], J-resistance curve [8] and tearing modulus [9], have been proposed. Of these, the J-resistance curve, crack tip opening angle (CTOA) or displacement (CTOD) were shown to be suited for modeling stable crack growth and instability during the fracture process [2,8,10]. Under large-scale yielding condition, however, there is no analytical solution available for stable crack growth analysis. Attempts have been made to extend the ductile fracture criteria for small-scale yielding and stable crack growth to large scale yielding. Particularly the resistance curve approach (in terms of J, COD or the likes) has been popular for evaluating stable crack growth and ductile fracture of metals in the presence of large plastic yielding. Questions have been raised, however, regarding the specimen size, loading condition and geometry dependence of the resistance curves

approach [10,11,12,13]. The purpose of this paper is to present experimental findings, using moire interferometry method, on crack tip parameters which control ductile crack tip initiation and stable crack growth. Of particular interests are the construction of crack tip displacement profiles during the loading stages, the determination of overall rotational factor, r_t , as well as the J- Δa and COD- Δa resistance curves using the moire fringes. The effect of specimen a/w ratio on the resistance curves, the rotational factor, and crack tip blunting, initiation and growth process were also discussed.

The J-integral: For two-dimensional problems of materials governed by nonlinear elasticity and deformation plasticity theory subjected to monotonically condition, the J-integral is defined as [14]

$$J = \int_{\Gamma} W dy - \vec{T} \cdot \frac{\partial \vec{u}}{\partial x} ds \quad (1)$$

where Γ : contour surrounding the crack tip

\vec{T} :

traction vector along the contour

\vec{u} : displacement vector on the contour

W : strain energy density on the contour

In the following, an experimental procedure for direct far- and near-field J-contour integral measurement is briefly outlined. Detailed discussions can be found in Refs. 15, 19 and 20.

Consider a rectangular line contour in a cracked body subjected to mode I loading conditions such as the dotted line shown in Fig. 1. The J-integral can be represented by

$$\begin{aligned} J &= J_V + J_H \\ &= -J_{V1} + J_{V2} - J_{V3} - J_{H1} + J_{H2} \end{aligned} \quad (2)$$

$$\text{where } J_{V\ell} = \int_{V\ell} \left[W - \left(\sigma_{xx} \frac{\partial u}{\partial x} + \sigma_{xy} \frac{\partial v}{\partial x} \right) \right] dy \quad (\ell=1,2,3)$$

$$\text{and } J_{H\ell} = \int_{H\ell} \left(\sigma_{yy} \frac{\partial v}{\partial x} + \sigma_{xy} \frac{\partial u}{\partial x} \right) dx \quad (\ell=1,2)$$

The moire J evaluation procedure is based on Eq. 2, and the stress terms and strain energy density W shown in Eq. 2 can be calculated as follows:

(a) Under elastic condition, i.e. $\sigma_e < \sigma_o$

$$\epsilon_{\ell j} = \frac{1+\nu}{E} S_{\ell j} + \frac{1-2\nu}{3E} \sigma_{kk} \delta_{\ell j}$$

$$W = \frac{1+\nu}{3E} \sigma_o^2 + \frac{1-2\nu}{6E} \sigma_{kk}^2$$

(b) At yielding, i.e. $\sigma_o \geq \sigma_e$

$$\begin{aligned}\epsilon_{ij} &= \frac{1+\nu}{E} S_{ij} + \frac{1-2\nu}{3E} \sigma_{kk} \delta_{ij} + \frac{3}{2} \alpha \left(\frac{\sigma_e}{\sigma_o} \right)^{N-1} \frac{S_{ij}}{E} \\ W &= \sigma_{ij} \epsilon_{ij} - \int_0^{\sigma_{ij}} \epsilon_{ij} d\sigma_{ij} \\ &= \frac{1+\nu}{3E} \sigma_e^2 + \frac{N}{N+1} \alpha \left(\frac{\sigma_e}{\sigma_o} \right)^{N-1} \frac{\sigma_e^2}{E} + \frac{1-2\nu}{6E} \sigma_{kk}^2\end{aligned}$$

where σ_e is the effective stress and $\sigma_e = \left(\frac{3}{2} S_{ij} S_{ij} \right)^{1/2}$, S_{ij} is the deviatoric stress, σ_o is the yield stress, ν is the Poisson's ratio, and E is the young's modulus.

Experimental Approach: Moire interferometry was used to obtain u- and v- displacement fields in slowly fracturing 5052-H32 and 2024-T3 aluminum SEN specimens. Fig. 2 shows schematic drawing of the moire test setup which consists of collimating optics, laser, a four-beam u-v moire interferometry unit capable of measuring u and v displacements simultaneously, recording camera, and a table-top loading frame. The measured moire fringes can be related to the surface deformation through

$$u = N/f$$

where u represents the displacement field generated by moire interferometry, N is the moire fringe number, and f is the reference grating frequency which is set to be 1200 lines/mm for this investigation, i.e. 0.85 $\mu\text{m}/\text{fringe}$ sensitivity. Ductile stable crack growth analyses by moire interferometry have been investigated by the author [15-18] and others [19-20]. The earlier studies were mainly focused on developing J-contour integral evaluation procedure and the construction of J- Δa , COD- Δa , and CTOD- Δa resistance curves. In this investigation, in addition to evaluate those fracture parameters, we also analyze ductile crack tip blunting, initiation, and growth as well as determine the overall rotational factor, r_t , based on the measured moire fringes. These will be discussed in the later sections.

Specimens: As shown in Fig. 1, pin-loaded single-edge-notched (SEN) tensile specimens with a/w ratios of 0.23, 0.47, and 0.67 were used for this experimental investigation. The materials used in this studies were 5052-H32 and 2024-T3 thin aluminum plates of thickness 0.8 mm. The material properties are shown in Table 1 which indicate that Al 5052-H32 is an elastic-perfectly plastic material and Al 2024-T3 is a strain hardening material.

Results: Figs 3, 4 and 5 show typical moire interferometry fringe patterns of the Al 5052-H32 and 2024-T3 SEN specimens under increasing load. Also shown in the figures are the contours used for J-integral evaluation. Previous studies [15,16,20] have demonstrated that the J values are path-independent using the J-evaluation procedure based on the moire interferometry fringes. However in those earlier experiments,

remaining ligament of the specimen was always under tension. In this investigation, deep crack specimens were used and tension and compression zones existed ahead of the crack tip, as clear shown in Figs. 4 and 5. Yet the J values evaluated from the three contours in Fig. 4 are 10.4 Mpa m, 11.3 Mpa m, and 12.1 Mpa m respectively with less than eight percent difference. The result shows that the moire J -contour evaluation procedure can be applied to bend-type specimens. Furthermore, the whole-field moire fringes also provide convenient ways to determine the crack mouth opening displacement (CMOD), COD and overall rotational factor, r_t . Experimental results of the measured J , COD, CMOD and r_t values. are shown in Tables 2, 3, 4 and 5.

Analysis and Discussion:

The rotational factor: The procedure to determine the rotational factor, r_t , is similar to the concept of plastic hinge model [21,22] which define the rotational factor as the point located at $r_t(w-a)$ ahead of crack tip where the two specimen halves rotate. As shown in Fig. 4, using moire fringes along the crack line, it is easy to construct the crack tip displacement profile (shown as dots in Fig. 4). The straight line portion of the profile is then extended (solid line in Fig. 4) to determine the location of the rotational center. Note that the whole-field moire fringe pattern also clearly indicates the existence of a rotational center and agrees well with the r_t determined from the plastic hinge model approach. Fig. 6 shows typical crack tip v-displacement profiles of an Al 5052-H32 SEN specimen ($a/w = 0.67$) under increasing load, and the locations of the overall rotational center. As shown in Fig. 6, the rotational center does not remain constant as the applied load increases. Fig. 7 shows r_t versus $\sqrt{J/E}$ plots of Al 2024-T3 (a strain hardening material) and 5052-H32 (a non-strain hardening material) SEN specimens. Also shown in Fig. 7 are onset of crack growth marks.

In plastic hinge model, the knowledge of rotational factor is essential for the evaluation of CTOD values from the measured CMOD values using clip gage. The British Standard for COD-testing [22] specifies that a plastic rotational factor, $r_p = 0.4$, be used for a bend specimen of a/w greater than 0.45 (note that under large plastic yielding, $r_t = r_p$). However experiments conducted by others showed conflicting results about the values of r_t and r_p [23,24]. As shown in Fig. 7, our experimental results indicate that r_t is affected by the material strain hardening. As for the Al 5052-H32 SEN specimens, r_t is independent of specimen a/w ratio up to the initial crack growth (an indication of similar crack tip blunting process) and for extended stable crack growth, r_t is strongly influenced by the specimen a/w ratios.

The J and COD resistance curves: Fig. 8 shows plots of J- Δa resistance curves of the Al 5052-H32 specimens, which consists of J- Δa curves evaluated from this investigation and those studied earlier [18]. Note that thickness of all the tested specimens is 0.8 mm, width of all the SEN specimens is 19 mm (Fig.1) and the effective width of the cruciform specimen is 140 mm. As shown in Fig. 8, the J_R curve of the large cruciform specimen started to deviate with the small SEN specimens after about 1 mm of crack extension while J_R curves of the SEN specimens are essentially independent of the specimen a/w ratio. Fig. 9 shows plots of the COD- Δa resistance curves. Similar observation of resistance curve deviation is noted. Based on Figs. 8 and 9, one may conclude that the J- Δa and COD- Δa resistance curves of Al 5052-H32 are specimen size and geometry independent up to the initial limited amount of crack growth of about 1 mm. This conclusion is reinforced by the detailed plots of crack tip v-displacement profiles of the Al 5052 H32 SEN specimens under increasing load, as shown in Figs. 10, 11 and 12. These plots show similar v-displacement profiles at the crack tip region during the loading stages, i.e. for the same specimen thickness, crack tip blunting, initiation and limited amount of crack growth are independent of specimen a/w ratios, even for a non-hardening material.

The theoretical base for the so-called resistance curves approach for stable crack growth is the condition of J-controlled crack growth [25,26]. Under such condition, nearly proportional loading must exist at the crack tip region and the amount of crack growth must be small compared to the region dominated by the HRR fields [27,28]. Within the condition of J-controlled crack growth, the J_R and the related COD resistance curve are meaningful parameters for characterizing the crack growth [25,26]. However, previous studies [16,20] have shown that a J-dominated zone does not exist in 5052-H32 aluminum specimens and this finding is in agreement with the theoretical prediction that J-dominated zone will shrink to zero for non-hardening material [29,30]. Also, the stress-strain field is not unique and varies with specimen geometries and type of loading conditions for a non-hardening material [31]. The J_R and COD resistance curves shown in Figs. 8 and 9 show deviations after approximate 1 mm crack growth, an indication that for a non-hardening material the crack tip growth process is specimen geometry dependent or the stress-strain field ahead of the growing crack tip is not unique (due to lack of a J-dominated zone). On the other hand, our results also indicate that for a non-hardening material with thin specimen thickness, the initial J- Δa and COD- Δa resistance curves are independent of specimen a/w ratios. This finding is further verified by the similar crack tip v-displacement profiles (with specimen a/w ratios ranging from 0.23 to 0.67) at the initial blunting and growth stages, even though for a non-hardening material, J-controlled crack growth theory is not valid.

Conclusion:

1. Moire Interferometry was applied to study crack tip blunting,

initiation and growth of Al 5052-H32 and 2024-T3 SEN specimens. Detailed v-displacement crack tip profiles indicate crack tip blunting and initial crack growth are independent of specimen a/w ratios.

2. A procedure for determining the overall rotational factor, r_t , from the recorded v-displacement field was developed. r_t is independent of specimen a/w ratio up to crack initiation and is strongly influenced by material strain hardening.

3. For a non-hardening material such as the Al 5052-H32, the J_R and COD resistance curves are not unique, however, for a small amount of crack growth, they are independent of specimen size, geometry and a/w ratios.

Acknowledgement: The work reported here was supported by the faculty initiation fund, Mechanical and Aerospace Engineering Department, West Virginia University.

Reference:

1. Green, G. and Knott, J.F., "On Effects of Thickness on Ductile Crack Growth in Mild Steel", Journal of the Mechanics and Physics of Solids, Vol 23, pp. 167-183, (1975).
2. de Koning, A.U., "A Contribution to the Analysis of Quasi-Static Crack Growth", Fracture 1977, Proceedings 4th International Conference on Fracture, University of Waterloo Press, Vol. 3, pp. 25-31, (1977).
3. Green, G. and Knott, J.F., "The Initiation and Propagation of Ductile Fracture in Low Strength Steels", Journal of Engineering Materials and Technology, Trans ASME, Series H 98, (1975).
4. McClintock, F.A. and Irwin, G.R., "Plasticity Aspects of Fracture Mechanics", Fracture Toughness Testing and Its Applications, ASTM STP 381, pp. 84-113, (1965).
5. Achenbach, J.D. and Dunayevsky, V., "Crack Growth Under Plane Stress Conditions in an Elastic Perfectly-Plastic Material", Journal of the Mechanics and Physics of Solids, Vol. 32, No. 2, pp. 89-100, (1984).
6. Broberg, K.B., "On Stable Crack Growth", Journal of the Mechanics and Physics of Solids, Vol. 23, pp. 215-237, (1975).
7. Kanninen, M.F., Rybicki, E.F., Stonesifer, R.B., Broek, D., Rosenfield, A.R., Marschall, C.W., and Hahn, G.T., "Elastic-Plastic Fracture Mechanics for Two-Dimensional Stable Crack Growth and Instability Problems", Elastic-Plastic Fracture, ASTM STP 668, pp. 121-150, (1979).
8. Shih, C.F., deLorenzi, H.G., and Andrew, W.R., "Studies on Crack Initiation and Stable Crack Growth", Elastic-Plastic Fracture, ASTM STP 668, pp. 65-120, (1979).
9. Paris, P.C., Tada, H., Zahoor, A., and Ernst, H., "The Theory of Instability of the Tearing Mode of Elastic-Plastic Crack Growth", Elastic-Plastic Fracture, ASTM STP 668, pp. 5-36, (1979).

10. Davis, D.A., Joyce, J.A., and Hays, R.A., "Application of the J-Integral and the Modified J-Integral to Cases of Large Crack Extension and High Toughness Levels", ASTM, 21st National Symposium on Fracture Mechanics, Annapolis, MD, June (1988).
11. Etemad, M.R., and Turner, C.E., "Unique Elastic-Plastic R-Curves: Fact or Friction?", ASTM, 21st National Symposium on Fracture Mechanics, Annapolis, MD, June (1988).
12. Ernst, H.A., "Material Resistance and Instability Beyond J-Controlled Crack Growth", Elastic-Plastic Fracture: Second Symposium, Vol. 1 - Inelastic Crack Analysis, ASTM STP 803, American Society for Testing and Materials, Philadelphia, PA, pp. I-191-I-214, (1983).
13. Ernst, H.A., Schwalbe, K.H., Hellmann, D. and McCabe, D.E., "Modified J, J_M , Resistance Curves under Plane Stress Conditions," Int. Journal of Fracture, Vol.37, pp.83-100, (1988).
14. Rice, J.R., "A Path Independent Integral and the Approximate Analysis of Strain Concentration by Notches and Cracks," Journal of Applied Mechanics, pp.379-386, (1968).
15. Kang, B.S., Kobayashi, A.S. and Post, D., "Stable Crack Growth in Aluminum Tensile Specimens", Experimental Mechanics, 27(3), pp. 234-245, (1987).
16. Kang, B.S.-J., and Kobayashi, A.S., "J-estimation Procedure Based on Moire Interferometry Data," ASME, Journal of Pressure Vessel Technology, 110(3), pp.291-300, (1988).
17. Kang, B.S.-J., "Experimental Investigation of Ductile Fracture by White Light Moire Interferometry," to be published in the special moire interferometry volume of Laser and Optics in Engineering.
18. Kang, B.S.-J., Dadkhah, M.S., Kobayashi, A.S., "J-resistance Curves of Aluminum Specimens Using Moire Interferometry," Proceedings of the 1989 SEM Spring Conference on Experimental Mechanics, Cambridge, MA, pp.317-322, (1989).
19. Dadkhah, M.S., Kobayashi, A.S., Wang, F.X. and Graesser, D.L., "J-Integral Measurement Using Moire Interferometry", Proceedings of the VI International Congress on Experimental Mechanics, Portland, OR, pp. 227-234, (1988).
20. Dadkhah, M.S., "Analysis of Ductile Fracture Under Biaxial Loading Using Moire Interferometry", Ph.D. dissertation, University of Washington, (1988).
21. Dawes, M.G., "Elastic-Plastic Fracture Toughness Based on the COD and J-contour Integral Concepts," Elastic-Plastic Fracture, ASTM STP 668, pp.307-333, (1979).
22. BS 5762: 1979, Methods for Crack Opening Displacement (COD) Testing. The British Standards Institution (1979).

23. Kolednik, O., "On the Calculation of COD from the Clip-Gauge Displacement in CT and Bend Specimen," *Engineering Fracture Mechanics*, 29(2), pp.173-188, (1988).
24. Pandey, R.K., Pratap, C.R., and Chinadurai, R., "Significance of Rotational Factor r in CTOD Determination and The Effect of Material and Loading Geometry on r ," *Engineering Fracture Mechanics*, 31(1), pp.105-118, (1988).
25. Hutchinson, J.W. and Paris, P.C. "Stability Analysis of J-Controlled Crack Growth," *Elastic-Plastic Fracture*, ASTM STP 668, American Society for Testing and Materials, Philadelphia, Pa., pp.37-64, (1979).
26. Shih, C.F. and German, M.D., "Requirements for a One Parameter Characterization of Crack Tip Field by The HRR Singularity," *International Journal of Fracture*, 17(1), pp.27-43, (1981).
27. Hutchinson, J.W., "Singular Behavior at the End of a Tensile Crack in a Hardening Material," *Journal of Mechanics and Physics of Solids*, Vol.16, pp.13-31, (1968).
28. Rice, J.R. and Rosegren, G.F., "Plane Strain Deformation near a Crack Tip in a Power-Law Hardening Material," *Journal of Mechanics and Physics of Solids*, Vol.16, pp.1-12, (1968).
29. Rice, J.R., "Stresses Due to a Sharp Notch in a Work-Hardening Elastic-Plastic Material Loaded by Longitudinal Shear," *Journal of Applied Mechanics*, Vol.34, pp.287-298, (1967).
30. Amazigo, J.C., "Some mathematical Problems of Elastic-Plastic Crack Growth," *Fracture Mechanics 12*, SIAM-AMS Proceedings, R. Burridge Editor, pp.125, (1978).
31. McClintock, F.A., "Plasticity Aspects of Fracture," *Fracture - An Advanced Treatise*, edited by H. Leibowitz, Vol.3, pp.47-225, (1971).

Table 1. Material Properties of Aluminum Specimens

Aluminum	Yield Stress (MPa)	Young's Modulus (MPa)	α	N
2024-T3	337	75000	1.0	4
5052-H32	190	70200	0.4	15

$$\epsilon_{YY} = \frac{\sigma_{YY}}{E} + \alpha \frac{\sigma_{YY}}{E} \left(\frac{\sigma_{YY}}{\sigma_0} \right)^{N-1}$$

Table 2. Measured applied load, Δa , J, COD, CMOD and rotational factor of 5052-H32 Al SEN Specimen with $a/w = 0.23$

P (N)	Δa (mm)	J (MPa-m)	COD (mm)	CMOD (mm)	r_t
493	0	0.000431	0.005	0.010	0.27
617	0	0.000677	0.008	0.020	0.31
751	0	0.001000	0.014	0.028	0.37
884	0.198	0.006128	0.030	0.054	0.44
986	0.346	0.007914	0.044	0.076	0.48
1017	0.495	0.011490	0.050	0.107	0.52
1066	0.544	0.013543	0.075	0.117	0.54
1097	0.692	0.019333	0.115	0.153	0.56
1231	0.989	0.036240	0.143	0.208	0.57
1262	1.088	0.045704	0.163	0.268	0.59
1293	1.137	0.46425	0.177	0.273	0.60

Table 3. Measured applied load, Δa , J, COD, CMOD and rotational factor of 5052-H32 Al SEN Specimen with $a/w = 0.47$

P (N)	Δa (mm)	J (MPa-m)	COD (mm)	CMOD (mm)	r_t
84	0	0.000080	0.001	0.030	0.24
217	0	0.000541	0.005	0.040	0.35
355	0	0.001431	0.012	0.063	0.39
480	0	0.002708	0.020	0.122	0.47
533	0.221	0.006951	0.046	0.157	0.49
568	0.388	0.009172	0.075	0.223	0.51
662	0.814	0.023671	0.107	0.318	0.53
706	0.985	0.035897	0.147	0.413	0.55
751	1.241	0.053723	0.185	0.502	0.56

Table 4. Measured applied load, Δa , J, COD, CMOD and rotational factor of 5052-H32 Al SEN Specimen with $a/w = 0.67$

P (N)	Δa (mm)	J (MPa-m)	COD (mm)	CMOD (mm)	r_t
8	0	0.000015	0.00016	0.010	0.19
45	0	0.000140	0.00033	0.030	0.21
66	0	0.000324	0.0005	0.040	0.26
111	0	0.000883	0.010	0.070	0.31
155	0	0.001745	0.015	0.100	0.39
200	0	0.003181	0.020	0.140	0.46
222	0.148	0.003740	0.030	0.168	0.49
257	0.316	0.009046	0.042	0.258	0.51
275	0.346	0.009522	0.055	0.297	0.55
284	0.396	0.011295	0.057	0.318	0.56
297	0.495	0.014573	0.076	0.363	0.60
324	0.544	0.015977	0.088	0.430	

Table 5. Measured applied load, Δa , J, COD, CMOD and rotational factor of 2024-T3 Al SEN Specimen with $a/w = 0.69$

P (N)	Δa (mm)	J (MPa-m)	COD (mm)	CMOD (mm)	r_t
89	0	0.000564	0.004	0.040	0.26
155	0	0.001587	0.007	0.068	0.31
200	0	0.002251	0.009	0.085	0.35
244	0	0.003557	0.013	0.103	0.37
311	0.239	0.006357	0.017	0.140	0.40
351	0.288	0.008757	0.019	0.156	0.43
395	0.336	0.010147	0.022	0.175	0.45
440	0.383	0.013765	0.029	0.206	0.46
480	0.431	0.015071	0.035	0.222	0.47
524	0.479	0.195391	0.039	0.266	0.47
578	0.502	0.237339	0.052	0.350	0.49

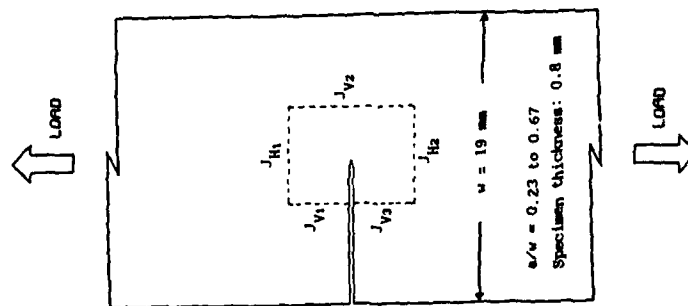


Fig. 1 Single edge-notched (SEN) specimen.

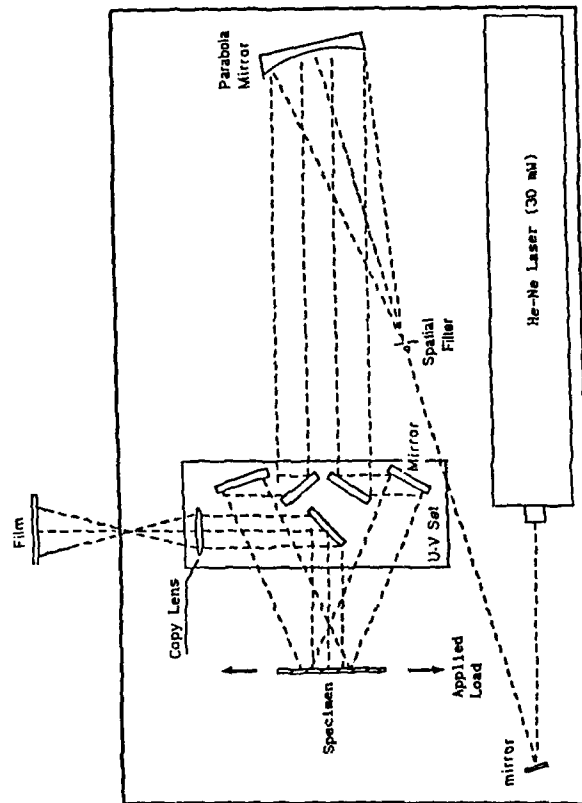
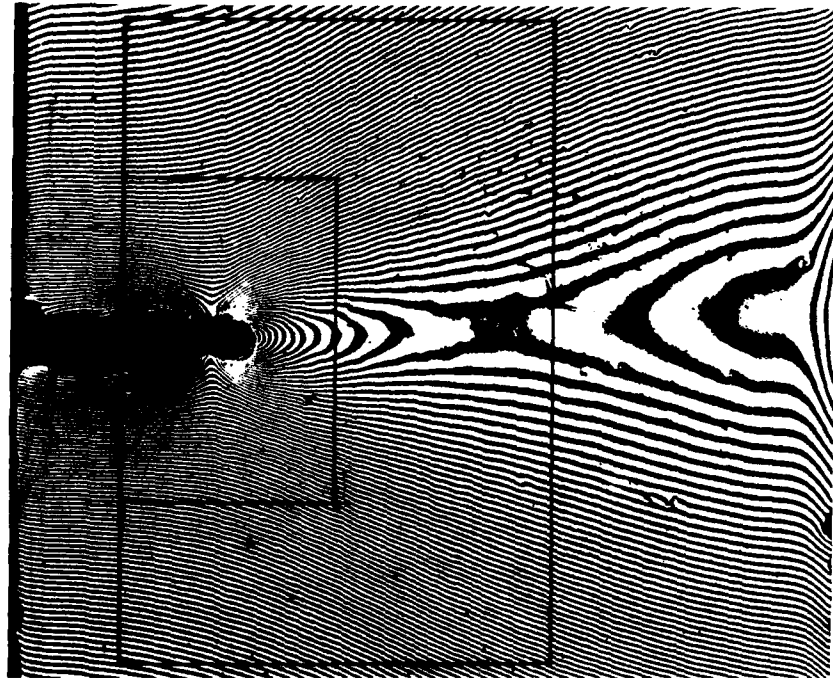
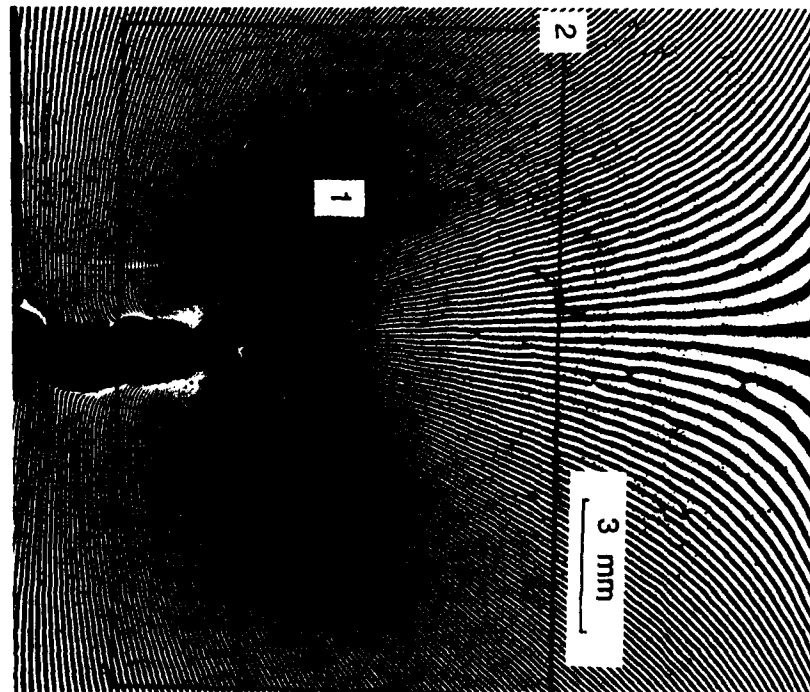


Fig. 2 Optical setup for moiré interferometry test.

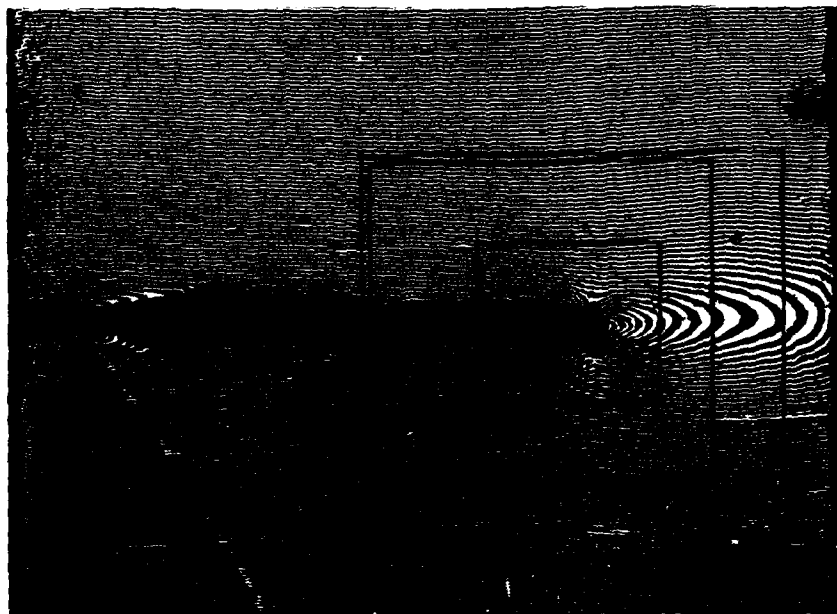


(u-displacement)

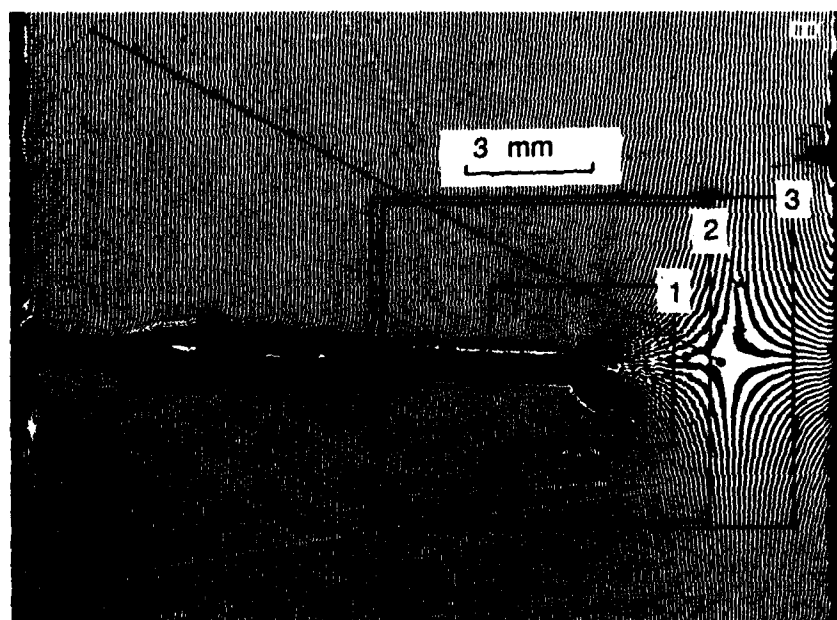


(v-displacement)

Fig. 3 Moiré fringe patterns of an Al 5052-H32 SEN specimen under increasing load. ($a/w = 0.23$, $P = 1066$ N)

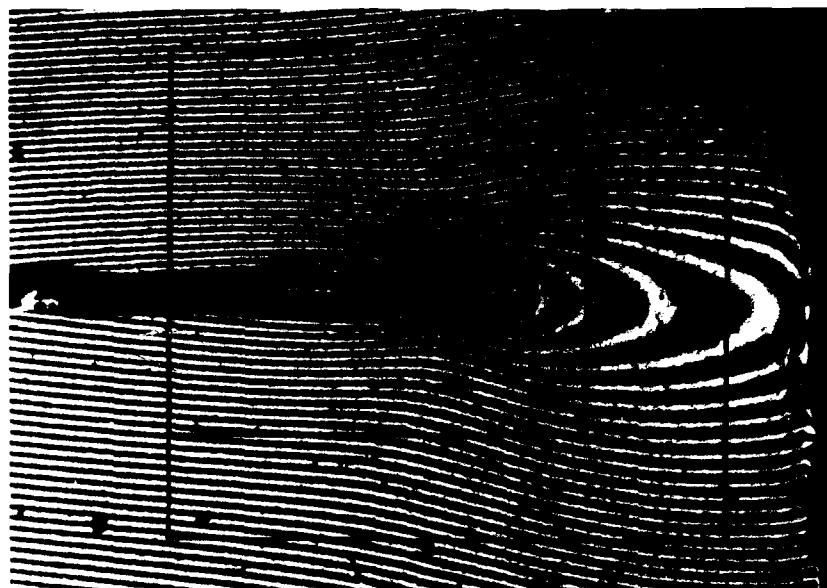


(u-displacement)

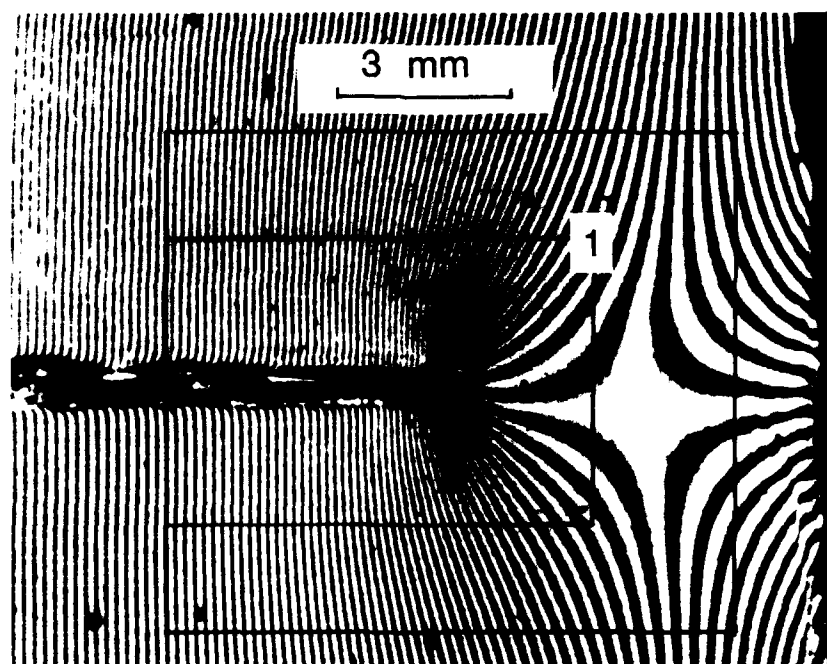


(v-displacement)

Fig. 4 Moire fringe patterns of an Al 5052-H32 SEN specimen under increasing load. ($a/w = 0.67$, $P = 284$ N)

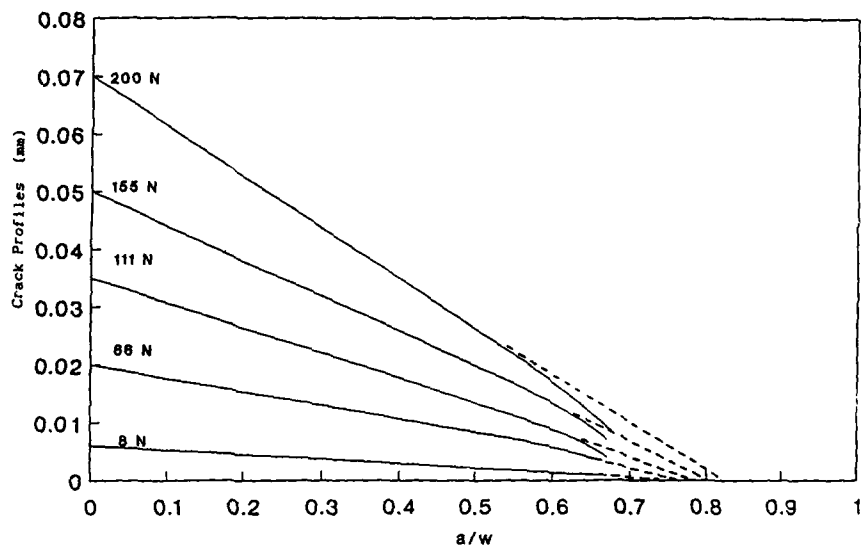


(u-displacement)

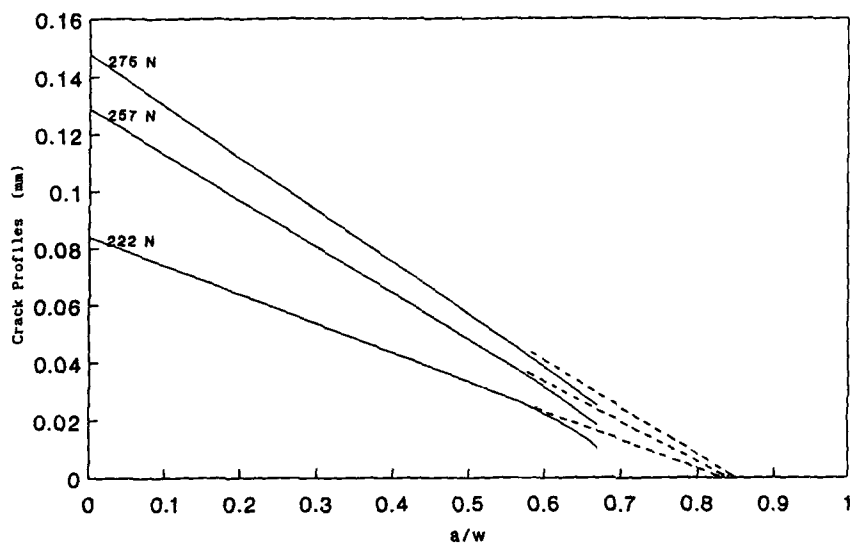


(v-displacement)

Fig. 5 Moire fringe patterns of an Al 2024-T3 SEN specimen under increasing load. ($a/w = 0.69$, $P = 351$ N)



(a) Crack Tip Blunting



(b) Crack Growth

Fig. 6 v -displacement crack line profiles of an Al 5052-H32 SEN specimen under increasing load and the extended dot lines for rotational factor determination. Specimen $a/w = 0.67$

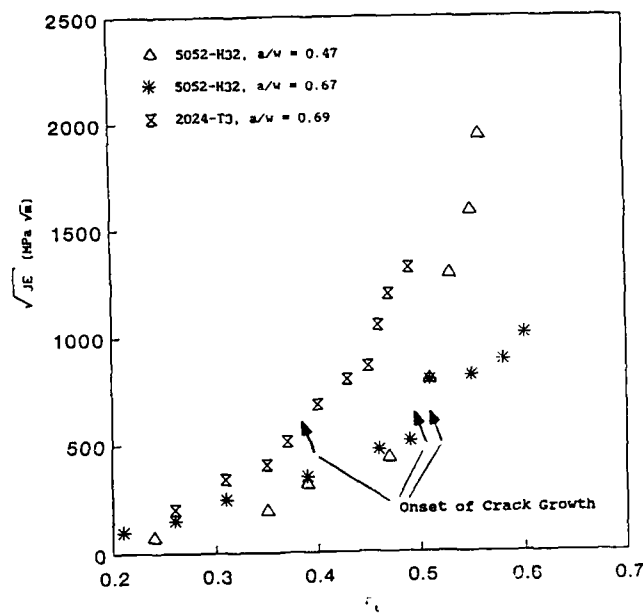


Fig. 7 Plots of r_t versus \sqrt{JE} of Al 5052-H32 and 2024-T3 SEN specimens.

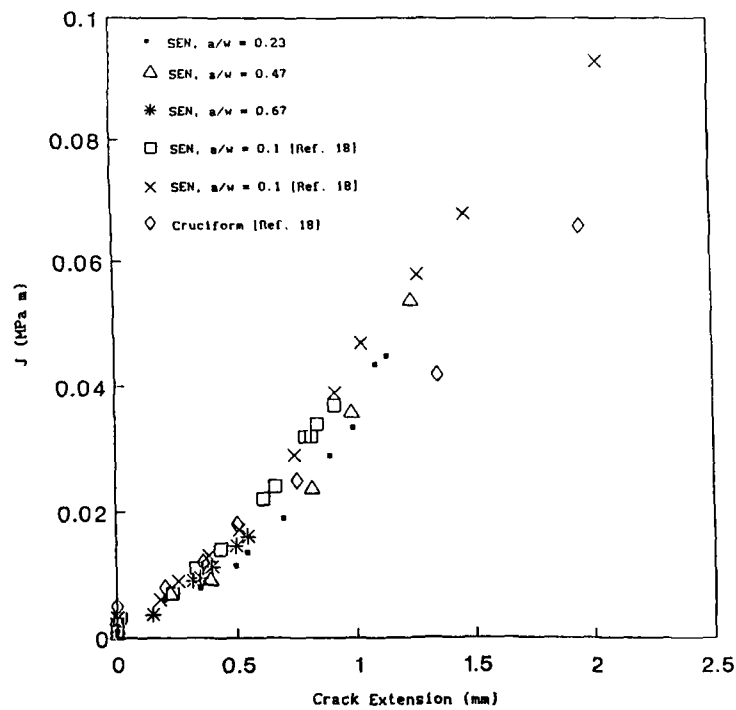


Fig. 8 J_R resistance curves of Al 5052-H32 SEN specimens.

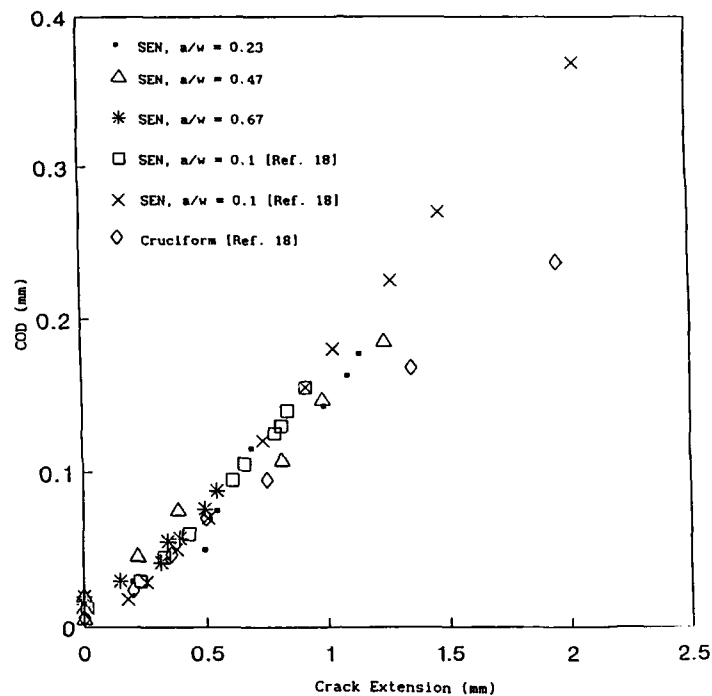


Fig. 9 COD resistance curves of Al 5052-H32 SEN specimens.

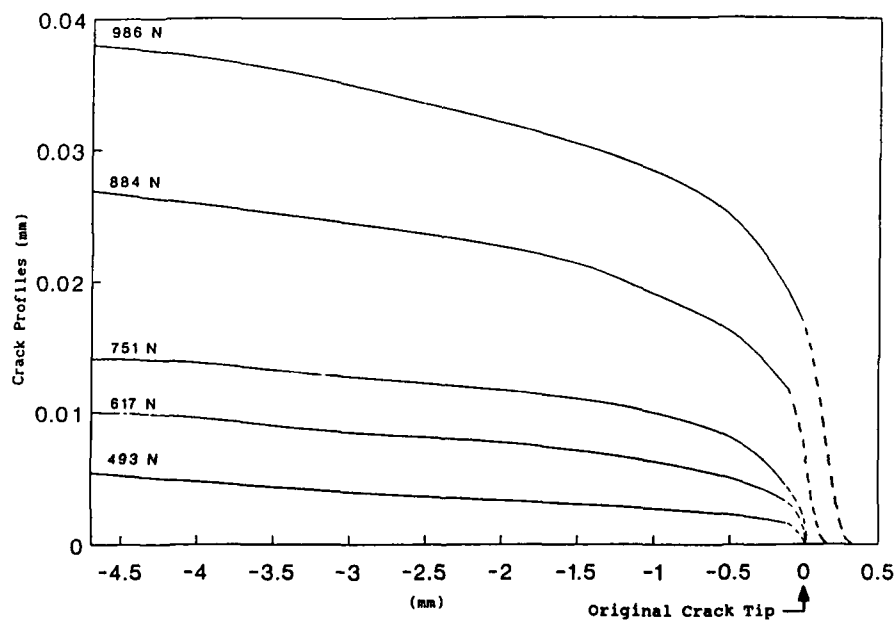


Fig. 10 v-displacement profiles of crack tip blunting, initiation and growth of an Al 5052-H32 SEN specimen under increasing load. Specimen $a/w = 0.23$

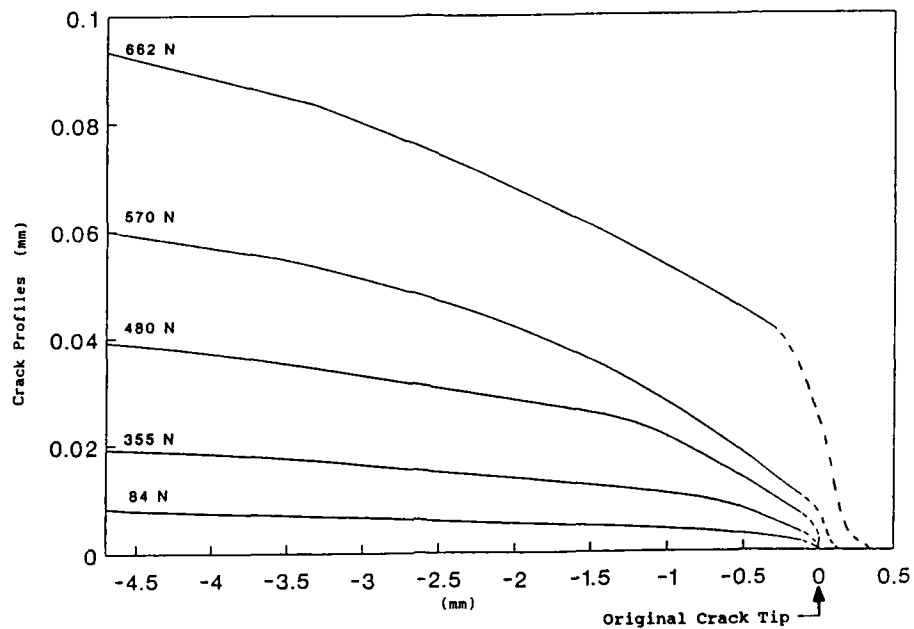


Fig. 11 v-displacement profiles of crack tip blunting, initiation and growth of an Al 5052-H32 SEN specimen under increasing load. Specimen $a/w = 0.47$

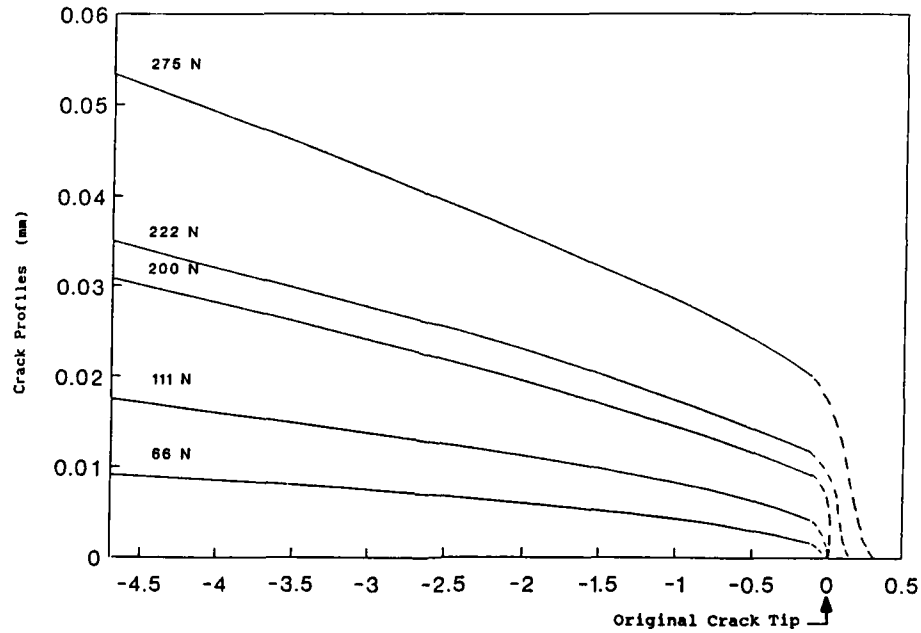


Fig. 12 v-displacement profiles of crack tip blunting, initiation and growth of an Al 5052-H32 SEN specimen under increasing load. Specimen $a/w = 0.67$

**ADVANCES IN PREVENTING PREMATURE FAILURE OF
PEEK BASED COMPRESSOR VALVE PLATES**

Roy S. Klein, Harry P. Wertheimer
and Derek Woollatt, PhD

Dresser-Rand Company
100 Chemung Street
Painted Post, New York 14870

Abstract: Failures of PolyEther Ether Ketone (PEEK) thermoplastic valve plates are principally caused by impact and/or fatigue loads during seating. Recent advances in preventing premature failure focused on reducing manufacturing defects and improving the accuracy of predicting service conditions. An aggressive total quality system was implemented to insure tough moldings, free from harmful defects in critical areas. A computer model of the reciprocating compressor cycle has been refined to account for pulsations, better estimates of "sticktion", and to accept more valve description parameters. This program serves to minimize incorrect applications and to help evaluate potentially beneficial new valve design features.

Key words: Flutter; impact velocity; mass damping; mer; PEEK; reciprocating compressor; sticktion; thermoplastic; valve dynamics; valve plate.

Introduction: The recent introduction of PEEK valve elements promises much longer life and wider successful window of applications. This is largely due to PEEK's inherent superiority to pre-existing valve plate materials. PEEK is stronger and more heat resistant than nylon. PEEK can also tolerate impacts better than metals.

Further, PEEK is more corrosion resistant than other polymers or metals. Yet plates made from this apparently ideal material can fail prematurely. Two principle causes for premature failure have been identified: misapplication of the valve and manufacturing defects. This paper describes Dresser-Rand's recent advances in applying and producing HITEMP™ valve plates based on PEEK plastic.

Predicting Valve Plate Motion: The calculation of valve dynamics has become routine during the design and application engineering of valves for large reciprocating compressors. Each application, whether for a new unit of aftermarket retrofit, is different and the valve dynamics is calculated to assist the design of the valve components for the application, thus reducing, and in most cases eliminating, the need for trial and error in the field. The major factors affecting valve reliability have been known for many years and several of these, the impact

velocity of the moving elements on the seat and guard, and the amount of flutter are determined by the valve dynamics calculation. These calculations also give the influence of the valves on compressor capacity and power.

For effective prediction of valve reliability, details of the valve movement, in particular the impact velocities, must be accurately calculated. Ignoring second order effects can lead to improper valve selection.

The computer program used is a general purpose compressor cycle simulation program. The calculation proceeds in the traditional way using a time step integration of the flow, heat transfer, energy, and motion equations. It is assumed that the flow through the valve and in the cylinder is quasi steady so equivalent area and drag coefficients obtained from steady flow tests can be used.

The motion of each valve plate is assumed to have only one degree of freedom as characterized by its lift. The valve dynamics calculation is set up to include the effects of:

- i) Non-linear springs, including dual springs
- ii) Viscous damping that varies with lift
- iii) Plate drag coefficients that vary with lift
- iv) A non-linear equivalent area against lift relationship
- v) Mass damping
- vi) Sticktion (or viscous adhesion) to the seat and guard
- vii) Rebound from the seat and guard
- viii) Pulsations

The basic method used to integrate the equation of motion for the plate is similar to that used previously (1). Variation of mass damping and coefficients with lift are accommodated by dividing the lift into up to 19 portions. Figure 1 illustrates how an integration time step is subdivided as necessary when a discontinuity occurs within it.

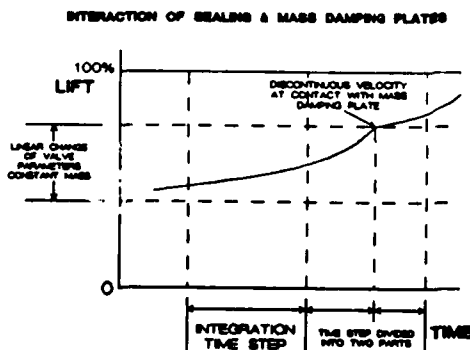


Figure 1.

The classical, although suspect, approach is used for seat sticktion. This assumes a zero absolute pressure in the sealing surface. We use the area ratio (Seat slot area/Plate area) as an independent sticktion parameter, the value of which is determined from experimental results.

Sticktion on the guard is calculated by assuming that the integral with time of the force/unit plate area acting to close the valve, starting when this force becomes positive, must reach a critical value before

the plate breaks away from the guard. This critical value, is determined from experimental diagrams of lift against crank angle.

The flow in the cylinder passages is assumed to be unsteady, one dimensional and homentropic, and a non-mesh time domain solution (2) based

on the method of characteristics is used. This has several advantages over the usual mesh methods in that systems consisting of different length short pipes can be modelled accurately, and equal time steps can be used without loss of precision or the possibility of numerical instability.

Experimental Methods to Study Plate Motion: A 9.25 inch (235 mm) bore CUB compressor cylinder on a closed loop test facility was used with 5.25 inch (133 mm) nominal size standard production valves to examine valve plate motion. This valve has three independent plate elements or rings made of HITEMP PEEK-based resin. To measure plate motion, an optical probe system based on reflected light intensity was used, aimed at the innermost ring of the valve.

The measured motion of the inner ring of the outer end discharge valve was compared to the motion calculated with the program described. Several different assumptions for pulsations and sticktion were input to the program to see which gave the best match to the experimentally observed valve plate motion.

At 600 rpm: Valve flutter occurs when speeds are low and spring forces are high relative to conditions. Figure 2 typifies the valve motion in a flutter situation. The heavy solid line represents the observed motion.

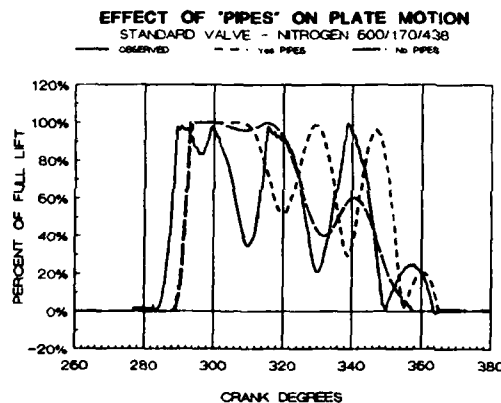


Figure 2.

The notation "600/170/438" at the top of the figure shows the compressor speed/inlet gage pressure/discharge gage pressure (RPM/psig/psig). The curve on the figure with long dashes is the motion calculated without considering pulsations. This curve does not agree well with the observed motion, especially with regard to the closing (seat) impact.

Much improved agreement is seen when the piping algorithm is used to generate pressure pulsations similar to those known to occur in the inlet and discharge valve plenum chambers. This (dotted curve on figure 2) agrees well except for a period of dwell at full lift and a later opening as compared with the observed motion.

A slightly better match can be obtained with adjustment of the guard rebound coefficient but, clearly, there are factors not yet taken into account. When flutter exists, extremely accurate prediction of motion is difficult. This applies especially to the estimating of seat impact velocities, which is highly dependent on the phase relationship of the flutter cycles.

At 1200 rpm: In figure 3 again, the heavy solid line shows the observed valve motion. The dotted line is the simplest model, no piping and no sticktion. At this operating condition, the effect of the piping model is seen to be all but negligible. However, when a sticktion value

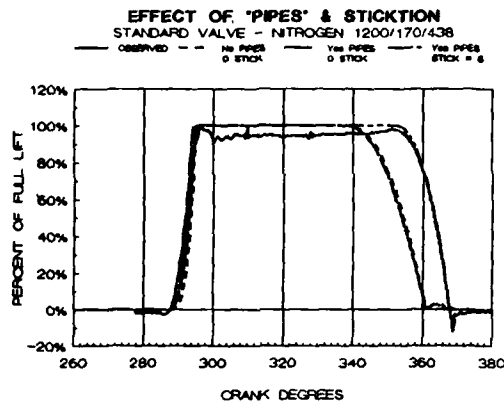


Figure 3.

pipings was used but no sticktion, and last (on the right end) both piping and sticktion are input to the computer model.

Referring now to figure 4, it is apparent that with neither pipes nor sticktion, predicted seat impacts fall considerably short of the observed values at all speeds.

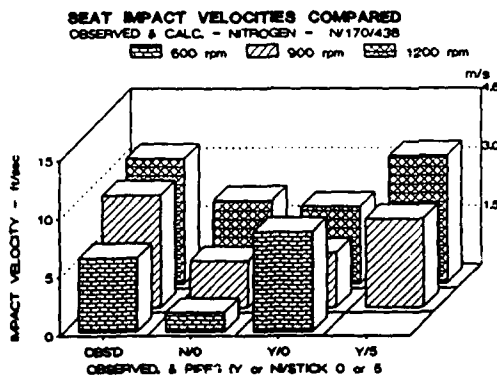


Figure 4.

side pair of bars in figure 5 shows that with seat sticktion, guard impacts are calculated that are 3 or 4 times the measured values. The use of seat sticktion, based on the actual seat port to plate face area of the valve tested, also caused the calculated opening point to be 15° later than the observed start-to-open.

New Design Compared to Production Valve: A new valve design has been defined which features a one piece ported plate of the same material as the standard valve plates. This valve has a maximum design lift of 0.140 inch (3.6 mm), the same nominal size as the 5.25 inch (133 mm) standard valve, and an equivalent flow area of 3.0 in² (1935 mm²) which is slightly less than the standard valve in this size. The new design valve employs a set of secondary springs that engage at a lift of 0.110

of 5 psi-ms (34.5 kPa-ms) is entered, the prediction (dash-dot-dot line) falls almost on top of the observed line.

Impact Velocities: The velocity with which the plate hits the seat or the guard has a strong bearing on durability of the plate in any given compressor application. Figures 4 and 5 are arranged to have increasing rpm from the front row to the back row of bars. The impacts for the observed data are on the left. Second from the left is the case of no piping or sticktion used as input for calculation. Then comes the case where

adding sticktion is required for good agreement with the experimentally measured impacts. At 600 rpm, the piping model generates an impact close to but above that observed. At 900 and 1200 rpm the piping contributes almost nil toward a match with the observed impacts. But, adding sticktion is required for good agreement with the experimentally measured impacts.

Guard impacts are accurately forecast with, but not without piping, as seen in figure 5. Not shown, but not surprising, is the fact that guard impact velocity is not influenced at all by guard sticktion as an input to the model. The right

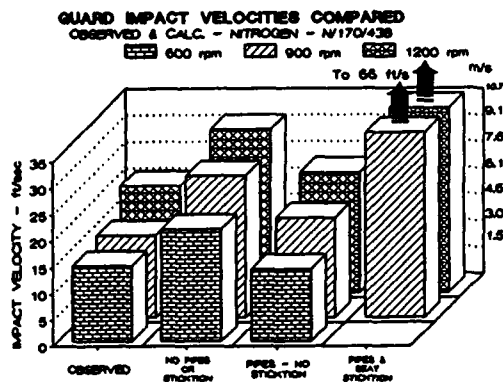


Figure 5.

This edge is lost when the pipes are considered, but regained when sticktion to the guard is factored in. Putting high rate springs in the standard valve reduces the calculated seat impact, but still not to the level of the new design.

Although mass damping appears to lower seat impacts with the new design, the higher mass gives a higher impact to the seat, suggesting that there will be conditions where a mass damped valve would have as high or higher seat impacts as a valve without this feature.

As seen before, figure 7 shows lower guard impacts with the piping model, and no effect from guard sticktion. In this figure it is seen that the higher rate springs in the standard production valve reduce guard impact somewhat. The damping mass equal to the seal plate mass approximately halves the guard impact of the new design and tripling that damper plate mass cuts the guard impact to about one fourth of the value without mass damping.

Space limitations preclude a detailed discussion of effects on compressor capacity, power requirements, and efficiency, though these parameters are calculated by the program described previously. Figure 8 is a comparison of effects on power

inch (2.8 mm). These springs have a very high rate and are intended to prevent sticktion to the guard and thus avoid late closing with its attendant high seat impacts.

Bars in the front row are for the new design, and those in the back represent the standard valve in figures 6, 7, and 8. Comparing predicted seat impacts for the new design against the standard valve, it is seen, in figure 6, that modeling without pipes or sticktion shows an advantage for the new design.

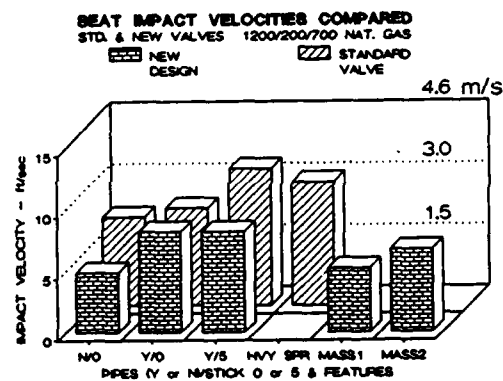


Figure 6.

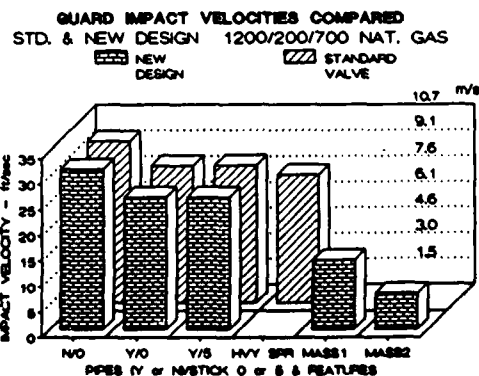


Figure 7.

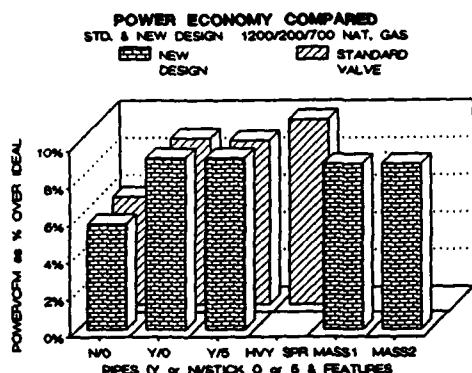


Figure 8.

plate - resistance to heat and chemicals combined with outstanding dynamic properties - make the resin difficult to polymerize and mold. Table I. After initial synthesis, it took 20 years to commercially introduce PEEK, in 1982, at 10 times Nylon's price. Early successes in static applications in the severe "downhole" environment led to attempts at valve plates. However, producing reliable plates met 3 obstacles. First, PEEK technology was aimed at static service. Second, quality PEEK molding is demanding. Finally, high resin cost deterred molders from process development for dynamic applications.

Table I.

Selected Valve Service and
Moldability Characteristics
of HITEMP and Nylon

Characteristic	HITEMP	Nylon
Impact Str. ft-lbs	2.7	1.8
264psi Defl. Temp., °F	600	450
Molding Temp., °F	710	550
Viscosity at Molding Temp, poise	4500	900

to insure production plates deliver maximum reliability.

economy or the brake power per unit of gas delivery. The standard production and new design valves are seen to be comparable in power economy, and it appears that calculation without consideration of piping will lead to optimistic predictions. The high rate springs cost a little increase in power economy for the standard valve. The mass damping has almost no effect on this efficiency parameter.

Manufacturing Development Program: The characteristics that make PEEK so useful as a valve

Therefore, in 1987 Dresser-Rand, working with selected vendors, launched an extensive program to optimize PEEK plate-making. Initially a detailed review of PEEK was conducted to help understand processing problems, and a summary follows. Then, vendors were selected on their technical proficiency. Mean-while an innovative accelerated life test method shortcut the evaluation of several processing parameters. The resulting manufacturing protocol was incorporated into a proprietary HITEMP line of PEEK-based valve plates and Total Quality System was implemented

Understanding PEEK: PEEK's properties, derive from its molecular architecture. Like all plastics, PEEK consists of long, chain-like molecules. Chains of most plastics are relatively light, based on a carbon atom backbone covalently bonded together. But PEEK chains contain links which are themselves small organic molecules. Figure 9. Therefore, PEEK chains are inherently bulkier and heavier. Bulky chains are more resistant to thermally induced motion, resulting in higher creep strength and thermal resistance. The usual practice of adding glass fibers results in glass-PEEK plates which are substan-

Typical Link, or MER,
in PEEK Chain

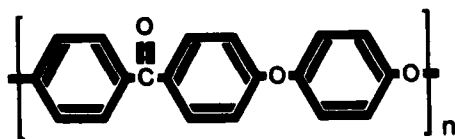


Figure 9.

tially stronger at normal compressor temperatures of 250°F than older resins like Nylon. Conversely, as shown below, molding must overcome heat resistance and high viscosity.

PEEK has an inherently chemically stable structure because constituent atoms and molecules are bonded in the strong covalent format. Consequently, PEEK is compatible

with almost all common gases such as natural gas, propane, nitrogen, carbon dioxide. Unlike metals, PEEK is immune to chloride-induced stress cracking and/or pitting. Unlike Nylon, PEEK is virtually unaffected by moisture or hot water and tolerates steam exposure.

The regular structure of PEEK chains permits forming a crystalline arrangement. If allowed to solidify slowly, chains fold into a repetitive pattern similar to the crystal structure of a metal. This metal-like structure partially accounts for PEEK's excellent dynamic properties. With glass reinforcing, PEEK exhibits one of the highest fatigue strengths of any plastic. Similarly, the crystal structure provides the restoring force underlying good impact strength. Added impact resistance derives from PEEK's molecular architecture. Recall that Oxygen atoms bond the small organic molecules together. In plastics, this type Oxygen bond permits the adjoining molecules to flex under impact. Thus each molecule of the chain absorbs impact, enhancing PEEK's ability to withstand impact loads without gross deformation or fracture.

Resin Factors: Testing was required to optimize both PEEK grade selection and resin handling. The resin maker, responding to demand from molders without adequate press capacity, introduced a low viscosity grade of PEEK called "Easy Flow". Since PEEK's bulky molecule results in flow resistance, the resin maker could only lower viscosity by decreasing the average chain length. Based on equivalent results from routine static tensile and impact tests shown in Table II, the resin maker claimed Easy Flow as strong as the high viscosity, longer chain grade. Similarly, based on static service results, the resin supplier felt that molders could continue the routine practice of cutting cost by blending reground runners and scrap parts with virgin PEEK resin.

Both these practices raised concerns for dynamic applications. Short chains tend to have less crystallinity and lower dynamic properties than long chains. Similarly, the high temperatures and pressures that occur during PEEK regrinding can lower toughness if the polymer is oxidized or the notch sensitive glass fibers are nicked. The routine method of testing these hypotheses, extensive life testing in service conditions, could have taken years.

However, Dresser-Rand's Valve Endurance Tester (VET) was applied for accelerated life testing (3). The VET simulates compressor operation with a rotating dually ported steel disk that directs the flow of air from a high volume compressor to open and close 3 valves mounted in a fixture. This system provides 6,000 valve cycles per minute, 5 to 10 times faster than compressor speeds. Plate motion was monitored by the

optical probe system described above. The VET permits control of pressure differentials so that plate seating impacts approximating service conditions could be obtained.

A VET test protocol of side-by-side testing of rings molded from different resin grades and both virgin and regrind resin was used. As shown in Figure 10, Easy-Flow grade proved far too brittle. Long chain PEEK ran almost 7 times longer under the same conditions. Similarly, regrind cut the average life by about 40%. Thus, VET testing led to the timely optimization of resin factors in a laboratory environment and eliminated 2 potential causes of premature service failures.

Table II.
Resinmaker's Mechanical
Test Results

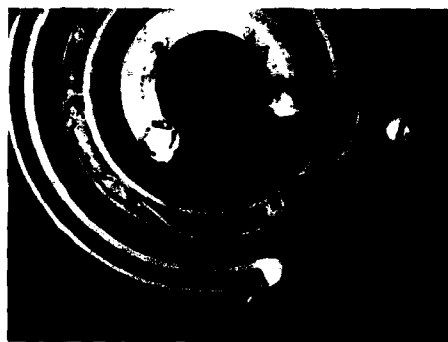
PEEK Grade	Tensile Strength psi	Notched Izod, ft-lb
HITEMP Base	22,800	2.1
Easy Flow	23,800	1.8

Reinforcement: Control of glass reinforcement yielded two improvements in service life. First, a proprietary additive was discovered which retards the pro-pagation of radial cracks. Second, fiber orientation control made ring shaped plates more impact resistant. During molding, fibers become oriented parallel to resin flow. Rings can be gated as tubes or disks. Electron microscopy revealed fibers oriented "on end" in tubular moldings whereas disk gating oriented fibers parallel to the seating surface. Figure 11. Testing showed that rings made from tubes, which maximized impacts on the ends of the fibers, were far more prone to edge chipping than rings molded as disks.

Molding: Improper molding can embrittle PEEK. Recall that PEEK crystallizes during slow cooling. Proper molding requires a mold uniformly preheated to 400°F. Many molders tried to use lower mold temperatures for several reasons. Expensive, sophisticated mold design is required to attain temperature uniformity. Preheating a ton of steel to 400°F is cumbersome and results in challenging handling problems. Finally, a cold mold produced a flatter plate molding because the chains are virtually frozen in place, replicating the mold. A slow cooled molding tends to distort as the orientation of the crystals from the flow pattern of molding causes non-uniform contraction. Commonly, properly crystallized plates must be machined to attain the required flatness for reliable sealing.

Char: PEEK requires molding temperatures and pressures so high that the resin can burn or "char". Charring can be so severe that the basic hydrocarbon structure of PEEK is destroyed. Indeed, charred resin

D-R Accelerated Testing

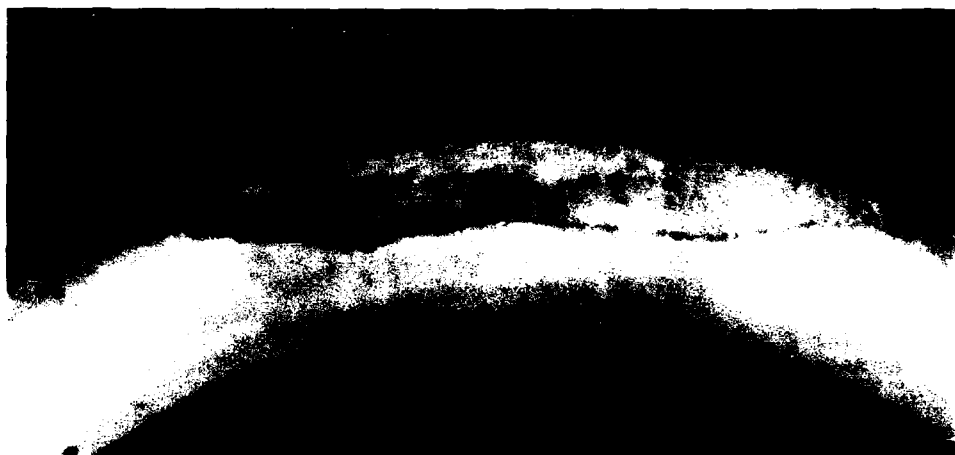


Inner and outer Easy Flow rings broke. HITEMP middle ring lasted almost 7 times longer.

Figure 10.

changes from a light grayish tan to a dark black. These char defects can be discontinuities in the structure that will grow into cracks when subjected to fatigue or impact loads.

Effect of Fiber Orientation



"On edge" orientation of glass fibers resulted in premature edge chipping of ring plate seating areas.

Figure 11.

The char control program has 2 phases. First, optimum processing and process control is needed. For example, molding press selection has several factors. First, the press should have sufficient capacity so that minimum injection temperatures are used and the resin need not be overheated to lower viscosity. Second, to minimize resin dwell time at injection temperature, the barrel of the machine must be sized to volume of the "shot" to be molded. Finally, appropriate temperature and pressure control devices are a necessity.

Since char is an inherent problem with PEEK, a 3 part inspection system was developed. First, only the light, natural colored resin is used. Some molders added colorants for product differentiation. However, colorants make it difficult to visually detect char specks in the

Char Inspection Criteria

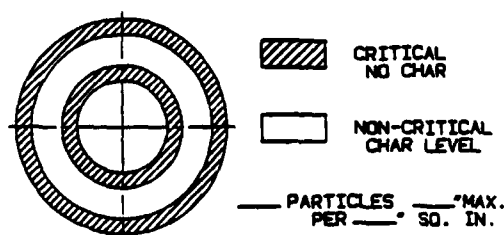


Figure 12.

plates. Second, the resin cleanliness is checked prior to molding. Finally, all finished plates are visually inspected for char to standards that maximize reliability. Figure 12. Stresses are highest in the seating areas. Since plates can seat non-uniformly, highly localized impact and bending loads may arise. Therefore, the inspection standard forbids any observable char particles from being present in the seating areas. In the lower stress areas, a limited number of char specks are permitted.

Total Quality System: Plate making is controlled by a Total Quality System co-developed with the supplier network. In processing, records are kept of critical factors like mold temperature and injection temperature for each run of plates. Resin lot numbers are tracked throughout the process. Then the finished plates are permanently marked with a Quality Batch Number for traceability. Thus HITEMP PEEK plates are made with same type of quality system as critical metal parts. Finally, suppliers are audited both during receiving inspection and monthly visits.

Conclusions:

- 1) The refined computer model is an important tool to aid selection of valve parameters that promote durability, or conversely, too simple a model may result in an overly optimistic estimate of impact velocities or otherwise lead to short life.
- 2) Optimizing and controlling HITEMP's PEEK resin base and manufacturing method significantly improved reliability by eliminating causes of premature failure.
- 3) Refined analysis techniques combined with today's best plate valve plate materials will lead to new compressor valve designs with superior durability compared to valves presently available for many applications.

References:

1. Woollatt, D., "A Simple Numerical Solution for Compressor Valves with One Degree of Freedom", Compressor Technology Conference, Purdue University, 1974.
2. Woollatt, D., "Unsteady Flow in Branched Systems", Ph.D. Thesis, University of Liverpool, U. K., 1962.
3. Hartshorn, K., "An Experimental Device for Accelerated Endurance Evaluation of Compressor Valve Assemblies", International Compressor Engineering Conference, Purdue University, 1986.

DIAGNOSTICS LOOK AT ENGINE CONDITION

James L. Pettigrew, PE
Howell Instruments, Inc.
3479 West Vickery Boulevard
Fort Worth, Texas 76107

Abstract: Since 1986, the U.S. Army has been evaluating digital data recording systems for the detection, diagnosis and prognosis of faults on T53 engines installed in helicopters. On-board use of digital data systems makes test cell quality instrumentation available for testing installed engines. Electronic data recording and transfer of accurate performance information into a personal computer allows the use of Artificial Intelligence methods to form and interpret the significance of the data. The resulting information is being successfully used to provide previously unobtainable diagnostic capabilities for maintenance decisions. Standardized engine testing and formatting of data helps low experience technicians see the relative internal condition of a gas turbine engine at a glance.

The computational capability of the personal computer allows expert logic to be applied in data reduction to yield Referred Engine Diagnostic Data (REDD). REDD compares the engine under test to a normal, installed specification engine. REDD may not detect all engine problems experienced but has shown its ability to identify many hidden faults, thereby enhancing propulsion system management. Field testing has suggested that inaccurately installed indicating systems cause many maintenance actions (or decisions to take NO action) to be made in error.

The digital data system includes vibration monitoring capability. Data have shown that vibration limits alone are of little value in understanding the meaning of observed vibration levels. The operating/flight conditions exert significant influence on the level of vibration experienced. Since the data system records operational data along with the vibration data, flight conditions which accompany or cause high vibration can be identified. Abnormal vibration indications, when compared to fleet averages in like conditions, have identified and confirmed impending failures. The abnormal values for the problem engines were still less than 1/3 of the published limits.

This paper presents results from 1989 testing of helicopter turbine engines with digital data recording systems. Engine maintenance management based on the demonstrated capability of REDD to provide knowledge of each turbine engine's internal condition has essentially improved operational reliability, maximized flight safety, reduced Remove and Replace (R & R) troubleshooting, while producing an excellent return on investment.

Key words: Turbine engine diagnostics, data acquisition, turbine engine testing, reliability enhancement, impending failure detection, vibration signature analysis, expert analysis, artificial intelligence application.

Introduction: The U.S. Army Aviation Systems Command (AVSCOM)/AMCPM UH-1H and AH-1S program management selected the Portable Engine Analyzer Test Set (PEATS) to provide performance data for the management of T53 equipped weapon systems in a technical competition among 10-plus companies at the Corpus Christi Army Depot (CCAD) in late 1985. Procurement and testing of Howell's off-the-shelf Portable Engine Analyzer Test Set (PEATS) was under Army contract DAAJ09-87-C-A145.

AVSCOM/(AMSAV-MR) completed an initial PEATS verification on March 2, 1989. AVSCOM/AMSAV-E has provided airworthiness releases and completed Qualitative Electromagnetic Compatibility (EMC) tests for PEATS on both UH-1H and AH-1S aircraft.

Personnel in the Corpus Christi Army Depot Engineering and RCM Support Office (DERSO) continued their technical evaluation of PEATS until AVSCOM-AMSAV-MRP released the technical findings showing that PEATS performs accurately, providing the type of data necessary to determine an engine's internal condition. The accurate PEATS data provides a new level of confidence in an installed engine's performance potential.

Instrumentation description: The digital data recording system used by the U.S. Army is an instrumentation package which can be installed on Bell UH-1H and AH-1S helicopters without permanent changes in the aircraft configuration. It provides equivalent test cell instrumentation for testing installed engines and adds Referred Engine Diagnostic Data (REDD). This REDD data is capable of indicating at any power setting the health of the engine relative to operating limits at maximum power. See figures 1, 2 & 3 for an AH-1S helicopter, a PEATS unit, and memory module with computer interface unit.

PEATS application: A typical installed engine test requires PEATS installation on the aircraft, inspection, ground test run, test flight, post flight ground test, removal and a post removal inspection to return the aircraft to flight ready status.

PEATS installation, by two aircraft mechanics with PEATS experience, requires approximately 75 minutes. Installation inspection by a technical inspector (TI) takes 15 minutes. Ground test by a test pilot and PEATS operator (mechanic or TI) requires approximately 30 minutes, flight test takes 30 minutes, and post flight ground test takes 10 minutes. Removal by two mechanics or electricians requires 30 minutes and post removal inspection takes 15 minutes. The total time to perform a PEATS test is 3.5 hours (6.2 man-hours).

PEATS output is available in real time on the display, in printed format from 3-inch PEATS tape, and in a memory module. The module stores and transports more than 150 readings of monitored parameters for electronic transfer into a personal computer data base. Actual data on engine operating performance can be transmitted over telephone lines to a central data base where expert propulsion people can do a detailed analysis of the individual engine's operating condition.

U.S. ARMY test objectives: The objectives of testing were to verify that PEATS accurately measures engine data required for maintenance decisions, manipulates and presents the data in a manner that significantly enhances engine diagnostics, and can be fielded in the current Army maintenance environment. Decisions required in the maintenance environment are shown in figure 4.

To accomplish these objectives, PEATS was used in engine test cells, on aircraft with newly installed engines and on aircraft with known engine performance problems. PEATS was used for successive tests on a UH-1 engine at Fort Rucker over a period of several hundred flight hours. It was also tested under simulated fielding conditions and used for diagnostic testing on field engines, then used again after the repair to verify that the problem was fixed.

PEATS software: Programs which produce referred engine diagnostics data are provided under license to PEATS users. The factory-loaded microchips (firmware) operate PEATS, display all engine instrument data, normalize and refer the data. The accuracy of real time displays are traceable to the National Bureau of Standards and can, therefore, be used as an accuracy check of aircraft instruments. The diskette/software for an IBM PC calculates and displays the difference between the baseline engine performance curves (ideal engine curves) and the data (observed performance) from a particular engine test. The PC's printout shows an engine's calculated parameters and the operating ranges (\pm XXXX) in which a normal engine should operate. See figure 5 for a normal engine REDD data. This provides immediate and specific identification of an engine's variance from the norm and is called Referred Engine Diagnostic Data (REDD). Some REDD values are available on the PEATS display in real time as the test is being performed. Additionally, the software records, calculates, and displays all required HIT and TEAC data.

The IBM PC compatible software provided on diskettes is composed of several programs which transfer test data from the PEATS memory module to the computer, format the test data for display and printing, and aid in analyzing the data. Also, once the data is in the computer, it can be transferred to remote locations via computer networks or modem connections. Figure 6 illustrates the relationships between the computer and REDD data.

Enhanced diagnostic capabilities: The PEATS Referred Engine Diagnostic Data (REDD) concept is based on expert system theory and has been proven to significantly improve engine diagnostics. It also provides a level of confidence not

previously possible in the performance potential of an installed engine. It gives the operator a way, under almost any conditions, to verify that they have a good engine. The concept and equipment work.

PEATS REDD presents the test data in a way that allows the user to determine easily that his engine is good, thus leading to a decision to fly. See figure 7 for an illustrative problem engine REDD data summary. REDD helps the user to interpret exactly what is wrong and to decide what will correct the problem and restore airworthiness. PEATS and REDD make possible accurate, expert troubleshooting and analysis of an engine's gas path.

Successful use of PEATS depends on field maintenance personnel's ability to turn PEATS information into maintenance decisions. In the case of a good engine, verified by PEATS, the decision is easy -- fly it. But, when PEATS identifies an unhealthy engine, the line mechanic may want expert capability to help identify the best corrective action. It is essential to isolate the failure so that the real problem will be repaired properly. Correct diagnostics which identify the problem without remove and replace troubleshooting will maximize system utilization potential and minimize the system down time.

Results from PEATS testing: Data from the PEATS project revealed several misconceptions and erroneous conclusions regarding the current maintenance, installed performance and operation of T53-L-13B and T53-L-703 engines. This knowledge should influence changes which will improve future maintenance practices and decisions.

Cockpit instrumentation errors: PEATS testing identified a large number of inaccurate cockpit indicating systems suggesting that many maintenance actions (or decisions to take no action) have been based on faulty information and have, therefore, been performed in error. The accurate and precise PEATS display of engine and related parameters made an initial impact on almost every group of users, especially pilots. PEATS duplicates all engine instruments, except oil pressure. Additionally, it duplicates free air temperature (FAT), altitude (pressure altitude), and rotor speed. PEATS also adds fuel flow and pressure, gas producer (GP or N1) and power turbine (PT or N2) radial vibration, outside air temperature at the inlet particle separator screen, variable inlet guide vane (VIGV) and bleed band positions, plus compressor discharge pressure and temperature.

Using PEATS, all cockpit engine instrumentation can be checked at one time against a reference traceable to the National Bureau of Standards. In many cases during the test project, a number of suspected "bad" engines turned out to be cases of inaccurate or out of tolerance instrumentation. At one PEATS test facility, the maintenance officer said that he would not fly an aircraft until the instrumentation had been verified with PEATS. A field engine mechanic suggested the PEATS would pay for itself just in the identification of bad instruments. Problems with the current Huey and Cobra instrumentation were probably the most frequently

repeated concerns of field personnel, i.e. an aviation support facility tested 14 aircraft in a 6-month period and found 11 (80%) had one or more cockpit indicator reading out of acceptable tolerances.

Examples of the many cockpit instruments found operating outside of acceptable tolerances are: 1) a cockpit power turbine tachometer read 2% low, causing the pilot to unknowingly operate in an undetected overspeed condition, 2) an engine was rejected on a Turbine Engine Analysis Check (TEAC) because corrosion in an electrical connector caused the torque gauge to read 4 psi low. These faulty cockpit indications obviously inhibit the pilot's ability to make valid decisions about his engine's condition based on the aircraft instrumentation.

Rebaselining invalidates HIT: The Health Indication Test (HIT) is the pilot's primary tool for determining engine condition on a daily basis. It utilizes changes in EGT from a baseline EGT to check for changes in the engine's gas path. The baseline EGT is determined when the engine is first installed. Whenever gas path or fuel flow components are changed or modified, it is common field practice to re-establish the baseline. When the HIT is rebaselined, previous changes in exhaust gas temperature (EGT) are dropped from consideration. For instance, if an engine's EGT has gradually increased 10°, then an unrelated fuel control failure requires rebaselining and the initial 10° rise will effectively be lost. If EGT continues to rise another 7° and the VIGV is found out of rig and is rerigged, the HIT is rebaselined and, again, the additional 7° effectively disappears. Now the engine is operating 17° hotter than when new, but this change is not considered in checking the engine's condition because the HIT was rebaselined twice. There can now be another 20° rise before concerns are raised when in actuality, the engine will be running 37° hotter than when first installed.

Flight with unchecked engines: The Turbine Engine Analysis Check (TEAC) requires that the pilot climb at full power until the engine can no longer maintain constant rotor speed, at which time the engine or rotor is said to droop or top. The TEAC results in a single baseline performance point (the droop point) and allows later performance comparison at that point only. Instrument readings, recorded when the engine droops, are normalized and compared to previous TEACs to verify engine health and performance potential. TEAC tests require high ceilings for climbing to make the engine droop, but in some geographical areas, days or weeks may pass before weather conditions permit a topping. Often, in the case of the T53-L-703, even if there is no cloud cover, the engines have so much power reserve that the mandated altitude limit of 10,000 feet is reached before the engine droops. Either way, the TEAC cannot be performed and the engine's performance potential or degradation remains an unknown. When conditions preclude engine topping, field manuals allow the sign-off of a deferred TEAC and a return to flight-ready status.

With PEATS, successive data comparisons can be made at any performance setting. If no degradation occurs, the engine will maintain the same performance

in relation to its baseline over its operating range. Successive flights with PEATS installed and operating will ensure knowledge of actual performance and identify any degradation. Drooping is not required and the ceiling is not an issue. PEATS can measure an engine performance condition without reaching TEAC flight conditions.

Performance analysis misconception: A commonly held misconception is that the gas generator on a faulty engine runs faster than it would on a good engine. Most Army T53 users assume that as the compressor loses efficiency, the gas producer (GP or N1) system "speeds up" to make up for the decreased airflow. PEATS data has shown that in reality, slower operation occurs. PEATS indicates that for a constant power output, the GP system does not speed up, but actually slows down as the compressor loses efficiency. Less airflow accompanies the slower speed. Increased fuel flow (richer mixture) and the resulting higher combustor temperature combine with lower compressor power consumption to allow the power turbine to make power with the lower airflow. An engine operating with an inefficient compressor has lower stall margin and increased hot end thermal stress. The required power is produced well within all operating limits, but at a lower gas generator speed and higher interturbine gas temperature.

PEATS vibration capability: PEATS uses a vibration tracking filter supported by an analysis capability that can show how an aircraft was being operated when any abnormal vibration occurred. Since many operational parameters are recording along with vibration, graphs can be plotted which include vibs vs. time, vib vs. altitude, vibs vs. NPT, vibs vs. gas generator speed, and vibs vs. engine torque. Each series of plots reveals something different in the vibration. Vibs vs. altitude shows where in relation to altitude the vibration occurred. Vibs vs. time shows when in relation to time it occurred, and vibs vs. torque shows at what power level it occurred. Other combinations are possible. PEATS uses velocity units-Inches Per Second (IPS) to record and display vibration readings. The data can also be plotted with the data points sequentially joined by lines, giving a picture of the time pattern of occurrence. Note that this combination of plots shows when, under what conditions, and how much the aircraft vibrated during the entire flight instead of at a single point as given by a spectrum analysis.

Typical vibration levels: Vibration graphs from aircraft flown with PEATS show that the power turbine has a typical high vibration which commonly occurs during the low power descents. The vibration observed for the gas generator at speeds above 90% RPM is normally less than 0.5 IPS.

Army Field Manual TM 55-2840-229-23's ENGINE VIBRATION TEST DATA SHEET gives vibration limits in displacement MIL values. These field manual limits, converted to velocity values, Inches Per Second (IPS), range from about 2.5 to 4 IPS, depending on the speed at which the component is operating.

Vibration experience: PEATS data from an engine test six hours before an in-flight bearing failure resulted in an off-airport emergency landing showed a gas generator vibration untypically greater than 1 IPS. While the 1 IPS limit is far less than the 4 IPS field manual limit, it is about twice what is seen for most normal engines. The test also showed the typical high power turbine vibration during low torque descent at 4 plus IPS which was judged to be insignificant. The 1 IPS vibration of the gas generator (twice the normal observed values), while only one-fourth the limit, did show that the engine was operating with an unusual vibration condition before the failure. See figures 8-12 for data from this engine which show both the how, when and where vibration capability and this engine's signature six hours before failure.

Teardown and visual inspection of engines from two other aircraft grounded because vibration was observed above normal values have supported the contention that the lower limits should be used. One engine with gas generator vibration above 1.3 IPS had, on teardown, internal compressor/case seal rub. Another tested with NG vibs at 1.3 IPS and NPT vibration above 2.5 IPS had significant internal damage, including a large diffuser crack. Both engines, at high power, had the gas generator RPM stagnated (RPM constant with increasing fuel flow, EGT, and torque) when the vibration reached the 1.3 IPS value.

Apparently when vibration approaches the 1.3 IPS value, rotors are displaced off-center enough to cause tip rub. The off-center rotor operation moves all the tip clearances to one side, increasing tip leakage lowers the compressor ratio at a given gas generator speed. Tip rub wear increases compressor clearances, reducing efficiency even when operating without the high vibration. Graphs in figures 13-16 show the vibration and performance associated with one of these engines which stagnated at high power.

Experience with PEATS data and engine problems has shown that the installed 4 IPS per the broad band limits from the FM were probably set to accommodate the highest reading seen in the flight envelope at low power operation. TM 55-2840-229-23, page 1-235, gives vibration limits in IPS for the T53-L-703 on a test stand as 1.3 IPS maximum NG vibs and 2.5 IPS as maximum NPT vibs. Internal engine condition found on teardown has supported the use of these lower values as limits for vibration measured in velocity units (IPS) on the aircraft.

Conclusions: PEATS REDD values provide the basis for discovery of hidden engine gas path deterioration with an indication of what component is weak. Early discovery of what is bad allows for decisive repair action without remove and replace troubleshooting and before secondary damage has occurred.

REDD values from PEATS testing prior to scheduled downtime can identify problems for correction without degrading the operational ready rate. Early problem repair improves operational reliability, reduces in-flight problems, and increases flight safety. Aircraft operating free from engine deterioration will have increased reliability, combat capability, and lower life cycle cost.

Vibration data, when simultaneously recorded with other operating parameters, can be formatted to show what conditions accompany the high vibration. When operating conditions are not available with vibration readings, limits may be set higher to allow for the maximum acceptable reading under any condition. PEATS testing shows that these higher limits may not be reached when serious internal conditions exist. Recorded vibration levels for the problem engines, while well below field manual limits, have been abnormal when compared to a fleet average for like engines operating in the same flight conditions.

Summary: Since weapon systems are effective only when they are operational, keeping system reliability at a maximum is vital. Declining numbers of skilled personnel able to troubleshoot and maintain weapon systems makes the improved capability of the Portable Engine Analyzer highly desirable because it provides accurate condition assessments and pinpoints problems which can reduce system down-time. The PEATS is relatively simple to use and is very cost effective when compared with the data recording errors and lack of accuracy inherent in current manual methods. The REDD data from PEATS offers a reference and accurate data which can define the internal condition of a turbine engine. This knowledge allows maintenance personnel the ability to detect, identify and repair equipment deficiencies which may not be found under current maintenance practices. Verification of cockpit instrument calibration alone will have a major impact on system operation. The improvements in fleet readiness, the lower life cycle costs (to include reduced pipe line assets and number of spare engines that a unit must deploy to the field), and the reduction in the unnecessary removal of good parts will provide a good return on investment (ROI) by paying back many times over the cost of using PEATS recording and diagnostic capability. The current reliability improvement initiatives to make the older single engine aircraft safer in the adverse low level flight environment can successfully be implemented with PEATS.

Bibliography:

Oates, Gordon C., Ed, The Aerothermodynamics of Aircraft Gas Turbine Engines, AFAPI TR 78-52, Wright-Patterson AFB, AF Aero Propulsion Lab, 1978.

Pettigrew, James L., (Big Jim), "Diagnostic Monitoring's Potential Impact on Reliability and Performance," 43rd Annual Forum and Technology Display of the American Helicopter Society, St. Louis, MO, May 1987.

-----, "Digital Data Exposes Engine Condition," 35th International Instrumentation Symposium, Instrument Society of America (ISA), Orlando, FL, ISA, 1989.

-----, "Is EMS the Key to Operational Readiness for Less Money with On-Condition Maintenance?", 14th Annual International Logistics Symposium, Clearwater, FL, 1979.

NOTE: Readers with questions or comments can reach Mr. Pettigrew at (817) 336-7411.

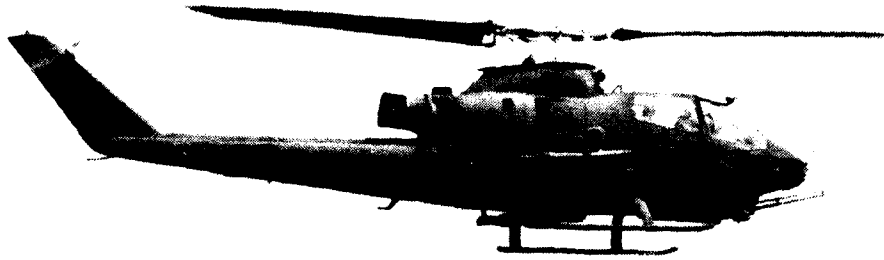


Figure 1. Bell AH-1 Helicopter.

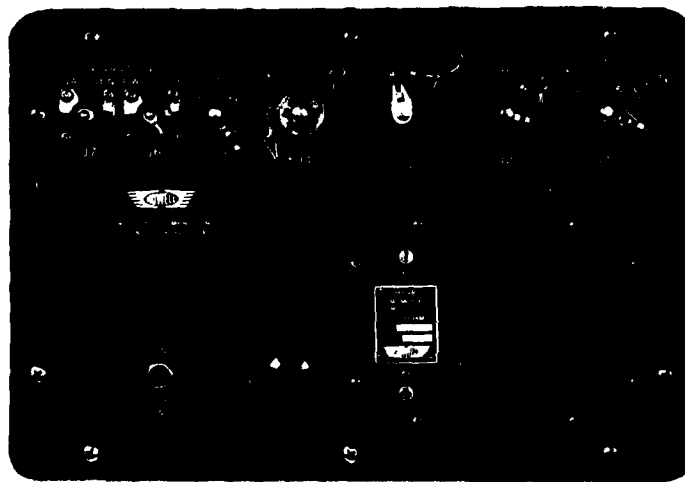


Figure 2. Portable Engine Analyzer Test Set (Peats) display and controls.

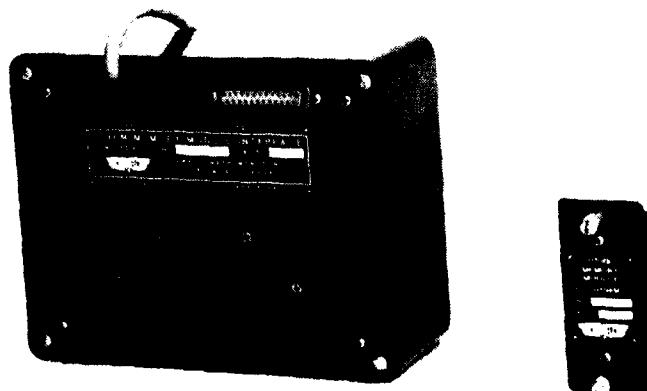


Figure 3. Solid state memory module and memory module interface to RS-232 computer port.

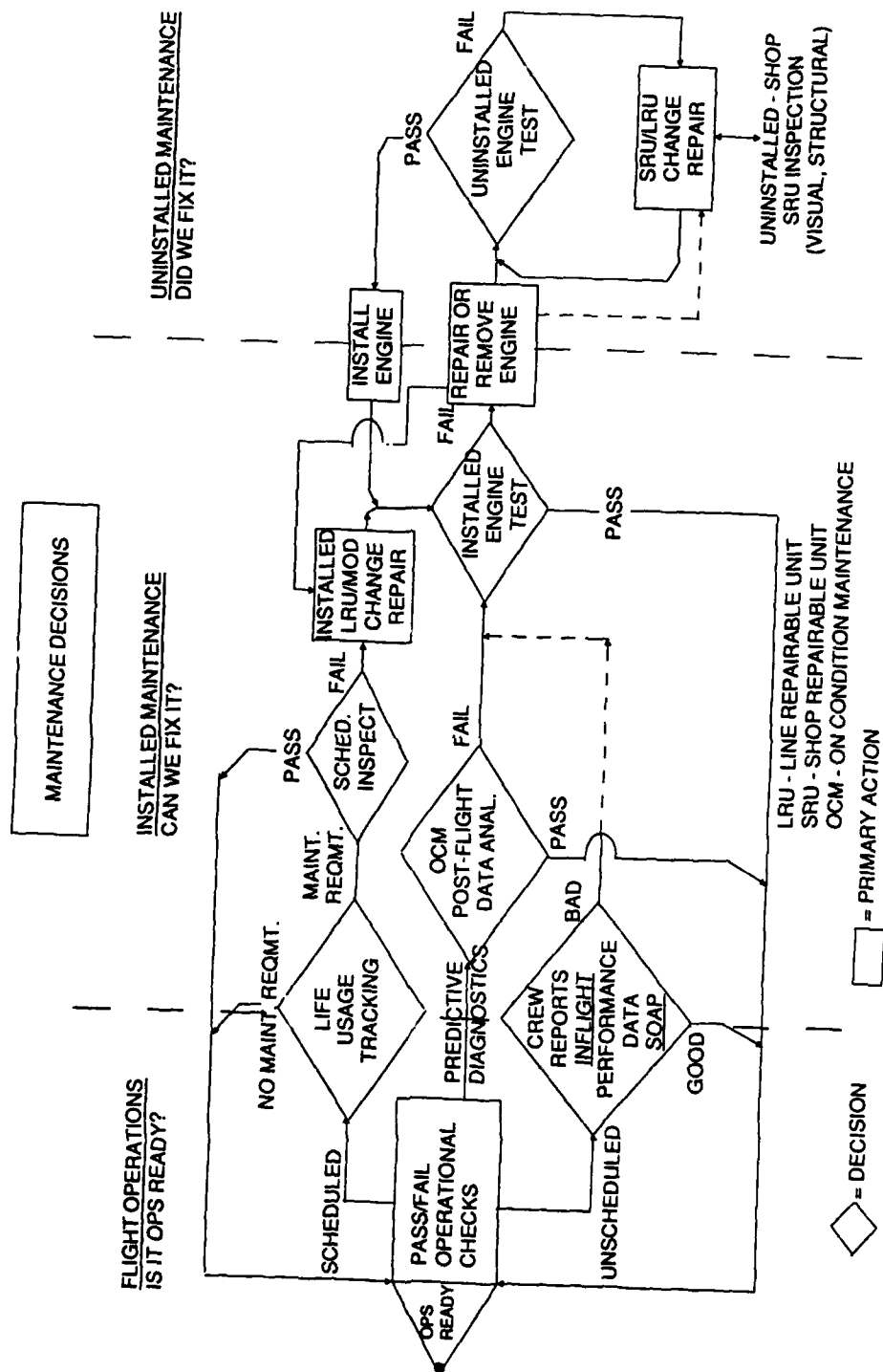


Figure 4. Maintenance decisions required in an aircraft environment.

DATE: 01/22/88 Location: AUS
ACFT# UH-1H 59602 ENG# 15291 TOTAL HRS 7190.47

High Power Performance Summary REFERRED ENGINE DIAGNOSTIC DATA (REDD)

Compressor Parameters 3,4,6,7,P,R

```

.....63.P..R47.....
/\          (-)          0          (+)          /\

```

Turbine Parameters 2,5,F,T

```

.....5.....T.....2..F.....
/\          (-)          0          (+)          /\

```

Overall Parameters 1,E,G,W,M

```

.....E...1G...W.....
/\          (-)          0          (+)          /\

```

NOTE: Points beyond '/' are not scaled
Used 13 Records in Calculations

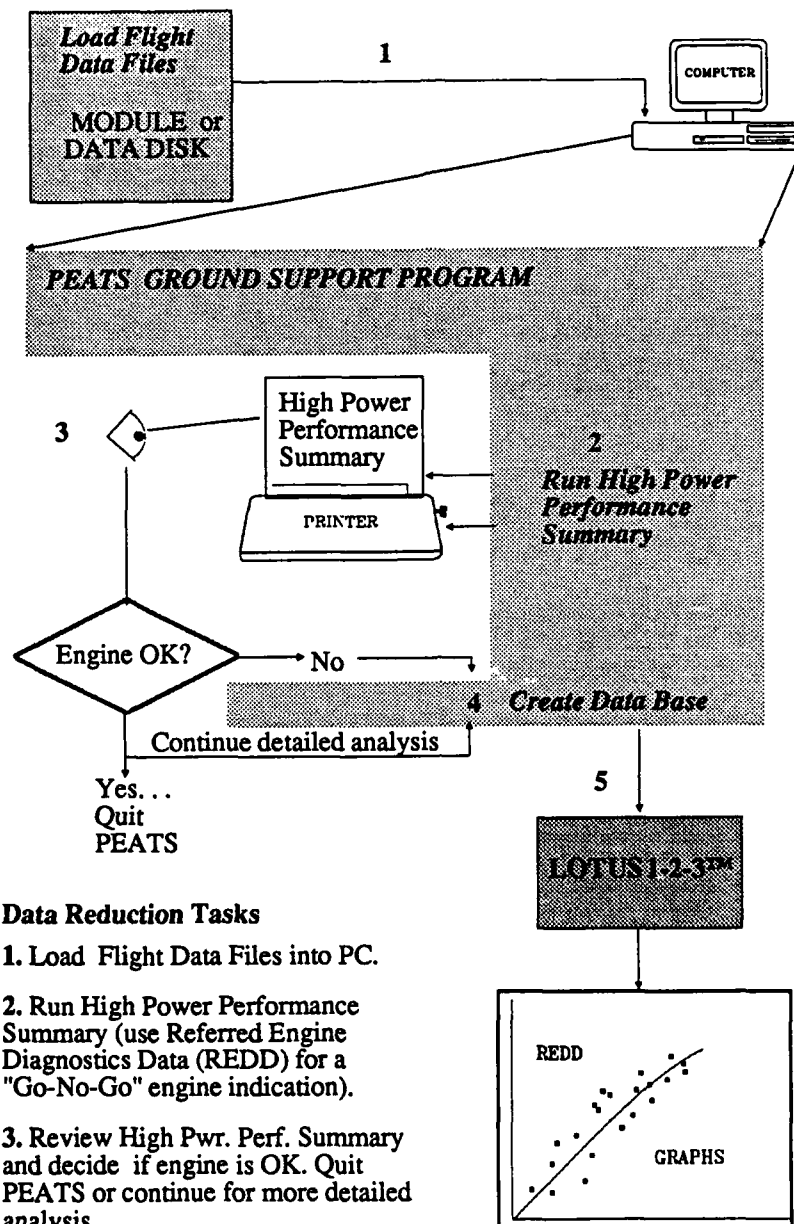
Deltas @ 99.2% Ngc		Deltas @ Qc = 54.7 (psi)	
1 dEGTc:Ngc	(+/-30 degC) 8	5 dNgc:Qc	(+/-1.3%) -0.4
2 dQc:Ngc	(+/-4 psig) 1.5	E dEGTc:Qc	(+/-25 degC) 2
3 dCTR:Ngc	(+/-0.04) -0.013	6 dCPR:Qc	(+/-0.5) -0.171
P dCPR:Ngc	(+/-0.4) -0.091	7 dFFc/CPR:Qc	(+/-8) -0.7
4 dFFc/CPR:Ngc	(+/-8) 0.3		
Delta @ 96% Ngc		Deltas @ FFc = 811 (pph)	
W dEGTc:Ngc	(+/-30 degC) 16	G dEGTc:FFc	(+/-25 degC) 8
EGT Harness Check OK		F dQc:FFc	(+/-3 psig) 1.5
		T dNgc:FFc	(+/-1.3%) -0.0
HIT-CKc BL (STD 488) SET 500		Deltas @ CPR = 6.824	
H dHIT-CKc	(+/-20 degC) -4	R dCTR:CPR	(+/-0.05) -0.00
Margins		FP @ 639 FF (pph)	
EGTc	(>+1 degC) 48	M FP (165 to 235 psia)	****
Ngc	(>+1.0%) 2.4		
TEAC @ 6400 Npt		SHPc @625degC (Ref: 1468) 1621	
Manual- Not Accomplished		SFC SDAY SL (Ref: 0.647) 0.617	
Auto- Not Accomplished			
Vibs (ips) @ 96.0% Ng		Vibs (ips) @ 99.2% Ng	
Ng	(<1.3) 0.45	Ng	(<1.3) 0.54
Np	(<2.5) 0.89	Np	(<2.5) 1.07

c ---- Equivalent Standard Sea-Level Value
* - Indicates Abnormal Engine Performance
**** - Value out of Expected Range-- Check Instrumentation

Comments/Actions Taken

PEATS installed upon completion of Phase 1 inspection. Acft hrs 7189.3
TBO 1485.3. AVCRAD replaced Ng gear box and fixed leak on Npt gear box
during phase. Also xmsn change.

Figure 5. Referred Engine Diagnostic Data (REDD) from a normal engine.



Data Reduction Tasks

1. Load Flight Data Files into PC.
2. Run High Power Performance Summary (use Referred Engine Diagnostics Data (REDD) for a "Go-No-Go" engine indication).
3. Review High Pwr. Perf. Summary and decide if engine is OK. Quit PEATS or continue for more detailed analysis.
4. Create Data Base for REDD graphs.
5. Import data into LOTUS 1-2-3™ and run automatic REDD analysis.

Figure 6. Referred Engine Diagnostic Data (REDD) software capabilities.

DATE: 11/16/89 Location: AUS
ACFT# UH-1H 59602 ENG# 22351 TOTAL HRS 7487.73

High Power Performance Summary REFERRED ENGINE DIAGNOSTIC DATA (REDD)

Compressor Parameters 3,4,6,7,P,R

6P.....3.....R47
/\ (-) 0 (+) /\

Turbine Parameters 2,5,F,T

.....5.....T.....F.....2.....
/\ (-) 0 (+) /\

Overall Parameters 1,E,G,W,M

.....M.....E.....G.....W.....1.....
/\ (-) 0 (+) /\

NOTE: Points beyond '/' are not scaled
Used 18 Records in Calculations

Deltas @ 99.8% Ngc		Deltas @ Qc = 54.7 (psi)	
1 dEGTc:Ngc (+/-30 degC)	30	*5 dNgc:Qc (+/-1.3%)	-1.4
*2 dQc:Ngc (+/-4 psig)	4.9	E dEGTc:Qc (+/-25 degC)	10
3 dCTR:Ngc (+/-0.04)	0.032	*6 dCPR:Qc (+/-0.5)	-0.993
*P dCPR:Ngc (+/-0.4)	-0.738	*7 dFFc/CPR:Qc (+/-8)	17.1
*4 dFFc/CPR:Ngc (+/-8)	20.0		
Delta @ 96% Ngc		Deltas @ FFc = 804 (pph)	
W dEGTc:Ngc (+/-30 degC)	24	G dEGTc:FFc (+/-25 degC)	14
EGT Harness Check OK		F dQc:FFc (+/-3 psig)	1.0
		T dNgc:FFc (+/-1.3%)	-1.1
HIT-CKc BL (STD 488) SET 480		Deltas @ CPR = 6.929	
*H dHIT-CKc (+/-20 degC)	38	*R dCTR:CPR (+/-0.05)	0.11
Margins		FP @ 700 FF (pph)	
EGTc (>+1 degC)	40	M FP (209 to 286 psia)	250
Ngc (>+1.0%)	3.4		
TEAC @ 6400 Npt		SHPc @625degC (Ref: 1342) 1599	
Manual- Not Accomplished		SFC SDAY SL (Ref: 0.625) 0.603	
Q auto (45.4 + 3.0 psig) = 47.8			
Vibs (ips) @ 96.0% Ng		Vibs (ips) @ 99.8% Ng	
Ng (<1.3)	0.14	Ng (<1.3)	0.14
Np (<2.5)	0.80	Np (<2.5)	1.07

c ---- Equivalent Standard Sea-Level Value
* - Indicates Abnormal Engine Performance
*** - Value out of Expected Range-- Check Instrumentation

Comments\Actions Taken

Engine removed from aircraft at CCAD - REPAIRED AND RETURNED TO SERVICE.
L703 PARTS USED IN 13B #2 BEARING AREA - TURBINE COOLING AIR IS HIGHER
EGT harness has loss of insulation fidelity at top end - indicates 35 degs
low. If EGT reading was correct- engine would not top for high Temp.

Figure 7. Referred Engine Diagnostic Data (REDD) for a problem engine with excessive compressor cooling air bleed.

DATE: 06/21/88 Location: AUS
ACFT# UH-1H 17090 ENG# 22367 TOTAL HRS 5102.65

High Power Performance Summary REFERRED ENGINE DIAGNOSTIC DATA (REDD)

Compressor Parameters 3,4,6,7,P,R

```

.....4..7.....P.....6.....R.3.....
/\      (-)          0          (+)      /\

```

Turbine Parameters 2,5,F,T

```

.....2.....F.....5.....T.....
/\      (-)          0          (+)      /\

```

Overall Parameters 1,E,G,W,M

```

.....W..1.....E.GM.....
/\      (-)          0          (+)      /\

```

NOTE: Points beyond '/' are not scaled
Used 20 Records in Calculations

Deltas @ 99.8% Ngc		Deltas @ Qc = 54.7 (psi)	
1 dEGTc:Ngc	(+/-30 degC) -17	*3 dNgc:Qc	(+/-1.3%) 1.6
*2 dQc:Ngc	(+/-4 psig) -5.4	E dEGTc:Qc	(+/-25 degC) -2
3 dCTR:Ngc	(+/-0.04) 0.035	6 dCPR:Qc	(+/-0.5) 0.193
P dCPR:Ngc	(+/-0.4) -0.090	7 dFFc/CPR:Qc	(+/-8) -6.6
*4 dFFc/CPR:Ngc	(+/-8) -8.3		
Delta @ 96% Ngc		Deltas @ FFc = 804 (pph)	
W dEGTc:Ngc	(+/-30 degC) -23	G dEGTc:FFc	(+/-25 degC) 2
EGT Harness Check OK		F dQc:FFc	(+/-3 psig) 1.2
		*T dNgc:FFc	(+/-1.3%) 1.9
HIT-CKc BL (STD 488) SET 462		Deltas @ CPR = 6.929	
H dHIT-CKc	(+/-20 degC) 9	R dCTR:CPR	(+/-0.05) 0.04
Margins		FP @ 634 FF (pph)	
EGTc	(>+1 degC) 52	M FP (175 to 246 psia)	215
*Ngc	(>+1.0%) 0.4		
TEAC @ 6400 Npt		SHPc @625degC (Ref: 1151) 1628	
*Q man	(43.7 + 3.0 psig) = 41.3	SFC SDAY SL (Ref: 0.625) 0.654	
Auto- Not Accomplished			
Vibs (ips) @ 96.0% Ng		Vibs (ips) @ 99.8% Ng	
Ng	(<1.3) 0.87	Ng	(<1.3) 1.19
Np	(<2.5) 1.44	Np	(<2.5) 1.37

c ---- Equivalent Standard Sea-Level Value
* - Indicates Abnormal Engine Performance
**** - Value out of Expected Range-- Check Instrumentation

Comments/Actions Taken

PEATS installed at completion of Phase 2 inspection. Acft time 5101.5, engine 1840.5 TSO,TSN 4440.5. This is the first acft that has been tested under the PEATS program where both acft and PEATS instrumentation were OK. Six hours after this test, this aircraft had an off airfield emergency landing due to Gas Generator bearing failure and engine siezure.

Figure 8. Referred Engine Diagnostic Data (REDD) for engine six hours before bearing failure caused emergency landing.

PEATS - T53 - VIBRATION ANALYSIS

ACFT# 17090, ENG# 22367, 21-JUN-88

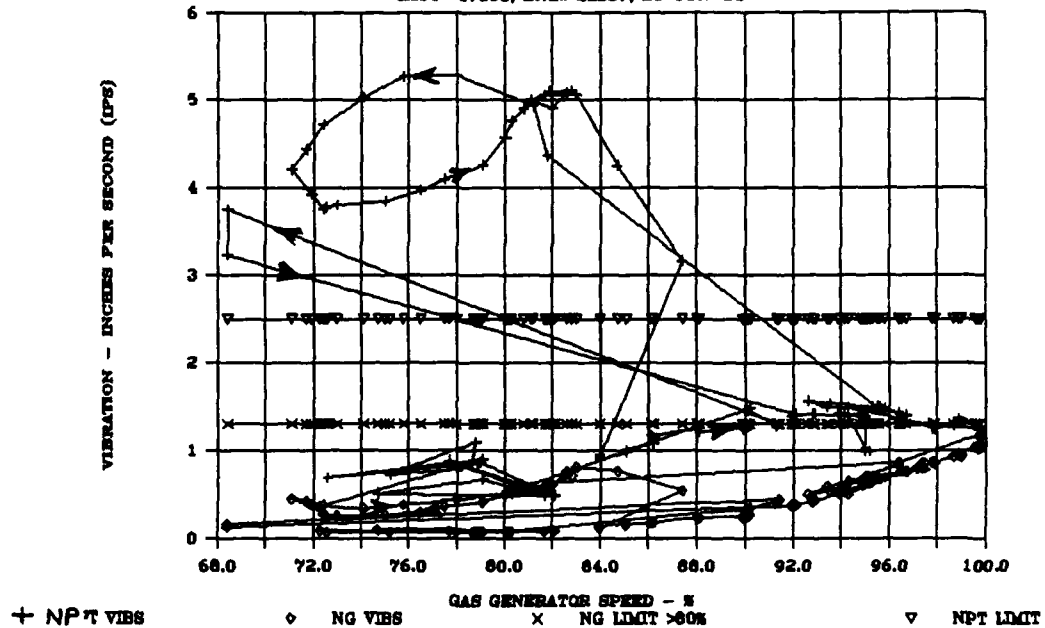


Figure 9. Graph of vibration versus gas generator speed from engine six hours before bearing failure.

PEATS - T53 - VIBRATION ANALYSIS

ACFT# 17090, ENG# 22367, 21-JUN-88

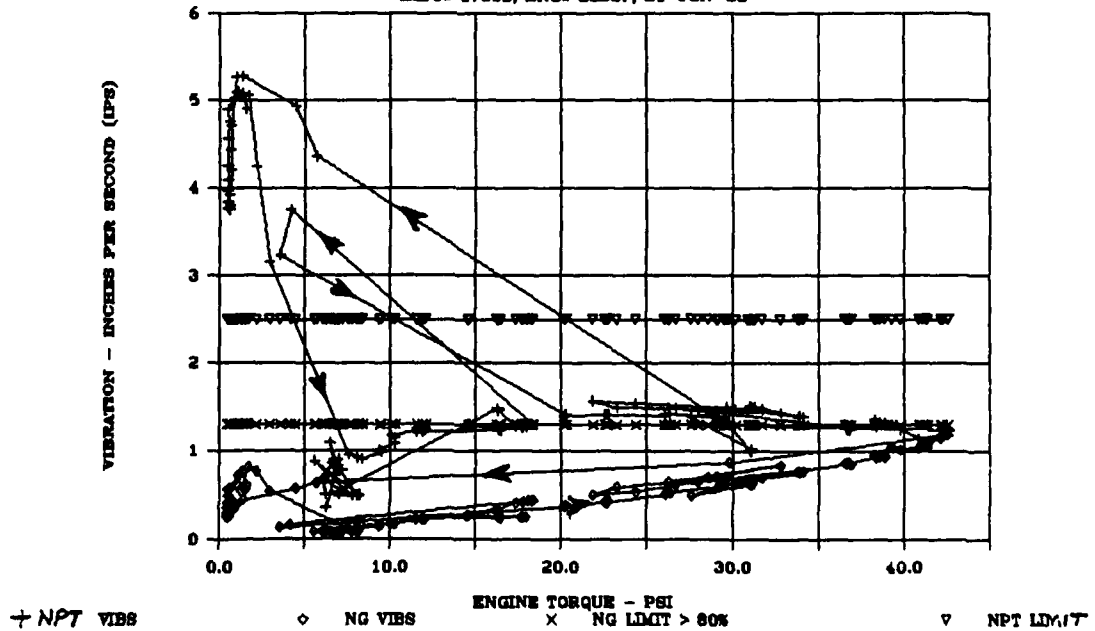


Figure 10. Graph of vibration versus engine torque from engine six hours before bearing failure.

PEATS - T53 - VIBRATION ANALYSIS

ACFT# 17090, ENG# 22367, 21-JUN-88

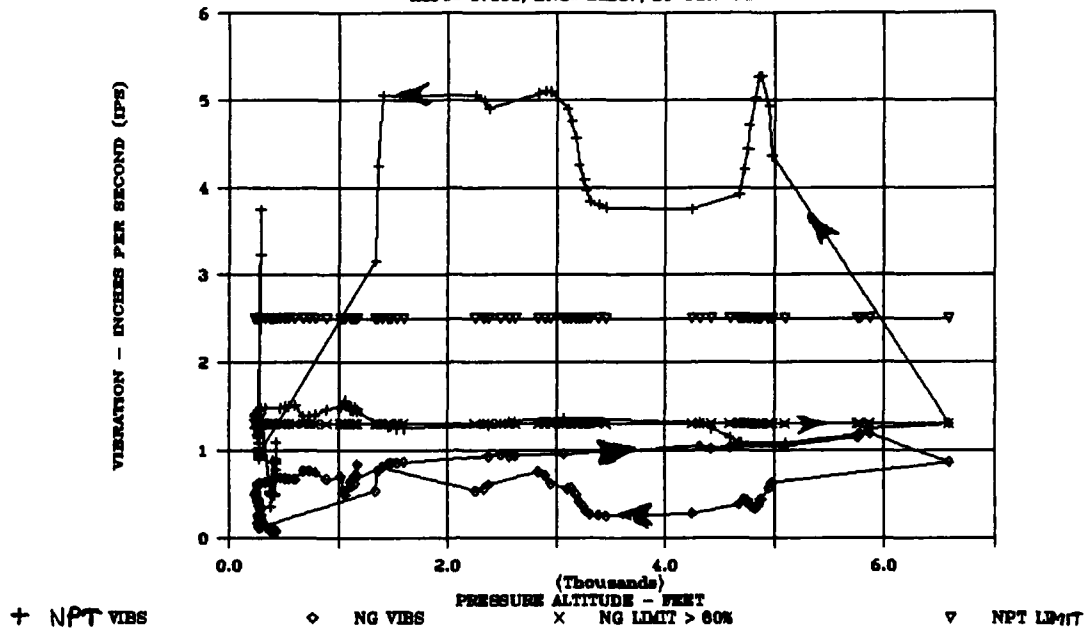


Figure 11. Graph of vibration versus altitude from engine six hours before bearing failure.

PEATS - T53 - VIBRATION ANALYSIS

ACFT# 17090, ENG# 22367, 21-JUN-88

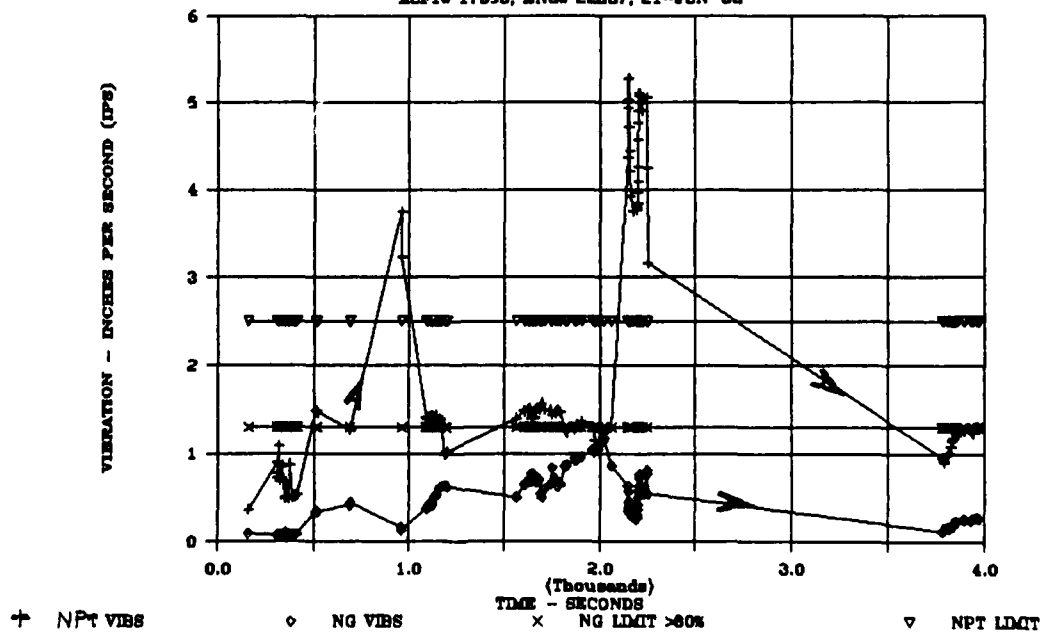


Figure 12. Graph of vibration versus time after start from engine six hours before bearing failure.

PEATS - L13B - ENGINE ANALYSIS

ACFT# 15262, ENG# 16502, 23-JUN-89

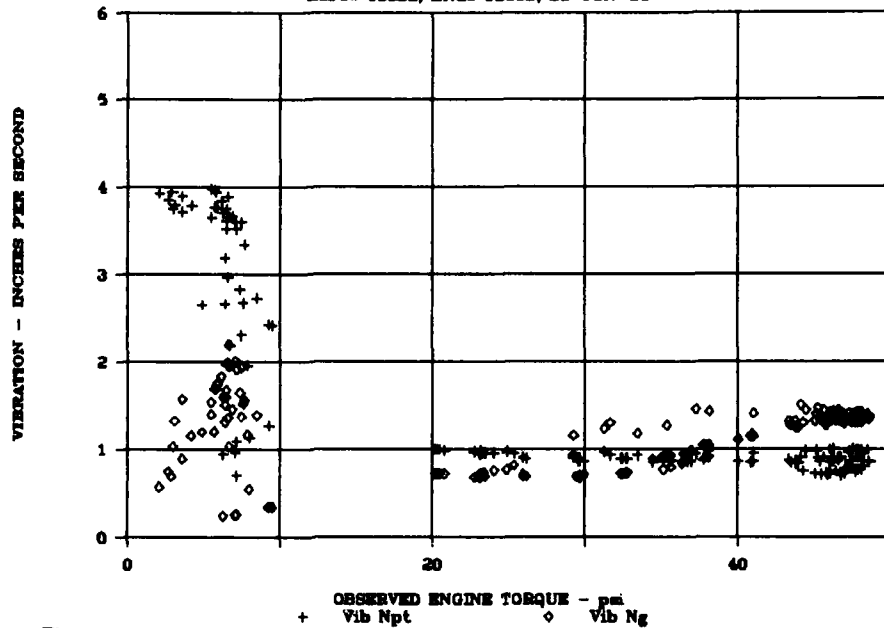


Figure 13. Graph of vibration versus torque for engine experiencing NG speed stagnation at high power.

PEATS - L13B - ENGINE ANALYSIS

ACFT# 15262, ENG# 16502, 23-JUN-89

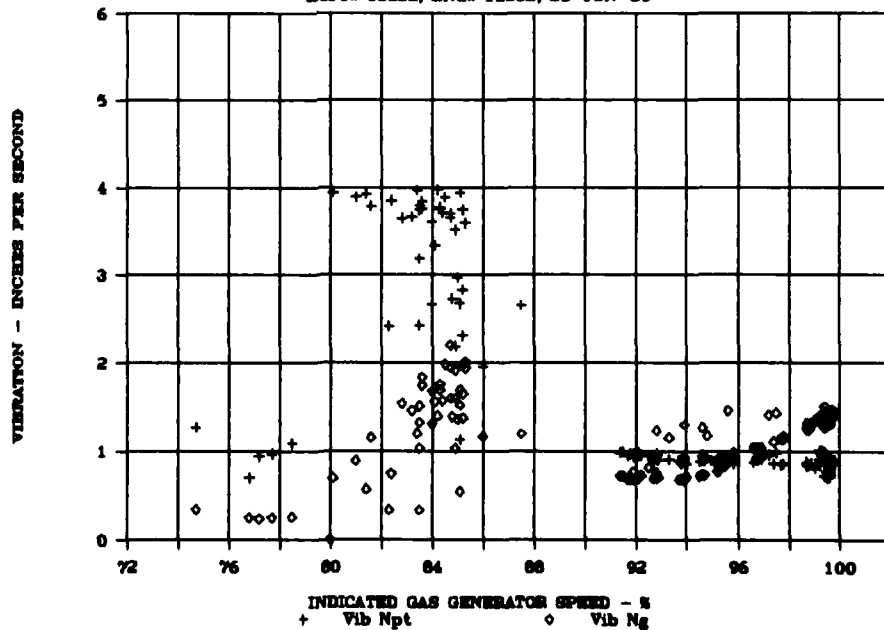


Figure 14. Graph of vibration versus gas generator speed for engine experiencing NG speed stagnation at high power.

PEATS - L13B - ENGINE ANALYSIS

ACFT# 15362, ENG# 16502, 23-JUN-89

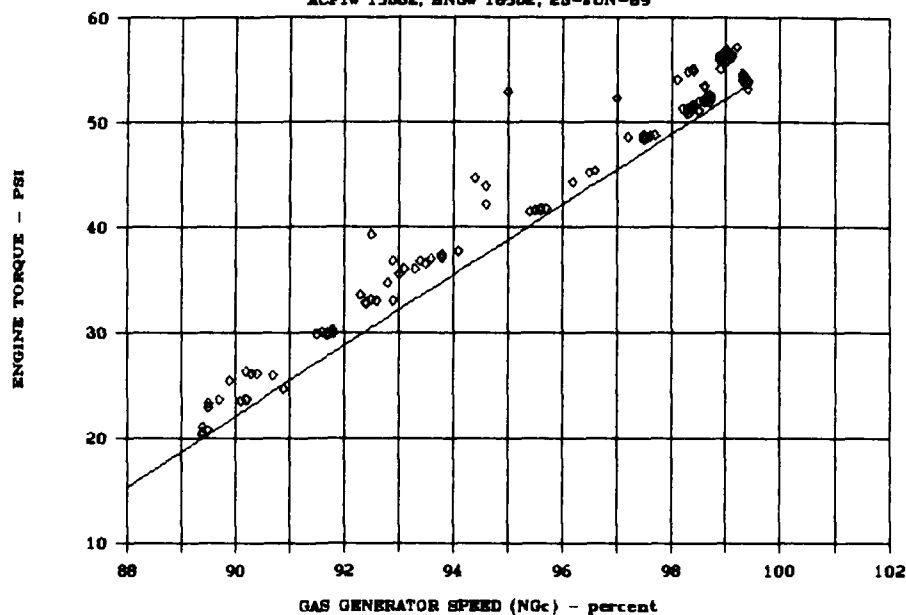


Figure 15. Graph of torque versus NG speed for engine experiencing NG speed stagnation.

PEATS - L13B - ENGINE ANALYSIS

ACFT# 15362, ENG# 16502, 23-JUN-89

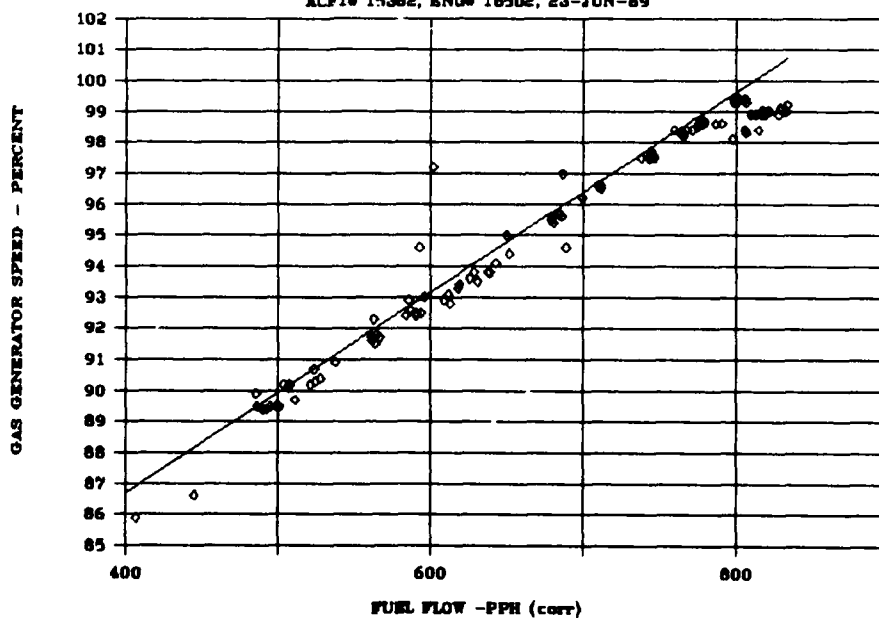


Figure 16. Graph of NG speed versus fuel flow for engine experiencing NG speed stagnation. Note the half percent slow down after 800 PPH .

PREDICTIVE MAINTENANCE

Chairman: John S. Mitchell
Palomar Technology International

FIFTEEN PROVEN PREDICTIVE MAINTENANCE TECHNOLOGIES

John W. Flude, P.E.
NUS Corporation
Gaithersburg, MD 20877

Abstract: This paper discusses the application of fifteen predictive maintenance technologies that have been productively used in industry to monitor equipment parameters. These technologies contain the diagnostic and trending capabilities to turn a labor intensive preventive maintenance program into a labor saving predictive maintenance program.

This paper discusses the physical phenomenon these technologies uses, their limitations, some applications, and the implementation techniques. The paper also discusses the facility of these programs to such techniques as trending, correlation of data, computer loading, storage, display, and analysis. Also discussed will be problems in the introduction of these technologies, both technical and practical.

Key Words: Emission-acoustic, filtration, flow-measurement, leak-detection, maintenance, oil-analysis, predictive, radiography, temperature, timing-testing, trace-element, vibration, visual-inspection

Background: Every organization with operating equipment has some kind of maintenance program. These maintenance programs are a combination of corrective maintenance and preventive maintenance. **Corrective** maintenance restores failed equipment to an operable condition. **Preventive** maintenance consists of **scheduled** maintenance and **predictive** maintenance. Scheduled maintenance is performed on a prescribed time or operating hours schedule to reduce the likelihood of failure. Predictive maintenance refers to the measurement of relevant parameters (monitoring) to detect degradation which will lead to failure. Maintenance performed on degraded but un-failed equipment as a result of predictive maintenance monitoring to prevent failure is called **on-condition** maintenance.

Introduction: The concept of predictive maintenance is rapidly gaining acceptance throughout industry. A good predictive maintenance program can reduce total operating and maintenance costs. Setting up a predictive maintenance program typically involves a review of technical guidance and operating history, the establishment of proper criteria or limits, the selection of proper tests, and the use of proper maintenance and surveillance procedures. Three of the four above steps -- criteria, test, and procedures -- depend on the proper selection of a predictive maintenance technology for their success.

This paper discusses the application of fifteen predictive maintenance technologies that have been productively used in industry to monitor equipment parameters. These technologies contain the diagnostic and trending capabilities to turn a labor intensive preventive maintenance program into a labor saving predictive maintenance program.

Vibration / Shock Pulse Analysis: Of all of the technologies in this paper, vibration analysis probably comes to mind first when someone mentions "predictive maintenance." This technology is well established and widely used as a predictive maintenance tool.

Shock pulse analysis is a special form of vibration analysis which looks at the noise pattern \$shock pulse\$ set up by an individual defect in a specific part such a bearing ball.

The results of such testing are numerical, making them easy to trend. Equipment exists in the commercial marketplace to automatically take, record, analyze, and display the data. Often this equipment is portable. Due to standardization, data from one machine, or taken at one time, can be compared to other, similar data.

In fact, the biggest problem with vibration analysis is its apparent simplicity coupled with its actual complexity. The automated equipment, which seems to supply the requisite sophistication is actually a trap unless the operator and the analyst fully understand the equipment and the phenomenon. Not that many people do. Not only is vibration analysis very complex, it is rapidly changing. It is extremely difficult to keep up with all the new developments in this field.

Furthermore, vibration analysis is expensive. Although the savings in avoided operating costs and capital equipment replacement costs can far outweigh the costs of the monitoring equipment, vibration monitoring still costs a lot of money. As equipment increases in sophistication, costs go up quickly. At the same time training and qualification costs multiply. Equipment line-ups must be modified -- although some automated equipment is designed to minimize this. If management cannot see the cost benefits of vibration monitoring, [predictive maintenance,] they are not likely to pay for it.

Oil Analysis / Debris Analysis / Tribology: Oil analysis includes several forms of analysis -- spectroscopy, chemical analysis, ferrography, and particle counting. All of these, except for some forms of chemical analysis, are based on the fact that oil transports worn parts of the machinery, or broken down particles of lubricant, out of the machine. The major difference between the technologies is in the size of the particles detected and analyzed.

Every piece of equipment that moves produces rubbing and

wear. Analysis of the lubricant can yield important insight into the condition of the lubricated surfaces. Overheating and contamination can also be detected.

Spectrographic oil analysis generates a large amount of numeric data which can be easily trended. An analyst must be careful, however, because many types of analysis equipment produce widely varying data (scatter). For this reason, users of spectrographic analysis are often prompted by their laboratories to "send another sample."

Ferrography produces evolving indications of progressive wear, but its indications tend to be more subjective and "adjective" based, which are hard to computerize.

Particle counting usually is an alarm that indicates that the machine has already failed. Trending is usually not feasible.

Typically, providing for a means of taking the sample is the largest problem in starting an oil analysis program. The location must be safe for the technician, must provide a truly representative sample, and must provide an uncontaminated sample.

Advanced Filtration Systems: Small pore, high efficiency filters can be used to augment wear and contamination monitoring systems such as oil analysis. Whereas oil analysis techniques take a sample at a given point in time, these filter systems are, in effect, always on. Material given off only once or intermittently may be missed by an oil analysis.

On the downside, the filter systems are hard to install unless they replace another filter. The filter may be hard to monitor (replace) in some inaccessible systems. And, of course, the entrained material will not be detected until the filter is retrieved and analyzed. This may be after the unit has failed.

Trace Element Sensing: Like oil analysis trace element sensing monitors wear or contamination. Trace element sensing utilizes a monitor in the flow stream typically keyed to only one type of wear or contamination. The target element may be part of the normal composition of one component. In another use of trace element sensing, an indicator is introduced into one side of a component such as a heat exchanger. If the heat exchanger leaks internally, the trace element will be detected on the other side.

Typically this monitor does not provide data on the amount of the trace element present but only senses presence of the element and provides an alarm.

Contact Pyrometry / Infrared Imaging / Temperature Measurement: Whenever the failure mode of a failed or failing part generates heat, that heat can be detected by the proper instrument. Occasionally, installed thermometers or resistance temperature detectors (RTDs) can be used. More often, however, sensors such as a thermocouple must be placed on a suspected heated surface, or stand-off sensing with infrared detectors may be used. Calibration of the sensors is typically critical for these applications. Sensor calibration can vary for a variety of reasons: thermometers are subject to drift, thermocouples also can drift and, in addition, must have a reference standard, and infrared sensors must be calibrated against a "black body."

Implementation, except for calibration, is usually simple as long as the equipment is accessible. Once in place and calibrated the temperature can be recorded at some other location.

Individual temperatures are easy to trend, if allowances for data scatter are made. With technologies such as infrared imaging, however, the data are often in the form of a two-dimensional image -- a photograph or monitor screen -- and a system must be used to define the location of the object of interest in the photo. This will require manual input.

Electronic / Sonic Leak Detection / Analysis: As a fluid flows through a small orifice such as a leak, the pressure in the fluid drops. The fluid may actually produce flow noises which can be detected by sensitive equipment. More often the leak detection instrument detects cavitation caused by the severe pressure drop flashing the fluid into vapor. As the leak hole size, and the leakage, increases the noise level will increase due to the increased flow. Eventually, however, there will be less pressure drop, reducing the intensity of cavitation. Therefore, as the leak path effective diameter increases, the sound level will increase up to a certain maximum and then decrease.

With the present state of the art it is very hard to quantify the leakage rate from the sound level. While this technology works well at detecting leakage, nearly ideal conditions are required to quantify the leakage accurately enough to trend the data. This technology is successful at determining the leak rate if the operator is able to compare the signal with known reference signals from the same or very similar components -- normally valves. The area must not have excessive background noise.

Different fluids produce cavitation noises that differ in the quality or "timbre" of the sound. Also as the sound producing phenomenon changes from strong cavitation to weak cavitation to primarily flow noise, the timbre will change. Nevertheless, even experienced operators will not be able to

tell the leakage rate from the quality of the sound alone.

Nonintrusive Flow Measurement of Fluids: There are several types of nonintrusive flow measurement devices.

Doppler flow meters actively transmit sound into the fluid stream and measure the flow induced frequency shift of the signal echoed off of material in the fluid stream.

Time difference flow meters transmit acoustic signals upstream and downstream in the fluid path and measure the difference in time that each signal requires.

Vortex flow meters measure the rate of creation of flow vortexes downstream of an induced obstruction.

Flow noise flow meters measure the intensity of flow noise inside the pipe.

Doppler and time-difference meters are the most widely used non-intrusive types in use today. Doppler flow meters are the flow meters of choice in fluid streams with large amounts of undissolved matter or air bubbles since they rely on this material to reflect the signal. Time difference flow meters are best where the fluid is clear because the suspended matter interferes with the transmission of the signal between the transducer pairs.

The results are easily trendable. If used for pump performance testing, full pump head-flow curves should be developed. An individual curve is useful for diagnosing a pump problem, or the pump-head at a particular flow can be plotted for trending.

All flow transducers are sensitive to the flow profile (the net velocity along the axis of the pipe vs position of the flow vector relative to the centerline of the pipe) of the measured fluid. Transducers selection and control of the factors affecting the flow profile are critical to any type of flow meter.

Hyperbaric Dew Point Measurement: Compressed air stored in a container at a site will very likely contain some amount of dissolved water. This water can cause problems with the storage container, other handling equipment, or with processes. If the air is expanded [the pressure reduced] the weight of water per unit weight of air does not change but the weight of water per unit volume of air does change. Most moisture testing equipment measures water quantity per unit volume.

To avoid corrosion, the air within these components must not approach the dew point. Monitoring dew point can either be done at high storage pressure or at a reduced pressure. Test equipment capable of measuring dew point at high pressure

is highly specialized and expensive. Equipment capable of measuring dew point at a reduced, or even atmospheric, pressure is more moderately priced, however the results obtained must be corrected to the pressure within the equipment.

Precise Timing Testing and Trending / Sequential Testing: If valve packing becomes old and stiff, if a valve stem corrodes or galls, if a power operator degrades, if the voltage to a power operator drops, or if its internal wiring insulation resistance drops, if the valve stems bends, if the internal fluid flow or pressure increases, or if mechanical or electrical indication deforms or becomes loose, indicated actuation time will be effected. Often actuation time is the only accessible indication of internal component condition. Trending the actuation time of equipment is an old technique, but it must be used carefully. Many factors can affect operating time and it is usually hard to determine which one is causing a change.

Sequential testing uses timing testing techniques to measure the elapsed time of a series of events in sequence to verify the occurrence and the time of operation of each event.

Installed switches, light cells, pressure or magnetic switches, and photocells can all replace the human eye in timing testing to increase precision and repeatability. It is important that these items be accurately placed and that their location be understood in terms of the movement of the tested component. For instance, does a valve start to come open before any indication is received? Can other factors cause an indication? The results of this testing can easily be recorded and trended, but the user of such data should be aware of how the data were taken and the potential for error.

Visual and Remote Visual Inspection / Fiber Optics / Mini TV / Video / Camera Recording: Sometimes the best predictive maintenance and monitoring system is to look at the component of system and observe its condition.

Sometimes this is not possible. The item to be inspected is inaccessible or is in a dangerous location. Remote sensors allow the inspector to be in one place and to inspect another place. These systems can be relatively simple devices -- such as fiber optic equipment -- or can be as sophisticated as remotely operated, self-contained robots with installed cameras and other sensors (e.g. radiation or explosives detectors).

The biggest drawback of direct observation also affects remote visual observation: the results are typically subjective and not amenable to objective analysis or trending.

Dynamic Radiography: Dynamic radiography is similar to the fluoroscopy used in the medical profession. A radiation source is placed to project through the object under test with the detector placed on the other side. The sensor will have a screen or will be directed to a screen. Motions of objects inside the component will be apparent. This can be a large improvement over the single view given by conventional radiography. The image obtained can also be recorded for later evaluation or comparison. One of the best uses for dynamic radiography equipment is to show the source of other signals or to confirm a problem.

The equipment used with this technology is, as might be expected, quite large and expensive. Operators must access two sides of the equipment. Furthermore, the device produces a semi-transparent image of the internal parts of the component under test which must be interpreted by an experienced operator.

Electrical System / Cable Condition Monitoring: Electrical cables, cable connections, and internal wiring and insulation of components are subject to deterioration with age. Impedance and insulation resistance readings monitor the present condition of these component parts. Temperature corrections should be applied where needed.

Often, to monitor electrical system and cabling conditions the equipment must be secured and tagged out for the duration of testing. This can be quite expensive.

Acoustic Emission / Strain Gauging / Interferographs: As micro-crystalline material, such as steel, is put under tension or compression beyond the yield point, the crystals begin to break and tear along their crystal boundaries. Sensitive instruments can detect this energy in the form of sound waves known as acoustic emission. Note that the yielding may be very localized and may not affect the overall integrity of the component.

Deformation prior to reaching the yield point can be measured with strain gauges.

Interferographs produce two electronic images of equipment -- before and after a load is applied. The device displays deformation by electronically cancelling out all parts of a piece of equipment that do not move and displaying only the parts that do move.

These systems provide data on the severity of loads and on the number of cycles undergone by equipment. The data are most useful as an alarm or for comparison to other data such as timing or vibration.

Fotonic Sensors: Fotonic sensors count. They may count drops of lubricating oil, a target on a rotation shaft, or the number of objects moving down a conveyor. They may also be used to detect the presence of something which might trigger an action, an alarm, or another test to be performed.

This type of testing is easy to set up. A video camera, with a light source if required by the equipment, must be installed. Rarely is any disruption to any equipment required.

Break-away Analysis / Coast-Down Testing: All bearings have some friction and most steam valves on turbines leak to some extent. Steam leakage can be compared to another time period or another machine by simple testing.

Steam is applied to the closed steam throttle valves. If the valves did not leak, the turbine would not rotate. A small amount of leakage will cause the turbine to begin rotating. The revolution rate after a fixed amount of time can then be used as a comparative measure of the leakage rate.

Similarly, the reverse throttle valves can be tested by measuring the revolution rate after a period of time (or by the time required to stop) of a turbine that is coasting down.

The biggest advantage of this test is that it requires very little equipment except a means of measuring turbine speed and a stopwatch. One disadvantage is that the test can only be run when the turbine is being shut down. The biggest disadvantage is that many factors not under the control of the tester can effect test results. The test is best used as an indicator of the need for other testing or when no other test can be done.

Trending: Since the purpose of predictive maintenance is to avoid failure, the data collected up to the present must be projected or extrapolated into the future to be of value. If the data collected are purely numeric, and the degradation process is well understood, the analyst can use a mathematical model. Although mathematical projections may be used for alert purposes, it is rarely the case that the failure mechanism is understood well enough to predict the exact point in time when failure will occur. Obviously when analyzing subjective data, and even when analyzing numeric data, only the well-trained human mind has the capacity to assimilate and synthesize the amount of data presented and come to a valid conclusion.

Correlation of data: One of the advantages of collecting data through a number of different technologies is the ability to correlate the data -- to compare the output of one technology to the output of another.

One obvious application of this is where one technology

produces an alert (or alarm) and then another technology can be used for diagnostics or close monitoring. Such is the case with trace element sensing and oil analysis or leak diagnostics. When a trace element is sensed in rotating equipment, the frequency of oil testing can be increased. If a trace element is sensed on the opposite side of a heat exchanger from which it has been introduced, then a search for the leakage path can begin.

Often, indications from different technologies can complement each other. If a bearing in a piece of rotating equipment begins to fail, simultaneous indications will often be seen in the vibration monitoring and in the oil analysis.

Implementation Politics: Predictive maintenance systems cost money. Engineers often have trouble justifying the expense of a predictive maintenance program which has an intangible payoff. This a problem that needs to be faced straight-on. Engineers, used to working in the real world with real equipment, must learn that intangibles have value. If someone asserts that, because a potential system has only intangible benefits, and therefore should not be used in a cost-benefit analysis, then they are assigning a real value of zero to that system. This is just as inaccurate as the engineers' tendency to assign the most optimistic value to the project. Implementation of a new predictive maintenance program should be subjected to the same cost-benefit analysis of any other program, but the intangible benefit require special handling. Expected value (the product of potential value and probability of occurrence), averted costs (downtime, turnover), competitive advantage or advantage lost, range of potential value, and a realistic presentation of all associated costs are all part of the cost-benefit equation and should be used.

APPENDIX

MFFG PUBLICATIONS

Both printed and microfiche copies of the following MFFG publications (1-12) whose catalog numbers start with either "AD" or "COM" may be obtained from the National Technical Information Service (NTIS).

NTIS
5285 Port Royal Road
Springfield, Virginia 22161

1. Glossary of Terms AD 721 354
2. Proceedings of Meeting Nos. 1-9 (set of five) AD 721 359
Meeting Nos. 1-5 Papers and discussion on Failure
Analysis and Control
Meeting No. 6 "Detection, Diagnosis and Prognosis"
December 6, 1968
Meeting No. 7 "Failure Mechanisms as Identified with
Helicopter Transmissions"
March 27, 1969
Meeting No. 8 "Critical Failure Problem Areas in the
Aircraft Gas Turbine Engine"
June 25-26, 1969
Meeting No. 9 "Potential for Reduction of Mechanical
Failure through Design Methodology"
November 5-6, 1969
3. Proceedings of Meeting No. 10 AD 721 912
"Vibration Analysis Systems"
January 21-22, 1970
4. Proceedings of Meeting No. 11 AD 724 475
"Failure Mechanisms: Fatigue"
April 7-8, 1970
5. Proceedings of Meeting No. 12 AD 721 913
"Identification and Prevention of Mechanical
Failures in Internal Combustion Engines"
July 8-9, 1970
6. Proceedings of Meeting No. 13 AD 724 637
"Standards as a Design Tool in Surface Specifi-
cation for Mechanical Components and Structures"
October 19-20, 1970
7. Proceedings of Meeting No. 14 AD 721 355
"Advances in Decision-Making Processes in
Detection, Diagnosis and Prognosis"
January 25-26, 1971

8. Proceedings of Meeting No. 15 AD 725 200
"Failure Mechanisms: Corrosion"
April 14-15, 1971
9. Proceedings of Meeting No. 16 AD 738 855
"Mechanical Failure Prevention
through Lubricating Oil Analysis"
November 2-4, 1971
10. Proceedings of Meeting No. 17 AD 750 411
"Effects of Environment upon Mechanical
Failures, Mechanisms and Detection"
April 25-27, 1972
11. Proceedings of Meeting No. 18 AD 772 082
"Detection, Diagnosis and Prognosis"
November 8-10, 1972
12. Proceedings of Meeting No. 19 (NBS SP 394) COM-74-50523
"The Role of Cavitation in
Mechanical Failures"
October 31-November 2, 197

Printed copies of the following publications may be obtained from the
U. S. Government Printing Office.

Superintendent of Documents
U. S. Government Printing Office
Washington, DC 20402

Microfiche copies of these publications may be obtained from the NTIS.

13. Proceedings of Meeting No. 20 (NBS SP 423) . . . SN003-003-01451-6
"Mechanical Failure - Definition
of the Problem"
May 8-10, 1974
14. Proceedings of Meeting No. 21 (NBS SP 433) . . . SN003-003-01639-0
"Success by Design: Progress
through Failure Analysis"
November 7-8, 1974
15. Proceedings of Meeting No. 22 (NBS SP 436) . . . SN003-003-01556-3
"Detection, Diagnosis and Prognosis"
April 23-25, 1975
16. Proceedings of Meeting No. 23 (NBS SP 452) . . . SN003-003-01664-1
"The Role of Coatings in the Pre-
vention of Mechanical Failures"
October 29-31, 1975

17. Proceedings of Meeting No. 24 (NBS SP 468) . . . SN003-003-01760-4
"Prevention of Failures in Coal
Conversion Systems"
April 21-24, 1976
18. Proceedings of Meeting No. 25 (NBS SP 487) . . . SN003-003-01829-5
"Engineering Design"
November 3-5, 1976
19. Proceedings of Meeting No. 26 (NBS SP 494) . . . SN003-003-01844-9
"Detection, Diagnosis and Prognosis"
May 17-19, 1977
20. Proceedings of Meeting No. 27 (NBS SP 514) . . . SN003-003-01935-6
"Product Durability and Life"
November 1-3, 1977
21. Proceedings of Meeting No. 28 (NBS SP 547) . . . SN003-003-02083-4
"Detection, Diagnosis and Prognosis"
November 28-30, 1978
22. Proceedings of Meeting No. 29 (NBS SP 563) . . . SN003-003-02120-2
"Advanced Composites"
May 23-25, 1979
23. Proceedings of Meeting No. 30 (NBS SP 584) . . . SN003-003-02272-1
"Joint Conference on Measurements and
Standards for Recycled Oil/Systems
Performance and Durability"
October 23-26, 1979
24. Proceedings of Meeting No. 31 (NBS SP 621) . . . SN003-003-02428-7
"Failure Prevention in Ground
Transportation Systems"
April 22-24, 1980
25. Proceedings of Meeting No. 32 (NBS SP 622) . . . SN003-003-02361-2
"Detection, Diagnosis and Prognosis:
Contribution to the Energy Challenge"
October 7-9, 1980
26. Proceedings of Meeting No. 33 (NBS SP 640) . . . SN003-003-02425-2
"Innovation for Maintenance
Technology Improvements"
April 21-23, 1981
27. Proceedings of Meeting No. 34 (NBS SP 652) . . . SN003-003-02488-1
"Damage Prevention in the
Transportation Environment"
October 21-23, 1981

Printed copies of the following MFPG publications are available from Cambridge University Press, 110 Midland Avenue, Port Chester, NY 10573.

- 28. Proceedings of Meeting No. 35
"Time Dependent Failure Mechanisms
and Assessment Methodologies"
April 20-22, 1982
- 29. Proceedings of Meeting No. 36
"Technology Advances in Engineering and
Their Impact on Detection, Diagnosis
and Prognosis Methods"
December 6-10, 1982
- 30. Proceedings of Meeting No. 37
"Mechanical Properties, Performance
and Failure Modes of Coatings"
May 10-12, 1983

Note: The proceedings of meeting no. 38 were not published because of the format of the meeting.

- 31. Proceedings of Meeting No. 39
"Failure Mechanisms in High
Performance Materials"
May 1-3, 1984
- 32. Proceedings of Meeting No. 40
"Use of New Technology to Improve
Mechanical Readiness, Reliability
and Maintainability"
April 16-18, 1985
- 33. Proceedings of Meeting No. 41
"Detection, Diagnosis and Prognosis
of Rotating Machinery to Improve
Reliability, Maintainability, and
Readiness through the Application
of New and Innovative Techniques"
October 28-30, 1986

The proceedings of meeting nos. 42 and 43 are in press.

- 34. Proceedings of Meeting No. 42
"Technology Innovation - Key to
International Competitiveness"
September 15-17, 1987
- 35. Proceedings of Meeting No. 43
"Advanced Technology in
Failure Prevention"
October 3-6, 1988

SECURITY CLASSIFICATION OF THIS PAGE

REPORT DOCUMENTATION PAGE				
1a REPORT SECURITY CLASSIFICATION Unclassified		1b RESTRICTIVE MARKINGS None		
2a SECURITY CLASSIFICATION AUTHORITY		3 DISTRIBUTION/AVAILABILITY OF REPORT Unclassified/Unlimited		
2b DECLASSIFICATION/DOWNGRADING SCHEDULE				
4 PERFORMING ORGANIZATION REPORT NUMBER(S) MFPG-44		5 MONITORING ORGANIZATION REPORT NUMBER(S)		
6a NAME OF PERFORMING ORGANIZATION Vibration Institute	6b OFFICE SYMBOL (If applicable)	7a NAME OF MONITORING ORGANIZATION Office of Naval Research		
6c ADDRESS (City, State, and ZIP Code) 6262 S. Kingery Hwy. Willowbrook, IL 60514		7b ADDRESS (City, State, and ZIP Code) Arlington, VA 22217-5000		
8a NAME OF FUNDING/SPONSORING ORGANIZATION Office of Naval Research	8b OFFICE SYMBOL (If applicable)	9 PROCUREMENT INSTRUMENT IDENTIFICATION NUMBER Grant No: N00014-90-J-1611		
8c ADDRESS (City, State, and ZIP Code) Arlington, VA 22217-5000		10 SOURCE OF FUNDING NUMBERS		
		PROGRAM ELEMENT NO	PROJECT NO	TASK NO WORK UNIT ACCESSION NO
11 TITLE (Include Security Classification) Current Practices and Trends in Mechanical Failure Prevention				
12 PERSONAL AUTHOR(S) Compiled by Henry C. Pusey and Sallie C. Pusey				
13a TYPE OF REPORT Conference Proceedings	13b TIME COVERED FROM 1/1/90 TO 4/2/90	14 DATE OF REPORT (Year, Month, Day) 90/4/2	15 PAGE COUNT 370	
16 SUPPLEMENTARY NOTATION				
17 COSATI CODES			18 SUBJECT TERMS (Continue on reverse if necessary and identify by block number)	
FIELD	GROUP	SUB-GROUP	Rotating equipment, motors, detection, diagnosis, prognosis, failure mechanisms, current monitoring, oil analysis, gearboxes, durability, machine tools	
19 ABSTRACT (Continue on reverse if necessary and identify by block number) This document is the proceedings of the 44th Meeting of the Mechanical Failures Prevention Group (MFPG) which was held at Virginia Beach, VA on April 3-5, 1990. The proceedings contains featured papers on the high cost of failures of rotating equipment, legal liability of the design engineer, detection, diagnosis, and prognosis: an evaluation of current technology, and plasticity in failure mechanisms. Session papers on motor driven equipment diagnostics, oil analysis in machinery diagnostics, methodology for improved durability, fault diagnosis, condition monitoring, mechanisms of failure, and predictive maintenance are included in the proceedings.				
20 DISTRIBUTION/AVAILABILITY OF ABSTRACT <input checked="" type="checkbox"/> UNCLASSIFIED/UNLIMITED <input type="checkbox"/> SAME AS RPT <input type="checkbox"/> DTIC USERS			21 ABSTRACT SECURITY CLASSIFICATION Unclassified/unlimited	
22a NAME OF RESPONSIBLE INDIVIDUAL Peter Schmidt			22b TELEPHONE (Include Area Code) 202/696-0285	22c OFFICE SYMBOL

DD FORM 1473, 84 MAR

83 APR edition may be used until exhausted
All other editions are obsolete

SECURITY CLASSIFICATION OF THIS PAGE

U.S. Government Printing Office: 1985-00P-007